Reactions of rhodium(I) with diynes and studies of the photophysical behavior of the luminescent products

Dissertation zur Erlangung des naturwissenschaftlichen Doktorgrades

der Julius-Maximilians-Universität Würzburg

vorgelegt von

Florian Tobias Kerner

aus Memmingen

Würzburg, 2020

Eingereicht bei der Fakultät für Chemie und Pharmazie der Julius-Maximilians-Universität Würzburg am: _____

Gutachter der schriftlichen Arbeit

1. Gutachter: Prof. Dr. Dr. h. c. Todd B. Marder
2. Gutachter: Prof. Dr. Udo Radius

Prüfer des öffentlichen Promotionskolloquiums

1. Prüfer: Prof. Dr. Dr. h. c. Todd B. Marder
2. Prüfer: Prof. Dr. Udo Radius
3. Prüfer:

Datum des öffentlichen Promotionskolloquiums

am: _____

Doktorurkunde ausgehändigt

am: _____

"Thinking is the hardest work there is,

which is probably the reason why so few engage in it."

Henry Ford

Für meine Familie & Lina

Die Experimente zur vorliegenden Arbeit wurden in der Zeit von Juni 2016 bis Juni 2020 am Institut für Anorganische Chemie der Julius-Maximilians-Universität Würzburg unter der Aufsicht von Prof. Dr. Dr. h. c. Todd B. Marder durchgeführt.

Abbreviations

A	Absorbance
Å	Ångström, 1 Å = 10^{-10} m
ACN	Acetonitrile
abs	Absorption
acac	Acetylacetonate
a.u.	Arbitrary units
APCI	Atmospheric-pressure chemical ionization
BINAP	2,2′-Bis(diphenylphosphino)-1,1′-binaphthyl
BHT	3,5-Di-*tert*-butyl-4-hydroxytoluene
bpy	Bipyridine
°C	Degrees Celsius
c	Concentration, mol l^{-1}
CCDC	Cambridge Crystallographic Data Center
COD	Cyclooctadiene
COE	Cyclooctene
Cp	Cyclopentadienyl
Cp*	Pentamethylcyclopentadienyl
Cy	Cyclohexyl
d	Doublet
DCE	1,2-Dichloroethylene
DCM	Dichloromethane
dd	Doublet of doublets
DFT	Density functional theory
dt	Doublet of triplets
DTBM-Segphos	5,5′-Bis[di(3,5-di-tert-butyl-4-methoxyphenyl)phosphino]-4,4′-bi-1,3-benzodioxole
dtc	Diethyldithiocarbamate
Ebthi	Ethylenebistetrahydroindenyl
EtOH	Ethanol
em	Emission
eV	Electron volt, 1 eV = 1.60 x 10^{-19} J
equiv.	Equivalent
F	Fluorescence

f	Oscillator strength
GCMS	Gas chromatography mass spectrometry
h	Hour
H_8-BINAP	2,2'-Bis(diphenylphospino)-5,5',6,6',7,7',8,8'-octahydro-1,1'-binaphthyl
HDDA	Hexadehydro Diels-Alder
HOMO	Highest occupied molecular orbital
HRMS	High-resolution mass spectrometry
Hz	Hertz, 1 Hz = 1 s^{-1}
IMes	1,3-Dimesitylimidazol-2-ylidene
I	Intensity, a.u.
IC	Internal conversion
IL	Intra ligand
IR	Infrared
IRF	Instrument response factor
ISC	Inter-system crossing
J	*J*-coupling constant, Hz
K	Kelvin
k	Rate constant
kcal	Kilocalorie, 1 kcal = 4.1868 kJ
k_{IC}	Internal conversion rate constant, s^{-1}
k_{ISC}	Intersystem-crossing rate constant, s^{-1}
k_F	Fluorescence rate constant, s^{-1}
k_P	Phosphorescence rate constant, s^{-1}
k_{nr}	Non-radiative decay rate constant, s^{-1}
k_r	Radiative rate constant, s^{-1}
LF	Ligand field
LIFDI	Liquid injection field desorption ionization
LMCT	Ligand-to-metal charge-transfer
LUMO	Lowest unoccupied molecular orbital
$[M]^+$	Molecular ion
M	Metal
M	Molar concentration, 1 M = 1 mol L^{-1}
m	Multiplet
Me_2Im	1,3-Dimethylimidazolin-2-ylidene

MHz	Mega Hertz
min	Minute, 1 min = 60 s
MLCT	Metal-to-ligand charge-transfer
MO	Molecular orbital
mol%	Percentage by amount
m/z	Mass to charge ratio
µs	Microseconds
NHC	N-heterocyclic carbene
nm	Nanometer
NMR	Nuclear magnetic resonance
$^{n}Pr_2Im$	1,3-Di-*n*-propylimidazolin-2-ylidene
nr	Non-radiative
ns	Nanosecond
ox	Oxalate
P	Phosphorescence
ppm	Parts per million
ppy	2-Phenyl pyridine
rt	Room temperature
s	Second
SOC	Spin orbit coupling
S_0	Ground state
S_1	1st singlet excited state
S_n	nth Singlet (excited) state
T	Temperature
TCSPC	Time-correlated single photon counting
TD	Time dependent
THF	Tetrahydrofuran
TMS	Trimethylsilyl
T_1	1st triplet excited state
T_n	nth Triplet (excited) state
Tp^{Me2}	Hydrotris(3,5-dimethylpyrazolyl)borate
UV-vis	Ultraviolet-visible
V	Volt, 1 V = J C^{-1}
wt%	Percentage by weight

Δ	Heat
ΔH^0	Standard enthalpy
ΔE	Difference in energy, eV or cm^{-1}
δ	Chemical shift, ppm
ε	Extinction coefficient, M^{-1} cm^{-1}
η	Hapticity of a ligand
λ	Wavelength, nm
λ_{em}	Emission wavelength, nm
λ_{ex}	Excitation wavelength, nm
λ_{max}	The longest-wavelength maximum, nm
τ	Excited state lifetime
Φ	Quantum yield of photoluminescence
χ^2	Chi-squared (statistical tool)

Table of contents

Chapter 1

1 Introduction

1.1 Metallacycles

Cyclic compounds comprise a series of atoms connected to form a ring, the size of which can vary from three to several 100 atoms. These ring systems can consist of only carbon (carbocycle), no carbon at all (inorganic cyclic compounds), or carbon and non-carbon atoms (heterocycles).[1-3] Heterocycles containing carbon and metal atoms are called metallacycles. The metal is usually bound into a cyclic structure with two metal-carbon bonds.[4] These ring-systems can be aromatic or non-aromatic. Aromaticity, which is well known in pure organic compounds, can also be found in metal-containing compounds. Metallaaromatics are aromatic compounds in which one of the ring atoms is a transition metal and its metal d-orbitals are involved in the π-delocalization. In metallabenzenes, for example, a CH-unit is replaced with an isolobal transition metal fragment. The classes of metallabenzenes, fused-ring metallabenzenes, heterometallabenzenes and metallabenzynes have been investigated in detail.[5]

Metallacycles have a multi-faceted structural chemistry and they play an important role in different catalytic processes, e.g., polymerization, oligomerization and metathesis reactions of olefins and alkynes. Metallacyclobutanes, for example, occur as intermediates in olefin metathesis. For their elucidation of the mechanism, and the discovery of highly effective catalysts, Yves Chauvin, Robert H. Grubbs and Richard R. Schrock were awarded with the Nobel Prize in Chemistry in 2005 (Scheme 1-1).[6]

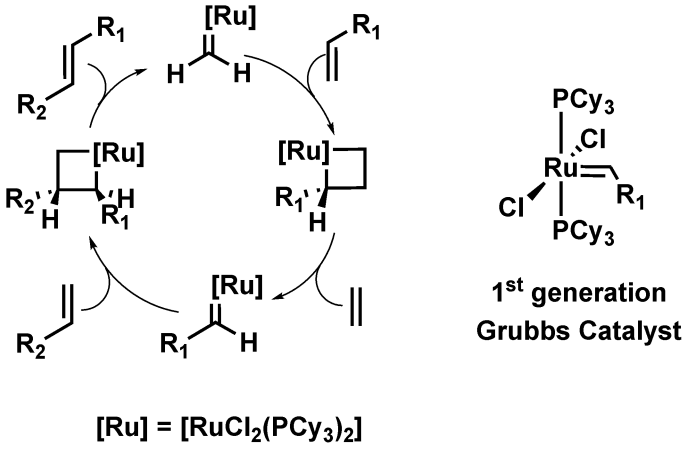

Scheme 1-1: Mechanistic cycle for the alkene metathesis reaction (left) with Grubbs 1st generation catalyst (right).

Furthermore, metallacycles have been used as precursors for alkylidenes, alkylidynes, vinylidenes, and η^5-vinyl complexes, and employed for the synthesis of main group heterocycles, organic molecules and functionalized polymers.[7-8]

1.1.1 Metallacyclopropenes

For transition metal complexes with disubstituted acetylenes, two extreme bond types can be formulated (Scheme 1-2), which can be distinguished by single-crystal X-ray diffraction analysis, or by the infrared stretching frequencies of the coordinated acetylene.

The π-bound type is considered as a monodentate ligand, bound in an η^2-fashion, and does not alter the oxidation state of the metal. The angular geometry of the acetylene is not greatly influenced by the bonding and the infrared stretching frequencies of the coordinated acetylene, compared to the unbound acetylene are only slightly reduced by ca. 100 – 200 cm^{-1}.

In the σ-bound type, two metal-carbon bonds are formed and the formal oxidation state of the metal increases from "n" to "n+2". The angular geometry of the acetylene exhibits a strong distortion of the acetylenic bond angles from 180 to ca. 120° and an elongation of the C-C triple-bond length from ca. 1.20 to 1.40 Å. The infrared stretching frequencies of the coordinated acetylene are dramatically lowered by ca. 500 cm^{-1}.[9-10]

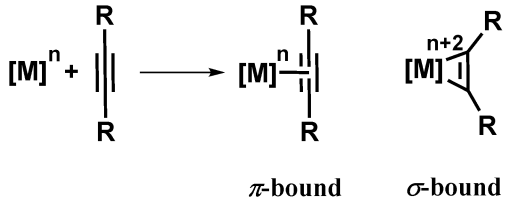

Scheme 1-2: Two extreme types of acetylene bonding to a transition metal [M]: π-bound and σ-bound.

The smallest possible ring size is a three-membered ring, a metallacyclopropene. These complexes are usually reactive and often used as precursors for the synthesis of larger ring systems. Nonetheless, various examples of such systems have been characterized,[11] such as the titanocene and zirconocene bis(trimethylsilyl)acetylene complexes shown in Scheme 1-3.[4, 12] These unstable complexes can be used as precursors for the synthesis of five-membered titana- and zirconacycles.[13]

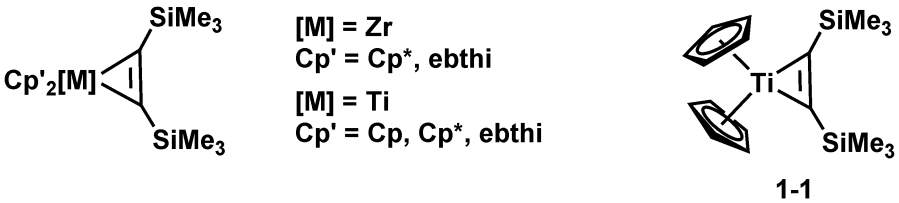

Scheme 1-3: The smallest possible, three-membered metallacycle (left). The metallocene [M(Cp'$_2$] is stabilized by bis(trimethylsilyl)acetylene. The structure of [Ti(η^5-Cp)$_2$(η^2-bis(trimethylsilyl)acetylene)] **1-1** (right).

A stable complex with a metallacyclopropene core structure is [ReCp*(CO)$_2$(η^2-CPhCHPh)]BF$_4$ **1-2**, formed in the reaction of [ReCp*(CO)$_2$(η^2-PhCCPh)] with HBF$_4$[14] or [RhCp(P(^{i}Pr)$_3$)$_2$(η^2-MeCCMe)] **1-3** formed in the reaction of [RhCl(P(^{i}Pr)$_3$)$_2$(η^2-MeCCMe) with NaCp (Scheme 1-4).[15]

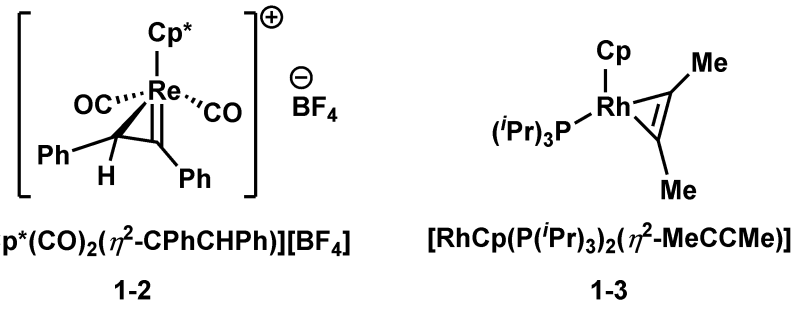

[ReCp*(CO)$_2$(η^2-CPhCHPh)][BF$_4$] **1-2**

[RhCp(P(^{i}Pr)$_3$)$_2$(η^2-MeCCMe)] **1-3**

Scheme 1-4: Stable metallacyclopropene complexes [ReCp*(CO)$_2$(η^2-CPhCHPh)]BF$_4$ and [RhCp(P(^{i}Pr)$_3$)$_2$(η^2-MeCCMe)].

Such metallacyclopropenes can not only be formed with substituted alkynes, but also with substituted buta-1,3-diynes. As already described for the reactions with alkynes, when using buta-1,3-diynes, it is possible to form compounds which are either stable over a longer period of time, or are just short-lived intermediates.

Werner *et al.* synthesized various square planar 16-electron rhodium complexes with η^2-bound alkynes, resulting in rhodacyclopropenes **1-4** to **1-7** (Scheme 1-5)[16-19] as well as an iridium analogue of compound **1-4**.[20] Complex **1-4** was found to be only slightly air-sensitive and even stable on deactivated Al_2O_3.[16] Furthermore, it was found that compound **1-6** is an intermediate in the trimerization of methylpropiolate forming a hexadienyne derivative.[18]

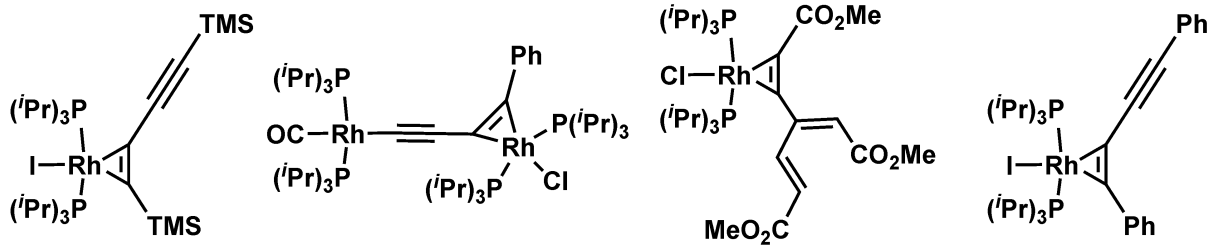

1-4 **1-5** **1-6** **1-7**

Scheme 1-5: Various square planar 16-electron rhodium complexes with η^2 bound alkynes **1-4** – **1-7** synthesized by Werner and co-workers.

Ward reported the formation of the 18-electron, trigonal bipyramidal [Rh(PMe_3)$_3$Cl((1,2-η^2)-*p*-F_3C–C_6H_4–CC–CC–C_6H_4-*p*-CF_3)] **1-8** and [Rh(PMe_3)$_3$Cl]$_2$(μ-(1,2-η^2):(1,2-η^2)-*p*-F_3C–C_6H_4–CC–CC–C_6H_4-*p*-CF_3) **1-9** complexes in solution, from the reaction of the salt [Rh(PMe_3)$_4$]Cl with CF_3-substituted 1,4-diphenylbuta-1,3-diyne. However, a third species, [Rh(PMe_3)$_3$Cl]$_2$(μ-(1,2-η^2):(3,4-η^2)-*p*-F_3C–C_6H_4–CC–CC–C_6H_4-*p*-CF_3) **1-10** was obtained as single-crystals suitable for X-ray diffraction analysis (Scheme 1-6).[21]

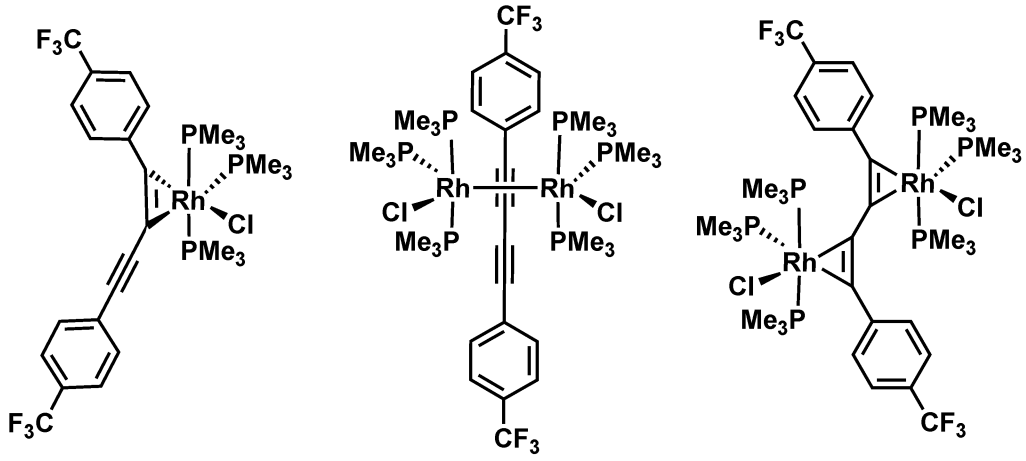

1-8 **1-9** **1-10**

Scheme 1-6: Formation of different π-complex in the reaction of [Rh(PMe_3)$_4$Cl] with CF_3-substituted 1,4-diphenylbuta-1,3-diyne.

1.1.2 Metallacyclobutenes

Metallacyclobutenes are proposed to be intermediates in metal-catalyzed C-C bond forming reactions, e.g. enyne/"ynene" metathesis, cyclopropenation, alkyne polymerization or titanium-catalyzed carboamination and hydrophosphination of diphenylacetylene. With an appropriate combination of metals, ligands and ring substituents, it is possible to study the formation and reactivity of those unsaturated metallacycles, or even isolate and characterize them.[22] Although the number of metallacyclobutenes is limited, various synthetic pathways for the formation have been employed. Complexes of the form of **1-11** were prepared by Tebbe and co-workers in the reaction of [$TiCp_2CH_2AlClMe_2$] with alkynes.[23-25] Hughes *et al.* synthesized **1-12** and **1-13** *via* the oxidative addition of perfluorocyclopropene to [$Pt(C_2H_4)(PR_3)_2$][26] and [$IrCl(PR_3)_2CO$].[27] Metallacyclobutenes of the form of **1-14** can be synthesized by the addition of nucleophiles to rhenium-,[28-29] platinum- and iridium[25] allenyl or propargyl complexes. By treating the cobalt-alkyne species [$CoCp(PPh_3)(\eta^2$-TMS-$CCSO_2Ph)$] with ethyl diazoacetate, O'Connor and co-workers synthesized **1-15**.[30] The phospha-metallacyclobutene complex **1-16** is formed in the [2+2] cycloaddition reaction of the terminal phosphido complex [$Ru(\eta^5$-indenyl$)(PPh_3)(PR_2)$] with acetylenes.[31]

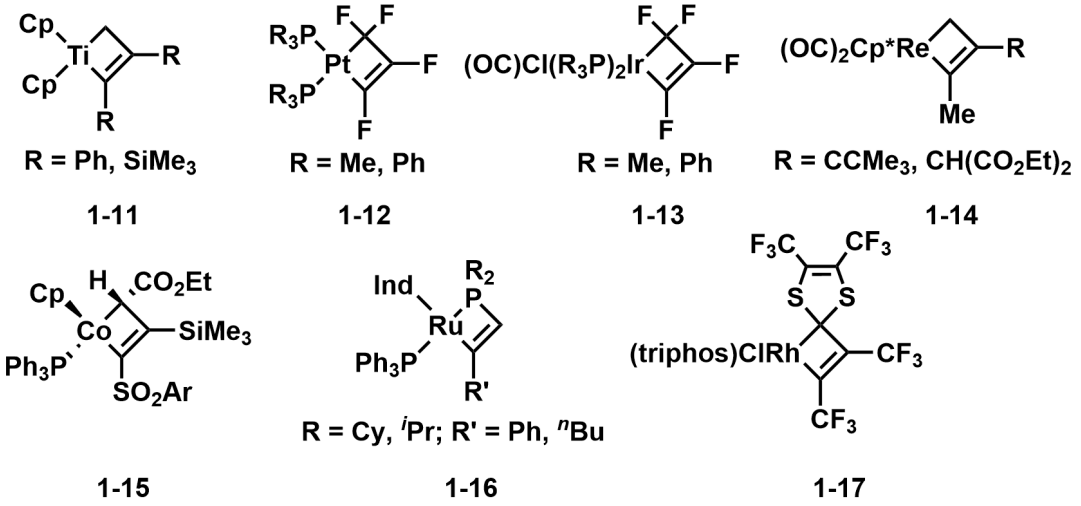

Scheme 1-7: Metallacyclobutene complexes **1-11** – **1-17**.

Examples for rhodacyclobutenes are rare. The only complex reported **1-17** was described by Sabat and co-workers in 1985, and was prepared *via* the addition of two equivalents of hexafluorobut-2-yne to [$RhCl(triphos)(\eta^2$-$CS_2)$] (Scheme 1-7).[32]

1.1.3 Metallacyclopentadienes

A wide range of transition metals have been used in the past for synthesizing metallacyclopentadienes e.g. Ti,[33] Zr,[34] Hf,[35] Pt,[36] Pd,[37] Ir,[38] Ru,[39] W,[40] Fe,[41] Au,[42] Rh,[43] and Co.[44]

Nishihara and co-workers synthesized three regioisomeric diethynylcobaltacyclopentadienes and one insoluble polymer as the major product, by reductive coupling of two equivalents of diphenylbuta-1,3-diyne with [Co(Cp)(PPh_3)$_2$] **1-18** (Scheme 1-8).

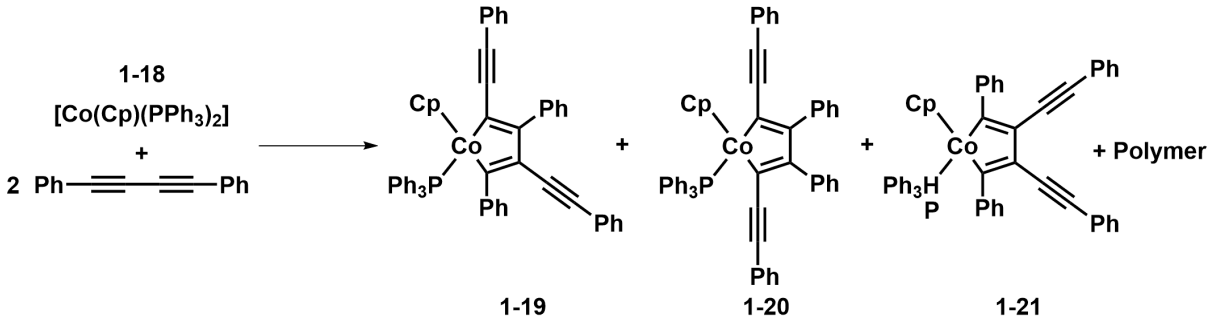

Scheme 1-8: Reductive coupling of diphenylbuta-1,3-diyne with [Co(Cp)(PPh_3)$_2$] **1-18** and the resulting three regioisomers **1-19**, **1-20** and **1-21**, and an insoluble polymer as the main product.

At 40 °C, with two equivalents diphenylbuta-1,3-diyne, the major isomer formed was the unsymmetric 2,4-bis(phenylethynyl)cobaltacyclopentadiene **1-19**, and the minor product was the symmetric 3,4-bis(phenylethynyl) complex **1-21**. The symmetric 2,5-bis(phenylethynyl) complex **1-20** was only formed as the minor product at elevated temperatures in addition to **1-19** and **1-21** which where the major isomers.[45] Replacing the phenyl group with the bulkier trimethylsilyl (TMS) group, led to the 2,4-bis(trimethylsilylethynyl) complex as only isomer **1-22** (Scheme 1-9). When Me-CC-CC-Me was used, the 2,5-bis(methylethynyl) complex **1-23** was the only isomer formed.[45]

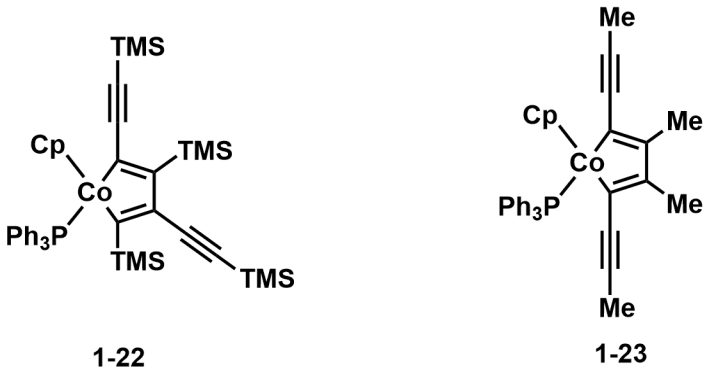

Scheme 1-9: Major isomers formed in the reaction of [Co(Cp)(PPh_3)$_2$] **1-18** with TMS-CC-CC-TMS and Me-CC-CC-Me.

The structural selectivity for the main isomers in Schemes 1-8 and 1-9 can be explained by findings from Wakatsuki *et al.* They proposed that the formation of the cobaltacyclopentadiene is controlled by steric rather than electronic factors and the bulky substituent of the acetylene is found at the 2- and 4-positon of the cobaltacyclopentadiene.[46]

Similar results were observed in the reaction of the labile titanium precursor **1-1** with two equivalents of bis(trimethylsilyl)buta-1,3-diyne. The 2,4-(trimethylsilylacetylene)titanocyclo-pentadiene complex **1-24** was formed exclusively (Scheme 1-10).[47-48]

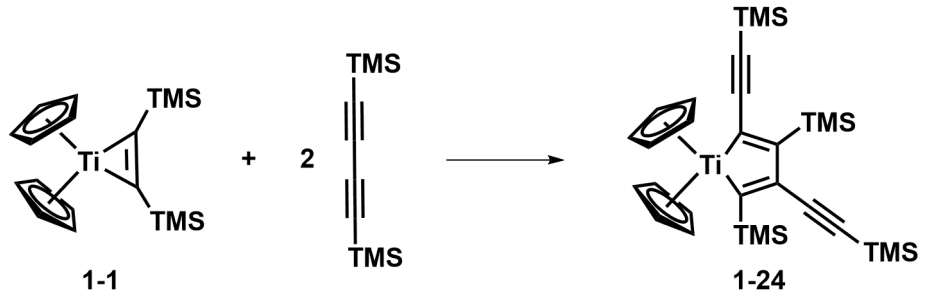

Scheme 1-10: Formation of the asymmetric 2,4-bis(trimethylsilylethynyl)titanocyclopentadiene **1-24**.

In the reaction of diphenylbuta-1,3-diene with $[Ru_3(CO)_{10}(NCMe)_2]$ in the presence of trimethylamine oxide (NMe_3O), a mononuclear 2,5-bis(phenylethynyl)ruthenacyclopentadiene complex **1-25** formed in ca. 4% yield, along with various other complexes.[49] In 2007, Hill and co-workers were more successful with their regioselective synthesis of a 2,5-bis(phenylethynyl)ruthenacyclopentadiene **1-26** by varying the metal precursor. The 2,5-isomer is formed exclusively in 80% yield in the reaction of $[Ru(CO)_2(PPh_3)_3]$ with an excess of diphenylbuta-1,3-diyne at elevated temperatures (Scheme 1-11).[50]

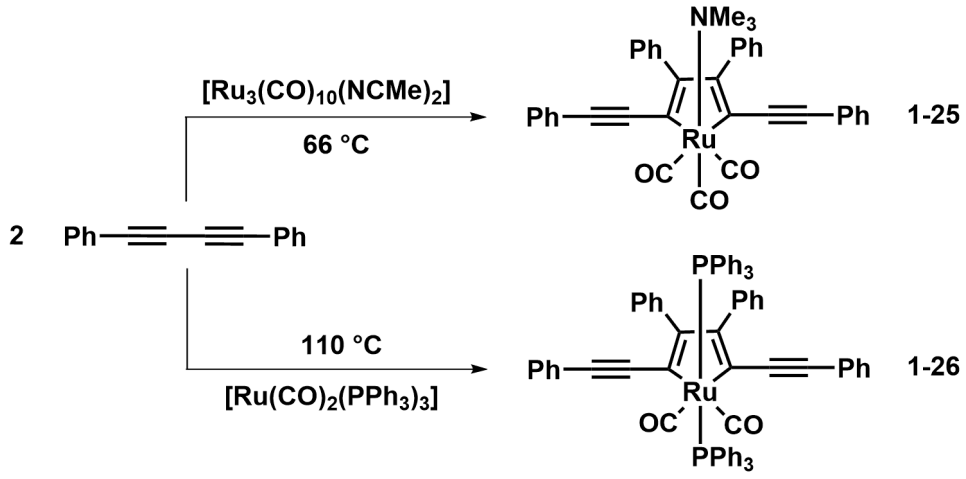

Scheme 1-11: Non-regiospecific formation of 2,5-bis(phenylethynyl)ruthenacyclopentadiene **1-25** and the regiospecific formation of 2,5-bis(phenylethynyl)ruthenacyclopentadiene **1-26**.

Although there is a wide variety of different metallacyclopentadienes and different routes for their synthesis are known, the knowledge of their photophysical and excited-state properties is

less well explored.[51] This is astonishing, as they are structurally related to main group EC_4 systems such as boroles,[52] siloles,[53] phospholes[54] and thiophenes[55] (Scheme 1-12), whose optical and electron-transporting properties have been explored in considerable detail. In addition, 2,5-bis(arylethynyl) conjugated ring systems are of special interest due to their linear and nonlinear optical properties.[56]

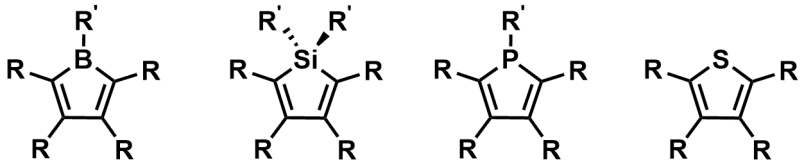

Scheme 1-12: Borole, silole, phosphole and thiophene structures.

1.1.4 Rhodacyclopentadienes

In 2001, Marder and co-workers successfully developed a high-yield, one-pot synthesis of a luminescent 2,5-bis(*p*-tolylethynyl)rhodacyclopentadiene **1-30a** *via* the regiospecific reductive coupling of two equivalents of di-*p*-tolylbuta-1,3-diyne with [Rh(CCSiMe$_3$)(PMe$_3$)$_4$] **1-28a**. The complex formed within minutes at room temperature, and only the 2,5-bis(arylethynyl)metallacyclopentadiene isomer was observed (Scheme 1-13).[57]

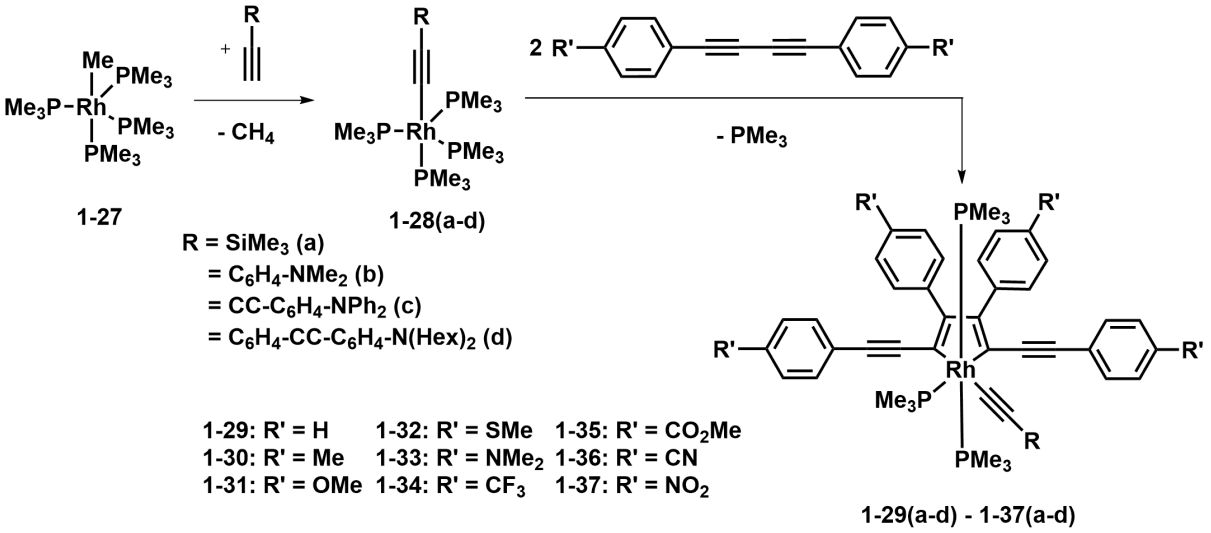

Scheme 1-13: Regiospecific reductive coupling of *para*-substituted 1,4-diphenylbuta-1,3-diynes with the rhodium(I) complexes **1-28(a-d)** forming 2,5-bis(arylethynyl)rhodacyclopentadienes **1-29(a-d)** – **1-37(a-d)**.

In the course of further research, functionalization at the metal bound alkynyl ligand (R = SiMe$_3$, *p*-C$_6$H$_4$-NMe$_2$, CC-(*p*-C$_6$H$_4$-NPh$_2$), *p*-C$_6$H$_4$-CC-*p*-C$_6$H$_4$-N(Hex)$_2$) and at the *para*-substituted 1,4-diphenylbuta-1,3-diynes (R'= H, Me, OMe, SMe, NMe$_2$, CF$_3$, CO$_2$Me, CN and NO$_2$) were explored leading to the synthesis of **1-28(a-d)** and 2,5-bis(arylethynyl)rhodacyclopentadienes **1-29(a-d)** – **1-37(a-d)**. Remarkably, in all cases, only the 2,5-bis(arylethynyl)rhodacyclopentadiene isomer was formed quantitatively and regiospecifically at room temperature, which was confirmed by $^{31}P\{^1H\}$ NMR spectroscopy. When R' was a donor, the reaction was slower than for R' being an acceptor. This is a result of the diminished π-backbonding from the electron-rich rhodium(I) center in the precursor diyne π-complexes. Complexes **1-29a**,**b** – **1-37a**,**b** were found to be robust and insensitive to air and moisture in the solid state, and the acceptor-substituted complexes **1-34a**,**b – 1-37a**,**b** are also stable in THF and toluene solutions over a period of several months. However, with longer conjugated substituents R on the rhodium metal, complexes **1-29c**,**d** – **1-37c**,**d** are rather sensitive to air.

Complexes **1-38**, **1-39** and **1-40** were synthesized to determine whether they possess liquid-crystal behavior and for further investigations on the influence of longer π-conjugation of the ligand on the photophysical behavior. However, no evidence for liquid-crystal phase behavior was observed. Complexes **1-38**, **1-39** and **1-40** are sensitive to air and moisture (Scheme 1-14).

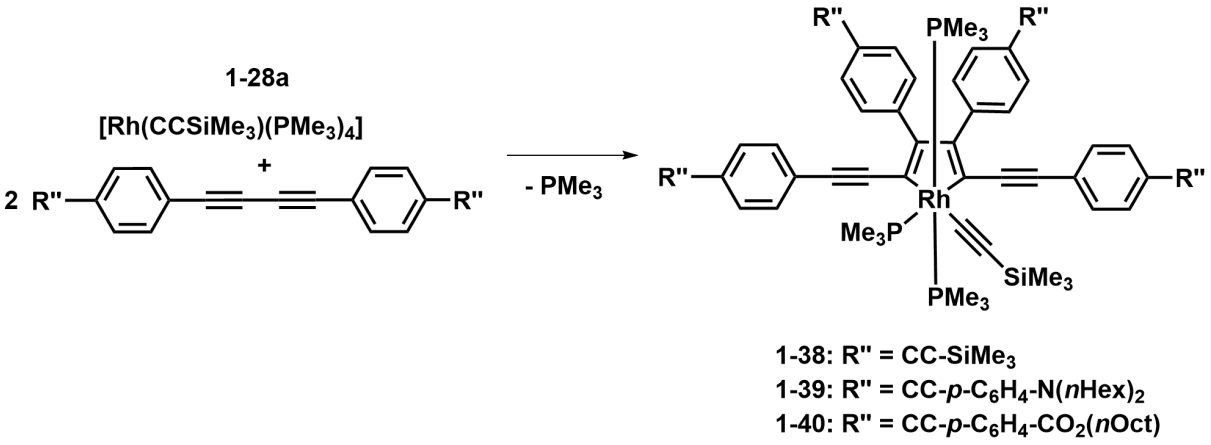

Scheme 1-14: Synthesis of 2,5-bis(arylethynyl)rhodacyclopentadienes **1-38**, **1-39** and **1-40**.

Reaction of [RhCl(PMe$_3$)$_4$], the precursor of **1-27**, with *para*-substituted 1,4-diphenylbuta-1,3-diynes was only successful for R' being CF_3 and at 80 °C for four days, yielding moderate amounts of the desired chloro-substituted 2,5-bis(arylethynyl)rhodacyclopentadiene. This limitation for the chloro-substituted complexes can be avoided by the reaction of [RhMe(PMe$_3$)$_4$] **1-27** with two equivalents of *para*-substituted 1,4-diphenylbuta-1,3-diynes (R' = H, Me, OMe, SMe, NMe_2, CF_3, CO_2Me) at 80 °C for 3 – 12 hours yielding rhodacyclopentadienes **1-41(a-g)**, followed by the addition of HCl·Et_2O, resulting in the chloro-substituted rhodacyclopentadienes **1-42(a**, **c**, **d**, **f** and **g**) (Scheme 1-15).[56]

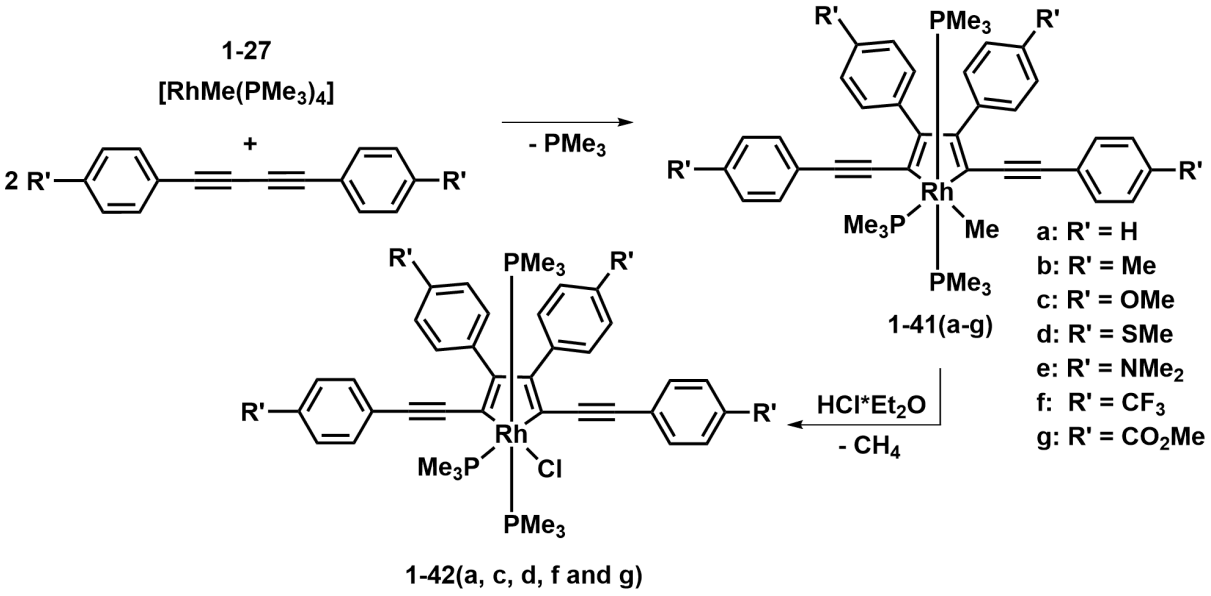

Scheme 1-15: Synthesis of methyl-**1-41(a-g)** and chloro-**1-42(a**, **c**, **d**, **f** and **g)** substituted 2,5-bis(arylethynyl)rhodacyclopentadienes.

Further modification of the *para*-substituted 1,4-diphenyl-1,3-butadiynes resulted in the synthesis of *α,ω*-bis(arylbutadiynyl)alkanes (*α,ω*-tetraynes) **1-43(a-d)**, in which the 1,3-butadiyne units are connected by a butyl chain.

By reacting [Rh(CCSiMe$_3$)(PMe$_3$)$_4$] **1-28a** with *α,ω*-tetraynes **1-43(a-d)** the rhodacyclopentadienes **1-45(a-d)** are formed in 23 – 82% yield (Scheme 1-16, top). The introduction of the *α,ω*-tetraynes results in a rigidification of the rhodacycle backbone which leads to more efficient fluorescence (see section 1.3.2). In order to investigate the effect of modulating the metal participation in the frontier orbitals, the -CC-R ligand in **1-28** was replaced with a diethyldithiocarbamate ligand (dtc), which is a strong *σ*- and *π*-donor, resulting in the rhodium(I) complex [Rh(S$_2$CNEt$_2$)(PMe$_3$)$_2$] **1-44**. The dtc ligand destabilizes the filled d-orbitals of the rhodium atom. Reacting the *α,ω*-tetraynes **1-43(a**, **b** and **d)** with **1-44** at 90 °C over night, the dtc-substituted rhodacyclopentadienes **1-46(a**, **b** and **d)** were obtained in an atom-economical click type reaction in 55 – 82% yield (Scheme 1-16, bottom).[58]

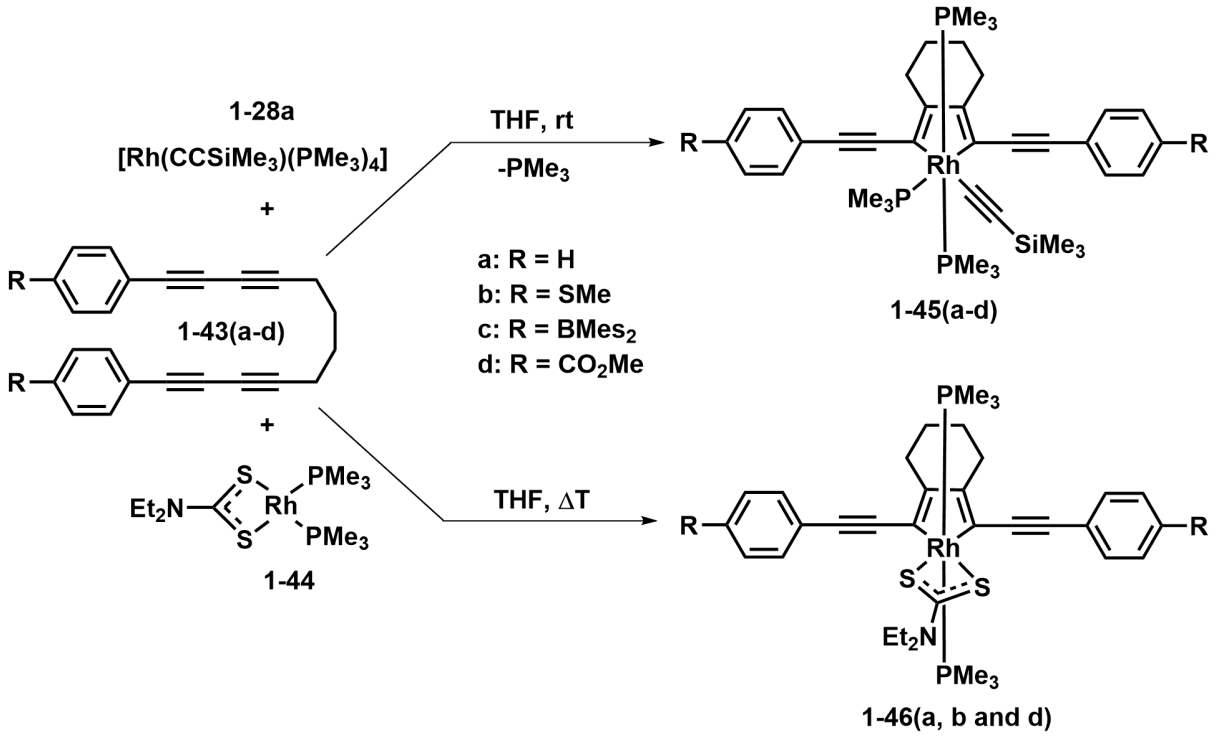

Scheme 1-16: Synthesis of 2,5-bis(arylethynyl)rhodacyclopentadienes **1-45(a-d)** and **1-46(a**, **b** and **d)**.

Reacting **1-44** at room temperature with the *α,ω*-tetraynes **1-47(a-e)**, which were shortened by one CH$_2$-unit in the backbone compared to **1-43**, results in the formation of rhodacyclopentadienes **1-48(a-e)**. The reaction with donor-substituted *α,ω*-tetraynes **1-47(a-c)** took ca. 2 – 3 weeks and, therefore, this reaction was repeated in the microwave reactor. The result was a reduced reaction time of only 15 – 24 hours at 40 °C for the synthesis of the 2,5-bis(arylethynyl)rhodacyclopentadienes (Scheme 1-17, top).

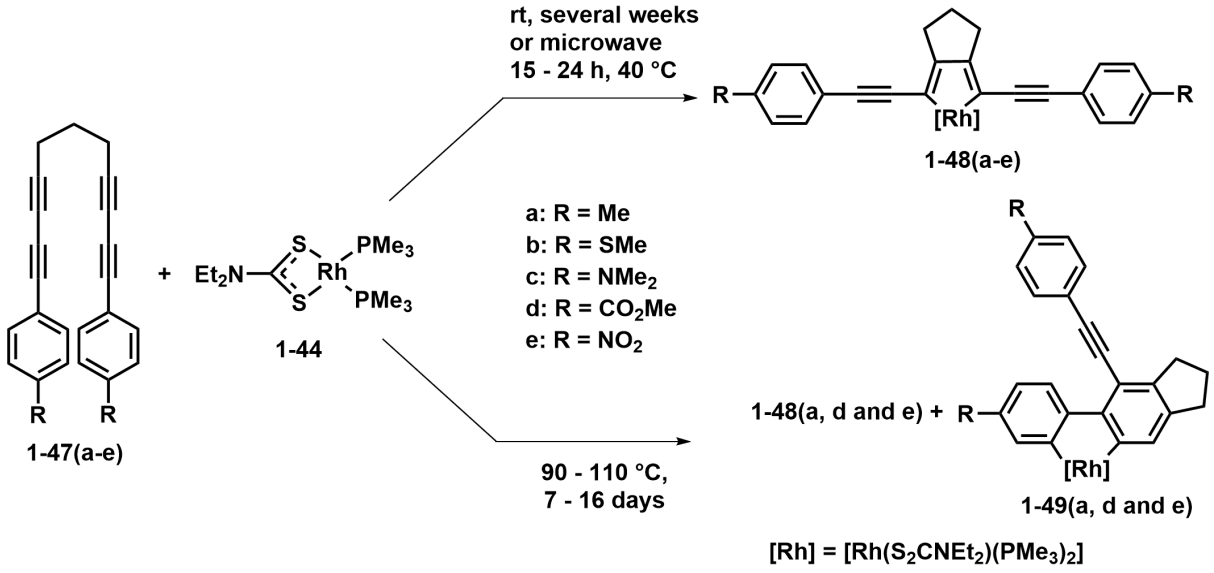

Scheme 1-17: Synthesis of 2,5-bis(arylethynyl)rhodacyclopentadienes **1-48(a-e)** and **1-49(a**, **d** and **e)**.

Heating the reaction of **1-44** with **1-47(a**, **d** and **e)** to 90 – 110 °C for several days, results in a significantly different outcome of the reaction. The 2,5-bis(arylethynyl)rhodacyclopentadienes **1-48(a**, **d** and **e)** were no longer formed exclusively. Additionally, an isomeric dibenzo-rhodacyclopentadiene **1-49(a**, **d** and **e)**, is formed in 20 – 30% yield according to $^{31}P\{^{1}H\}$ NMR spectroscopy, (Scheme 1-17, bottom). Dibenzometallacyclopentadiene complexes are difficult to synthesize due to limited synthetic methods, and their photophysical properties are hence rather less well investigated.[51, 59]

The rhodacyclopentadienes originate from a [2+2] reductive coupling and, are thus structurally related to well established intermediates in metal-mediated alkyne cyclotrimerization.[4, 60-63] The formation of the dibenzorhodacyclopentadienes is more complicated. While the group initially considered a bimetallic pathway, the most likely possibility is *via* a Hexadehydro-Diels-Alder (HDDA) reaction followed by a C-H activation and a β-H-shift as depicted in Scheme 1-18. HDDA reactions usually occur at elevated temperatures, even in the presence of metal complexes.[64-67]

In the first step of the rhodium-mediated HDDA reaction a [2+2+2] cycloaddition takes place, resulting in a benzyne coordinated to the rhodium metal center. This would be followed by an *ortho* C-H activation and loss of one trimethylphosphine ligand. Finally, a β–H sift and re-coordination of PMe_3 forms the dibenzorhodacyclopentadiene complex.

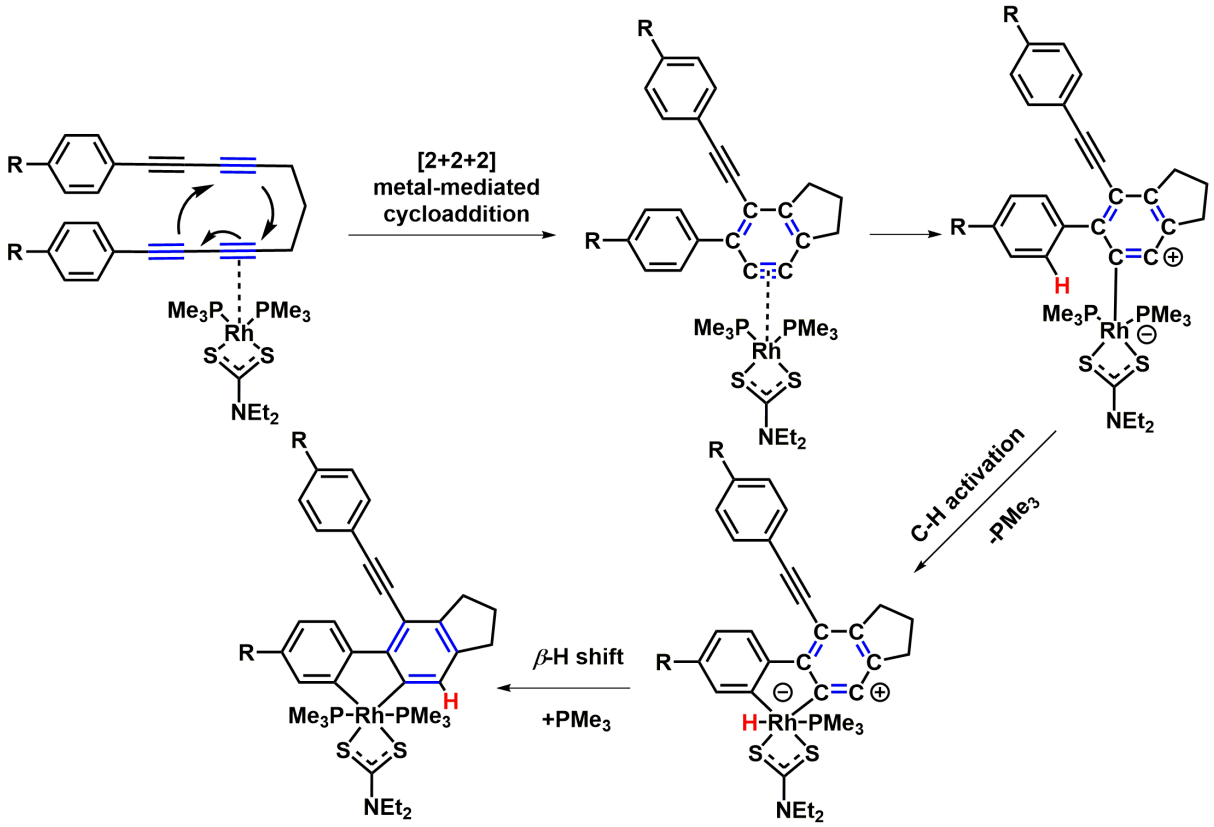

Scheme 1-18: Plausible mechanism for the formation of the dibenzorhodacyclopentadienes *via* an HDDA mechanism.

Investigations of the mechanism led to the synthesis of *α,ω*-tetrayne **1-47f** (Scheme 1-19). With this *α,ω*-tetrayne the *ortho*-C-H activation would not be possible. Surprisingly, the reaction of **1-44** with **1-47f** at room temperature resulted in the formation of a bimetallic complex **1-50** as the main species in the reaction mixture. It was possible to isolate and characterize **1-50** by multi-nuclear NMR spectroscopy and single-crystal X-ray diffraction analysis. One rhodium center is part of a six-membered ring with two trimethylphosphine ligands being *trans* disposed, while the second rhodium atom is part of a four-membered ring with *cis*-phosphines. Both rhodium atoms are bound to the same *α,ω*-tetrayne. This intermediate further reacts upon heating to give the 2,5-bis(arylethynyl)rhodacyclopentadiene **1-48f** as the main isomer. Schwenk proposed a plausible mechanism for the formation of the dibenzorhodacyclopentadiene from the bimetallic complex **1-50**. However, no experiments at 90 – 100 °C were reported, the temperature range which is usually applied for the formation of the dibenzorhodacyclopentadienes.[68-69]

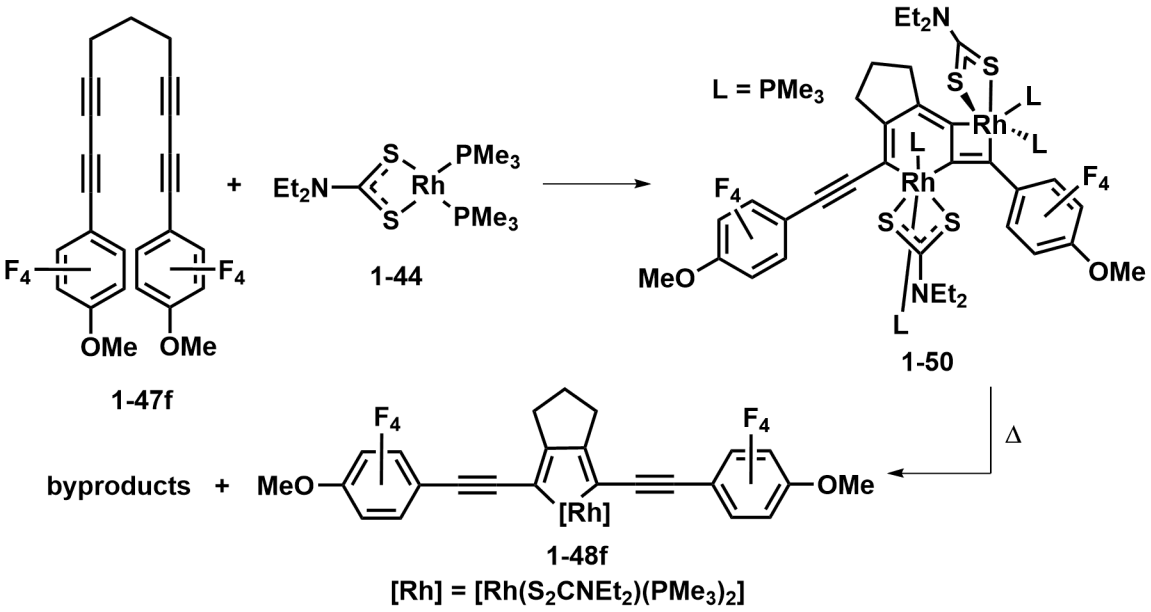

Scheme 1-19: Formation of a bimetallic intermediate **1-50** in the reaction of [Rh(S_2CNEt_2)(PMe_3)$_2$] **1-44** with **1-47f**, followed by the formation of the 2,5-bis(arylethynyl)rhodacyclopentadiene **1-48f** as the major product.

To investigate in more detail the influence of the ligand sphere around the rhodium metal center upon the rhodacycle formation and its photophysical properties, another π-electron-donating group, namely acac (acetylacetonate), was introduced *via* the rhodium(I) precursor, [Rh(acac)(PMe_3)$_2$)] **1-51**. While in the reaction of **1-44** with **1-43** no dibenzorhodacyclopentadiene was observed, and with **1-47** it was only formed at elevated temperature, the reaction of **1-51** with **1-43b**,**d** and **1-47b**,**d** results in the formation of 2,5-bis(arylethynyl)rhodacyclopentadienes **1-52b**,**d** – **1-53b**,**d** and dibenzorhodacyclopentadienes **1-54b**,**d** – **1-55b**,**d** at room temperature and at elevated temperatures (Scheme 1-20). In the reaction of **1-51** with the α,ω-tetraynes **1-43b**,**d**, in equimolar amounts, the product ratio depends on the temperature and the substituents (CO_2Me and SMe) on the aryl rings. The electron withdrawing CO_2Me group favors the dibenzorhodacyclopentadiene while an electron donating SMe group results in the predominance of the 2,5-bis(arylethynyl)-rhodacyclopentadiene. In contrast, in the reaction of **1-51** with **1-47b**,**d**, the dibenzorhodacyclopentadiene is favored, regardless of temperature and substituent. The reaction with an electron withdrawing group in *para*-position of the aryl moiety is always faster than with an electron donating group. Additionally, the reaction of **1-51** with **1-47b**,**d** is faster (< 3days) than with **1-43b**,**d** (several weeks).[59]

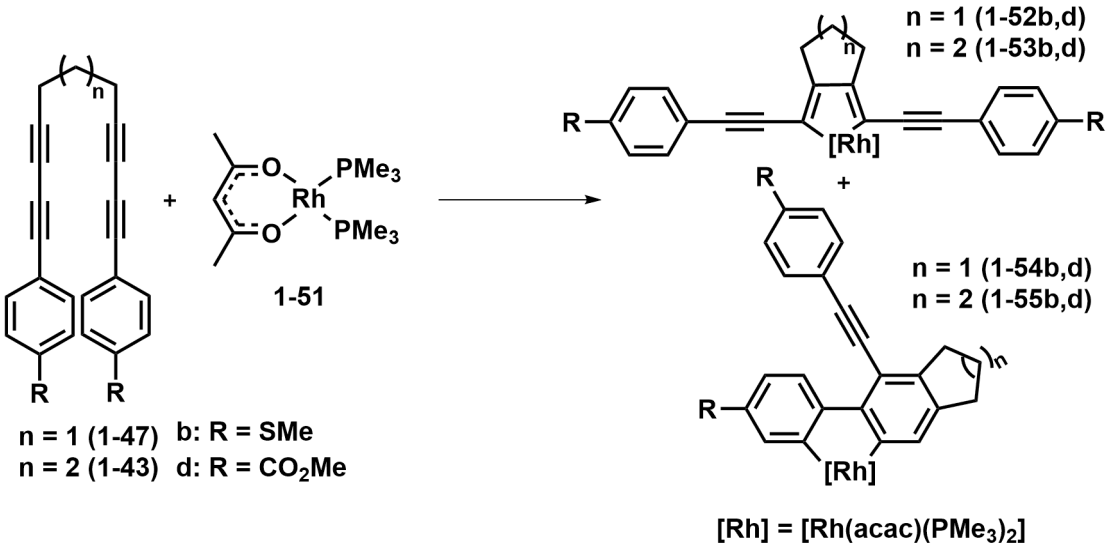

Scheme 1-20: Synthesis of 2,5-bis(arylethynyl)rhodacyclopentadienes **1-52b,d** – **1-53b,d** and dibenzorhodacyclopentadienes **1-54b,d** – **1-55b,d**.

In the reaction of **1-51** with **1-47f** it was possible to isolate single-crystals suitable for X-ray diffraction analysis of an acac-analogue species of **1-50**.[69] However, efforts to isolate larger quantities of this complex for further mechanistic studies were not successful, as numerous other rhodium-phosphine species were present in the reaction mixture, according to $^{31}P\{^{1}H\}$ NMR spectroscopy.[70]

In order to provide convenient access to 2,5-bis(arylethynyl)rhodacyclopentadienes **1-52** and to overcome the separation of the two isomers, an alternative synthesis route was established. Therefore, the reaction of [Rh(acac)(P(*p*-tolyl)$_3$)$_2$] **1-56** with the α,ω-tetraynes **1-47b**,**d** provides a selective reaction to the tri(*p*-tolyl)phosphine-substituted 2,5-bis(arylethynyl)rhodacyclopentadienes **1-57b**,**d**. A ligand exchange reaction was observed, when excess of PMe_3 was added and the reaction mixture heated at 60 °C (Scheme 1-21). Due to a weaker Rh-P bond with the P(*p*-tolyl)$_3$-ligand compared to complexes with a PMe_3-ligand, a facile ligand exchange reaction is possible.[70-71] The same route can be applied for the synthesis of the rhodacyclopentadienes **1-53** *via* the reaction of **1-56** with **1-43** followed by the addition of PMe_3 and heating.[70] Diethyldithiocarbamate-substituted rhodacyclopentadienes follow the same scheme.[68]

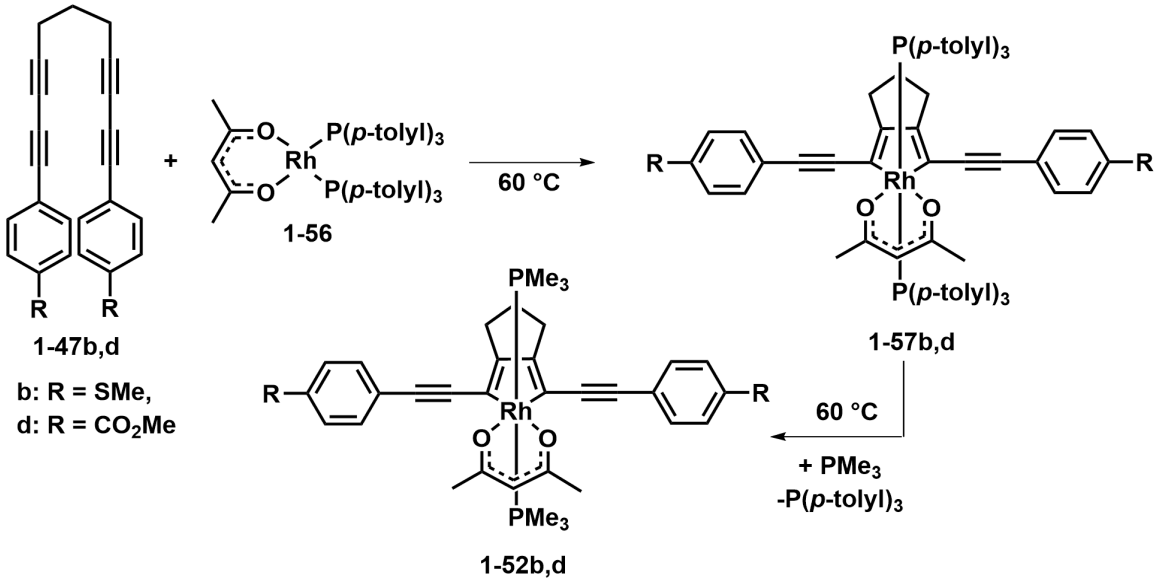

Scheme 1-21: Synthesis of 2,5-bis(arylethynyl)rhodacyclopentadienes **1-52b**,**d** *via* the reaction of [Rh(acac)(P(p-tolyl)$_3$)$_2$] **1-56** with α,ω-tetraynes **1-47b**,**d** for three days at 60 °C, followed by phosphine ligand exchange reaction.

Reactions of the SMe-substituted 2,5-bis(arylethynyl)rhodacyclopentadiene **1-57b** with NHCs (N-heterocyclic carbenes) as even stronger *σ*-donors than phosphines, were also investigated. Addition of an excess of either 1,3-di(methyl)imidazol-2-ylidene (Me_2Im) or 1,3-di(*n*-propyl)imidazol-2-ylidene ($^nPr_2Im$) to a solution of **1-57b** in toluene at room temperature led to the release of one equivalent of P(*p*-tolyl)$_3$ and to the quantitative formation of the mono-substituted NHC rhodium complexes **1-58**.[71] Attempts to replace both phosphines by gentle heating to 60 °C resulted in the formation of a black precipitate and a complex of the form [Rh($^nPr_2Im$)$_4$][acac] (Scheme 1-22).[72]

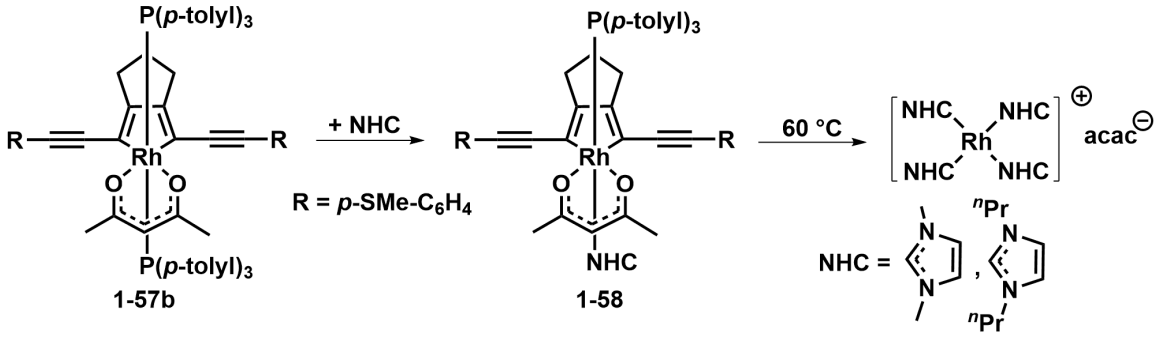

Scheme 1-22: Synthesis of the mono-NHC, mono-P(*p*-tolyl)$_3$ 2,5-bis(arylethynyl)rhodacyclopentadienes **1-58** and the formation of a decomposition product [Rh($^nPr_2Im$)$_4$][acac] after heating to 60 °C.

An NHC-phosphine exchange reaction was also observed by Schwenk in the reaction of a dtc-substituted rhodacyclopentadiene with $^nPr_2Im$ at 60 °C. Surprisingly, a *cis*-NHC-phosphine complex formed but not a *trans*-NHC-phosphine one, and no decomposition was observed, as reported by Sieck. Further studies by Schwenk revealed the possibility to exchange the acac-ligand in 2,5-bis(arylethynyl)rhodacyclopentadienes and dibenzorhodacyclopentadienes with the dtc-ligand using an excess of dtc at elevated temperature.[68]

1.2 Catalytic [2+2+2] cycloaddition reactions

The first reported cyclotrimerization was the formation of benzene from acetylene by Berthelot, in 1866.[73] In this uncatalyzed reaction, harsh thermal conditions (ca. 400 °C) were applied. About 80 years later, Reppe reported a nickel(II)-catalyzed cyclotrimerization of alkynes under milder conditions, resulting in different benzene derivatives.[74]

Cycloaddition can be promoted by, among others, heat, light, Lewis acids, high pressure, or sonication. These reaction conditions require the presence of polarized functional groups in the substrate in order to facilitate the transformation. In general, the reaction of unactivated olefins, dienes, and acetylenes requires extreme conditions, or special methods, to achieve good yields, as homodimerization of two unactivated species is a competitive reaction pathway.[61]

The thermal cyclotrimerization of acetylene forming benzene is symmetry allowed,[75] but enthalpic and entropic factors hinder this process. The reaction is extremely exothermic with ΔH° = -143 kcal mol^{-1},[76] but only occurs at temperatures above 400 °C and to a very small extent, along with the formation of various other hydrocarbons.[73] The activation barrier is calculated to lie in the 60 – 80 kcal mol^{-1} range and results from the large HOMO-LUMO gap (HOMO: highest occupied molecular orbital, LUMO: lowest unoccupied molecular orbital).[76-77] This gap prevents significant charge-transfer interactions, which are necessary for a reaction, and the overlap of filled orbitals additionally destabilizes the system. As a consequence, the acetylenes have to distort considerably before the HOMO-LUMO gap is sufficiently decreased, and stabilizing interactions overcome the destabilizing ones.[76]

The metal-promoted, atom-economical [2+2+2] cyclization strategy is a popular method for the preparation of functionalized arenes. Numerous transition metal catalysts based on Ni, Co, Pd, Cr, Rh, Fe, Zr, Nb, Ir and Ta have been developed for the [2+2+2] cyclotrimerization. The scope of the reaction is not only limited to alkynes, but can also incorporate other unsaturated molecules, including carbon dioxide, ketones, nitriles, isocyanates and olefins.[61, 78-82]

1.2.1 Mechanistic investigations on the [2+2+2] cyclotrimerization

Various mechanisms were proposed by, for example, Schrauzer[83] and Meriwether.[84] Collman *et al*. intensely studied the Ni-catalyzed mechanism proposed by Meriwether in 1968, employing isotopically labelled substrates in combination with rhodium(I) and iridium(I) precursors. Scheme 1-23 (left) shows the catalytic cycle proposed by Collman and co-workers for the metal-catalyzed cyclotrimerization of acetylenes. The presence of **1-I1**, as a possible intermediate, was confirmed by the reaction of $[IrCl(PPh_3)_2N_2]$ with dimethyl acetylenedicarboxylate. Collman was able to rule out a nickel η^4-cyclobutadiene intermediate proposed by Meriwether, on the basis of NMR spectroscopic findings, and the metallacyclopentadiene intermediate was confirmed by synthesis and characterization of rhoda- and iridacyclopentadienes **1-I2**. By subsequent reaction of these metallacyclopentadienes with dimethyl acetylenedicarboxylate, he verified their catalytic activity. Experiments using CO verified the mechanism requiring complexation of the third alkyne to the metal center, in contrast to a Diels-Alder-based mechanism. Carbon monoxide blocks the free coordination site which is required for the alkyne complexation. Colmann *et al.* pointed out that the transformation from complex **1-I3** to the cyclotrimerization product and the re-formation of the catalytic active species is complicated.[38]

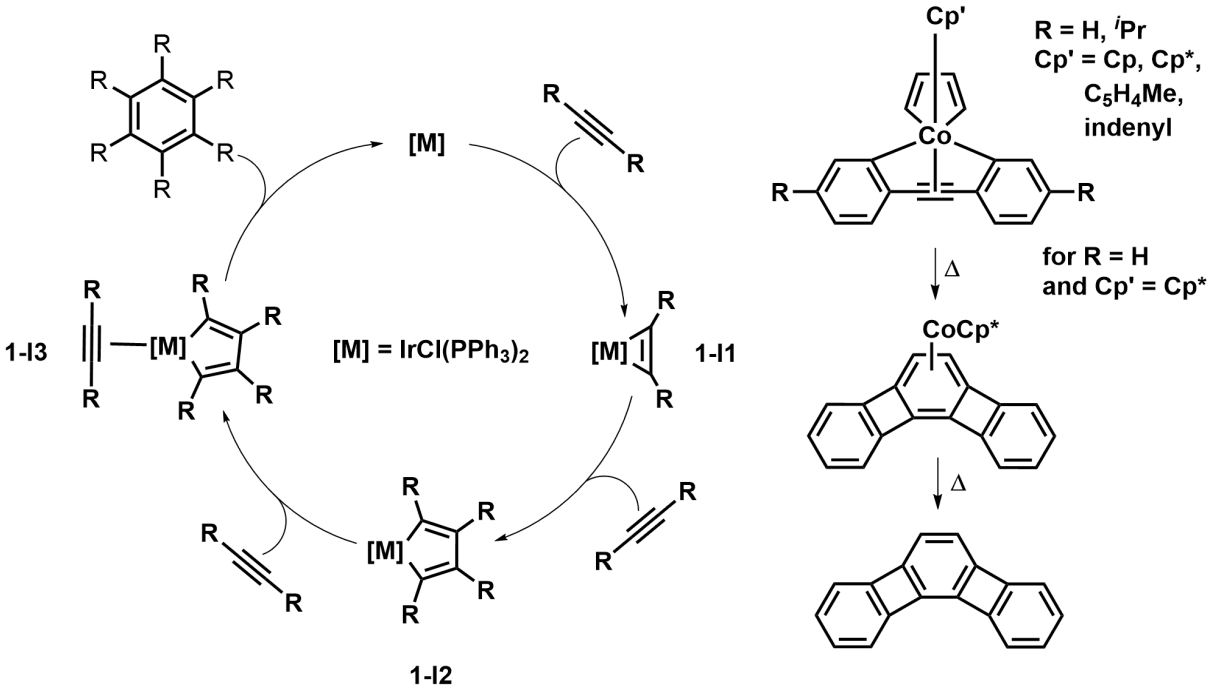

Scheme 1-23: Proposed catalytic cycle for the cyclotrimerization of alkynes by Collman, whereas [M] = $IrCl(PPh_3)_2$ and an isolated Co analogue of the suggested intermediate **1-I3** in the cyclotrimerization.

The last crucial intermediate **1-I3** in Collman's proposed catalytic cycle, which he was not able to synthesize, was clarified ca. 30 years later by Vollhardt and co-workers. They were able to isolate different cobaltacyclopentadienes bearing a π-bound alkyne moiety (Scheme 1-23, right), which forms after heating the [$CoCp^*(\eta^4$-arene)] complex, and is followed by the release of the arene species after further heating.[85]

Scheme 1-24 describes a general mechanism proposed for the CpRuCl- and CpCo-catalyzed [2+2+2] cycloaddition reactions. Sequential reaction of two alkynes results in the formation of a metallacyclopentadiene **1-I2**, followed by the coordination of a third alkyne yielding complex **1-I3**. The ring-closing step, i.e., the incorporation of the third alkyne into the metallacyclopentadiene can proceed *via* two pathways: (1) insertion forming a seven-membered metallacycloheptatriene **1-I4**; or (2) [4+2] cycloaddition resulting in the norbornadiene complex **1-I5**. After reductive elimination, complex **1-I6** is formed in both cases. Finally, decoordination from the metal affords the alkyne cyclotrimerization product and regenerates the catalytic active metal-species.

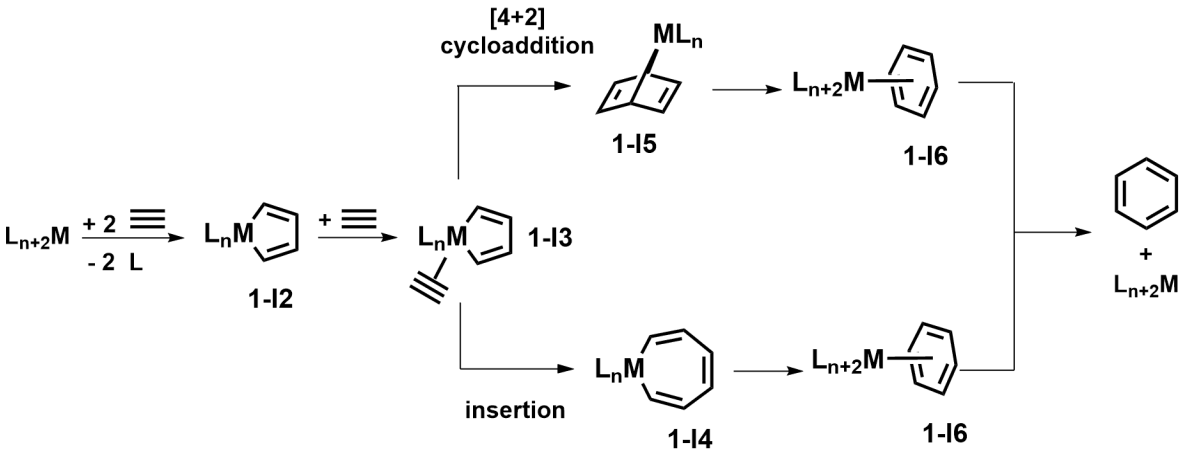

Scheme 1-24: General pathway for the CpRuCl- and CpCo-catalyzed [2+2+2] cycloaddition reaction *via* insertion and [4+2] cycloaddition.

Although this catalytic cycle was studied various times, its complete elucidation has remained elusive, as it was not possible to isolate all proposed intermediates. Computational studies help to provide further insight into the species involved in the mechanism. However, a combination of experimental studies and computational techniques is likely the best way to ascertain the mechanism.[86]

Cobalt complexes of the type [$CoCpL_2$] (L = CO, PR_3, alkenes) are probably the most studied catalytic system for the [2+2+2] cyclotrimerization of alkynes.[46, 87-94] In these studies, it was possible to isolate intermediates in the proposed catalytic cycle (Scheme 1-25). In the reaction of [$CoCp(PPh_3)_2$] with 2-butyne, it was possible to detect the monoalkyne-species **1-59** and to

isolate the cobaltacyclopentadiene **1-60**.[95] When 2-butyne was reacted with [CoCp(C_2H_4)$_2$] at -10 °C it was possible to isolate the paramagnetic, 20-electron sandwich complex **1-61**.[96] While using dimethyl acetylenedicarboxylate, an η^4-arene complex **1-62** was obtained,[97] an analogous CoCp*-complex as described in Scheme 1-23, right. Additionally, kinetic studies by Bergmann *et al.* provide evidence for the process proceeding *via* a [4+2] mechanism by the reaction of the cobaltacyclopentadiene [CoCp(C_4Me_4)(PR_3)] (R = Me, Et, Ph) with 2-butyne and dimethyl acetylenedicarboxylate.[98]

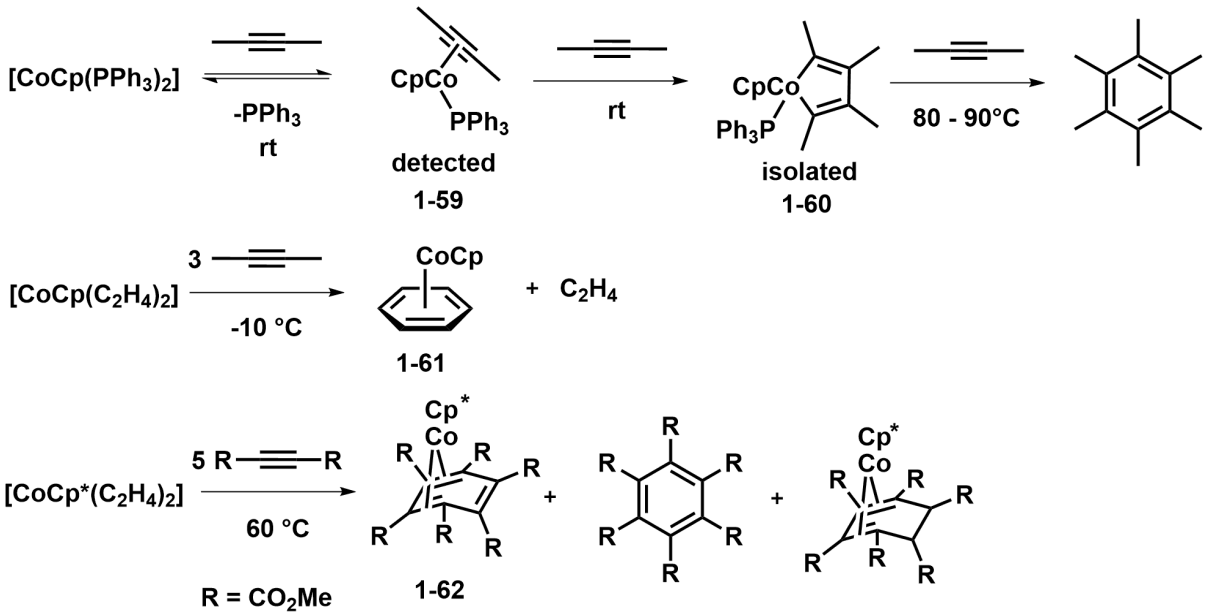

Scheme 1-25: Experimental results of the reaction of 2-butyne and dimethyl acetylenedicarboxylate with different CoCp catalysts.

A DFT study by Gandon and Vollhardt on the cobalt-catalyzed [2+2+2] cyclotrimerization of alkynes fully explains the experimental findings and further describes the already detailed computational description of the mechanism by Albright from 1999, by removing the restrictions of closed-shell species.[99] Two parallel mechanisms (Scheme 1-26) describe the cycloaddition depending on the type of ligand (L) bound to the metal center and the electronic properties of the alkynes used for the reaction. In both pathways, a cobaltacyclopentadiene **1-I8** is formed *via* oxidative coupling of a bisalkyne complex **1-I7**, which spontaneously relaxes to the triplet ground state ^{3}[**1-I8**]. For strong σ-donating ligands (PR_3 and CO) and σ-donor solvents (THF), the 18-electron complex **1-I9** is formed faster than reaction with π-donors (alkyne, alkene and arene). The cobaltanorbornene **1-I10** is obtained in an *intermolecular* [4+2] cycloaddition of a dienophilic alkyne with **1-I9**. The catalytic cycle is complete by a change in the spin state of **1-I10**, which results in the liberation of benzene and [CpCoL]. For weak σ-donating ligands and electron poor alkynes, the other catalytic cycle takes over by which

^{3}[**1-I8**] reacts to give the π-complex **1-I11**, which forms the η^4-benzene complex **1-I12** by an *intramolecular* metal-assisted [4+2] cycloaddition. Intermediate **1-I12** transforms into the 20-electron sandwich complex ^{3}[**1-I12**] by a spin change. Finally, benzene is liberated and CpCo re-enters the catalytic cycle.[100] However, it should be noted that Clark and co-workers found a third possible pathway, which will not be discussed further.[101]

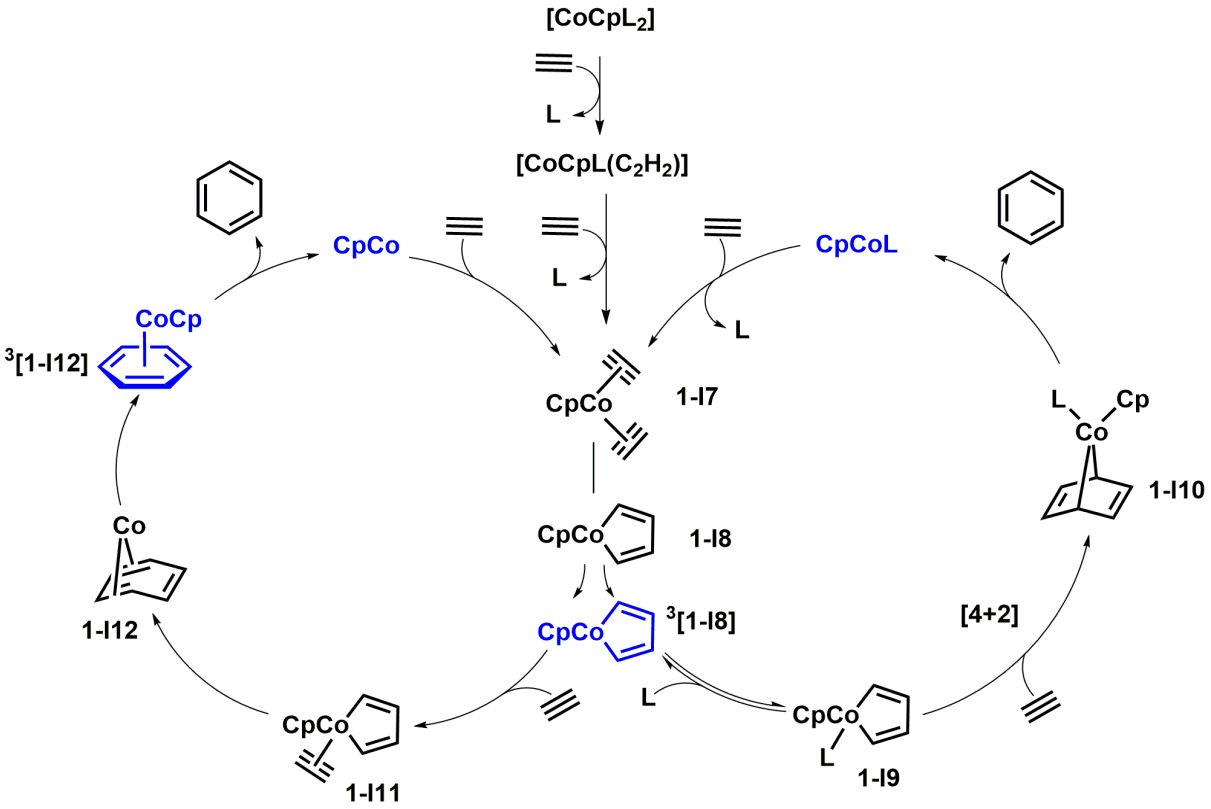

Scheme 1-26: Two parallel mechanisms for the CoCp-catalyzed [2+2+2] cyclotrimerization of acetylene to benzene with triplet species highlighted in blue.

A general catalytic cycle for the [RuCpClL$_2$] catalyzed [2+2+2] cyclotrimerization of acetylene to benzene is depicted in Scheme 1-27. In the first step, a bisacetylene complex **1-I13** is formed by the replacement of two labile ligands L with acetylene from the initial [RuCpClL$_2$] complex. The ruthenacycle **1-I14** is formed in an oxidative coupling. This coordinatively saturated 18-electron complex, can be regarded as a five-membered aromatic compound rather than a metallacyclopentatriene. With the coordination of a third alkyne, complex **1-I15** is formed, which isomerizes giving a ruthenabicyclo[3.2.0]heptatriene **1-I16** and, by subsequent scission of the central ruthenium-carbon bond, the seven-membered ruthenacycle **1-I17** is formed. Reductive elimination gives the η^2-benzene complex **1-I18**, which liberates benzene after the coordination of two new acetylene molecules and regenerates the initial catalytic active species **1-I13**. An *intramolecular* Diels-Alder type cyclization from **1-I15** to **1-I18** is not likely, as the activation energy for this step is 14.5 kcal mol^{-1}, while the activation energy for the formation

of the bicyclic intermediate **1-I16** from **1-I15** is only 0.1 kcal mol^{-1}.[102-103] Related structures of **1-I14**,[104] **1-I16**[105] and **1-I17**[105-106] were obtained and characterized by single-crystal X-ray diffraction analysis.

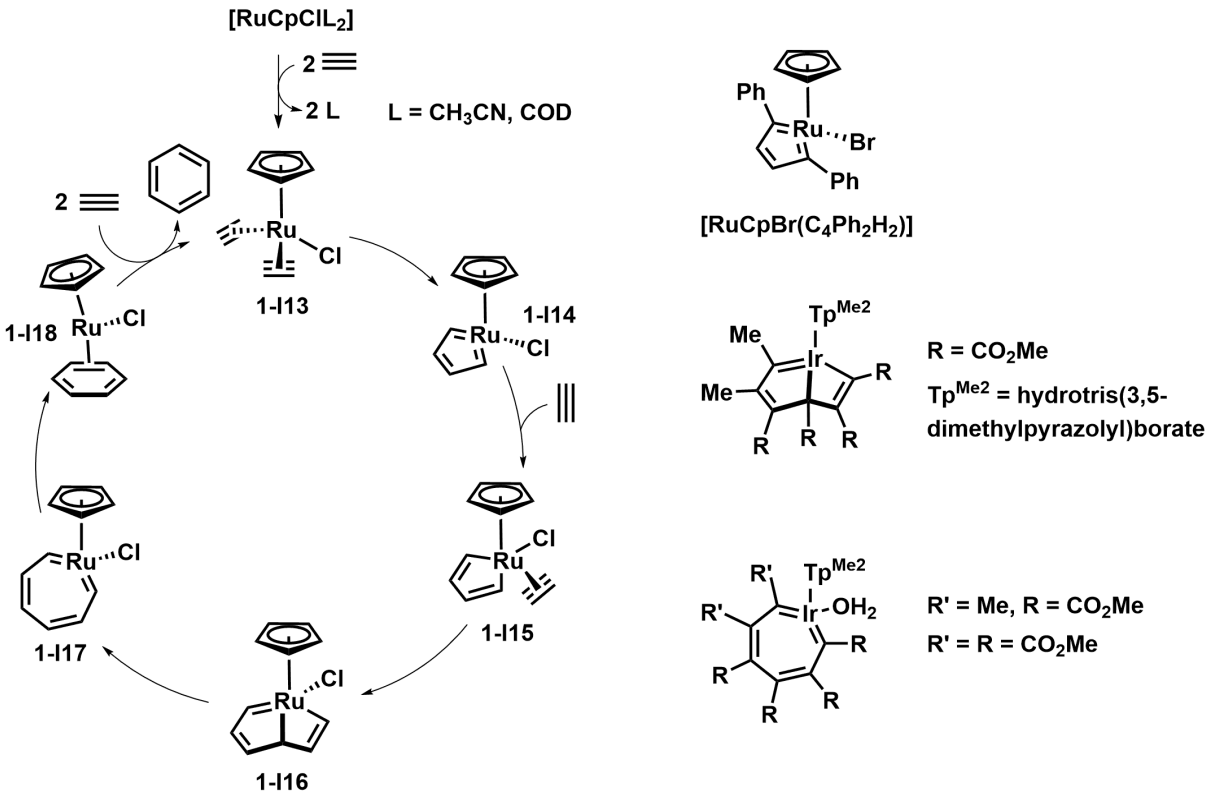

Scheme 1-27: Catalytic cycle for the RuCpCl-catalyzed [2+2+2] cyclotrimerization of acetylene to benzene and related characterized complexes.

Comparing the CpCo- (for weak σ-donating ligands and solvents) with and RuCpCl-catalyzed acetylene trimerization, numerous differences can be found. The formation of a five-membered metallacycle as the first key intermediate from the oxidative coupling of two alkyne ligands varies with the metal fragment: with CpCo it is a metallacyclopentadiene, while with RuCpCl a five-membered aromatic ruthenacycle is formed. The addition of a third alkyne in an η^2 fashion is common to both metals, but the subsequent insertion of the alkyne differs markedly. While for CpCo the subsequent intermediate is formed in a [4+2] cycloaddition reaction, in the RuCpCl-system, a bicyclic system forms first, which rearranges and forms a metallaheptatetraene complex. The last intermediate before dissociation of benzene is an η^4- for CpCo and an η^2-coordinated benzene for RuCpCl.

The large variety of intermediates that are formed in the catalytic cycle for the ruthenium and the cobalt systems, respectively, may arise from the different valence-electron configurations of the respective metal cores and their different atomic radii. The smaller radius of Co (1.25 Å) compared to Ru (1.33 Å)[107] may control interligand interactions in a different way.[108]

As the atomic radii of ruthenium and rhodium (1.34 Å) are quite similar,[107] and due to the great interest in the chemical reactivity of rhodium complexes and its suitability for catalytic systems it is worth having a closer look at rhodium-mediated [2+2+2] cyclizations.

Half-sandwich rhodium(I) complexes of the form [RhCpL$_2$] (L = CO, C_2H_4, L_2 = COD) were experimentally assessed as efficient catalyst precursors for cyclization reactions.[109-110]

Scheme 1-28 shows two plausible catalytic cycles for the RhCp-mediated trimerization of alkynes.[111] The complex **1-I19** is formed in a stepwise ligand substitution of L with acetylene (Scheme 1-28, cycle I). An oxidative coupling of the two alkyne ligands forms the rhodacyclopentadiene **1-I20**, analogous to [CoCp(C_4H_4)] (Scheme 1-26, complex **1-I8**). This complex might also be in resonance with a biscarbene structure, the metallacyclopentatriene, analogous to [RuCpCl(C_4H_4)] (Scheme 1-27, complex **1-I14**). The stable complex [RhCp(η^4-C_4H_4)] **1-63** is formed by reductive elimination and represents a thermodynamic trap in the catalytic cycle.[112] Coordination of a third acetylene molecule to the metal center forms complex **1-I21**. The formation of compound **1-I23,** an η^4-benzene bound complex, might occur *via* a [4+2] cycloaddition reaction or, by insertion followed by reductive elimination from the rhodacycloheptatriene **1-I22**, as proposed by Schore.[113] Addition of another acetylene generates the η^2-benzene complex **1-I24**, which releases benzene after the addition of acetylene and finally regenerates the catalytically active species **1-I19**.

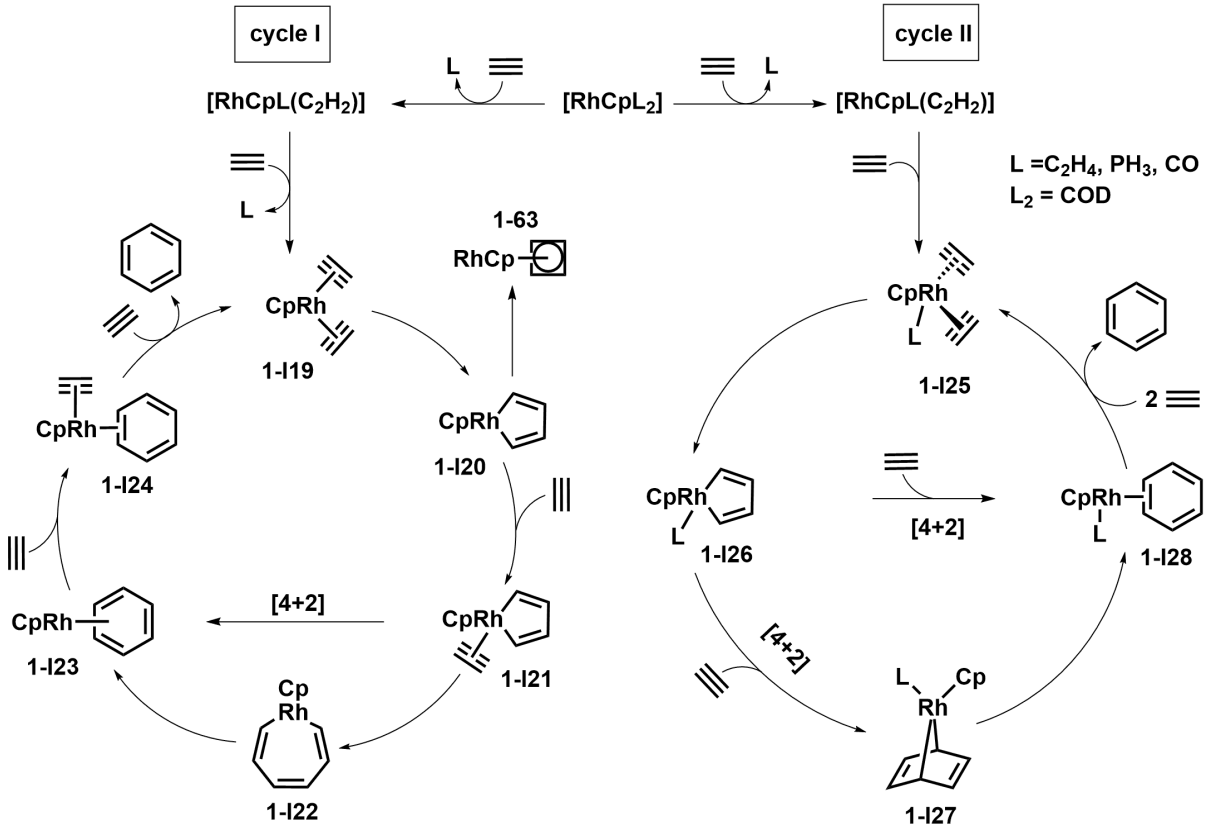

Scheme 1-28: Possible pathways for the RhCp-catalyzed acetylene cyclotrimerization to benzene.

Similar to the mechanistic investigations on [RuCpClL$_2$] (Scheme 1-27), and from experimental results of Booth and co-workers,[114] a nucleophilic ligand L (L = C_2H_4, PH_3, CO; L_2 = COD) on the rhodium-precursor might remain on the rhodium center throughout the catalytic cycle (Scheme 1-28, cycle II). As compound **1-I26** is already an 18-electron complex, and unfavorable 20-electron transition are usually avoided, there are two possibilities: (1) slippage to η^3- from an η^5-bound Cp ring, which leads to a free coordination site and, after coordination of a third acetylene to the rhodium metal center, *via* an *intramolecular* cycloaddition, to **1-I28**; or (2) by direct [4+2] cycloaddition reaction between **1-I26** and acetylene resulting in the rhodanorbornadiene **1-I27**, which forms **1-I28** by isomerization to an η^2-bound benzene. Subsequent addition of two alkynes results in the release of benzene and in the regeneration of the catalytically active species **1-I25**.

In 2007, Bickelhaupt and co-workers[111] conducted a theoretical investigation on the mechanism of [RhCp]-catalyzed cyclotrimerization of acetylene to benzene. In the absence of a strong σ-donor ligand, they found that the reaction occurs *via* **1-I19**, **1-I20**, **1-I21**, **1-I23**, **1-I24** and finally **1-I19**. Furthermore, the formation of the 16-electron rhodacyclopentadiene **1-I20** was found to be the rate determining step. The data for the calculated intermediates **1-I23** and **1-I24** fit nicely with reported X-ray structures of [Rh(η^4-C_6Me_6)(η^5-C_5Me_5)][115] and [Rh(η^5-C_5Me_5)(PMe_3)(η^2-C_6F_6)] (Scheme 1-29).[116]

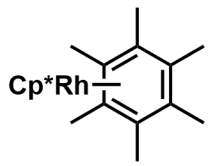

[Rh(η^4-C_6Me_6)(η^5-C_5Me_5)]

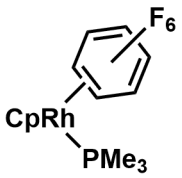

[Rh(η^5-C_5H_5)(PMe_3)(η^2-C_6F_6)]

Scheme 1-29: Complexes [Rh(η^4-C_6Me_6)(η^5-C_5Me_5)][115] and [Rh(η^5-C_5Me_5)(PMe_3)(η^2-C_6F_6)][116] characterized by single-crystal X-ray diffraction analysis.

The catalytic pathway *via* a rhodacycloheptatriene **1-I22**, as proposed by Schore,[113] and found for [RuCpCl][102] can be excluded, as reductive elimination for the rhodium-congener is more resistant.[111]

In the presence of a strong σ-donor ligand L (Scheme 1-28, cycle II), such as CO, it was found that the catalytic active species is [Rh(η^1-C_5H_5)(C_2H_2)$_2$(CO)] **1-I25**, which is formed from [Rh(η^5-C_5H_5)L(CO)] by replacement of L with acetylene, followed by addition of a second acetylene molecule.[111] During the addition of the second acetylene molecule, a haptotropic shift from η^5 to η^1 occurs, without any η^3-species as intermediate. During the oxidative coupling of the alkyne ligands forming the rhodacyclopentadiene species **1-I26**, the hapticity shifts back

from η^1 to η^5. As **1-I26** is an 18-electron complex, it has low reactivity for coordination of the third acetylene molecule and, again, a haptotropic shift from η^5 to η^1 would be required. However, this step is highly endothermic and thus not likely. A direct [4+2] cyclization from **1-I26** to **1-I28** resulted in a strained polycyclic aromatic intermediate.
A metallanorbornadiene intermediate **1-I27** was not found in the calculations. These results strongly indicate that if the vacant coordination site of the 16-electron rhodacyclopentadiene **1-I20** is blocked by a strong nucleophilic ligand, for example CO or PMe_3, as in **1-I26**, the mechanism is interrupted.[111]

Differences can be clearly seen when the [RuCpCl]- with the [RhCp]-catalyzed cyclotrimerizations of acetylene are compared. For example, in the [RuCpCl]-catalyzed cyclotrimerization, the seven-membered ruthenacycle plays a crucial role, while a similar species for the [RhCp]-catalyst can be excluded for energetic reasons. Hence, although the atomic radii of ruthenium (1.33 Å) and rhodium (1.34 Å) are quite similar,[107] the electronic structure of the metal core seems to be more important for the control of the mechanistic steps of the catalytic cycle as the atomic radii.[111]

1.2.2 Transition-metal-catalyzed [2+2+2] cycloaddition with alkynes

The transition-metal-catalyzed [2+2+2] cycloaddition is a powerful and atom-economical route for the construction of densely substituted six-membered carbo- and heterocycles. Heterocycles are often found as core structures in many natural products, in drugs or agrochemicals as well as in many biochemical molecules.[117] Therefore, one major objective in modern organic chemistry is to improve synthetic strategies for the formation of carbo- and heterocycles.[118]

In the past 20 years, rhodium(I)-based catalysts were thoroughly investigated for the [2+2+2] cyclizations.[119] In 1971, Müller and co-workers were the first to develop a protocol for this type of reaction using Wilkinson's catalyst $[Rh(PPh_3)_3Cl]$.[120-121] In 1984, Griggs and co-workers cyclotrimerized alkynes using catalytic amounts of $[Rh(PPh_3)_3Cl]$.[122]

The chemo- and regioselectivity of the intermolecular [2+2+2] cycloadditions of unsymmetric alkynes is difficult to control. It was found that a cationic rhodium(I) species, $[Rh(COD)_2]BF_4$, and H_8-BINAP were shown to be an efficient combination for the chemo- and regioselective [2+2+2] cycloaddition of two molecules of an electron-rich terminal alkyne with diethyl acetylenedicarboxylate at room temperature (Scheme 1-30).[119]

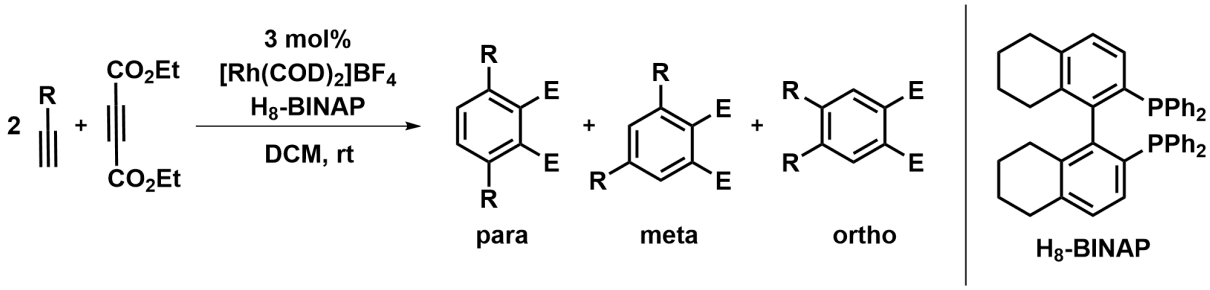

Scheme 1-30: Rhodium-catalyzed [2+2+2] cycloaddition of terminal alkynes with diethyl acetylenedicarboxylate.

Using different substituents at the terminal alkyne (R = *n*-$C_{10}H_{21}$, $(CH_2)_3Cl$, 1-cyclohexenyl, Ph, CH_2OAc and $SiMe_3$), moderate to good yields of 57 – 92% were obtained, as a mixture of *para*-, *meta*- and *ortho*-substituted benzenes. However, the *para*-substituted benzene was always obtained as the major product (ratio *p*:*m*:*o*: ca 0.9:0.08:0.02).[123] Similar results were obtained using $[Rh(COD)_2]BF_4$/BIPHEP (2,2'-bis(diphenylphosphino)-1,1'-biphenyl) and electron-rich 1,4-butyndiol derivatives and phenyl-substituted terminal alkynes, although a higher catalyst loading of 10 mol% was employed.[124]

In 1973, Wakatsuki and co-workers initially discovered the transition metal catalyzed [2+2+2] cycloaddition reaction of two alkynes with a nitrile.[125] This reaction has received considerable attention as it is a straightforward and atom economical route to substituted pyridines.[89] Various catalytic systems based on ruthenium, cobalt, rhodium, nickel, and iron amongst other transition metals have been used for the synthesis of different pyridine derivatives.[63, 81, 119, 126-127] The first reported example of a rhodium-catalyzed [2+2+2] cyclization of alkynes with nitriles was reported by Ingrosso and co-workers while using [RhCp]-systems in 1987.[109, 128] Different catalytic systems based on cationic rhodium(I)/BINAP-type systems were thoroughly used by Tanaka and co-workers.[129-133]

Aside from nitriles, isocyanates are also often used in the [2+2+2] cyclization due to their unique reactivity and their broad availability from commercial sources.[134] In the catalytic reaction of two molecules of alkynes and one molecule of isocyanate, 2-pyridones are formed.[135-136] Again, a variety of different transition metals such as cobalt, nickel, ruthenium and rhodium can catalyze the cyclization reaction.[137-142]

While the chemoselectivity of the cyclotrimerization of two or three different alkynes were accomplished by using suitable catalytic systems (*vide supra*) or stoichiometric amounts of transition metals,[143-145] the control of the chemo- and regioselectivity of the catalytic cyclotrimerization is still a formidable challenge.[103, 146]

1.2.3 Transition-metal-catalyzed [2+2+2] cycloaddition with diynes

To overcome the chemoselectivity issue, partial *intramolecular* cyclization of diynes with monoalkynes or complete intramolecular reactions by using triynes have been developed (Scheme 1-31).

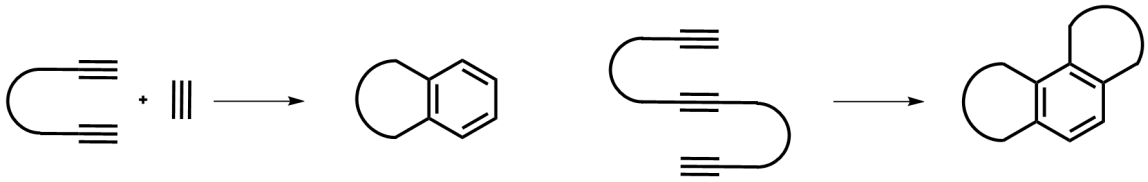

Scheme 1-31: Partial (left) or complete (right) intramolecular [2+2+2] alkyne cyclotrimerization.

Numerous stoichiometric intramolecular diyne-monoalkyne cyclotrimerization have been reported.[147-150] Müller and co-workers were the first to develop a protocol for this type of reaction by using Wilkinson's catalyst, $[Rh(PPh_3)_3Cl]$.[120-121]. However, various protocols for the catalytic intramolecular alkyne cyclotrimerization were realized in the following years, resulting in interesting polycyclic systems.[92, 122, 151-154]

In the reaction of heteroatom-linked 1,6-diynes with monoalkynes, substituted heterofluorenes were formed (Scheme 1-32). Substituted carbazoles can be synthesized from the reaction of tosylamide-linked 1,6-diynes with alkynes (conditions A).[155] Reactions of phenol-linked 1,6-diynes with alkynes under conditions B form substituted dibenzofurans.[156] Conditions C resulted in the formation of substituted dibenzothiophenes when thiophenol-linked 1,6-diynes were used.[157]

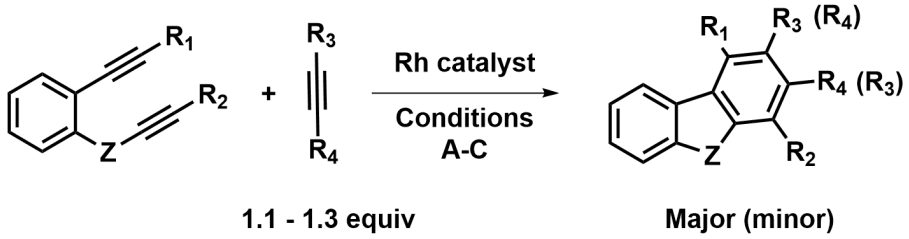

Scheme 1-32: Rhodium-catalyzed [2+2+2] cycloadditions of heteroatom-linked diynes with monoalkynes. Conditions: A: 3 - 5 mol% $[Rh(PPh_3)_3Cl]$, toluene, rt; B: 5 mol% $[Rh(COD)_2]BF_4/H_8$-BINAP, DCM, rt; C: 10 mol% $[Rh(COD)_2]BF_4$/BIPHEP, DCE, rt.

Using heterocumulenes, e.g. isocyanate, smooth conversion with 1,6-, 1,7- and 1,8-diynes at room temperature gave a variety of bicyclic 2-pyridones in moderate to high yields (Scheme 1-33).[158]

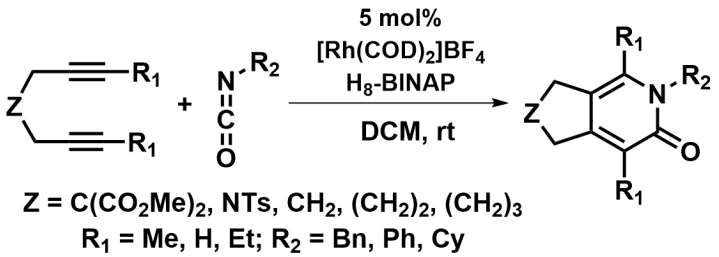

Scheme 1-33: Rhodium-catalyzed [2+2+2] cycloaddition of different diynes with isocyanate.

By a double [2+2+2] cycloaddition reaction it is possible to synthesize C_2-symmetric axially chiral biaryls with excellent enantioselectivity and good yields, by reaction of phosphonate- or ester-substituted 1,3-butadiynes with two molecules of an 1,6-diyne (Scheme 1-34).[159]

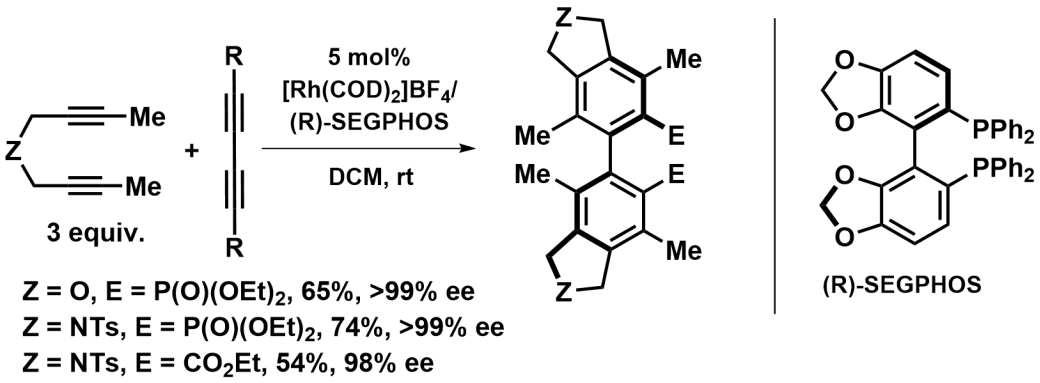

Scheme 1-34: Double rhodium-catalyzed [2+2+2] cycloaddition reaction of phosphonate- or ester-substituted 1,3-butadiynes with 1,6-diynes.

Steffen *et al.* reported that the reaction of **1-29a**, **1-34a** and **1-35b** with *para*-substituted 1,4-diphenylbuta-1,3-diynes at 80 °C for three weeks results in the formation of fully substituted 1,2,4-tris(*p*-R'-phenylethynyl)-3,5,6-tris(*p*-R'-phenyl)benzene.[56]

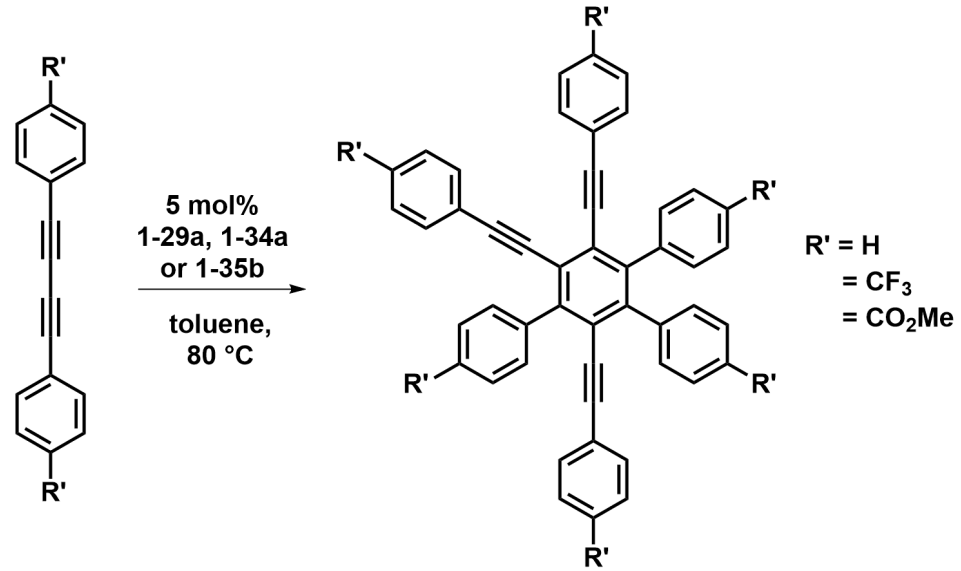

Scheme 1-35: Synthesis of 1,2,4-tris(arylethynyl)-3,5,6-tri(aryl)benzenes *via* the reaction of **1-29a**, **1-34a** and **1,35b** with *para*-substituted 1,4-diphenylbuta-1,3-diynes.

1.3 Fundamentals of photophysics

1.3.1 Photoactive transition-metal complexes

Transition-metal complexes of the 2nd and 3rd row play a major role in contemporary research,[160-168] owing to their broad applications as, for example, photocatalysts for CO_2 reduction,[169] water splitting,[170] in organic light emitting devices[168, 171] and as photosensitizers in dye-sensitized solar cells.[172] Photoactive transition-metal complexes also have applications in biotechnology and medicine.[173] They allow functional imaging of cells and tissues by e.g. DNA interactions[174] or provide a controlled photorelease of bioactive small molecules, such as CO[175-176] and NO.[177-178]

Absorption of electromagnetic radiation generates a photo-excited state. The emission of a photon from electronically excited states is called luminescence and is divided into two possible mechanisms: (1) fluorescence; and (2) phosphorescence, depending on the nature of the excited state. The process of the emission of a photon from a singlet excited state leading to a singlet ground state is called fluorescence. The emission rate constant k_F for fluorescence is usually ca. $10^8 – 10^9$ s^{-1} and the fluorescence lifetime τ_F ca. 1 – 10 ns. This process is spin allowed and thus happens quickly. Phosphorescence is the emission of a photon from a triplet excited state, leading to a singlet ground state. The transition to the ground state is normally spin forbidden. According to the selection rules, transitions between states of the same multiplicity are allowed, while transitions between different multiplicities are not.[179] Consequently, the emission rate constant for phosphorescence k_P is between $10^3 – 10^0$ s^{-1} and phosphorescence lifetime τ_P is typically milliseconds to seconds. Excited states are inherently unstable and there are competing processes to fluorescence and phosphorescence such as non-radiative decay, quenching, dissociation or isomerization.

Jablonski diagrams are often used to describe the fundamental radiative and non-radiative processes in molecules (Scheme 1-36). The singlet ground state is depicted by S_0, the first and all following singlet electronic states by S_1, …, S_n. The same nomenclature is used for the triplet states (T_1, …, T_n). The singlet and triplet energy levels have a different number of vibrational energy levels 0, 1, 2, etc. According to the Franck-Condon principle, the transition between states upon absorption of a photon occurs without a change in the positions of the nuclei in the molecular entity and its environment.[179] Those transitions occur in about 10^{-15} s and are illustrated by plain, vertical lines.

Absorption from S_0 occurs usually to higher vibrational levels of either S_1 or S_n. By a process called internal conversion (IC), which occurs within 10^{-12} s, a relaxation to the lowest vibrational level (n = 0) of S_1 is possible. According to Kasha's Rule, fluorescence/phosphorescence only occur from the lowest singlet or triplet excited states S_1 or T_1 with the lowest vibrational energy. That indicates that emission is independent of the excitation wavelength.[179] Fluorescence is slower than internal conversion, and therefore internal conversion takes place prior to emission.

A molecule in the S_1 state can undergo spin conversion. This process is called intersystem crossing (ISC) and results in the crossover from a singlet to a triplet state.

One can clearly see that the energy of the emission is smaller than of the absorption due to non-radiative decay. Phosphorescence appears at lower energies than fluorescence because of the lower energy of the excited triplet-state. The Stokes shift is the spectral shift to lower energy and longer wavelength between the absorbed light and the emitted light after interaction with a sample.[179]

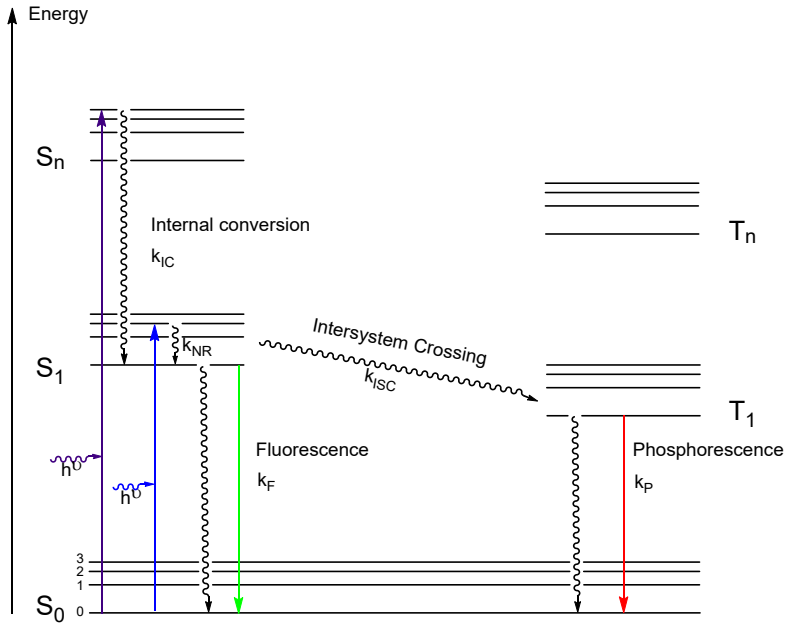

Scheme 1-36: Simplified Jablonski diagram illustrating the fundamental processes and their typical transitions in molecules after photoexcitation (F = fluorescence, IC = internal conversion, P = phosphorescence, ISC = intersystem crossing and NR = non-radiative decay).[70]

Other important characteristics of a luminophore are the photoluminescence quantum yield Φ, which is the number of emitted photons relative to the number of absorbed photons, and the lifetime τ, which is the average time a molecule spends in its excited state S_1/T_1 prior to returning to the ground state.[179-180]

For metal complexes additional aspects must be considered. Metal complexes show a relaxation of the spin-conversion rule because of the heavy atom effect. That means that the transition between S_n and T_n is now weakly forbidden and ISC is faster. The origin of this effect arises from the larger spin-orbit coupling (SOC) of heavy atoms such as transition metals. Additional symmetry selection rules also play an important part in this process.[179-180] Consequently, the stronger the SOC that is caused by the heavy atom, the more efficient is the ISC.[181] The typical rate constants k are also different $k_{IC} = 10^{-14} – 10^{-15}$ s, $k_{ISC} = 10^{-10} – 10^{-14}$ s, $k_F = 10^{-7} – 10^{-8}$ s and $k_P = 10^{-5} – 10^{-6}$ s. Because of the different photophysical and photochemical properties, it is important to distinguish fluorescence from phosphorescence. Excited triplet states have a lower-energy emission wavelength, longer lifetimes and different redox parameters, etc. compared to excited singlet states.[160, 182]

Electronic transitions occur between two molecular orbitals with different energies. Therefore, it is only possible to excite an electron from an occupied to a partially occupied or unoccupied orbital. There are different types of possible transitions in organometallic complexes: metal to ligand charge-transfer (MLCT), ligand to metal charge-transfer (LMCT), ligand field (LF) and intra-ligand (IL) (Scheme 1-37).[183]

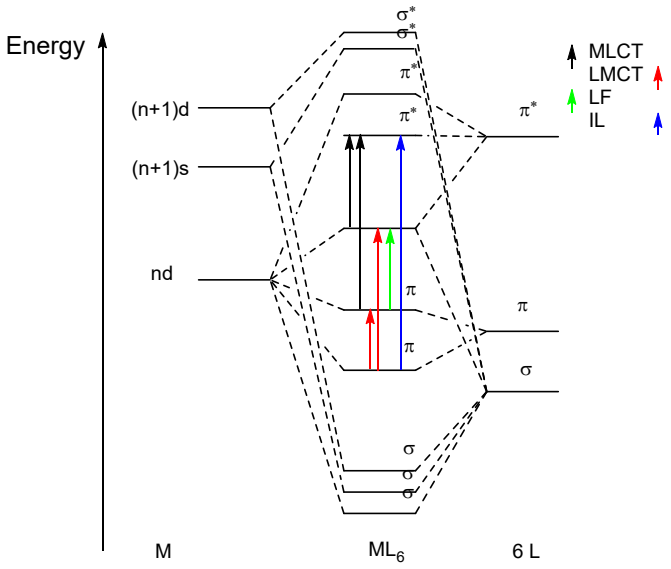

Scheme 1- 37: Molecular orbitals of an octahedral complex ML_6 and possible electronic transitions.[70]

Previous photophysical studies of cyclometallated d^6-rhodium complexes concentrated on bipyridine (bpy) and phenylpyridine (ppy) complexes of the type $[Rh(bpy)_{3-n}(ppy)_n]^{(3-n)+}$ (n = 0 – 3) and derivatives thereof.[184-188] These complexes usually exhibit weak luminescence at room temperature in solution and were therefore measured in a glass matrix at 77 K or in their crystalline form. They only show weak phosphorescence with emission lifetimes of

τ = 3 – 500 µs. In these complexes the major contribution to the excited state can be assigned to be of an intra-ligand π-π* transition while metal mixing is very limited, resulting in a very slow ISC from S_1 to T_1. The slow ISC, resulting in weak phosphorescence, is orders of magnitude slower than for other transition-meal complexes of ruthenium, iridium or platinum.[184] However, the SOC of rhodium is still large enough for efficient ISC from S_1 to T_1, as can be seen from ISC rate constants of 10^{11} s^{-1} found in $[RhX_2(bpy)_2)]$ with X = Cl and Br.[189]

1.3.2 Photophysical properties of rhodacyclopentadienes

Previous work demonstrated that 2,5-bis(arylethynyl)rhodacyclopentadienes with aryl moieties in the 3- and 4-position of the rhodacyclopentadiene and -CCTMS group in the equatorial plane **1-29a** – **1-37a**, show intense absorption bands in toluene at $\lambda_{abs,max}$ = 453 – 517 nm and exhibit extinction coefficients ε of 21000 – 35000 M^{-1} cm^{-1}. They emit in the visible region with $\lambda_{em,max}$ = 496 – 590 nm and have a small apparent Stokes shift of 1870 – 2390 cm^{-1}. The quantum yields are modest (Φ = 0.01 – 0.18) and the lifetimes τ_F = 0.45 – 1.21 ns. The *para* substitutents on the aryl rings induce a bathochromic shift of the absorption and emission spectra that is proportional to the increasing Hammet constant of the substituent, similar to structurally related 2,5-bis(phenylethynyl)thiophenes.[56] This arises from the influence of electron-withdrawing and electron-donating groups on the energy gap between the ground state and the emissive excited state.[190] The charge-transfer from the Rh-C_4 core to the phenyl moieties is more pronounced for electron-withdrawing groups.[59] This also implies that the energy gap between the S_1 and the S_0 state are decreased. This is a general phenomenon for all subsequently on discussed rhodacyclopentadienes. The small Stokes shifts and the short lifetimes τ_F in toluene suggest that the emission results from the singlet excited state S_1. Hence, the observed luminescence is fluorescence. As the quantum yield is not unity, some competitive processes take place during the relaxation of the excite state. For example, ISC to an excited triplet state or vibrational relaxation. A method to investigate the ISC after excitation is a singlet oxygen sensitization experiment, in which a triplet state of a compound is rapidly quenched by triplet (ground state) oxygen, generating singlet oxygen.[191] The quantum yields for singlet oxygen formation in O_2-saturated solutions were determined to be 0.57, 0.50 and 0.45 for **1-29a**, **1-32a** and **1-35a**, suggesting similar quantum yields for the ISC. Although the singlet oxygen sensitizing experiments indicate the formation of a T_1 state, no phosphorescence was observed. For late transition-metal complexes, this is rather unusual. Due to the spin-orbit coupling of the rhodium metal atom, very fast ISC from the S_1 to the T_1 excited state (10^{-14} – 10^{-10} s) and from there non-radiative decay or phosphorescence is expected. Nevertheless, the ISC from the S_1 to the T_1

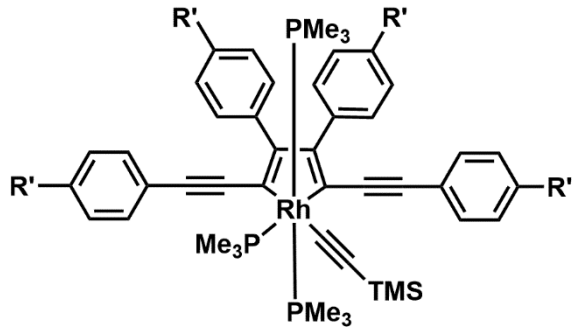

1-29a - 1-37a

1-29: R' = H **1-32: R' = SMe** **1-35: R' = CO_2Me**
1-30: R' = Me **1-33: R' = NMe_2** **1-36: R' = CN**
1-31: R' = OMe **1-34: R' = CF_3** **1-37: R' = NO_2**

state is several orders of magnitude slower (10^{-8} s), which results in a long-lived, emitting S_1 state. It was found that the HOMO and LUMO were ligand-centered π and π^* MOs with small metal contributions, which lie between the metal-centered filled and vacant orbitals. The S_1 and T_1 states originate from electronic transitions between the HOMO and LUMO.[182]

Attempts to increase the conjugation of the organic π–system of the ligand by introducing longer conjugated substituents at the *para*-position of the substituted 1,4-diphenylbuta-1,3-diynes resulted in the complexes **1-38 – 1-40**. Their absorption ($\lambda_{abs,max}$ = 478 – 500 nm) and emission ($\lambda_{em,max}$ = 526 – 556 nm) are bathochromically shifted compared to **1-29a** – **1-37a**. Furthermore, the extinction coefficients ε are increased (33000 – 48000 $M^{-1}\,cm^{-1}$), while the quantum yields decreased (Φ = 0.01 – 0.03). However, their fluorescence lifetime (τ_F = 0.06 – 1.64 ns) remains in the same short nanosecond range. These results indicate similar photophysical excited-state behavior as that of complexes **1-29a** – **1-37a**, although non-radiative decays are more efficient than in **1-29a** – **1-37a**, as indicated by the lower quantum yields. This results presumably from additional vibrational modes.[56]

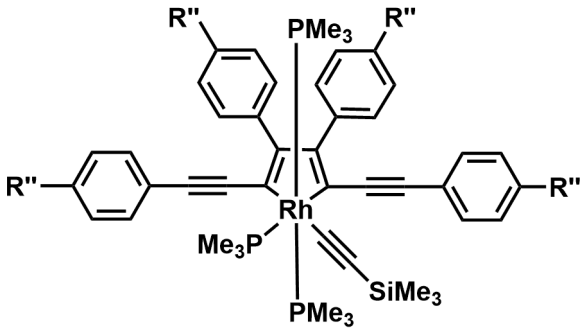

1-38: R'' = CC-SiMe$_3$
1-38': R'' = CC-H
1-39: R'' = CC-*p*-C$_6$H$_4$-N(*n*Hex)$_2$
1-40: R'' = CC-*p*-C$_6$H$_4$-CO$_2$(*n*Oct)

To clarify the influence of the σ-donor ligand in the equatorial plane of the metallacyclopentadiene and of the rhodium metal center on the photophysical behavior of the excited states, the CC-SiMe$_3$ ligand was replaced with ligands of different conjugation lengths and *σ-/π-donor* strengths (**b**: CC-(*p*-C$_6$H$_4$-NMe$_2$, **c**: CC-(*p*-C$_6$H$_4$-NPh$_2$ and **d**: CC-(*p*-C$_6$H$_4$)-CC-(*p*-C$_6$H$_4$)-N(*n*-hex)$_2$). The complexes **1-29b**,**d**, **1-30(b-d)**, **1-31b**,**d**, **1-32d**, **1-34b**,**d**, **1-35b**,**d** and **1-36d** show almost identical absorption and emission spectra, extinction coefficients and fluorescence lifetimes to **1-29a** – **1-37a** and **1-38** – **1-40**. Although the ligands in the equatorial plane have different electronic properties, they do not

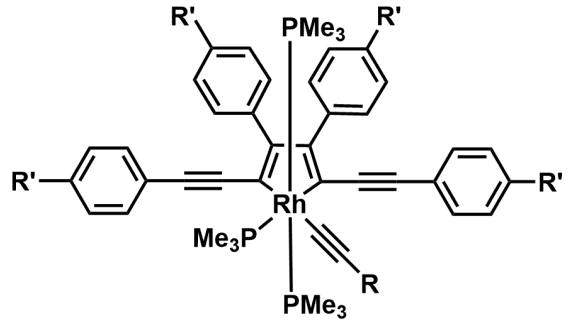

1-29(b-d) - 1-37(b-d)

b: R = C$_6$H$_4$-NMe$_2$, c: R = CC-C$_6$H$_4$-NPh$_2$
d: R = C$_6$H$_4$-CC-C$_6$H$_4$-N(Hex)$_2$

1-29: R' = H	**1-32: R' = SMe**	**1-35: R' = CO$_2$Me**
1-30: R' = Me	**1-33: R' = NMe$_2$**	**1-36: R' = CN**
1-31: R' = OMe	**1-34: R' = CF$_3$**	**1-37: R' = NO$_2$**

affect the photophysical properties, presumably because the aryl rings attached to the ligands are significantly rotated out of co-planarity with the metallacycle. Hence, the conjugation between the rhodium atom and the substitutents located on the acetylide ligand is not increased.[56]

Replacing the acetylene-unit with the stronger σ-donor methyl ligand, resulted in the formation of the complexes **1-41(a-g)**, and revealed a more pronounced effect. The increased electron density at the metal center increased the MLCT character of the emitting excited state and lead to higher ISC rates. The absorption and emission maxima for **1-41(a**, **c**, **e** and **g)** were bathochromically shifted by ca. 350 cm^{-1}, compared to the CC-$SiMe_3$ analogue complexes, and the fluorescence quantum yield is reduced to $\Phi < 0.01$. However, the singlet oxygen sensitizing experiment revealed similar quantum yields for the ISC compared to the CC-$SiMe_3$ substituted rhodacyclopentadienes. The low fluorescence quantum yield Φ results presumably from the very efficient non-radiative decay through C-H vibration in the methyl ligand and/or Rh-Me rotational modes. However, an isotope effect on the quantum yield by replacing CH_3 with CD_3 was not observed.[56]

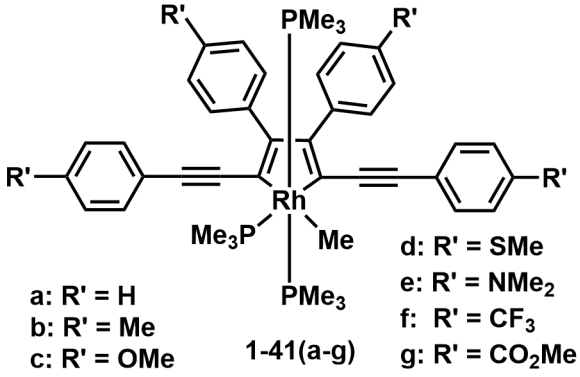

The photophysical properties of the rhodacyclopentadienes with the weak σ- and π-donating chloride ligand **1-42(a**, **c**, **d** and **f)**, are similar to that of their CC-$SiMe_3$ analogues. Absorption and emission spectra are bathochromically shifted by ca. 350 – 480 cm^{-1}. The fluorescence quantum yield strongly depends on the substituent in *para*-position of the aryl moiety and Φ is for the CO_2Me-substituted aryl moieties 0.22 and for the unsubstituted complex **1-42a** $\Phi < 0.01$. According to singlet oxygen sensitizing experiments, the ISC process occurs on the same time scale as for the other rhodacyclopentadienes (10^{-8} s). Additionally, a weak solvatochromic effect was observed, suggesting some CT character of the emission.

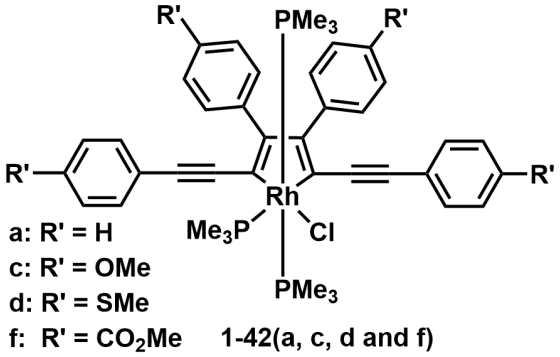

The complexes **1-45(a-c)** with a more rigid backbone and a CC-$SiMe_3$ group in the equatorial plane show intense absorption bands in toluene at $\lambda_{abs,max}$ = 456 – 497 nm with extinction coefficients ε of 22000 – 44000 M^{-1} cm^{-1}. They emit in the visible region with $\lambda_{em,max}$ = 501 – 560 nm and have a small Stokes shift of 2000 – 2300 cm^{-1}. The quantum yield was determined to be Φ = 0.33 – 0.69 and the lifetime τ_F = 1.2 – 3.0 ns. For compound **1-45c** a solvatochromic effect on going from *n*-hexane to acetonitrile (ACN) leads to an increased Stokes shift, therefore indicative of a charge-transfer character of the emissive excited-state. The small Stokes shifts, in toluene, suggests emission from the singlet excited states S_1 and this is further underpinned by the short lifetimes τ_F. Furthermore, the lifetime and quantum yield were not influenced by the presence of molecular oxygen. As the fluorescence quantum yield and the quantum yield for the singlet oxygen sensitizing sum to close to unity, only very little non-radiative decay is present. Additionally, it was found, that **1-45(a-c)** were potent singlet oxygen sensitizers and no phosphorescence was observed at room temperature or at 77 K in a glass matrix. Hence, a rigidification of the backbone leads to an increase in the fluorescence quantum yield, compared to **1-29a**, **1-32a** and **1-35a**.[58]

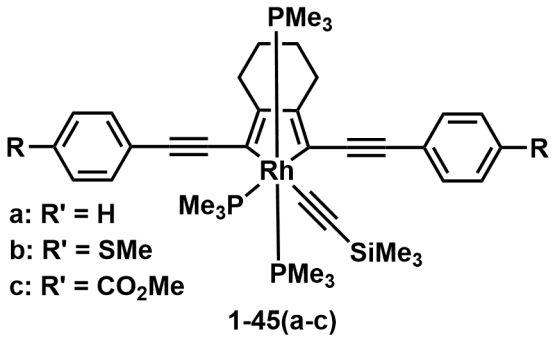

1-45(a-c)

By exchanging the CC-$SiMe_3$-unit and a PMe_3 ligand in the equatorial plane with a diethyldithiocarbamate ligand, a strong σ- and π-donor, the photophysical properties were only marginally altered, meaning that the metal contribution to the emissive excited state is, again, only small. They show intense absorption bands in toluene at $\lambda_{abs,max}$ = 476 – 518 nm and extinction coefficients ε of 15000 – 24000 M^{-1} cm^{-1}. Emission was observed in the visible region with $\lambda_{em,max}$ = 526 – 586 nm and is bathochromically shifted compared to **1-45(a-c)**. The Stokes shift is ca. 2000 cm^{-1}, the lifetimes τ_F are in the range from 0.4 – 2.5 ns and the fluorescence quantum yields Φ = 0.07 – 0.46. The singlet oxygen sensitizing ability is decreased compared to **1-45(a-c)**. Again, no phosphorescence was observed, even at 77 K in a glass matrix. It was found that the ligand exchange leads to a change in the lower lying occupied orbitals, but leaves the HOMO and LUMO of **1-46** unchanged, compared to **1-45**.[58]

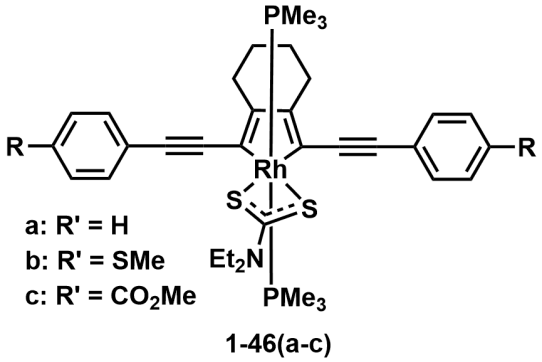

1-46(a-c)

The rhodacyclopentadienes **1-48(a-f)**, with only three CH_2 groups in the backbone, compared to **1-46**, show intense absorption bands in toluene at $\lambda_{abs,max}$ = 478 – 594 nm and exhibit extinction coefficients ε of 14000 – 33000 M^{-1} cm^{-1}. They emit in the visible region with $\lambda_{em,max}$ = 512 – 671 nm and small apparent Stokes shifts of 660 – 1900 cm^{-1}. The quantum yields were modest (Φ = 0.01 – 0.48) and the lifetimes τ_F = 0.38 – 1.41 ns.

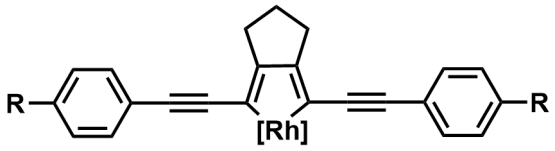

1-48(a-f)

a: R = Me **d: R = CO_2Me**
b: R = SMe **e: R = NO_2**
c: R = NMe_2 **f: R = *p*-OMe-C_6F_4**

[Rh] = [Rh(S_2CNEt_2)(PMe_3)$_2$]

For complexes **1-48b**,**d** the differences (minus one CH_2 group in the backbone) in the photophysical behavior, compared to **1-46b**,**c**, are small. Compound **1-48e** shows a strong red-shift in absorption and emission, compared to the other compounds in the series.[68]

The tri(*p*-tolyl)phosphine congeners **1-48'(b**, **d**, **e** and **f)** of the trimethylphosphine-substituted rhodacyclopentadienes **1-48(b**, **d**, **e** and **f)** show intense absorption bands in toluene at $\lambda_{abs,max}$ = 495 – 619 nm with extinction coefficients ε of 23000 – 31000 M^{-1} cm^{-1}. They emit in the visible region with $\lambda_{em,max}$ = 508 – 686 nm and experience only a small Stokes shift of 760 – 1600 cm^{-1}. The quantum yield was determined to be Φ = 0.04 for **1-48'e** and < 0.01 for **1-48'b**, **d** and **f**, and the lifetime τ_F < 2 ns.

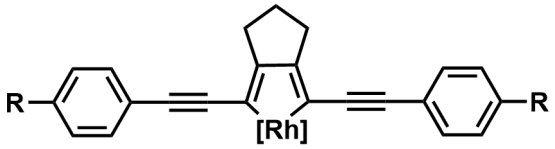

1-48'(b,d,e and f)

b: R = SMe **e: R = NO_2**
d: R = CO_2Me **f: R = *p*-OMe-C_6F_4**

[Rh] = [Rh(S_2CNEt_2)(P(*p*-tolyl)$_3$)$_2$]

Singlet oxygen sensitizing experiments conducted with **1-48d** and **1-48'd** in ACN revealed that the singlet oxygen quantum yield for **1-48d** is 0.27 and for **1-48'd** it is 0.37. This shows that the sum of the fluorescence and the singlet oxygen sensitizing quantum yield are not equal to 1 and therefore fluorescence and ISC are not the only pathways for relaxation in these derivatives. Other possibilities are vibrational and rotational non-radiative decay. That also explains the lower quantum yield of **1-48'**, compared to **1-48**. This presumably arises from additional vibrational modes of the tri(*p*-tolyl)phosphine ligands.

A strong solvatochromic effect was observed for **1-48e** and **1-48'e** in *n*-hexane, Me-cyclohexane, toluene and THF for the absorption and emission spectra. The apparent Stokes shifts for **1-48e** are 790 (n-hexane), 800 (Me-cyclohexane), 1900 (toluene) and 3900 cm^{-1} (THF), indicating a strong charge-transfer character of the emissive excited state. This was accompanied by a significant decrease of the quantum yields from ca. 0.2 for *n*-hexane and Me-cyclohexane over 0.07 in toluene. However, in THF no quantum yield was determined.

For **1-48'e** the Stokes shifts are comparable with the ones for **1-48e**. The quantum yield was determined to be ca. 0.03 in *n*-hexane, Me-cyclohexane and toluene, hence no trend corresponding to the solvent polarity was observed. The unusual strong solvatochromic effect of the complex **1-48e** is caused by the strong electron withdrawing NO_2-group, as the solvatochromic effect for the CO_2Me-analogue complex is smaller.[68]

Complexes **1-53b**,**d** show intense absorption bands in toluene at $\lambda_{abs,max}$ = 481 and 514 nm with extinction coefficients ε of 23000 and 34000 M^{-1} cm^{-1}. They emit in the visible region at $\lambda_{em,max}$ = 534 and 579 nm and experience only a small Stokes shift of 2060 and 2180 cm^{-1}. The quantum yields were determined to be Φ = 0.13 and 0.50 and the lifetimes τ_F were determined to be 2.0 (25%) and 0.5 (75%) ns for **1-53b** and 2.5 ns for **1-53d**. The complexes **1-52b**,**d** and **1-52'**, which is a donor-acceptor system, show intense absorption bands in toluene at $\lambda_{abs,max}$ = 503, 535 and 498 nm with extinction coefficients ε of 33500, 37600 and 31000 M^{-1} cm^{-1}. They emit in the visible region at $\lambda_{em,max}$ = 522, 563 and 576 nm and consequently have small Stokes shifts of 720, 930 and 2720 cm^{-1}. The quantum yields were determined to be Φ = 0.07 (**1-52b**), 0.54(**1-52d**), and 0.22 (**1-52'**) and the lifetimes τ_F = 0.3 (77%) and 0.1 (23%) (**1-52b)**, 1.7 ns (**1-52d**) and 0.8 ns (**1-52'**). The donor/acceptor complex **1-52'** shows a strong intra-ligand charge-transfer, which results in a large bathochromic shift in emission with $\lambda_{em,max}$ = 576 nm (toluene), $\lambda_{em,max}$ = 600 nm (PMMA film) and $\lambda_{em,max}$ = 651 nm (2-Me-THF). Interestingly, the bathochromic shift at 77 K in 2-Me-THF, is comparable with that in toluene solution at room temperature. This suggests that the charge-transfer in polar solvents at room temperature is accompanied by a significant geometrical reorganization in the excited state, which is hampered at 77 K in the glass matrix. The quantum yield and the emission lifetime of complexes **1-52** and **1-53** show no major difference at room temperature in a 2-Me-THF solution, the solid state and in PMMA films to toluene. Additionally, no phosphorescence was detected at 77 K in a glass matrix, and dioxygen has no influence on the luminescent properties.[59, 72]

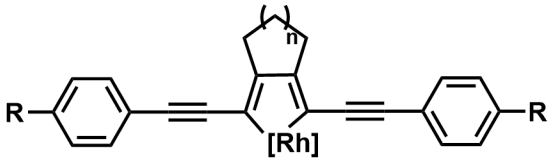

n = 1 (1-52), n = 2 (1-53)
b: R = SMe, d: R = CO_2Me

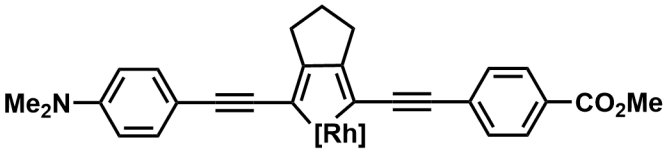

1-52'
[Rh(acac)(PMe_3)$_2$]

The tri(*p*-tolyl)phosphine congeners **1-57b**,**d** of the rhodacyclopentadienes **1-52b**,**d** show intense absorption bands in toluene at $\lambda_{abs,max}$ = 525 and 563 nm and exhibit an extinction coefficient ε of 32500 M^{-1} cm^{-1}. They emit in the visible region at $\lambda_{em,max}$ = 550 and 583 nm and thus have only a small apparent Stokes shift of 866 and 609 cm^{-1}. The quantum yields were determined to be $\Phi < 0.01$ and the lifetimes τ_F < 1 ns.[71-72] No additional phosphorescence was observed at 77 K. The photophysical properties of **1-57** are similar to **1-48'**.

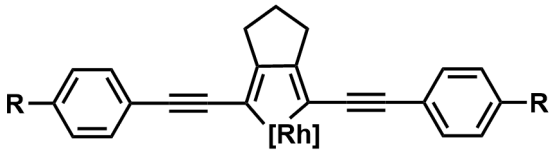

1-57b,d
b: R = SMe, d: R = CO_2Me
[Rh(acac)(P(*p*-tolyl)$_3$)$_2$]

Similar photophysical behavior and pure IL(π-π*) transitions were also found in structurally related main-group 2,5-bis(arylethynyl)boroles, siloles, phospholes, and thiophenes (see Scheme 1-12). The fluorescent properties of transition-metal complexes are not only limited to the rhodacyclopentadienes. It was also observed in rhenium,[192] osmium, [193-194] iridium[195-198] and platinum[199-201] complexes. By the introduction of a spacer unit, it was possible to electronically isolate the chromophore from the metal center, resulting in a pure IL state by inhibiting the SOC of the metal atom. There are only a few examples of rhodium complexes with intra-ligand fluorescence and phosphorescence described in the literature. However, their properties were only described by the luminescent spectra, without details on lifetime and quantum yield.[202-204] A recent publication by Otero and co-workers describes the formation of fluorescent rhenacyclopentadienes from the reaction of a dirhenium carbonyl complex $[Re_2(CO)_8(CH_3CN)_2]$ with different octa-1,7-diynes, resulting in 2,5-(bisaryl)rhenacyclopentadienes. However, the reported Stoke shifts are in the range from 16600 – 24900 cm^{-1}, indicative of phosphorescence, although no lifetimes were reported.[205]

In contrast to the rhodacyclopentadienes described above, the dibenzorhodacyclopentadienes show pure phosphorescence as expected for a second-row transition metal.

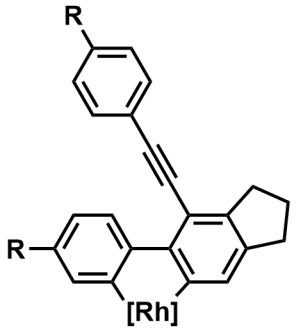

1-49d,e
d: R = CO_2Me, e: R = NO_2
[Rh] = [Rh(S_2CNEt_2)(PMe_3)$_2$]

Complexes **1-49d**,**e** show intense absorption bands in toluene at $\lambda_{abs,max}$ = 370 and 379 nm and exhibit extinction coefficients ε of 23000 and 19000 M^{-1} cm^{-1}, respectively. They emit in the visible region at $\lambda_{em,max}$ = 541 and 592 nm and exhibit large Stokes shifts of 8500 and 9500 cm^{-1}, respectively. The quantum yields were determined to be Φ = 0.14 and 0.23, and the phosphorescence lifetimes τ_P = 185 µs and 94 µs.[68]

The complexes **1-55b**,**d** show intense absorption bands in toluene at $\lambda_{abs,max}$ = 390 and 410 nm with extinction coefficients ε of 11400 and 8430 M^{-1} cm^{-1}. They emit in the visible region at $\lambda_{em,max}$ = 542 and 545 nm and display large Stokes shifts of 7190 and 6040 cm^{-1}. The quantum yields were determined to be Φ = 0.01 and 0.12, and the phosphorescence lifetimes τ_P = 43 (40%) and 119 µs (60%) ns for **1-55b** and 162 µs for **1-55d**.

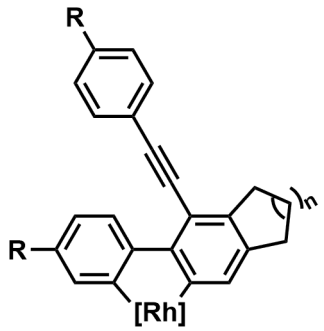

n = 1 (1-54), n = 2 (1-55)
b: R = SMe, d: R = CO_2Me

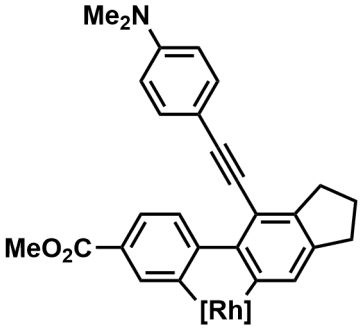

1-54'

[Rh] = [Rh(acac)(PMe_3)$_2$]

Complexes **1-54b**,**d** and **1-54'** show intense absorption bands in toluene at $\lambda_{abs,max}$ = 382, 377 and 371 nm and exhibit extinction coefficients ε of 12000, 9600 and 16300 M^{-1} cm^{-1}, respectively. They emit in the visible region at $\lambda_{em,max}$ = 535, 540 and 536 nm and thus have large Stokes shifts of 7480, 8000 and 8300 cm^{-1}, respectively. The quantum yields were determined to be Φ = 0.02, 0.14 and 0.29 and lifetimes τ_P were determined to be 61 (98%) and 163 µs (2%) ns for **1-54b**, 181 µs for **1-54d** and for **1-54'** 164(12%) and 496 (88%) µs.[59, 72] The dibenzorhodacyclopentadienes **1-54**, **1-55** and **1-54'** were chemically sensitive to dioxygen in solution. The *para*-substituents of the phenyl rings have only a small influence on the absorption and emission, in contrast to **1-52** and **1-53**. Furthermore, it was found that **1-54d** and **1-54'** were the most efficient phosphorescent rhodium complexes and the most efficient metal biphenyl triplet emitters to date.[59, 72]

A detailed TD-DFT study of the acac-substituted rhodacyclopentadienes and dibenzorhodacyclopentadienes explains the different luminescence pathways. Marder and co-workers reported that in the fluorescent rhodacyclopentadienes, despite the presence of the heavy rhodium metal, the excited S_1 and T_1 states are pure intra-ligand in nature. The HOMO and the LUMO are nearly pure π and π^* orbitals and the HOMO is well separated from the filled rhodium d-orbitals. This excludes low-energy MLCT transitions, which could contribute to the nature of the emissive state and additionally facilitate SOC and hamper the ISC process. For the dibenzorhodacyclopentadienes an energetic proximity of the filled frontier molecular orbitals was found, which are mixtures of ligand π and metal d-orbitals. This results in several triplet excited states with some MLCT contribution, which connects S_1 with the emitting T_1 state. As no fluorescence was detected, even at low temperature, ISC from the S_1 to the T_n state must be faster than fluorescence and non-radiative decay. However, the very small radiative rate constants of 110 – 770 s^{-1} of the complexes **1-54**, **1-55** and **1-54'** in toluene, indicate that the nature of the T_1 state is purely intra-ligand, with only a small contribution of the rhodium atom.[59, 72]

Chapter 2

2 A rhodium-mediated all-carbon “click-reaction”

2.1 Abstract

The formation of fluorescent 2,5-bis(arylethynyl)rhodacyclopentadienes from the reaction of [Rh(R)(PMe_3)$_4$] (R = Me, CC-$SiMe_3$, CC-*p*-C_6H_4-NMe_2, CC-CC-(*p*-C_6H_4-NPh_2), CC-*p*-C_6H_4-CC-*p*-C_6H_4-$N(Hex)_2$) with various *para*-substituted 1,4-diphenylbuta-1,3-diynes (diynes) were reported previously. However, using [Rh(acac)(PMe_3)$_2$] as the rhodium precursor resulted in a drastically altered outcome of the reaction. At room temperature, a complex containing a bidentate organic fulvene moiety, composed of two diynes, *σ*-bound to the rhodium center is formed in an all-carbon [3+2] type cyclization reaction. In addition, a complex containing an organic indene moiety, composed of three diynes, attached to the rhodium center in a bis-*σ*-manner is formed in a [3+2+3] cyclization process. Reactions at 100 °C reveal that the third diyne inserts between the rhodium center and the bis-*σ*-bound organic fulvene moiety. Furthermore, the formation of a 2,5-bis(arylethynyl)rhodacyclopentadiene and a 2,4-bis(arylethynyl)rhodacyclopentadiene is observed. This unique [3+2] cyclization product was used for the synthesis of a highly conjugated organic molecule, which is hard to access or even inaccessible by conventional methods. Thus, at elevated temperatures, reaction of the [3+2] product with *para*-tolyl isocyanate led to the formation of a purple organic compound containing the organic fulvene structure and one equivalent of *para*-tolyl isocyanate.

The blue and green [3+2+3] complexes show an unusually broad absorption from 500 – 1000 nm with extinction coefficients ε of up to 11000 M^{-1} cm^{-1}. The purple organic molecule shows an absorption spectrum similar to those of known diketopyrrolopyrroles.

Additionally, the reaction of [Rh(acac)(PMe_3)$_2$] with *para*-tolyl isocyanate was investigated. A *cis*-phosphine complex of the form *cis*-[Rh(acac)(PMe_3)$_2$(isocyanate)$_2$] with an isocyanate dimer bound to the rhodium center by one carbon and one oxygen atom was isolated.

Replacing the trimethylphosphine ligands in [Rh(acac)(PMe_3)$_2$] with the stronger *σ*-donating NHC ligand Me_2Im (1,3-dimethylimidazolin-2-ylidene), again, drastically alters the reaction. Similar [3+2] and [3+2+3] products to those discussed above could not be unambiguously assigned, but *cis*- and *trans*-*π*-complexes, which are in an equilibrium with the two starting materials, were formed.

2.2 Previous work and motivation

One main field in the Marder research group is the synthesis of rhodacyclopentadienes. In 2001, a high-yield, one-pot synthesis of 2,5-bis(arylethynyl)rhodacyclopentadienes *via* reaction of a rhodium(I) precursor with two equivalents of *para*-substituted 1,4-diphenylbuta-1,3-diynes was reported.[57] In order to enhance the photophysical properties, an alkyl chain was used to link the two diynes.[51] These rhodacyclopentadienes show intense fluorescence due to slow intersystem crossing. These unusual findings can be attributed to the pure intra-ligand nature of the relevant excited states (S_1 and T_1). The rhodium d-orbitals are well separated in energy from the ligand based HOMO and LUMO orbitals. Further investigations of the influence of the ligand sphere around the rhodium center included the introduction of π-donating groups such as diethyldithiocarbamate[68] and acetylacetonate,[59] in order to increase the electron density around the rhodium metal center and raise the metal d-orbitals closer to the organic, ligand-based orbitals. Surprisingly, not only the expected fluorescent rhodacyclopentadienes were formed, but phosphorescent dibenzorhodacyclopentadienes were formed as well.[51, 59, 68, 71] In order to investigate this finding, the group went one step back and used *para*-substituted 1,4-diphenylbuta-1,3-diynes again in reactions with [Rh(acac)(PMe_3)$_2$]. Interestingly, this time, no 2,5-bis(arylethynyl)rhodacyclopentadienes or dibenzorhodacyclopentadienes formed but instead, an unusual [3+2] cyclization at the rhodium metal took place and an organic fulvene-like molecule was trapped at the metal center as the major product (Scheme 2-1). In further investigations, it was possible to elucidate some aspects of the mechanism of the formation of the unusual all-carbon [3+2] annulation complexes. Initially, two isomeric π-complexes with *cis*-PMe_3 ligands form $\mathbf{I_{cis}a}$ and $\mathbf{I_{cis}b}$, which rearrange to a *trans*-π-complex. Two of these *trans*-complexes react in a bimetallic process to form the desired product.[206]

Further efforts were made to convert this [3+2] cycloaddition complex into a pure organic product. Okorn investigated the reactions of the [3+2] complex with different types of substrates to detach the organic fulvene moiety from the metallacyclobutene,[207] and *para*-tolyl isocyanate was found to be a promising substrate for this purpose.

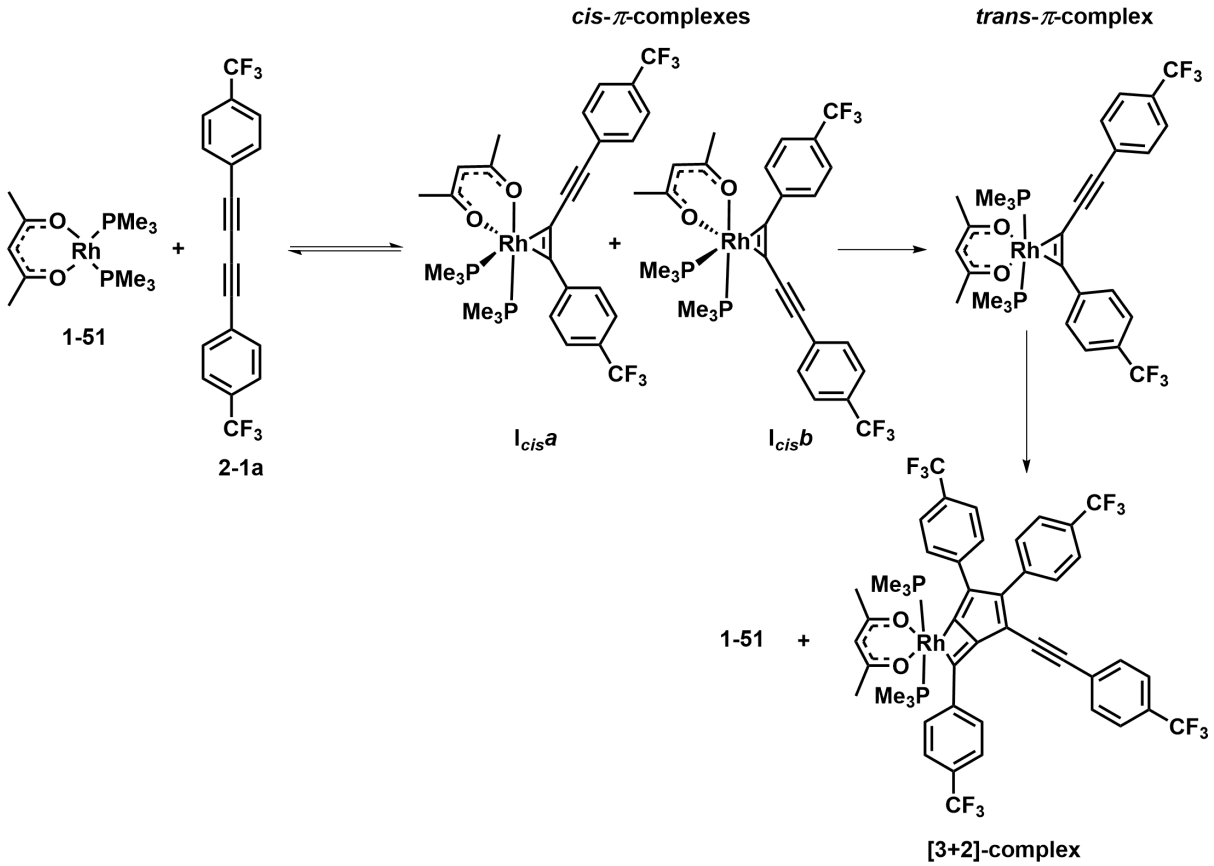

Scheme 2-1: Proposed reaction pathway for the formation of the all-carbon [3+2] annulation reaction.

The aim of Chapter 2 of this thesis was to continue the work of Okorn regarding the isolation and characterization of a pure organic compound derived from the reaction of the [3+2] complex with *para*-tolyl isocyanate. Furthermore, the minor product from the reaction of [Rh(acac)(PMe_3)$_2$] with CF_3-*para*-substituted 1,4-diphenylbuta-1,3-diyne was to be isolated and characterized.

2.3 Results and discussion

2.3.1 Synthesis and structural characterization of rhodium-mediated alkyne annulation products

2.3.1.1 Reactions of [Rh(acac)(PMe$_3$)$_2$] with *para*-substituted 1,4-diphenylbuta-1,3-diynes at room temperature

In the reaction of [Rh(acac)(PMe$_3$)$_2$] **1-51** with two equivalents of *para*-substituted 1,4-diphenylbuta-1,3-diynes **2-1a**,**b** at room temperature, the formation of a minor side product was observed in ca. 6 – 10% yield (according to ^{31}P{^{1}H} NMR spectroscopy) with a similar ^{31}P chemical shift compared to the major product **2-2a**,**b** (Scheme 2-2).[206] The isolation of this unknown compound was not successful with the previously applied methods (washing with different solvents and recrystallization from different solvents). By flash column chromatography it was possible, in the current study, to separate and isolate the desired compound. While complexes **2-2a** and **2-2b** were isolated in 74 and 51% yield, respectively, as analytically pure dark yellow solids, complexes **2-3a** and **2-3b** were isolated analytically pure in 4 and 8% yield as a blue and blue/green solid and were fully characterized by multinuclear NMR spectroscopy, high-resolution mass spectrometry (HRMS), elemental analysis and, for **2-3a**, additionally by single-crystal X-ray diffraction analysis.

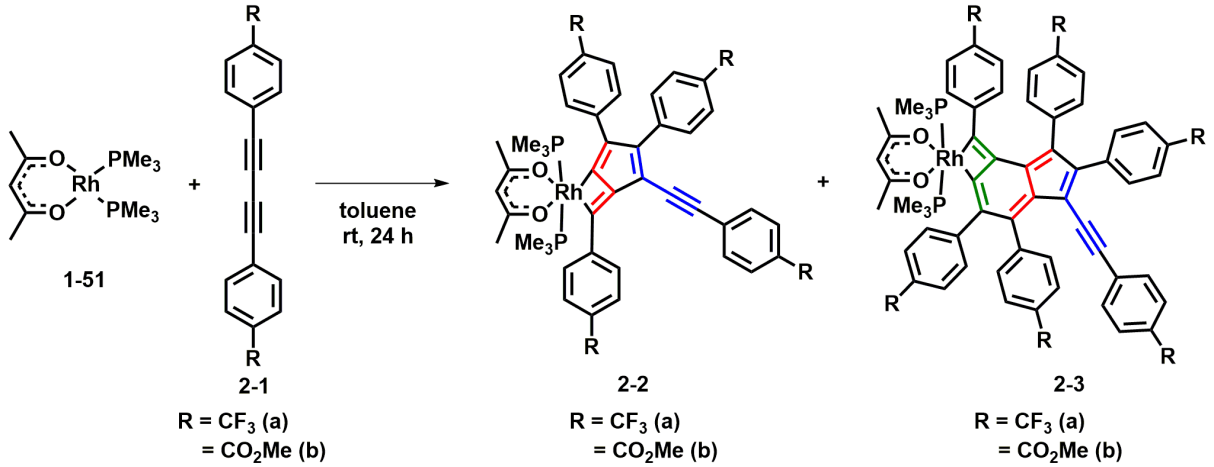

Scheme 2-2: Synthesis of complexes **2-2a**,**b** and **2-3a**,**b** *via* the reaction of [Rh(acac)(PMe$_3$)$_2$] **1-51** with *para*-CF$_3$-substituted 1,4-diphenylbuta-1,3-diynes **2-1a**,**b**. The former 1,3-butadiyne units are highlighted in different colors.

Inspection of the ^{1}H NMR spectroscopic data in THF-d$_8$ revealed unsymmetrical complexes for **2-3a** and **2-3b** as indicated by two sets of signals for the acac-CH$_3$ hydrogen atoms at 1.51 and 1.88 ppm for **2-3a**, and 1.51 and 1.85 ppm for **2-3b**. A virtual triplet with an integral of 18 is observed for the two trimethylphosphine ligands at ca 1.14 ppm for both complexes. Signals for the CO$_2$Me groups of **2-3b** resonate at 3.81 (6H), 3.80 (3H), 3.79 (3H), 3.77 (3H) and 3.74

ppm (3H). The single acac-CH group gives rise to a singlet at 5.09 and 5.07 ppm for **2-3a** and **2-3b**, respectively, integrating to one. For complex **2-3a** eight multiplets in the aromatic region from 7.56 – 6.69 ppm and for **2-3b** nine multiplets in the region from 7.85 – 6.62 ppm with a total number of 24 hydrogen atoms are observed. In the $^{13}C\{^{1}H\}$ NMR spectra, the acac-CH groups resonate at 98.8 and 97.8 ppm for **2-3a** and **2-3b**, respectively. In the ^{19}F NMR spectrum of **2-3a**, six signals are observed, of which four are singlets (-62.9, -63.0, -63.1 and -63.5 ppm) and two are quartets (-62.9 and -63.4 ppm, $J_{F\text{-}F}$ = 3.7 Hz). The $^{31}P\{^{1}H\}$ NMR resonances of compounds **2-3a** and **2-3b** are observed at 0.50 and 0.55 ppm, respectively, with ^{103}Rh-^{31}P coupling constants of 111 and 112 Hz, being in agreement with the data obtained for other octahedral rhodacyclopentadienes.[56, 59, 71]

By HRMS and elemental analysis it could be concluded that a third *para*-substituted 1,4-diphenylbuta-1,3-diyne had attached to the complexes **2-2a** and **2-2b** in this side product.

As already indicated by NMR spectroscopic data, single-crystal X-ray analyses confirmed that an additional third diyne had been incorporated between the rhodium metal center and the organic fulvene part of **2-2a** and **2-2b**. The complexes **2-3a** and **2-3b** exhibit an indene structure attached to the rhodium metal center in a bis-σ-manner as depicted in Scheme 2-2 and are formed in a [3+2+3] cyclization process.

Single-crystals suitable for X-ray diffraction were obtained by vapor diffusion of *n*-hexane into a THF solution of **2-3a**. Complex **2-3a** crystallizes in the monoclinic space group $P2_1/n$. The molecular structures of complexes **2-2a** and **2-3a** are shown in Figure 2-1 and selected bond lengths and angles listed are in Table 2-1 and Table 2-2.

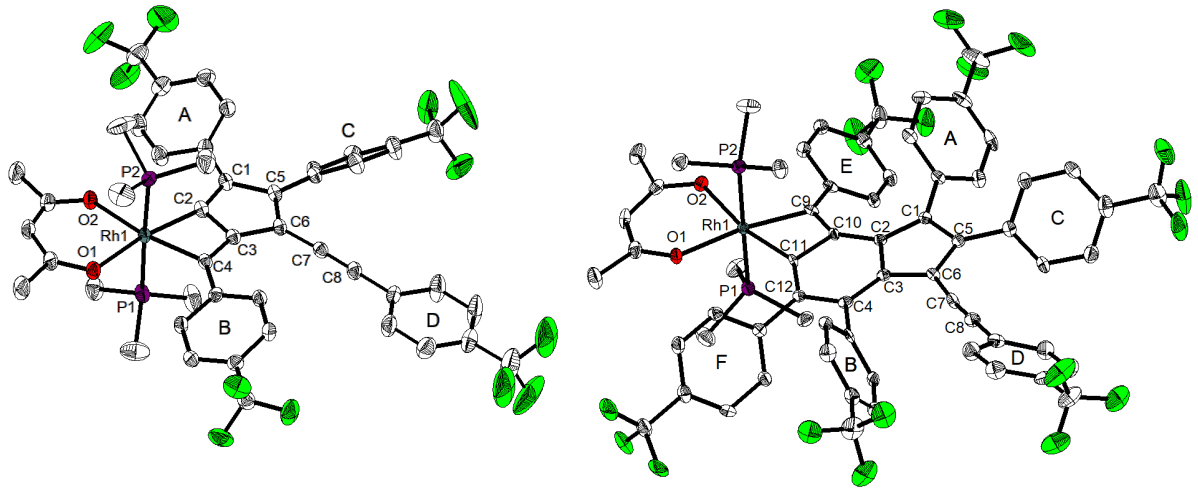

Figure 2-1: Molecular structure of complexes **2-2a**[206] (left) and **2-3a** (right) in the solid state at 100 K. Hydrogen atoms, THF solvent molecules and minor disordered CF_3 groups are omitted for clarity. Atomic displacement ellipsoids are drawn at the 50% probability level.

The molecular geometries of **2-2a** and **2-3a** are very similar, with the rhodium atom being in an octahedral coordination environment with *trans*-disposed phosphine ligands. The bond

distances in **2-2a** and **2-3a** are also very similar (Table 2-1). The Rh1-P bond distances are in the range of 2.3167(17) – 2.3498(17) Å, the Rh1-O bond distances are in the 2.1303(16) – 2.153(3) Å range and the Rh1-C bond distances are in the range of 2.008(4) – 2.044(2) Å and therefore in the same range as in acac- and PMe_3-substituted rhodacyclopentadienes (**1-52** and **1-53**) and dibenzorhodacyclopentadienes (**1-54** and **1-55**).[59, 71-72] The carbon-carbon bond distances in the five membered rings are in the range of 1.374(3) – 1.486(3) Å for **2-2a** and 1.391(6) – 1.462(6) Å for **2-3a**, respectively. In the six-membered ring in **2-3a**, the carbon-carbon distances are in the range of 1.377(6) – 1.462(6) Å. The C-C single bonds are very similar to typical conjugated C=C(sp^2)-C(sp^2)=C bonds and the C=C double bonds are characteristic for heterocyclic pyrrole C(sp^2)=C(sp^2) bonds, as they are quite long for double bonds. The distance between carbon atoms C7 and C8 are 1.202(3) and 1.195(6) Å, respectively, indicating carbon-carbon triple bonds as expected.[208]

Table 2-1: Selected bond lengths [Å] of complexes **2-2a**[206] and **2-3a** determined by single-crystal X-ray diffraction at 100 K with esd's in parentheses.

	2-2a	**2-3a**		**2-2a**	**2-3a**
Rh1-O1	2.1309(16)	2.135(3)	C2-C10	-	1.435(6)
Rh1-O2	2.1303(16)	2.153(3)	C3-C4	1.371(3)	1.381(6)
Rh1-P1	2.3323(7)	2.3167(17)	C3-C6	1.471(3)	1.452(6)
Rh1-P2	2.3196(6)	2.3498(17)	C4-C12	-	1.448(6)
Rh1-C2	2.025(2)	-	C5-C6	1.395(3)	1.391(6)
Rh1-C4	2.044(2)	-	C6-C7	1.413(3)	1.421(6)
Rh1-C9	-	2.011(5)	C7-C8	1.202(3)	1.195(6)
Rh1-C11	-	2.008(4)	C9-C10	-	1.393(6)
C1-C2	1.374(3)	1.402(6)	C10-C11	-	1.450(6)
C1-C5	1.486(3)	1.445(6)	C11-C12	-	1.377(6)
C2-C3	1.437(3)	1.462(6)			

The O1-Rh1-O2 angles of the complexes **2-2a** and **2-3a** are 88.21(6) and 86.21(12)°, the P1-Rh1-P2 angles are 177.82(2) and 179.44(5)°, the O1-Rh1-P1 angles are 89.38(5) and 90.15(10)° and the O2-Rh1-P2 angles are 91.69(5) and 88.37(10)°, respectively. The O1-Rh1-C angles are 103.62(8) and 105.02(15)°, the C-Rh-C angles are 65.81(9) and 65.05(17)° and the C-Rh1-O2 angles are 102.35(8) and 103.77(15)°, respectively. The sum of the angles within the four membered rhodacyclobutene is 360° and it is therefore planar. The small C-Rh-C angle in the rhodacyclobutene moiety can also be found in the bimetallic rhodium complex **1-50** (Scheme 1-19), synthesized by Schwenk, from the reaction of [Rh(S_2CNEt_2)(PMe_3)$_2$] **1-44** with 1,11-bis(4-(*p*-methoxy-tetrafluorophenyl))undeca-1,3,8,11-tetrayne **1-47f** (C-Rh-C: 63.19(14)°).[68]

Defining the organic core of the compounds **2-2a** and **2-3a** as plane "Z" and determining the rotation of the substituted phenyl rings out of this plane, it is striking that the angles for **2-2a**, of 5.2(1) – 44.2(8)° are, in general, smaller than for **2-3a** for which they are 33.6(3) – 70.3(1)°. This indicates that the substituted phenyl rings in **2-3a** are more crowded than in **2-2a** and rotate out of plane in order to minimize steric interactions. This finding is supported by the ^{19}F NMR spectrum, which shows six signals in total, of which four show a singlet and two show multiplets which originate from through space ^{19}F-^{19}F coupling. The distance between the carbon atom of the CF_3 groups of rings A and E is 4.278(9) Å.

Table 2-2: Selected angles [°] of complexes **2-2a** and **2-3b** determined by single-crystal X-ray diffraction at 100 K with esd's in parentheses.

	2-2a	**2-3a**		**2-2a**	**2-3a**
O1-Rh1-O2	88.21(6)	86.21(12)	∡ Z-A	27.9(1)	49.6(2)
P1-Rh1-P2	177.82(2)	179.44(5)	∡ Z-B	19.6(9)	70.3(1)
O1-Rh1-P1	89.38(5)	90.15(10)	∡ Z-C	44.2(8)	44.8(2)
O2-Rh1-P2	91.69(5)	88.37(10)	∡ Z-D	5.2(1)	33.6(3)
O1-Rh1-C4	103.62(8)	-	∡ Z-E	-	42.3(1)
C2-Rh1-C4	65.81(9)	-	∡ Z-F	-	62.0(1)
C2-Rh1-O2	102.35(8)	-			
O1-Rh1-C11	-	105.02(15)			
C9-Rh1-C11	-	65.05(17)			
C9-Rh1-O2	-	103.77(15)			

For compound **2-2a** the "Z"-plane is that of the fulvene core and for **2-3a** that of the indene core.

2.3.1.2 Reactions of [Rh(acac)(PMe_3)$_2$] with *para*-substituted 1,4-diphenylbuta-1,3-diynes at elevated temperature and different ratios

Because complexes **2-3a**,**b** are only formed in small quantities under the above mentioned conditions (6 – 10% according to $^{31}P\{^1H\}$ NMR spectroscopy) and a quantitative isolation during the workup is not possible, it was necessary to develop alternative reaction conditions in order to obtain more of the desired products. Preliminary studies at room temperature showed that adding more equivalents of the *para*-substituted 1,4-diphenylbuta-1,3-diyne **2-1a** to [Rh(acac)(PMe_3)$_2$] **1-51** did not increase the quantity of **2-3a**, but only increased the reaction rate for the formation of **2-2a**.[206] In this study, it was found that increasing the temperature and the number of equivalents at the same time resulted in formation of a larger amount of the desired complex **2-3a**. It was found that 100 °C was convenient regarding the progress of the reaction, and that at lower temperatures (80 and 85 °C), the reaction progress was very slow.[207] The solid compounds [Rh(acac)(PMe_3)$_2$] **1-51** (28.2 µmol) and *para*-substituted 1,4-diphenylbuta-1,3-diyne **2-1a** (two, three and five equivalents) were mixed in a J-Young's tap NMR tube in an argon-filled glovebox, 0.7 mL of toluene-d_8 were added, the NMR tubes were sealed, removed from the glovebox and heated in an aluminum block at 100 °C. The conversion and product ratios were calculated from the $^{31}P\{^1H\}$ NMR spectrum of the crude products, using the integration range from 2.1 – -5.1 ppm and the integration range of one signal of the respective doublet (see for an example Figure A1 for **1-51** + **2-1a** and Figure A2 for **2-2a** + **2-1a**).

Using two equivalents of **2-1a** and heating the reaction for one day results, according to the $^{31}P\{^1H\}$ NMR spectrum, in remaining starting material **1-51** (5%), **2-2a** (41%), **2-3a** (31%), and two other compounds **2-SYM^{CF3}** and **2-UNSYM^{CF3}** (Scheme 2-3, **2-SYM** and **2-UNSYM** will be discussed in more detail at the end of section 2.3.1.2) in 4 and 5% yields, respectively, and other minor side products (14%) that could yet not be identified (Table 2-3, entry 1). Heating the reaction for an additional two days showed no further progress (entry 2).

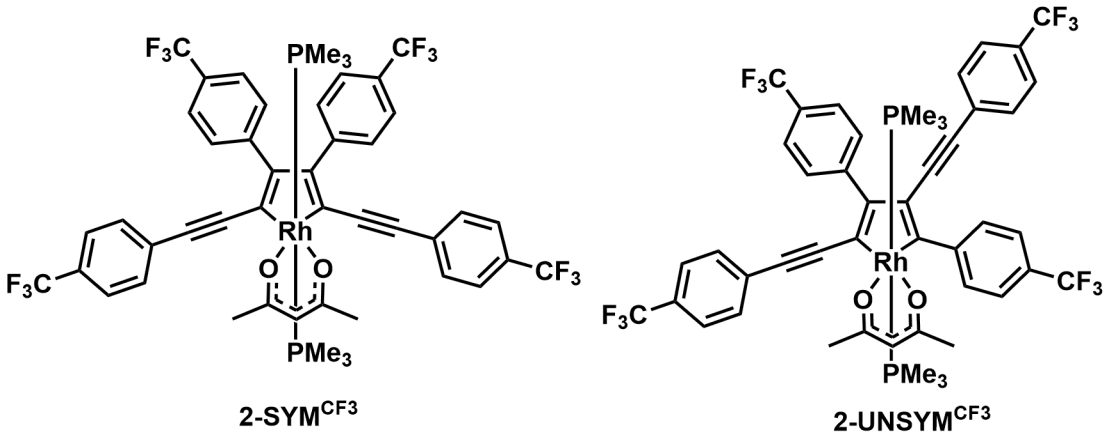

Scheme 2-3: Chemical structures of 2,5- and 2,4-bis(arylethynyl)rhodacyclopentadienes **2-SYM^{CF3}** and **2-UNSYM^{CF3}**.

Using three equivalents of complex **2-1a** and heating the reaction for one day results, according to the $^{31}P\{^{1}H\}$ NMR spectrum, in **2-2a** (24%), **2-3a** (50%) as well as **2-SYM^{CF3}** and **2-UNSYM^{CF3}** in 6 and 10% yields, respectively, and other minor side products (10%) (entry 3). Over a total period of eleven days, nearly all of **2-1a** was consumed, **2-SYM^{CF3}** shows no change, the amount of **2-2a** decreases further (24 – 2%), and the amount of **2-3a** increases (50 – 62%) as well as **2-UNSYM^{CF3}** (10 – 12%) and **2-Rest** (10 – 18%) (entries 4 – 8).

Adding five equivalents of **2-1a** and heating the reaction for 24 hours (entry 9) results, according to the $^{31}P\{^{1}H\}$ NMR spectrum, in **2-2a** (28%), **2-3a** (46%) as well as **2-SYM^{CF3}** and **2-UNSYM^{CF3}** in 6 and 10% yields, respectively, and other minor side products (10%). Over a total period of eleven days the amount of **2-2a** decreases (28 – 2%), the amount of **2-3a** increases (46 – 58%) as well as for **2-SYM^{CF3}** and **2-UNSYM^{CF3}** (6 – 8% and 10 – 14 %), and the amount of unidentified byproducts increases from 10 – 18% (entries 9 – 14).

From Table 2-3, entries 1 and 2 it can be concluded that, in order to obtain complete consumption of starting material [Rh(acac)(PMe_3)$_2$] **1-51** at 100 °C, more than two equivalents of **2-1a** are necessary. A further outcome from entries 3 – 8 and 9 – 14 is that more **2-3a** is formed (entry 6) when three equivalents of **2-1a** are used instead of five equivalents and that, after six days, the maximum amount of **2-3a** is formed and the amount of byproducts increases.

Mixing a solution of two equivalents of **2-1a** in toluene at 100 °C with a solution of [Rh(acac)(PMe_3)$_2$] **1-51** in toluene at 100 °C *via* cannulation and further heating for 24 hours results in **1-51** (2%), **2-2a** (60%), **2-3a** (20%), **2-SYM^{CF3}** (2%), **2-UNSYM^{CF3}** (2%) and 14% of unidentified byproducts. Comparing these results with those from Table 2-3 entry 1 shows, that more **2-2a** was formed, while the amount of **1-51**, **2-3a**, **2-SYM^{CF3}** and **2-UNSYM^{CF3}** is reduced. The amount of unidentified byproducts stayed unchanged with 14%.

The yields in Table 2-3 clearly indicate that the amount of **2-2a** decreases, **2-3a** increases and various new species are formed over the time which could not be further identified (except **2-SYM^{CF3}** and **2-UNSYM^{CF3}**) when more than two equivalents of *para*-substituted 1,4-diphenylbuta-1,3-diyne **2-1a** are used at 100 °C. This leads to the conclusion that complex **2-3a** as well as **2-SYM^{CF3}** and **2-UNSYM^{CF3}** are formed from complex **2-2a**.

Table 2-3: Results of the reaction of [Rh(acac)(PMe$_3$)$_2$] **1-51** with two, three and five equivalents of *para*-substituted 1,4-diphenylbuta-1,3-diyne **2-1a** at 100 °C in toluene-d$_8$ at different stages of the reaction.

1-51 : 2-1a	**entry**	**days**	**1-51** [%]	**2-2a** [%]	**2-3a** [%]	**2-SYM^{CF3}** [%]	**2-UNSYM^{CF3}** [%]	**2-REST** [%]
1 : 2 equiv. (100 °C; tol-d$_8$)	1	1	5	41	31	4	5	14
	2	3	5	41	31	4	5	14
1 : 3 equiv. (100 °C; tol-d$_8$)	3	1	0	24	50	6	10	10
	4	2	0	16	58	6	10	10
	5	3	0	12	60	6	12	10
	6	6	0	6	64	6	12	12
	7	8	0	4	62	6	12	16
	8	11	0	2	62	6	12	18
1 : 5 equiv. (100 °C; tol-d$_8$)	9	1	0	28	46	6	10	10
	10	2	0	16	54	6	12	12
	11	3	0	12	56	6	12	14
	12	6	0	4	60	8	14	14
	13	8	0	2	60	8	14	16
	14	11	0	2	58	8	14	18

In order to investigate this finding, complex **2-2a** was reacted with *para*-substituted 1,4-diphenylbuta-1,3-diyne **2-1a** under the above mentioned conditions, and the results are summarized in Table 2-4.

Entries 1 – 5 (Table 2-4) represent a ratio of 1:2 at 100 °C in toluene-d$_8$ over a period of eleven days. During this time span 94% of **2-2a** was consumed and 68% of **2-3a**, 4% of **2-SYM^{CF3}** and 10% **2-UNSYM^{CF3}** were formed as well as 12% of as yet unidentified compounds.

Entries 6 – 8 represent the reaction in a ratio of 1:3 at 100 °C in toluene-d$_8$ over a period of eleven days. During this time span, 99% of **2-2a** was consumed and 64% of **2-3a**, 6% of **2-SYM^{CF3}** and 16% **2-UNSYM^{CF3}** as well as 13% of as yet unidentified compounds were formed.

A ratio of 1:5 results in a complete consumption of complex **2-2a** after eleven days, and the formation of 52% of **2-3a**, 8% of **2-SYM^{CF3}** and 22% of **2-UNSYM^{CF3}** (entries 9 – 11) as well as 18% of as yet unidentified compounds.

Table 2-4: Results of the reaction of complex **2-2a** with two, three and five equivalents of *para*-substituted 1,4-diphenylbuta-1,3-diyne **2-1a** at 100 °C in toluene-d_8 at different stages of the reaction.

2-2a : 2-1a	**entry**	**days**	**2-2a** [%]	**2-3a** [%]	**2-SYM^{CF3}** [%]	**2-UNSYM^{CF3}** [%]	**2-REST** [%]
1 : 2 equiv. (100 °C; tol-d_8)	1	1	82	14	1	2	1
	2	2	64	26	2	4	4
	3	3	48	40	2	4	6
	4	5	28	54	4	8	6
	5	11	6	68	4	10	12
1 : 3 equiv. (100 °C; tol-d_8)	6	2	50	34	2	6	8
	7	7	8	62	6	14	10
	8	11	1	64	6	16	13
1 : 5 equiv. (100 °C; tol-d_8)	9	2	44	34	4	10	8
	10	7	4	54	8	20	14
	11	11	0	52	8	22	18

The assumption that complex **2-3a** is formed from compound **2-2a** (Table 2-3) at 100 °C can be confirmed by the findings from Table 2-4. Complexes **2-SYM^{CF3}** and **2-UNSYM^{CF3}** are both formed in the reaction of [Rh(acac)(PMe_3)$_2$] **1-51** and complex **2-2a**, respectively, with *para*-substituted 1,4-diphenylbuta-1,3-diyne **2-1a**. In both reactions, **2-UNSYM^{CF3}** is always favored over **2-SYM^{CF3}**. While the formation of **2-3a** from **2-2a** can be proposed to occur by insertion of an unbound *para*-substituted 1,4-diphenylbuta-1,3-diyne into the rhodium-carbon σ-bonds, the formation pathway for **2-SYM^{CF3}** and **2-UNSYM^{CF3}** remains unclear. However, it seems likely that an organic component dissociates and [Rh(acac)(PMe_3)$_2$] **1-51** then reacts with *para*-substituted 1,4-diphenylbuta-1,3-diyne **2-1a** at 100 °C.

Table 2-3 and 2-4 also indicate that, the more equivalents of *para*-substituted 1,4-diphenylbuta-1,3-diyne **2-1a** are used at 100 °C the more of the complexes **2-SYM^{CF3}** and **2-UNSYM^{CF3}** are formed.

To verify the hypothesis that a third *para*-substituted 1,4-diphenylbuta-1,3-diyne inserts between the metal and the organic fulvene core of complex **2-2a**, *para*-CO_2Me-substituted 1,4-diphenylbuta-1,3-diyne **2-1b** (5 equiv.) was added to **2-2a** and the reaction was stirred for a period of 14 days at 100 °C. By flash column chromatography, it was possible to separate and isolate the desired compound **2-3c** as a pale green solid (Scheme 2-4). Further purification resulted in analytically pure **2-3c** in 14% yield. The complex was fully characterized by multinuclear NMR spectroscopy, HRMS, elemental analysis and single-crystal X-ray diffraction analysis.

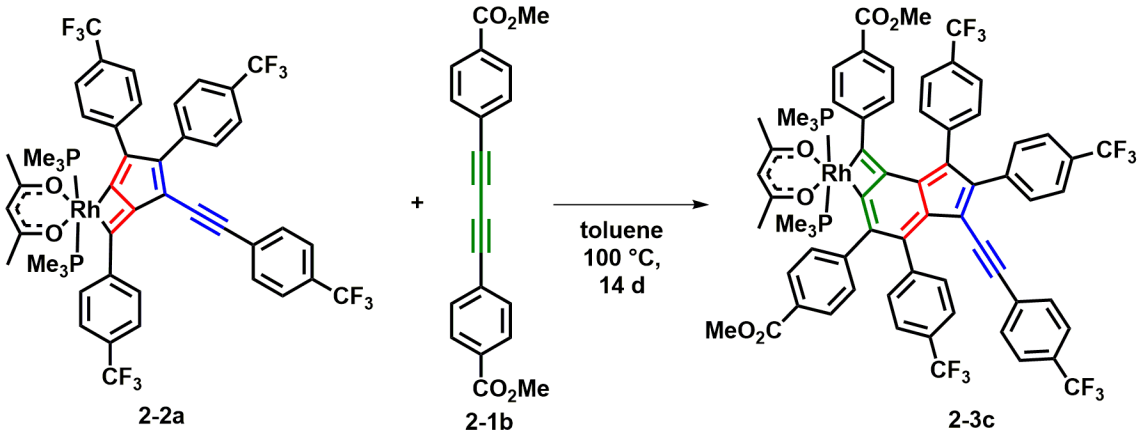

Scheme 2-4: Synthesis of complex **2-3c** *via* the reaction of complex **2-2a** with *para*-CO_2Me-substituted 1,4-diphenylbuta-1,3-diyne **2-1b**. The former 1,3-butadiyne units are highlighted in different colors.

Inspection of the ^{1}H NMR spectroscopic data in THF-d_8 revealed **2-3c** to be an unsymmetrical complex, as indicated by two sets of signals in the ^{1}H NMR spectrum for the acac-CH_3 hydrogen atoms at 1.50 and 1.86 ppm as well as for the CO_2Me groups at 3.78 and 3.80 ppm. A virtual triplet with an integral of 18 is observed for the two trimethylphosphine ligands at 1.14 ppm. The single acac-CH group gives rise to a singlet at 5.07 ppm, integrating to one, identical to complex **2-3b**. Additionally, 24 hydrogen atoms in the aromatic region from 7.75 – 6.70 ppm gives rise to nine multiplets. In the $^{13}C\{^{1}H\}$ NMR spectrum, the acac-CH group resonates at 98.7 ppm. In the ^{19}F NMR spectrum, there are four singlets at -62.7, -62.91, -62.93 and -63.5 ppm. The spectrum shows no ^{19}F-^{19}F through space coupling, as the shortest distance between the carbon atoms of the two closest neighboring CF_3 groups (Figure 2-2, rings B and D) is 4.73(1) Å, hence ca. 0.45 Å longer than the shortest distance in **2-3a**. The $^{31}P\{^{1}H\}$ NMR resonance of compound **2-3c** is observed at 0.55 ppm with a ^{103}Rh-^{31}P coupling constant of 112 Hz being in agreement with the data obtained for other octahedral rhodacycles[56, 59, 71] and the similar complexes **2-3a**,**b**.

By HRMS and elemental analysis it could be concluded that the *para*-CO_2Me-substituted 1,4-diphenylbuta-1,3-diyne **2-1b** had attached to the complex **2-2a**.

As already indicated by NMR spectroscopic data, single-crystal X-ray analyses confirmed that the additional third *para*-substituted 1,4-diphenylbuta-1,3-diyne **2-1b** had been incorporated between the rhodium metal center and the organic fulvene part of complex **2-2a**. Resulting an indene structure bound to the rhodium metal center in a bis-*σ*-manner as for the complexes **2-3a**,**b**. Single-crystals suitable for X-ray diffraction were obtained by vapor diffusion of *n*-hexane into a THF solution of **2-3c**. Complex **2-3c** crystallizes in the monoclinic space group *C*2/*c* and the molecular structure is shown in Figure 2-2 and selected bond lengths and angles are listed in Table 2-5.

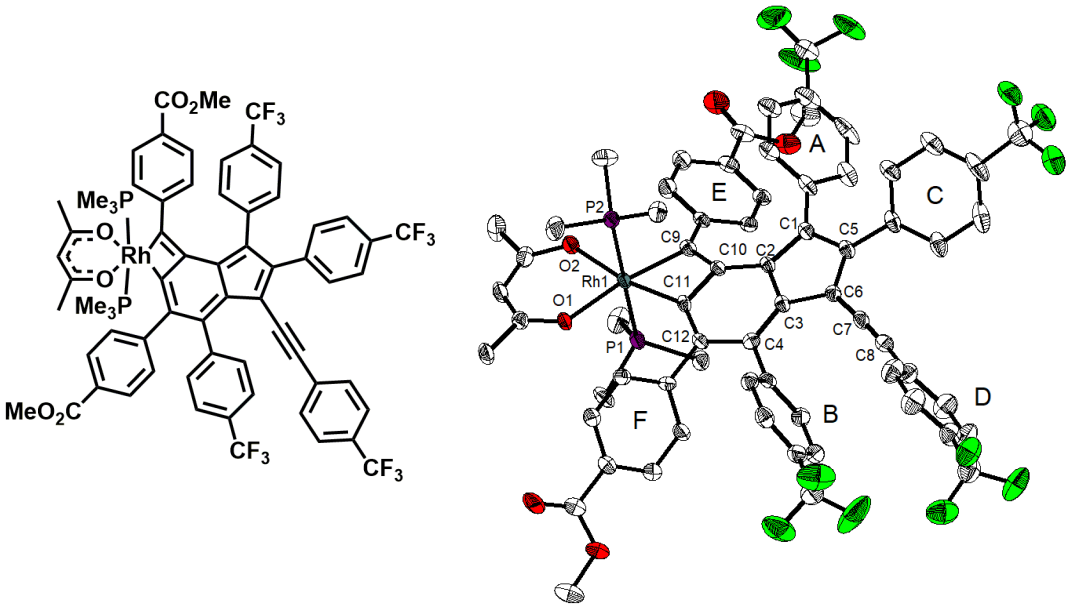

Figure 2-2: Chemical and molecular structure of complex **2-3c** in the solid state at 100 K. Hydrogen atoms, THF solvent molecules and minor disordered CF_3 groups are omitted for clarity. Atomic displacement ellipsoids are drawn at the 50% probability level.

The molecular geometries of **2-3a** and **2-3c** are very similar. The bond lengths of **2-3c** listed in Table 2-5 and the bond lengths of **2-3a** listed in Table 2-1 are the same, as are the bond angles and the angles between the indene core and the attached phenyl rings (Table 2-2), except for ring D. For **2-3a**, this angle is 33.6(3)° and for **2-3c** it is 71.1(2)°.

Table 2-5: Selected bond lengths [Å] and angles [°] of complex **2-3c** determined by single-crystal X-ray diffraction at 100 K with esd's in parentheses.

	2-3c		**2-3c**
Rh1-O1	2.126(3)	C9-C10	1.389(7)
Rh1-O2	2.137(3)	C10-C11	1.454(6)
Rh1-P1	2.3238(16)	C11-C12	1.369(7)
Rh1-P2	2.3414(16)	O1-Rh1-O2	87.44(13)
Rh1-C9	2.014(5)	P1-Rh1-P2	179.32(5)
Rh1-C11	2.021(5)	O1-Rh1-P1	90.9(1)
C1-C2	1.395(6)	O2-Rh1-P2	89.10(9)
C1-C5	1.444(7)	O1-Rh1-C11	104.01(16)
C2-C3	1.462(6)	C9-Rh1-C11	65.39(19)
C2-C10	1.441(6)	C9-Rh1-O2	103.15(16)
C3-C4	1.391(6)	∡ Z-A	47.3(1)
C3-C6	1.455(6)	∡ Z-B	72.4(1)
C4-C12	1.449(7)	∡ Z-C	48.7(1)
C5-C6	1.393(7)	∡ Z-D	71.1(2)
C6-C7	1.421(7)	∡ Z-E	39.8(1)
C7-C8	1.191(7)	∡ Z-F	61.4(1)

For compound **2-3c** the "Z"-plane is that of the indene core.

During the purification of **2-3c** it was possible to isolate small amounts of an orange solid. This solid turned out to be a mixture containing the complexes **2-SYM^{CO2Me}** and **2-UNSYM^{CO2Me}**. By washing this fraction with acetone, it was possible to reduce the amount of **2-UNSYM^{CO2Me}**. Complex **2-SYM^{CO2Me}** was characterized by multinuclear NMR spectroscopy, HRMS and single-crystal X-ray diffraction.

Inspection of the ^{1}H NMR spectroscopic data revealed a symmetrical complex to be the main product as indicated by only one signal with an integral of six for the two acac-CH_3 groups at 1.92 ppm and two singlets for the two different methoxy groups at 3.48 and 3.45 ppm, each integrating to six. A virtual triplet with an integral of 18 is observed for the two trimethylphosphine ligands at ca. 0.94 ppm. The single acac-CH group gives rise to a singlet at 5.16 ppm, integrating to one. Four sets of multiplets, each with an integral of four resonate in the aromatic region from 8.24 – 7.42 ppm (two sets for A/D and two sets for B/C). (Figure 2-3). The ^{31}P{^{1}H} NMR spectrum (Figure 2-4) shows a dominating doublet at -1.8 ppm for **2-SYM^{CO2Me}** and a smaller doublet at -3.4 ppm for **2-UNSYM^{CO2Me}**, respectively, with the ^{103}Rh-^{31}P coupling constants of 110 and 109 Hz being in agreement with those of other octahedral rhodacycles bearing trimethylphosphine ligands.[56, 59, 71]

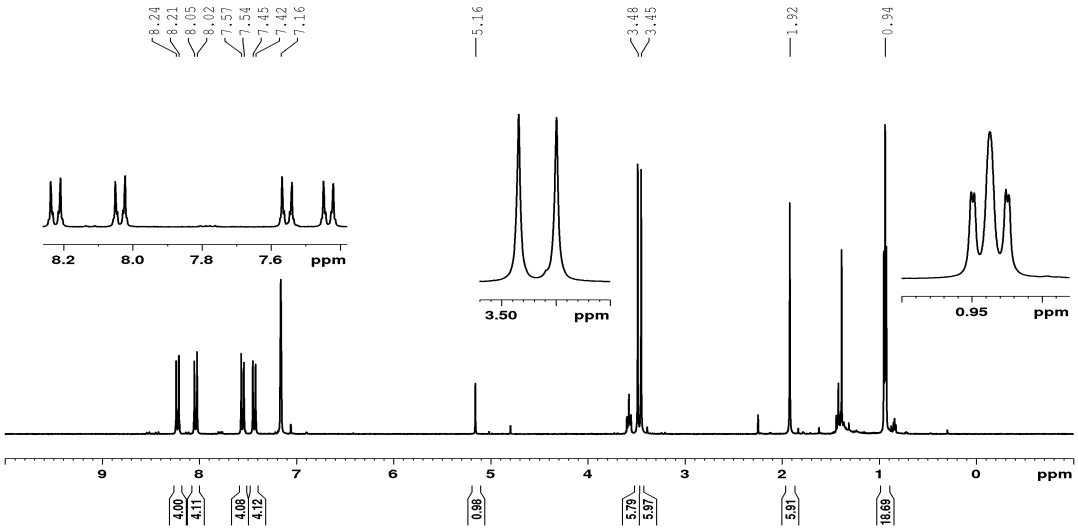

Figure 2-3: ^{1}H NMR spectrum (300 MHz, C_6D_6) of complex **2-SYM^{CO2Me}** with small amounts of **2-UNSYM^{CO2Me}** and residual amounts THF and BHT (stabilizing agent in THF).

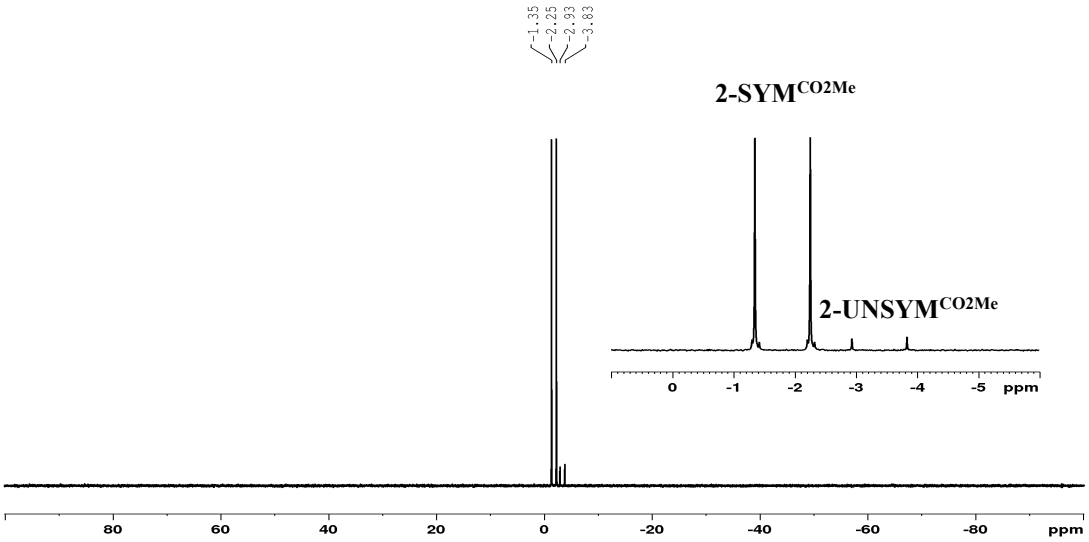

Figure 2-4: $^{31}P\{^{1}H\}$ NMR spectrum (121 MHz, C_6D_6) of complex **2-SYM^{CO2Me}** with small amounts of **2-UNSYM^{CO2Me}**.

Furthermore, it was possible to isolate orange-colored single-crystals suitable for X-ray diffraction by vapor diffusion of *n*-hexane into a THF solution of the mixture of **2-SYM^{CO2Me}** and **2-UNSYM^{CO2Me}**. The molecular structure of complex **2-SYM^{CO2Me}** is shown in Figure 2-5 and selected bond lengths and angles are listed in Table 2-6.

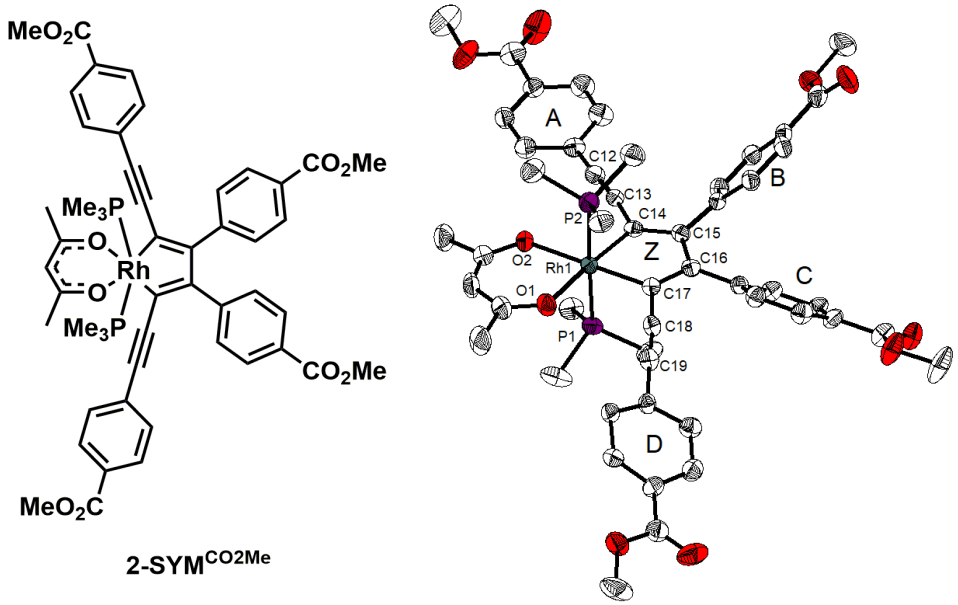

Figure 2-5: Chemical and molecular structure of complex **2-SYM^{CO2Me}** in the solid state at 100 K. Hydrogen atoms are omitted for clarity. Atomic displacement ellipsoids are drawn at the 50% probability level.

Complex **2-SYM^{CO2Me}** crystallizes in the triclinic space group $P\bar{1}$. The rhodium atom is in an octahedral coordination environment with *trans*-disposed PMe_3 ligands. The Rh1-P bond distances are 2.3048(14) and 2.3150(14) Å, the Rh1-O bond distances are 2.137(2) and 2.149(2) Å, and the Rh1-C bond distances are 1.996(3) and 2.001(3) Å and, therefore, in the same range as in acac- and PMe_3-substituted rhodacyclopentadienes (**1-52** and **1-53**) and dibenzorhodacyclopentadienes (**1-54** and **1-55**).[59, 72] The carbon-carbon distances in the five membered ring are 1.367(5) and 1.380(5) Å for the C=C double bonds and 1.469(5) Å for the C-C single bond. Hence, the C=C double bonds are very similar to typical cyclopenta-1,3-diene $C(sp^2)=C(sp^2)$ bonds, and the single C-C bond is characteristic for an endocyclic $C(sp^2)$-$C(sp^2)$ bond. The distances between the carbon atoms C12-C13 and C18-C19 are 1.193(5) and 1.188(5) Å, respectively, indicating carbon-carbon triple bonds.[208]

The O1-Rh1-O2 angle is 88.10(9)°, the P1-Rh1-P2 angle is 177.32(4)°, the O1-Rh1-P1 angle is 93.20(8)°, the O2-Rh1-P2 angle is 91.83(8)°, the O1-Rh1-C17 angle is 95.84(12)° and the C14-Rh1-O2 angle is 96.41(12)°. The C-Rh-C angle is 79.71(14)°, while the other angles in the rhodacyclopentadiene are within the range of 113.4(3) – 117.0(3)°and larger than the expected 108° for a regular planar, five-membered ring. This finding is similar to other rhodacyclopentadienes.[59, 72] Nevertheless, the sum of all five angles is 540°.

In this complex, aryl ring A connected to the alkyne group is nearly coplanar with 7.2(2)° with the rhodacyclopentadiene, while the aryl moiety D is twisted by 28.1(3)°. Similar findings in related rhodacyclopentadienes formed from the reaction of [Rh(acac)(P(*p*-tolyl)$_3$)$_2$] **1-56** or [Rh(acac)(PMe_3)$_2$] **1-51** with *para*-CO_2Me-substituted α,ω-bis(arylbutadiynyl)alkanes **1-43d** and **1-47d** in which angles of 8.2(1)° and 23.2(1)° as well as 6.5(2)° and 14.1(2)°, respectively, are found.[59, 71-72] The phenyl rings in positions 3 and 4 are rotated by 47.0(3)° (B) and 39.0(3)° (C) out of the rhodacyclopentadiene plane, which can also be found in similar rhodacyclopentadienes formed from the reaction of different rhodium(I) complexes with *para*-CO_2Me-substituted 1,4-diphenylbuta-1,3-diyne **2-1b** (44.2(2) – 56.0(2)°).[56, 209]

Table 2-6: Selected bond lengths [Å] and angles [°] of complex **2-SYM^{CO2Me}** determined by single-crystal X-ray diffraction at 100 K with esd's in parentheses.

	2-SYM^{CO2Me}		**2-SYM^{CO2Me}**
Rh1-O1	2.137(2)	O1-Rh1-O2	88.10(9)
Rh1-O2	2.149(2)	P1-Rh1-P2	177.32(4)
Rh1-P1	2.3048(14)	O1-Rh1-P1	93.20(8)
Rh1-P2	2.3150(14)	O2-Rh1-P2	91.83(8)
Rh1-C14	2.001(3)	O1-Rh1-C17	95.84(12)
Rh1-C17	1.996(3)	C14-Rh1-C17	79.71(14)
C12-C13	1.193(5)	C14-Rh1-O2	96.41(12)
C13-C14	1.417(5)	∢ Z-A	7.2(2)
C14-C15	1.380(5)	∢ Z-B	47.0(3)
C15-C16	1.469(5)	∢ Z-C	39.0(3)
C16-C17	1.367(5)	∢ Z-D	28.1(3)
C17-C18	1.421(5)		
C18-C19	1.188(5)		

The formation of the 2,4-bis(arylethynyl)rhodacyclopentadiene **2-UNSYM** is surprising. In the reaction of similar rhodium(I)-phosphine complexes, e.g. [Rh(CCSiMe$_3$)(PMe$_3$)$_4$] **1-28a** with different *para*-substituted 1,4-diphenylbuta-1,3-diynes, only the 2,5-substituted rhodacyclopentadienes **1-29a** – **1-37a** were observed (Scheme 1-13).[56] However, in the reaction of [Rh(acac)(P(*p*-tolyl)$_3$)$_2$] **1-56** with *para*-CF$_3$-substituted 1,4-diphenylbuta-1,3-diyne **2-1a**, the tri(*p*-tolyl)phosphine analogues of **2-SYM^{CF3}** and **2-UNSYM^{CF3}** were observed as intermediates in the catalytic cyclotrimerization of **2-1a**. Addition of PMe$_3$, and gentle heating resulted in **2-SYM^{CF3}** and **2-UNSYM^{CF3}**.[209]

In order to verify the finding of the two rhodacyclopentadienes **2-SYM^{CO2Me}** and **2-UNSYM^{CO2Me}**, especially of **2-UNSYM^{CO2Me}**, as it was not possible to obtain a single-crystal X-ray structure, [Rh(acac)(P(*p*-tolyl)$_3$)$_2$] **1-56** was reacted with *para*-substituted 1,4-diphenylbuta-1,3-diyne **2-1b** for three days at 50 °C before PMe$_3$ was added and the mixture stirred for another 24 hours at 50 °C (Scheme 2-5). The outcome of this reaction are the complexes **SYM^{CO2Me}** and **UNSYM^{CO2Me}** as was shown by Hartmann for the CF$_3$-substituted congeners.[209]

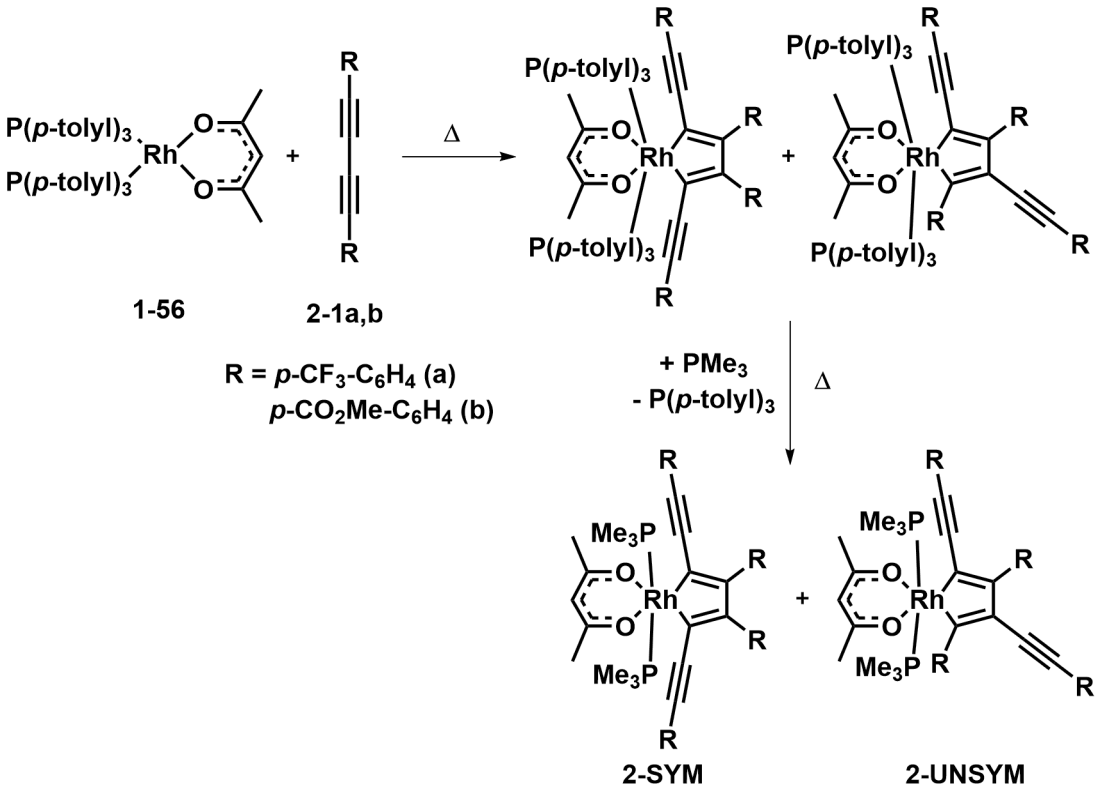

Scheme 2-5: Synthesis of PMe_3-substituted rhodacyclopentadienes **2-SYM** and **2-UNSYM** *via* ligand exchange reaction.

Figure 2-6 displays the *in-situ* $^{31}P\{^1H\}$ NMR spectra in toluende-d_8 of the reactions of complex **2-2a** with *para*-substituted 1,4-diphenylbuta-1,3-diyne **2-1a** (black spectrum) and complex **2-2a** with **2-1b** (blue spectrum) at 100 °C after 48 hours. The reaction of [Rh(acac)(P(*p*-tolyl)$_3$)$_2$] **1-56** with **2-1a** at 50°C for three days, followed by the addition of PMe_3 and additional 24 hours at 50 °C is presented in the red spectrum, and the reaction of [Rh(acac)(P(*p*-tolyl)$_3$)$_2$] **1-56** with **2-1b** followed by the addition of PMe_3 is displayed in the purple spectrum.

In the purple spectrum, two doublets at -1.6 ppm ($^1J_{Rh\text{-}P}$ = 110 Hz) and -3.2 ppm ($^1J_{Rh\text{-}P}$ = 110 Hz) for **2-SYM^{CO2Me}** and **2-UNSYM^{CO2Me}** are observed. In Figure 2-4, similar resonances and coupling constants in C_6D_6 were found, with the lower field shifted resonance being that of **2-SYM^{CO2Me}** (*vide supra*).

In the blue NMR spectrum, the crossover product **2-3c** (-0.3 ppm, $^1J_{Rh\text{-}P}$ = 113 Hz) is apparent besides resonances at -1.6 ppm with $^1J_{Rh\text{-}P}$ = 110 Hz and at -3.2 ppm with $^1J_{Rh\text{-}P}$ = 109 Hz, representing **2-SYM^{CO2Me}** and **2-UNSYM^{CO2Me}**, respectively.

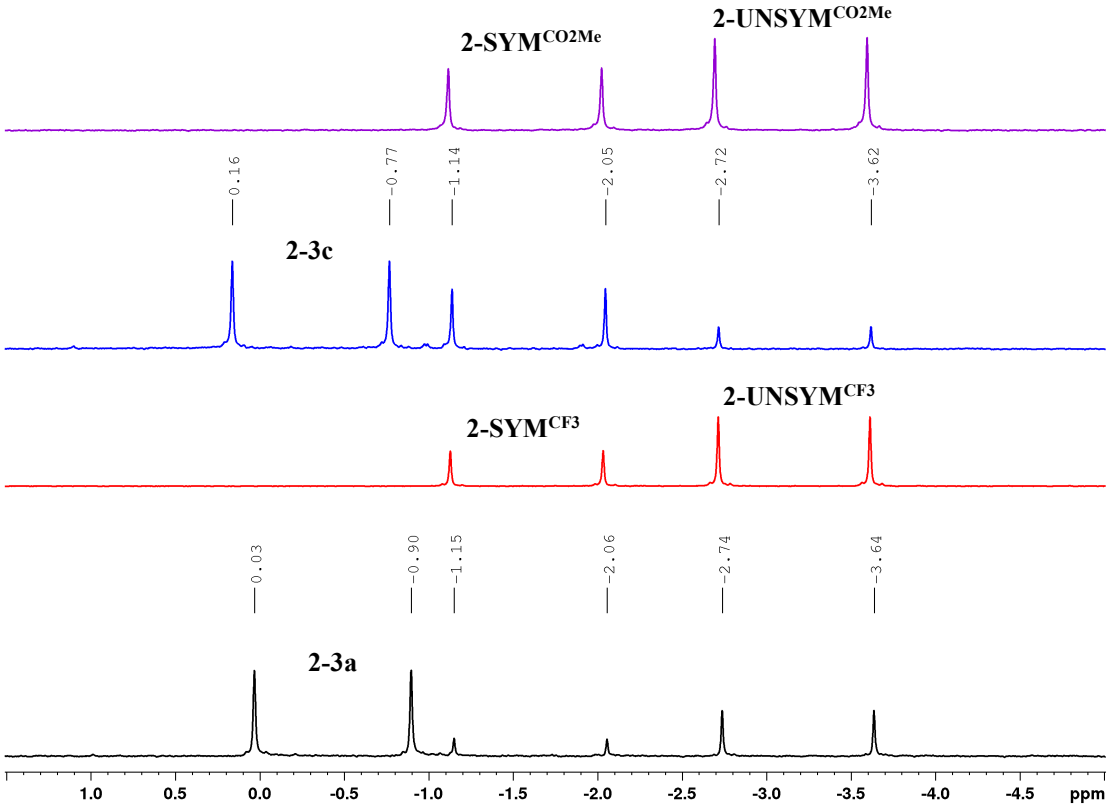

Figure 2-6: Portion of the $^{31}P\{^{1}H\}$ NMR spectra (121 MHz, toluene-d_8) of the reactions of complex **2-2a** with *para*-substituted 1,4-diphenylbuta-1,3-diyne **2-1a** (black) and of complex **2-2a** with **2-1b** (blue) at 100 °C after 48 hours, and reactions of [Rh(acac)(P(*p*-tolyl)$_3$)$_2$] **1-56** with **2-1a** and PMe_3 (red) and **1-56** with **2-1b** and PMe_3 at 50 °C after 4 days (purple).

The red spectrum displays two doublets at -1.6 ppm with $^{1}J_{Rh\text{-}P}$ = 110 Hz and at -3.2 ppm with $^{1}J_{Rh\text{-}P}$ = 109 Hz, respectively. Hartmann found similar resonances in C_6D_6, representing **2-SYM^{CF3}** and **2-UNSYM^{CF3}**.[209] In the black spectrum, compound **2-3a**, resonating at -0.4 ppm with $^{1}J_{Rh\text{-}P}$ = 113 Hz, **2-SYM^{CF3}**, resonating at -1.6 ppm with $^{1}J_{Rh\text{-}P}$ = 110 Hz and **2-UNSYM^{CF3}**, resonating at -3.2 ppm with $^{1}J_{Rh\text{-}P}$ = 109 Hz are apparent.

The resonances for the two **2-SYM** and **2-UNSYM** complexes formed in the reaction of the different *para*-substituted 1,4-diphenylbuta-1,3-diynes **2-1a**,**b** are identical in toluene-d_8 and only slightly shifted to low field in C_6D_6. The formation of a species of the formula [Rh(acac)(PMe_3)$_2$(2-1a,b)] in the reaction of [Rh(acac)(PMe_3)$_2$] **1-51** with **2-1a**,**b** and PMe_3 was also confirmed by HRMS of the crude reaction mixture.

Okorn already observed signals for the complexes **2-3a** and **2-UNSYM^{CF3}** in the reaction of [Rh(acac)(PMe_3)$_2$] **1-51** with the *para*-substituted 1,4-diphenylbuta-1,3-diyne **2-1a** at elevated temperatures. However, in his work, the resonances could not be assigned to specific species.[207] Interestingly, in order to obtain the complexes **2-SYM** and **2-UNSYM**, rhodium(I) starting material [Rh(acac)(PMe_3)$_2$] **1-51** needs to be present, hence the organic fulvene part of

complex **2-2a** must be released from the metal center. Unfortunately, it was not possible to isolate or identify any organic compound containing the fulvene system in these reactions.
Attempts to add a fourth diyne to the rhodium metal by adding three equivalents of *para*-substituted 1,4-diphenylbuta-1,3-diyne **2-1a** to a solution of complex **2-3a** in toluene at 100 °C for three weeks results, according to $^{31}P\{^{1}H\}$ NMR spectroscopy, in **2-SYM^{CF3}**, **2-UNSYM^{CF3}**, unreacted **2-3a** and further, low intensity doublets that could not be further assigned. However, by HRMS, a signal for a $[Rh(acac)(PMe_3)_2(2\text{-}1a)_4]$ species was detected.

The results of the reactions described in section 2.3.1.1 and 2.3.1.2 are summarized in Scheme 2-6. In the reaction of $[Rh(acac)(PMe_3)_2]$ **1-51** with the *para*-substituted 1,4-diphenylbuta-1,3-diyne **2-1a** at ambient temperatures, **2-2a** and **2-3a** were formed exclusively, while at 100 °C **2-SYM^{CF3}** and **2-UNSYM^{CF3}** were also formed. At 100 °C, the reaction of complex **2-2a** with an excess of *para*-CF_3-substituted 1,4-diphenylbuta-1,3-diyne **2-1a** results in **2-3a**, **2-SYM^{CF3}** and **2-UNSYM^{CF3}**. With an excess of *para*-CO_2Me-substituted 1,4-diphenylbuta-1,3-diyne **2-1b**, the crossover complex **2-3c** is formed in addition to the CO_2Me-substituted complexes **2-SYM^{CO2Me}** and **2-UNSYM^{CO2Me}**. In the reaction of complex **2-3a** with an excess of **2-1a**, again, **2-SYM^{CF3}** and **2-UNSYM^{CF3}** formed, in addition to trace amounts of a species with the formula $[Rh(acac)(PMe_3)_2(2\text{-}1a)_4]$.
The results obtained indicate that at elevated temperatures, the formation of the complexes **2-SYM** and **2-UNSYM** are favored, compared to the formation of complex **2-2a**. Furthermore, it is possible to extend the conjugated fulvene π-system in **2-2a** at least, to an indene π-system as in **2-3a**. Additionally, it can be concluded that the extension of the π-system occurs *via* an insertion between the rhodium metal center and the bis-σ-bound organic fulvene moiety.

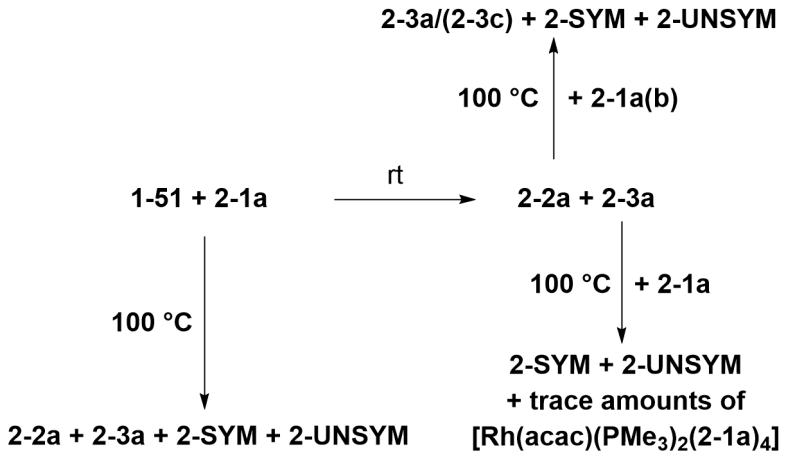

Scheme 2-6: Reaction overview of the reactions in section 2.3.1.1 and 2.3.1.2.

2.3.1.3 Reaction of complex **2-2a** with *para*-tolyl isocyanate

Previous work already dealt with the separation of the organic part from the rhodium metal in complexes **2-2a** and **2-2b**. The reaction of **2-2a** with alkyne derivatives leads to complicated product mixtures with oligomers and polymers, to degradation, or no reaction at all, according to NMR spectroscopy. The collected data suggested that steric factors may be responsible for the slow and unspecified reactions, indicating that small substrates may be more reactive.[210] Therefore, the very small H_2-molecule was tested. Under an atmospheric pressure of H_2 and at elevated temperature, a reaction took place, but further identification of the reaction products was unsuccessful. However, isocyanates are often used in rhodium-catalyzed intermolecular [2+2+2] cycloaddition reactions with alkynes to provide pyridones.[138, 142, 158, 211-212] Promising results from the reaction of **2-2a** with 1.4 equivalents of *para*-tolyl isocyanate **2-4** at elevated temperatures were observed by Okorn.[207]

In this work, four equivalents of *para*-tolyl isocyanate **2-4** were reacted with **2-2a** at 80 °C for three days. By flash column chromatography, it was possible to separate and isolate a purple compound. Further purification yielded analytically pure **2-5** in 13% yield (Scheme 2-7).

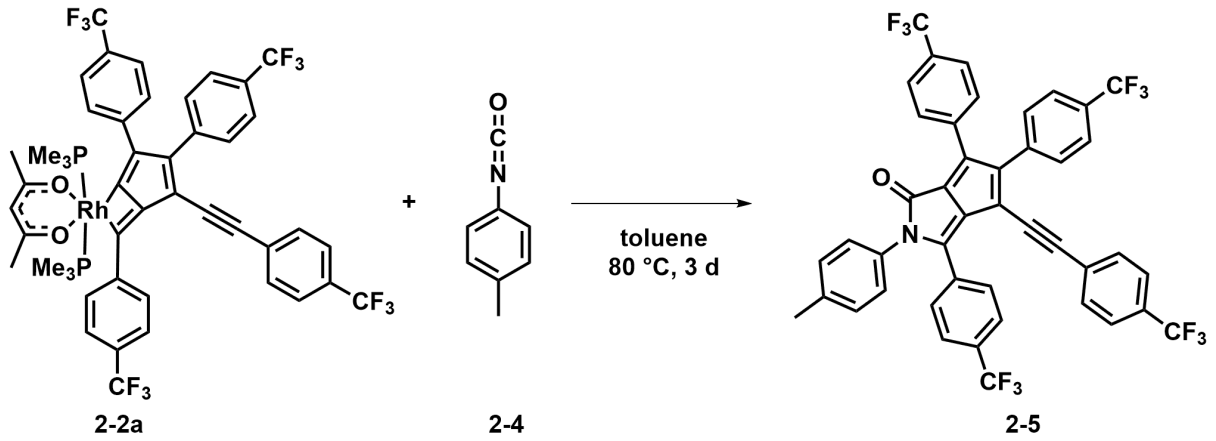

Scheme 2-7: Synthesis of cyclopentapyrrolone **2-5** *via* the reaction of complex **2-2a** with *para*-tolyl isocyanate **2-4**.

Inspection of the ^{1}H NMR spectroscopic data in C_6D_6 revealed a singlet at 1.95 ppm with an integral of three and eight multiplets with a total number of 20 hydrogen atoms in the aromatic region from 7.69 – 6.75 ppm. In the ^{19}F NMR spectrum, there are four singlets at -62.1, -62.5, -62.7 and -63.1 ppm, respectively, which are shifted slightly upfield compared to those of **2-2a** (-61.6, -61.9, -62.2 and -62.3 ppm).

HRMS and elemental analysis indicated the formation a compound derived from the organic fulvene part of complex **2-2a** plus one equivalent of **2-4**.

Single-crystals suitable for X-ray diffraction were obtained by vapor diffusion of *n*-hexane into a toluene solution of **2-5**, and the molecular structure is shown in Figure 2-7 and selected bond lengths and angles are listed in Table 2-7. Compound **2-5** crystallizes in the triclinic space group $P\bar{1}$.

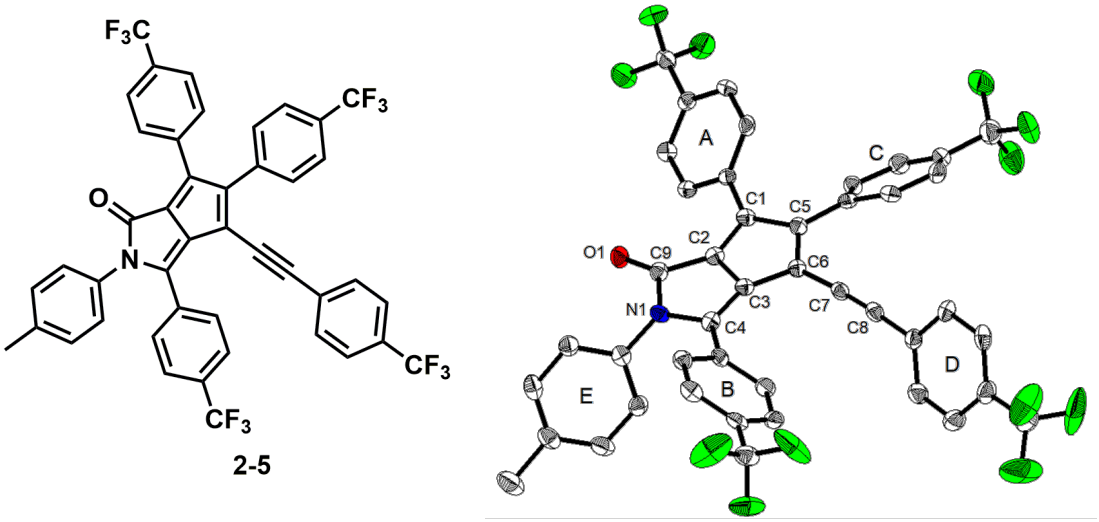

Figure 2-7: Chemical and molecular structure of compound **2-5** in the solid state at 100 K. Hydrogen atoms, toluene solvent molecules and minor disordered CF_3 groups are omitted for clarity. Atomic displacement ellipsoids are drawn at the 50% probability level.

A cyclopentapyrrolone core is found for compound **2-5**, in which the carbon-carbon distances in the five membered rings are between 1.384(5) – 1.401(5) Å for the double bonds and 1.425(5) – 1.473(5) Å for the single bonds. The carbon-carbon distances in the all-carbon five membered ring are the same as in the respective five membered rings in **2-2a** and **2-3a**. The distances within the N-heterocyclic five membered ring are identical with those in diketopyrrolopyrroles (*vide infra*). The C7-C8 distance is 1.206(5) Å, indicating a carbon-carbon triple bond and the C9-O1 distance is 1.199(4) Å, indicating a C=O bond. The C4-N1 and C9-N1 distances of 1.397(4) and 1.451(5) Å, respectively, indicating C-N single bonds.[208]

Table 2-7: Selected bond lengths [Å] and angles [°] of the cyclopentapyrrolone **2-5** determined by single-crystal X-ray diffraction at 100 K with esd's in parentheses.

	2-5		**2-5**
C1-C2	1.384(5)	C7-C8	1.206(5)
C1-C5	1.469(5)	C9-O1	1.199(4)
C2-C3	1.425(5)	C9-N1	1.451(5)
C2-C9	1.473(5)	∡ Z-A	37.2(1)
C3-C4	1.387(5)	∡ Z-B	41.5(1)
C3-C6	1.440(5)	∡ Z-C	34.2(1)
C4-N1	1.397(4)	∡ Z-D	52.9(1)
C5-C6	1.401(5)	∡ Z-E	57.0(1)
C6-C7	1.425(5)		

For compound **2-5** the "Z"-plane is that of the cyclopentapyrrolone core.

The angles within the cyclopentapyrrolone are all close to the expected 108° for a regular planar, five-membered ring. The aryl moieties are twisted in different directions out of the pyrrolone plane by 37.2(1) – 57.0(1)°.

Neutral, purple organic molecules are relatively rare. However, 2,3,4,5-tetraphenylcyclopenta-2,4-dien-1-one **2-6** (Scheme 2-8) is also purple,[213] but it has a different core structure. The only molecules found with a cyclopentapyrrolone core structure similar to compound **2-5** that were found, is the class of diketopyrrolopyrrole (DPP) **2-7**. DPPs were reported by Farnum, Metha and co-workers in 1974.[214] They are usually substituted with aromatic moieties at the 3- and 6-positions, and are used as high-performance pigments for lacquers and plastics.[215-216] Substituting the hydrogen atom at the nitrogen atom with alkyl- or aryl-substituents increases the solubility of the compounds. In combination with 2-thiophenes at the 3- and 6-positions, these compounds are used in photovoltaic devices[216] or for cell imaging studies.[217]

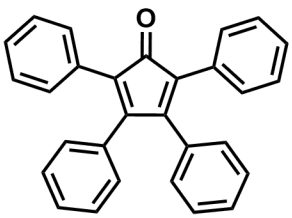

2-6

2,3,4,5-tetraphenylcyclopenta-2,4-dien-1-one

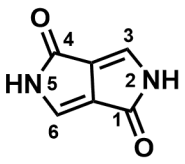

2-7

Diketopyrrolopyrrole (DPP)

Scheme 2-8: Chemical structures of 2,3,4,5-tetraphenylcyclopenta-2,4-dien-1-one **2-6** and diketopyrrolopyrrole **2-7**.

In a DPP with aryl moieties at positions 2, 3, 5 and 6, synthesized by Smith an co-workers (monoclinic space group, $P2_1/n$),[218] the phenyl rings are twisted, in the same direction, out of plane of the planar heterocyclic system by 43.75(8)° and 47.23(7)° (the second half of the molecule is generated by an inversion center). The bond length of the N-C(O) bond was found to be 1.439(3) Å and for the N-C(C) bond 1.413(3) Å, respectively. The C=C bond distance is 1.371(4) Å, the C-C bond is 1.404(5) Å and the C-C(O) bond is 1.449(4) Å.

DPPs only substituted with an aryl moiety in positions 3 and 6, and a N-H unit, show head-to-tail double H-bonds to two neighbors, π-π stacking,[219] and only a small twist of the *para*-substituted aryl rings out of plane of the planar heterocyclic system (3.3(2) – 10.57(8)°).[219-222]

Figure 2-8 shows the course of the reaction of complex **2-2a** with *para*-tolyl isocyanate **2-4** at 80 °C in C_6D_6 over a period of three days, monitored by ^{19}F NMR spectroscopy. The black and the red spectra represent the starting material **2-2a** and the product **2-5**. After 24 hours (green spectrum), most of the starting material was already consumed and **2-5** is the dominant species present. In the purple spectrum (after 48 hours), hardly any **2-2a** is visible while, after 72 hours (blue spectrum) the rhodium starting material was completely consumed. Heating the reaction for more than 72 hours showed no further progress of the reaction according to ^{19}F NMR spectroscopy.

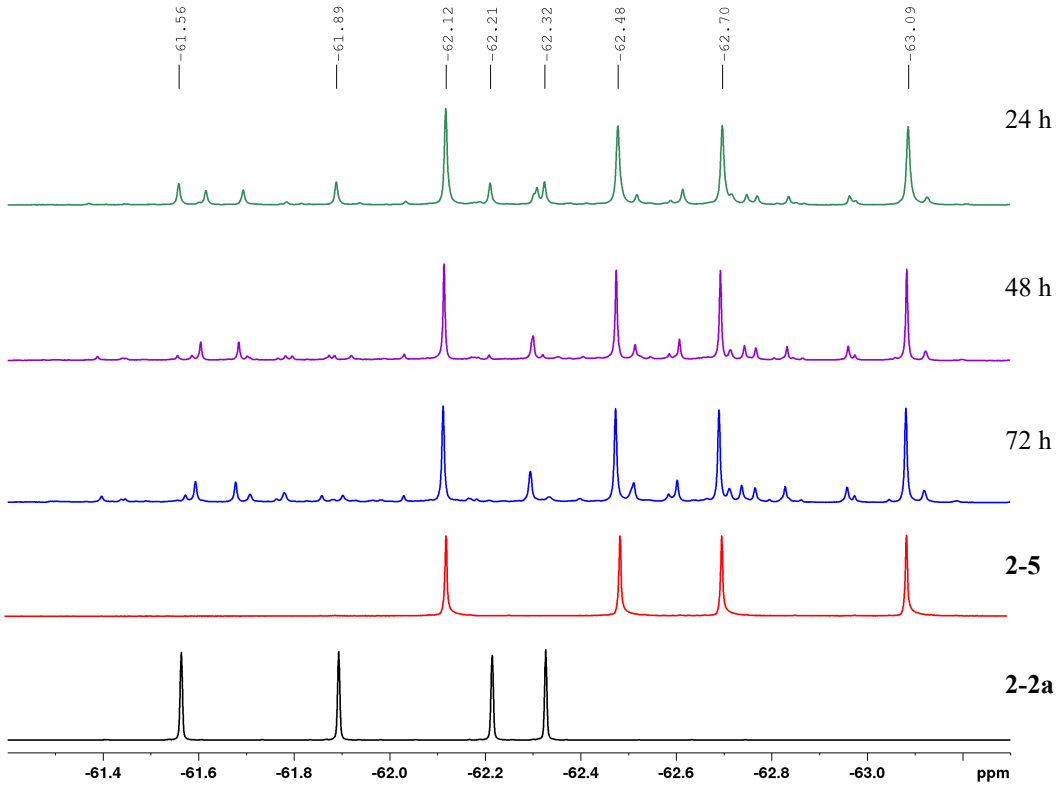

Figure 2-8: ^{19}F NMR spectra (377 MHz, C_6D_6) of the reaction of complex **2-2a** (black) with four equivalents of *para*-tolyl isocyanate **2-4** at 80 °C after 24 hours (green), 48 hours (purple), and 72 hours (blue) as well as isolated cyclopentapyrrolone **2-5** (red).

Monitoring the reaction by $^{31}P\{^1H\}$ NMR spectroscopy (Figure 2-9) shows after 24 hours at 80 °C (black spectrum), starting material **2-2a** and three sets of two doublets of doublets. One major set is visible at 15.9 ppm ($^1J_{Rh\text{-}P}$ = 136 Hz, $^2J_{P\text{-}P}$ = 40 Hz) and 12.5 ppm ($^1J_{Rh\text{-}P}$ = 143 Hz, $^2J_{P\text{-}P}$ = 40 Hz). Two minor sets are observed at 14.7 ppm ($^1J_{Rh\text{-}P}$ = 136 Hz, $^2J_{P\text{-}P}$ = 40 Hz) and 3.7 ppm ($^1J_{Rh\text{-}P}$ = 127 Hz, $^2J_{P\text{-}P}$ = 40 Hz) as well as at 6.0 ppm ($^1J_{Rh\text{-}P}$ = 141 Hz, $^2J_{P\text{-}P}$ = 40 Hz) and 5.2 ppm ($^1J_{Rh\text{-}P}$ = 145 Hz, $^2J_{P\text{-}P}$ = 40 Hz), respectively. The major set shows a sharp doublet of doublets at 15.9 ppm and a broad doublet of doublets at 12.5 ppm. The latter shifts to lower field and broadens over time (red and blue spectra), indicating some dynamic process. The

starting material **2-2a** decreases as do the doublet of doublets at 15.9 and 12.5 ppm, while the set of doublet of doublets at 14.7 and 3.7 ppm grow in intensity. Usually ^{103}Rh-^{31}P coupling constants close to 140 Hz indicate neutral rhodium(I) species with P *trans* to P as in Wilkinson's catalyst[223] and coupling constants of around 40 Hz ($^{2}J_{P\text{-}P}$) indicate *cis*-standing phosphines. The presence of two doublets of doublets indicate two phosphines in different chemical environments.

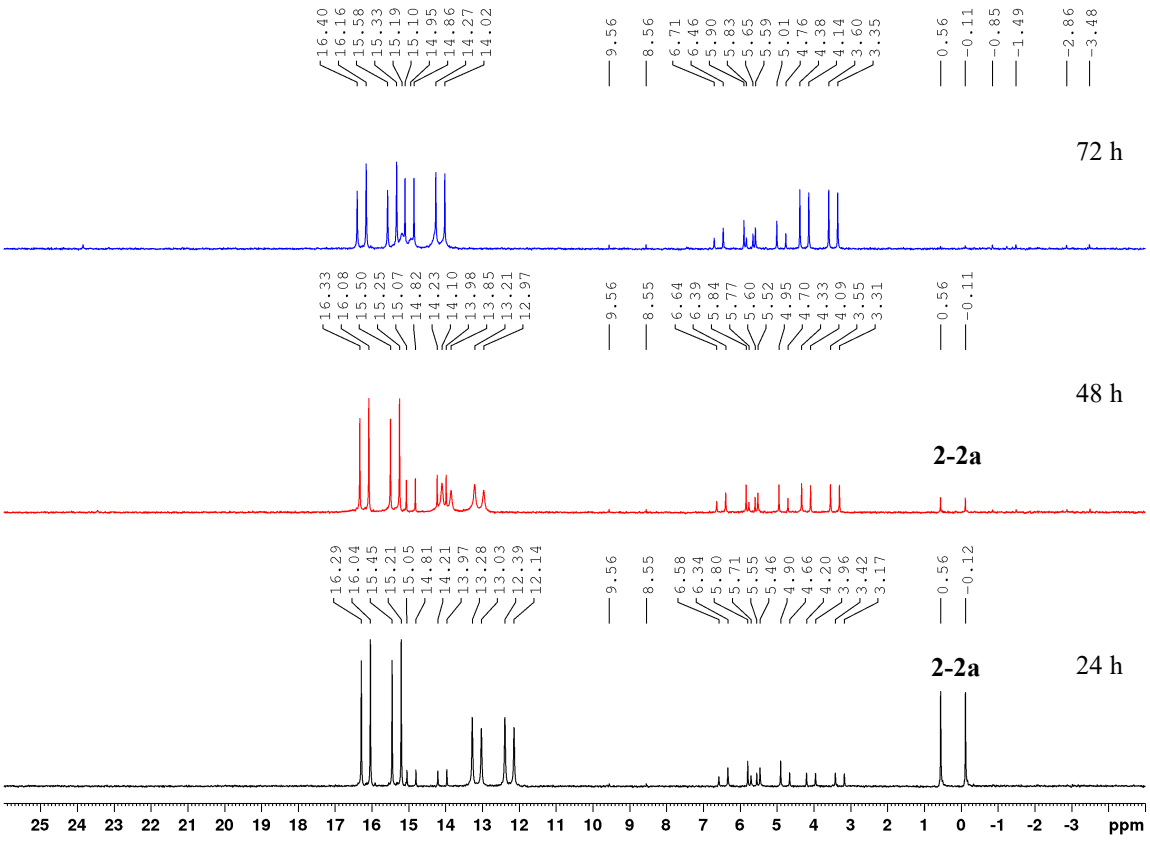

Figure 2-9: $^{31}P\{^{1}H\}$ NMR spectra (162 MHz, C_6D_6) of the reaction of complex **2-2a** with four equivalents of *para*-tolyl isocyanate **2-4** at 80 °C after 24 hours (black), 48 hours (red), and 72 hours (blue).

In contrast to the ^{19}F NMR spectra, there is still progress detectable after three days in the $^{31}P\{^{1}H\}$ NMR spectra (Figure 2-10). New doublets form in the region of 0 – -4 ppm, indicating *trans*-phosphine ligands and a coupling constant of 103 Hz (-1.1 and -1.5 ppm) and 101 Hz (-3.1 ppm), indicate neutral rhodium(III) species (black spectrum). A new set of doublet of doublets appears at 23.9 ppm ($^{1}J_{Rh\text{-}P}$ = 145 Hz, $^{2}J_{P\text{-}P}$ = 40 Hz) and 16.3 ppm ($^{1}J_{Rh\text{-}P}$ = 125 Hz, $^{2}J_{P\text{-}P}$ = 40 Hz), indicative of another rhodium species with *cis*-phosphines (red spectrum). The set of doublet of doublets at 14.7 and 3.7 ppm becomes the main signal in the spectrum (blue spectrum). It was not possible to isolate or crystallize any of the phosphorus-containing compounds from this reaction.

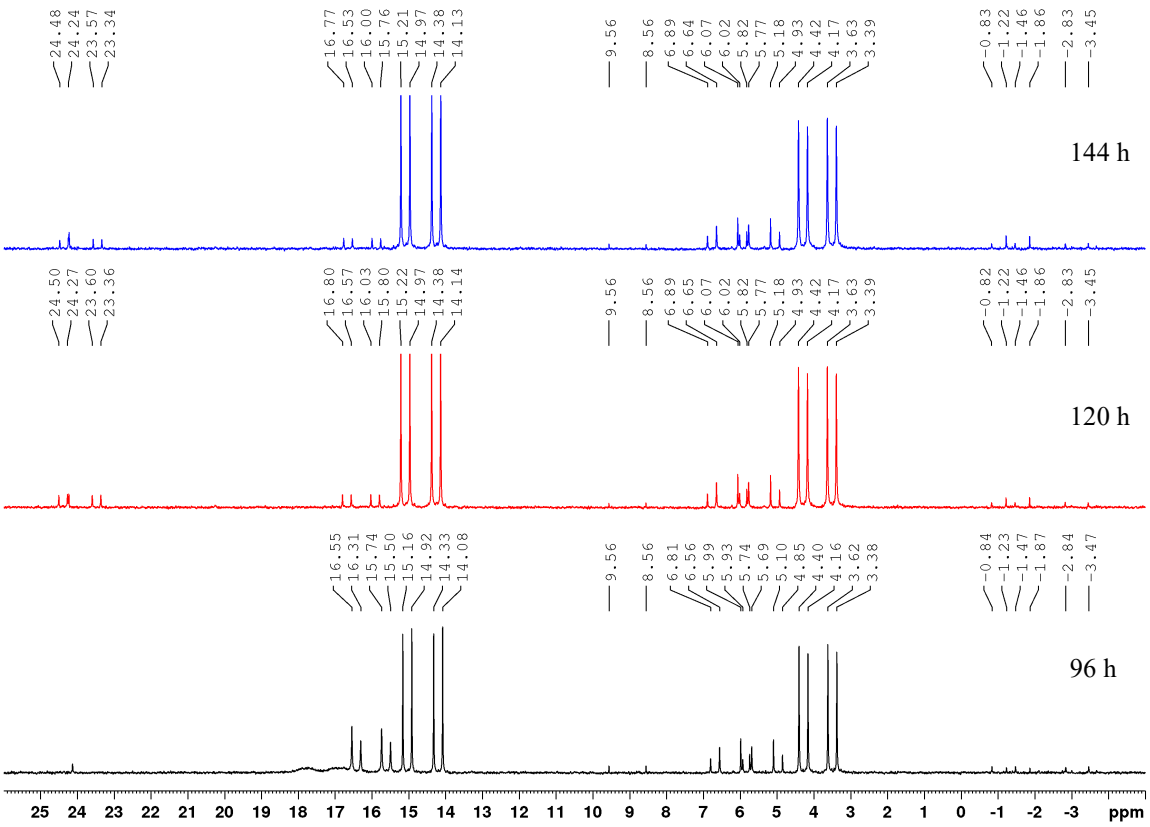

Figure 2-10: $^{31}P\{^{1}H\}$ NMR spectra (162 MHz, C_6D_6) of the reaction of complex **2-2a** with four equivalents of *para*-tolyl isocyanate **2-4** at 80 °C after 96 hours (black), 120 hours (red) and 144 hours (blue).

During the workup of the reaction it was found by Okorn, that 1,3,5-tris(*p*-tolyl)-1,3,5-triazine-2,4,6-trione **2-8** was also formed, and it was possible to isolate single-crystals suitable for X-ray diffraction analysis.[207] It is a cyclotrimerization product of *para*-tolyl isocyanate **2-4** (Figure 2-11).

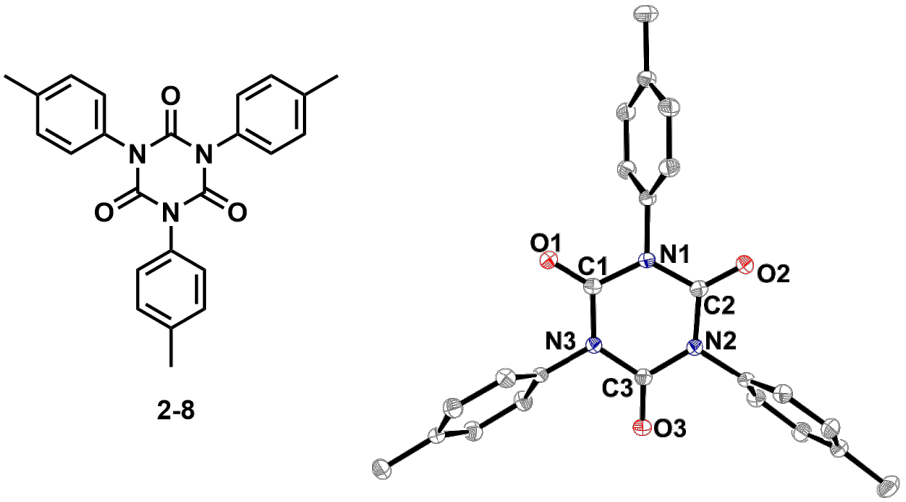

Figure 2-11: Chemical and molecular structure of compound **2-8** in the solid state at 100 K. Hydrogen atoms are omitted for clarity. Atomic displacement ellipsoids are drawn at the 50% probability level. Selected mean bond lengths [Å] and angles [°] with esd's in parentheses: C-O 1.2032(16) – 1.2079(16), C-N 1.3851(16) – 1.3934(17), C-N-C 124.82(11) – 124.94(11), N-C-N 114.86(11) – 115.27(11), O-C-N 122.15(12) – 122.74(11).[207]

The finding led to the conclusion that some participant in the reaction catalyzes this trimerization. Having a closer look at Scheme 2-7, it appears that after removing the organic fulvene part from the rhodium metal center, the starting material [Rh(acac)(PMe_3)$_2$] **1-51** is released. Therefore, **1-51** may be involved in the trimerization of *para*-tolyl isocyanate **2-4**.
The cyclotrimerization of isocyanates forming isocyanurates is atom-economical. These compounds are used as additives in polyurethane foams and coating materials[224-225] and are key components in various applications, e.g. medicines,[226-227] drug delivery,[228-229] and microporous materials.[230-231] A closer investigation of the cyclotrimerization process will be discussed in the following section.

Besides 1,3,5-tris(*p*-tolyl)-1,3,5-triazine-2,4,6-trione **2-8**, it was possible to isolate orange colored single-crystals, of another byproduct, suitable for X-ray diffraction, of a pure organic compound **2-9**, which were obtained by vapor diffusion of *n*-hexane into a dichloromethane solution of **2-9**. The molecular structure is shown in Figure 2-12 and selected bond lengths and angles are listed in Table 2-8. Compound **2-9** crystallizes in the monoclinic space group $P2_1/n$. It is formally a dimer of **2-5**. Three of the former buta-1,3-diyne units are colored in red, blue and green. A closer look at the carbon atom chain, connecting the aryl rings F and G, shows that there is no buta-1,3-diyne motif remaining. The mechanism of this reaction has not yet been investigated.

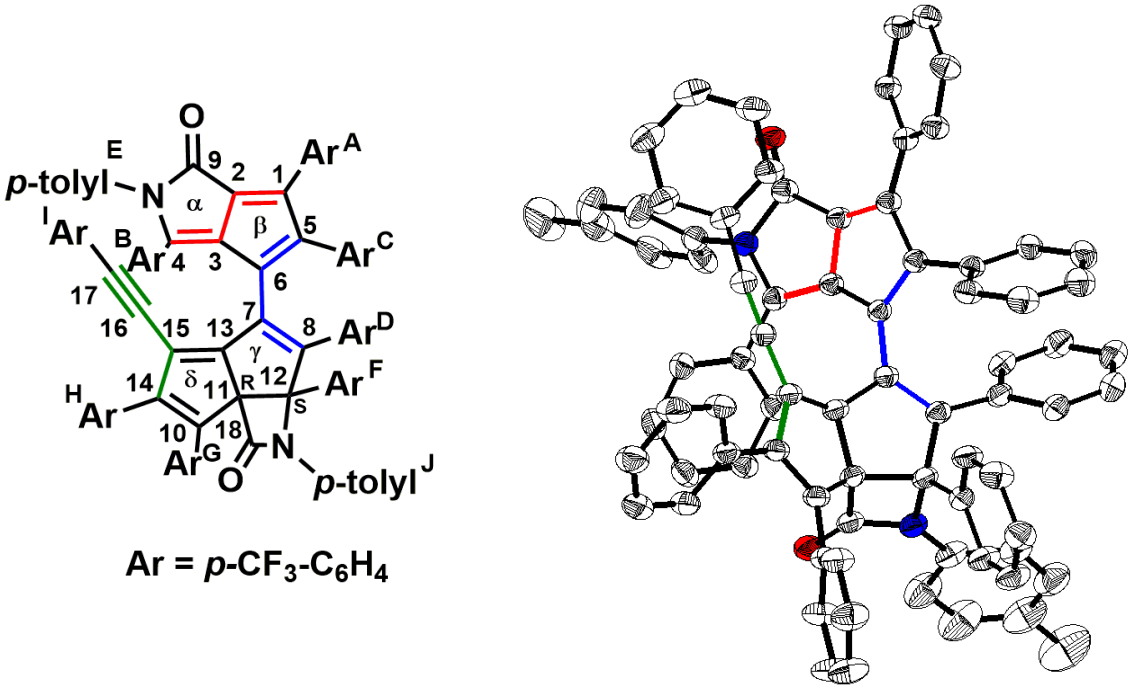

Figure 2-12: Chemical and molecular structure of compound **2-9** in the solid state at 100 K. Hydrogen atoms and CF_3 groups are omitted for clarity. Atomic displacement ellipsoids are drawn at the 50% probability level. The former buta-1,3-diyne units are highlighted in different colors.

The carbon-carbon bond lengths within the cyclopentapyrrolone ring are between 1.384(3) and 1.459(3) Å, the C4-N1 and C9-N1 bond lengths are 1.385(3) and 1.441(3) Å, respectively, and the C9-O1 bond distance is 1.213(3) Å, hence similar to compound **2-5**. In the pentalene moiety, the carbon-carbon bond lengths are between 1.359(3) – 1.575(3) Å. The carbon-carbon distances in the pentalene ring are in the range of 1.359(3) – 1.360(3) Å for the double bonds. For the "single" bonds, the distances are in the range of 1.457(3) – 1.575(3) Å, while the distances between the bonds C7-C13, C10-C11 and C14-C15 are 1.457(3), 1.494(3) and 1.492(3) Å and the distance for the bonds C8-C12 and C11-C12 (part of the four-membered ring) are 1.541(3) and 1.575(3) Å, respectively. The C6-C7 bond length is 1.474(3) Å.

In the four membered ring, the C12-N2 and C18-N2 bond distances are 1.492(3) and 1.366(3) Å, respectively. The C18-O2 and C11-C18 bond distances are 1.204(3) and 1.552 Å, respectively (Table 2-8).

The absolute stereochemistry for C11 is R and for C12 is S in the molecule shown in Figure 2-13, but the other enantiomer is also present in the crystal by symmetry.

Table 2- 8: Selected bond lengths [Å] and angles [°] of compound **2-9** determined by single-crystal X-ray diffraction at 100 K with esd's in parentheses.

	2-9		**2-9**
C1-C2	1.384(3)	C13-C15	1.359(3)
C1-C5	1.458(3)	C14-C15	1.492(3)
C2-C3	1.422(3)	C10-C14	1.359(3)
C2-C9	1.459(3)	C10-C11	1.494(3)
C3-C4	1.379(3)	C15-C16	1.424(3)
C3-C6	1.445(3)	C16-C17	1.196(3)
C4-N1	1.385(3)	C11-C12	1.575(3)
C5-C6	1.392(3)	C7-C13	1.457(3)
C6-C7	1.474(3)	∡ (α+β)-A	32.1(1)
C7-C8	1.360(3)	∡ (α+β)-B	57.2(2)
C9-O1	1.213(3)	∡ (α+β)-*C*	62.5(1)
C9-N1	1.441(3)	∡ (α+β)-E	69.5(1)
C8-C12	1.541(3)	∡ (γ+δ)-D	49.7(2)
C12-N2	1.492(3)	∡ (γ+δ)-F	77.5(1)
N2-C18	1.366(3)	∡ (γ+δ)-G	71.6(1)
C18-O2	1.204(3)	∡ (γ+δ)-H	52.0(2)
C18-C11	1.552(3)	∡ (γ+δ)-I	47.4(1)
C11-C13	1.485(3)		

While the two five-membered rings α and β are nearly planar (9.8(1)°), and similar to those in **2-5** (4.0(1)°), the angle between rings γ and δ is 31.2(1)°. The angle between γ and the four membered ring is 66.4(4)°. The angles within the five-membered rings are all around 108°, as expected for a regular, five-membered ring. The angles within the four membered ring are between 84.50(15) and 94.64(16)°, and sum to 360°. The aryl moieties are twisted out of the cyclopentapyrrolone ring plane by 32.1(1) – 69.5(1)°. The aryl moieties attached to the pentalene ring system are rotated out of the pentalene plane by 47.4(1) – 77.5(1)°. Rings β and γ are rotated by 51.5(1)°.

A ^{19}F NMR spectrum of the orange colored crystals in C_6D_6 shows eight intense signals at -62.3, -62.5, -62.71, -62.74, -62.77, -62.83, -63.0 and -63.1 ppm (Figure 2-13, black spectrum), respectively, which are shifted to high field compared to the signals of the monomer at -62.1, -62.5, -62.7 and -63.1 ppm. These signals are also observed in the reaction progress (Figure 2-13 (red) and Figure 2-8), hence it can be excluded that the compound formed during the workup under ambient conditions.

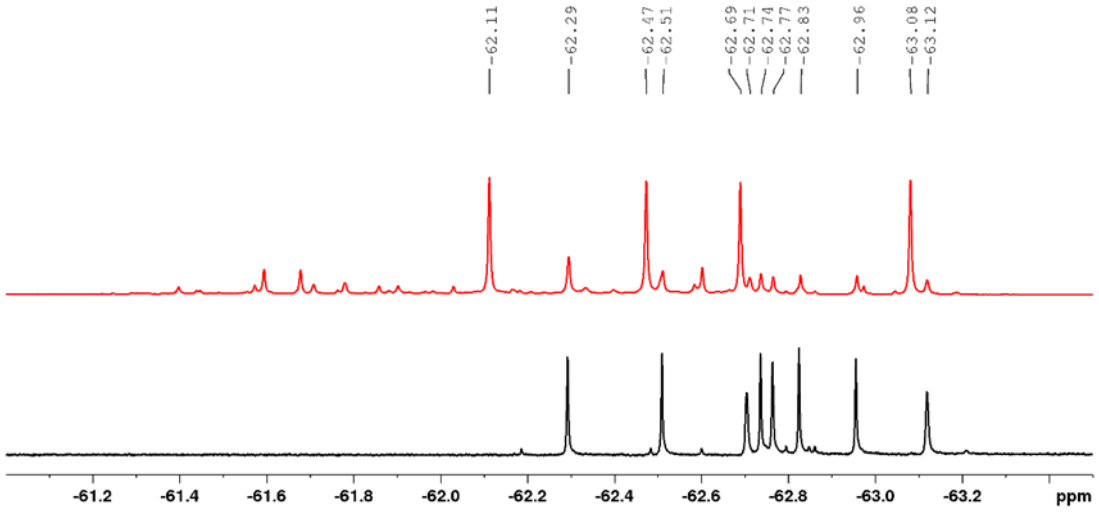

Figure 2-13: ^{19}F NMR spectra (377 MHz, C_6D_6) of the reaction of complex **2-2a** with four equivalents of *para*-tolyl isocyanate **2-4** at 80 °C after 72 hours (red, see also Figure 2-8) and of the isolated single-crystals of **2-9** (black).

HRMS (APCI$^-$) shows an intense signal at *m/z* 1485.2632 and a weaker signal at *m/z* 1618.3160. The latter represents the molecular ion, while the other represents the molecule minus one *para*-tolyl isocyanate unit.

2.3.1.4 Reaction of [Rh(acac)(PMe$_3$)$_2$] with *para*-tolyl isocyanate

In the reaction of [Rh(acac)(PMe$_3$)$_2$] **1-51** with two equivalents of *para*-tolyl isocyanate **2-4** at room temperature for 24 hours, three isomeric compounds are formed, indicated by doublets of doublets in the $^{31}P\{^1H\}$ NMR spectrum, each with two inequivalent, *cis*-phosphine ligands per complex (ca. $^1J_{Rh\text{-}P}$ = 130 Hz, $^2J_{P\text{-}P}$ = 40 Hz) can be detected and some starting material **1-51** remains (Figure 2-14, black spectrum). Rhodium-phosphine coupling constants of ca. 130 Hz are usually observed in neutral rhodium(I) complexes (*vide supra*).

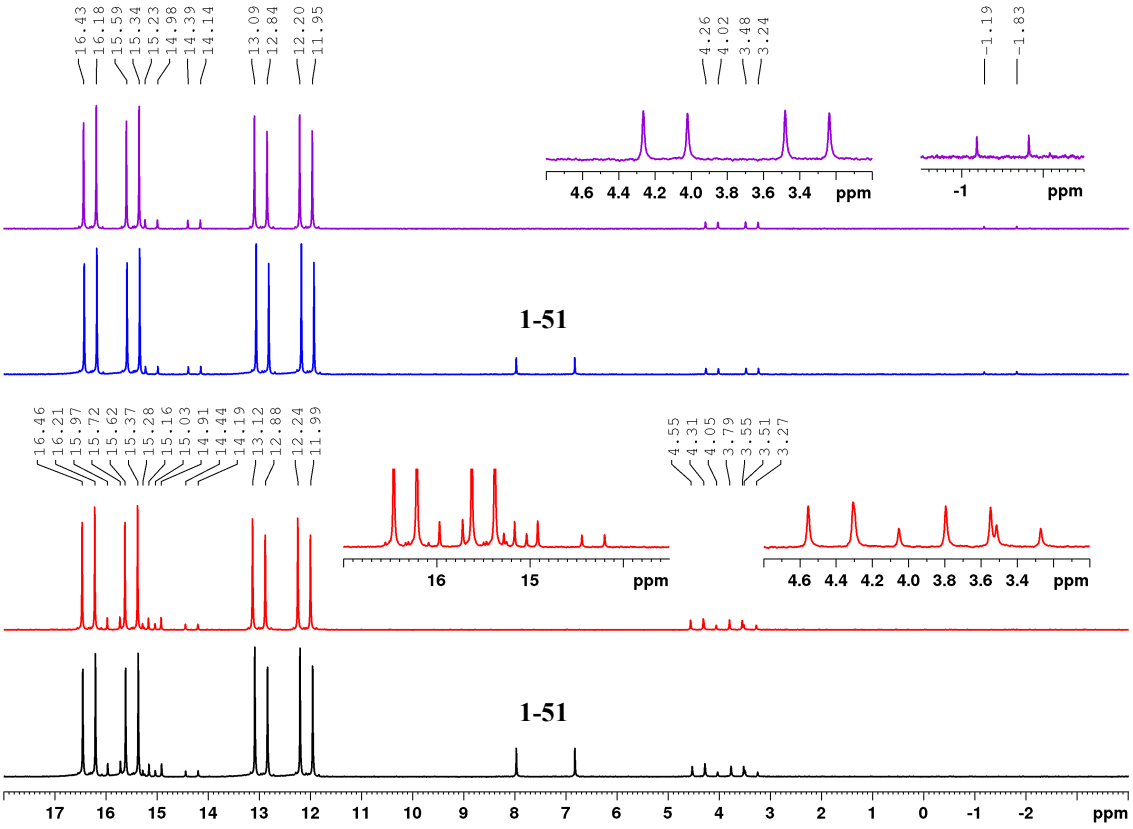

Figure 2-14: $^{31}P\{^1H\}$ NMR spectra (162 MHz, C_6D_6) of the reaction of [Rh(acac)(PMe$_3$)$_2$] **1-51** with two equivalents of *para*-tolyl isocyanate **2-4** at room temperature for 24 hours (black), and with the addition of two more equivalents of **2-4** after an additional 24 hours at room temperature (red). Reaction of **1-51** with two equivalents of **2-4** at 80 °C for 24 hours (blue) and with the addition of two more equivalents of **2-4** after an additional 24 hours at 80 °C(purple).

The major compound appears at 15.9 ($^1J_{Rh\text{-}P}$ = 136 Hz, $^2J_{P\text{-}P}$ = 40 Hz) and 12.5 ppm ($^1J_{Rh\text{-}P}$ = 143 Hz, $^2J_{P\text{-}P}$ = 40 Hz), and two minor isomers at 15.4 ($^1J_{Rh\text{-}P}$ = 131 Hz, $^2J_{P\text{-}P}$ = 40 Hz) and 4.0 ppm ($^1J_{Rh\text{-}P}$ = 123 Hz, $^2J_{P\text{-}P}$ = 40 Hz) as well as 14.7 ($^1J_{Rh\text{-}P}$ = 136 Hz, $^2J_{P\text{-}P}$ = 40 Hz) and 3.7 ppm ($^1J_{Rh\text{-}P}$ = 127 Hz, $^2J_{P\text{-}P}$ = 40 Hz) (Figure 2-12, black spectrum), respectively. Adding two additional equivalents of isocyanate to the reaction mixture results in complete consumption of [Rh(acac)(PMe$_3$)$_2$] **1-51** and no further reaction according to $^{31}P\{^1H\}$ NMR

spectroscopy (red spectrum). HRMS reveals signals for 1,3,5-tris(*p*-tolyl)-1,3,5-triazine-2,4,6-trione **2-8**, [Rh(acac)(PMe_3)$_2$(2-4)$_2$], and [Rh(acac)(PMe_3)$_2$] **1-51**.

Immediately heating of the reaction to 80 °C of [Rh(acac)(PMe_3)$_2$] **1-51** with two equivalents of *para*-tolyl isocyanate **2-4**, for 24 hours results in the formation of only two isomeric compounds. The first appears at 15.9 ($^1J_{Rh-P}$ = 136 Hz, $^2J_{P-P}$ = 40 Hz) and 12.5 ppm ($^1J_{Rh-P}$ = 143 Hz, $^2J_{P-P}$ = 40 Hz) and the second at 14.7 ($^1J_{Rh-P}$ = 136 Hz, $^2J_{P-P}$ = 40 Hz) and 3.7 ppm ($^1J_{Rh-P}$ = 127 Hz, $^2J_{P-P}$ = 40 Hz). Besides these two sets of doublets of doublets, a doublet for [Rh(acac)(PMe_3)$_2$] **1-51** and a doublet at -1.5 ppm ($^1J_{Rh-P}$ = 103 Hz), indicating a rhodium(III) species with trans phosphine ligands, are visible (blue spectrum). Adding two additional equivalents of *para*-tolyl isocyanate to this reaction mixture and heating to 80 °C for another day led to consumption of [Rh(acac)(PMe_3)$_2$] **1-51** (purple spectrum). HRMS revealed that the compounds responsible for the spectrum are 1,3,5-tris(*p*-tolyl)-1,3,5-triazine-2,4,6-trione **2-8**, [Rh(acac)(PMe_3)$_2$(2-4)$_2$] and [Rh(acac)(PMe_3)$_2$] **1-51**.
Heating the room temperature reaction with four equivalents of *para*-tolyl isocyanate **2-4** (red spectrum) to 80 °C for 24 hours, results in vanishing of the doublets of doublets at 15.4 and 4.0 ppm, while no doublet at -1.5 ppm is formed.
At room temperature and at 80 °C, the reactions of [Rh(acac)(PMe_3)$_2$] **1-51** with two equivalents of *para*-tolyl isocyanate **2-4** show both remaining **1-51** after 24 hours, which is consumed after addition of two more equivalents of **2-4**. Furthermore, the two sets of doublets of doublets at 15.9 and 12.5 ppm, and 14.7 and 3.7 ppm are present at 80 °C, and are also visible in the room temperature reaction. Additionally, the doublets of doublets at 15.4 and 4.0 ppm, which are only visible at room temperature, diminish after heating at 80 °C. The doublet at -1.5 ppm is only formed while heating the reaction right from the beginning at 80 °C.

The corresponding ^{1}H NMR spectra (Figure 2-15) of the ^{31}P{^{1}H} NMR spectra of Figure 2-14 exhibit resonances in the aliphatic region of 2.30 – 0.80 ppm, corresponding to the signals for the acac-CH_3, the *p*-tolyl-CH_3 of the isocyanate and *cis*-PMe_3 groups.
The presence of three (for the reaction at room temperature) and two (for the reaction 80 °C) different rhodium-acac species is indicated by signals at 5.19, 4.67 and 4.66 ppm, and 5.19 and 4.67 ppm, respectively, for the acac-CH group (Figure 2-15). A resonance for [Rh(acac)(PMe_3)$_2$] **1-51** can be located at 5.41 ppm for the reactions with two equivalents of *para*-tolyl isocyanate **2-4**.

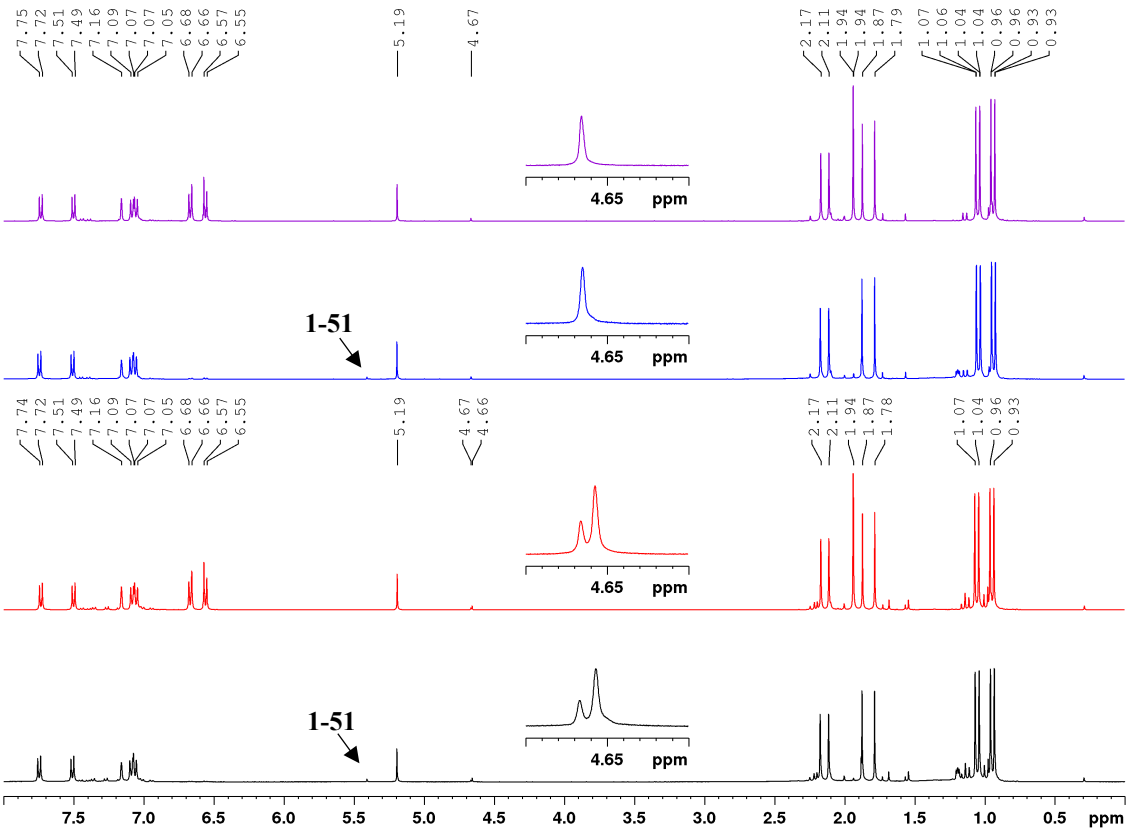

Figure 2-15: ^{1}H NMR spectrum (400 MHz, C_6D_6) of the reaction of [Rh(acac)(PMe_3)$_2$] **1-51** with two equivalents of *para*-tolyl isocyanate **2-4** at room temperature for 24 hours (black), and after the addition of two more equivalents of **2-4** after an additional 24 hours at room temperature (red). Reaction of **1-51** with two equivalents of **2-4** at 80 °C for 24 hours (blue) ,and after the addition of two more equivalents of **2-4** after an additional 24 hours at 80 °C (purple).

In the aromatic region from 8.00 – 6.30 ppm (Figure 2-16), three multiplets at 7.74, 7.50 and 7.07 ppm stand out. The multiplet at 6.62 ppm is assigned to the aromatic-CH groups of *para*-tolyl isocyanate **2-4**, which is visible in all four spectra, even for the reaction with only two equivalents of isocyanate, although in small amounts. Close to the solvent signal (C_6D_6, 7.16 ppm), in all four spectra, a small shoulder is visible at ca 7.17 ppm, which, together with another multiplet at 6.95 ppm, results from 1,3,5-tris(*p*-tolyl)-1,3,5-triazine-2,4,6-trione **2 8**.[232] Additionally, various smaller multiplets are visible, but due to their overlap and low intensities, no further assignment is possible.

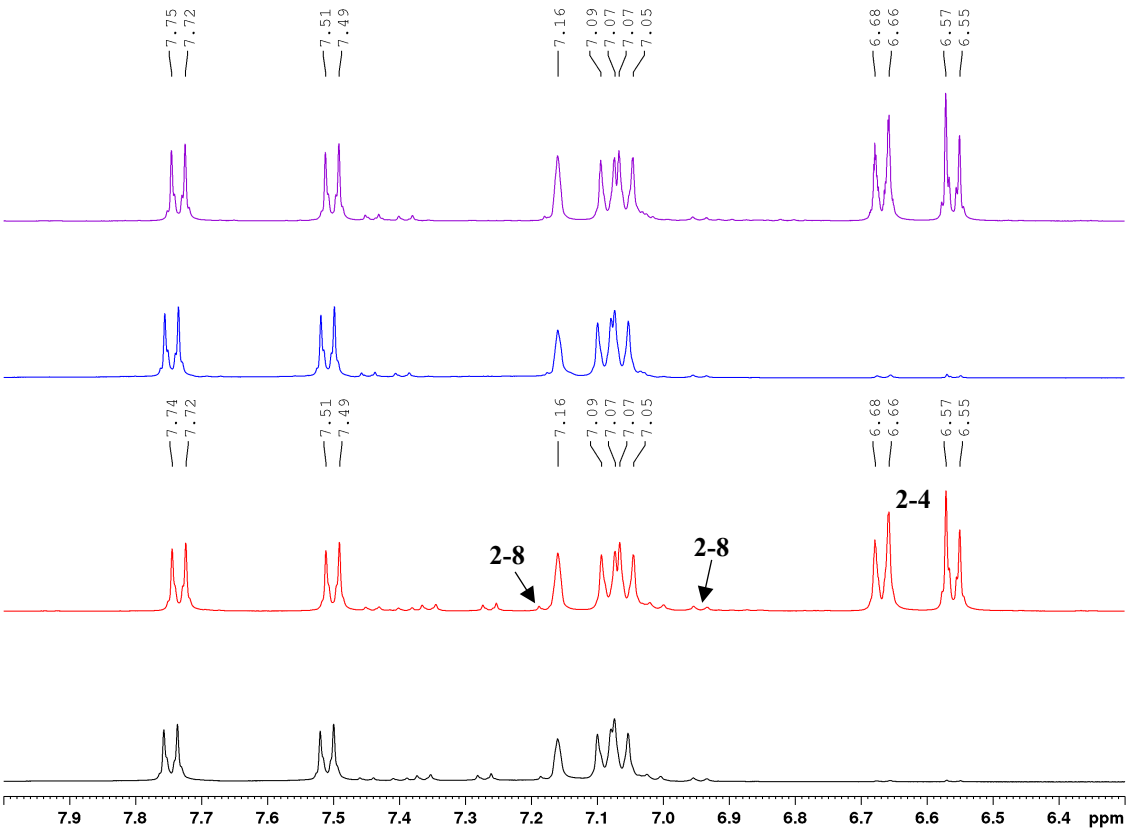

Figure 2-16: Portion (8.00 – 6.30 ppm) of the ^{1}H NMR spectrum (400 MHz, C_6D_6) of the reaction of [Rh(acac)(PMe_3)$_2$] **1-51** with two equivalents of *para*-tolyl isocyanate **2-4** at room temperature for 24 hours (black), and after the addition of two more equivalents of **2-4** after an additional 24 hours at room temperature(red). Reaction of **1-51** with two equivalents of **2-4** at 80 °C for 24 hours (blue), and after the addition of two more equivalents of **2-4** after an additional 24 hours at 80 °C(purple).

In the reaction of [Rh(acac)(PMe_3)$_2$] **1-51** with two equivalents of *para*-tolyl isocyanate **2-4**, resonances at 0.94, 1.05, 1.78, 1.87, 2.11 and 2.17 ppm dominate in the aliphatic and at 5.19, 7.07, 7.50 and 7.74 ppm in the acac and aromatic region. In the reaction with four equivalents of **2-4**, additional intense signals at 1.94 and 6.62 ppm for **2-4** are clearly visible. Signals for 1,3,5-tris(*p*-tolyl)-1,3,5-triazine-2,4,6-trione **2-8** are visible in all spectra.

HRMS data indicates the incorporation of two equivalents of isocyanate into the rhodium starting material [Rh(acac)(PMe_3)$_2$] **1-51**, ^{31}P{^{1}H} NMR spectroscopy indicates the formation of rhodium complexes bearing *cis*-PMe_3 ligands and in the ^{1}H NMR spectra resonances for the acac-CH group and *cis*-PMe_3 groups are displayed. From these findings, two possible complexes, **2-10a** and **2-10b**, bearing two isocyanates, *cis*-phosphines and an acac ligand are depicted in Scheme 2-9.

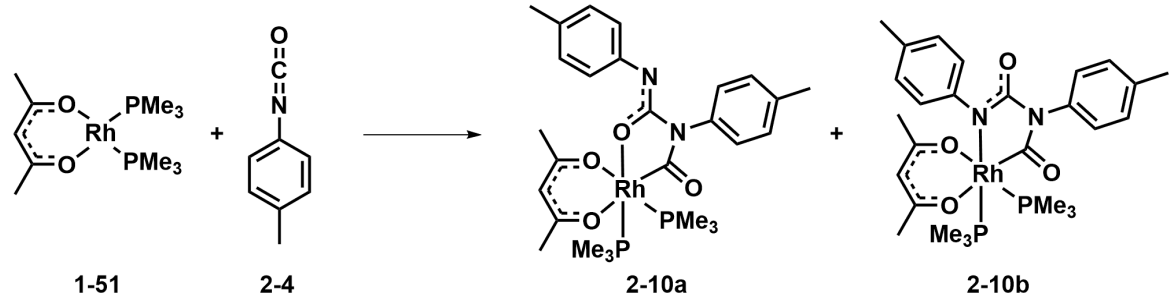

1-51 2-4 2-10a 2-10b

Scheme 2-9: Reaction of [Rh(acac)(PMe_3)$_2$] **1-51** with *para*-tolyl isocyanate **2-4** forming two possible *cis*-[Rh(acac)(PMe_3)$_2$(2-4)$_2$] complexes **2-10a** and **2-10b**.

Due to remaining [Rh(acac)(PMe_3)$_2$] **1-51** when using two equivalents of *para*-tolyl isocyanate **2-4** at room temperature, and the formation of 1,3,5-tris(*p*-tolyl)-1,3,5-triazine-2,4,6-trione **2-8**, it is clear that trimerization is caused by **1-51**. Nevertheless, the amount of trimerization product formed is small, as the signals in the ^{1}H NMR spectrum are quite small compared to other signals, and no precipitation of the trimer, due to low solubility in C_6D_6, was observed. The set of doublet of doublets at 15.4 and 4.0 ppm is only present at room temperature, and this signal set might represent a complex in which three equivalents of isocyanate are incorporated into a rhodium complex, while at elevated temperature this complex liberates the trimerization product and is therefore not detectable in the NMR spectra.

It was possible to isolate a complex from the reaction mixture, after multiple washing and recrystallization steps, as a colorless, crystalline solid in 36% yield. The complex was characterized by multinuclear NMR spectroscopy, HRMS, elemental analysis and by single-crystal X-ray diffraction analysis.

Inspection of the ^{1}H NMR spectroscopic data in C_6D_6 revealed two doublets of doublets at 0.93 and 1.03 ppm for two inequivalent PMe_3 ligands. Two singlets for the acac-CH_3 groups at 1.79 and 1.87 ppm, respectively, and two singlets for the CH_3 groups of the *para*-tolyl moieties are displayed at 2.11 and 2.17 ppm, respectively. A resonance for the acac-CH group gives rise to a singlet at 5.20 ppm. Eight hydrogen atoms for the aryl moieties, represented by three multiplets at 7.08, 7.52 and 7.76 ppm, are displayed in the 7.08 – 7.78 ppm range. In the ^{13}C{^{1}H} NMR spectrum, the acac-CH group resonates at 98.9 ppm. The ^{31}P{^{1}H} NMR resonances for this compound are observed at 15.8 and 12.3 ppm as doublets of doublets, with the ^{103}Rh-^{31}P coupling constants of 136 and 143 Hz, respectively, and the ^{31}P-^{31}P coupling constant is 40 Hz.

As the resonances of this isolated complex are slightly shifted compared to the *in-situ* spectra, and in order to confirm, that the isolated species is present in the reaction mixtures, [Rh(acac)(PMe_3)$_2$] **1-51** and *para*-tolyl isocyanate **2-4** were added to the isolated complex in

C_6D_6 at room temperature, which resulted in the observation of three sets of doublets of doublets. Furthermore, although the resonances in the *in-situ* spectra are slightly shifted, the coupling constants are always identical.

Single-crystals suitable for X-ray diffraction were obtained by vapor diffusion of *n*-hexane into a THF solution of the compound, which crystallizes in the triclinic space group $P\bar{1}$. The molecular structure of the complex is shown in Figure 2-17 and selected bond lengths and angles are listed in Table 2-9. The isolated species corresponds to the suggested complex **2-10a** (Scheme 2-9).

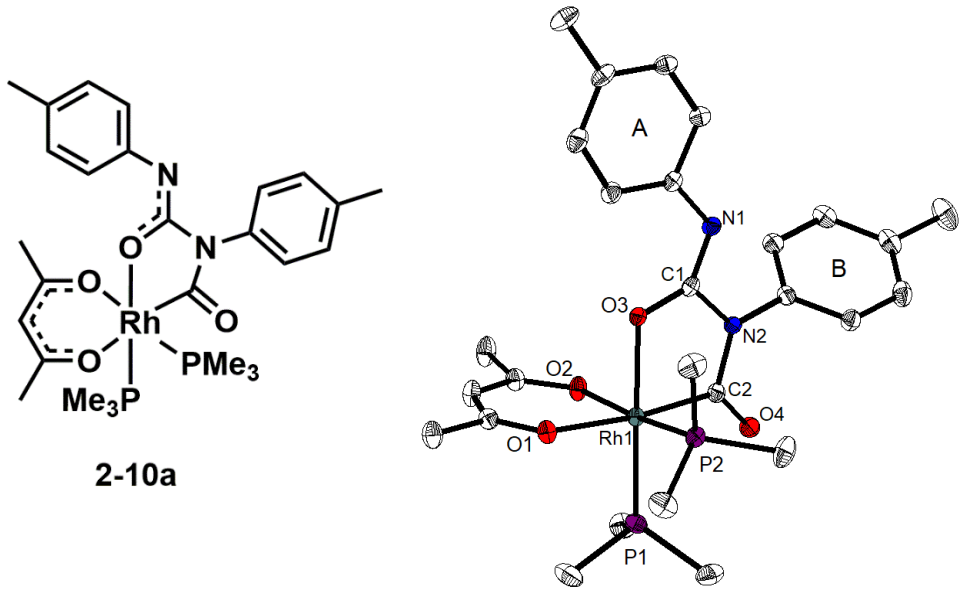

Figure 2-17: Chemical and molecular structure of complex **2-10a** in the solid state at 100 K. Hydrogen atoms and solvent molecules are omitted for clarity. Atomic displacement ellipsoids are drawn at the 50% probability level.

The acac Rh-O bond lengths are Rh-O1 2.1516(14) and Rh-O2 2.0760(14) Å. Compared to other rhodacycles in this chapter, for which the acac Rh-O bond length is ca. 2.13 Å, the Rh-O2 distance in **2-10a** is significantly shorter due to the lower *trans*-influence of the phosphine ligand compared to C2. The Rh-O1 bond is in accordance with the distances reported previously. The Rh1-O3 distance is 2.0639(14) Å. Both, Rh1-O2 and Rh1-O3, have a phosphine ligand *trans* to oxygen. The Rh1-P1 and Rh1-P2 bond distances are 2.2588(10) and 2.2499(9) Å, respectively, hence shorter than the Rh-P bonds in the previously discussed rhodacycles, since the phosphine ligands have oxygen atoms in *trans*-position (less *trans*-influence of O *trans* to P compared to P *trans* to P). The Rh1-C2 bond distance is 1.9680(18) Å and therefore similar to the aforementioned rhodacycles and other rhodacyclopentadienes.[59, 72]. The different angles around the rhodium metal center in **2-10a**, are similar to other rhodacyclopentadienes.[59, 72] Of noteworthy mention are the *cis*-disposed trimethylphosphine ligands with a P-Rh-P angle of 96.69(3)°.

Table 2-9: Selected bond lengths [Å] and angles [°] of complex **2-10a** determined by single-crystal X-ray diffraction at 100 K with esd's in parentheses.

	2-10a		**2-10a**
Rh1-O1	2.1516(14)	O1-Rh1-O2	90.19(6)
Rh1-O2	2.0760(14)	P1-Rh1-O3	172.81(3)
Rh1-P1	2.2588(10)	O1-Rh1-P1	93.27(5)
Rh1-P2	2.2499(9)	O2-Rh1-O3	85.58(5)
Rh1-O3	2.0639(14)	O3-Rh1-C2	83.22(6)
Rh1-C2	1.9680(18)	P1-Rh1-P2	96.69(3)
C1-O3	1.290(2)	P2-Rh1-C2	91.63(6)
C1-N1	1.296(2)	O3-Rh1-P2	88.70(4)
C1-N2	1.430(2)		
C2-N2	1.408(2)		
C2-O4	1.223(2)		

Complex **2-10a**, as depicted in Figure 2-17, is a rhodium(III)-complex. The ^{103}Rh-^{31}P coupling constants of the isolated species of 136 and 143 Hz, respectively, are usually observed in neutral rhodium(I) compounds with P *trans* P, as in Wilkinson's catalyst.[233] Therefore, the solid state structure of complex **2-10a** cannot unambiguously be assigned to the species present in solution.

Similar bond lengths as for **2-10a** were found for the rhodium(III) complex **2-11** (Figure 2-18).[234] Unfortunately, no NMR data are available.

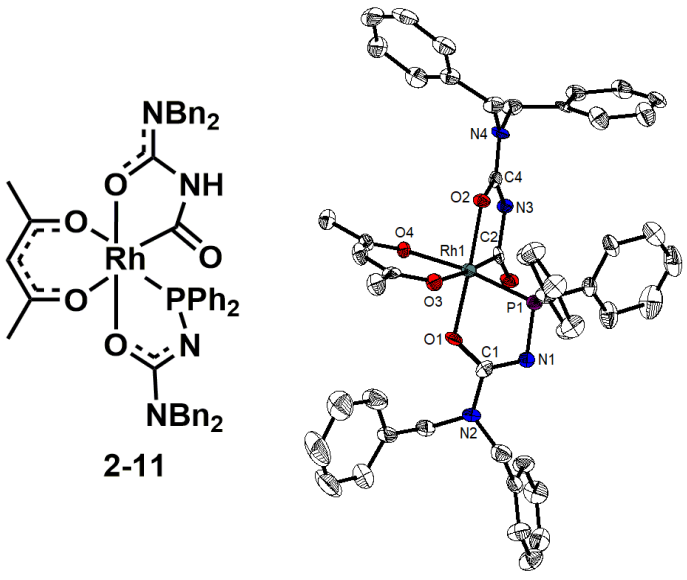

Figure 2-18: Chemical and molecular structure of complex **2-11** (CCDC 1058712) in the solid state at 110 K. Hydrogen atoms, solvent molecules and a second molecule in the unit cell are omitted for clarity. Atomic displacement ellipsoids are drawn at the 50% probability level. Selected bond lengths [Å] with esd's in parentheses: Rh1-O2: 2.045(4), Rh1-C2: 1.953(5), Rh1-P1: 2.212(4), Rh1-O1: 2.027(4), Rh1-O3: 2.135(4), Rh1-O4: 2.112(4) and O1-C1: 1.293(7).

Other similar compounds in which structures with a benzoyl isocyanate bound to rhodium were reported previously. Ishii and co-workers synthesized complex **2-12** in a two-step reaction.

Using benzoyl isocyanate and Wilkinson's catalyst [$RhCl(PPh_3)_3$] yields first the dimer [$RhCl(PPh_3)_2(PhCONCO)]_2$, which was further reacted with sodium tetraphenylborate and bipyridine resulting in [$Rh(bpy)(PPh_3)${-C(O)NC(Ph)O-}]BPh_4 (Scheme 2-10).[235] Werner and co-workers reported the reaction of [$Rh(Cp)(CO)PMe_3$] with $PhCON_3$ yielding [$Rh(Cp)PMe_3${-C(O)NC(Ph)O-}] **2-13**.[236]

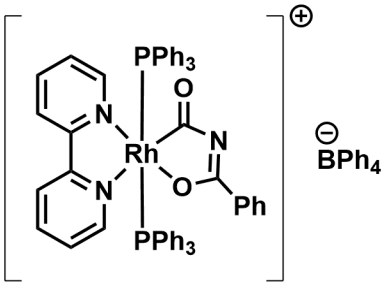

2-12

[Rh(bpy)(PPh$_3$)$_2${-C(O)NC(Ph)O-}]BPh$_4$

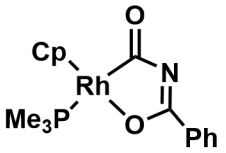

2-13

[Rh(C$_5$H$_5$)PMe$_3${-C(O)NC(Ph)O-}]

Scheme 2-10: Chemical structures of previously synthesized rhodium-benzoyl isocyanate complex **2-12** by Ishii and co-workers and of complex **2-13** by Werner and co-workers.

Metallacyclic complexes containing isocyanate units are reported to be key intermediates in the cyclotrimerization of isocyanates. This trimerization can be promoted by main-group,[237-240] rare-earth[241-245] and transition metals[235, 246-252] as well as in metal-free processes.[253-257]

The reactivity of isocyanates with group 10 metals was particularly well studied in the early 1990's,[134] in order to synthesize different types of heterocycles. This was extensively examined using Ni(0) catalysts by Hoberg,[258-267] who reported various five-membered nickelacycles bearing dimeric organic isocyanate structures (Scheme 2-11).

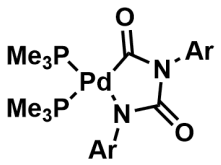

Ar = C$_6$H$_5$, *p*-Me-C$_6$H$_4$, *p*-Cl-C$_6$H$_4$ **2-14** **2-15**

[Pd(PMe$_3$){-C(O)N(Ar)C(O)N(Ar)-}]

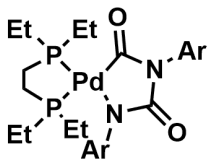

Ar = *p*-Cl-C$_6$H$_4$ **2-16**

[Pd(depe){-C(O)N(Ar)C(O)N(Ar)-}]

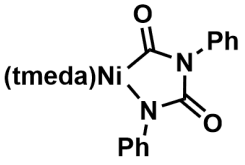

2-17

[Ni(tmeda){-C(O)N(Ph)C(O)N(Ph)-}]

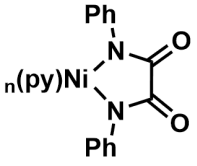

2-18

[Ni(py)$_n${-N(Ph)C(O)C(O)N(Ph)-}]

Scheme 2-11: Chemical structures of a selection of [Pd(isocyanate)$_2$] and [Ni(isocyanate)$_2$] complexes: [$Pd(PMe_3)_2${-C(O)N(Ar)C(O)N(Ar)-}] **2-14**, **2-15**,[268] [Pd(depe){-C(O)N(Ar)C(O)N(Ar)-}] **2-16**,[268] [Ni(tmeda){-C(O)N(Ph)C(O)N(Ph)-}] **2-17**[258] and [$Ni(py)_n${-N(Ph)C(O)C(O)N(Ph)-}] **2-18**.[259]

The rhodium-mediated cyclotrimerization of isocyanates has not previously been reported. Of particular interest is that the isocyanate dimer is bound to the rhodium metal center by one carbon and one oxygen atom (see Figure 2-17). So far, there have been no reports on isolated and structurally characterized complexes of this type. Usually, coordination occurs *via* the nitrogen, rather than the oxygen atom (*vide supra*).

However, in an extended experimental and theoretical study, Paul, Floch and co-workers[269] predicted an oxygen bound isomer, analogous to **2-10a**, to be the catalytically active intermediate in isocyanate cyclotrimerization catalyzed by a palladium complex. The palladium analogue of the nitrogen bound isomer **2-10b** was isolated, but it was shown not to be active in the trimerization for thermodynamic reasons. One has to keep in mind, however, that in both cases (O-bound and N-bound), Paul, Floch *et al.* were dealing with four coordinate d^8-systems, while compounds **2-10a** and **2-10b** are d^6-octahedral complexes.

It was already mentioned that small amounts of *para*-tolyl isocyanate **2-4** were still present in the mixture even when two equivalents were used, besides [Rh(acac)(PMe_3)$_2$] **1-51** (*vide supra*). It seems that the catalytic reaction depends on the amount of isocyanate left in solution. This was already observed by Hofmann in 1885[270] and also later by, for example, Paul, Floch and co-workers.[269]

Further studies showed that precipitation of the trimerization product 1,3,5-tris(*p*-tolyl)-1,3,5-triazine-2,4,6-trione **2-8** was observed after 24 hours when 15 equivalents of *para*-tolyl isocyanate **2-4** were added to a solution of [Rh(acac)(PMe_3)$_2$] **1-51** in C_6D_6 at either room temperature or 80 °C. When ten equivalents of *para*-tolyl isocyanate were used, it took ca. 36 hours at room temperature to form a considerable amount of precipitate.

Whereas, when four equivalents of *para*-tolyl isocyanate **2-4** were added to complex **2-10a** in C_6D_6 at 80 °C for twelve days, and then allowed to cool to room temperature, a precipitate formed within 36 hours.

Compound **1-51** and **2-10a** both appear to catalyze the trimerization of *para*-tolyl isocyanate. However, publications from Hofmann in 1870 and subsequent years,[270-273] noted that triethylphosphine can catalyze the dimerization of phenyl isocyanate. However, when 10 mol% of trimethylphosphine was added to *para*-tolyl isocyanate **2-4** in C_6D_6, precipitation was observed after a couple of minutes at room temperature. Inspection of the ^{1}H NMR spectrum revealed the formation of trimerization product **2-8** and a second species, presumably the dimer 1,3-bis(*p*-tolyl)-1,3-diazetidine-2,4-dione **2-19** (Scheme 2-12). At 80 °C, the same reaction yields additional products besides dimer and trimer, according to ^{1}H NMR spectroscopy.

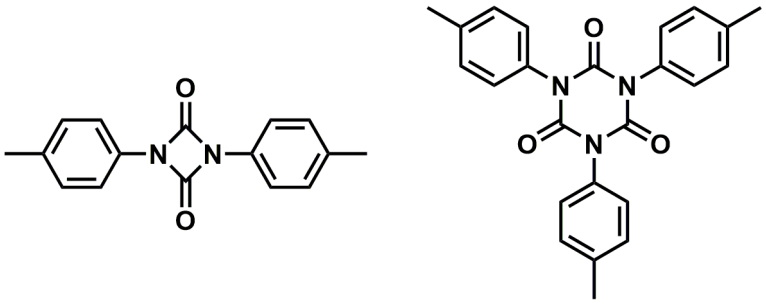

2-19 **2-8**

Scheme 2-12: Chemical structures of compounds 1,3-bis(*p*-tolyl)-1,3-diazetidine-2,4-dione **2-19** and 1,3,5-tris(*p*-tolyl)-1,3,5-triazine-2,4,6-trione **2-8**.

Finally, it needed to be clarified whether the different species (according to $^{31}P\{^{1}H\}$ NMR spectroscopy) from the reaction of [Rh(acac)(PMe_3)$_2$] **1-51** with *para*-tolyl isocyanate **2-4** are also formed in the reaction of complex **2-2a** with **2-4**, and whether the formation of trimerized *para*-tolyl isocyanate can be explained with these findings. Therefore, the *in-situ* $^{31}P\{^{1}H\}$ NMR spectra of the reaction of complex **2-2a** with *para*-tolyl isocyanate **2-4** at 80 °C after 24 hours (blue spectrum) and after seven days (purple spectrum), and [Rh(acac)(PMe_3)$_2$] **1-51** with **2-4** at 80 °C after 24 hours (black spectrum) and after seven days (red spectrum) are compared, and similarities are clearly recognizable (Figure 2-19).

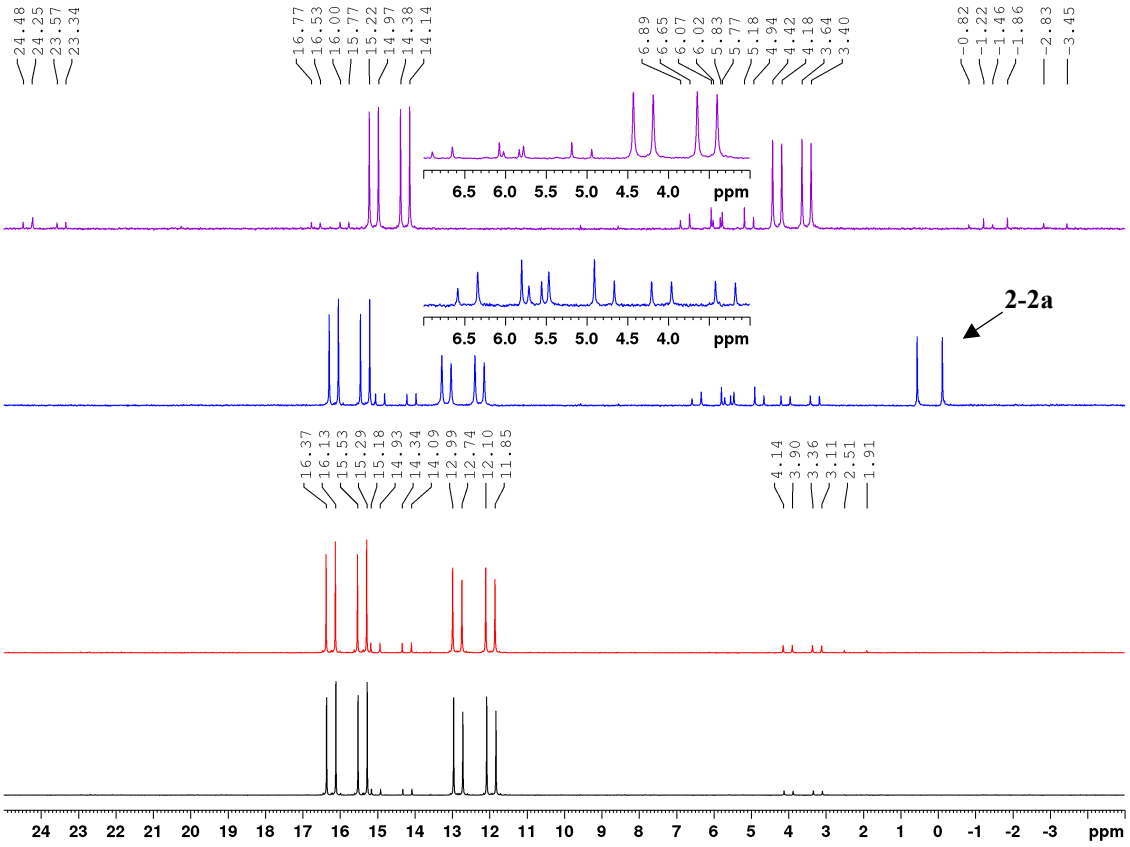

Figure 2-19: $^{31}P\{^{1}H\}$ NMR spectra (377 MHz, C_6D_6) of the reaction of [Rh(acac)(PMe_3)$_2$] **1-51** with four equivalents of *para*-tolyl isocyanate **2-4** at 80 °C for 24 hours (black), at 80 °C after 7 days (red). Complex **2-2a** with four equivalents of **2-4** at 80 °C after 24 hours (blue) and at 80 °C after 7 days (purple).

According to $^{31}P\{^{1}H\}$ NMR spectroscopy, the two doublets of doublets in the black spectrum at 15.9 ($^{1}J_{Rh\text{-}P}$ = 136 Hz, $^{2}J_{P\text{-}P}$ = 40 Hz) and 12.5 ppm ($^{1}J_{Rh\text{-}P}$ = 143 Hz, $^{2}J_{P\text{-}P}$ = 40 Hz), representing, presumably **2-10a**, as well as at 14.7 ($^{1}J_{Rh\text{-}P}$ = 136 Hz, $^{2}J_{P\text{-}P}$ = 40 Hz) and 3.7 ppm ($^{1}J_{Rh\text{-}P}$ = 127 Hz, $^{2}J_{P\text{-}P}$ = 40 Hz) are also visible in the blue spectrum, in the *in-situ* reaction of complex **2-2a** with *para*-tolyl isocyanate **2-4** at 80 °C after 24 hours. The minor doublet of doublets in the black and blue spectra at 14.7 and 3.7 ppm is the main species in the purple spectrum. The two sets of doublets of doublets in the purple spectrum at 23.9 ($^{1}J_{Rh\text{-}P}$ = 145 Hz, $^{2}J_{P\text{-}P}$ = 40 Hz) and 16.3 ppm ($^{1}J_{Rh\text{-}P}$ = 125 Hz, $^{2}J_{P\text{-}P}$ = 40 Hz), and 6.0 ($^{1}J_{Rh\text{-}P}$ = 141 Hz, $^{2}J_{P\text{-}P}$ = 40 Hz) and 5.2 ppm ($^{1}J_{Rh\text{-}P}$ = 145 Hz, $^{2}J_{P\text{-}P}$ = 40 Hz) only appear in the reaction of complex **2-2a** with *para*-tolyl isocyanate **2-4** at 80 °C, as do the two doublets at -1.1 ($^{1}J_{Rh\text{-}P}$ = 104 Hz) and -3.1 ppm ($^{1}J_{Rh\text{-}P}$ = 104 Hz) (see also Figure 2-10). A third doublet in the purple spectrum at -1.5 ppm ($^{1}J_{Rh\text{-}P}$ = 104 Hz) is also visible in the red spectrum, but very low in intensity (see also Figure 2-14).

Therefore some reactant in the reaction of complex **2-2a** with *para*-tolyl isocyanate **2-4** is able to push the minor doublet of doublets at 14.7 and 3.7 ppm in the blue spectrum to become the main doublet of doublets in the purple spectrum. However, this does not occur in the reaction of [Rh(acac)(PMe_3)$_2$] **1-51** with *para*-tolyl isocyanate **2-4**, in which complex **2-10a** is the major complex (black and red spectra).

During the reaction of complex **2-2a** with *para*-tolyl isocyanate **2-4**, [Rh(acac)(PMe_3)$_2$] **1-51** is released, which reacts with **2-4** and forms different [Rh(acac)(PMe_3)$_2$(isocyanate)$_n$] complexes, and finally, the isocyanate trimer. It cannot be completely excluded that trimethylphosphine, which is liberated at some point in the reaction, catalyzes the trimerization. The formation of different [Rh(acac)(PMe_3)$_2$(isocyanate)$_n$] complexes and the trimerization product explain the need for the four-fold excess of isocyanate during the reaction. However, it is difficult to simulate the exact process for the reaction of **1-51** with **2-4**, as **1-51** is liberated stepwise (over three days) in the reaction of complex **2-2a** with **2-4**.

2.3.1.5 Reactions of [Rh(acac)(Me$_2$Im)$_2$] with *para*-substituted 1,4-diphenylbuta-1,3-diynes

Previous work dealt with the reaction of [Rh(acac)(^{n}Pr$_2$Im)$_2$] **2-20** with SMe- and CO_2Me-substituted α,ω-bis(arylbutadiynyl)alkanes **1-47b**,**d**. After five days at room temperature, the rhodium(I) starting material was consumed and a mixture of *cis* and *trans*-rhodacyclopentadienes was formed (Scheme 2-13). For the latter it was possible to isolate single-crystals suitable for X-ray diffraction analysis and to prove the connectivity. However, separation of the *cis*- and *trans*-rhodacyclopentadiene isomers was not possible. DFT calculations showed a very small preference for the *cis*-isomer (0.6 kcal/mol).[72]

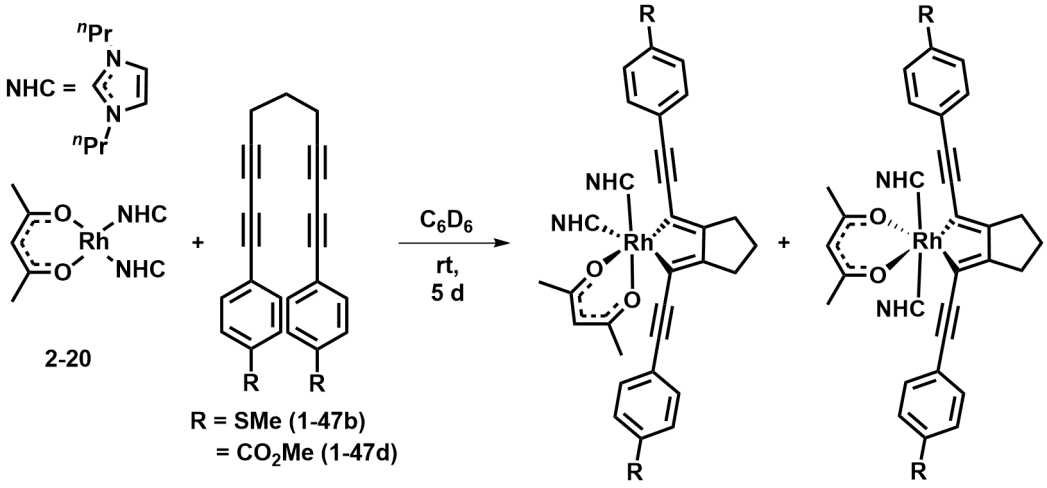

Scheme 2-13: Reaction of [Rh(acac)(^{n}Pr$_2$Im)$_2$] **2-20** with CO_2Me- and SMe-substituted α,ω-bis(arylbutadiynyl)alkanes **1-47b**,**d** forming *cis*- and *trans*-NHC-substituted rhodacyclopentadienes.

Due to the observation of different isomers, while using para-substituted α,ω-bis(arylbutadiynyl)alkanes, the reaction of [Rh(acac)(Me$_2$Im)$_2$] **2-21** with *para*-substituted 1,4-diphenylbuta-1,3-diynes **2-1a**,**b** was conducted and further investigated.

Complex [Rh(acac)(Me$_2$Im)$_2$] **2-21** was synthesized in an analogous fashion to [Rh(acac)(^{n}Pr$_2$Im)$_2$] **2-20** and [Rh(acac)(phosphine)$_2$] complexes.[59, 71] In the reaction of [Rh(acac)(COE)$_2$] with two equivalents of 1,3-dimethylimidazol-2-ylidene (Me$_2$Im) in THF at room temperature, an orange solid was obtained in 96% yield (Scheme 2-14). Complex **2-21** was characterized by multinuclear NMR spectroscopy, HRMS, elemental analysis, and single-crystal X-ray diffraction analysis.

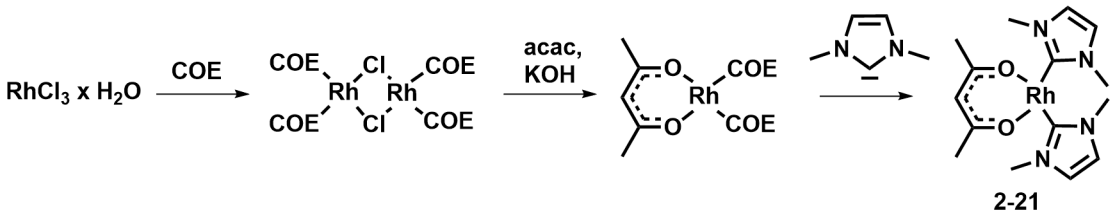

2-21

Scheme 2-14: Synthesis of rhodium(I) complex [Rh(acac)(Me_2Im)$_2$] **2-21**.

Inspection of the ^{1}H NMR spectroscopic data of **2-21** in C_6D_6 revealed a symmetrical complex as indicated by only one signal with an integral of six for the acac-CH_3 hydrogen atoms at 1.91 ppm and a singlet for the four methyl groups of the NHC ligand at 3.52 ppm with an integral of 12. The single acac-CH group resonates at 5.54 ppm with an integral of one. The hydrogen atoms of the unsaturated NHC-backbone give rise to a resonance at 6.09 ppm with an integral of four. The advantage of [Rh(acac)(Me_2Im)$_2$] **2-21** over the previously synthesized [Rh(acac)($^n Pr_2Im$)$_2$] **2-20** is the simplified ^{1}H NMR spectrum, as only one signal is expected for the methyl groups, while in [Rh(acac)($^n Pr_2Im$)$_2$] **2-20** the methyl groups give rise to a triplet and the two CH_2 groups to multiplets. *In-situ* characterization of reaction mixtures will be easier to analyze due to less signals in the aliphatic region.

In the $^{13}C\{^1H\}$ NMR spectrum of [Rh(acac)(Me_2Im)$_2$] **2-21**, the NHC carbene carbon atom gives rise to a doublet at 192.3 ppm with a rhodium-carbon coupling constant of 61 Hz in the same region as that for [Rh(acac)($^n Pr_2Im$)$_2$] **2-20** synthesized by Sieck.[72] The signal for the acac-CH carbon atom is located at 99.7 ppm.

Elemental analysis and HRMS data are also consistent with the formulation of [Rh(acac)(Me_2Im)$_2$].

Single-crystals suitable for X-ray diffraction were obtained by vapor diffusion of *n*-hexane into a THF solution of **2-21**. The complex crystallizes in the triclinic space group $P\bar{1}$, and the molecular structure is shown in Figure 2-20 and selected bond lengths and angles are listed in Table 2-10.

The rhodium atom has a square planar coordination environment with *cis*-disposed NHC ligands and a chelating acac ligand. The rhodium to carbene-carbon atom bond lengths for Rh1-C1 and Rh1-C10 are 1.950(2) and 1.9459(18) Å, respectively. The rhodium oxygen bond lengths are 2.0754(17) Å for Rh1-O1 and for Rh1-O2 2.0856(14) Å. Both the Rh-C as well as Rh-O bond length are identical with those of the previously synthesized complex [Rh(acac)($^n Pr_2Im$)$_2$] **2-20** (see Table 2-10).[72]

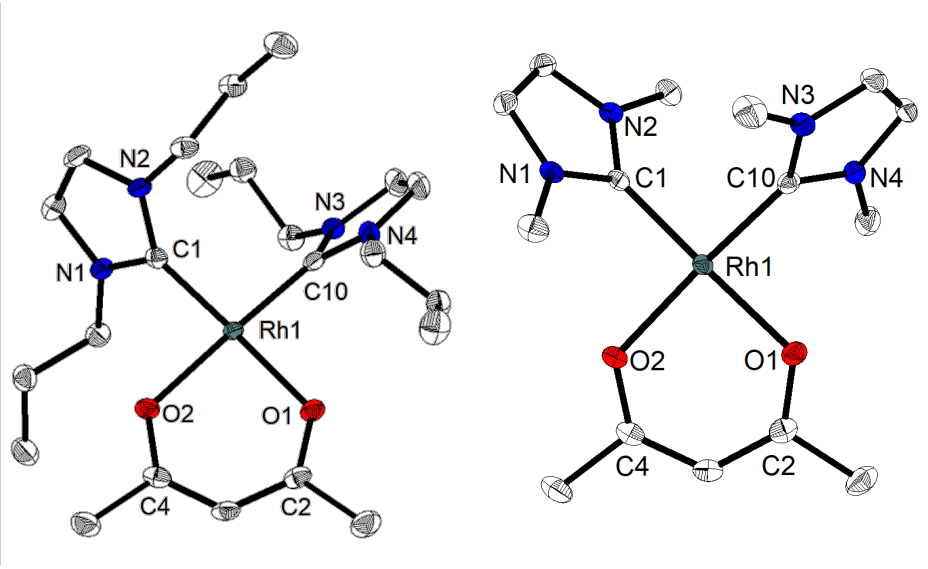

Figure 2-20: Molecular structures of complexes [Rh(acac)(^{n}Pr$_2$Im)$_2$] **2-20**[72] (left) and [Rh(acac)(Me$_2$Im)$_2$] **2-21** (right) in the solid state at 100 K. Hydrogen atoms and other molecules in the unit cell are omitted for clarity. Atomic displacement ellipsoids are drawn at the 50% probability level.

The rhodium to carbene-carbon atom bond distances are shorter than the distance in other rhodium(I)-NHC complexes, e.g. [Rh(PPh$_3$)$_2$(IMes)Cl] with 2.0527(14) Å,[274] in which the NHC is *trans* to a triphenylphosphine ligand. The larger Rh-C distance in [Rh(PPh$_3$)$_2$(IMes)Cl] originates from the stronger *trans*-influence of the phosphine, compared to the acac ligand in [Rh(acac)(^{n}Pr$_2$Im)$_2$] **2-20** and [Rh(acac)(Me$_2$Im)$_2$] **2-21**.

Table 2-10: Selected bond lengths [Å] and angles [°] of complexes [Rh(acac)(^{n}Pr$_2$Im)$_2$] **2-20**[72] and [Rh(acac)(Me$_2$Im)$_2$] **2-21** determined by single-crystal X-ray diffraction at 100 K with esd's in parentheses.

	2-20	**2-21**
Rh1-O1	2.0821(14)	2.0754(17)
Rh1-O2	2.0848(14)	2.0856(14)
Rh1-C1	1.951(2)	1.950(2)
Rh1-C10	1.948(2)	1.9459(18)
C1-N1	1.369(3)	1.370(2)
C1-N2	1.373(2)	1.369(2)
C10-N3	1.370(2)	1.371(2)
C10-N4	1.376(3)	1.371(3)
O1-C2	1.269(2)	1.268(2)
O2-C4	1.269(2)	1.271(2)
O1-Rh1-O2	89.61(5)	89.73(6)
C1-Rh1-C10	91.65(8)	91.23(8)
O1-Rh1-C1	177.83(7)	178.48(7)
O2-Rh1-C10	176.93(7)	177.35(7)

The reaction of [Rh(acac)(Me_2Im)$_2$] **2-21** with *para*-CF_3-substituted 1,4-diphenylbuta-1,3-diyne **2-1a** in a 1:2 ratio at room temperature in C_6D_6 was investigated. Initially, a clear red solution is formed, which turns dark red over the time.

In the ^{1}H NMR spectrum of the reaction after 15 minutes (Figure 2-21, bottom), two intense singlets, each with an integral of three, for the acac-CH_3 groups are observed at 1.68 and 2.03 ppm, indicating, similar to complexes **2-2a** and **2-3a**, an unsymmetrical environment *trans* to the acac ligand. The acac-CH group gives rise to a signal at 5.18 ppm with an integral of one. For the two NHC ligands, signals for the methyl groups are observed at 2.83, 3.05, 3.83 and 4.31 ppm, each with an integral of three, and the CH groups of the unsaturated NHC backbone resonate at 5.87 (2H), 6.05 (1H) and 6.30 (1H) ppm. In the aromatic region, there are three multiplets at 7.26 – 7.34 with an integral of four, and 7.45 – 7.47 and 8.09 – 8.12 ppm with an integral of two for each multiplet. The multiplet at 7.02 – 7.10 ppm results from unreacted *para*-substituted 1,4-diphenylbuta-1,3-diyne **2-1a**.

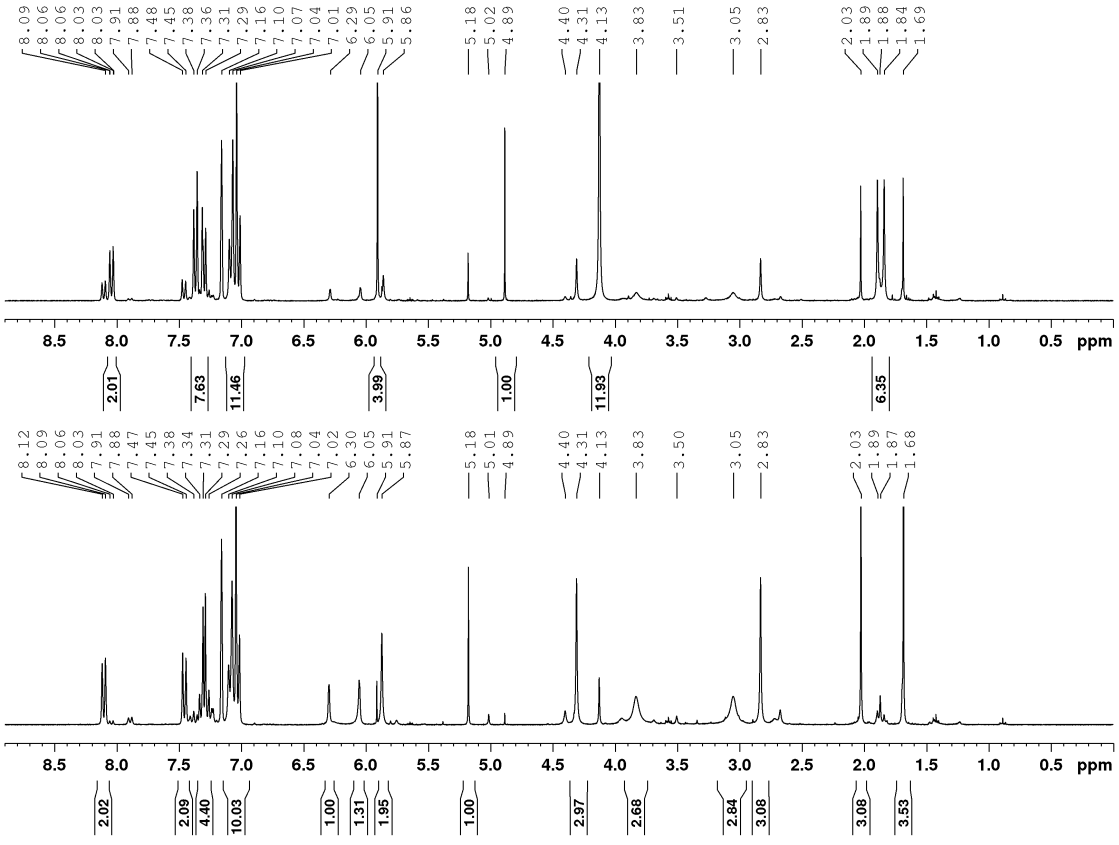

Figure 2-21: *In-situ* ^{1}H NMR spectra (400 MHz, C_6D_6) of the reaction of [Rh(acac)(Me_2Im)$_2$] **2-21** with *para*-substituted 1,4-diphenylbuta-1,3-diyne **2-1a** in a 1:2 ratio at room temperature after 15 minutes (bottom) and 20 hours (top).

At room temperature after 20 hours (Figure 2-21, top), a major species appears which is different from the species in the bottom spectrum. There are two singlets, each with an integral of three, for the acac-CH_3 groups at 1.84 and 1.89 ppm and a singlet for the acac-CH group at

4.89 ppm with an integral of one. The four methyl groups of the NHC ligand give rise to a singlet at 4.13 ppm with an integral of 12, and the four unsaturated NHC-backbone CH groups give rise to a singlet at 5.91 ppm with an integral of four. A multiplet at 7.29 – 7.38 with an integral of eight (overlapping with other signals) and another at 8.09 – 8.12 ppm with an integral of two are found in the aromatic region. Signals for *para*-substituted 1,4-diphenylbuta-1,3-diyne **2-1a** are still present. Further assignment of other signals is not possible due to their low intensity and overlapping resonances.

From the ^{1}H NMR spectra in Figure 2-21, it is clear that, after 15 minutes, a *cis*-NHC complex is the dominant species in solution, as the signals for the methyl and CH groups of the NHC ligand split into four and three sets, respectively. However, after 20 hours, a *trans*-complex is the dominant species in the reaction mixture, as only one signal for the methyl and one signal for the CH groups are visible, meaning that the *cis*-species isomerized to a *trans*-species. Two possible *cis*-complexes and a *trans*-complex are shown in Scheme 2-15.

The *trans*-complex is already visible in the reaction after 15 minutes, and the major *cis*-species is still observable after 20 hours. A signal at 5.01 ppm is visible in both NMR spectra, the intensity of which is higher in the bottom NMR spectrum than in the top spectrum. This signal might be due to an acac-CH group of a second *cis*-isomer. Monitoring the reaction for another 24 hours or heating the reaction to 60 or 80 °C results in no visible change in the ^{1}H NMR spectrum compared to the spectrum after 20 hours. The ratio of *cis*- to *trans*-product is ca. 0.37:1.

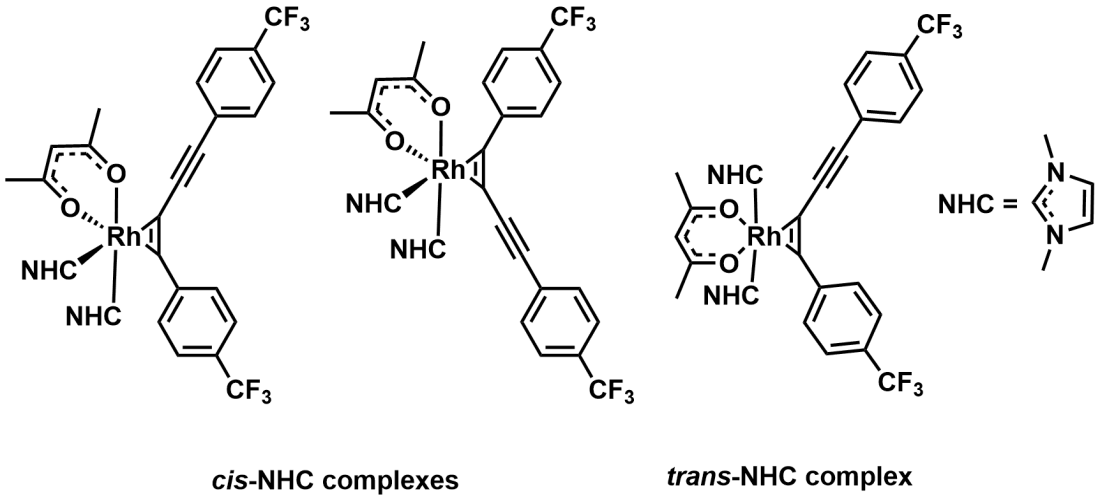

Scheme 2-15: Chemical structures of two possible *cis*-NHC complexes and a *trans*-NHC complex.

The *in-situ* ^{19}F NMR spectra after 15 minutes (Figure 2-22, bottom) and after 20 hours (Figure 2-20, top) both display singlets at -61.61, -61.63, -61.71, -62.07, -62.21, -62.23 and -62.85 ppm. In the spectrum acquired after 15 minutes, the signal at -62.85 ppm is broad compared to the

one observed after 20 hours, indicating a dynamic process at the beginning of the reaction. Additional signals of very low intensity are visible at -60.85 and -62.31 ppm in the spectrum after 20 hours.

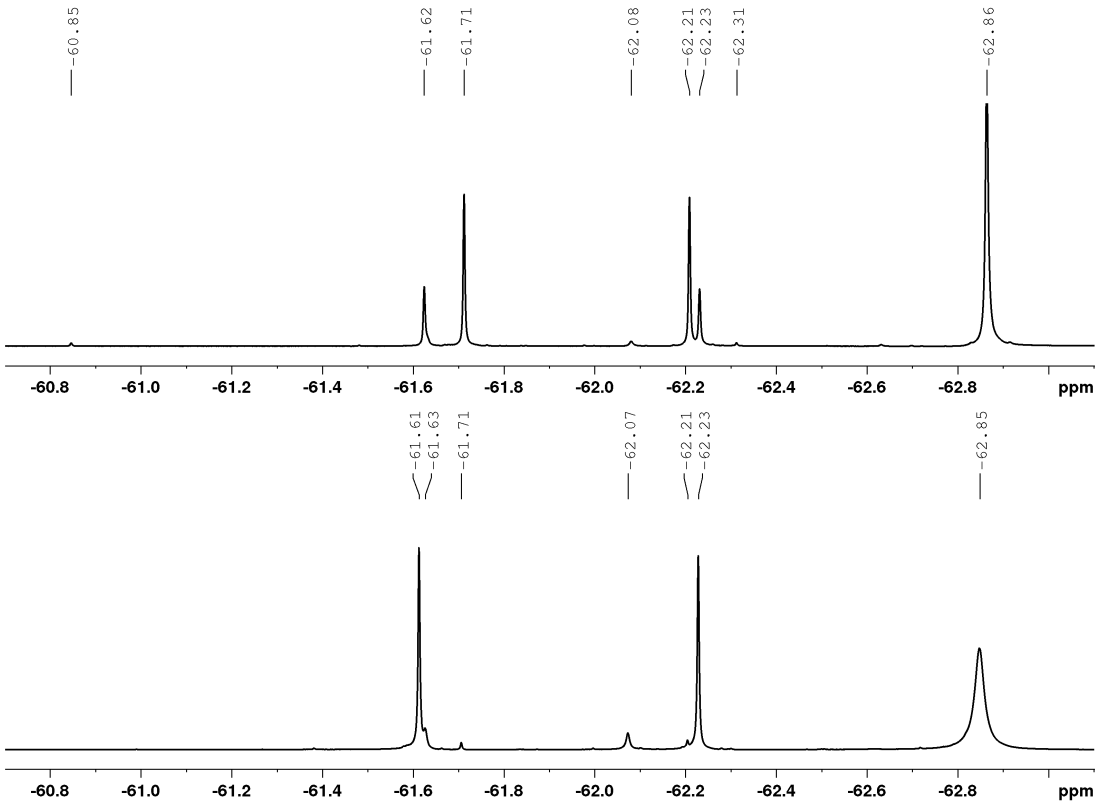

Figure 2-22: *In-situ* ^{19}F NMR spectra (377 MHz, C_6D_6) of the reaction of [Rh(acac)(Me_2Im)$_2$] **2-21** with *para*-substituted 1,4-diphenylbuta-1,3-diyne **2-1a** in a 1:2 ratio at room temperature after 15 minutes (bottom) and 20 hours (top).

With the findings from the ^1H NMR spectra (Figure 2-21), the ^{19}F NMR spectra (Figure 2-22) can be explained. At the beginning of the reaction (Figure 2-22, bottom), two singlets at -61.61 and -62.23 ppm result from the dominant species which is the major *cis*-complex. Two signals at -61.63 and -62.07 ppm can be attributed to the minor *cis*-complex, and signals at -61.71 and -62.21 ppm result from the *trans*-complex. The broad signal at -62.85 ppm is due to residual *para*-substituted 1,4-diphenylbuta-1,3-diyne **2-1a**. After 20 hours (Figure 2-22, top), the *trans*-complex is the major metal-containing complex in solution. The major *cis*-compound is still visible, while the signals for the minor *cis*-compound are very weak. The signals at -60.85 and -62.31 ppm could result from a species with the formula [Rh(acac)(NHC)$_2$(2-1a)$_2$].

HRMS of the reaction mixture after 20 hours indicates that both [Rh(acac)(NHC)$_2$(2-1a)] and [Rh(acac)(NHC)$_2$(2-1a)$_2$] are present. However, in the LIFDI HRMS, both signals are very weak and the signal for [Rh(acac)(Me_2Im)$_2$] **2-21** is the strongest signal, although the rhodium(I) starting material appears to be completely consumed, according to ^1H NMR

spectroscopy. Some dissociation of diyne from the complex in the mass spectrometer is possible.

Attempted purification by washing the crude residue with *n*-hexane after evaporating the solvent *in vacuo* failed. According to ^{1}H NMR spectroscopy, a ca. 1:1 *cis*:*trans* ratio was observed in the compound recovered from the washing solution, but isomerization over 12 hours, again, resulted in a *cis*:*trans* ratio of 0.36:1.

Reacting [Rh(acac)(Me$_2$Im)$_2$] **2-21** with *para*-substituted 1,4-diphenylbuta-1,3-diyne **2-1a** in a 1:1 ratio at room temperature in C_6D_6 results, after 15 minutes, in the formation of a *cis*-complex as a major product which isomerizes over 10 hours giving the *trans*-complex as the major product (Figure 2-23), similar to the reaction in a 1:2 ratio. In contrast to the reaction with two equivalents of *para*-substituted 1,4-diphenylbuta-1,3-diyne **2-1a**, both starting materials **2-1a** and **2-21** are still visible (**2-21**:*cis*:*trans* 0.12:0.53:1*)*. Adding a second equivalent of **2-1a** results in the complete consumption of **2-21** and in a *cis*:*trans* ratio of 0.36:1 for the buta-1,3-diyne π-complexes.

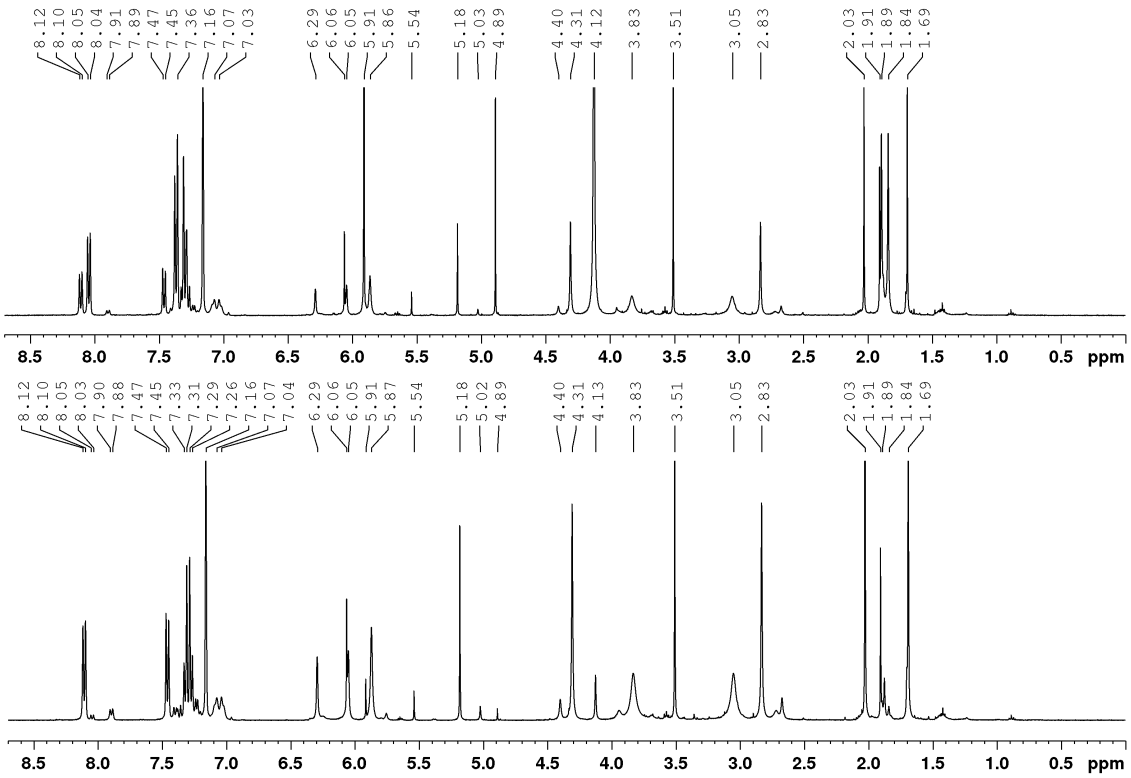

Figure 2-23: *In-situ* ^{1}H NMR spectra (400 MHz, C_6D_6) of the reaction of [Rh(acac)(Me$_2$Im)$_2$] **2-21** with *para*-substituted 1,4-diphenylbuta-1,3-diyne **2-1a** in a 1:1 ratio after 15 minutes (bottom) and 10 hours (top).

By 2D NMR spectroscopy of the *in-situ* reaction of [Rh(acac)(Me_2Im)$_2$] **2-21** with *para*-substituted 1,4-diphenylbuta-1,3-diyne **2-1a** in a 1:1 ratio after 10 hours, it was possible to confirm the formation of three different rhodium-acac species. A signal in the $^{13}C\{^1H\}$ NMR spectrum at 97.4 ppm correlates with the singlet at 4.89 ppm in the ^1H NMR spectrum, and signals at 98.2 and 99.8 ppm in the $^{13}C\{^1H\}$ spectrum correlate with the singlets at 5.18 and 5.03 ppm in the ^1H NMR spectrum. The ^1H and the $^{13}C\{^1H\}$ NMR shifts are similar to those in related rhodacyclopentadienes bearing an acac ligand.[59, 71] Additionally, it was possible to observe two doublets in the $^{13}C\{^1H\}$ NMR at 108.1 and 72.6 ppm with coupling constants of 23 and 20 Hz, respectively, indicating that one triple bond is bound to the rhodium metal center in an η^2 fashion. Similar shifts and coupling constants were reported by Werner and co-workers for the square-planar *trans*-[RhCl(η^2-$Me_3SiC{\equiv}CC{\equiv}CSiMe_3$)($P^iPr_3$)$_2$] **1-4** in $CDCl_3$.[16]

Using two equivalents of *para*-CO_2Me-substituted 1,4-diphenylbuta-1,3-diyne **2-1b** gives similar results compared to *para*-CF_3-substituted 1,4-diphenylbuta-1,3-diyne **2-1a**. After 15 minutes, a *cis*-complex is the major species present, which isomerizes over 10 hours forming a *trans*-complex as the major species. The color of the reaction mixture is not dark red, as in the reaction of [Rh(acac)(Me_2Im)$_2$] **2-21** with *para*-substituted 1,4-diphenylbuta-1,3-diyne **2-1a**, but instead it is dark purple after 10 hours. HRMS of the reaction mixture after 10 hours indicates that the two species [Rh(acac)(NHC)$_2$(2-1b)] and [Rh(acac)(NHC)$_2$(2-1b)$_2$] are present in solution. However, in the LIFDI spectrum, both signals are very weak in intensity and the signal for **2-21** was the main one. Some dissociation of *para*-substituted 1,4-diphenylbuta-1,3-diyne **2-1b** from the complex in the mass spectrometer is possible.

The results obtained strongly indicate an equilibrium between the different species. Therefore, a crossover experiment was conducted, similar to section 2.3.1.2. Compound [Rh(acac)(Me_2Im)$_2$] **2-21** was reacted with two equivalents of *para*-CF_3-substituted 1,4-diphenylbuta-1,3-diyne **2-1a** for 24 hours at room temperature and, after the complete consumption of **2-21**, this was followed by addition of two equivalents of *para*-CO_2Me-substituted 1,4-diphenylbuta-1,3-diyne **2-1b**. By using ^1H NMR spectroscopy, it was possible to identify the *cis*- and *trans*-isomers of [Rh(acac)(Me_2Im)$_2$(2-1b)]. The color of the solution changed from dark red to purple. This finding shows that although the rhodium(I) starting material **2-21** is completely consumed by **2-1a** initially, the buta-1,3-diyne must be labile, in order for reaction with **2-1b** to take place, confirming the idea of an equilibrium between the two starting materials and the different *cis*- and *trans*-complexes.

In order to obtain a better understanding of the reaction of [Rh(acac)(Me_2Im)$_2$] **2-21** with two equivalents of *para*-substituted 1,4-diphenylbuta-1,3-diyne **2-1a**, a variable temperature NMR experiment was conducted. Therefore, **2-21** was dissolved in THF-d_8 in a J-Young's tap NMR tube and cooled to -95 °C before solid **2-1a** was added. At -90 °C (Figure 2-24, black spectrum), the rhodium(I) starting material was completely consumed, while some **2-1a** remains unreacted in solution (7.84 ppm). Strong signals were observed at 1.51, 1.88, 3.08, 3.18, 3.98, 4.32, 4.93, 6.98, 7.05, 7.12 and 7.34 ppm and a weaker set at 1.55, 1.74 (overlapping with solvent signal), 3.01, 3.11, 4.16, 4.42, 4.77, 6.93, 7.17, 7.22 and 7.39 ppm. Signals in the aromatic region at 7.57 – 7.89 ppm belong to both new species and unreacted **2-1a**.

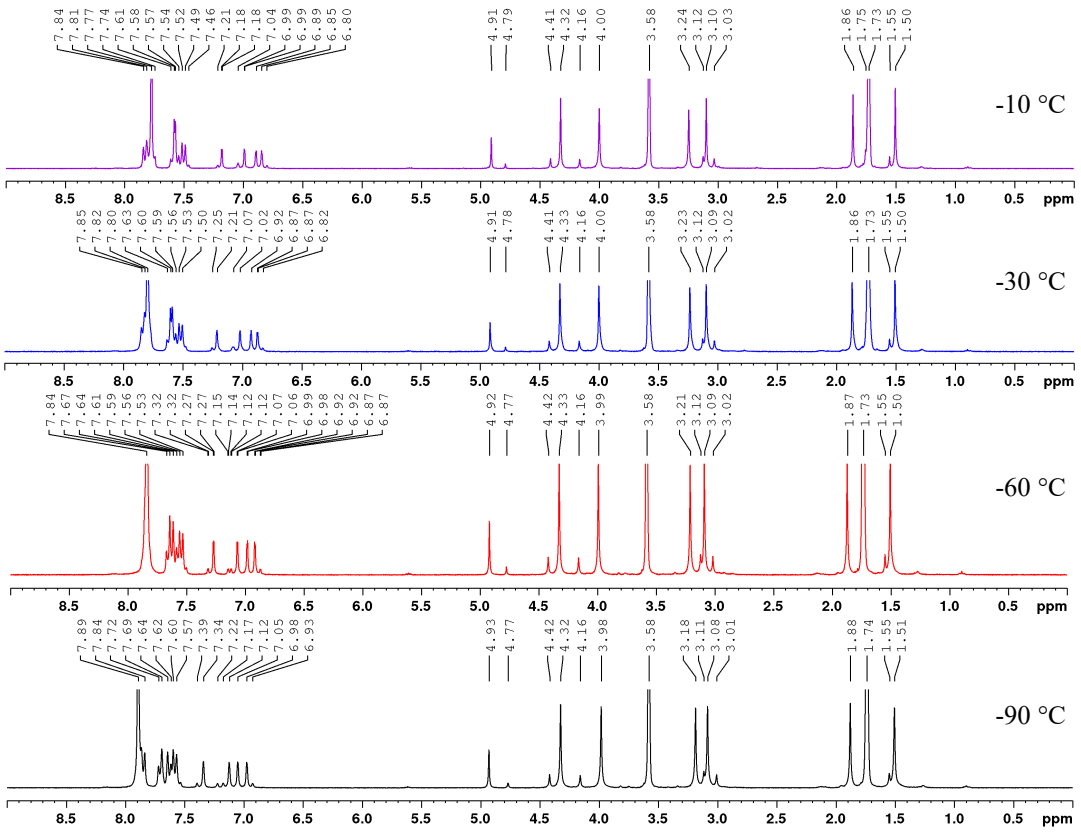

Figure 2-24: Variable temperature ^{1}H NMR spectra (300 MHz, THF-d_8) of the reaction of [Rh(acac)(Me_2Im)$_2$] **2-21** with *para*-substituted 1,4-diphenylbuta-1,3-diyne **2-1a** in a 1:2 ratio at -90 (black), -60 (red), -30 (blue) and -10 °C (purple).

In the black spectrum signals at 4.77 and 4.93 ppm can be assigned to the single acac-CH group and indicate two rhodium-acac species. The signals from 1.51 – 1.89 ppm integrate to three for each species and can be assigned to the acac-CH_3 groups. From 3.01 – 4.42 ppm, eight signals in total are observed, integrating to three each, which are due to the NHC-CH_3 groups. From 6.93 – 7.39 ppm, there are eight singlets with an integral of one for each species, due to the CH groups of the NHC backbone.

The observation of four different singlets for the NHC backbone CH groups, as well as for the methyl groups, for each species, indicate the presence of two *cis*-complexes. Similar signals were observed in the reaction of [Rh(acac)(Me_2Im)$_2$] **2-21** with *para*-substituted 1,4-diphenylbuta-1,3-diyne **2-1a** in C_6D_6 at room temperature after 15 minutes (Figure 2-21 and 2-23). There is no visible progress in the ^{1}H NMR spectrum until the temperature is raised from -90 to -10 °C.

Inspection of the variable temperature ^{1}H NMR spectra at +10 °C (black), +25 °C (red) and +35 °C (blue) shows a new signal in the acac-CH region at 5.14 ppm, which begins to grow at +10 °C, and a second additional singlet in this area at 4.68 ppm starting to arise at +25 °C (Figure 2-25). In the temperature range from +10 – +35 °C, the signal at 5.14 ppm is always more intense than the signal at 4.68 ppm. Further assignment is rather complicated due to the large number of overlapping signals.

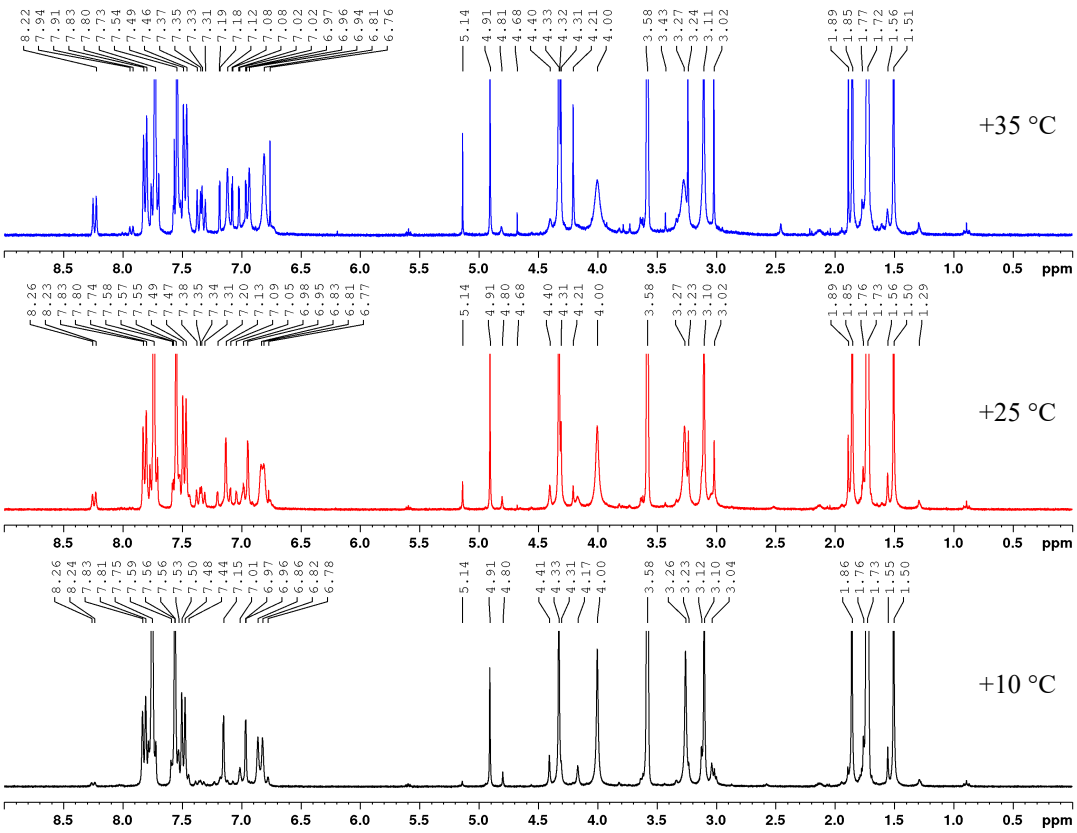

Figure 2-25: Variable temperature ^{1}H NMR spectra (300 MHz, THF-d_8) of the reaction of [Rh(acac)(Me_2Im)$_2$] **2-21** with *para*-substituted 1,4-diphenylbuta-1,3-diyne **2-1a** in a 1:2 ratio at +10 °C (black), +25 °C (red) and +35 °C (blue).

Figure 2-26 displays the spectra acquired at +45 °C (black), +55 °C (red), +60 °C (blue) and then after cooling to +25 °C (purple). With an increase in temperature (black to blue spectrum), the intensity of the singlet at 4.90 ppm decreases, while the intensity of the singlets at 5.14 and 4.68 ppm increase. While at +35 °C, a signal for the minor *cis*-compound is still visible at

4.81 ppm, it vanishes at higher temperatures and is visible again after cooling the solution to 25 °C, although in very low intensity. The spectrum at +60 °C (blue) was further heated for additional 40 minutes, and, compared to the ^{1}H NMR spectrum after cooling back to 25 °C (purple), shows only a sharper signal for the singlet at 4.90 ppm. Sharp and intense singlets are visible in the purple spectrum at 6.77 and 4.21 ppm. When integrating the resonance at 4.68 ppm, representing an acac-CH group, to one, the signal at 6.77 ppm integrates to four and the signal at 4.21 ppm to 12, representing the NHC-CH backbones and NHC-CH_3 groups hydrogen atoms, respectively, implying that these signals correspond to the *trans*-[Rh(acac)(Me_2Im)$_2$(2-1a)] complex.

The singlet at 5.14 ppm begins to appear before the signal for the *trans*-complex at 4.68 ppm, suggesting the formation of an intermediate during the *cis-trans* isomerization process.

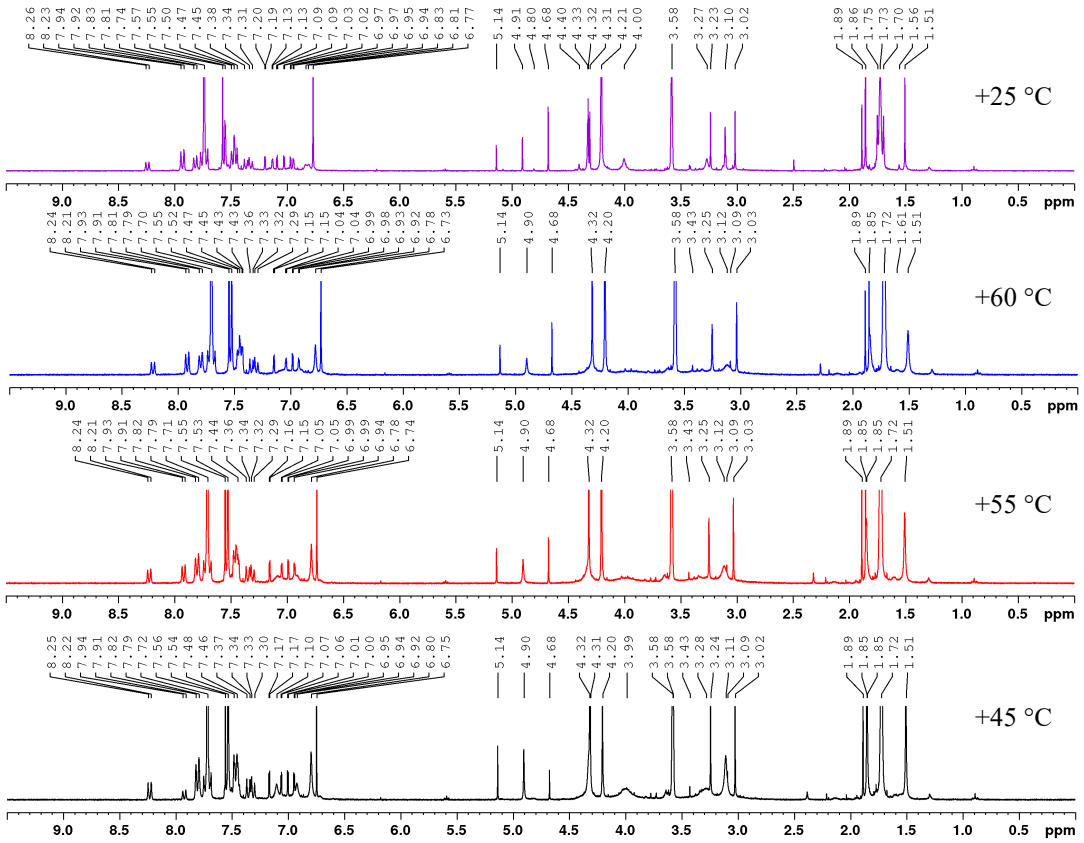

Figure 2-26: Variable temperature ^{1}H NMR spectra (300 MHz, THF-d_8) of the reaction in a 1:2 ratio of [Rh(acac)(Me_2Im)$_2$] **2-21** with *para*-substituted 1,4-diphenylbuta-1,3-diyne **2-1a** at +45 (black), +55 (red), +60 (blue) and +25 °C (purple).

However, evaporating THF-d_8, and dissolving the residue in C_6D_6 and recording a ^{1}H NMR spectrum shows one additional signal in the acac region (compared to acac-CH region of the top NMR spectrum in Figure 2-21) at 5.04 ppm. This indicates that a species forms in THF-d_8, which was not formed in the reaction in C_6D_6, which could be somewhat with a THF solvent molecule as ligand as a stable intermediate during the formation of the *trans*-complex.

Following the proposed reaction pathway for the formation of the all-carbon [3+2] annulation reaction (Scheme 2-1) as well as the observations of an equilibrium and those from the variable temperature NMR study, the following reaction pathway is proposed. The *para*-substituted 1,4-diphenylbuta-1,3-diyne **2-1a** binds in a η^2 fashion to the low valent rhodium(I) complex [Rh(acac)(Me_2Im)$_2$] **2-21**, forming the two *cis*-isomers **2-I$_{cis}$a** and **2-I$_{cis}$b**. Dissociation of one NHC ligand and rearrangement of the other ligands is accompanied by THF solvent binding to a vacant site at the rhodium metal center forming a stable intermediate, before a second NHC ligand replaces the solvent molecule and forms the final *trans*-complex (Scheme 2-16).

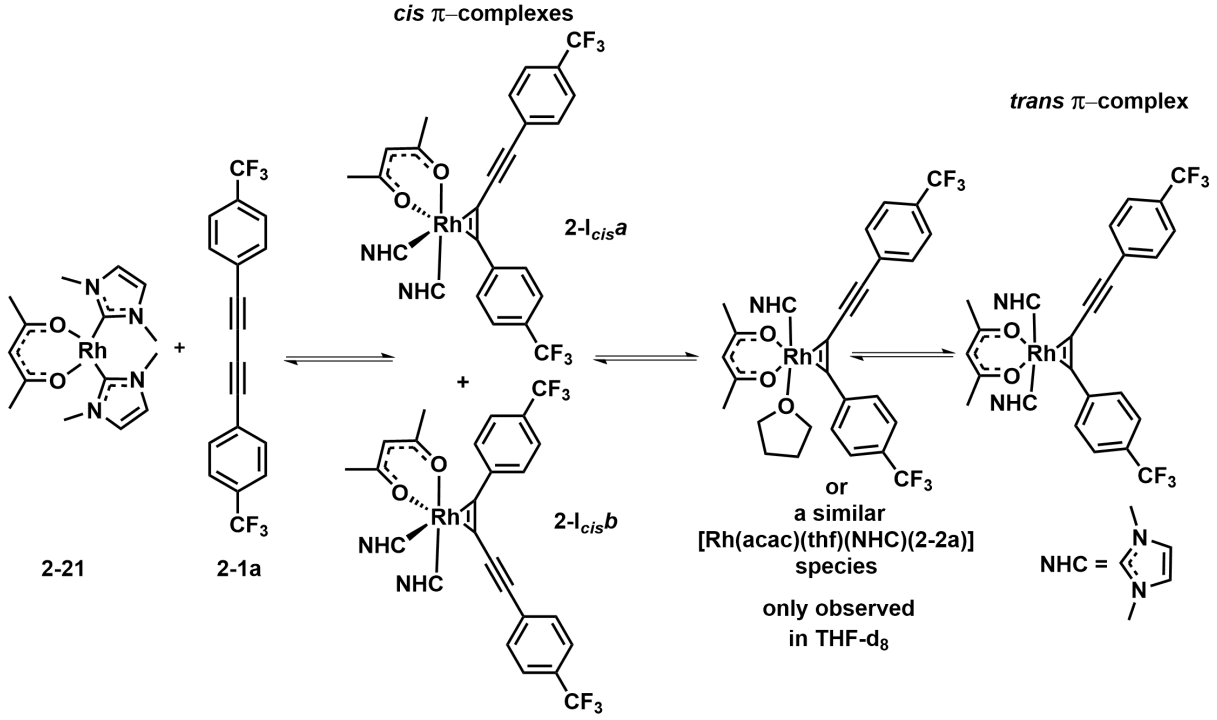

Scheme 2-16: Proposed reaction pathway for the formation of the *trans*-[Rh(acac)(Me_2Im_2)$_2$(2-1)] complex *via* reaction of [Rh(acac)(Me_2Im)$_2$] **2-21** with *para*-substituted 1,4-diphenylbuta-1,3-diyne **2-1a** in THF-d$_8$.

Reacting [Rh(acac)(Me_2Im)$_2$] **2-21** with one equivalent of *para*-substituted 1,4-diphenylbuta-1,3-diyne **2-1a** in -30 °C cold toluene, stirring the solution for 15 seconds before layering it with -30 °C cold *n*-hexane, and placing the mixture in a freezer at -30 °C over night, resulted in the formation of orange colored single-crystals suitable for X-ray diffraction analysis. The complex crystallizes in the monoclinic space group $P2_1/n$, and the molecular structure is shown in Figure 2-27 and selected bond lengths and angles are listed in Table 2-11.

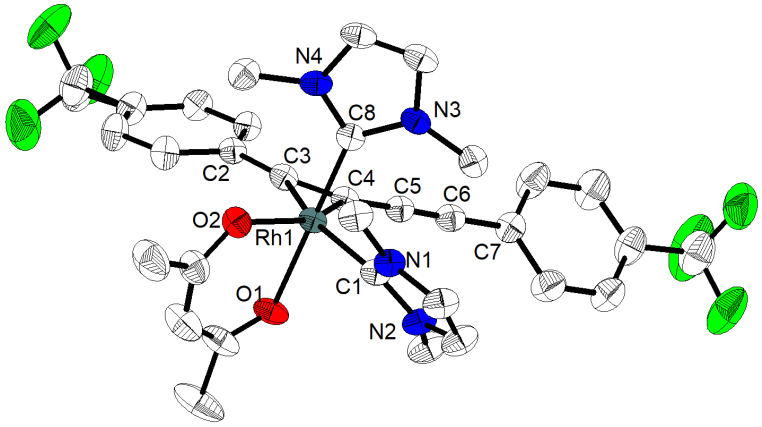

Figure 2-27: Molecular structure of complex **2-I$_{cis}$b** in the solid state at 100 K. Hydrogen atoms, toluene solvent molecules and a second molecule in the unit cell are omitted for clarity. Atomic displacement ellipsoids are drawn at the 50% probability level.

The molecular structure in the solid state confirms the conclusion from the ^{1}H NMR spectroscopic data that a *cis*-compound, namely **2-I$_{cis}$b**, is the major species at low temperature. The distances of the rhodium atom to the carbene-carbon atoms are Rh1-C1 2.090(3) and Rh1-C8 1.959(3) Å. The acac-rhodium bond distances are 2.132(2) and 2.180(2) Å for Rh1-O1 and Rh1-O2, respectively. The C3-C4 bond distance is 1.311(5) Å, which is significantly longer than 1.20 Å normally found for a carbon-carbon triple bond, and close to the value of 1.34 Å, typical of a C=C double bond, and is an indication of very strong π-backbonding from the electron-rich rhodium metal center to the alkyne moiety. Likewise, the C2-C3-C4 and C3-C4-C5 angles are 138.4(3) and 146.7(3)°, and hence deviate significantly from linearity, whereas the C4-C5-C6 and C5-C6-C7 angles are close to 180°, being 175.4(3) and 178.5(4)°, respectively. The C2-C3-C4 angle is significantly smaller than the ones reported by Schwenk for *trans*-[Rh(S$_2$CNEt$_2$)(PMe$_3$)$_2$(diyne)] **2-22** and **2-23** being 149.8(5) and 152.0(4)°, respectively (*vide infra*). The Rh1-C3 and Rh1-C4 bond lengths of 2.072(3) and 2.038(3) Å, respectively, and the C3-Rh1-C4 angle of 37.2(1)° are identical with the bond lengths and angles reported by Schwenk.[68]

The Rh-C1 bond distance is the same as in an octahedral rhodium(III) complex with an NHC ligand *trans* to a P(*p*-tolyl)$_3$ ligand and an acac ligand lying in the equatorial plane,[72] as the phenyl-substituted C3 carbon atom and the phosphine ligand both have a strong *trans*-influence. However, the distance for Rh1-C8, in which the NHC ligand is *trans* to an oxygen atom of the acac ligand, is significantly shorter, due to the weaker *trans*-influence of the oxygen atom compared to C3. The Rh1-O1 distance for the oxygen atom *trans* to the NHC ligand is significantly shorter than the Rh1-O2 bond length for the oxygen atom *trans* to C4.

Table 2-11: Selected bond lengths [Å] and angles [°] of complex **2-I$_{cis}$b** determined by single-crystal X-ray diffraction at 100 K with esd's in parentheses.

	2-I$_{cis}$b		**2-I$_{cis}$b**
Rh1-O1	2.132(2)	O1-Rh1-O2	87.78(9)
Rh1-O2	2.180(2)	C1-Rh1-C8	88.68(12)
Rh1-C1	2.090(3)	C2-C3-C4	138.4(3)
Rh1-C8	1.959(3)	C3-C4-C5	146.7(3)
Rh1-C3	2.072(3)	C3-Rh1-C4	37.21(12)
Rh1-C4	2.038(3)	C4-C5-C6	175.4(3)
C2-C3	1.444(4)	C5-C6-C7	178.5(4)
C3-C4	1.311(5)	C4-Rh1-O2	152.85(11)
C4-C5	1.381(4)	C3-Rh1-C1	155.97(13)
C5-C6	1.208(5)		
C6-C7	1.424(5)		

In contrast, with [Rh(acac)(PMe$_3$)$_2$] **1-51** it was only possible, by $^{31}P\{^1H\}$ NMR spectroscopy, to identify two *cis*-complexes and one *trans*-complex of the form [Rh(acac)(PMe$_3$)$_2$(2-1a)] at low temperatures as intermediates in the formation of the complexes **2-2a**. By $^{13}C\{^1H\}$ NMR spectroscopy, it was possible to assign the main species observed in the $^{31}P\{^1H\}$spectrum to **I$_{cis}$a** (Scheme 1-2). Generally, the phenyl-substituted carbon exerts a stronger *trans*-influence than the phenylethynyl substituted carbon atom. Thus, the **I$_{cis}$b** species with PMe$_3$ *trans* to the phenyl-substituted carbon is less stable than the one with PMe$_3$ ligand *trans* to the phenylethynyl-substituted carbon **I$_{cis}$a**. These results were also supported by theoretical calculations.[206]

Interestingly, the solid state structure of **2-I$_{cis}$b** represents the NHC analogue of the less stable *cis*-phosphine species **I$_{cis}$b**, as the NHC ligand is *trans* to the phenyl-substituted carbon atom C3. Although the π-acceptor ability of NHCs is, in general, lower than that of phosphines.[275-277]

As the quantity of single-crystals obtained was quite large, and diffraction data was collected on several different crystals, all of which had the same unit cell, it seems likely that **2-I$_{cis}$b** is also the main isomer in solution.

However, Schwenk successfully isolated single-crystals suitable for X-ray diffraction analysis of two *trans*-phosphine complexes **2-22** and **2-23** of the form [Rh(S$_2$CNEt$_2$)(PMe$_3$)$_2$(diyne)] (Figure 2-28) from reactions of [Rh(S$_2$CNEt$_2$)(PMe$_3$)$_2$] **1-44** with different *para*-substituted 1,4-diphenylbuta-1,3-diynes (methyl and naphthyl groups in the *para*-positions). The two possible *cis*-compounds were only observed in very small quantities along with an intense signal for the *trans*-complex in low temperature (-80 – -40 °C) NMR studies. Furthermore, purification

attempts of the *trans*-complex always yielded a mixture of the starting materials, the *trans*-species, and decomposition products, as decomposition of the complexes begins at ca. -20 °C.[68]

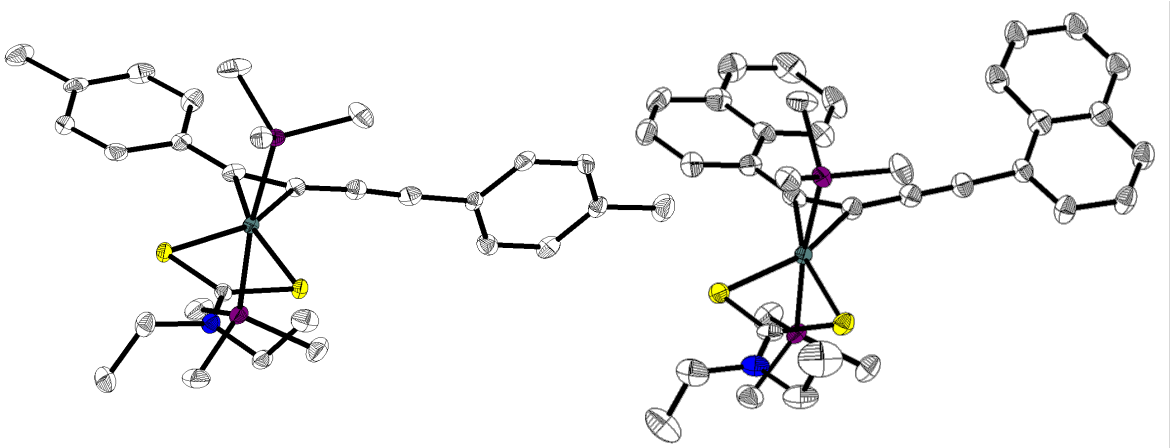

Figure 2-28: Molecular structures of complexes **2-22** (left) and **2-23** (right) in the solid state at 100 K. Hydrogen atoms and a second molecule in the unit cell (for **2-23**) are omitted for clarity. Atomic displacement ellipsoids are drawn at the 50% probability level.

Attempts to add a second *para*-CO_2Me-substituted 1,4-diphenylbuta-1,3-diyne to a *trans*-[$Rh(S_2CNEt_2)(PMe_3)_2$(2-1b)] complex resulted in a mixture of different compounds under the conditions used, according to $^{31}P\{^1H\}$ NMR spectroscopy. It was not possible to separate the mixture completely, but it was possible to identify the major product in the reaction mixture as an unsymmetric rhodium(III)-complex with the formula [$Rh(S_2CNEt_2)(PMe_3)_2$(2-1b)$_2$] by ^1H NMR spectroscopy. In the $^{31}P\{^1H\}$spectrum, a doublet at -5.0 ppm with a rhodium phosphorus coupling constant of 104 Hz was observed. In the work of Schwenk, it remained unclear whether the main product is connected in a 2,4 manner (**2-UNSYM**) or is analogous to complexes **2-2a**,**b**.[68]

In this work, attempts were made to clarify these findings by reacting [$Rh(acac)(PMe_3)_2$] **1-51** with *para*-CO_2Me-substituted 1,4-diphenylbuta-1,3-diyne **2-1b** at 40 °C for 22 hours, followed by the addition of sodium diethyldithiocarbamate and further heating at 80 °C. In the $^{31}P\{^1H\}$ NMR spectrum, aside from several small doublets, an intense doublet at -5.0 ppm with a Rh-P coupling constant of 102 Hz was observed. HRMS of the reaction mixture confirmed the presence of a species with the formula [$Rh(S_2CNEt_2)(PMe_3)_2$(2-1b)$_2$]. The same signal in the $^{31}P\{^1H\}$ NMR spectrum was observed by Schwenk in the reaction of [$Rh(S_2CNEt_2)(PMe_3)_2$] with **2-1b** at room temperature,[68] indicating that the [3+2] compound is also formed. Hence, in the reaction of [$Rh(S_2CNEt_2)(PMe_3)_2$] **1-44** with **2-1b**, a *trans*-compound is also only an intermediate leading to the formation of a complex similar to complexes **2-2a**,**b** and unlike in the reaction of [$Rh(acac)(Me_2Im)_2$] **2-21** with **2-1b**, for which it was only possible to observe a [$Rh(acac)(NHC)_2$(2-1b)$_2$] species by HRMS.

2.4 Photophysical studies of the luminescent products

The UV-visible absorption spectra of the compounds **2-2a** and **2-2b** in THF are generally very similar (Figure 2-29a)). Complex **2-2a** shows four absorption bands at 252 (ε = 33000 M^{-1} cm^{-1}), 318 (ε = 36100 M^{-1} cm^{-1}), 375 (ε = 23700 M^{-1} cm^{-1}) and 466 nm (ε = 14000 M^{-1} cm^{-1}), while **2-2b** shows also four absorption bands at 242 (ε = 44700 M^{-1} cm^{-1}), 339 (ε = 32800 M^{-1} cm^{-1}), 400 (ε = 31500 M^{-1} cm^{-1}) and 477 nm (ε = 15500 M^{-1} cm^{-1}). Additionally, the complexes **2-2a**,**b** show a weak absorption from 540 – 700 nm with extinction coefficients ε in the range of 800 – 2000 M^{-1} cm^{-1}. Comparing **2-2a** with **2-2b** the absorption band with the highest energy at 252 nm is hypsochromically shifted, while the other three low energy absorption bands are all bathochromically shifted. The extinction coefficients ε are all in the same range, and both compounds show a weak absorption from 540 – 700 nm low extinction coefficients.

The UV-visible absorption spectra of the compounds **2-3a**, **2-3b** and **2-3c** in THF are also generally very similar (Figure 2-29b)). Complex **2-3a** shows an absorption band at 331 nm (ε = 40100 M^{-1} cm^{-1}), while **2-3b** shows one high energy absorption band at 243 nm (ε = 70000 M^{-1} cm^{-1}) and a second band at 364 nm (ε = 54100 M^{-1} cm^{-1}). Complex **2-3c** shows an absorption band at 350 nm (ε = 46700 M^{-1} cm^{-1}). All three complexes show broad absorptions from around 500 – 1000 nm with extinction coefficients ε of up to 11000 M^{-1} cm^{-1}. The absorption band from the pure CF_3-substituted complex **2-3a** at 331 nm is hypsochromically shifted, compared to 350 nm for the mixed CO_2Me-CF_3-substituted complex **2-3c**, and to 364 nm for the pure CO_2Me-substituted complex **2-3b**.

For compound **2-5** the UV-visible absorption spectrum in THF shows a maximum at 314 nm (ε = 40500 M^{-1} cm^{-1}), a second band at 514 nm (ε = 15000 M^{-1} cm^{-1}) and a broad absorption from around 570 – 750 nm with an extinction coefficient ε of up to 4200 M^{-1} cm^{-1}. This broad absorption is very unusual for small organic compounds (Figure 2-29c)).

A combination of the UV-visible absorption spectra of the three CF_3-only compounds **2-2a**, **2-3a** and **2-5** leads to an absorption of light from 215 – 1000 nm with a minimum extinction coefficient ε of ca. 11000 M^{-1} cm^{-1} (Figure 2-29d)). Thus, the system could be useful for light harvesting processes. Various systems bearing a metal center were already described in the literature.[278-279]

Compounds **2-2a**, **2-2b**, **2-3(a-c)** and **2-5** do not emit in THF and 2-Me-THF at room temperature or at 77 K in a 2-Me-THF glass matrix.

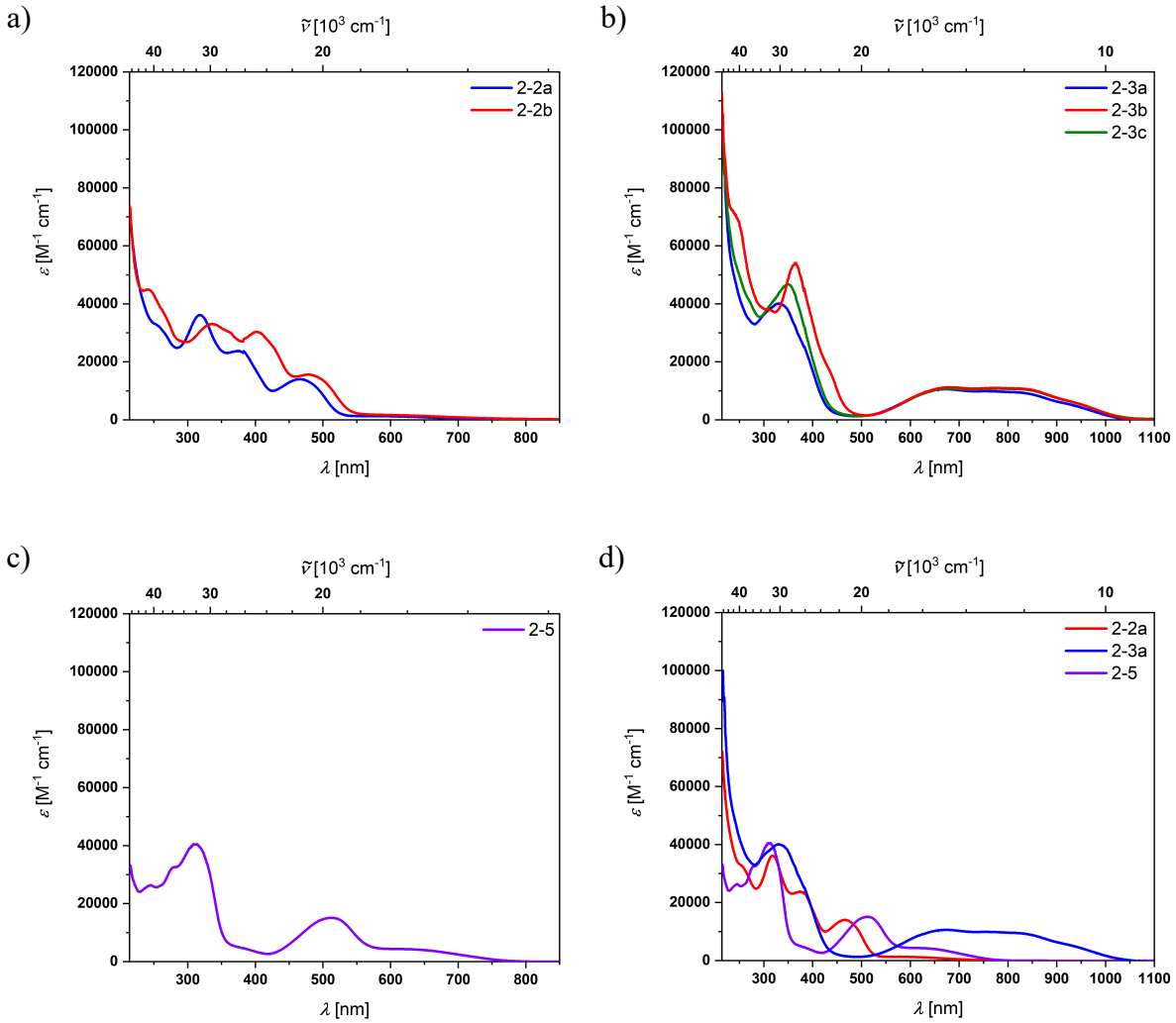

Figure 2-29: UV-visible absorption spectra in dry, degassed THF at room temperature of the compounds a) **2-2a** and **2-2b**, b) **2-3a**, **2-3b** and **2-3c**, c) **2-5**, and d) **2-2a**, **2-3a** and **2-5**.

Figure 2-30 shows the different compounds **2-2a**, **2-3a**, **2-5**, **2-3c**, **2-2b** and **2-3b** in THF solution.

Figure 2-30: From left to right: Compounds **2-2a**, **2-3a**, **2-5**, **2-3c**, **2-2b** and **2-3b** in THF.

Broad absorptions with $\lambda_{abs,max}$ = 464 and 485 nm and extinction coefficients ε of 23000 and 21000 M^{-1} cm^{-1}, respectively, were previously reported for CF_3 and CO_2Me-substituted 2,5-bis(arylethynyl)rhodacyclopentadienes **1-34a** and **1-35a** in toluene, obtained from the reaction

of [Rh(CCSiMe$_3$)(PMe$_3$)$_4$] **1-28a** with *para*-CF$_3$ and CO$_2$Me-substituted 1,4-diphenylbuta-1,3-diynes **2-1a**,**b**. Compared to the complexes **2-2a**,**b** and **2-3(a-c)**, $\lambda_{abs,max}$ is shifted hypsochromically and the respective extinction coefficients are roughly double. Additionally, **2-2a**,**b**, show weak absorptions tailing to 700 nm and complexes **2-3(a-c)** moderate absorption bands from 500 – 1000 nm.

The shape of the UV-visible absorption spectrum of compound **2-5** is similar to those of known DPPs.[280] DPPs exhibit fluorescence and the extinction coefficients of the high energy bands in DPPs are larger or at least comparable to that of the low energy band.[217, 281-282] The high energy band corresponds to a $\pi \rightarrow \pi^*$ transition and the low energy band to a charge-transfer transition.[281]

TD-DFT (time-dependent density functional theory) calculations (B3LYP/6-31G+(d), gas phase) were carried out in order to obtain information on the nature of the optical transitions, and to compute the UV-visible absorption spectrum of compound **2-5** in order to compare it with the experimental spectrum. The purple color of **2-5** is due to three broad bands in the red (658 nm), green (538 nm) and UV-blue region (428 nm) of the electromagnetic spectrum (see Appendix, Table A11). The first three transitions are HOMO, HOMO-1 and HOMO-2 to LUMO transitions (Figure A142). The oscillator strength *f* is smaller for $S_1 \leftarrow S_0$ than for $S_2 \leftarrow S_0$ and $S_3 \leftarrow S_0$. According to the calculations, the three lowest energy π-π^* excitations exhibit moderate to weak charge-transfer character. The incorporation of the nitrogen donor and the carbonyl moiety as acceptor in conjunction with the large conjugation and delocalization of the π- and π^*-system (see frontier orbital contour plots Figure A141) is the reason for those transitions occurring at such low energies.

From the calculated oscillator strengths (Figure 2-31, green bars), the simulated extinction coefficients (cyan spectrum) in the gas phase are in good agreement with the experimental determined ones (purple spectrum) in dry, degassed THF of compound **2-5**.
The simulated spectrum of compound **2-5** in the gas phase shows a band with a large extinction coefficient at 340 nm (ε = 63000 M^{-1} cm^{-1}). Further bands are visible at 430 nm (ε = 10000 M^{-1} cm^{-1}), 540 nm (ε = 20000 M^{-1} cm^{-1}) and a broad shoulder from 590 – 800 nm (ε = 8000 M^{-1} cm^{-1}). The simulated data are in in good agreement with the experimental data in the region from 450 – 800 nm. The extinction coefficient for the highest energy band around 300 nm is overestimated compared with the experimentally obtained data. The calculated

absorption at 428 nm (f = 0.1528) might represent the small shoulder at ca. 375 nm in the experimental spectrum.

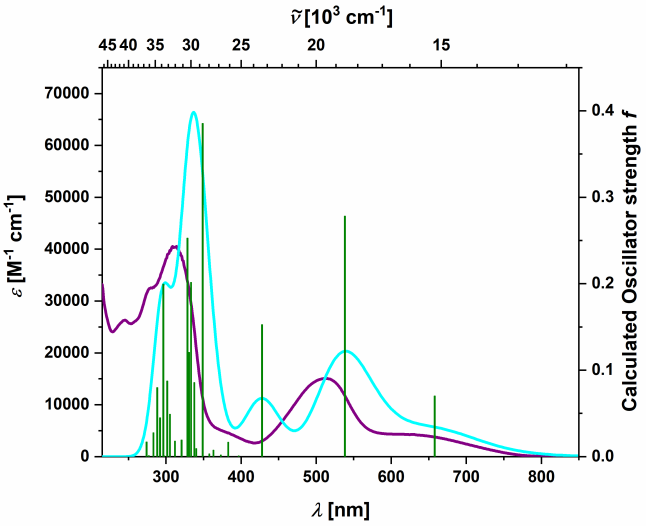

Figure 2-31: Simulated absorption spectrum (cyan, FHWM = 3000 cm^{-1}) from the calculated oscillator strengths f (green bars) in the gas phase and experimentally determined extinction coefficient of **2-5** (purple) in dry, degassed THF.

2.5 Redox properties of selected complexes

The cyclic voltammetry measurements of complex **2-2a** show that only the first reduction is reversible (Figure 2-32a) and Table 2-12) and all following reductions at 250 mV/s (-2.46, -2.95, -3.13 and -3.29 V) are irreversible. The first reduction occurs at $E_{1/2}$ = -1.89 V in THF (Figure 2-32b) and Table 2-12).

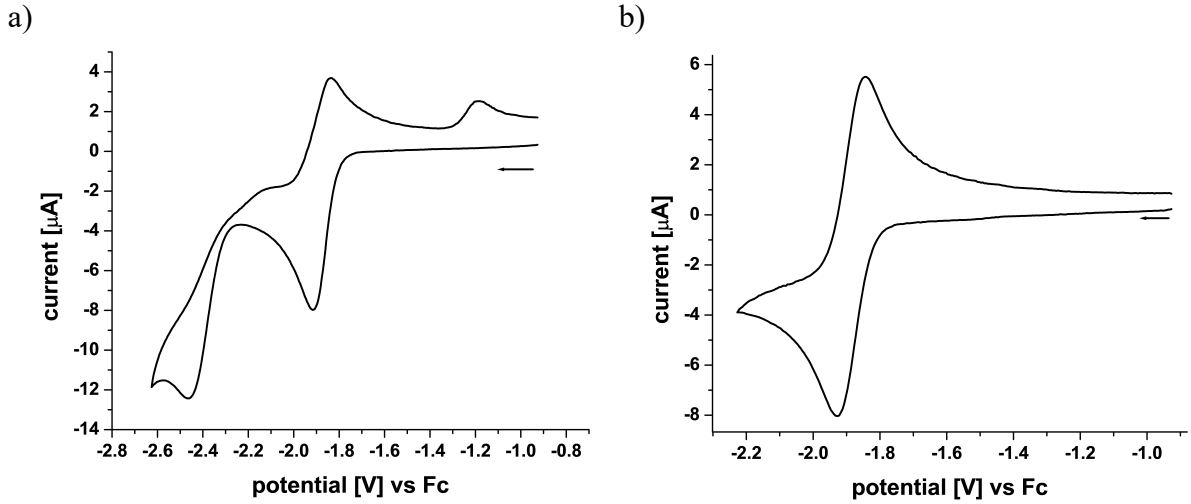

Figure 2-32: Cyclic voltammograms at 250 mV s^{-1} of the first two reductions (left) and the first reduction (right) of compound **2-2a** relative to the Fc/Fc^+ couple in 0.1 M tetrabutylammonium hexafluorophosphate THF solutions.

Compound **2-2a** is reversibly oxidized at $E_{1/2}$ = 0.29 V relative to the Fc/Fc^+ couple in THF (Figure 2-33).

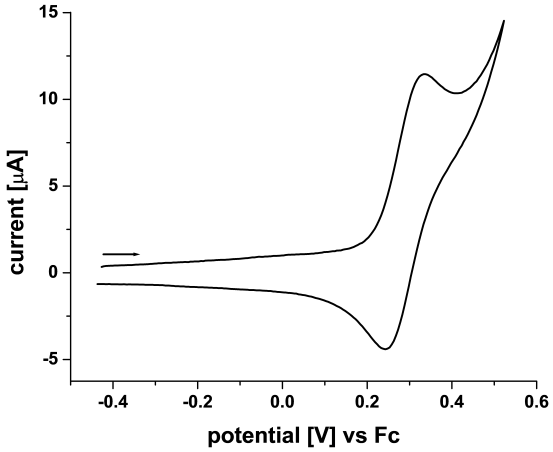

Figure 2-33: Cyclic voltammogram at 250 mV s^{-1} of the oxidation of compound **2-2a** relative to the Fc/Fc^+ couple in 0.1 M tetrabutylammonium hexafluorophosphate THF solutions.

Table 2-12: Summary of the electrochemical properties of compound **2-2a** derived from cyclic voltammetry relative to the Fc/Fc^+ couple in 0.1 M tetrabutylammonium hexafluorophosphate THF solutions.

	reduction			oxidation			other[b]
ν [mV s^{-1}]	$E_{1/2}$ [V]	ΔE_p [mV]	$\lvert i_{pa}/i_{pc}\rvert$	$E_{1/2}$ [V]	ΔE_p [mV]	$\lvert i_{pc}/i_{pa}\rvert$[a]	
100	-1.88	74	0.96				-2.46; -2.95; -3.13 and -3.29 V.
250	-1.89	83	0.95	0.29	91	0.59	
500	-1.88	83	0.96				
1000	-1.88	96	0.95				

a: With the signal being close to the solvent window, the determination of the peak current for the re-reduction was significantly impacted.
b: E_{pc} values [V] of irreversible reductions at 250 mV s^{-1}.

The cyclic voltammetry measurements of complex **2-3a** show that there is only one reversible reduction at $E_{1/2}$ = -1.42 V (Figure 2-34 and Table 2-13) and one reversible oxidation at $E_{1/2}$ = 0.13 V relative to the Fc/Fc^+ couple in THF.

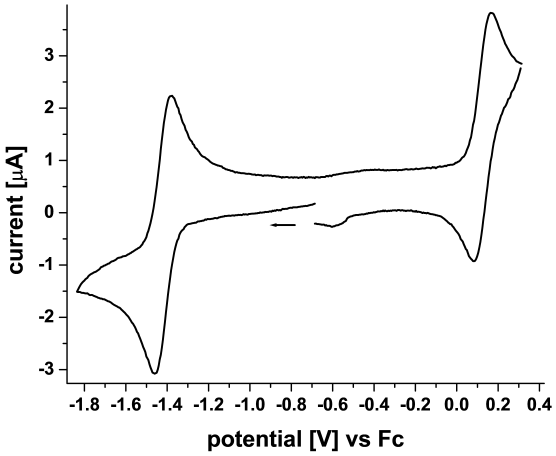

Figure 2-34: Cyclic voltammogram at 250 mV s^{-1} of the reduction and oxidation of compound **2-3a** relative to the Fc/Fc^+ couple in 0.1 M tetrabutylammonium hexafluorophosphate THF solutions.

Table 2-13: Summary of the electrochemical properties of compound **2-3a** derived from cyclic voltammetry relative to the Fc/Fc^+ couple in 0.1 M tetrabutylammonium hexafluorophosphate THF solutions.

	reduction			oxidation		
ν [mV s^{-1}]	$E_{1/2}$ [V]	ΔE_p [mV]	$\lvert i_{pa}/i_{pc}\rvert$	$E_{1/2}$ [V]	ΔE_p [mV]	$\lvert i_{pc}/i_{pa}\rvert$[a]
150	-1.42	82	0.97	0.12	83	0.67
250	-1.42	81	1.03	0.13	85	0.75
500	-1.42	84	0.98	0.13	93	0.72
1000	-1.42	90	0.98	0.13	95	0.73

a: With the signal being close to the solvent window, the determination of the peak current of the re-reduction was significantly impacted.

Inspection of the pure organic compound **2-5** reveals two fully reversible reductions at $E_{1/2}$ = -1.05 and -1.70 V, respectively, relative to the Fc/Fc^+ couple in THF (Figure 2-35 and Table 2-14).

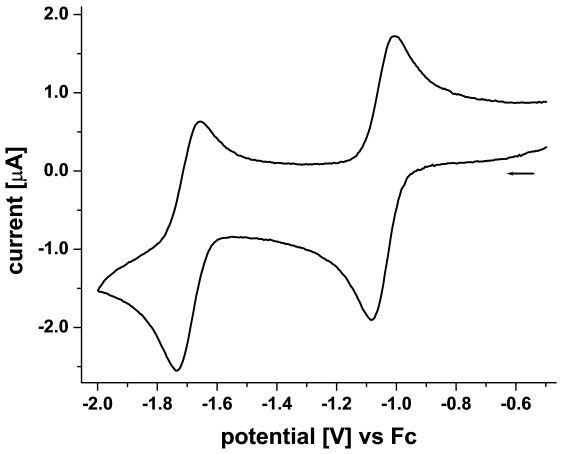

Figure 2-35: Cyclic voltammogram at 250 mV s^{-1} of both reductions of compound **2-5** relative to the Fc/Fc^+ couple in 0.1 M tetrabutylammonium hexafluorophosphate THF solutions.

Table 2-14: Summary of the electrochemical properties of compound **2-5** derived from cyclic voltammetry relative to the Fc/Fc^+ couple in 0.1 M tetrabutylammonium hexafluorophosphate THF solutions.

	first reduction			second reduction		
ν [mV s^{-1}]	$E_{1/2}$ [V]	ΔE_p [mV]	$\lvert i_{pa}/i_{pc}\rvert$	$E_{1/2}$ [V]	ΔE_p [mV]	$\lvert i_{pa}/i_{pc}\rvert$
50	-1.04	68	0.80	-1.69	70	0.71
150	-1.05	69	0.88	-1.70	75	0.75
250	-1.05	76	0.88	-1.70	78	0.83
500	-1.04	82	0.89	-1.70	86	0.89
1000	-1.04	87	0.93	-1.70	92	0.88

Due to the fact, that the pure organic compound **2-5** shows only reduction, and the metal containing complexes **2-2a** and **2-3a** show oxidation, it is likely that the oxidation occurs at the metal center.

Chapter 3

3 Synthesis and structural characterization of 2,5-bis(aryl)rhodacyclopentadienes

3.1 Abstract

The formation of highly fluorescent 2,5-bis(arylethynyl)rhodacyclopentadienes and phosphorescent rhodium 2,2'-biphenyl complexes from the reaction of [Rh(acac)(PMe_3)$_2$] with α,ω-bis(arylbutadiynyl)alkanes (α,ω-tetraynes) was previously reported. Furthermore, a convenient route to access only the PMe_3-substituted 2,5-bis(arylethynyl)rhodacyclopentadienes *via* the reaction of [Rh(acac)(P(*p*-tolyl)$_3$)$_2$] with α,ω-tetraynes followed by a subsequent ligand exchange of P(*p*-tolyl)$_3$ with PMe_3 was previously established. In the reaction of α,ω-bis(arylethynyl)alkanes (α,ω-diynes) with [Rh(acac)(PMe_3)$_2$] the formation of only one isomer had been observed, namely weakly fluorescent 2,5-bis(aryl)rhodacyclopentadienes.

In this chapter, the influence of the backbone of the α,ω-diynes on the formation and photophysical properties of 2,5-bis(aryl)rhodacyclopentadienes is discussed. Therefore, different α,ω-diynes were reacted with [Rh(acac)(PMe_3)$_2$] and [Rh(acac)(P(*p*-tolyl)$_3$)$_2$] in equimolar amounts. In general, a faster consumption of the rhodium(I) starting material is observed while using preorganized α,ω-diynes with electron withdrawing substitutents in the backbone. The isolated PMe_3-substituted rhodacyclopentadienes exhibit fluorescence, despite the presence of the heavy atom rhodium, with lifetimes τ_F of < 1 ns and photoluminescence quantum yields Φ of < 0.01 as in previously reported P(*p*-tolyl)-substituted 2,5-bis(arylethynyl)rhodacyclopentadienes. However, an isolated P(*p*-tolyl)-substituted 2,5-bis(aryl)rhodacyclopentadiene shows multiple lifetimes and different absorption and excitation spectra leading to the conclusion that different species may be present.

Reaction of [Rh(acac)(Me_2Im)$_2$] with dimethyl 4,4'-(naphthalene-1,8-diylbis(ethyne-2,1-diyl))dibenzoate, results in the formation of a mixture *trans*- and *cis*-NHC-substituted 2,5-bis(aryl)rhodacyclopentadienes.

3.2 Previous work and motivation

Since 2001, with the development of a high-yield one-pot synthesis forming *para*-substituted 2,5-bis(arylethynyl)rhodacyclopentadienes from a rhodium(I) precursor with two equivalents of *para*-substituted 1,4-diphenylbuta-1,3-diynes, the Marder group has successfully modified these rhodacyclopentadienes. For example, connecting two *para*-substituted phenylbuta-1,3-diynes *via* a propyl- or butyl-chain, results in a rigidification of the rhodacyclopentadiene backbone. They have also altered the substituents in *para*-position of the aryl moiety, the ligand sphere by using π-electron donating groups such as acetylacetonato or diethyldithiocarbamate, and replaced the trimethylphosphine with tri(*p*-tolyl)phosphine ligands or even stronger σ-donor NHC ligands.[51, 56-59, 68, 71-72, 182]

Previous work demonstrated that the reaction of $[Rh(acac)(PMe_3)_2]$ with α,ω-tetraynes results in the formation of highly fluorescent 2,5-bis(arylethynyl)rhodacyclopentadiene and phosphorescent rhodium 2,2'-biphenyl complexes. However, by using stoichiometric amounts of $[Rh(acac)(P(p\text{-tolyl})_3)_2]$, only the weakly fluorescent 2,5-bis(arylethynyl)rhodacyclopentadiene isomer is formed.[59, 71] Intrigued by the finding of two different isomers while using $[Rh(acac)(PMe_3)_2]$, the α,ω-tetraynes were shortened by one triple bond per side, resulting in α,ω-diynes. Reacting these α,ω-diynes with $[Rh(acac)(PMe_3)_2]$ led to the formation of only one isomer, the weakly fluorescent 2,5-bis(aryl)rhodacyclopentadienes.[72]

So far, the only variation in the backbone of the α,ω-tetraynes was the linker length of three and four CH_2 groups. In order to investigate further the luminescent properties of the *para*-substituted 2,5-bis(aryl)rhodacyclopentadienes and the limits of the rhodacycle formation, various α,ω-diynes with different backbones were synthesized according to literature known methods and reacted with $[Rh(acac)(PMe_3)_2]$ and $[Rh(acac)(P(p\text{-tolyl})_3)_2]$ in equimolar amounts. The complexes obtained were purified and their photophysical behavior explored.

The reaction of α,ω-diynes with $[Rh(PPh_3)_3Cl]$ was previously reported by Müller in 1974. However, spectroscopic evidence is rare. The complexes were only described by their color and melting point. Solely for compound **3-IV** (Scheme 3-1) was it possible to carry out an X-ray diffraction analysis, confirming the trigonal bipyramidal rhodacyclopentadiene structure with *trans*-disposed tris(triphenyl)phosphine ligands. The Rh-C bond lengths are 2.006 and 2.002 Å, the Rh-P bond lengths are 2.38 and 2.40 Å, and the Rh-Cl bond length is 2.41 Å. Esd's are not

given in the publication,[121, 283] and the deposited cif file in the CCDC database (CCDC Number: 1223372) contains insufficient data.

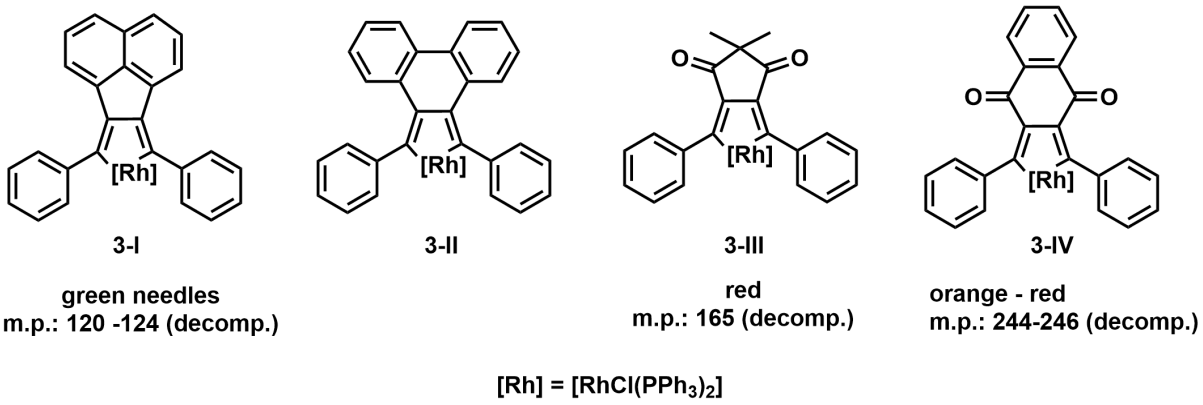

Scheme 3-1: Chemical structures of rhodacyclopentadienes **3-I** – **3-IV** synthesized by Müller in 1974.

3.3 Results and discussion

3.3.1 Synthesis of aryl-substituted α,ω-diynes

The compounds **3-1** and **3-3** (Scheme 3-2) were synthesized from methyl 4-ethynylbenzoate[284] and the diiodo species, 1,8-diiodonapthalene[285] and commercially available 1,2-diiodobenzene, in a Sonogashira cross-coupling reaction in 98 and 93% yields, respectively as colorless solids after purification. The compound 1,8-bis(4-(methylthio)phenyl)octa-1,7-diyne **3-4** was synthesized in 61% yield by a Sonogashira cross-coupling reaction of 4-iodothioanisole with octa-1,7-diyne. For compounds **3-2** and **3-5**, the diyne backbones dimethyl 2,2-di(prop-2-yn-1-yl)malonate and 3-(prop-2-yn-1-yloxy)prop-1-yne were first prepared according to modified literature procedures by reaction of dimethylmalonate with propargylbromide,[286] and propargylic alcohol with propargylbromide,[287] respectively, which were further reacted with methyl 4-iodobenzoate in Sonogashira cross-coupling reactions yielding 66% and 3%, respectively, of colorless solids after purification. The compounds were characterized by multinuclear NMR spectroscopy, HRMS, elemental analysis and, for **3-1**, additionally by single-crystal X-ray diffraction analysis. Scheme 3-2 shows the five α,ω-diynes with different backbones, which were synthesized.

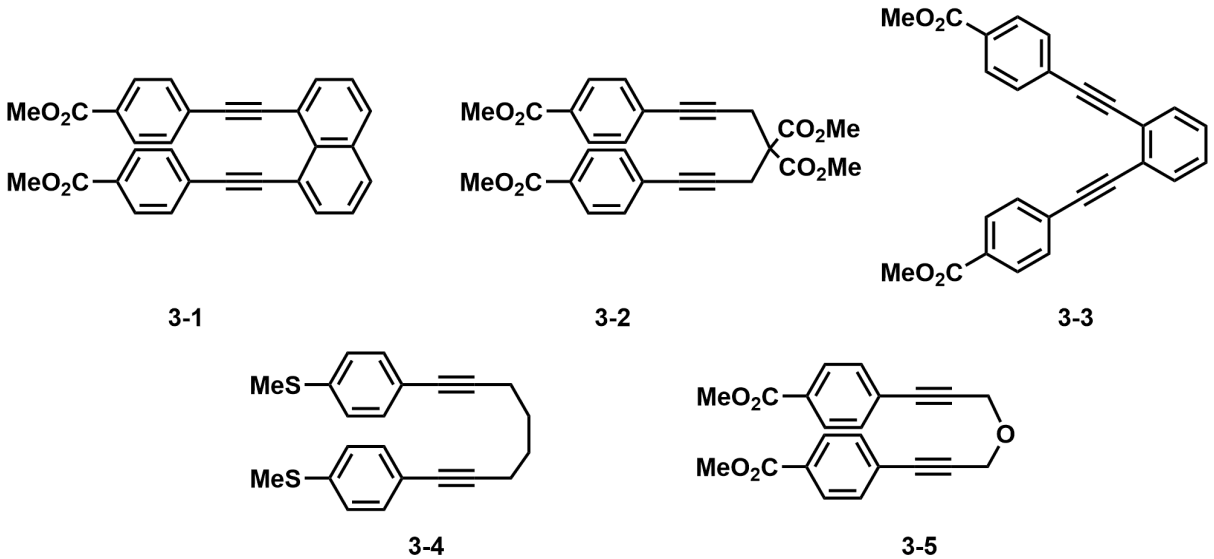

Scheme 3-2: Chemical structures of the α,ω-diynes dimethyl 4,4'-(naphthalene-1,8-diylbis(ethyne-2,1-diyl))dibenzoate **3-1**, dimethyl 2,2-bis(3-(4-(methoxycarbonyl)phenyl)prop-2-yn-1-yl)malonate **3-2**, dimethyl 4,4'-(1,2-phenylenebis(ethyne-2,1-diyl))dibenzoate **3-3**, 1,8-bis(4-(methylthio)phenyl)octa-1,7-diyne **3-4** and dimethyl 4,4'-(oxybis(prop-1-yne-3,1-diyl))dibenzoate **3-5**.

Single-crystals suitable for X-ray diffraction of **3-1** were obtained by diffusion of *n*-hexane into a solution of **3-1** in THF and the molecular structure is shown in Figure 3-1.

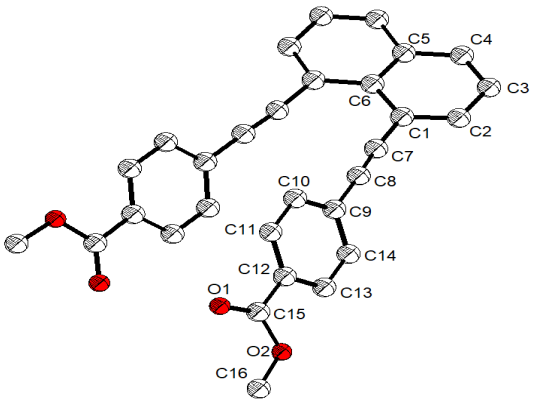

Figure 3-1: Molecular structure of *α,ω*-diyne **3-1** in the solid state determined by single-crystal X-ray diffraction with thermal ellipsoids drawn at the 50% probability level. Hydrogen atoms are omitted for clarity.

The molecule crystallized in the monoclinic space group *C*2/*c*, and the second half of the molecule is generated by symmetry. The C7-C8 bond length is 1.1968(18) Å, indicative of a triple bond. The C1-C7 and C8-C9 bond lengths are similar, being 1.4372(18) and 1.4355(18) Å, respectively. The bond lengths in the naphthalene backbone are in the range of 1.3603(18) Å for C3-C4 and 1.4367(15) Å for C1-C6. The *para*-CO_2Me-substituted aryl moiety (C9 – C14) is twisted out of the naphthalene-backbone plane (C1 – C6) by 52.05(4)°. The bond lengths for the *para*-substituted phenyl ring range between 1.3843(18) Å for C10-C11 and 1.4031(18) Å for C9-C10. All bond length are in the expected region.[208]

Compared to the w-shape of the *α,ω*-diynes[72] or *α,ω*-tetraynes[56, 68, 71] employed thus far in the Marder group (Figure 3-2), compounds **3-1**, **3-2**, **3-3** and **3-5** have a fixed u-shape, meaning that no reorganization for the rhodacycle formation during the [2+2+M] mechanism is necessary, hence the consumption of the rhodium(I) starting material and the formation of the rhodacyclopentadiene should proceed faster.

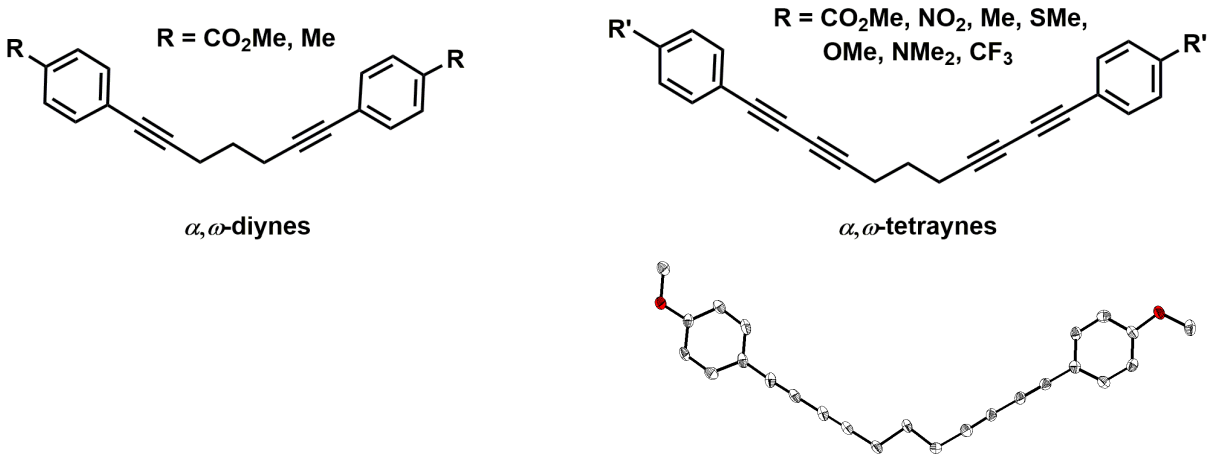

Figure 3-2: Typical w-shape of the *α,ω*-diynes and *α,ω*-tetraynes employed thus far in the Marder group, and the molecular structure of 1,11-bis(4-methoxyphenyl)undeca-1,3,8,10-tetrayne in the solid state determined by single-crystal X-ray diffraction with thermal ellipsoids drawn at the 50% probability level. Hydrogen atoms are omitted for clarity. The structure only serves as a proof of connectivity.

3.3.2 Reactions of [Rh(acac)(PMe$_3$)$_2$] with aryl-substituted α,ω-diynes

$^{31}P\{^1H\}$ NMR spectroscopic data for the reaction of [Rh(acac)(PMe$_3$)$_2$] **1-51** with the α,ω-diynes **3-1** and **3-2** in equimolar amounts at 60 °C for 24 hours (Scheme 3-3) revealed the formation of the desired 2,5-bis(aryl)rhodacyclopentadienes **3-6** and **3-7**. The complexes were purified by several washings with *n*-hexane and recrystallization from THF layered with *n*-hexane at -30 °C to give samples of very high purity for photophysical investigations in good isolated yields of 47 and 70%, respectively.

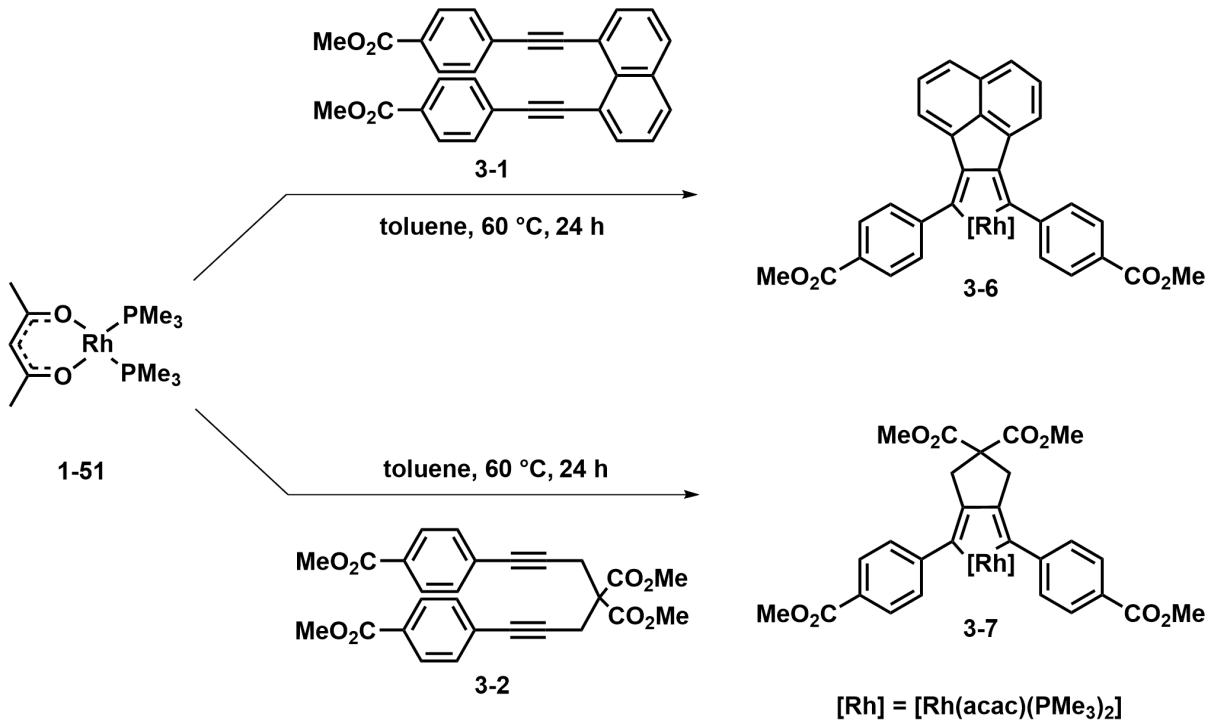

Scheme 3-3: Synthesis of 2,5-bis(aryl)rhodacyclopentadienes **3-6** and **3-7** *via* reaction of [Rh(acac)(PMe$_3$)$_2$)] **1-51** with α,ω-diynes **3-1** and **3-2**, respectively.

Inspection of the NMR spectroscopic data in C_6D_6 revealed the formation of a C_{2v} symmetric complex, as indicated by a single resonance for the acac-CH_3 group at 1.55 and 1.60 ppm as well as a single resonance for the CO_2Me groups, located at the aryl moiety, at 3.59 and 3.56 ppm integrating to six for **3-6** and **3-7**, respectively. Additionally, for complex **3-7**, there is only one singlet for the CO_2Me group located at the backbone at 3.33 ppm with an integral of six. A virtual triplet with an integral of 18 is observed for the two trimethylphosphine ligands at ca 0.77 ppm for both complexes. The single acac-CH group gives rise to a singlet at 4.88 and 4.95 ppm for **3-6** and **3-7**, respectively, integrating to one. For complex **3-6** five multiplets in the aromatic region from 8.36 – 7.18 ppm with a total number of 14 hydrogen atoms are observed and for **3-7** two multiplets at 8.26 and 7.62 ppm with a total number of eight hydrogen atoms are observed. In the $^{13}C\{^1H\}$ NMR spectra, the acac-CH groups resonate at ca. 90 ppm

for both complexes. In the $^{31}P\{^{1}H\}$ NMR spectra a doublet at -3.4 and -2.9 ppm for **3-6** and **3-7**, respectively, with a Rh-P coupling constant of 113 Hz for both complexes indicates a rhodium(III) species with *trans*-disposed trimethylphosphine ligands (see Chapter 2). Single-crystals suitable for X-ray diffraction analysis were obtained by diffusion of *n*-hexane into a solution of **3-6** in toluene and by diffusion of *n*-hexane into a solution of **3-7** in THF. Complex **3-6** crystallizes in the triclinic space group $P\bar{1}$ and **3-7** in the monoclinic space group $P2_1/c$. The molecular structures are shown in Figure 3-3 and selected bond lengths and angles are listed in Table 3-1.

The molecular geometries of the complexes **3-6** and **3-7** are very similar, the rhodium atom being in an octahedral environment with *trans*-disposed phosphine ligands. The acac-Rh bond distances range from 2.1218(16) – 2.1632(16) Å, with the Rh1-O1 bond length in **3-7** being 2.1632(16) Å and the other three Rh-O bonds being ca. 2.12 Å. The Rh-P bond distances range

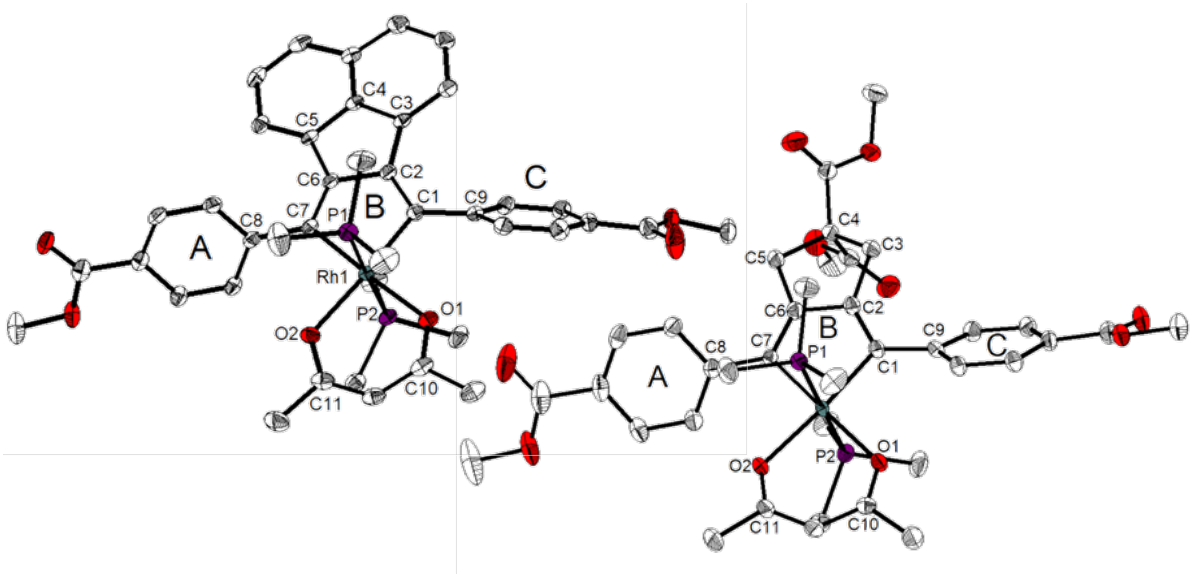

Figure 3-3: Molecular structure of 2,5-bis(aryl)rhodacyclopentadienes **3-6** (left) and **3-7** (right) in the solid state determined by single-crystal X-ray diffraction with thermal ellipsoids drawn at the 50% probability level. Hydrogen atoms are omitted for clarity.

from 2.2916(9) – 2.3297(7) Å and are therefore in agreement with similar rhodacyclopentadienes bearing trimethylphosphine ligands (ca. 2.306 Å).[56, 59, 71-72] In **3-6** and **3-7**, the C-Rh-C angle in the rhodacyclopentadiene moiety is ca. 82° and the O-Rh-O angle is ca. 88°. The other angles within the rhodacyclopentadiene-unit range from 111.90(15) – 117.32(19)°. The C-Rh-C angle is smaller than the expected 108° for a regular five-membered ring, while the other angles are larger. However, the sum of all angles within the rhodacyclopentadiene is 540° in both complexes.

The bond lengths and angles are similar to those of 2,5-bis(aryl)rhodacyclopentadienes **3-10** and **3-11** previously synthesized by Sieck (Scheme 3-4),[72] and only the rotation of the rings A

and C with respect to the rhodacyclopentadiene plane for complex **3-6** are larger than for the others (see Table 3-1). This likely result from the steric interactions between the aromatic C-H bonds of the naphthalene backbone and the aryl rings A and C.

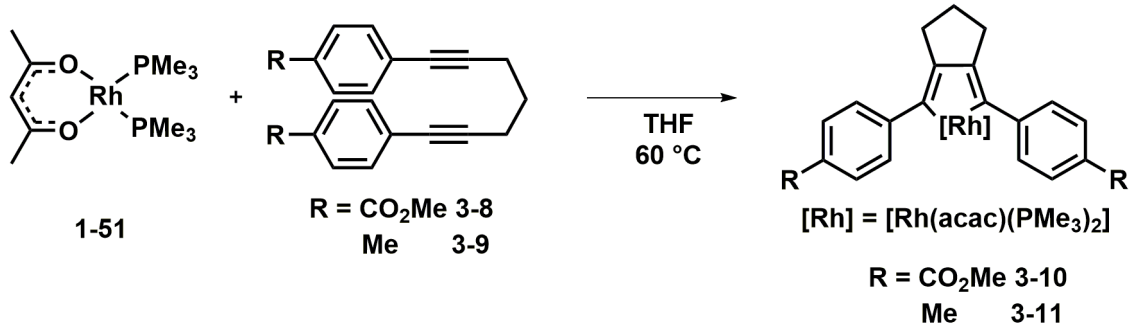

Scheme 3-4: 2,5-bis(aryl)rhodacyclopentadienes **3-10** and **3-11** previously reported by Sieck *via* reaction of [Rh(acac)(PMe_3)$_2$] **1-51** with α,ω-diynes **3-8** and **3-9**, respectively.[72]

Table 3-1: Selected bond lengths [Å] and angles [°] of 2,5-bis(aryl)rhodacyclopentadienes **3-6**, **3-7**, **3-10**[72] and **3-11**[72] determined by single-crystal X-ray diffraction at 100 K with esd's in parentheses.

	3-6	**3-7**	**3-10**	**3-11**
Rh1-O1	2.1250(15)	2.1632(16)	2.1428(13)	2.1458(19)
Rh1-O2	2.1274(15)	2.1218(16)	2.1492(12)	2.1443(19)
Rh1-P1	2.3120(9)	2.3231(9)	2.3140(9)	2.2983(8)
Rh1-P2	2.3297(9)	2.2916(9)	2.3036(8)	2.2966(8)
Rh1-C1	2.044(2)	2.035(2)	2.0474(15)	2.050(3)
Rh1-C7	2.038(2)	2.042(2)	2.0447(16)	2.045(3)
O1-C10	1.275(3)	1.260(3)	1.2659(19)	1.260(4)
O2-C11	1.274(2)	1.264(3)	1.2651(19)	1.259(4)
C1-C2	1.366(3)	1.355(3)	1.356(2)	1.346(4)
C2-C6	1.472(3)	1.441(3)	1.452(2)	1.454(4)
C6-C7	1.359(3)	1.351(3)	1.354(2)	1.352(4)
C7-C8	1.474(3)	1.472(3)	1.4778(19)	1.482(4)
C1-C9	1.480(3)	1.468(3)	1.4740(19)	1.482(4)
O1-Rh1-O2	89.26(6)	87.52(6)	87.24(4)	87.15(8)
C1-Rh1-C7	81.58(8)	81.69(8)	81.40(6)	81.56(11)
Rh1-C1-C2	113.34(15)	111.90(15)	112.5(1)	112.2(2)
C1-C2-C6	115.31(18)	117.32(19)	116.74(13)	117.1(3)
C2-C6-C7	116.71(18)	116.54(18)	116.62(13)	116.7(3)
C6-C7-Rh1	113.03(15)	112.27(14)	112.74(10)	112.4(2)
∡ A-B	60.24(7)	41.7(3)	45.5(1)	46.8(3)
∡ C-B	50.6(1)	42.2(3)	36.5(1)	38.0(4)

The "B"-plane is that of the rhodacyclopentadiene moiety.

Figure 3-4 shows selected *in-situ* $^{31}P\{^{1}H\}$ NMR spectra of the reaction of [Rh(acac)(PMe_3)$_2$] **1-51** with *α,ω*-diyne **3-1** in equimolar amounts at room temperature in C_6D_6 monitored over a period of seven days.

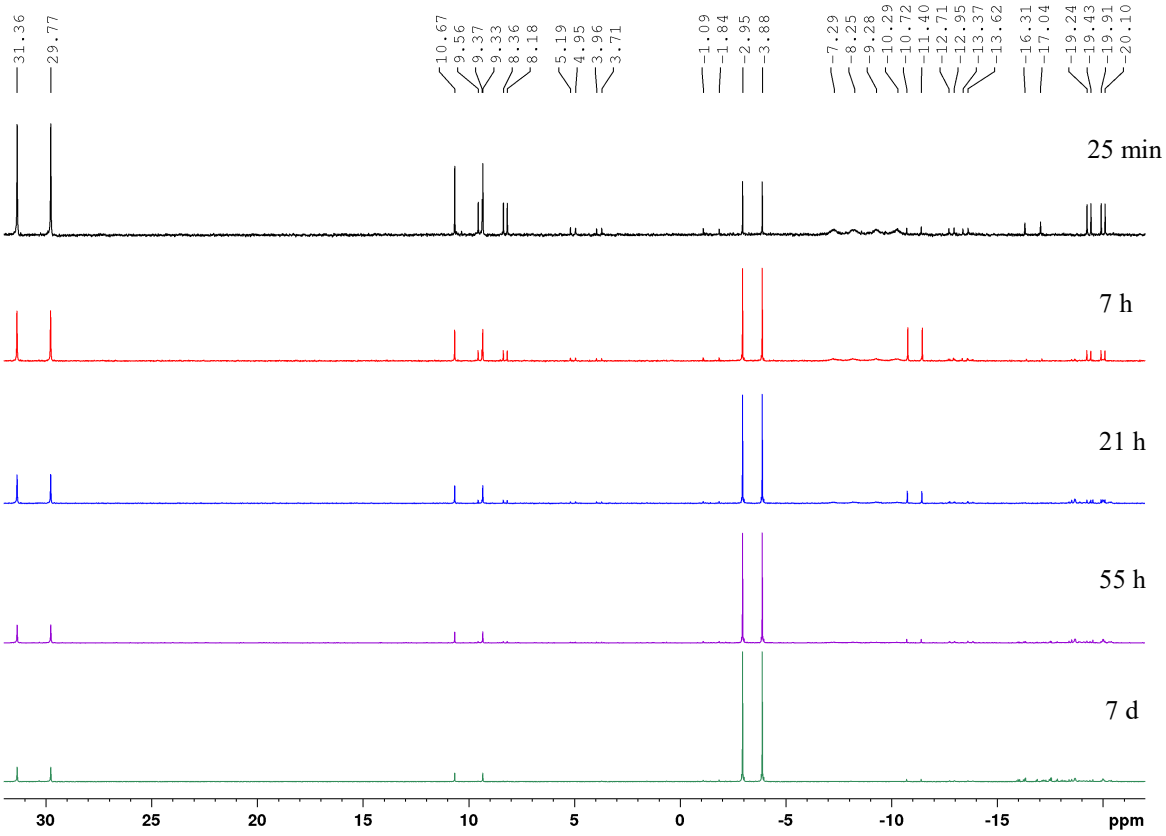

Figure 3-4: *In-situ* $^{31}P\{^{1}H\}$ NMR spectra (121 MHz, C_6D_6) of the reaction of [Rh(acac)(PMe_3)$_2$] **1-51** with *α,ω*-diyne **3-1** at room temperature after 25 minutes (black), 7 hours (red), 21 hours (blue), 55 hours (purple), 7 days (green).

The black spectrum shows ten signal sets of signals of significant intensity between 31 and -21 ppm as well as broad signals in the range of -7 – -11 ppm. A doublet at 30.6 ppm with a Rh-P coupling constant J = 193 Hz and a doublet at 10.0 ppm with J = 162 Hz indicate two rhodium(I) species. Two sets of two doublets of doublets are observed at 8.9 ppm ($^{1}J_{Rh\text{-}P}$ = 145 Hz, $^{2}J_{P\text{-}P}$ = 23 Hz) and -19.7 ppm ($^{1}J_{Rh\text{-}P}$ = 82 Hz, $^{2}J_{P\text{-}P}$ = 23 Hz), and at 4.5 ppm ($^{1}J_{Rh\text{-}P}$ = 150 Hz, $^{2}J_{P\text{-}P}$ = 30 Hz) and -13.2 ppm ($^{1}J_{Rh\text{-}P}$ = 80 Hz, $^{2}J_{P\text{-}P}$ = 30 Hz), indicating rhodium species with *cis*-disposed phosphine ligands. The three doublets at -1.5, -11.1 and -16.7 ppm with coupling constants of 91, 83 and 89 Hz, respectively, also represent rhodium(III) species. The doublet at -3.4 ppm with a Rh-P coupling constant of 113 Hz is assigned to the rhodacyclopentadiene **3-6**. Over time (black to green spectra), the intensities of all resonances diminish or even decrease, while the doublet for **3-6** grows in intensity. In the region of -16 – -20 ppm various, not yet identified, species begin to form (blue to green spectra).

In the work of Schwenk, similar coupling constants of 130 and 80 Hz (for $^{1}J_{Rh\text{-}P}$) were observed from the reaction of [Rh(S_2CNEt_2)(PMe_3)$_2$] **1-44** with dimethyl 4,4'-(undeca-1,3,8,10-tetrayne-1,11-diyl)dibenzoate **1-47d**.[68] These signals were attributed to different *cis*-π-complexes. Consistent with these finding, the reaction of [Rh(acac)(PMe_3)$_2$] **1-51** with *para*-substituted 1,4-diphenylbuta-1,3-diynes **2-1a**,**b** reveals the formation of two different *cis*-π-complexes **I$_{cis}$a** and **I$_{cis}$b** at -50 °C (Scheme 2-1). It was found, that the more downfield shifted phosphine is arranged *trans* to one of the acac oxygen atoms, while the second phosphine atom is *trans* to a carbon atom. Furthermore, it was found that the phosphine of the main isomer has a Rh-C-C≡C-Ar unit *trans* to it as its electronegativity is larger.[206] Based on these observations, the *cis*-π-complexes **3-I$_{cis}$a** and **3-I$_{cis}$b** can be postulated (Scheme 3-5), resulting from the reaction depicted in Scheme 3-3 (top). Assuming that the methyl benzoate-substituted carbon atom has a lower *trans*-influence, the major set of doublet of doublets at 8.9 and -19.7 ppm correspond to **3-I$_{cis}$a**, while the minor set of doublet of doublets at 4.5 and -13.2 ppm correspond to **3-I$_{cis}$b**. Generally, for each *cis*-complexes two different orientations are possible: "outside" and "inside" to the α,ω-diyne. The "inside" orientations would lead to rhodacyclopentadiene formation, while the "outside" formation does not. In the $^{31}P\{^{1}H\}$ NMR spectra, likely the "outside"-complexes are visible, and the inside not, as the "inside"-complexes react very fast to the rhodacyclopentadiene **3-6**.

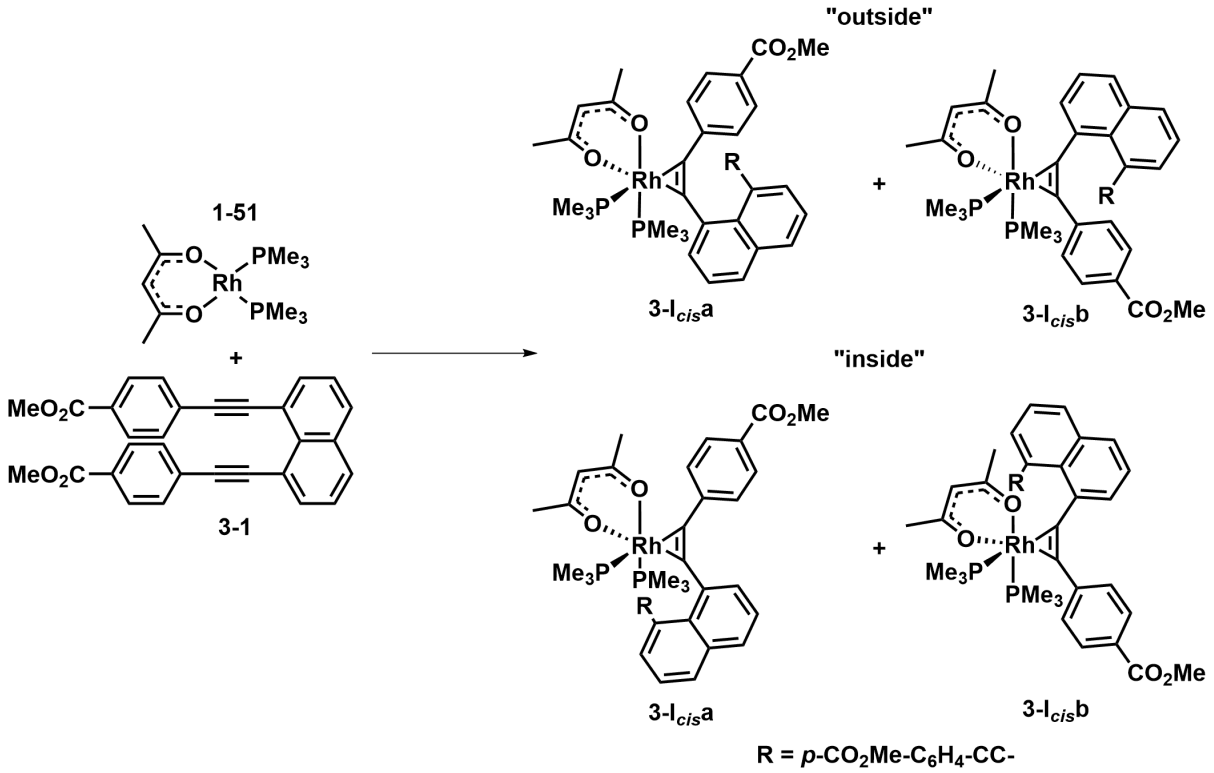

Scheme 3-5: Proposed α,ω-diyne *cis*-π-complexes **3-I$_{cis}$a** and **3-I$_{cis}$b** for the "outside" and "inside" orientation.

In each of the two possible orientations for the π-complexes, one phosphine ligand lies in the equatorial plane, whereas the other occupies an axial position and one oxygen atom of the acetylacetonato ligand lies in the equatorial plane, while the other oxygen atom occupies the axial position.

Signals for a *trans*-π-complex, indicated by a doublet close to the rhodacycle **3-6** and a similar Rh-P coupling constant as **3-6**, are not observable using **3-1** as they were in the work of Schwenk[68] and Sieh.[206]

The reaction of [Rh(acac)(PMe_3)$_2$] **1-51** with α,ω-diyne **3-1** results in a complete consumption of the rhodium(I) starting material within 25 minutes and, at the same time, in the formation of various signals of high intensity, which diminish after seven days at room temperature to a major part, forming the 2,5-bis(aryl)rhodacyclopentadiene **3-6**.

Figure 3-5 shows selected *in-situ* $^{31}P\{^1H\}$ NMR spectra of the reaction of [Rh(acac)(PMe_3)$_2$] **1-51** with α,ω-diyne **3-8** in equimolar amounts at room temperature in C_6D_6 (Scheme3-6).

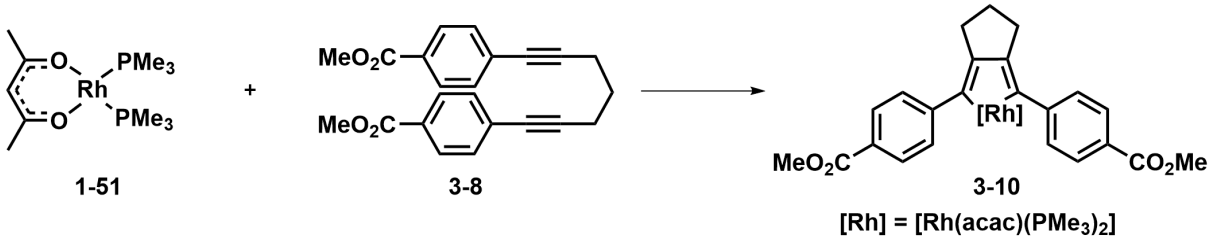

Scheme 3-6: Reaction of [Rh(acac)(PMe_3)$_2$] **1-51** with α,ω-diyne **3-8**.

In the black spectrum (reaction after 24 hours), a doublet at -3.6 ppm with a Rh-P coupling constant of J = 115 Hz, indicates the formation of the rhodacyclopentadiene **3-10**. A broad signal, indicating a dynamic process, e.g. diyne coordination and/or decoordination, from ca. 9 - 5 ppm is observed for the starting material [Rh(acac)(PMe_3)$_2$] **1-51**. Four additional weak intensity doublets, at 31.4 ($^1J_{Rh\text{-}P}$ = 198 Hz), 13.0 ($^1J_{Rh\text{-}P}$ = 167 Hz), 12.9 ($^1J_{Rh\text{-}P}$ = 134 Hz) and at -2.5 ppm ($^1J_{Rh\text{-}P}$ = 115 Hz) are visible. The red spectrum (after seven days) displays one additional doublet at 14.1 ppm ($^1J_{Rh\text{-}P}$ = 136 Hz). The broad signal for the starting material diminished in intensity, but is still present.

The signals at 31.4, 13.0, 12.9 (black spectrum) and 14.1 ppm (red spectrum) with large Rh-P coupling constants of 134 – 198 Hz represent rhodium(I) species, while the doublet at -2.5 ppm, close to the product signal, with a Rh-P coupling constant of 115 Hz represents a rhodium(III) species.

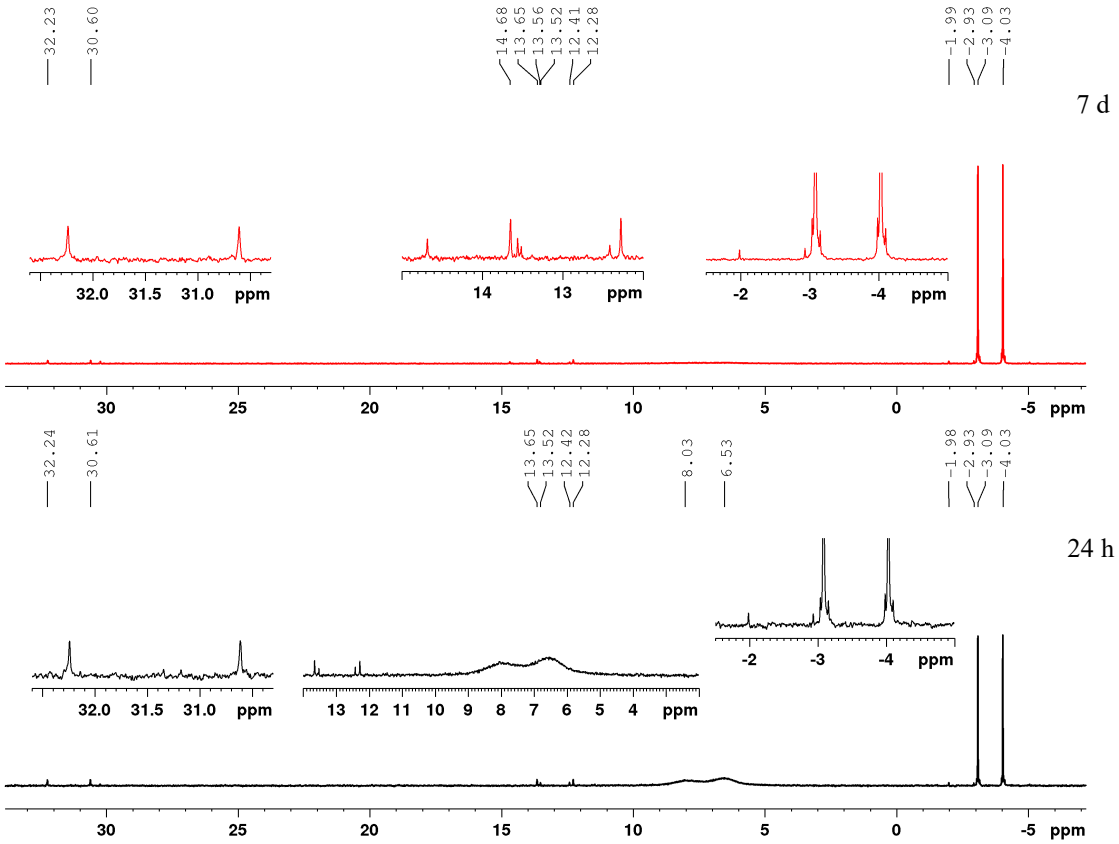

Figure 3-5: *In-situ* $^{31}P\{^{1}H\}$ NMR spectra (121 MHz, C_6D_6) of the reaction of [Rh(acac)(PMe_3)$_2$] **1-51** with α,ω-diyne **3-8** at room temperature after 24 hours (black) and 7 days (red).

Figure 3-6 shows selected *in-situ* $^{31}P\{^{1}H\}$ NMR spectra of the reaction of [Rh(acac)(PMe_3)$_2$] **1-51** with α,ω-diyne **3-2** in equimolar amounts at room temperature in C_6D_6 (Scheme 3-7).

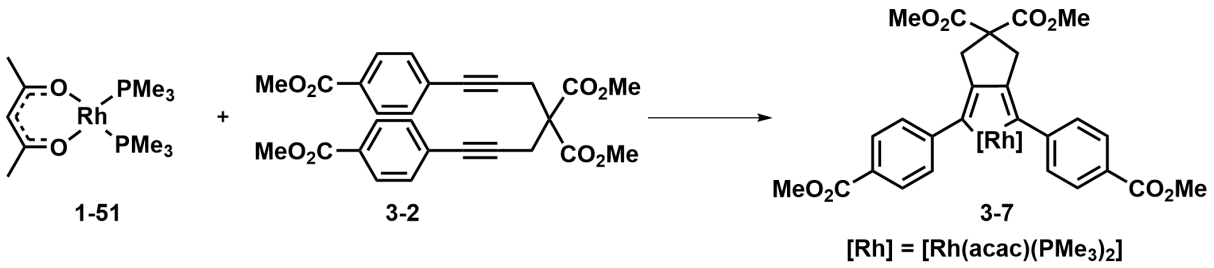

Scheme 3-7: Reaction of [Rh(acac)(PMe_3)$_2$] **1-51** with α,ω-diyne **3-2**.

In the black spectrum (reaction after 24 hours), a doublet at -2.9 ppm with a Rh-P coupling constant J = 113 Hz, indicates the formation of the rhodacyclopentadiene **3-7**. A broad signal from ca. 9 – 5 ppm represents the starting material. Four weak intensity doublets, at 33.5 ($^{1}J_{Rh\text{-}P}$ = 199 Hz), 14.1 ($^{1}J_{Rh\text{-}P}$ = 136 Hz), 13.9 ($^{1}J_{Rh\text{-}P}$ = 139 Hz) and 13.0 ppm ($^{1}J_{Rh\text{-}P}$ = 164 Hz) are visible, and a doublet of doublets at 11.2 ppm ($^{1}J_{Rh\text{-}P}$ = 128 Hz, $^{2}J_{P\text{-}P}$ = 18 Hz) and a doublet of triplets at -22.6 ppm ($^{1}J_{Rh\text{-}P}$ = 72 Hz, $^{2}J_{P\text{-}P}$ = 18 Hz). The red spectrum (reaction after seven days) shows an additional doublet at 14.1 ($^{1}J_{Rh\text{-}P}$ = 139 Hz) as well as four doublets close to the

product signal at -2.4 ($^1J_{Rh-P}$ = 115 Hz), -3.4 ($^1J_{Rh-P}$ = 115 Hz), -5.7 ($^1J_{Rh-P}$ = 116 Hz) and -7.9 ppm ($^1J_{Rh-P}$ = 107 Hz). The broad signal for the starting material is no longer visible.

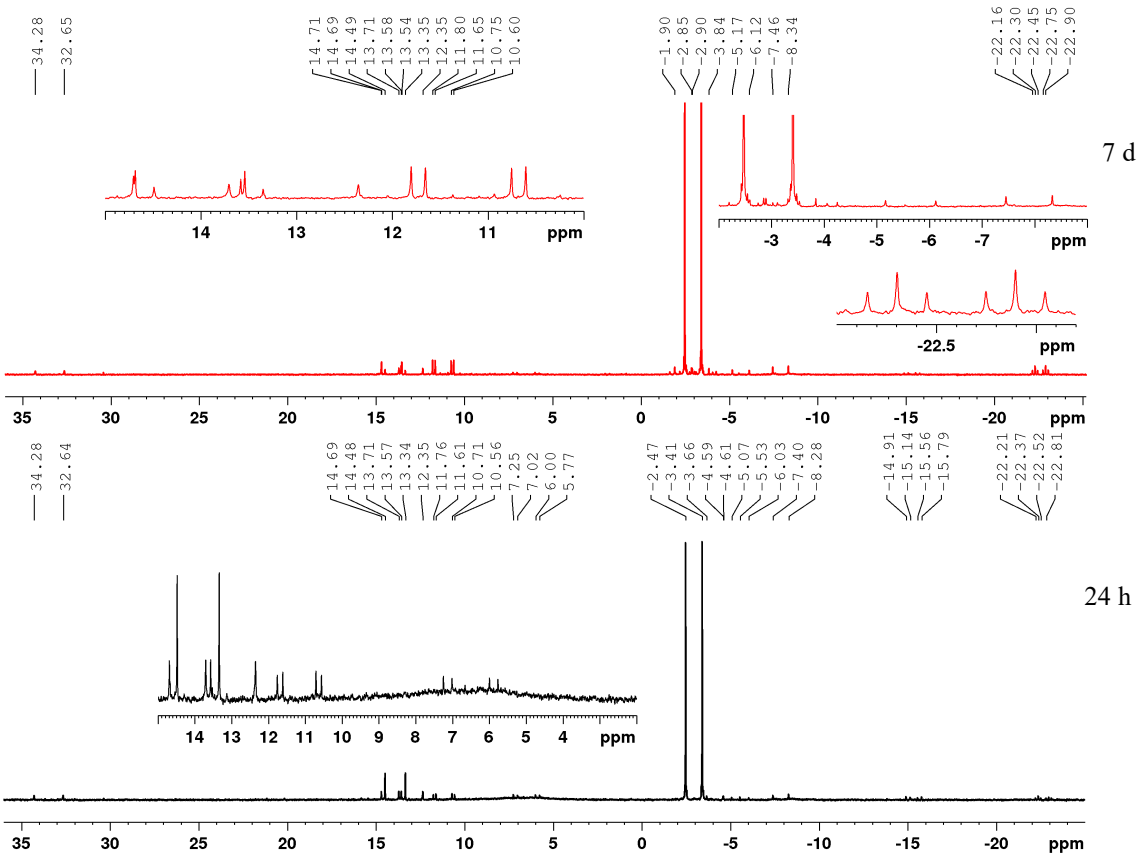

Figure 3-6: *In-situ* $^{31}P\{^1H\}$ NMR spectra (121 MHz, C_6D_6) of the reaction of [Rh(acac)(PMe_3)$_2$] **1-51** with *α,ω*-diyne **3-2** at room temperature after 24 hours (black) and 7 days (red).

The signals at 33.5, 14.1, 13.9 and 13.0 ppm with Rh-P coupling constants of 136 – 199 Hz represent rhodium(I) species, while the doublets in the range of -2 – -8 ppm with Rh-P coupling constants of ca. 115 Hz represent rhodium(III) species. The doublet of doublets and the doublet of triplets results from a single species, in which three phosphine ligands are attached to one rhodium(I) species, two equivalent phosphines giving rise to the doublet of doublets and a unique phosphine ligand resulting in the doublet of triplets.

In the reactions of [Rh(acac)(PMe_3)$_2$] **1-51** with *α,ω*-diynes **3-8** and **3-2** doublets at 31.4 and 33.5 ppm with $^1J_{Rh-P}$ = 198 and 199 Hz are visible as well as doublets at ca. 13.0 ppm with $^1J_{Rh-P}$ = 130 – 170 Hz. Two doublets occur in both spectra, the first at 14.1 ppm ($^1J_{Rh-P}$ = 136 and 139 Hz) and a second at 13.0 ppm ($^1J_{Rh-P}$ = 167 and 164 Hz), indicating, in both cases, two very similar rhodium-phosphine complexes. Doublets close to the product signal, with similar coupling constants to that in the product, which might represent a *trans*-phosphine-complex, are also present in both reactions.

The reaction of [Rh(acac)(PMe_3)$_2$] **1-51** with α,ω-diyne **3-2** results in a complete consumption of rhodium(I) starting material **1-51** after seven days, however, when α,ω-diyne **3-8** was used, **1-51** was still present (~30%) after seven days. This difference likely results from the electron withdrawing effect of the CO_2Me groups attached to the backbone and/or on the fixed u-shape of the α,ω-diyne.

In the reaction of [Rh(acac)(PMe_3)$_2$] **1-51** with α,ω-diyne **3-1** a doublet is visible at 30.6 ppm with $^1J_{Rh\text{-}P}$ = 193 Hz, among other signals. A similar resonance was also observed in the reactions of **1-51** with α,ω-diynes **3-2** and **3-8**.

Comparing the reactions of [Rh(acac)(PMe_3)$_2$] **1-51** with α,ω-diynes **3-1**, **3-2** and **3-8** indicates that the preorganization of the α,ω-diyne enhances the rate of consumption of the rhodium(I) starting material. Interestingly, in the reaction of [Rh(acac)(PMe_3)$_2$] **1-51** with α,ω-diyne **3-1**, the rhodium(I) starting material is completely consumed within 25 minutes, while for α,ω-diyne **3-2** this takes seven days, during which it is visible as a broad doublet. Using the preorganized α,ω-diyne **3-2** results in the observation of more species in the $^{31}P\{^1H\}$ NMR spectra at room temperature, meaning that more intermediates and/or byproducts are stable.

A doublet at ca. 30 ppm ($^1J_{Rh\text{-}P}$ ~ 195 Hz) is visible in all three reactions. Reaction of [Rh(acac)(PMe_3)$_2$] **1-51** with α,ω-diynes **3-8** and **3-2** results in the appearance of doublets at 14.1 and 13.0 ppm with rhodium-phosphorus coupling constants of ca. 140 and 165 Hz, respectively, in both reactions. Using α,ω-diyne **3-1**, two sets of signals each representing a *cis*-π-complex are visible but no *trans*-π-complexes are observed, but for α,ω-diynes **3-2** and **3-8** the opposite is observed.

Figure 3-7 displays *in-situ* $^{31}P\{^{1}H\}$ NMR spectra of the three reactions described above at room temperature for seven days with further heating at 60 °C for 24 hours. For the reaction of [Rh(acac)(PMe_3)$_2$] **1-51** with *α,ω*-diynes **3-1** and **3-8**, this results in complete conversion of all species to the rhodacyclopentadienes **3-6** (blue spectrum) and **3-10** (red spectrum). The black spectrum shows the reaction of [Rh(acac)(PMe_3)$_2$] **1-51** with *α,ω*-diyne **3-2**. The doublet of doublets and doublet of triplets disappear, but signals at ca. 15 and -3 ppm are still present.

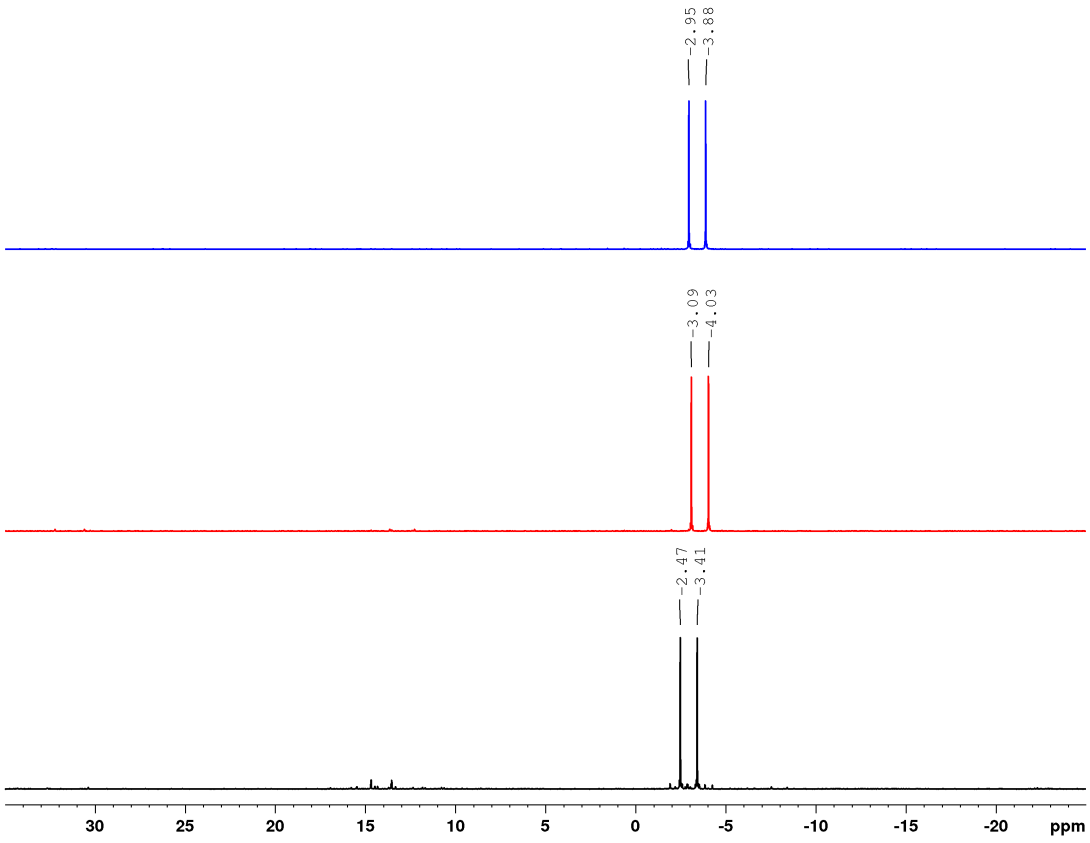

Figure 3-7: *In-situ* $^{31}P\{^{1}H\}$ NMR spectra (121 MHz, C_6D_6) of the reactions of [Rh(acac)(PMe_3)$_2$] **1-51** with *α,ω*-diynes **3-1** (blue), **3-2** (black) and **3-8** (red) at room temperature for 7 days and at 60 °C for 24 hours.

In the reactions of [Rh(acac)(PMe_3)$_2$] **1-51** with the two *α,ω*-diynes **3-1** and **3-8**, after heating, complete conversion of all intermediates/byproducts to the rhodacyclopentadienes **3-6** and **3-10** was observed. However, for the reaction with **3-2**, more side products are observed, even after heating, indicating a less selective reaction.

According to $^{31}P\{^{1}H\}$ NMR spectroscopy, the reaction of [Rh(acac)(PMe_3)$_2$] **1-51** with α,ω-diyne **3-4** in equimolar amounts in C_6D_6 (Scheme 3-8) does not result in rhodacycle formation nor the formation of any other species after four days at room temperature (Figure 3-8). However, heating the reaction mixture at 60 °C for seven days in C_6D_6 results in the appearance of a doublet at 28.1 ppm with a Rh-P coupling constant of 196 Hz, indicative of a rhodium(I) species, and two small doublets at -4.2 and -5.4 ppm with $^{1}J_{Rh\text{-}P}$ of 118 and 106 Hz (blue spectrum).

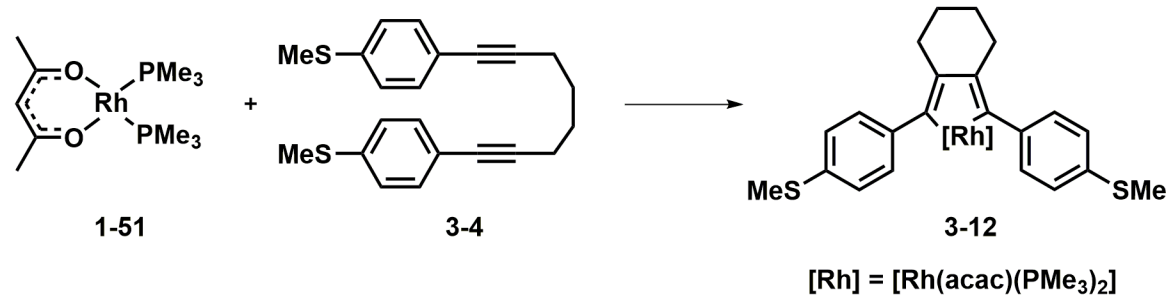

Scheme 3-8: Reaction of [Rh(acac)(PMe_3)$_2$] **1-51** with α,ω-diyne **3-4**.

The doublet at -4.2 ppm with $^{1}J_{Rh\text{-}P}$ = 118 Hz could represent the desired rhodacyclopentadiene **3-12**. A resonance similar to the doublet at 28.1 ppm with $^{1}J_{Rh\text{-}P}$ = 196 Hz was also observed in the reactions previously mentioned in this section.

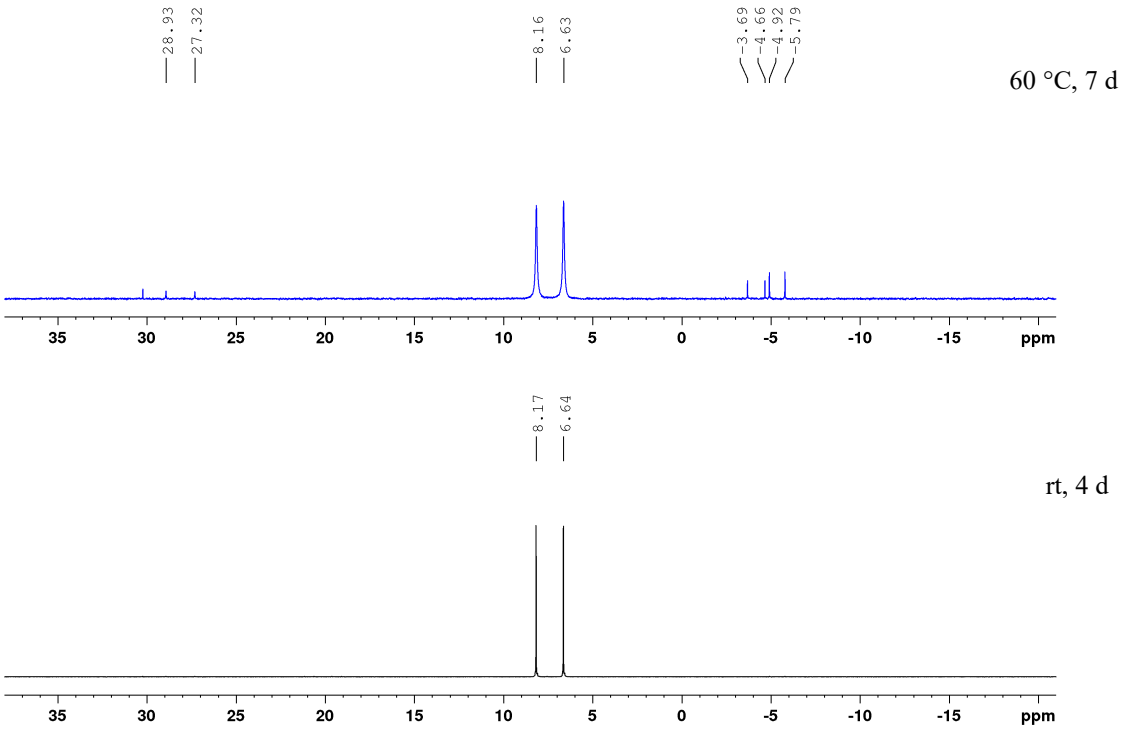

Figure 3-8: *In-situ* $^{31}P\{^{1}H\}$ NMR spectra (121 MHz, C_6D_6) of the reaction of [Rh(acac)(PMe_3)$_2$] **1-51** with α,ω-diyne **3-4** at room temperature after 4 days (black) and at 60 °C for 7 days (blue).

This behavior was not expected, as the reaction of different rhodium(I) precursors with *para*-SMe-substituted 1,12-diphenyldodeca-1,3,9,11-tetrayne **1-43b** usually forms the expected rhodacycles.[58-59, 70] In addition, the reaction of [Rh(acac)(PMe_3)$_2$] **1-51** with α,ω-diyne **3-9** forms rhodacyclopentadiene **3-11** (Scheme 3-4),[72] suggesting that the donor-group is not responsible for this behavior, but the increased chain lengths from three to four CH_2 groups is. It is known that donor-substituted α,ω-diynes, α,ω-tetraynes [68, 72] as well as *para*-donor-substituted 1,4-diphenylbuta-1,3-diynes react more slowly with a low valent rhodium(I) precursor at ambient temperature.[206] Therefore, heating is required due to the electron rich triple bond.

Following the reaction of [Rh(acac)(PMe_3)$_2$] **1-51** with α,ω-diyne **3-5** (Scheme 3-9) in equimolar amounts in C_6D_6 by $^{31}P\{^1H\}$ NMR spectroscopy, shows, after one hour (Figure 3-9, black spectrum) doublets at 12.6 ($^1J_{Rh\text{-}P}$ = 164 Hz) and -3.4 ppm ($^1J_{Rh\text{-}P}$ = 113 Hz) and two doublets of doublets at 5.9 ppm ($^1J_{Rh\text{-}P}$ = 151 Hz, $^2J_{P\text{-}P}$ = 28 Hz) and -15.6 ppm ($^1J_{Rh\text{-}P}$ = 78 Hz, $^2J_{P\text{-}P}$ = 28 Hz). Two broad signals, the first around 7.8 ppm and a second at -8.4 ppm, are also visible.

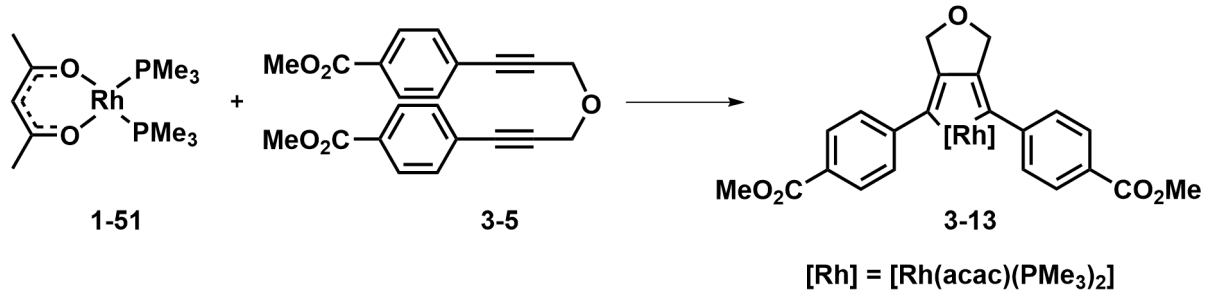

Scheme 3-9: Reaction of [Rh(acac)(PMe_3)$_2$] **1-51** with α,ω-diyne **3-5**.

Close to the doublet at -3.4 ppm, which represents complex **3-13**, smaller signals at -1.8, -2.1 and -2.6 are also visible, likely, a doublet of doublets (one signal is overlapping with the signal at -2.9 ppm) with $^1J_{Rh\text{-}P}$ = 99 Hz and $^2J_{P\text{-}P}$ = 40 Hz. A corresponding second set cannot be identified in the spectrum. After 24 hours (blue spectrum), the two broad signals decrease in intensity and the doublet at -3.4 ppm grows in intensity. The broad signal at 7.8 ppm disappears within 48 hours, and by that time, the doublet of doublets at ca. 2 ppm also disappears (red spectrum). No visible change was observed by NMR spectroscopy over the following five days at room temperature. Heating the reaction mixture at 60 °C for 24 hours did not result in a visible change in the NMR spectrum. Further heating for 48 hours resulted in a slow decrease of the intensity of the broad signal at -8.4 ppm.

The rhodium(I) starting material [Rh(acac)(PMe$_3$)$_2$] **1-51** was consumed at room temperature within two days in the reaction with the preorganized α,ω-diyne **3-5** and a doublet appeared at 12.6 ppm ($^1J_{Rh-P}$ = 164 Hz). A similar resonance is also present in the reactions of **1-51** with α,ω-diynes **3-2** (13.0 ppm, $^1J_{Rh-P}$ = 164 Hz) and **3-8** (13.0 ppm, $^1J_{Rh-P}$ = 167 Hz). Several additional species formed, which only diminish very slow, even at elevated temperature.

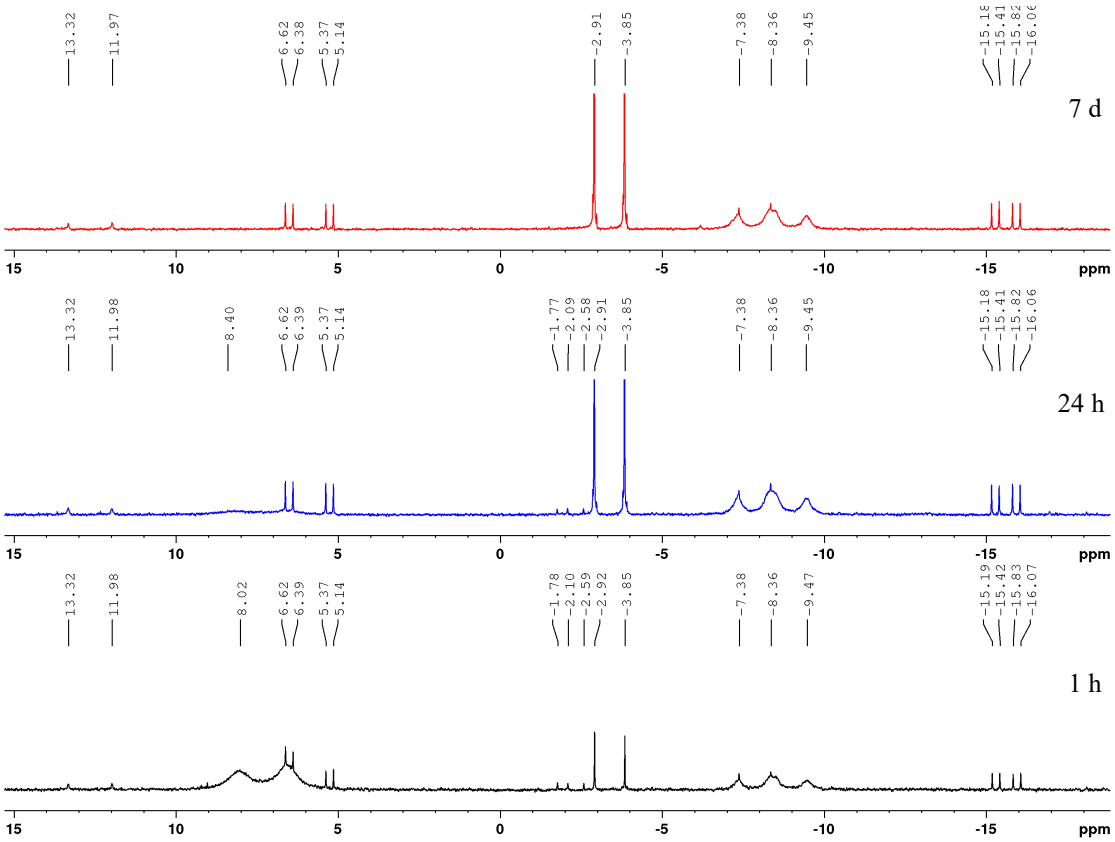

Figure 3-9: *In-situ* $^{31}P\{^1H\}$ NMR spectra (121 MHz, C_6D_6) of the reaction of [Rh(acac)(PMe$_3$)$_2$] **1-51** with α,ω-diyne **3-5** at room temperature after 1 hour (black), 24 hours (blue) and 7 days (red).

According to $^{31}P\{^1H\}$ NMR spectroscopy, the reaction of [Rh(acac)(PMe$_3$)$_2$] **1-51** with α,ω-diyne **3-3** (Scheme 3-10) in equimolar amounts at room temperature in C_6D_6 yields, in small amounts, only a species at -3.9 ppm with a ^{103}Rh-^{31}P coupling constant of 115 Hz, likely representing **3-14**. This is consistent with the data obtained for octahedral 2,5-bis(aryl)rhodacyclopentadienes **3-6** and **3-7** and those reported by Sieck ($^1J_{Rh-P}$ = 119 Hz for **3-10** and $^1J_{Rh-P}$ = 115 Hz for **3-11**).[72]

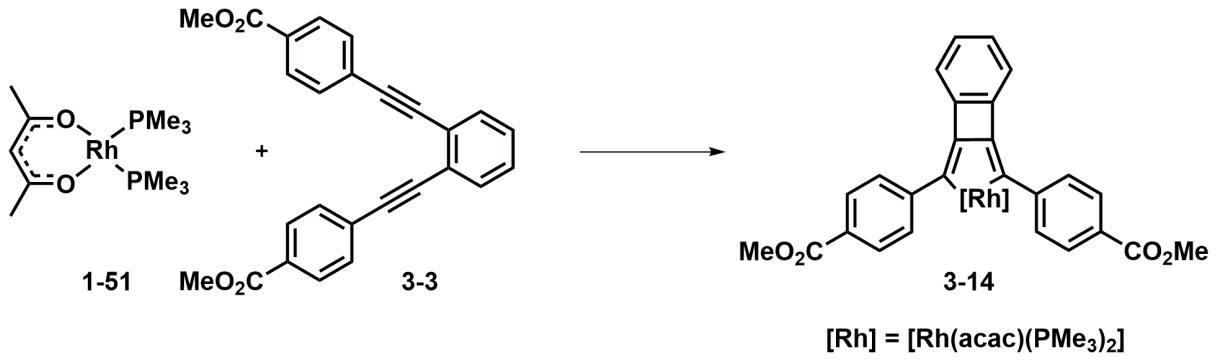

Scheme 3-10: Reaction of [Rh(acac)(PMe$_3$)$_2$] **1-51** with α,ω-diyne **3-3**.

Over a time span of seven days at room temperature, a new species starts to form, which gives rise to a doublet at 14.1 ppm with a ^{103}Rh-^{31}P coupling constant of 136 Hz (Figure 3-10, black spectrum). Heating the reaction mixture at 60 °C for 24 hours results in an additional doublet at 13.6 ppm with $^{1}J_{\text{Rh-P}}$ = 140 Hz. However, a high resolution mass spectrum indicated the presence of a species with the formula [Rh(acac)(PMe$_3$)$_2$(3-3)] and [Rh(acac)(PMe$_3$)(3-3)]. Further heating at 60 °C for eleven days resulted in the appearance of three new doublets at 13.7, 15.6 and 15.9 ppm with Rh-P coupling constants of 140, 137 and 141 Hz, respectively, while heating, the signal for the doublet at -3.9 ppm decreased in intensity and the doublet at 13.6 ppm grew in intensity.

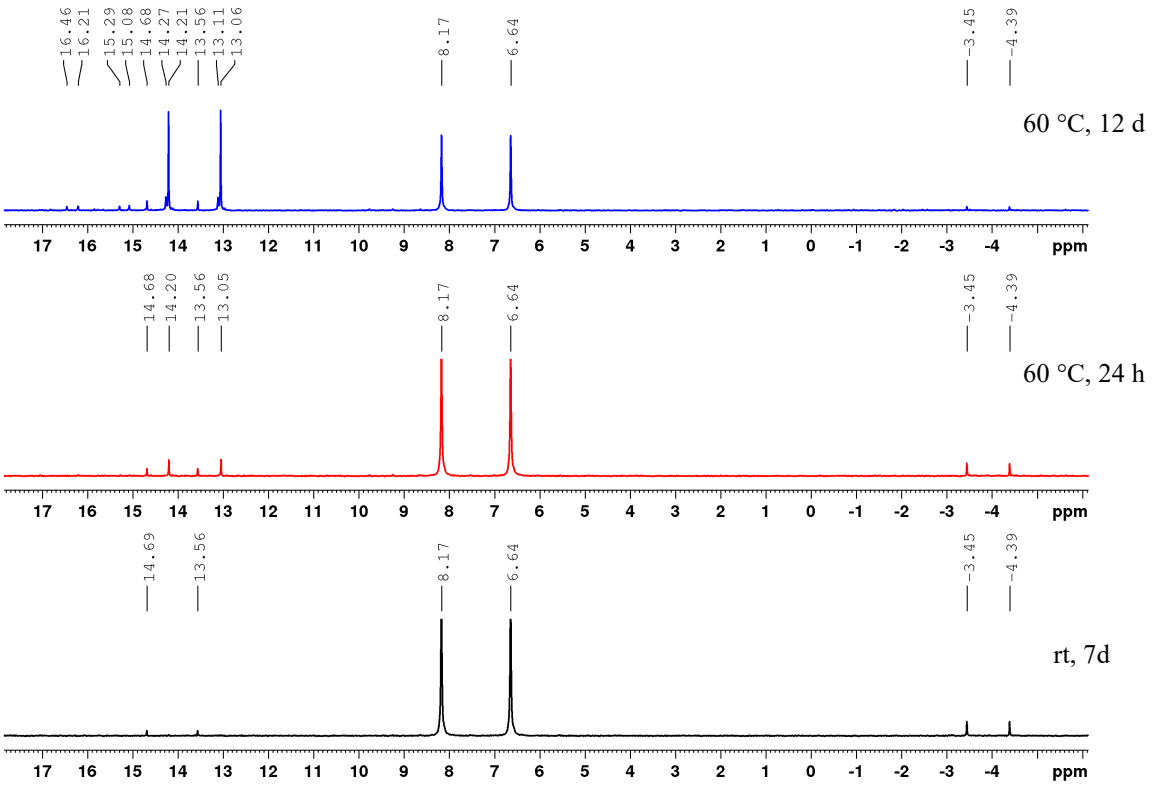

Figure 3-10: *In-situ* ^{31}P{^{1}H} NMR spectra (162 MHz, C_6D_6) of the reaction of [Rh(acac)(PMe$_3$)$_2$] **1-51** with α,ω-diyne **3-3** at room temperature after 7 days (black), at 60 °C for 24 hours (red) and at 60 °C for 12 days (blue).

Heating the reaction at 60 °C for several days did not result in the formation of larger amounts of the desired rhodacyclopentadiene **3-14**, but several species formed with coupling constants indicative of rhodium(I) complexes, and the signal for what is assumed to be **3-14** diminished. Similar coupling constants to those observed for signals in the 13.6 – 15.9 ppm region with $^{1}J_{Rh\text{-}P}$ = 140 Hz were also observed in the reactions of [Rh(acac)(PMe_3)$_2$] **1-51** with α,ω-diynes **3-2** and **3-8**.

While it was possible to isolate the 2,5-bis(aryl)rhodacyclopentadienes **3-6**, **3-7**, **3-10** and **3-11** the isolation of **3-12**, **3-13** and **3-14** was not possible, due to its low yield and the presence of various other rhodium-phosphine complexes. However, the formation of cyclic six-membered[58-59] and five-membered rhodacycles with heterocyclic-backbone was already described in the literature.[121]

Inspection of the core structure of rhodacyclopentadiene **3-14** shows a strained four-membered ring, flanked by benzene and the rhodacyclopentadiene moiety. Due to the strained double bonds, this rhodacyclopentadiene does not seem to be stable under the conditions employed. In addition, similar, pure organic analogues such as 2*H*-cyclopenta-3,4-cyclobuta-1,2-bezenes, have not been reported. On the other hand, replacing the carbon at position 1 with sulfur results in stable benzo-3,4-cyclobutathiophenes.[288-289] Other, related polycyclic hydrocarbons, such as biphenylene, are well known (Scheme 3-11).[290-296]

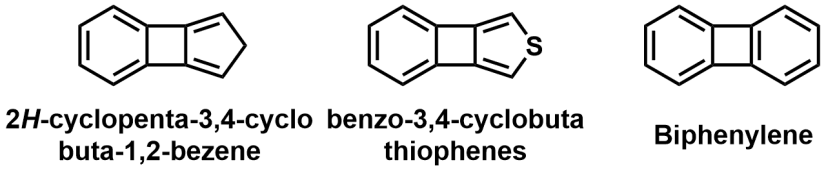

Scheme 3-11: Strained polycyclic aromatic compounds related to rhodacycle **3-14**.

3.3.3 Reactions of [Rh(acac)(P(*p*-tolyl)$_3$)$_2$] with aryl-substituted α,ω-diynes

The reaction in a 1:1 ratio of [Rh(acac)(P(*p*-tolyl)$_3$)$_2$] **1-56** with different aryl-substituted α,ω-diynes will be described in this section. Generally, using a bulkier phosphine ligand, namely tri(*p*-tolyl)phosphine, in place of the smaller trimethylphosphine ligand gave different outcomes of the reaction. The complex [Rh(acac)(P(*p*-tolyl)$_3$)$_2$] **1-56** is known to be a catalyst for the cycloisomerization of α,ω-diynes and α,ω-tetraynes.[68, 72] However, the catalytic reaction itself, in which dimer and trimer of the organic starting material were obtained, will be discussed in more detail in section 4.3.2.

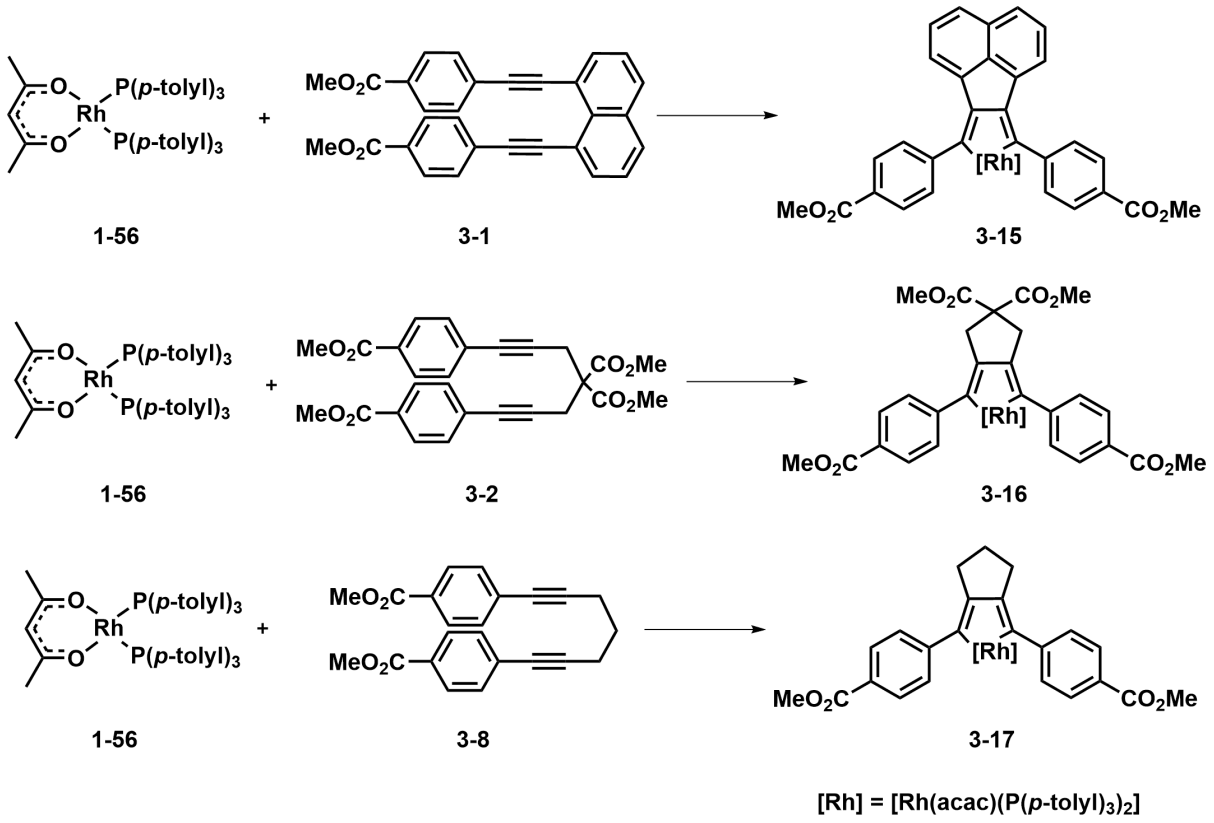

Scheme 3-12: Reaction of [Rh(acac)(P(*p*-tolyl)$_3$)$_2$] **1-56** with α,ω-diynes **3-1**, **3-2** and **3-8**, respectively.

According to $^{31}P\{^1H\}$ NMR spectroscopy, reactions of [Rh(acac)(P(*p*-tolyl)$_3$)$_2$] **1-56** with α,ω-diynes **3-1**, **3-2** and **3-8** (Scheme 3-12) at room temperature in C_6D_6 for 56 hours result in different outcomes (Figure 3-11). In the reaction of **1-56** with α,ω-diyne **3-1**, two doublets at 54.8 ($^1J_{Rh\text{-}P}$ = 195 Hz) and 19.8 ppm ($^1J_{Rh\text{-}P}$ = 117 Hz) are visible (black spectrum). The reaction of **1-56** with α,ω-diyne **3-2** led to doublets at 54.8 ($^1J_{Rh\text{-}P}$ = 195 Hz), 31.2 ($^1J_{Rh\text{-}P}$ = 170 Hz) and 18.6 ppm ($^1J_{Rh\text{-}P}$ = 118 Hz) as well as a singlet at -7.8 ppm (blue spectrum). Similarly, the reaction of **1-56** with α,ω-diyne **3-8** shows the same number of signals, i.e., doublets at 54.8 ($^1J_{Rh\text{-}P}$ = 195 Hz), 31.4 ($^1J_{Rh\text{-}P}$ = 173 Hz) and 25.4 ppm ($^1J_{Rh\text{-}P}$ = 120 Hz) as well as a singlet at -7.8 ppm (red spectrum).

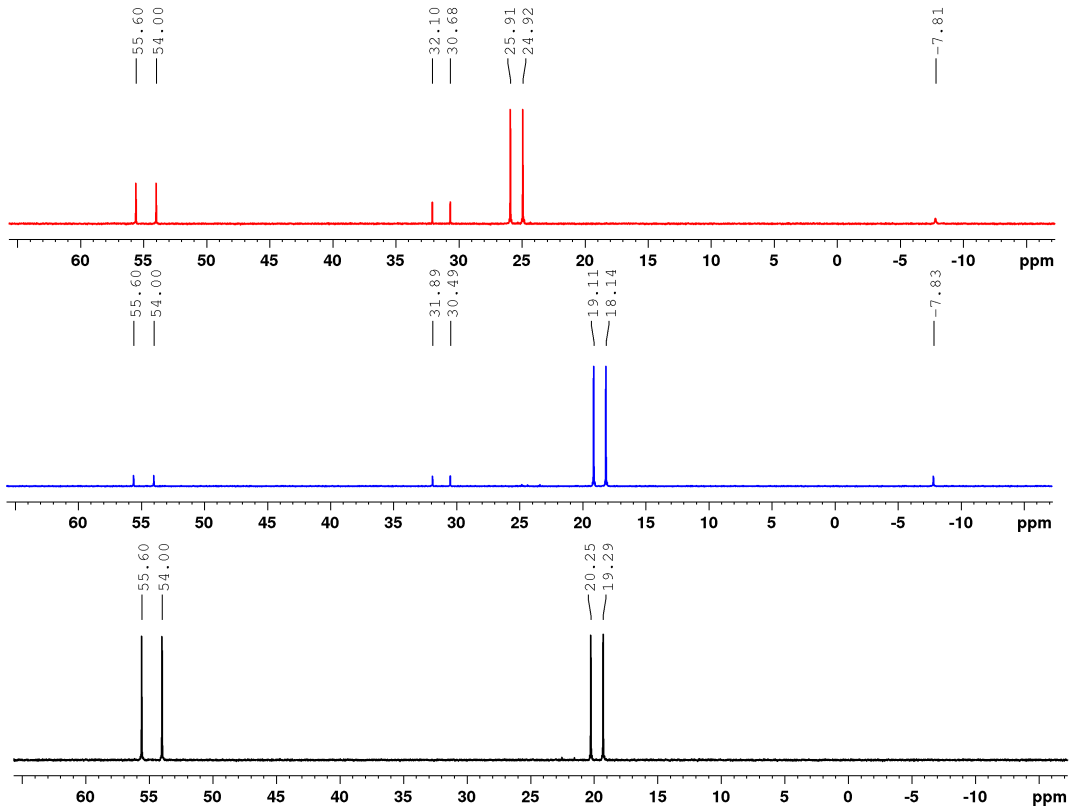

Figure 3-11: *In-situ* $^{31}P\{^{1}H\}$ NMR spectra (121 MHz, C_6D_6) of the reactions of [Rh(acac)(P(*p*-tolyl$_3$)$_2$)] **1-56** with *α,ω*-diynes **3-1** (black), **3-2** (blue) and **3-8** (red) at room temperature after 56 hours.

The doublet at 54.8 ppm represents the starting material [Rh(acac)(P(*p*-tolyl)$_3$)$_2$] **1-56** and the doublets at 19.8, 18.6 and 25.4 ppm with coupling constants of ca. 120 Hz correspond to the tri(*p*-tolyl)phosphine-substituted 2,5-bis(aryl)rhodacyclopentadienes **3-15**, **3-16** and **3-17**, respectively. In the reaction of **1-56** with *α,ω*-diynes **3-2** and **3-8** a doublet at ca. 30 ppm with a Rh-P coupling constant of 170 Hz, indicating a rhodium(I) species, and a singlet at ca. -7.8 ppm representing tri(*p*-tolyl)phosphine were observed. Both signals have similar integrated areas (blue spectrum: 1:0.97 and red spectrum: 1:0.77), indicating that the species at ca. 30 ppm is a monophosphine complex and the second equivalent of phosphine is unbound.

According to the $^{31}P\{^{1}H\}$ NMR spectra, two rhodium-phosphine complexes are present in the black spectrum and three rhodium-phosphine complexes in the blue and red spectra. In all spectra, signals for [Rh(acac)(P(*p*-tolyl)$_3$)$_2$] **1-56** and the respective rhodacyclopentadiene are visible. In the reaction of **1-56** with *α,ω*-diynes **3-2** and **3-8**, an additional rhodium(I)-phosphine complex bearing, presumably, only one phosphine is present.

In the corresponding ^{1}H NMR spectra (Figure 3-12), various signals in the aromatic (9.00 – 6.50 ppm), acac-CH (5.80 – 4.50 ppm), carboxymethoxy (4.00 – 3.00 ppm), and aliphatic (2.00 – 1.00 ppm) regions are visible, arising from the different rhodium species, free

tri(*p*-tolyl)phosphine and dimers and trimers of the organic starting material (for *α*,*ω*-diynes **3-2** and **3-8**).

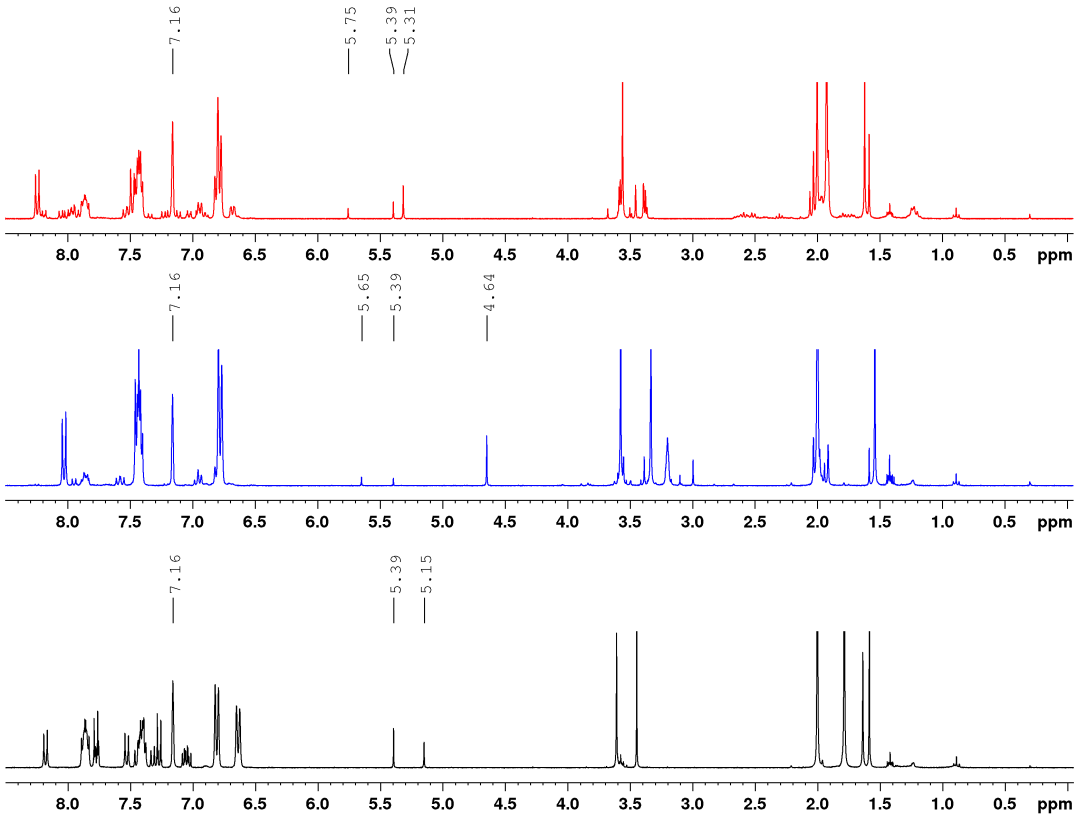

Figure 3-12: *In-situ* ^{1}H NMR spectra (300 MHz, C_6D_6) of the reactions of [Rh(acac)(P(*p*-tolyl$_3$)$_2$)] **1-56** with *α*,*ω*-diynes **3-1** (black), **3-2** (blue) and **3-8** (red) at room temperature after 56 hours.

The following discussions focus on the signals in the acac-CH region (5.80 – 4.50 ppm) as further assignment of other signals is difficult due to the large amount of overlapping resonances. In the black spectrum, two singlets at 5.39 and 5.15 ppm are visible. In the blue spectrum, three singlets at 5.65, 5.39 and 4.64 ppm are apparent and, in the red spectrum, there are three singlets at 5.75, 5.39 and 5.31 ppm. The signal at 5.39 ppm represents the acac-CH group of the rhodium(I) starting material [Rh(acac)(P(*p*-tolyl)$_3$)$_2$] **1-56** and the upfield signals at 5.15, 4.64 and 5.31 ppm represent the tri(*p*-tolyl)phosphine-substituted 2,5-bis(aryl)rhodacyclo-pentadienes **3-15**, **3-16** and **3-17**. It is important to note that the organic starting material is still visible after 56 hours for *α*,*ω*-diyne **3-1**, whereas for **3-8**, only trace amounts remain, while **3-2** shows only trace amounts after six hours. After consumption of the organic starting material, no change in the NMR spectra is visible.

The observation of two and three different rhodium-phosphine species in the ^{31}P{^{1}H} NMR spectra can be expanded by findings from the ^{1}H NMR spectra, from which it is clear that all of them bear an acetylacetonato ligand.

According to the $^{31}P\{^{1}H\}$ NMR spectra, heating the reactions at 60 °C for seven hours resulted in the complete disappearance of the doublet at ca. 30 ppm and the singlet at -7.8 ppm (for *α,ω*-diynes **3-2** and **3-8**), and only the signals for the rhodium(I) starting material [Rh(acac)(P(*p*-tolyl)$_3$)$_2$] **1-56** and the rhodacyclopentadienes **3-15**, **3-16** and **3-17** remain.
In the corresponding ^{1}H NMR spectra (Figure 3-13), the singlets at 5.65 and 5.75 ppm (see Figure 3-12, blue and red spectrum) diminished, and both spectra show fewer signals in all three regions compared to the reaction at room temperature. For all three reactions, the intensity of the rhodacyclopentadiene signals increased compared to the room temperature reaction.

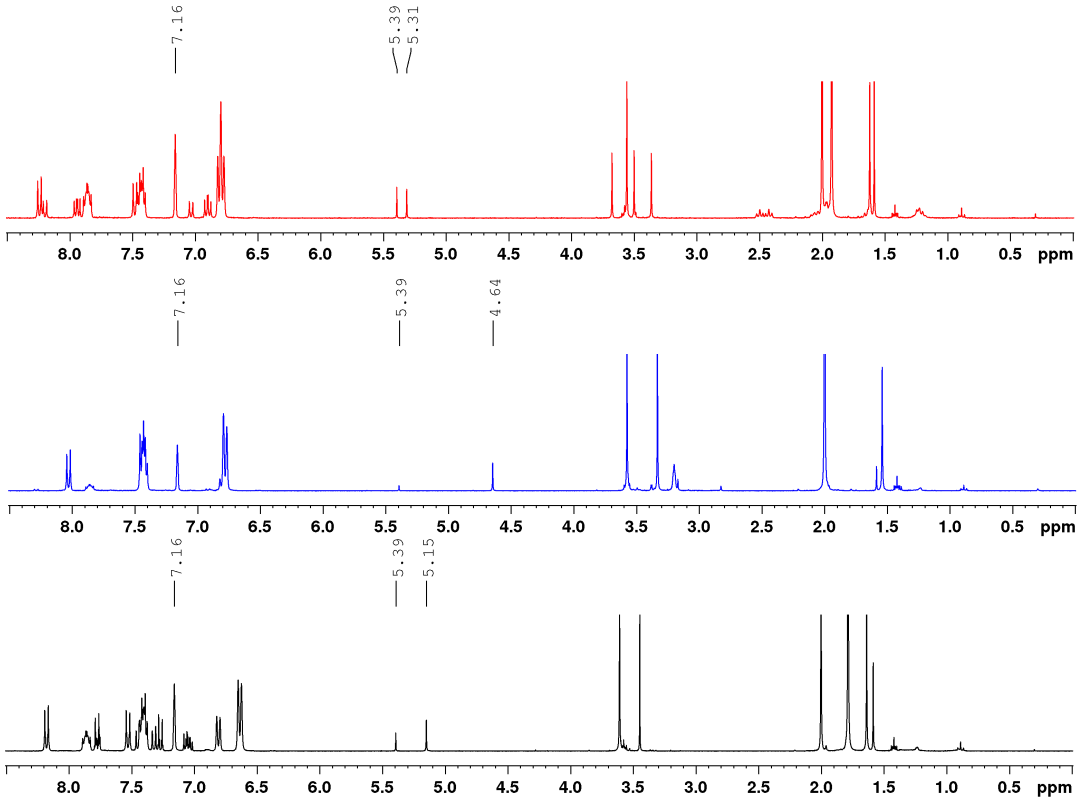

Figure 3-13: *In-situ* ^{1}H NMR spectra (300 MHz, C_6D_6) of the reaction of [Rh(acac)(P(*p*-tolyl$_3$)$_2$)] **1-56** with *α,ω*-diynes **3-1** (black), **3-2** (blue) and **3-8** (red) at room temperature after 56 hours and at 60 °C 7 hours.

A closer analysis shows, that for the reactions of [Rh(acac)(P(*p*-tolyl)$_3$)$_2$] **1-56** with *α,ω*-diynes **3-2** and **3-8**, the organic starting material was completely consumed, **1-56** still remained present and no further progress of the reactions were observed. Cycloisomerization products of the organic starting materials are visible, indicated by resonances at ca. 3.5 ppm, for the CO_2Me groups. The signal intensity for the trimer of *α,ω*-diyne **3-8** (red spectrum) is higher than for the trimer of *α,ω*-diyne **3-2** (only trace amounts, blue spectrum). In accordance with this finding, the intensity of **1-56** is higher in the red than in the blue spectrum (Figure 3-13), as the consumption of *α,ω*-diyne **3-8** is slower than for *α,ω*-diyne **3-2**. A plausible mechanism for the dimerization and trimerization will be discussed in section 4.3.2.

With the diminishing of the signals from the $^{31}P\{^{1}H\}$ and ^{1}H NMR spectra, the singlet at 5.65 ppm (blue spectrum, Figure 3-12) can be linked to the doublet at 31.2 ppm (blue spectrum, Figure 3-11), and the singlet at 5.75 ppm (red spectrum, Figure 3-12) can be linked to the doublet at 31.4 ppm (red spectrum, Figure 3-11). The Rh-P coupling constant of 170 Hz indicates a rhodium(I) species. The fact that the number of aromatic signals decreased (Figure 3-12 vs. 3-13) can be attributed to a re-coordination of tri(*p*-tolyl)phosphine, the disappearance of the species giving rise to the signals at 5.65 and 5.75 ppm, respectively, and the consumption of the dimer of the organic starting material. With a decrease of dimer, the intensity of the signals of the trimer, of the respective *α*,*ω*-diynes, increased.

According to the $^{31}P\{^{1}H\}$ NMR spectrum, the reaction of [Rh(acac)(P(*p*-tolyl)$_3$)$_2$] **1-56** with *α*,*ω*-diyne **3-8** in THF-d_8 instead of C_6D_6 does not result in a doublet with a coupling constant of ca. 170 Hz. Only signals for **1-56** and rhodacyclopentadiene **3-17** were observed at room temperature after 56 hours.

Similar to the reactions described above, the $^{31}P\{^{1}H\}$ NMR spectrum of the reaction of [Rh(acac)(P(*p*-tolyl)$_3$)$_2$] **1-56** with *α*,*ω*-diyne **3-5** at room temperature in C_6D_6 after 56 hours shows three doublets at 54.8 ($^{1}J_{Rh\text{-}P}$ = 195 Hz), 30.8 ($^{1}J_{Rh\text{-}P}$ = 171 Hz) and 24.7 ppm ($^{1}J_{Rh\text{-}P}$ = 117 Hz) and a singlet at -7.8 ppm. In the ^{1}H NMR spectrum, three significant signals in the acac region are observed at 5.75, 5.39 and 5.30 ppm. The organic starting material is consumed within 40 minutes.

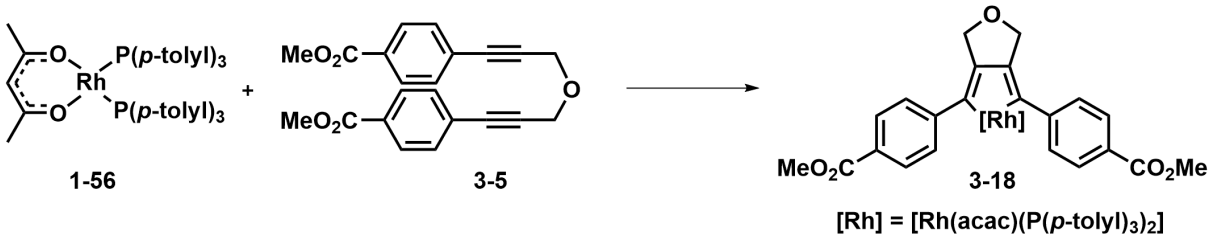

1-56 **3-5** **3-18**

[Rh] = [Rh(acac)(P(*p*-tolyl)$_3$)$_2$]

Scheme 3-13: Reaction of [Rh(acac)(P(*p*-tolyl)$_3$)$_2$] **1-56** with *α*,*ω*-diyne **3-5**.

According to $^{31}P\{^{1}H\}$ NMR spectroscopy, heating the reaction mixture at 60 °C for seven hours results in the disappearance of the doublet at 30.8 ppm and the singlet at -7.8 ppm and, in the ^{1}H NMR spectrum, the singlet at 5.75 ppm is also gone. There are less signals in the aromatic and aliphatic regions, and signals for the organic trimerization product appear. Furthermore, only small amounts of [Rh(acac)(P(*p*-tolyl)$_3$)$_2$] **1-56** remained in the reaction mixture, similar to the reaction of **1-56** with *α*,*ω*-diyne **3-2**.

In the $^{31}P\{^{1}H\}$ NMR spectrum of the reaction of [Rh(acac)(P(*p*-tolyl)$_3$)$_2$] **1-56** with *α*,*ω*-diyne **3-4** at room temperature in C_6D_6 for four days, small doublets at 48.8 ppm ($^{1}J_{Rh-P}$ = 190 Hz) and 29.5 ppm ($^{1}J_{Rh-P}$ = 127 Hz) as well as a singlet at -7.8 ppm are observed in addition to resonances due to **1-56**. Similar to the previously mentioned reactions, two doublets and one singlet appear, although this time only at low intensity. The resonances are downfield shifted and the coupling constants are larger. In the $^{31}P\{^{1}H\}$ NMR spectrum, after heating the reaction mixture at 60 °C for seven days, results in the disappearance of the signals at 48.8, 29.5 and -7.8 ppm. In the ^{1}H NMR spectrum, additional signals, small in intensity, in the aromatic region as well as in the region from 2.0 – 1.8 ppm are visible, pointing to the formation of cycloisomerization products of the organic compound **3-4**.

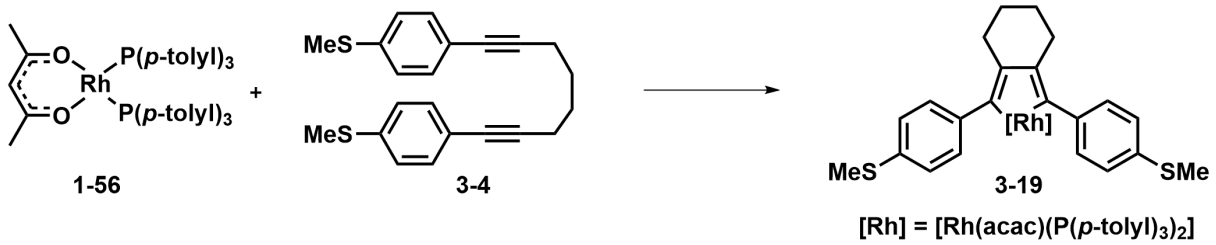

1-56 **3-4** **3-19**

[Rh] = [Rh(acac)(P(*p*-tolyl)$_3$)$_2$]

Scheme 3-14: Reaction of [Rh(acac)(P(*p*-tolyl)$_3$)$_2$] **1-56** with *α*,*ω*-diyne **3-4**.

For the reaction of [Rh(acac)(P(*p*-tolyl)$_3$)$_2$] **1-56** with *α*,*ω*-diyne **3-1** no cycloisomerization products were observed, either by HRMS or by NMR spectroscopy. The only species left after both reactants were consumed is the tri(*p*-tolyl)phosphine-substituted 2,5-bis(aryl)rhodacyclopentadiene **3-15** (Scheme 3-15).

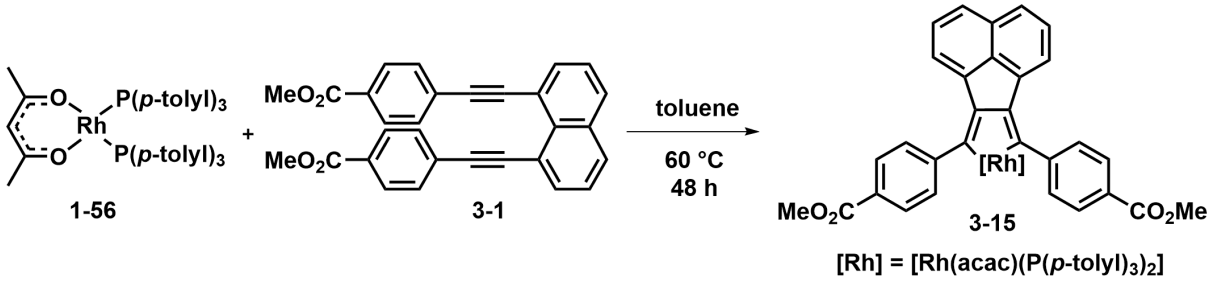

Scheme 3-15: Synthesis of 2,5-bis(aryl)rhodacyclopentadiene **3-15** *via* reaction of [Rh(acac)(P(*p*-tolyl$_3$)$_2$)] **1-56** with *α*,*ω*-diyne **3-1**.

Analytically pure **3-15** was isolated in 77% yield as a red solid and was characterized by multinuclear NMR spectroscopy, HRMS, elemental analysis and single-crystal X-ray diffraction analysis.

Inspection of the ^{1}H NMR spectroscopic data in C_6D_6 revealed the formation of a C_{2v} symmetric complex as indicated by only one set of signals for the acac-CH_3 groups at 1.64 ppm with an integral of six and for the CO_2Me groups at 3.61 ppm (6H). A singlet with an integral of 18 is observed for the methyl groups of the tri(*p*-tolyl)phosphine ligands at 1.79 ppm. The single acac-CH group gives rise to a singlet at 5.15 ppm, integrating to one. In the aromatic region, five multiplets in the 8.19 – 6.62 ppm range integrating to 38 are displayed. In the ^{13}C{^{1}H} NMR spectrum, the acac-CH group resonates at 101.1 ppm. The ^{31}P{^{1}H} NMR resonance of **3-15** is observed at 19.8 ppm with a ^{103}Rh-^{31}P coupling constant of 117 Hz being in agreement with the data obtained for similar tri(*p*-tolyl)phosphine-substituted octahedral 2,5-bis(arylethynyl)rhodacyclopentadienes.[70-72]

Elemental analysis, as well as HRMS data are also consistent with the formulation of [Rh(acac)(P(*p*-tolyl)$_3$)$_2$(3-1)].

Single-crystals suitable for X-ray diffraction analysis were obtained by vapor diffusion of *n*-hexane into a solution of **3-15** in toluene. Complex **3-15** crystallizes in the monoclinic space group $P2_1/c$. The molecular structure is shown in Figure 3-14 and selected bond lengths and angles are listed in Table 3-2.

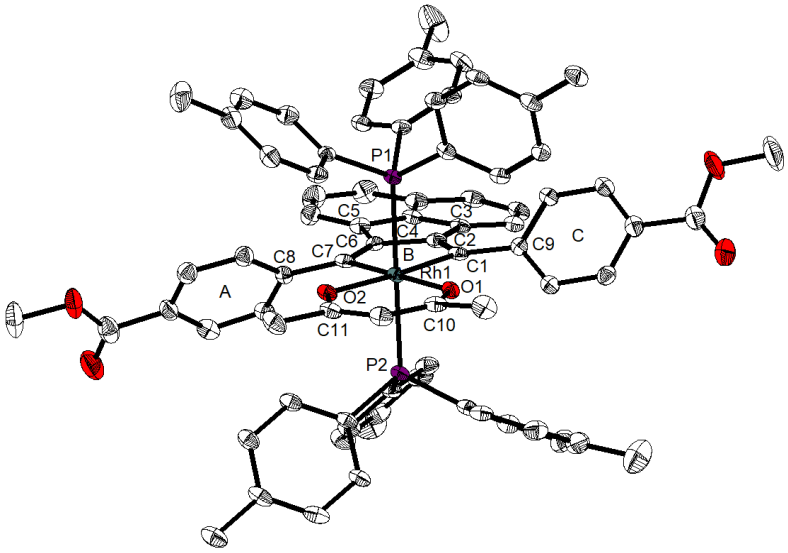

Figure 3-14: Molecular structure of 2,5-bis(aryl)rhodacyclopentadiene **3-15** in the solid state determined by single-crystal X-ray diffraction with thermal ellipsoids drawn at the 50% probability level. Hydrogen atoms and solvent molecules are omitted for clarity.

The rhodium atom is in an octahedral environment with *trans*-disposed phosphine ligands. The Rh-O1 and Rh-O2 bond distances are 2.121(3) and 2.133(3) Å, respectively, and therefore identical with the bond lengths in 2,5-bis(aryl)rhodacyclopentadienes **3-6** and **3-7**. The Rh-P1 bond distance is 2.3704(16) Å and the Rh-P2 bond length is 2.3943(16) Å. The Rh-P bond lengths are longer, compared to similar rhodacyclopentadienes bearing trimethylphosphine ligands (ca. 2.306 Å, see Table 3-1), due to the weaker σ-donor ability and larger steric constraints of the tri(*p*-tolyl)phosphine ligand. The Rh-P bond lengths obtained for **3-15** are also longer than those in similar tri(*p*-tolyl)phosphine-substituted 2,5-bis(arylethynyl)rhodacyclopentadienes synthesized by Sieck with 2.3464(8) – 2.3637(8) Å.[72] The carbon-carbon distances in the five membered ring are 1.360(5) and 1.353(5) Å for the C=C double bonds and 1.466(6) Å for the C-C single bond. Hence, the C=C double bonds are very similar to typical cyclopenta-1,3-diene C(sp^2)=C(sp^2) bonds and the single C-C single bond is characteristic of an endocyclic C(sp^2)-C(sp^2) bond.[208] The O1-Rh1-O2 angle is 86.67(11)°, the P1-Rh1-P2 angle is 177.49(4)° and the C-Rh-C angle is 81.57(16)°, while the other angles in the rhodacyclopentadiene range from 112.1(3) to 116.9(3)° and are larger than the expected 108° for a regular planar, five-membered ring. Nevertheless, the sum of all five angles is 540°.This finding is similar to those for **3-6**, **3-7**, and other acac-substituted rhodacyclopentadienes.[59, 72]

The rotation of the rings A and C with respect to the rhodacyclopentadiene plane in **3-15** are 51.9(3) and 44.7(2)°, and hence are larger than those in **3-7**, **3-10** and **3-11**, but also smaller than that for **3-6**, the PMe_3-analogue of **3-15**, which can be explained by the larger cone angle of the tri(*p*-tolyl)phosphine ligand compared to the trimethylphosphine ligand.

Table 3-2: Selected bond lengths [Å] and angles [°] of 2,5-bis(aryl)rhodacyclopentadiene **3-15** determined by single-crystal X-ray diffraction at 100 K with esd's in parentheses.

	3-15		**3-15**
Rh1-O1	2.121(3)	O1-Rh1-O2	86.67(11)
Rh1-O2	2.133(3)	C1-Rh1-C7	81.57(16)
Rh1-P1	2.3704(16)	Rh1-C1-C2	112.1(3)
Rh1-P2	2.3943(16)	C1-C2-C6	116.6(3)
Rh1-C1	2.067(4)	C2-C6-C7	116.9(3)
Rh1-C7	2.047(4)	C6-C7-Rh1	112.8(23)
O1-C10	1.273(5)	P1-Rh1-P2	177.49(4)
O2-C11	1.269(5)	∢ A-B	51.9(3)
C1-C2	1.360(5)	∢ C-B	44.7(2)
C2-C6	1.466(6)		
C6-C7	1.353(5)		
C7-C8	1.467(6)		
C1-C9	1.467(5)		

The "B"-plane is that of the rhodacyclopentadiene moiety.

3.3.4 Reactions of [Rh(acac)(Me$_2$Im)$_2$] with aryl-substituted α,ω-diynes

NMR spectroscopic investigations of the reaction of [Rh(acac)(^{n}Pr$_2$Im)$_2$] **2-20** with the CO$_2$Me- and SMe-substituted α,ω-tetraynes showed that *cis*- and *trans*-NHC-substituted 2,5-bis(arylethynyl)rhodacyclopentadienes were formed (Scheme 2-13). However, it was not possible to isolate either of the two isomers. This part of Chapter 3 deals with the reaction of [Rh(acac)(Me$_2$Im)$_2$] **2-21** with the α,ω-diyne **3-1**.

Room temperature and 60 °C reactions of [Rh(acac)(Me$_2$Im)$_2$] **2-21** with α,ω-diynes **3-3** and **3-8** resulted in various signals which could not be assigned. However, room temperature reaction of [Rh(acac)(Me$_2$Im)$_2$] **2-21** with α,ω-diyne **3-1** (Scheme 3-16) results in the formation of two new species identified by ^{1}H {^{1}H} NMR spectroscopy (Figure 3-15). In the reaction at room temperature after three days (black spectrum), various overlapping signals in the aromatic region (8.30 – 7.00 ppm), which cannot be further assigned, are visible.

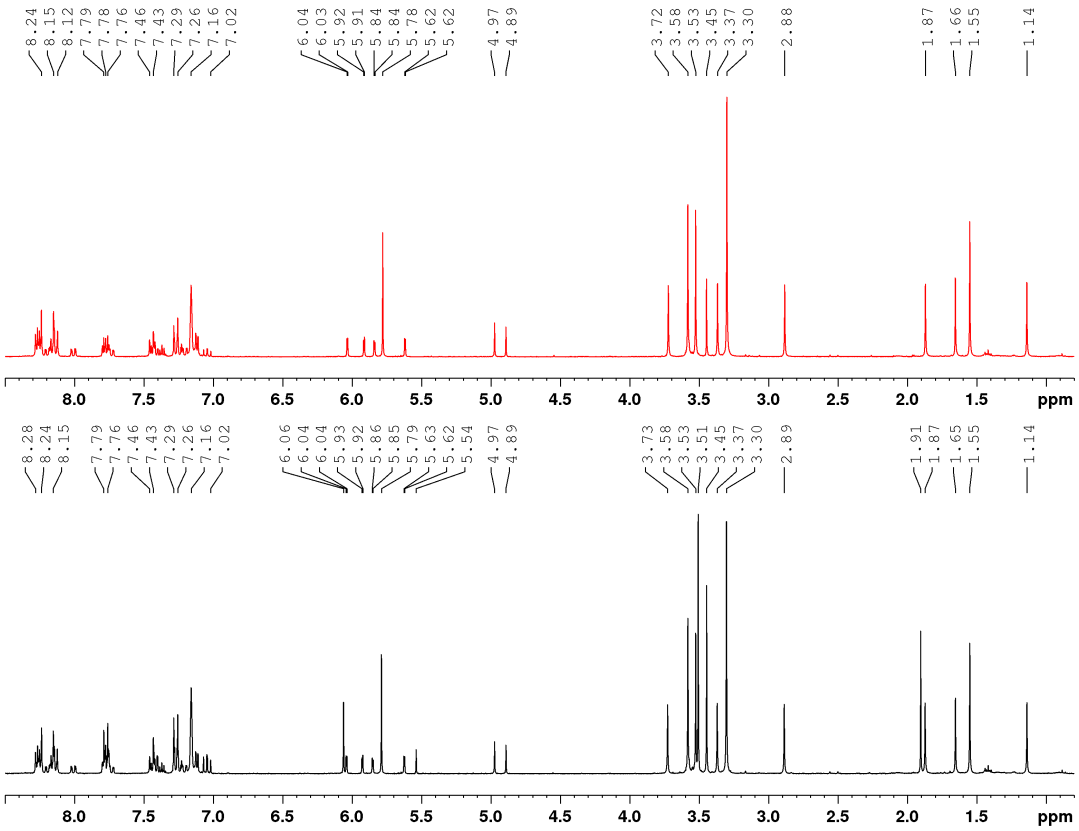

Figure 3-15: *In-situ* ^{1}H NMR spectra (300 MHz, C$_6$D$_6$) of the reaction of [Rh(acac)(Me$_2$Im)$_2$] **2-21** with α,ω-diyne **3-1** at room temperature after 3 days (red) and 14 days (black).

A singlet at 5.79 ppm and four doublets at 6.04, 5.93, 5.86 and 5.63 result from the unsaturated NHC backbone. Two singlets at 4.97 and 4.89 ppm are assigned to acac-CH groups, and signals for the carboxymethoxy and methyl groups of the NHC ligand are apparent between 3.80 –

1.87 ppm. In the range from 1.65 – 1.14 ppm the resonances for the different acac-CH_3 groups are visible. Signals for the starting materials at 1.91, 3.51, 5.54 and 6.06 ppm for [Rh(acac)(Me_2Im)$_2$] **2-21** and at 3.45 ppm for the CO_2Me resonances of α,ω-diyne **3-1** are also present. Inspection of the ^{1}H NMR spectrum after three days, already reveals the formation of a *cis*- and *trans*-rhodium-NHC complex, similar to the reaction of [Rh(acac)(Me_2Im)$_2$] **2-21** with *para*-substituted 1,4-diphenylbuta-1,3-diynes **2-1a**,**b** described in section 2.3.1.5.

After 14 days (red spectrum), the rhodium(I) starting material was completely consumed, and only signals for small amounts of the organic starting material **3-1** and the above mentioned *cis*- and *trans*-compounds remain. The ratio of *cis*:*trans* complexes is 1:0.83.
Four doublets at 6.04, 5.92, 5.84 and 5.62 ppm each with an integral of one and singlets at 3.72, 3.37, 2.88 and 1.87 ppm with an integral of three, are assigned to the NHC backbone and methyl groups of the *cis*-NHC rhodium species. A singlet at 4.97 ppm with an integral of one and singlets at 1.14 and 1.66 ppm with an integral of three correspond to the acac-CH group and the two inequivalent acac-CH_3 groups. The resonance at 3.58 ppm with an integral of six can be assigned to the carboxymethoxy group.
The singlet at 5.78 with an integral of four and at 3.30 ppm with an integral of 12 are assigned to the NHC backbone and the four methyl groups of the NHC ligand of the *trans*-NHC rhodium species. At 4.89 ppm with an integral of one and at 1.55 ppm with an integral of six are resonances assigned to the acac-CH and methyl groups of the acac ligand. The carboxymethoxy groups resonate at 3.53 ppm with an integral of six.

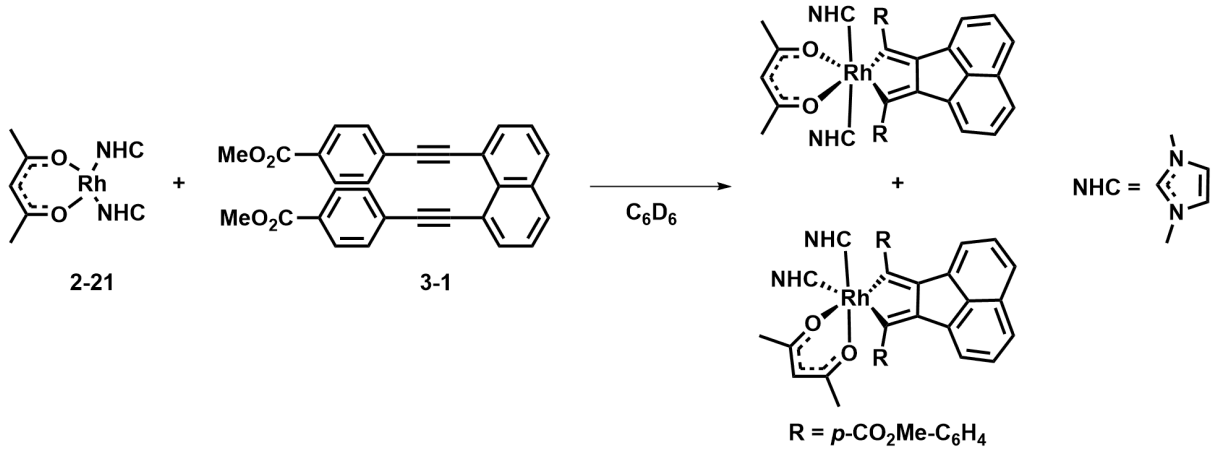

Scheme 3-16: Reaction of [Rh(acac)(Me_2Im)$_2$] **2-21** with α,ω-diyne **3-1** resulting in a *trans*- and *cis*-NHC-substituted 2,5-bis(aryl)rhodacyclopentadiene.

Heating the reaction at 60 °C for six days resulted in a *cis*:*trans* ratio of 1:0.25. Further heating at 80 °C for 24 hours resulted in a *cis*:*trans* ratio of 1:0.10, and additional heating did not change the ratio but resulted in decomposition. While in the reaction of [Rh(acac)(Me_2Im)$_2$] **2-21** with *para*-substituted 1,4-diphenylbuta-1,3-diynes **2-1a**,**b** the *trans*-species was the thermodynamic favored species, in this reaction the *cis*-species seems to be favored.

By $^{13}C\{^1H\}$ NMR spectroscopy it was not possible to identify any carbon atoms in the 110 - 60 ppm range which would indicate the presence of a triple bond, implying that a rhodacyclopropene was formed.

Similar to the reactions of [Rh(acac)(^{n}Pr$_2$Im)$_2$] **2-20** with the CO_2Me- and SMe-substituted α,ω-tetraynes, it was not possible to separate the different species.

3.4 Photophysical studies of the 2,5-bis(aryl)rhodacyclopentadienes

Previous studies of Sieck showed that replacing trimethylphosphine with a tri(*p*-tolyl)phosphine ligand in CO_2Me-substituted 2,5-bis(arylethynyl)rhodacyclopentadienes shifts $\lambda_{abs,max}$ bathochromically by 930 cm^{-1} and $\lambda_{em,max}$ by 609 cm^{-1} in toluene. The quantum yield Φ drops from 0.54 to less than 0.01, and the lifetime τ_F shortens from 1.7 to less than 1 ns (see section 1.3.2). The PMe_3-substituted 2,5-bis(aryl)rhodacyclopentadiene **3-10** shows an intense absorption band at $\lambda_{abs,max}$ = 476 nm and emission in the visible region at $\lambda_{em,max}$ = 517 nm in toluene. An extinction coefficient ε was not determined. The quantum yield Φ and the lifetime τ_F were determined to be < 0.01 and < 1 ns. Comparing the CO_2Me and PMe_3-substituted 2,5-bis(arylethynyl)rhodacyclopentadiene **1-52d** with the 2,5-bis(aryl)rhodacyclopentadiene **3-10** (Scheme 3-17) indicates that, in the latter, $\lambda_{abs,max}$ is shifted hypsochromically by 2317 cm^{-1} and $\lambda_{em,max}$ by 1580 cm^{-1}. Again, the quantum yield Φ drops from 0.54 to less than 0.01 and the lifetime τ_F shortens from 1.7 to less than 1 ns (Table 3-3). Hence, replacing the trimethylphosphine with tri(*p*-tolyl)phosphine and shortening of the π-system have a similar influence on the quantum yield and lifetime.

Table 3-3: Selected photophysical data of PMe_3- and CO_2Me-substituted 2,5-bis(arylethynyl)rhodacyclopentadiene **1-52d**, $P(p\text{-tolyl})_3$- and CO_2Me-substituted 2,5-bis(arylethynyl)rhodacyclopentadiene **1-57d**, and PMe_3- and CO_2Me-substituted 2,5-bis(aryl)rhodacyclopentadiene **3-10** in dry, degassed toluene.[59, 71-72]

Compound	$\lambda_{abs,max}$ [nm]	$\lambda_{em,max}$ [nm]	ε [M^{-1} cm^{-1}]	Φ	τ_F [ns]	Stokes shift [cm^{-1}]
1-52d	535	563	37600	0.54	1.7	930
1-57d	563	583	32500	< 0.01	< 1	609
3-10	476 476*	517 523*	-	< 0.01	< 1	1666 1888*

*in THF

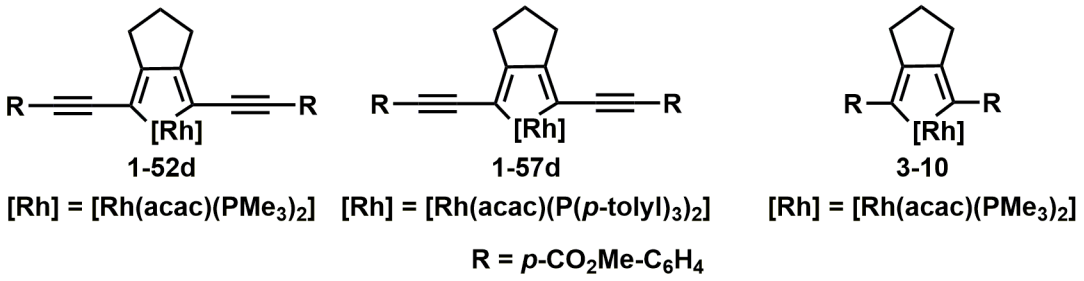

Scheme 3-17: Chemical structures of rhodacyclopentadienes **1-52d**, **1-57d** and **3-10** previously synthesized by Sieck.[59, 71-72]

The lower quantum yield as well as the shorter lifetime of **1-57d** compared to **1-52d** results from additional vibrational modes of the tri(*p*-tolyl)phosphine ligand which lead to higher rate constants for non-radiative decay. The surprisingly low quantum yield and short lifetime of **3-10** compared to **1-52d** may result from additional vibrational or rotational modes of the aryl

rings directly bound to the rhodacyclopentadiene moiety leading to higher rate constants for non-radiative decay. No phosphorescence was observed in a 2-Me-THF glass matrix at 77 K (Figure 3-16).[59, 71-72]

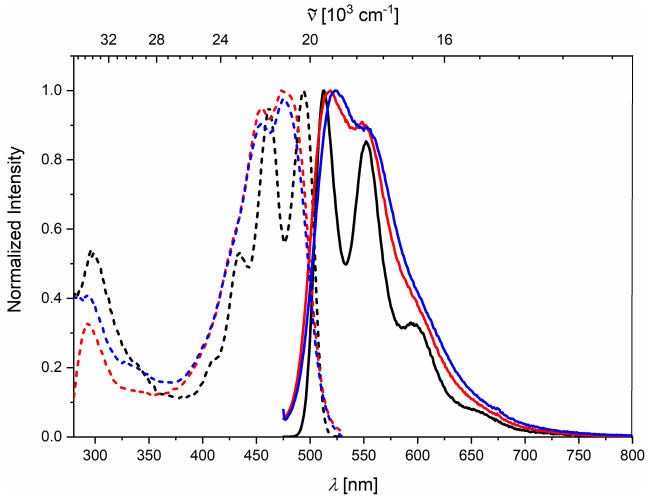

Figure 3-16: Absorption (dashed lines) and emission spectra (solid lines) of **3-10** in dry, degassed toluene (red) and dry, degassed THF (blue) at room temperature, and in a 2-Me-THF glass (black) at 77 K.[72]

The photophysical properties of complexes **3-6**, **3-7** and **3-15** were investigated to see whether they are influenced by altering the backbone.

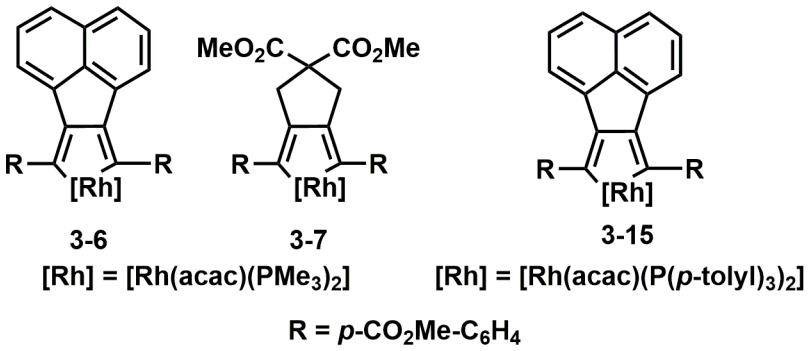

3-6 **3-7** **3-15**

[Rh] = [Rh(acac)(PMe$_3$)$_2$] **[Rh] = [Rh(acac)(P(*p*-tolyl)$_3$)$_2$]**

R = *p*-CO$_2$Me-C$_6$H$_4$

Scheme 3-18: Chemical structures of rhodacyclopentadienes **3-6**, **3-7** and **3-15**.

Complex **3-6** shows a low-energy absorption band in the visible region of the electromagnetic spectrum with $\lambda_{abs,max}$ = 467 nm and a small shoulder at ca. 504 nm in THF with extinction coefficients ε of 10600 M^{-1} cm^{-1} and 7500 M^{-1} cm^{-1}, respectively. A broad emission band is observed between 500 – 800 nm with $\lambda_{em,max}$ = 555 nm and a shoulder at ca. 590 nm. The apparent Stokes shift is ca. 1800 cm^{-1}.

In toluene, compound **3-6** shows an absorption band with $\lambda_{abs,max}$ = 471 nm and a small shoulder at ca. 507 nm and an emission band with $\lambda_{em,max}$ = 549 nm and a shoulder at ca. 585 nm. The apparent Stokes shift is ca. 1500 cm^{-1} (Figure 3-17).

Rhodacyclopentadiene **3-6** exhibits a low quantum yield of Φ < 0.01 and very short emission lifetimes τ_F of less than 1 ns at room temperature. Such short lifetimes and the small Stokes shifts strongly indicate fluorescence.

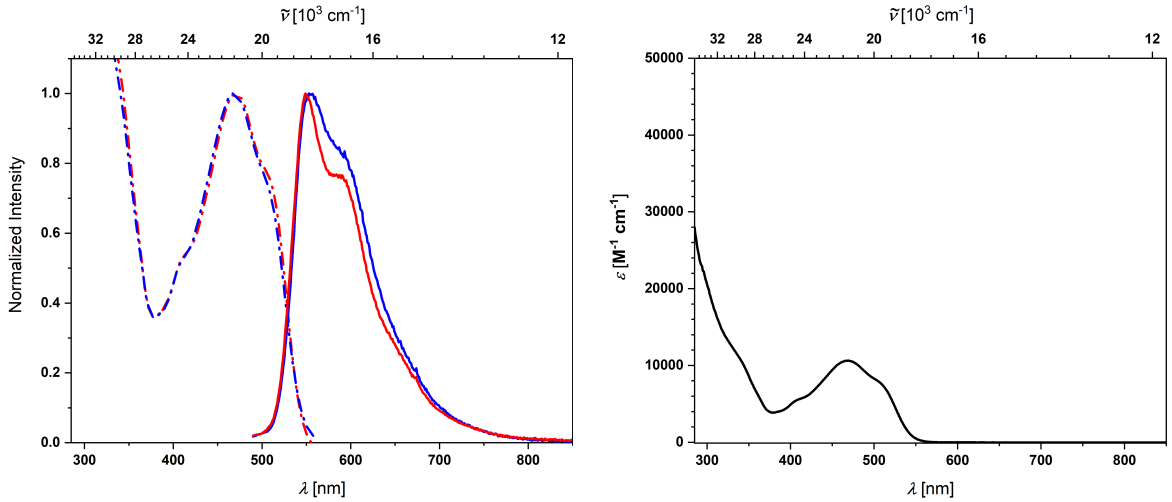

Figure 3-17: Absorption (dashed lines) and emission spectra (solid lines) of **3-6** in dry, degassed toluene (red) and dry, degassed THF (blue) at room temperature (left). Molar extinction coefficient of **3-6** in dry, degassed THF at room temperature (right).

Complex **3-7** shows a low-energy absorption band in the visible region of the electromagnetic spectrum with two local maxima at $\lambda_{abs,max}$ = 451 and 475 nm in THF and extinction coefficients ε of 17000 M^{-1} cm^{-1} and 16500 M^{-1} cm^{-1}, respectively. A broad emission can be seen between 480 – 750 nm with two local emission maxima at $\lambda_{em,max}$ = 516 and 544 nm. The apparent Stokes shift is 1673 cm^{-1}.

In toluene, compound **3-7** shows an absorption band with two local maxima at $\lambda_{abs,max}$ = 450 and 475 nm and an emission band with two local maxima at $\lambda_{em,max}$ = 505 and 541 nm. The apparent Stokes shift is 1250 cm^{-1} (Figure 3-18).

Quantum yields Φ of < 0.01 and lifetimes τ_F < 1 ns were determined. The short lifetimes and small apparent Stokes shifts strongly indicate fluorescence.

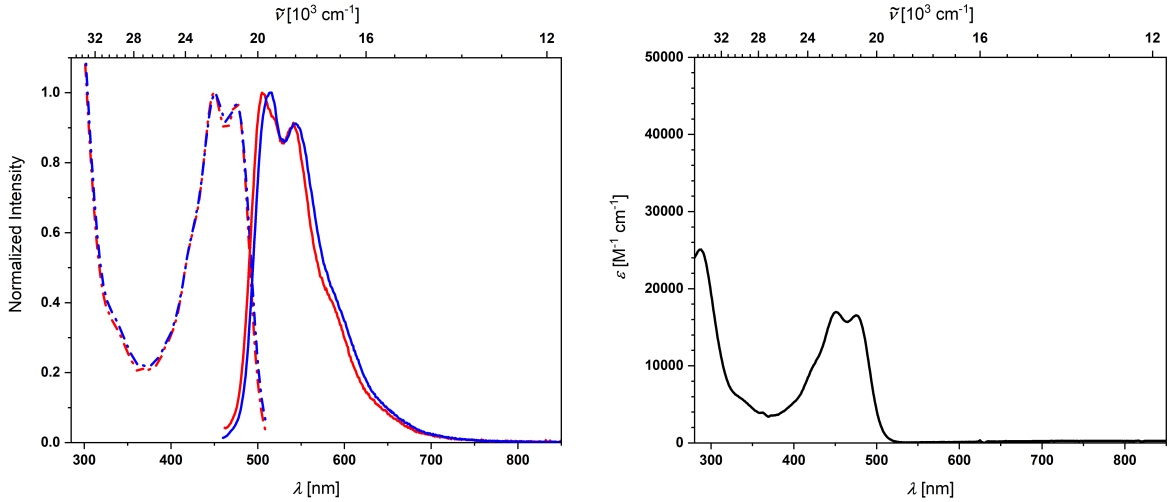

Figure 3-18: Absorption (dashed lines) and emission spectra (solid lines) of **3-7** in dry, degassed toluene (red) and dry, degassed THF (blue) at room temperature (left). Molar extinction coefficient of **3-7** in dry, degassed THF at room temperature (right).

Compared to compound **3-7**, complex **3-6** displays a bathochromic shift of the absorption and emission, and both have low quantum yields, very short emission lifetimes and small apparent Stokes shifts. For **3-6**, the extinction coefficient ε is 10600 M^{-1} cm^{-1} at 467 nm and for **3-7** it is 16500 M^{-1} cm^{-1} at 475 nm in THF.

Comparing complex **3-10**, characterized by Sieck, with **3-7** shows that they have similar photophysical properties.[72] Thus, replacing the CH_2 with a $C(CO_2Me)_2$ group in the rhodacyclopentadiene backbone does not significantly affect the photophysical properties of the compound.

Compound **3-15** shows two excitation bands with two local maxima with $\lambda_{exc,max}$ = 303 and 314 nm and $\lambda_{exc,max}$ = 380 and 391 nm as well as two absorption bands with $\lambda_{abs,max}$ = 397 and 454 nm in THF with extinction coefficients ε of 13200 $M^{-1}cm^{-1}$ and 9800 $M^{-1}cm^{-1}$, respectively. A broad emission is observed between 400 – 700 nm with an emission maximum $\lambda_{em,max}$ = 443 nm and a shoulder at 466 nm (Figure 3-19).
A quantum yield Φ of 0.02 and emission lifetimes τ_F of 1.79 ns (32%), 5.81 ns (63%) and 13.12 ns (5%) were obtained. Such short lifetimes strongly indicate fluorescence. It was not possible to detect any emission from compound **3-15** in toluene.

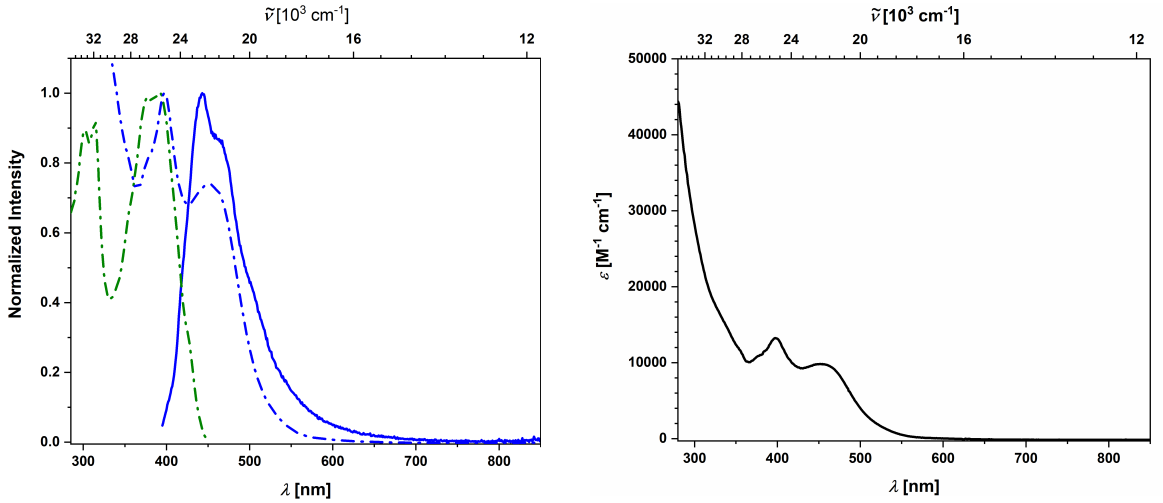

Figure 3-19: Excitation (green dashed line), absorption (blue dashed line) and emission spectrum (blue solid line) of **3-15** in dry, degassed THF at room temperature (left). Molar extinction coefficient of **3-15** in dry, degassed THF at room temperature (right).

It is noteworthy, that the absorption and excitation spectra seem to have a difference. While the excitation ends at 450 nm the absorption ends at 600 nm. This finding is only present for compound **3-15**. However, the measurement of the excitation spectrum is restricted to the emission of the sample. As the sample emits at $\lambda_{em,max}$ = 443 nm with a very low quantum yield

Φ = 0.02, the excitation was recorded until 450 nm only. Hence, it cannot be excluded that the absorption and excitation spectra have a more similar cutoff.

Compounds **3-6** and **3-15**, bearing different phosphine ligands, differ substantially in their photophysical properties. The absorption, excitation and emission spectra of **3-15** are hypsochromically shifted compared to **3-6**. Compound **3-15** exhibits a quantum yield of Φ = 0.02, while for **3-6** it is less than 0.01. The emission lifetime τ_F for **3-6** was determined to be less than 1 ns. For **3-15**, multiple lifetimes of 1.79 ns (32%), 5.81 ns (63%) and 13.12 ns (5%) were obtained (Table 3-4).

As the P(*p*-tolyl)$_3$ ligand is more labile than the trimethylphosphine ligand, and is therefore readily dissociable from rhodacycle **3-15**, it cannot be excluded that the recorded photophysical data for this compound result from a mixture of dissociation products. This assumption is strengthened by the fact that there is no emission in toluene, but emission was observed in THF which could possibly coordinate to a vacant side at the rhodium metal. Additionally, the longer Rh-P bond distance observed by single-crystal X-ray diffraction analysis facilitates dissociation of the phosphine ligand (see Table 3-2). The fact that the absorption and excitation spectra are different also leads to the conclusion that different species may be present. This finding has not been observed previously for any other rhodacycles.[56, 58-59, 68, 71-72, 182]

Table 3-4: Summary of the photophysical data of rhodacyclopentadienes **3-6**, **3-7** and **3-15**.

Compound	solvent	$\lambda_{abs,max}$ [nm]	$\lambda_{exc,max,}$ [nm]	$\lambda_{em,max}$ [nm]	ε [M^{-1} cm^{-1}]	Φ	τ_F [ns]
3-6	toluene	471, 507	470, 506	549, 585	-	< 0.01	< 1
	THF	467, 504	461, 508	555, 590	10600, 7500	< 0.01	< 1
3-7	toluene	450, 475	448,476	505, 541	-	< 0.01	< 1
	THF	451, 475	447, 476	516, 544	17000, 16500	< 0.01	< 1
3-15	toluene	-	-	-	-	-	-
	THF	397, 454	303, 314 380, 391	443, 466	13200, 9800	0.02	1.79(32%) 5.81(63%) 13.12(5%)

Chapter 4

4 Synthesis and structural characterization of dimers and trimers of aryl-substituted α,ω-diynes

4.1 Abstract

The formation of luminescent dimers and trimers in the reaction of *α*,*ω*-bis(arylbutadiynyl)alkanes (*α*,*ω*-tetraynes) with catalytic amounts of [$Rh(S_2CNEt_2)(PPh_3)_2$] was previously reported. Herein, the reaction of various acac- and diethyldithiocarbamate-substituted rhodium(I) catalysts bearing (chelating)phosphines with *α*,*ω*-bis(arylethynyl)alkanes (*α*,*ω*-diynes), yielding dimers and trimers, is described. The photophysical properties of dimers and trimers of the *α*,*ω*-diynes were investigated and compared to *para*-terphenyl, showing a lower quantum yield and a larger apparent Stokes shift. Compared to their *α*,*ω*-tetrayne analogues, in general, the absorptions and emissions are bathochromically shifted and the quantum yields are lower.

Furthermore, a bimetallic rhodium(I) complex of the form [$Rh_2(ox)(P(p\text{-tolyl})_3)_4$] (ox: oxalate) was reacted with a CO_2Me-substituted *α*,*ω*-tetrayne forming a complex in which only one rhodium(I) center reacts with the *α*,*ω*-tetrayne. The photophysical properties of this mixed rhodium(I)/(III) species shows only negligible differences compared to the P(*p*-tolyl)- and CO_2Me-substituted 2,5-bis(arylethynyl)rhodacyclopentadiene, previously synthesized by Marder and co-workers.

4.2 Previous work and motivation

Schwenk reported that the reaction of $[Rh(S_2CNEt_2)(PPh_3)_2]$ with the CO_2Me-substituted α,ω-tetrayne **1-47d** in equimolar amounts at room temperature after 24 hours formed the 2,5-bis(arylethynyl)rhodacyclopentadiene species exclusively. In the $^{31}P\{^1H\}$ NMR spectrum, small amounts of the rhodium(I) starting material were observed after additional six days at room temperature, and even more starting material appeared after additional seven days at 80 °C. In the reaction of the NMe_2-substituted α,ω-tetrayne **1-47c** with $[Rh(S_2CNEt_2)(PPh_3)_2]$ in equimolar amounts at room temperature, only low conversion to the 2,5-bis(arylethynyl)rhodacyclopentadiene was observed in seven days. Heating the system completely regenerated the rhodium(I) starting material. Initially, it was assumed that the triphenylphosphine-substituted 2,5-bis(arylethynyl)rhodacyclopentadiene is in equilibrium with the starting materials, but a closer analysis revealed that dimerization and trimerization of the organic starting material occurred and the $[Rh(S_2CNEt_2)(PPh_3)_2]$ complex serves as a catalyst for this process. Various dimers and trimers of different α,ω-tetraynes were isolated and characterized (Scheme 4-1).[68]

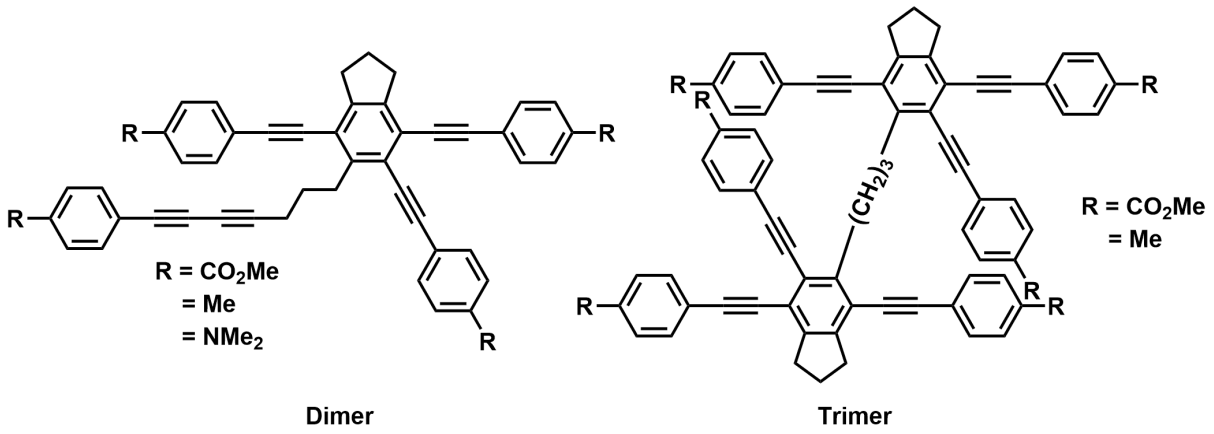

Scheme 4-1: Dimers and trimers of α,ω-tetraynes previously reported by Schwenk.

However, in preliminary studies, Sieck observed that the reaction of $[Rh(acac)(P(p\text{-tolyl})_3)_2]$ **1-56** with the CO_2Me-substituted α,ω-diyne **3-8** also formed dimer and trimer *via* a rhodium-mediated [2+2+2] cycloaddition reaction.

Usually, cationic rhodium(I) catalysts of the form $[Rh(COD)_2]X$ (X = BF_4 and Cl) or neutral species as $[Rh(C_2H_4)_2Cl]_2$ in combination with different phosphine ligands, e.g. BINAP, H_8-BINAP and DTBM-Segphos in DCM or DCE are used as catalyst precursors for such cyclotrimerization reactions.[78-79, 81] It is also possible to react the α,ω-diyne with other substrates, e.g. 1-alkynylphosphine sulfides,[297] H_2,[298] isocyanates[158] and trimethylsilylynamides.[299] The only report on the trimerization of an α,ω-diyne bearing two

phenyl groups was the reaction of 3,3'-oxybis(1-phenyl-1-propyne) with $RhCl_3$-Aliquat 336, which resulted in trimer besides dimer. Although, various phenyl-substituted α,ω-diynes with different backbones were used, a trimer was only found for the reaction depicted in Scheme 4-2.[300]

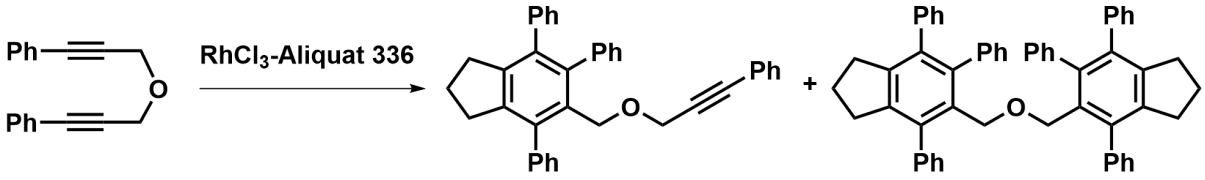

Scheme 4-2: Reaction of 3,3'-oxybis(1-phenyl-1-propyne) with $RhCl_3$-Aliquat 336 forming dimer and trimer.

The aim of this chapter is to follow up on the study initiated by Sieck. The different dimers and trimers of selected α,ω-diynes described in Chapter 3 were to be isolated, characterized and their photophysical properties compared to the dimers and trimers of the α,ω-tetraynes characterized by Schwenk. Furthermore, rhodium(I) complexes with chelating phosphines bearing acac- and diethyldithiocarbamate-ligand were to be synthesized and investigated with regard to their catalytic activity for the cycloisomerization of different α,ω-diynes.

4.3 Results and discussion

A former member of the Marder group, Prof. Dr. Stephen A. Westcott, had already synthesized several rhodium-acac complexes with chelating phosphines (dppm, dcpe, dppe, dppp, dppb and dppf) of which [Rh(acac)dppe] and [Rh(acac)dcpe] are also described in the following chapter. Furthermore, the synthesis of [Rh(acac)dppm], [Rh(acac)dppe] and [Rh(acac)dppp] was already described by Fennis *et al.* in 1990.[301]

4.3.1 Synthesis and structural characterization of rhodium(I) complexes bearing phosphines

The compounds [Rh(acac)dmpe] **4-1**, [Rh(acac)dcpe] **4-2**, [Rh(acac)dppe] **4-3** and [Rh(acac)(P(*p*-tolyl)$_3$)$_2$] **1-56** were all synthesized in several steps. First, reaction of $RhCl_3$ x H_2O with cyclooctene in a mixture of 2-propanol and water at elevated temperature, following a literature procedure,[302] yielding the rhodium(I) dimer [RhCl(COE)$_2$]$_2$. This rhodium dimer was reacted with a suspension of acetylacetone and finely powdered KOH in THF, yielding the monomeric species [Rh(acac)(COE)$_2$].[59] This precursor was reacted with the corresponding phosphine in THF, resulting in the desired complexes **4-1**, **4-2**, **4-3** and **1-56** as yellow solids in 88, 81, 96 and 94% yields, respectively.

The compound [Rh$_2$(ox)(COE)$_4$] **4-4** was synthesized by reaction of [Rh(acac)(COE)$_2$] with oxalic acid in THF resulting in 93% of a yellow solid, similarly to a procedure reported by Oro *et. al.* in 1985 for [Rh$_2$(ox)(COD)$_2$] starting with [Rh(acac)(COD)].[303] Compound **4-4** was further reacted with tri(*p*-tolyl)phosphine in THF yielding [Rh$_2$(ox)(P(*p*-tolyl)$_3$)$_4$] **4-5** as a pale orange solid in 89% yield. Alternatively, **4-5** can also be prepared in 81% yield by reaction of [Rh(acac)(P(*p*-tolyl)$_3$)$_2$] **1-56** with oxalic acid in degassed acetone (Scheme 4-3).

The compounds **4-1**, **4-2** and **4-3** were characterized by elemental analysis, HRMS, multinuclear NMR spectroscopy and single-crystal X-ray diffraction analysis. The molecular structures of **4-1**, **4-2** and **4-3** are shown in Figure 4-1, along with [Rh(acac)(PMe$_3$)$_2$] **1-51**, [Rh(acac)(PCy$_3$)$_2$) **4-6** and [Rh(acac)(P(*p*-tolyl)$_3$)$_2$] **1-56** for comparison. Selected bond distances and angles are listed in Table 4-1.

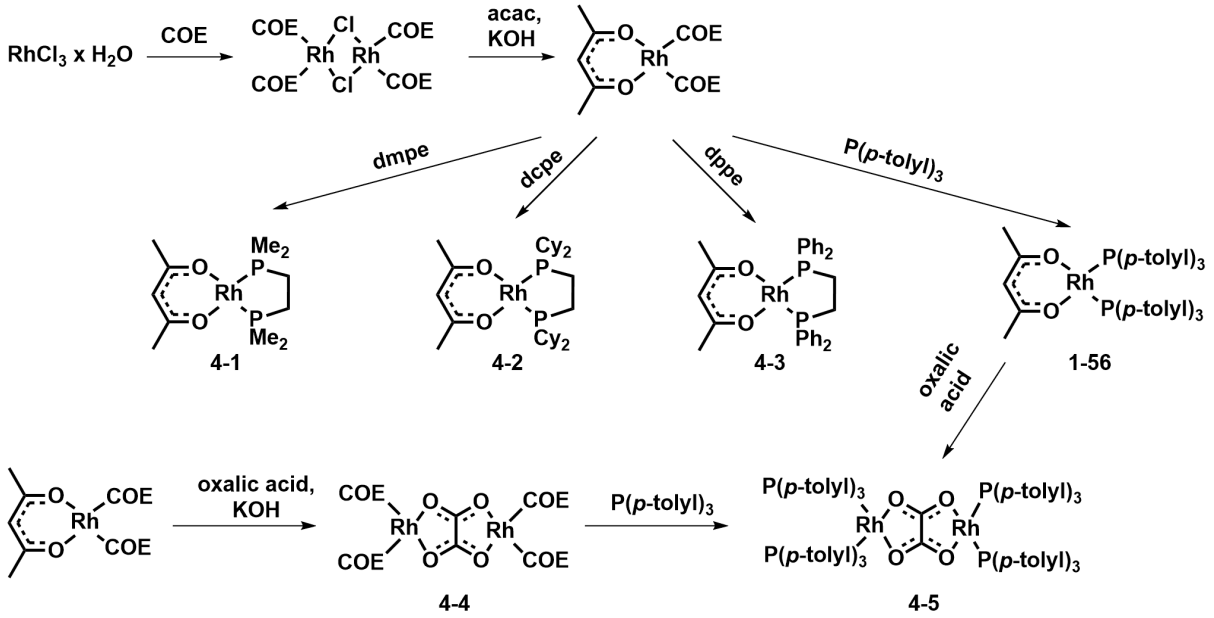

Scheme 4-3: Synthesis of [Rh(acac)dmpe] **4-1**, [Rh(acac)dcpe] **4-2**, [Rh(acac)dppe] **4-3**, [Rh(acac)(P(*p*-tolyl)$_3$)$_2$] **1-56**[71], [Rh$_2$(ox)(COE)$_4$] **4-4** and [Rh$_2$(ox)(P(*p*-tolyl)$_3$)$_4$] **4-5**.

The ^{1}H NMR spectra in C_6D_6 of [Rh(acac)dmpe] **4-1**, [Rh(acac)dcpe] **4-2** and [Rh(acac)dppe] **4-3** display a single resonance for the acac-CH_3 groups at ca. 1.90 ppm with an integral of six, and a singlet for the characteristic acac-CH group at ca. 5.40 ppm with an integral of one. For **4-1**, **4-2** and **4-3** a resonance for the C_2H_4-bridge of the chelating phosphine is located at 0.99, 2.49 and 1.83 ppm, respectively, with an integral of four. In the $^{13}C\{^1H\}$ NMR spectra, the carbonyl carbon atoms of the acac ligand resonate at ca. 185 ppm, and the acac-CH groups at ca. 100 ppm. The carbon atoms of the C_2H_4-bridge give rise to peaks at 29.7, 29.8 and 27.8 ppm, respectively. The $^{31}P\{^1H\}$ NMR spectra display doublets at 51.5, 91.7 and 70.2 ppm with Rh-P coupling constants of 190, 194 and 193 Hz, respectively, indicating rhodium(I) species. The ^{1}H, $^{13}C\{^1H\}$ and $^{31}P\{^1H\}$ NMR data are consistent with that for other square planar rhodium(I) complexes bearing phosphines and a chelating acac ligand.[71, 304-305] The $^{31}P\{^1H\}$ NMR shifts of **4-1**, **4-2** and **4-3** are downfield shifted compared to their PMe_3 (5.80 ppm), PCy_3 (49.9 ppm) and P(*p*-tolyl)$_3$ (54.8 ppm) analogues. The Rh-P coupling constants are around 190 Hz, as expected.

Elemental analysis as well as HRMS data are in accordance with the molecular formulae of the respective rhodium(I) compounds.

Single-crystals suitable for X-ray diffraction analysis were obtained by vapor diffusion of *n*-hexane into THF solutions of **4-1**, **4-2** and **4-3**. Complex **4-1** crystallizes in the orthorhombic space group $P2_12_12_1$, **4-2** in the monoclinic space group $P2_1/n$, and **4-3** in the tetragonal space group $I4_1/a$. The molecular structures are shown in Figure 4-1 and selected bond lengths and angles are listed in Table 4-1. The square-planar rhodium(I) metal centers in **4-1**, **4-2** and **4-3**

are coordinated by the bidentate acac ligand and by a chelating phosphine. The Rh-P distances are 2.1759(6) and 2.1807(6) Å for **4-1**, 2.1743(6) and 2.1770(8) Å for **4-2**, and 2.1836(5) and 2.1871(5) Å for **4-3**, respectively, and therefore significantly shorter than in [Rh(acac)(PMe_3)$_2$] **1-51**[305], [Rh(acac)(PCy_3)$_2$] **4-6**[304] and [Rh(acac)(P(*p*-tolyl)$_3$)$_2$] **1-56**[71] for which the analogous distances are 2.1950(5) and 2.1950(3) Å for **1-51**, 2.2523(12) and 2.2598(14) Å for **4-6**, and 2.2106(6) and 2.2203(6) Å for **1-56**, respectively. The Rh-P bond lengths in **4-1** and **4-2** are identical and slightly shorter than the Rh-P bond lengths in **4-3**, due to the stronger *σ*-donor abilities of the chelating phosphines in **4-1** and **4-2**, compared to the phenyl rings of the dppe ligand in **4-3**. The Rh-O bond distances in **4-1**, **4-2** and **4-3** are around the expected value of 2.086 Å as found for other square-planar [Rh(acac)(PR_3)$_2$]-complexes,[71, 304-305] and are not influenced by the shorter Rh-P bond distances. The O1-Rh1-O2 *β*-diketonato bite angle of 89° is similar to that of other related acac-substituted rhodium(I) complexes.[306-308]

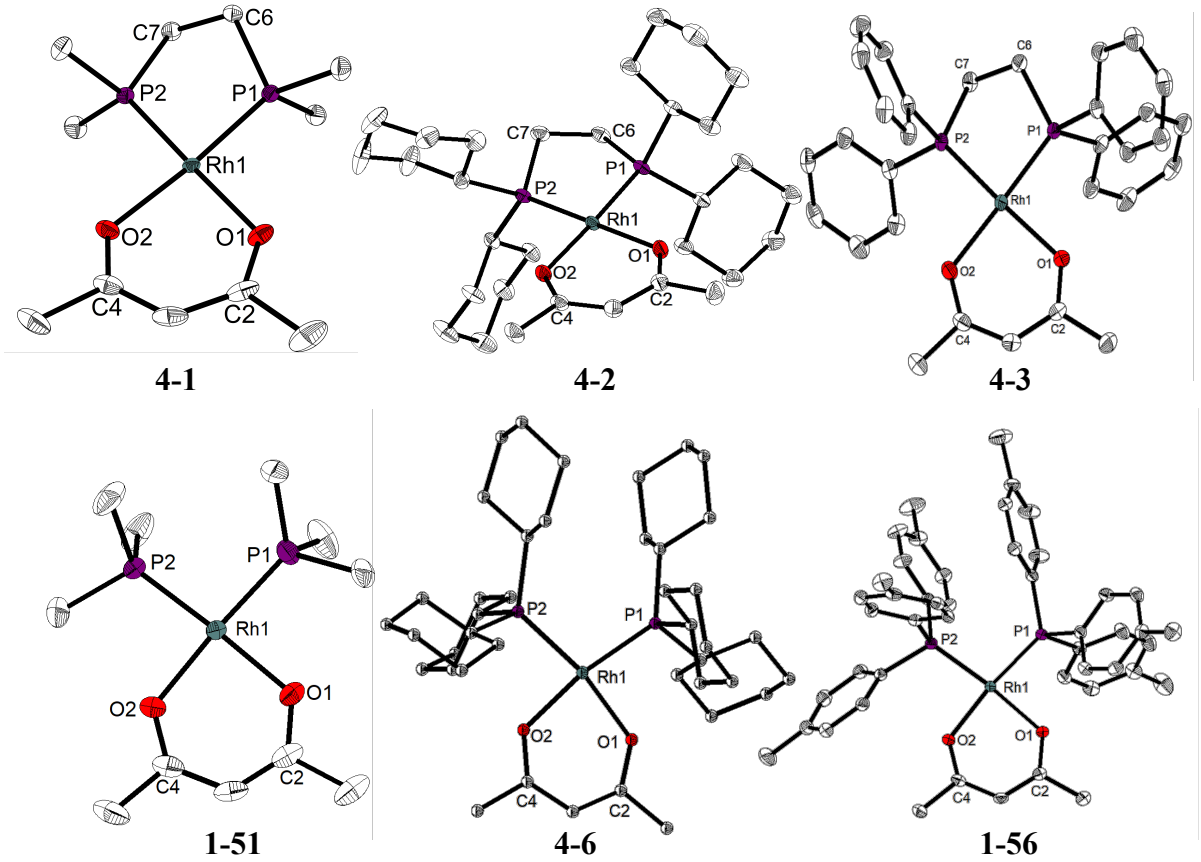

Figure 4-1: Molecular structures of [Rh(acac)dmpe] **4-1**, [Rh(acac)dcpe] **4-2**, [Rh(acac)dppe] **4-3**, [Rh(acac)(PMe_3)$_2$] **1-51**,[305] [Rh(acac)(PCy_3)$_2$] **4-6**[304] and [Rh(acac)(P(*p*-tolyl)$_3$)$_2$] **1-56**[71] in the solid state at 100 K. Hydrogen atoms and a THF solvent molecule (for **4-3**) are omitted for clarity. Atomic displacement ellipsoids are drawn at the 50% probability level.

The P1-Rh1-P2 phosphine angle in the complexes bearing a chelating phosphine is smaller 84.85(2), 86.40(3) and 84.588(2)° for **4-1**, **4-2** and **4-3**, respectively than those in complexes bearing two monodentate phosphines, for which the values are 94.716(15), 105.63(4) and 98.52(2)° for **1-51**, **4-6** and **1-56**, respectively. The bite angle in **4-1**, **4-2** and **4-3** is determined

by the C_2H_4-bridge connecting the two phosphorus atoms, while for **1-51**, **4-6** and **1-56** it results from steric constraints of phosphines. As a result of the large cone angle of PCy_3, **4-6** has the largest P1-Rh-P2 angle in the series.

Table 4-1: Selected bond lengths [Å] and angles [°] of [Rh(acac)dmpe] **4-1**, [Rh(acac)dcpe] **4-2**, [Rh(acac)dppe] **4-3**, [Rh(acac)(PMe_3)$_2$] **1-51**,[305] [Rh(acac)(PCy_3)$_2$] **4-6**[304] and [Rh(acac)(P(*p*-tolyl)$_3$)$_2$] **1-56**[71] determined by single-crystal X-ray diffraction at 100 K with esd's in parentheses.

	4-1	**4-2**	**4-3**
Rh1-O1	2.0925(16)	2.0838(11)	2.0844(15)
Rh1-O2	2.0876(16)	2.0870(12)	2.0927(15)
Rh1-P1	2.1807(6)	2.1770(8)	2.1871(5)
Rh1-P2	2.1759(6)	2.1743(6)	2.1836(5)
P1-C6	1.841(2)	1.8540(16)	1.855(2)
C6-C7	1.553(3)	1.539(2)	1.534(3)
P2-C7	1.840(2)	1.8464(15)	1.847(2)
O1-C2	1.271(3)	1.2693(18)	1.264(3)
O2-C4	1.265(3)	1.2673(18)	1.272(3)
O1-Rh1-O2	89.04(7)	88.85(5)	88.86(6)
P1-Rh1-P2	84.85(2)	86.40(3)	84.588(19)
O1-Rh1-P2	178.15(5)	178.57(3)	175.81(5)
O2-Rh1-P1	175.34(5)	177.10(3)	178.58(5)

	1-51	**4-6**	**1-56**
Rh1-O1	2.0850(11)	2.083(3)	2.0549(14)
Rh1-O2	2.0868(10)	2.089(4)	2.0857(14)
Rh1-P1	2.1953(5)	2.2598(14)	2.2106(6)
Rh1-P2	2.1950(5)	2.2523(12)	2.2203(6)
O1-C2	1.275(2)	1.279(6)	1.268(2)
O2-C4	1.2668(19)	1.276(6)	1.279(2)
O1-Rh1-O2	88.02(4)	85.91(12)	87.39(6)
P1-Rh1-P2	94.716(15)	105.63(4)	98.52(2)
O1-Rh1-P2	175.28(3)	169.98(9)	173.75(4)
O2-Rh1-P1	173.54(3)	169.26(9)	175.00(4)

The compounds $[Rh_2(ox)(COE)_4]$ **4-4** and $[Rh_2(ox)(P(p\text{-tolyl})_3)_4]$ **4-5** were characterized by elemental analysis, HRMS, multinuclear NMR spectroscopy and single-crystal X-ray diffraction analysis.

In the ^1H NMR spectrum of compound **4-4** in THF-d_8, the CH groups located at the double bond of the COE ligand give rise to a resonance at 2.50 ppm with an integral of eight. The CH_2 groups give rise to overlapping multiplets in the 2.15 – 1.25 ppm range, with a total integral of 48. In the $^{13}C\{^1H\}$ NMR spectrum, a resonance for the carbon atom of the bridging oxalate moiety is displayed at 174.5 ppm and of the olefin carbon atoms of the COE ligand resonate at 77.1 ppm. Singlets at 30.3, 27.7 and 27.1 ppm indicate the aliphatic COE-CH_2 carbon atoms.

In the ^1H NMR spectrum of compound **4-5** in THF-d_8, the tri(*p*-tolyl)phosphine ligands give rise to two multiplets at 7.37 – 7.31 and 6.83 – 6.81 ppm each with integral of 24 in the aromatic region. The CH_3 groups of the phosphine ligand give rise to a singlet at 2.25 ppm with an integral of 36. In the $^{13}C\{^1H\}$ NMR spectrum, the carbon atom of the bridging oxalate moiety resonates at 172.3 ppm. In the $^{31}P\{^1H\}$ NMR spectrum, a doublet at 54.7 ppm with a Rh-P coupling constant of 201 Hz is observed, indicating a rhodium(I) species. The ^1H, $^{13}C\{^1H\}$ and $^{31}P\{^1H\}$ NMR data are consistent with data for other square-planar rhodium(I) complexes.[71, 304-305] Elemental analysis and HRMS are also consistent with the formulations being $[Rh_2(ox)(COE)_4]$ and $[Rh_2(ox)(P(p\text{-tolyl})_3)_4]$.

Single-crystals suitable for X-ray diffraction analysis were obtained by vapor diffusion of *n*-hexane into THF solutions of **4-4** and **4-5**, respectively, and both crystallize in the triclinic space group $P\bar{1}$. The molecular structures are shown in Figure 4-2 and selected bond lengths and angles are listed in Table 4-2. The second halves of **4-4** and **4-5** are created by inversion centers located at the center of the C18-C20 bond.

The square-planar rhodium(I) metal center of complex $[Rh_2(ox)(COE)_4]$ **4-4** is coordinated to the bidentate oxalate ligand and to two η^2-bound cyclooctene ligands. The distances from the rhodium atom to the center of the C=C double bonds (C1-C8: X1 and C9-C16: X2) are 1.998(5) for Rh1-X1 and 1.999(6) Å for Rh1-X2, respectively. The Rh1-O1 and Rh1-O2 bond distances are 2.112(5) and 2.111(4) Å, respectively. The angles X1-Rh1-X2, O2-Rh1-X1, O1-Rh1-X2 and O1-Rh1-O2 are 95.29(3), 171.77(15), 171.56(15) and 79.20(17)°, respectively. Compared to the solid state structure of $[Rh(acac)(COE)_2]$, the Rh-X distances are in the same range and as those of other Rh-COE compounds. The Rh-O bond distances are somewhat shorter than those in $[Rh(acac)(COE)_2]$.[304] The O1-Rh1-O2 angles differ from those in known Rh(acac)-

complexes due to the different bite angle of the oxalate ligand, compared to that of the acetylacetonato ligand.

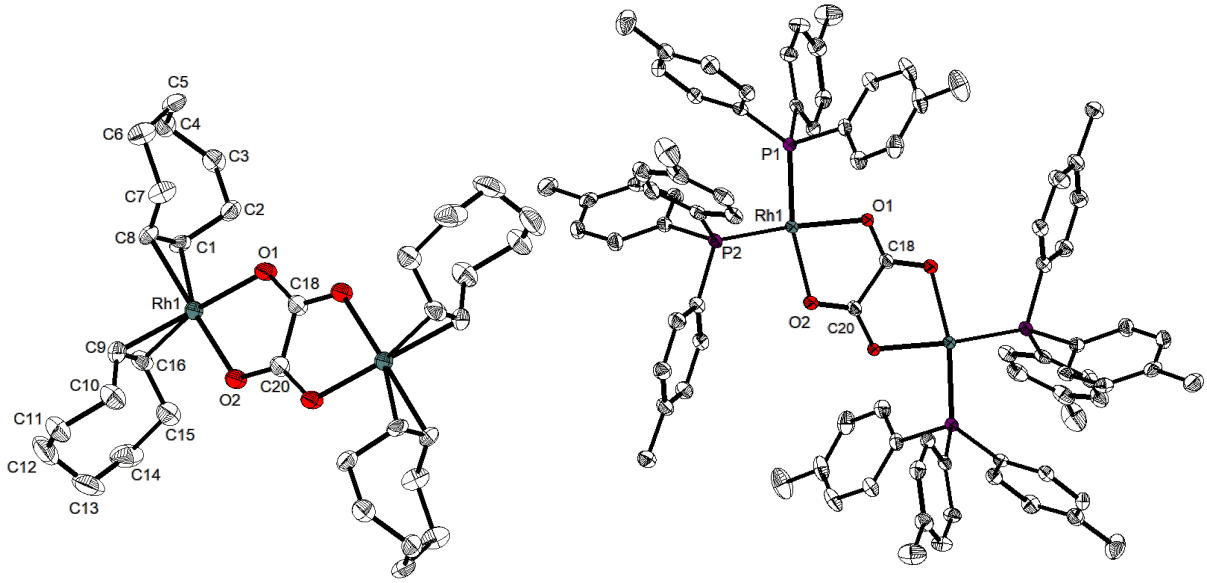

Figure 4-2: Molecular structure of $[Rh_2(ox)(COE)_4]$ **4-4** (left) and $[Rh_2(ox)(P(p\text{-tolyl})_3)_4]$ **4-5** (right) in the solid state at 100 K. Hydrogen atoms, THF solvent molecules and a second molecule in the unit cell (for **4-4**) are omitted for clarity. Atomic displacement ellipsoids are drawn at the 50% probability level.

The square-planar rhodium metal center of complex $[Rh_2(ox)(P(p\text{-tolyl})_3)_4]$ **4-5** is coordinated to the bidentate oxalate ligand and to two tri(*p*-tolyl)phosphine ligands. The Rh1-P1 and Rh1-P2 distances are 2.2046(14) and 2.1919(12) Å, respectively. The Rh1-O1 and Rh1-O2 bond distances are 2.147(2) and 2.144(2) Å, respectively. The P1-Rh1-P2, O1-Rh1-P2, O2-Rh1-P1 and O1-Rh1-O2 angles are 95.02(4), 175.20(5), 167.58(5) and 77.84(8)°, respectively. The Rh-P bond distances are similar and the Rh-O bond distances are larger than those of $[Rh(acac)(P(p\text{-tolyl})_3)_2]$ **1-56** (Table 4-1). The O1-Rh1-O2 angle is smaller, due to the bite angle of the oxalate ligand. The O1-Rh1-P2 angle is larger than the O2-Rh1-P1 angle. The same applies to the O2-Rh1-P2 and O1-Rh1-P1 angles.

Table 4-2: Selected bond lengths [Å] and angles [°] of [Rh_2(ox)$(COE)_4$] **4-4**, [Rh(acac)$(COE)_2$][304] and [Rh_2(ox)(P(*p*-tolyl)$_3)_4$] **4-5** determined by single-crystal X-ray diffraction at 100 K with esd's in parentheses.

	4-4	**Rh(acac)$(COE)_2$**		**4-5**
Rh1-O1	2.112(5)	2.0624(14)	Rh1-O1	2.147(2)
Rh1-O2	2.111(4)	2.0652(13)	Rh1-O2	2.144(2)
Rh1-C1	2.113(6)	2.1325(18)	Rh1-P1	2.2046(14)
Rh1-C8	2.117(6)	2.1347(19)	Rh1-P2	2.1919(12)
Rh1-C9	2.104(7)	2.1298(19)	O1-C18	1.255(3)
Rh1-C16	2.130(7)	2.1417(18)	O2-C20	1.257(3)
Rh1-X1	1.998(5)	2.0142(3)*	C18-C20	1.545(5)
Rh1-X2	1.999(6)	2.0163(3)*	-	-
O1-C18	1.260(8)	-	-	-
O2-C20	1.241(8)	-	-	-
C1-C8	1.391(10)	-	-	-
C9-C16	1.392(11)	-	-	-
C18-C20	1.543(12)	-	-	-
O1-Rh1-O2	79.20(17)	87.69(9)	O1-Rh1-O2	77.84(8)
X1-Rh1-X2	95.29(3)	93.614(9)*	P1-Rh1-P2	95.02(4)
O1-Rh1-X1	93.07(15)	90.15(4)*	O1-Rh1-P1	89.77(7)
O2-Rh1-X2	92.52(15)	89.47(4)*	O2-Rh1-P2	97.37(7)
O1-Rh1-X2*	171.56(15)	172.13(4)	O1-Rh1-P2	175.20(5)
O2-Rh1-X1*	171.77(15)	171.68(4)	O2-Rh1-P1	167.58(5)

X1: mid-point of C1-C8 and X2: mid-point of C9-C16. *due to two different values given in the publication of [Rh(acac)$(COE)_2$], the values were newly distinct.

In the Marder group, the common synthetic route to [Rh(S_2CNEt_2)(phosphine)$_2$] complexes is the reaction of [RhCl(COE)$_2$]$_2$ with a phosphine (PMe_3 or PPh_3) resulting in [Rh(PMe_3)$_3$Cl] or [Rh(PPh_3)$_3$Cl] which were further reacted with sodium diethyldithiocarbamate.[68] In order to avoid using an excess of phosphine (with regard to costs and purification) an alternative synthesis route was developed (Scheme 4-4). Thus, the reaction of [RhCl(COE)$_2$]$_2$ with sodium diethyldithiocarbamate, analogously to similar acac-complexes, resulted in the formation of a black solution, regardless of the solvent. Decomposition by COE dissociation in solution is described in the literature.[309] Therefore, the labile COE ligand in [RhCl(COE)$_2$]$_2$ was replaced with the stronger bidentate COD ligand yielding [RhCl(COD)]$_2$. Addition of sodium diethyldithiocarbamate to a solution of [RhCl(COD)]$_2$ in THF, and stirring the suspension for two days, results in [Rh(S_2CNEt_2)(COD)],[309] which was obtained as a yellow solid in 96% yield. The desired diethyldithiocarbamate-substituted rhodium(I)-phosphine compounds [Rh(S_2CNEt_2)dmpe] **4-7**, [Rh(S_2CNEt_2)dcpe] **4-8** and [Rh(S_2CNEt_2)dppe] **4-9** were obtained as yellow solids in 80, 89 and 89% yields, respectively (Scheme 4-4), by reaction of this rhodium monomer with the corresponding phosphine in THF.

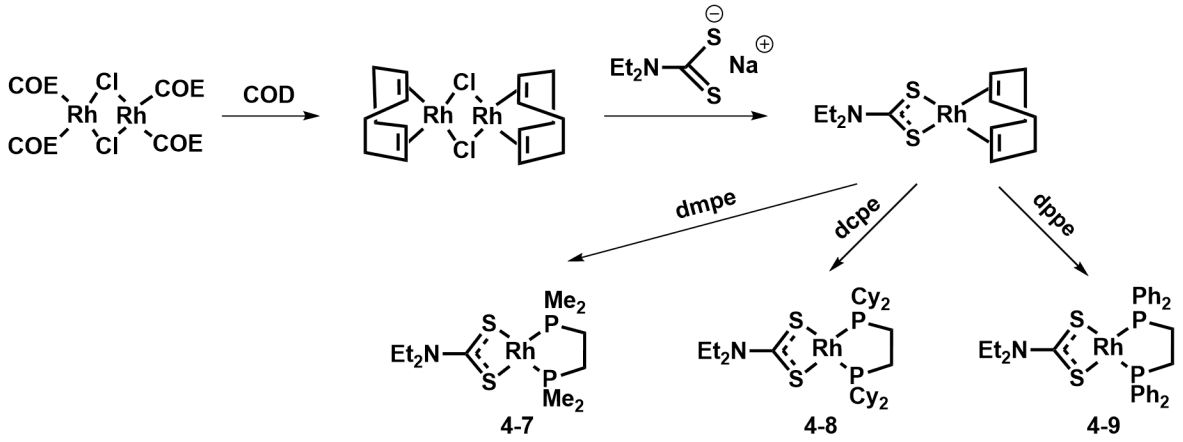

Scheme 4-4: Synthesis of [Rh(S_2CNEt_2)dmpe] **4-7**, [Rh(S_2CNEt_2)dcpe] **4-8** and [Rh(S_2CNEt_2)dppe] **4-9**.

An alternative to the reaction pathway shown in Scheme 4-4 is an acetylacetonato-diethyldithiocarbamate exchange reaction (Scheme 4-5). Therefore, an excess of the diethyldithiocarbamate salt (1.5 equiv.) was added to [Rh(acac)(phosphine)] in THF and the reaction was stirred at 60 °C for at least 24 hours. Purification was conducted by washing with ethanol or dissolving the crude product in toluene, followed by filtration and recrystallization from THF layered with *n*-hexane at -30 °C.

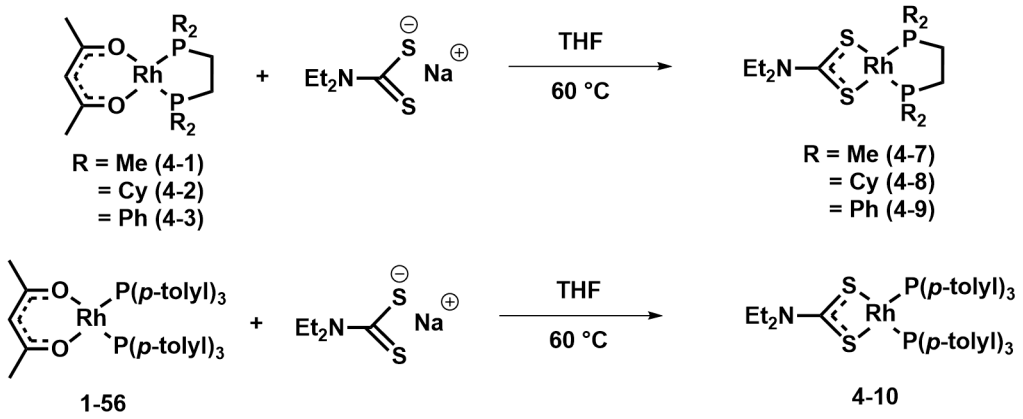

Scheme 4-5: Synthesis of [Rh(S2CNEt2)dmpe] **4-7**, [Rh(S2CNEt2)dcpe] **4-8**, [Rh(S2CNEt2)dppe] **4-9** and [Rh(S2CNEt2)(P(*p*-tolyl)3)2] **4-10** by an acetylacetonato-diethyldithiocarbamate exchange reaction.

The compounds [Rh(S2CNEt2)dmpe] **4-7**, [Rh(S2CNEt2)dcpe] **4-8**, [Rh(S2CNEt2)dppe] **4-9** and [Rh(S2CNEt2)(P(*p*-tolyl)3)2] **4-10** were characterized by elemental analysis (except **4-7**), HRMS, multinuclear NMR spectroscopy, and single-crystal X-ray diffraction analysis. The molecular structures of **4-7**, **4-8**, **4-9**, **4-10** and [Rh(S2CNEt2)(PMe3)2] **1-44**, for comparison, are shown in Figure 4-3 with selected bond distances and angles are listed in Table 4-3.

In the ^{1}H NMR spectra in C_6D_6 of the compounds **4-7**, **4-8**, **4-9** and **4-10**, the CH_2 groups of the diethyldithiocarbamate ligand give rise to quartets at 3.50, 3.47, 3.38 and 3.22 ppm, respectively, with a coupling constant of 7.1 Hz and an integral of four. The CH_3 groups give rise to triplets at 0.92, 0.87, 0.81 and 0.68 ppm, respectively, with a coupling constant of 7.1 Hz and an integral of six. The signals for the C_2H_4-bridges of the chelating phosphines in **4-7**, **4-8** and **4-9**, are located at 1.01, 2.47 and 1.93 ppm, respectively, with an integral of four. In the ^{13}C{^{1}H} NMR spectra, the carbon-atom attached to the two sulfur atoms in the diethyldithiocarbamate moiety gives rise to a doublet at ca. 215 ppm with a coupling constant of 5 Hz. The CH_2 groups of the diethyldithiocarbamate ligand resonate at ca. 43.2 ppm and the CH_3 groups resonate at 12.7 ppm. Resonances at 30.4, 30.2 and 28.7 ppm for **4-7**, **4-8** and **4-9**, respectively, can be assigned to the C_2H_4-bridges of the chelating phosphines. In the ^{31}P{^{1}H} NMR spectra of **4-7**, **4-8**, **4-9** and **4-10**, doublets are observed at 45.1, 91.1, 70.2 and 47.5 ppm with Rh-P coupling constants of 173, 180, 178 and 178 Hz, respectively, indicating rhodium(I) species. The ^{1}H, ^{13}C{^{1}H} and ^{31}P{^{1}H} NMR data are consistent with data for other square-planar rhodium(I) complexes bearing phosphines and a diethyldithiocarbamate ligand.[68] The ^{31}P{^{1}H} NMR shifts of the complexes **4-7** and **4-9** are shifted downfield compared to their PMe_3 (-5.00 ppm) and PPh_3 (49.0 ppm) analogues.[68] An analogous [Rh(S2CNEt2)(PCy3)2] complex was not found in the literature.

Single-crystals suitable for X-ray diffraction analysis were obtained by vapor diffusion of *n*-hexane or *n*-pentane into THF solutions of **4-7**, **4-8**, **4-9** and **4-10**. Complex **4-7** crystallizes in the orthorhombic space group *Pbca*, **4-8** in the triclinic space group $P\bar{1}$, **4-9** in the monoclinic space group $P2_1/c$, and **4-10** in the monoclinic space group $C2/c$. The molecular structures are shown in Figure 4-3 and selected bond lengths and angles are listed in Table 4-3.

The square-planar rhodium metal centers of complexes **4-7**, **4-8**, **4-9** and **4-10** are coordinated by the bidentate diethyldithiocarbamate ligand and by a chelating phosphine for **4-7**, **4-8** and **4-9** and by two tri(*p*-tolyl)phosphine ligands for **4-10**. Due to strong disorder in the solid state structure of **4-8**, the molecular structure shown in Figure 4-3 only serves as a proof of connectivity.

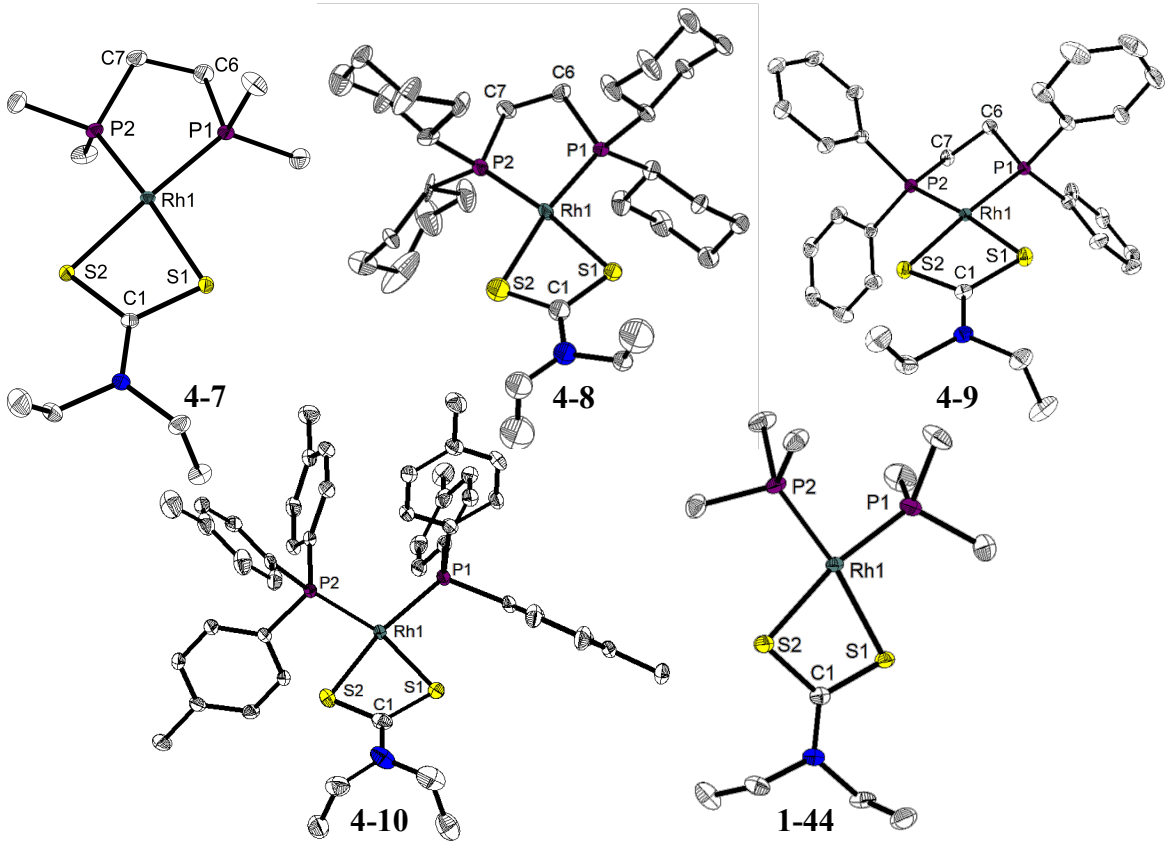

Figure 4-3: Molecular structure of [Rh(S$_2$CNEt$_2$)dmpe] **4-7**, [Rh(S$_2$CNEt$_2$)dcpe] **4-8**, [Rh(S$_2$CNEt$_2$)dppe] **4-9**, [Rh(S$_2$CNEt$_2$)(P(*p*-tolyl)$_3$)$_2$] **4-10** and [Rh(S$_2$CNEt$_2$)(PMe$_3$)$_2$] **1-44**[68] in the solid state at 100 K. Hydrogen atoms, solvent molecules (*n*-pentane for **4-10**) and a second molecule in the unit cell (for **1-44**) are omitted for clarity. Atomic displacement ellipsoids are drawn at the 50% probability level. The molecular structure of **4-8** only serves as a proof of connectivity.

The Rh-P bond distances are 2.1875(7) and 2.2048(6) Å for **4-7**, 2.2101(12) and 2.2066(12) Å for **4-9** and 2.2518(8) and 2.2406(9) Å for **4-10**, respectively. The Rh-P distances for **4-7** and previously reported **1-44** are similar, while for **4-9** the distances are significantly shorter than for **4-10**. The Rh-S bond distance for **4-7**, **4-9** and **4-10** is around the expected value of ca. 2.38 Å and the S1-Rh1-S2 dithiocarbamate bite angle of 74° is similar to that of other related diethyldithiocarbamate-chelated rhodium(I) complexes.[68] The P1-Rh1-P2 phosphine bite

angle is smaller (ca. 85°) in the complexes bearing a chelating phosphine, than in the complexes bearing two monodentate phosphines (102.31(3) and 95.53(2)° for **4-10** and **1-44**, respectively). The largest P1-Rh-P2 angle in the series is that for **4-10**, bearing the bulky monodentate triarylphosphine ligands.

Table 4-3: Selected bond lengths [Å] and angles [°] of [Rh(S_2CNEt_2)dmpe] **4-7**, [Rh(S_2CNEt_2)dppe] **4-9**, [Rh(S_2CNEt_2)(P(*p*-tolyl)$_3$)$_2$] **4-10** and [Rh(S_2CNEt_2)(PMe_3)$_2$] **1-44**[68] determined by single-crystal X-ray diffraction at 100 K with esd's in parentheses.

	4-7	**4-9**	**4-10**	**1-44**
Rh1-S1	2.3875(6)	2.3919(13)	2.3647(9)	2.3812(6)
Rh1-S2	2.3924(7)	2.3836(13)	2.3778(9)	2.3904(6)
Rh1-P1	2.1875(7)	2.2101(12)	2.2518(8)	2.2123(6)
Rh1-P2	2.2048(6)	2.2066(12)	2.2406(9)	2.2185(6)
P1-C6	1.8372(19)	1.8422(16)	-	-
C6-C7	1.525(3)	1.5334(19)	-	-
P2-C7	1.8430(18)	1.8439(17)	-	-
S1-C1	1.7247(17)	1.7273(15)	1.715(3)	1.722(2)
S2-C1	1.7235(16)	1.7219(15)	1.710(3)	1.727(2)
C1-N	1.3281(19)	1.3282(17)	1.327(4)	1.322(3)
S1-Rh1-S2	74.03(2)	73.86(5)	73.61(3)	73.89(2)
S1-C1-S2	113.14(9)	112.58(8)	112.11(17)	112.54(12)
P1-Rh1-P2	84.55(2)	85.10(5)	102.31(3)	95.53(2)
S1-Rh1-P1	98.97(2)	100.10(5)	93.19(3)	94.07(2)
S2-Rh1-P2	103.14(2)	101.00(5)	90.62(3)	96.55(2)
S1-Rh1-P2	174.041(16)	174.411(11)	164.09(3)	170.38(2)
S2-Rh1-P1	169.316(16)	173.721(12)	165.86(3)	167.60(2)

Table 4-4 shows a summary of characteristics of the different rhodium(I) complexes from section 4.3.1. For the acac-substituted rhodium complexes with chelating phosphines, the mean Rh-P distance is shorter and the P-Rh-P bite angle smaller than those for the corresponding complexes with two monodentate phosphines, whereas the mean O-Rh-P angle and the $^{31}P\{^{1}H\}$ NMR shifts are larger. The coupling constants are in the range of 186 – 195 Hz.

For the diethyldithiocarbamate-substituted rhodium(I)-phosphine complexes the same trends in bonds lengths, angles and $^{31}P\{^{1}H\}$ NMR shifts are observed. The coupling constants are in the range of 172 – 180 Hz, ca. 15 Hz smaller than those of the analogous acac-rhodium(I) complexes.

Table 4-4: Mean Rh-P distances [Å], mean P-Rh-P angle [°], mean O-Rh-P angle [°], $^{31}P\{^{1}H\}$ NMR shift in C_6D_6 [ppm] and $^{1}J_{Rh-P}$ [Hz] of the compounds [Rh(acac)dmpe] **4-1**, [Rh(acac)dcpe] **4-2**, [Rh(acac)dppe] **4-3**, [Rh(acac)(PMe_3)$_2$] **1-51**,[305] [Rh(acac)(PCy_3)$_2$] **4-6**,[304] [Rh(acac)(P(*p*-tolyl)$_3$)$_2$] **1-56,**[71] [Rh(S_2CNEt_2)dmpe] **4-7**, [Rh(S_2CNEt_2)dcpe] **4-8**, [Rh(S_2CNEt_2)dppe] **4-9**, [Rh(S_2CNEt_2)(PMe_3)$_2$] **1-44**[68] and [Rh(S_2CNEt_2)(P(*p*-tolyl)$_3$)$_2$] **4-10**. Additionally, $^{31}P\{^{1}H\}$ NMR shift of the unbound phosphine in C_6D_6 [ppm] and coordination chemical shift Δ [ppm].

	Mean Rh-P distance	Mean P-Rh-P angle	Mean O-Rh-P angle	$^{31}P\{^{1}H\}$ NMR shift	$^{1}J_{Rh-P}$	$^{31}P\{^{1}H\}$ NMR shift phosphine	Δ
				acac			
4-1	2.1783	84.85	176.75	51.5	189	-48.8	100.3
4-2	2.1757	86.40	177.84	91.7	194	1.0	90.7
4-3	2.1854	84.59	177.20	70.1	193	-12.8	82.9
1-51	2.1952	94.72	174.41	5.8	186	-62.7	68.5
4-6	2.2561	105.63	169.62	49.9	191	10.5	39.4
1-56	2.2155	98.52	174.38	54.8	195	-7.8	62.6
				S_2CNEt_2			
4-7	2.1962	84.55	171.68	45.1	173	-48.8	93.9
4-8	-	-	-	91.1	180	1.0	90.1
4-9	2.2084	85.10	174.07	70.2	178	-12.8	83.0
1-44	2.2154	95.53	168.99	-5.4	172	-62.7	57.3
4-10	2.2462	102.31	164.98	47.5	178	-7.8	55.3

Comparing the $^{31}P\{^{1}H\}$ NMR shifts of the rhodium-phosphine complexes with the unbound phosphines, it becomes obvious, that they are all shifted downfield. On bonding, the phosphorus atom of the phosphine donates electron density to the metal, which causes a deshielding of the phosphorus atom and, as a consequence, a downfield shift in its $^{31}P\{^{1}H\}$ NMR signal. The change in the NMR signal when a ligand binds to a metal is known as coordination chemical shift Δ and can be calculated by subtracting the shift of the unbound ligand from the shift of the complexed ligand. The larger the value of Δ, the more electron density is donated from the phosphorus atom to the metal center, hence, the shorter the Rh-P distance is expected to be.

This depends on both electronic and steric effects, i.e., the σ-donor properties of the substitutents of the phosphine and the ligand cone angle. A smaller cone angle of the phosphine results in a more stable Rh-P bond. The coordination chemical shift Δ also depends on the additional ligands attached to the metal center. Poorer electron donor groups result in a more deshielded complex with the same phosphine ligands, as more electron density from the phosphine can be donated to the metal center.[310-311] The ring size of the chelating phosphine has also an influence on the metal-phosphorus coupling. In general, in the order dppe, dppp and dppm the coupling constant increases.[311-312] The Rh-P coupling constant also reflects the Rh-P bond length. For a large $J_{Rh\text{-}P}$, in general, a shorter Rh-P bond distance is expected (see coupling constants[233] and distances[313] in $[RhCl(PPh_3)_3]$).

Comparing the acac- and the diethyldithiocarbamate-substituted rhodium(I) complexes with two monodentate phosphines, the latter are less deshielded, due to the better electron donor properties of the dithiocarbamate ligand, compared to the acac ligand, resulting in a lower Rh-P coupling constant. For the same reason, the Rh-P bond distances in the acac-complexes are always shorter than those in the analogues dithiocarbamate complexes. For these complexes, the Rh-P bond distances and the P-Rh-P angles correlate with the cone angle of the phosphines (PCy_3 > P(*p*-tolyl)$_3$ > PMe_3), hence, the smaller the cone angle, the shorter the Rh-P bond and the smaller the P-Rh-P angle.

The coordination chemical shifts Δ of the acac-substituted complexes $[Rh(acac)(PMe_3)_2]$ **1-51**, $[Rh(acac)(PCy_3)_2]$ **4-6** and [Rh(acac)(P(*p*-tolyl)$_3$)$_2$] **1-56** are 68.5, 39.4 and 62.6 ppm, respectively, and for the dithiocarbamate-substituted complexes $[Rh(S_2CNEt_2)(PMe_3)_2]$ **1-44** and $[Rh(S_2CNEt_2)$(P(*p*-tolyl)$_3$)$_2$] **4-10** they are 57.3 and 55.3 ppm, respectively. The larger the value of Δ, the shorter the Rh-P bond distance.

The coordination chemical shifts Δ of the acac-substituted complexes [Rh(acac)dmpe] **4-1**, [Rh(acac)dcpe] **4-2**, [Rh(acac)dppe] **4-3** are 100.3, 90.7 and 82.9 ppm, respectively, and for the dithiocarbamate-substituted complexes $[Rh(S_2CNEt_2)$dmpe] **4-7**, $[Rh(S_2CNEt_2)$dcpe] **4-8**, $[Rh(S_2CNEt_2)$dppe] **4-9** they are 93.9, 90.1 and 83.0 ppm, respectively. Again, a trend of a large Δ, and a short Rh-P bond length is observed, although the mean Rh-P bond length in **4-2** is shorter than in **4-1** and the value of Δ is smaller in **4-2** than in **4-1**. This discrepancy may arise from the standard uncertainties from the single-crystal X-ray structures.

For the acac- and the diethyldithiocarbamate-substituted rhodium(I) complexes with chelating phosphines, the Rh-P distances are significantly shorter and Δ larger than in the complexes with two monodentate phosphines.

Generally the acac- and dithiocarbamate-substituted rhodium(I)-phosphine complexes follow trends that are usually observed in such systems, but the cyclohexyl-substituted phosphine-complexes do not follow all trends strictly.

4.3.2 Reactions of rhodium(I) complexes with aryl-substituted *α,ω*-diynes

In section 3.3.3, the stoichiometric reaction of [Rh(acac)(P(*p*-tolyl)$_3$)$_2$] **1-56** with different aryl-substituted *α,ω*-diynes was described. It was found that, unlike in the reaction of **1-56** with different *α,ω*-tetraynes in equimolar amounts,[71-72] it was only possible to obtain clean formation of a tri(*p*-tolyl)phosphine-substituted 2,5-bis(aryl)rhodacyclopentadiene from the reaction with the *α,ω*-diyne **3-1**. In the reactions of *α,ω*-diynes **3-2**, **3-5** and **3-8** with **1-56**, rhodacyclopentadienes as well as cycloisomerization products were obtained. However, in the reaction of **1-56** with *α,ω*-diyne **3-4**, cyclization was only observed to a certain extend at elevated temperature. The rhodium(I) complexes [Rh(acac)dmpe] **4-1**, [Rh(acac)dcpe] **4-2**, [Rh(acac)dppe] **4-3**, [Rh(acac)(P(*p*-tolyl)$_3$)$_2$] **1-56**, [Rh(S$_2$CNEt$_2$)dcpe] **4-8**, [Rh(S$_2$CNEt$_2$)dppe] **4-9** and [Rh(S$_2$CNEt$_2$)(P(*p*-tolyl)$_3$)$_2$] **4-10** described in section 4.3.1 were used as catalysts, and the formation of dimers and trimers of *α,ω*-diynes were investigated. Due to the low solubility of [Rh(ox)(P(*p*-tolyl)$_3$)$_4$] **4-5** and the absence of an elemental analysis for [Rh(S$_2$CNEt$_2$)dmpe] **4-7** no investigations, regarding the catalytic activity were conducted. The compounds formed in the cycloisomerization reactions have a *para*-terphenyl core structure, with the newly formed benzene moiety being fully substituted (Scheme 4-6). The triple bond in the dimers **4-11a** – **4-14a** can be used for further modification by e.g., the reaction with metal-azides in a [3+2] click-type reaction.[314-315] By using different substituents at the *para*-position of the aryl moiety, modification can be conducted *via* Sonogashira cross-coupling reactions (*p*-Br), by the formation of azides (*p*-NH$_2$) or by methylation of secondary amines (*p*-NR$_2$).

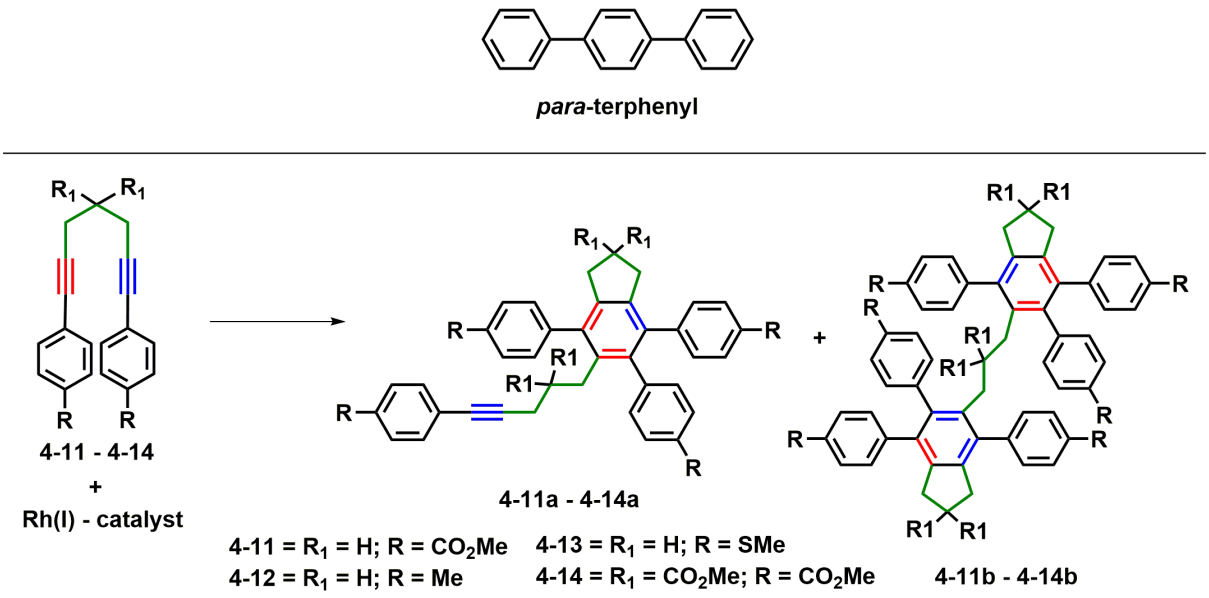

Scheme 4-6: Top: *para*-Terphenyl. Bottom: Reaction of *α,ω*-diynes **4-11** – **4-14** with rhodium(I)-catalyst forming dimers **4-11a** – **4-14a** and trimers **4-11b** – **4-14b**.

The formation of a dimer and trimer of *α,ω*-diynes was briefly mentioned in section 3.3.3. While in that section, attention was focused on the acac region (5.80 – 4.50 ppm), in this chapter, the region around 4.00 – 1.00 ppm is of greater importance for the identification of the different species. Figure 4-4 shows the ^{1}H NMR spectra of the reaction of [Rh(acac)(P(*p*-tolyl)$_3$)$_2$] **1-56** with the *α,ω*-diyne **4-11** at room temperature after 56 hours (purple spectrum), and at 60 °C after seven hours (blue spectrum), dimer **4-11a** (red spectrum) and trimer **4-11b** (black spectrum). Inspection of the carboxymethoxy region at room temperature from 3.70 – 3.30 ppm, shows formation of a dimer and trimer (more dimer than trimer) and, after heating, only trimer and a resonance for the CO_2Me group of the rhodacyclopentadiene **3-17**.

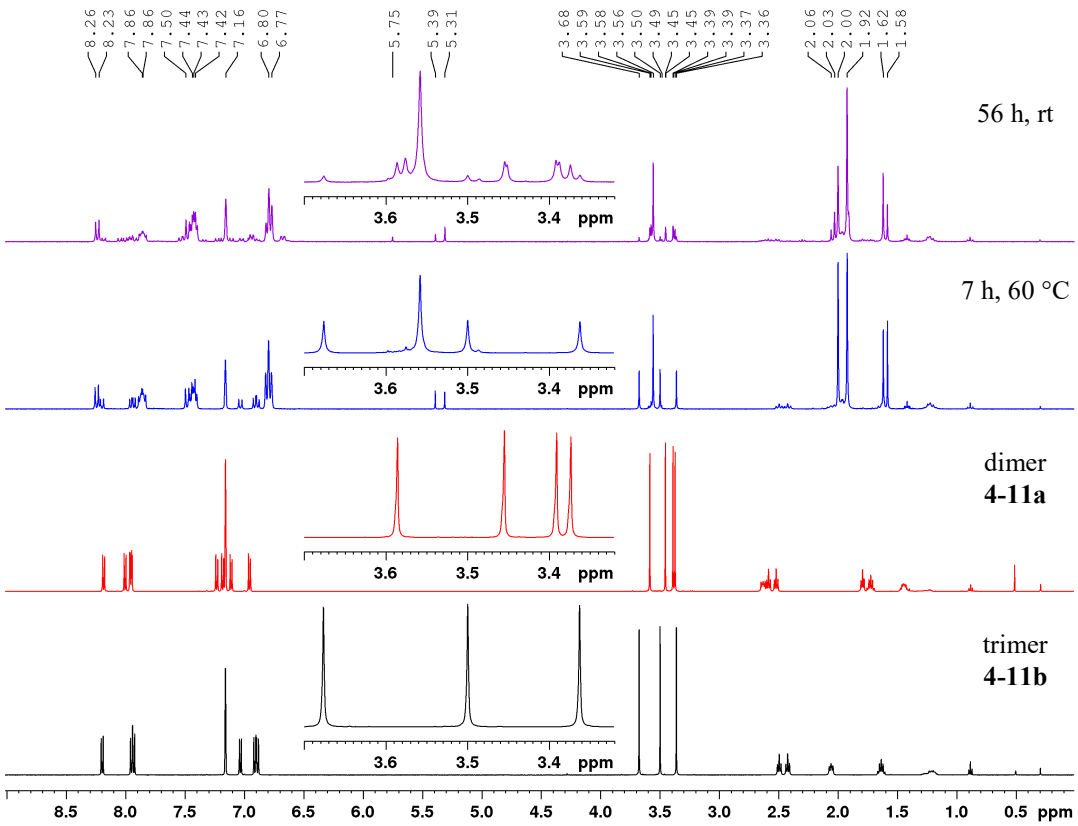

Figure 4-4: ^{1}H NMR spectra (300 MHz, C_6D_6) of the reaction of [Rh(acac)(P(*p*-tolyl)$_3$)$_2$] **1-56** with *α,ω*-diyne **4-11** in equimolar amounts at room temperature after 56 hours (purple), at 60 °C after 7 hours (blue), dimer **4-11a** (red) and trimer **4-11b** (black).

For a closer analysis of the catalytic reaction, the catalytic activities of [Rh(acac)(P(*p*-tolyl$_3$)$_2$] **1-56** and [Rh(S_2CNEt_2)(P(*p*-tolyl$_3$)$_2$] **4-10** were tested in first place with two different *α,ω*-diynes. Diynes **4-11** with an electron-withdrawing CO_2Me-group and **4-13** with an electron-donating SMe-group at the *para*-position of the aryl moiety were chosen as model substrates. Different catalyst loadings (1 and 10 mol%) and different temperatures (rt and 60 °C) were applied. J-Young's tap NMR tubes were used for reactions of 28.4 µmol of

α,ω-diyne in 1 mL of C_6D_6. Progress of the reactions were monitored *via* ^{1}H NMR spectroscopy. The reactions were considered to be complete when all of the *α,ω*-diyne starting material was consumed, according to the respective ^{1}H NMR spectrum. The ratio of dimer to trimer was determined *via* the integration of CO_2Me/SMe signals in the ^{1}H NMR spectrum.

Table 4-5 shows the results of the reactions with 10 mol% of the catalysts [Rh(acac)(P(*p*-tolyl$_3$)$_2$] **1-56** and [Rh(S_2CNEt_2)(P(*p*-tolyl$_3$)$_2$] **4-10** with the *α,ω*-diynes **4-11** and **4-13** at room temperature.

The cycloisomerization of **4-11** with **1-56** (Table 4-5, entry 1) was complete in 12 days, and that of **4-10** (entry 2) in eight days. The reaction of **4-13** with **1-56** (entry 3) was complete after 13 days, and that of **4-10** after 18 days. The dimer:trimer ratio for entries 1, 2 and 4 are ca. 1:0.45, while it is 1:0.14 for entry 3.

The cycloisomerization of the CO_2Me-substituted *α,ω*-diyne **4-11** is faster at room temperature with the diethyldithiocarbamate substituted catalyst than with the acac-substituted catalyst, while the dimer:trimer ratio is similar in both reactions. In contrast, the cycloisomerization of the SMe-substituted *α,ω*-diyne **4-13** was faster with the acac-substituted catalyst **1-56**.

Table 4-5: Results of the reaction of *α,ω*-diynes **4-11** and **4-13** with 10 mol% of [Rh(acac)(P(*p*-tolyl)$_3$)$_2$] **1-56** and [Rh(S_2CNEt_2)(P(*p*-tolyl)$_3$)$_2$] **4-10** at room temperature.

entry	diyne	catalyst-loading	catalyst	ratio dimer:trimer	reaction time until completion
1	**4-11**	10 mol%	**1-56**	1:0.42	12 d
2	**4-11**	10 mol%	**4-10**	1:0.45	8 d
3	**4-13**	10 mol%	**1-56**	1:0.14	13 d
4	**4-13**	10 mol%	**4-10**	1:0.50	18 d

The reactions with 1 mol% of catalyst loading did not reach completion at room temperature within a reasonable amount of time. Therefore, the reaction was stopped after 14 days and the results are summarized in Table 4-6.

In the reaction of **4-11** with **4-10**, more of the diyne was consumed and more trimer was formed than in the reaction with **1-56** after 14 days (Table 4-6, entries 1 and 2). In the reaction of *α,ω*-diyne **4-13** with **1-56**, more diyne was consumed and more trimer was formed than with the diethyldithiocarbamate-substituted catalyst **4-10** (entries 3 and 4). Although the reaction was not complete, it can be seen that the cycloisomerization of **4-11** with **4-10** and of **4-13** with **1-56** are faster than that of **4-11** with **1-56** and **4-13** with **4-10**. These results agree with those in Table 4-5.

Table 4-6: Results of the reaction of *α,ω*-diynes **4-11** and **4-13** with 1 mol% of [Rh(acac)(P(*p*-tolyl)$_3$)$_2$] **1-56** and [Rh(S$_2$CNEt$_2$)(P(*p*-tolyl)$_3$)$_2$] **4-10** at room temperature after 14 days.

entry	diyne	catalyst-loading	catalyst	ratio dimer:trimer:diyne
1	**4-11**	1 mol%	**1-56**	1:0.02:12.9
2	**4-11**	1 mol%	**4-10**	1:0.13:1.50
3	**4-13**	1 mol%	**1-56**	1:0.21:1.00
4	**4-13**	1 mol%	**4-10**	1:0.09:3.68

At 60 °C, the reactions of *α,ω*-diynes **4-11** and **4-13** with 10 mol% of the catalyst [Rh(acac)(P(*p*-tolyl)$_3$)$_2$] **1-56** were faster than those with [Rh(S$_2$CNEt$_2$)(P(*p*-tolyl)$_3$)$_2$] **4-10**. The dimer:trimer ratio for the reaction of **4-11** with **1-56** is 1:0.75 and for the others ca. 1:0.50 (Table 4-7).

Table 4-7: Results of the reaction of *α,ω*-diynes **4-11** and **4-13** with 10 mol% of [Rh(acac)(P(*p*-tolyl)$_3$)$_2$] **1-56** and [Rh(S$_2$CNEt$_2$)(P(*p*-tolyl)$_3$)$_2$] **4-10** at 60 °C.

entry	diyne	catalyst-loading	catalyst	ratio dimer:trimer	reaction time until completion
1	**4-11**	10 mol%	**1-56**	1:0.75	<12 h*
2	**4-11**	10 mol%	**4-10**	1:0.50	24 h
3	**4-13**	10 mol%	**1-56**	1:0.55	<12 h*
4	**4-13**	10 mol%	**4-10**	1:0.50	60 h

*the first NMR of the reaction was measured after 12 hours.

At 60 °C, the reactions of *α,ω*-diynes **4-11** and **4-13** with 1 mol% of the catalyst **1-56** were faster than those with **4-10** (Table 4-8, entries 1 – 4). Furthermore, the reaction time of diyne **4-11** is always shorter than with **4-13**. The dimer:trimer ratio is ca. 1:0.50 for the CO_2Me- and SMe-substituted diyne.

Table 4-8: Results of the reaction of *α,ω*-diynes **4-11** and **4-13** with 1 mol% of [Rh(acac)(P(*p*-tolyl)$_3$)$_2$] **1-56** and [Rh(S$_2$CNEt$_2$)(P(*p*-tolyl)$_3$)$_2$] **4-10** at 60 °C.

entry	diyne	catalyst-loading	catalyst	ratio dimer:trimer	reaction time until completion
1	**4-11**	1 mol%	**1-56**	1:0.42	2 d
2	**4-11**	1 mol%	**4-10**	1:0.45	3.5 d
3	**4-13**	1 mol%	**1-56**	1:0.46	5.5 d
4	**4-13**	1 mol%	**4-10**	1:0.52	7 d

At room temperature, the cycloisomerization of **4-11** was faster with [Rh(S$_2$CNEt$_2$)(P(*p*-tolyl)$_3$)$_2$] **4-10**, and of **4-13** with [Rh(acac)(P(*p*-tolyl)$_3$)$_2$] **1-56**, whereas the catalytic reactions at 60 °C were always faster with **1-56**, regardless of the substrate.

At 60 °C after 24 hours with a 10 mol% catalyst-loading, rhodium(I) complexes [Rh(acac)dcpe] **4-2**, [Rh(acac)dppe] **4-3**, [Rh(S_2CNEt_2)dcpe] **4-8** and [Rh(S_2CNEt_2)dppe] **4-9**, bearing a chelating phosphine, only gave trace amounts of the dimers of *α*,*ω*-diynes **4-11** and **4-13**, and no trimer and, therefore, they were not investigated further. However, in the reaction of the dmpe-substituted catalyst [Rh(acac)dmpe] **4-1** with *α*,*ω*-diyne **4-11** in a 1:1 ratio at room temperature for 24 hours, complete conversion to dimer and trimer was observed in a 1:0.50 ratio. In the $^{31}P\{^1H\}$ NMR spectra, no additional signals aside from those of the rhodium(I) catalyst were observed, in contrast to the findings in section 3.3.3. Using a catalyst-loading of 10 mol% resulted in complete consumption of *α*,*ω*-diyne **4-11** at room temperature in 5.5 days giving a 1:0.50 ratio of dimer:trimer. At 60 °C, the reaction with 1 mol% of **4-1** with **4-11** reached completion within 30 hours, resulting also in a dimer:trimer ratio of 1:0.50. Further investigations of the catalytic activity of [Rh(acac)dmpe] **4-1** were not conducted.

In summary, the catalytic reaction with 10 mol% of catalyst at room temperature is faster for the *α*,*ω*-diyne **4-11** with the diethyldithiocarbamate-substituted catalyst [Rh(S_2CNEt_2)(P(*p*-tolyl)$_3$)$_2$] **4-10** than with the acac-substituted catalyst [Rh(acac)(P(*p*-tolyl)$_3$)$_2$] **1-56**. The dimer:trimer ratio is ca. 1:0.45 for both reactions. The cycloisomerization of *α*,*ω*-diyne **4-13** is faster with **1-56** than with **4-10**. The dimer:trimer ratios are 1:0.14 and 1:0.50 (Table 4-5). The catalytic reaction with 1 mol% of catalyst at room temperature did not reach completion within 14 days. However, the reactions of *α*,*ω*-diyne **4-11** with **4-10** and of *α*,*ω*-diyne **4-13** with **1-56** are faster than those of *α*,*ω*-diyne **4-11** with **1-56** and of *α*,*ω*-diyne **4-13** with **4-10** (Table 4-6).
At 60 °C, using a catalyst loading of 10 mol%, the reactions of *α*,*ω*-diynes **4-11** and **4-13** is always faster with [Rh(acac)(P(*p*-tolyl)$_3$)$_2$] **1-56**. The reaction is complete within 12 hours with **1-56**, while the reaction with [Rh(S_2CNEt_2)(P(*p*-tolyl)$_3$)$_2$] **4-10** takes 24 and 60 hours for *α*,*ω*-diynes **4-11** and **4-13**, respectively (Table 4-7). At 60 °C, similar findings were observed for the catalytic reactions with 1 mol% of catalyst. The cycloisomerization with [Rh(acac)(P(*p*-tolyl)$_3$)$_2$] **1-56** appeared to be faster than that with [Rh(S_2CNEt_2)(P(*p*-tolyl)$_3$)$_2$] **4-10** (Table 4-8).

As only a low catalytic activity for the dcpe- and dppe-substituted rhodium(I) catalysts with *α*,*ω*-diynes **4-11** and **4-13** was observed, their reactivities with an OMe-substituted *α*,*ω*-tetrayne were investigated. In the reactions of [Rh(acac)dcpe] **4-2** and [Rh(S_2CNEt_2)dppe] **4-9** with the *α*,*ω*-tetrayne, complete conversion to dimer and trimer was observed, indicating that the neighboring triple bond plays an important role in the catalytic cycloisomerization.

Furthermore, the steric influence of the chelating phosphine also seems to play an important role in the catalytic reaction with *α,ω*-diynes as, for the sterically demanding dcpe- and dppe-substituted rhodium(I) catalysts, little reaction was observed, whereas the dmpe-substituted catalyst led to cycloisomerization.

Schwenk reported that it was not possible to observe an intermediate in the $^{31}P\{^{1}H\}$ NMR spectrum during the cycloisomerization of $[Rh(S_2CNEt_2)(PPh_3)_2]$ with *α,ω*-tetraynes. Furthermore, a catalyst loading of 1 mol% favored the formation of dimer, whereas a catalyst loading of 10 mol% results in a mixture of both dimer and trimer. Generally, electron-withdrawing groups tend to lead to more trimer. Unfortunately, the exact conditions (temperature and concentration of substrate) were not reported.[68]

With *α,ω*-diynes, it was possible to observe an intermediate in the cycloisomerization, at least for the rhodium(I) catalyst $[Rh(acac)(P(p\text{-tolyl})_3)_2]$ **1-56** (see section 3.3.3). A general trend for the ratio of dimer and trimer formed, in dependence on the catalyst loading were not observed for the *α,ω*-diynes studied.

In order to gain further insight into the mechanism of the dimerization and trimerization, a variable temperature NMR study was conducted on the reaction of [Rh(acac)(P(*p*-tolyl)$_3$)$_2$] **1-56** with *α,ω*-diyne **4-14** using a 10 mol% catalyst loading and 28.4 µmol of **4-14** in 1 mL of toluene-d$_8$.

The variable temperature ^{31}P{^{1}H} NMR spectra in the -90 – -60 °C range show only a doublet for the rhodium(I) starting material at 54.9 ppm with $^1J_{Rh\text{-}P}$ = 194 Hz (Figure 4-5, black spectrum is representing that range). At -40 °C, signals for a rhodium(III) species at 18.8 ppm with a Rh-P coupling constant of 118 Hz and a singlet at -8.3 ppm begin to grow. With a rise of temperature to -30 °C, the intensities of the doublet at 18.8 ppm and the singlet at -8.3 ppm (blue spectrum) increase. At -10 °C, two new doublets at 31.4 and 31.2 ppm with $^1J_{Rh\text{-}P}$ = 171 Hz begin to grow. Raising the temperature to 0 °C, increases the intensity of the resonances at 18.8 ppm, ca. 31 ppm and at 8.3 ppm, while the doublet from the starting material decreases (red spectrum). At +25 °C, the starting material is almost completely consumed, and the four resonances at 31.4, 31.2, 18.8 and -8.3 ppm are still present.

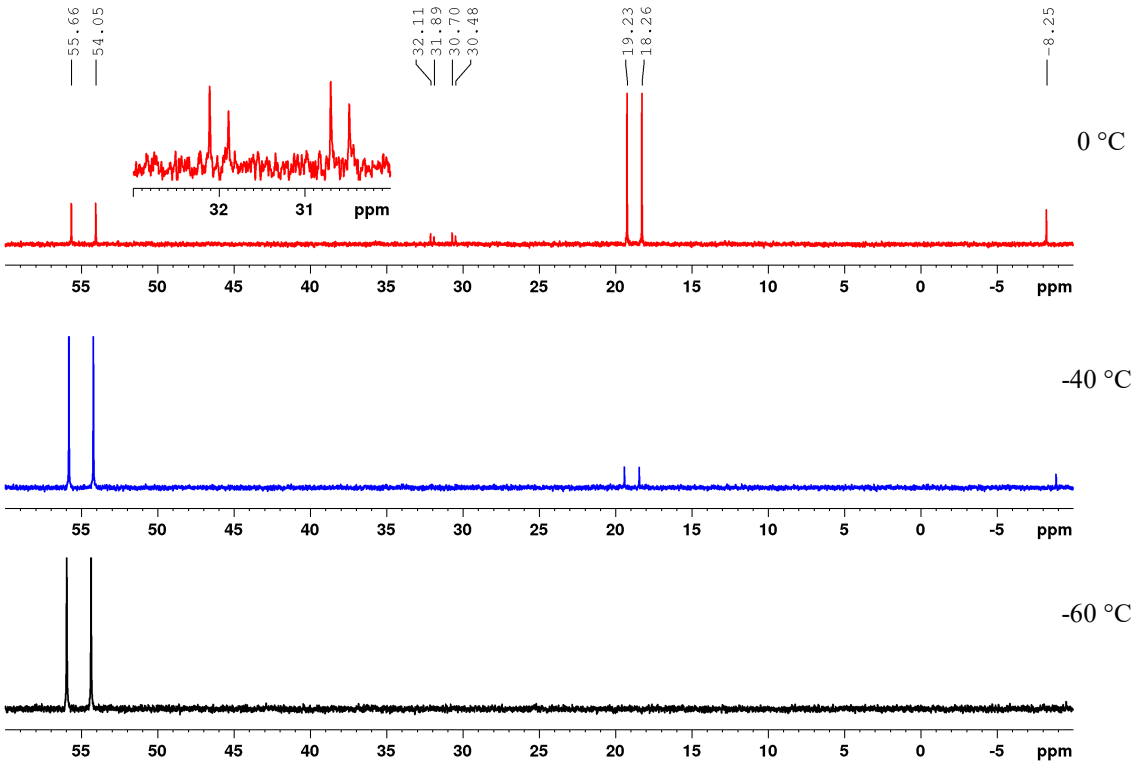

Figure 4-5: Variable temperature ^{31}P{^{1}H} NMR spectra (121 MHz, toluene-d$_8$) of the reaction of [Rh(acac)(P(*p*-tolyl)$_3$)$_2$] **1-56** and *α,ω*-diyne **4-14** at -60 °C (black spectrum), -40 °C (blue) and 0 °C (red).

The doublet at 18.8 ppm with a Rh-P coupling constant of 118 Hz represents the tri(*p*-tolyl)phosphine-substituted 2,5-bis(aryl)rhodacyclopentadiene **3-16**, and the singlet at -8.3 ppm, unbound tri(*p*-tolyl)phosphine. At -40 °C (blue spectrum), an additional mono-phosphine rhodium species represented by a doublet is expected, as unbound phosphine ligand

remains in solution. However, this species might be very broad and low in intensity due to dynamic processes, and therefore not visible. The two doublets at 31.4 and 31.2 ppm with $^{1}J_{Rh\text{-}P}$ = 171 Hz, indicate rhodium(I) species.

Inspection of the ^{1}H NMR spectrum at -60 °C (Figure 4-6, black spectrum) of the same reaction, shows only the two starting materials. For the following spectra (blue, red and purple), only the highlighted acac-CH region (5.90 – 4.90 ppm) will be discussed, as, due to overlapping signals and small quantities of the different species, further assignment of signals in other regions is not possible. At -40 °C (blue spectrum), an additional resonance at 4.58 ppm starts to grow. At 0 °C (red spectrum), low-field shifted resonances, compared to [Rh(acac)(P(*p*-tolyl)$_3$)$_2$] **1-56** (5.35 ppm), start to arise at ca. 5.70 ppm. At +25 °C (purple spectrum), the resonances at ca. 5.70 ppm increase in intensity, the singlet for the rhodium(I) starting material at 5.31 ppm (**1-56** shows a upfield shift from 5.39 to 5.31 ppm with increasing temperature) is almost gone, and a singlet at 4.58 ppm is the dominant signal in the acac-CH region.

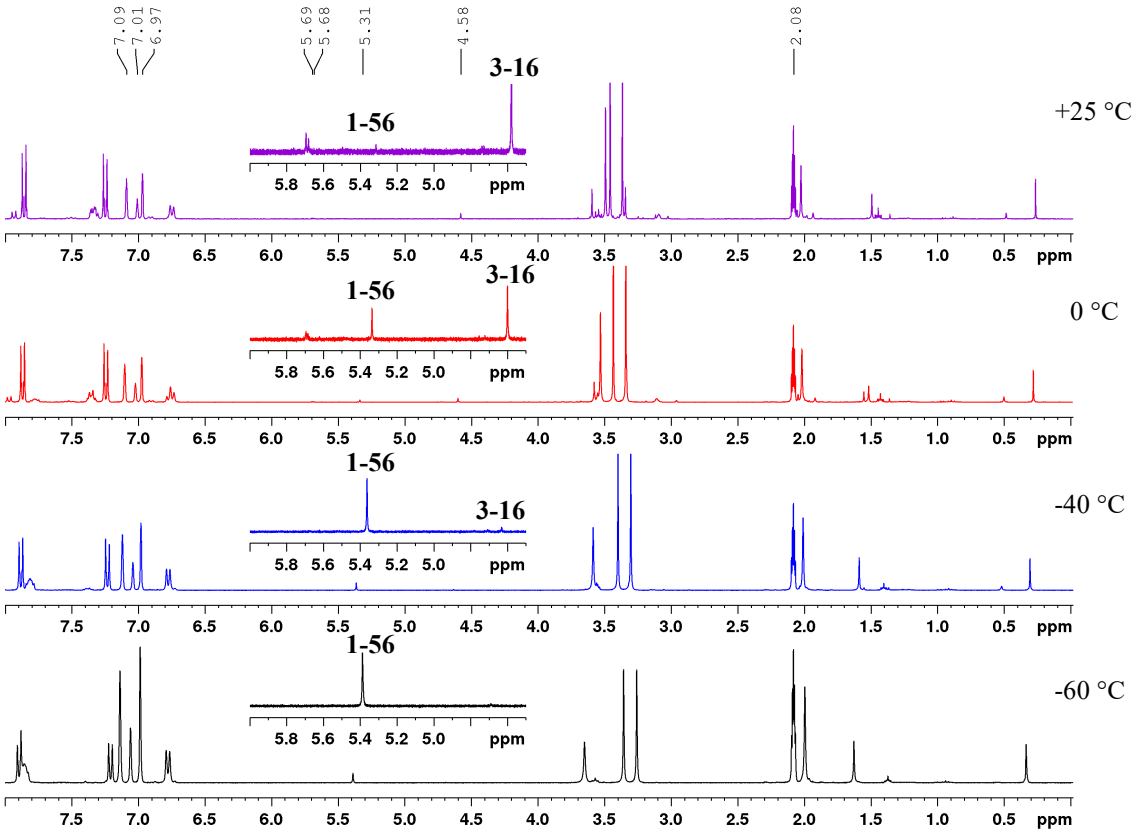

Figure 4-6: Variable temperature ^{1}H NMR spectra (300 MHz, toluene-d$_8$) of the reaction of [Rh(acac)(P(*p*-tolyl)$_3$)$_2$] **1-56** with *α,ω*-diyne **4-14** at -60 °C (black), -40 °C (blue), 0 °C (red) and +25 °C (purple).

In the blue spectrum, the signal at 4.58 ppm, which is shifted upfield compared with that of the starting material, can be assigned to the acac-CH group of the tri(*p*-tolyl)phosphine-substituted

2,5-bis(aryl)rhodacyclopentadiene **3-16**. The two resonances at 5.68 and 5.69 ppm indicate two rhodium-acac species.

Thus, in summary, in the variable temperature $^{31}P\{^{1}H\}$ NMR spectra, four different Rh-P species are observed and, in the variable temperature ^{1}H NMR spectra, four different resonances for the acac-CH group are observed. Aside from the rhodium(I) starting material [Rh(acac)(P(*p*-tolyl)$_3$)$_2$] **1-56** and the rhodacyclopentadiene **3-16**, two other rhodium-phosphine-acac complexes give rise to doublets at 31.4 and 31.2 ppm in the $^{31}P\{^{1}H\}$ NMR spectrum, and two singlets at 5.69 and 5.68 ppm in the ^{1}H NMR spectrum. The coupling constant, $^{1}J_{Rh\text{-}P}$ = 171 Hz, indicates a rhodium(I) species with no oxygen *trans* to the phosphine. The resonance for unbound tri(*p*-tolyl)phosphine ligand at -8.3 ppm, suggests two rhodium(I)-monophosphine-acac species at ca. 31 ppm.

Additionally, the variable temperature NMR experiment demonstrated that the species at ca. 31 ppm forms after, or at least simultaneously with the rhodacyclopentadiene **3-16**. This species may either be involved in the catalytic cycle, or in equilibrium with species which are, as it was not observed in the reaction of [Rh(acac)(P(*p*-tolyl)$_3$)$_2$] **1-56** with α,ω-diyne **3-1**, which resulted in no dimer and trimer. Furthermore, for the reaction in C_6D_6, only one doublet at ca. 30 ppm with $^{1}J_{Rh\text{-}P}$ = 170 Hz was observed (see section 3.3.3), and in toluene-d_8, two doublets were observed.

A plausible mechanism for the formation of dimers and trimers of α,ω-tetraynes was already established by Schwenk.[68] In Scheme 4-7, this mechanism is modified for α,ω-diynes. First, the 2,5-bis(aryl)rhodacyclopentadiene is formed in an oxidative [2+2+M] cyclization of [Rh(acac)(P(*p*-tolyl)$_3$)$_2$] **1-56** and an α,ω-diyne. In the second step, a tri(*p*-tolyl)phosphine ligand dissociates from the six-coordinate rhodium metal center, which leaves a vacant binding site. After coordination of a second α,ω-diyne to the rhodium center, a [4+2] cycloaddition reaction occurs forming a benzene-coordinated rhodium complex (Intermediate **4-I**). After re-addition of tri(*p*-tolyl)phosphine, the dimer is released and the catalyst is regenerated (similar to Scheme 1-28, left cycle). In order to form the trimer, a dimer is added instead of a α,ω-diyne in the second step, forming Intermediate **4-II**, which is then again released with the addition of phosphine, regenerating the rhodium(I) species.

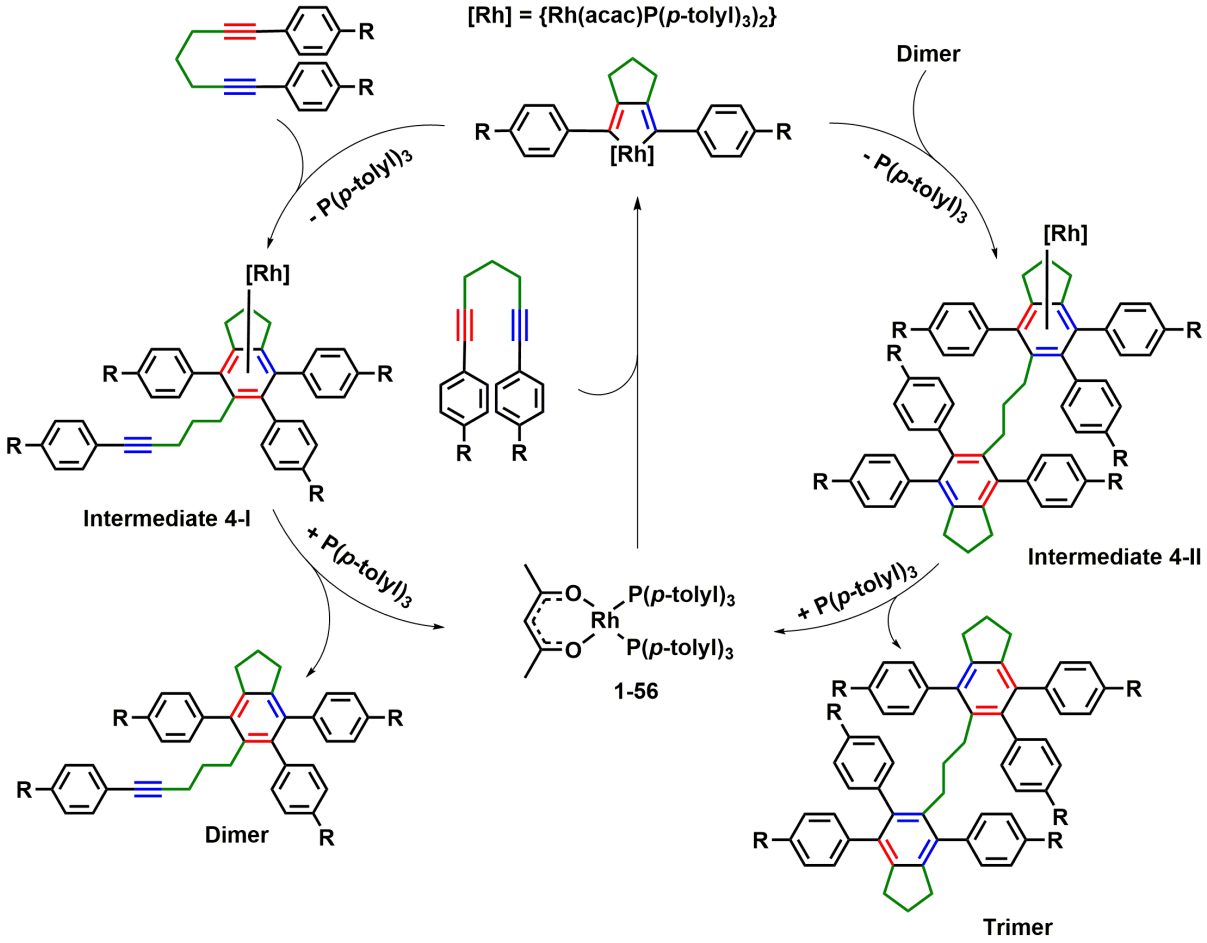

Scheme 4-7. Plausible mechanism for the dimerization and trimerization of α,ω-diynes catalyzed by [Rh(acac)(P(*p*-tolyl)$_3$)$_2$] **1-56**.

The observations made so far, are consistent with the proposed mechanism in Scheme 4-7. The formation of a rhodacyclopentadiene (Scheme 4-7, top middle) can be verified by the presence of a doublet at ca. 20 ppm with Rh-P coupling constants of ca. 120 Hz (e.g., Figures 4-5 and 3-11). The formation of trimer from dimer (Scheme 4-7, right cycle) is in accordance with the findings from Figure 4-4, displaying the reaction of [Rh(acac)(P(*p*-tolyl)$_3$)$_2$] **1-56** with *α,ω*-diyne **4-11** in equimolar amounts. At room temperature after 56 hours, dimer and trimer were present, whereas more dimer than trimer was formed. Heating the reaction at 60 °C for seven hours results in a complete consumption of dimer and only trimer remained.

According to the ^{1}H and ^{31}P{^{1}H} NMR spectra of the reaction of **1-56** with *α,ω*-diyne **4-14** in equimolar amounts in C_6D_6 at room temperature, dimer and trimer were present (Figure 3-12), and doublets at 54.8 ($^{1}J_{Rh\text{-}P}$ = 195 Hz), 31.2 ($^{1}J_{Rh\text{-}P}$ = 170 Hz) and 18.6 ppm ($^{1}J_{Rh\text{-}P}$ = 118 Hz), and a singlet at -7.8 ppm (Figure 3-11) were observed. The resonance at ca. 30 ppm was only present for *α,ω*-diynes that underwent dimerization and trimerization (Figure 3-11), and only in C_6D_6 and toluene-d_8. In THF-d_8 this species was not observed.

The cycloisomerization products **4-11a**,**b** – **4-14a**,**b** were synthesized in the reaction of [Rh(acac)(P(*p*-tolyl)$_3$)$_2$] **1-56** with the *α,ω*-diynes **4-11** – **4-14** and separated by flash column chromatography, and purified further by several recrystallization steps, resulting in good yields of 30 – 55% of the dimers and 30 – 40% yields of the trimers (Scheme 4-8).

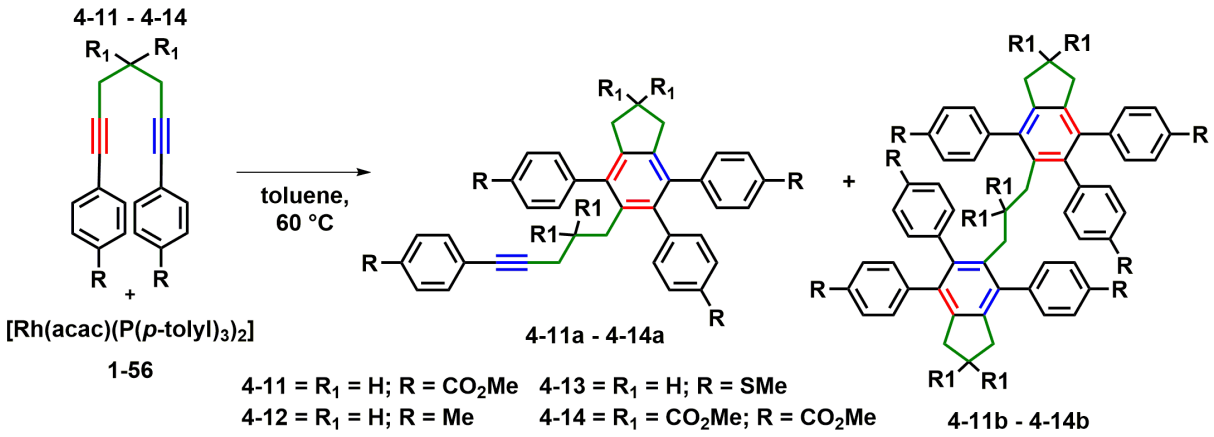

Scheme 4-8: Synthesis of dimers **4-11a** – **4-14a** and trimers **4-11b** – **4-14b** *via* reaction of [Rh(acac)(P(*p*-tolyl)$_3$)$_2$] **1-56** with *α,ω*-diynes **4-11** – **4-14**.

Compounds **4-11a**,**b** – **4-14a**,**b** were characterized by elemental analysis, HRMS and multinuclear NMR spectroscopy, and **4-12a**, **4-13a**,**b** and **4-14a** additionally by single-crystal X-ray diffraction analysis. Elemental analysis as well as HRMS data are in accordance with the molecular formulae of the respective dimers and trimers.

The dimer **4-11a** and trimer **4-11b** were chosen as model compounds for the description of the NMR spectra, as for the other cycloisomerization products the signals are less well separated, resulting in a large number of overlapping resonances.

The ^{1}H NMR spectrum of the dimer **4-11a** (Figure 4-7) shows the different CH_2 groups giving rise to resonances in the 2.65 ppm – 1.44 ppm range, each integrating to two. According to 2D NMR spectroscopy, the two multiplets at 2.65 – 2.62 and 1.47 – 1.42 ppm and the triplet at 1.79 ppm with $^3J_{H\text{-}H}$ = 6.5 Hz can be assigned to the $(CH_2)_3$-chain that is connected to the triple bond. The CH_2 groups of the cyclopentene moiety are displayed as two triplets at 2.59 and 2.52 ppm and as a quintet at 1.73 ppm with $^3J_{H\text{-}H}$ = 7.4 Hz. There are four singlets for the carboxymethoxy groups at 3.59, 3.45, 3.39 and 3.37 ppm, each integrating to three. Aromatic CH resonances in the 8.18 – 6.95 ppm range as seven multiplets with an integral of two and one multiplet integrating to four are displayed.

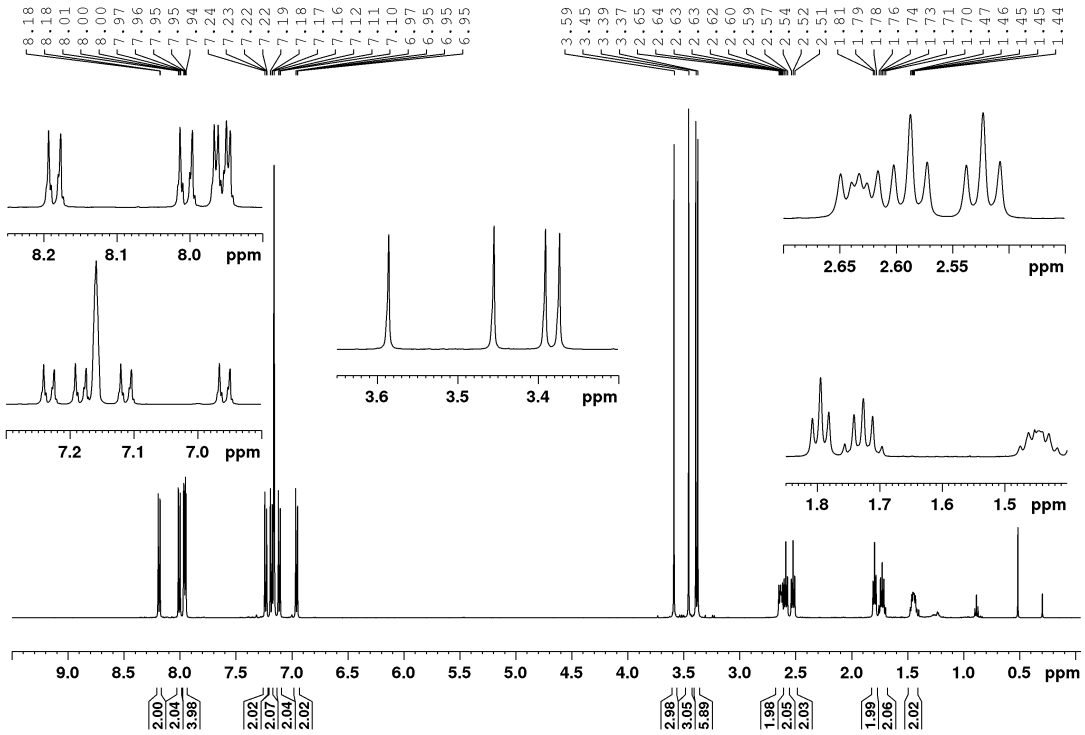

Figure 4-7: ^{1}H NMR spectrum (500MHz, C_6D_6) of dimer **4-11a**.

In the $^{13}C\{^{1}H\}$ NMR spectrum of **4-11a** (Figure 4-8), six singlets in the 33.5 – 19.7 ppm range represent the CH_2 groups of the backbone. Four resonances for the methoxy groups are observed at 51.8, 51.6, 51.51 and 51.47 ppm. The triple bonds give rise to signals at 92.6 and 81.2 ppm. In the aromatic region, 21 of the expected 22 signals are displayed. Due to fact that the resonances that are very close to each other, the missing signal is likely overlapped with another one. Four signals at 166.5, 166.31, 166.28 and 166.2 ppm represent the carbonyl carbon atoms of the carboxymethoxy groups.

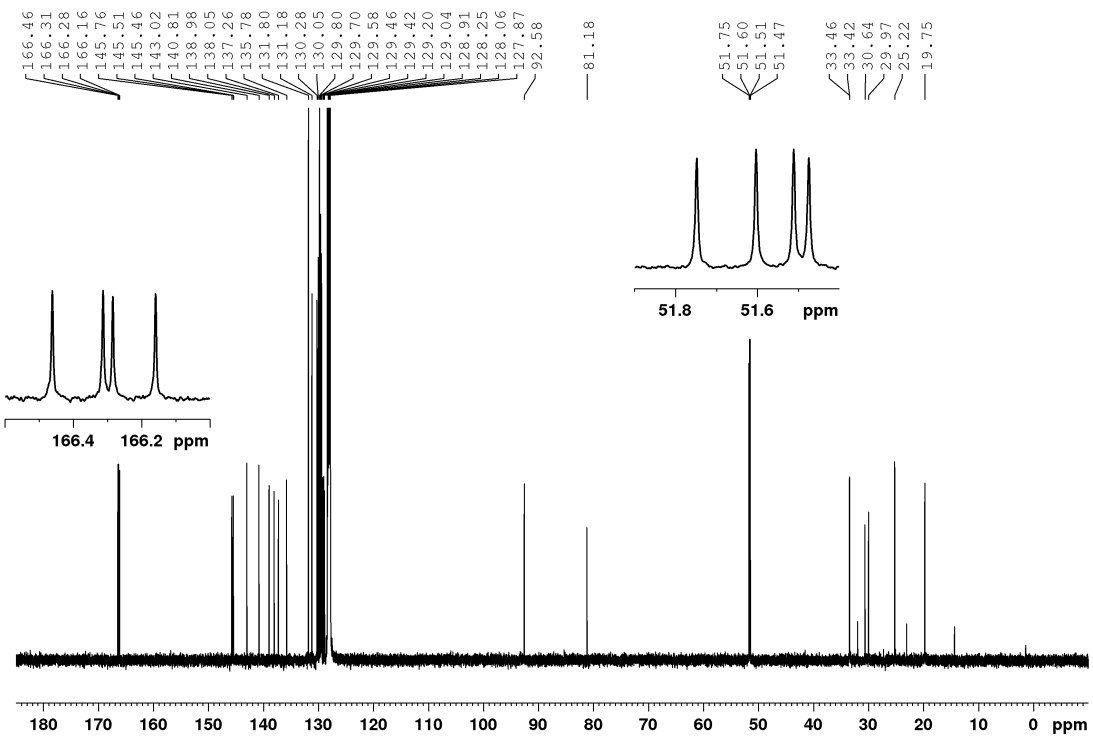

Figure 4-8: $^{13}C\{^{1}H\}$ NMR spectrum (125 MHz ,C_6D_6) of dimer **4-11a**.

An inversion center in the trimer, results in less signals in the ^{1}H and $^{13}C\{^{1}H\}$ NMR spectrum compared to that of the dimer.

The ^{1}H NMR spectrum of trimer **4-11b** (Figure 4-9) shows the different CH_2 groups giving rise to resonances in the 2.51 – 1.20 ppm range, each integrating to four except for a multiplet at 1.23 – 1.18 ppm (overlapping with *n*-hexane) which integrates to two, being the CH_2 group lying on the inversion center. According to 2D NMR spectroscopy, the multiplets at 1.23 – 1.18 and 2.08 – 2.04 ppm represent the $(CH_2)_3$-chain that connects the two benzene rings, while the two triplets at 2.49 and 2.42 ppm and a quintet at 1.64 ppm with $^{3}J_{H\text{-}H}$ = 7.4 Hz results from part of the cyclopentene moiety. There are three singlets for the six carboxymethoxy groups at 3.68, 3.50 and 3.36 ppm, each integrating to six. Four multiplets for the aromatic CH groups in the 8.21 – 6.88 ppm range are displayed. The multiplets at 8.21 – 8.19 and 7.04 – 7.02 ppm integrate to four and the multiplets at 7.96 – 7.92 and 6.92 – 6.88 ppm integrate to eight.

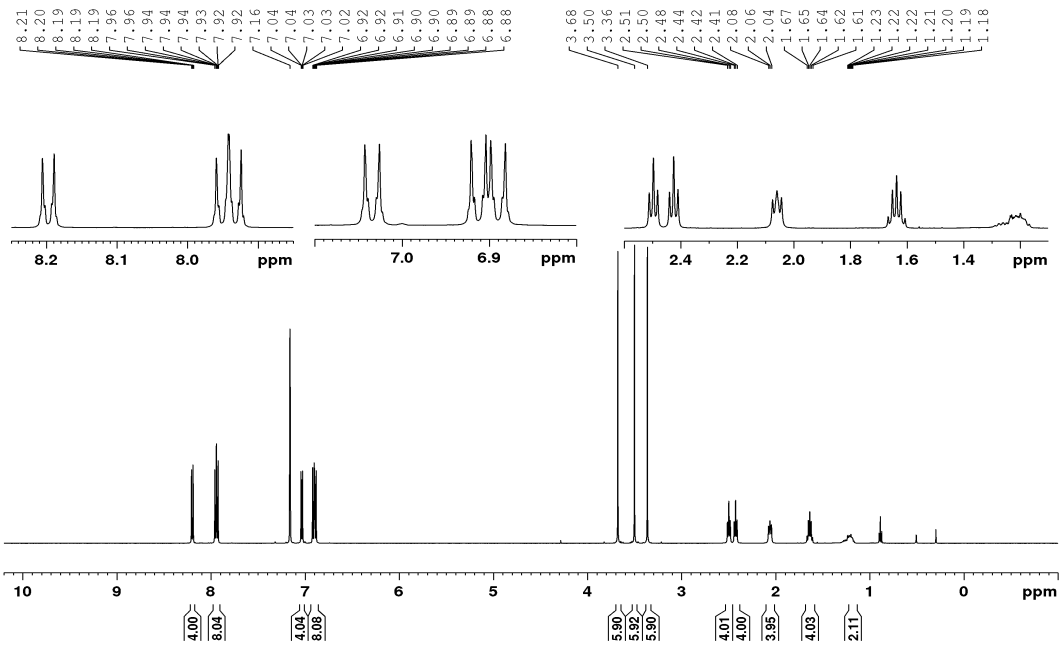

Figure 4-9: ^{1}H NMR spectrum (500 MHz, C_6D_6) of trimer **4-11b**.

In the $^{13}C\{^{1}H\}$ NMR spectrum of **4-11b** (Figure 4-10), five signals for the CH_2 groups are found in the region from 33.5 – 25.1 ppm and singlets for the methoxy carbon atoms are observed at 51.9, 51.6 and 51.4 ppm. All 18 expected resonances for the aromatic carbon-atoms are observed in the 145.9 – 128.9 ppm range. Three signals at 166.6, 166.4 and 166.3 ppm are observed for the six carbonyl carbon atoms of the carboxymethoxy groups.

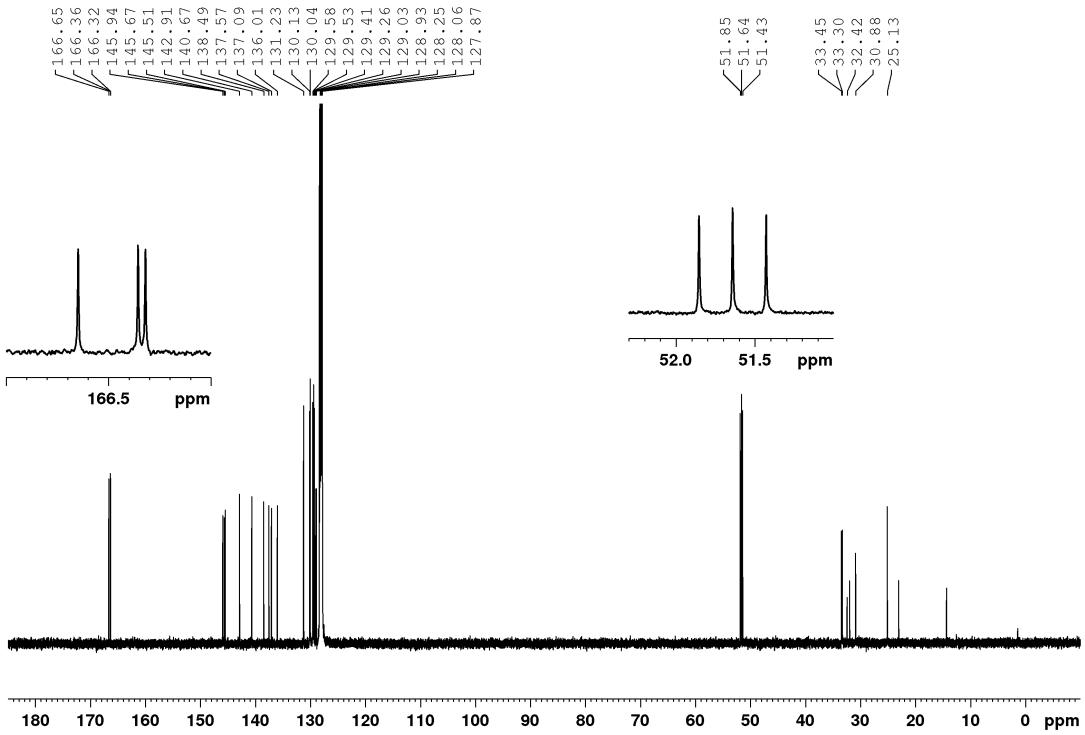

Figure 4-10: $^{13}C\{^{1}H\}$ NMR spectrum of trimer **4-11b** in C_6D_6 at 125 MHz.

The molecular structures of the dimers **4-12a**, **4-13a** and **4-14a** are shown in Figure 4-11, and selected bond distances and angles are listed in Table 4-13. The dimers **4-12a** and **4-13a** crystallize in the triclinic space group $P\bar{1}$ and **4-14a** in the monoclinic space group *C*2/*c*. For compound **4-12a** the aryl moiety E shows disorder therefore, the bond lengths will not be discussed.

The aromatic C-C bond distances of the dimers **4-12a**, **4-13a** and **4-14a** in rings A range from 1.381(2) – 1.397(2) Å, for rings B from 1.3904(3) – 1.415(3) Å, for rings C from 1.384(3) – 1.4015(5) Å, for rings D from 1.381(2) – 1.399(3) Å and for rings E from 1.382(3) – 1.4011(3) Å. The C1-C2, C8-C9 and C10-C11 distances are ca. 1.490 Å. The C3-C4, C4-C5, C5-C6 and C6-C7 bond distances are in the range of 1.509(2) – 1.553(2) Å. The C-C distances for C12-C13, C13-C14, C14-C15 range from 1.5133(4) – 1.565(2) Å. The C15-16 and C16-C17 bond lengths are ca. 1.464 and 1.195 Å, respectively. For **4-13a** and **4-14a**, the C17-C18 distances are 1.4381(4) Å and 1.443(2) Å, respectively. The distances from the methyl substituents to the carbon atoms of the aryl moiety of **4-12a** are in the range of 1.508(3) – 1.514(3) Å. For compound **4-13a**, the distances from the sulfur substituents to the carbon atoms of the aryl moieties is in the 1.7579(5) – 1.7632(5) Å range, and the distances from the methyl groups to the sulfur atom are in the range of 1.7896(5) – 1.7957(4) Å. In the dimer **4-14a**, the distances from the carboxymethoxy carbonyl atoms to the carbon atoms of the aryl moieties are in the 1.482(3) – 1.493(2) Å range. The distances from the carboxymethoxy carbonyl atoms to

the carbon atoms of the alkyl chain are in the range of 1.524(2) – 1.536(2) Å. All of the reported bond lengths are in the expected range.[208] The rotation of the rings A, C and D with respect to the central benzene core are in the 57.1(1) – 86.29(1)° range, due to steric overcrowding.

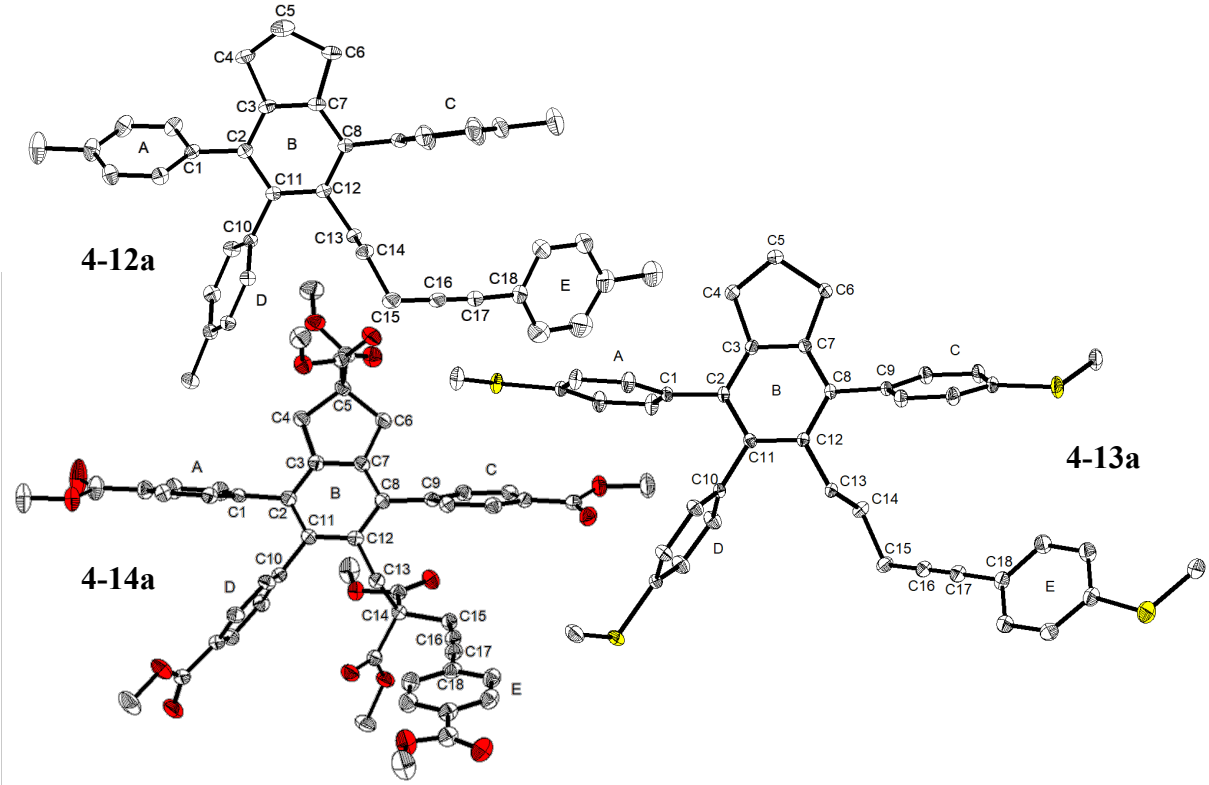

Figure 4-11: Molecular structures of dimers **4-12a**, **4-13a** and **4-14a** in the solid state at 100 K. Hydrogen atoms, solvent molecules (*n*-pentane for **4-14a**) and minor disordered parts (aryl moiety of ring E for **4-12a**) are omitted for clarity. Atomic displacement ellipsoids are drawn at the 50% probability level.

Whereas the *para*-terphenyl molecule shows only a small rotation of the rings attached to the central aryl moiety of ca. 1° (Figure 4-12).[316]

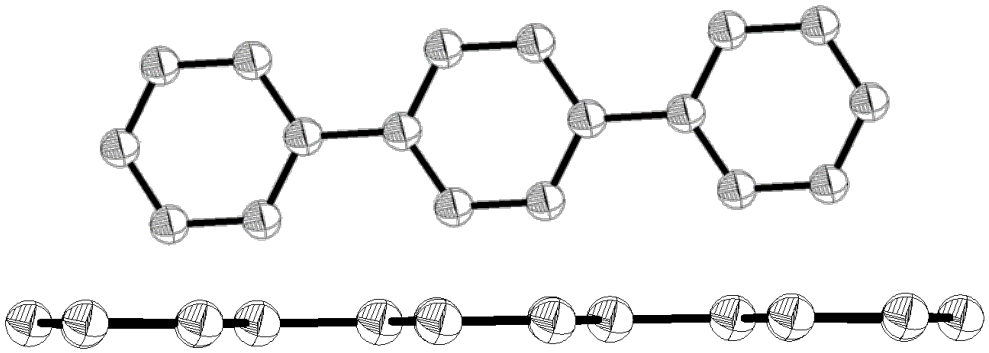

Figure 4-12: Molecular structure of *para*-terphenyl in the solid state. Top view (top) and side view (bottom) of *para*-terphenyl.[316]

Table 4-9: Selected bond lengths [Å] and angles [°] of dimers **4-12a**, **4-13a** and **4-14a** determined by single-crystal X-ray diffraction at 100 K with esd's in parentheses.

	4-12a	**4-13a**	**4-14a**
C1-C2	1.492(3)	1.4903(4)	1.490(2)
C2-C3	1.394(3)	1.3917(4)	1.394(2)
C2-C11	1.415(3)	1.4079(3)	1.408(2)
C3-C7	1.394(3)	1.3936(4)	1.391(2)
C7-C8	1.395(3)	1.3904(3)	1.396(2)
C8-C9	1.495(3)	1.4886(4)	1.495(2)
C8-C12	1.413(3)	1.4109(4)	1.414(2)
C11-C12	1.412(3)	1.4060(4)	1.407(2)
C10-C11	1.495(3)	1.4935(4)	1.499(2)
C12-C13	1.514(3)	1.5133(4)	1.518(2)
C13-C14	1.534(3)	1.5302(4)	1.565(2)
C14-C15	1.533(3)	1.5331(4)	1.558(2)
C15-C16	1.460(4)	1.4643(4)	1.468(2)
C16-C17	1.192(4)	1.1979(4)	1.195(2)
C17-C18	-	1.4381(4)	1.443(2)
∡ A-B	63.80(7)	86.29(5)	62.5(1)
∡ C-B	82.12(8)	66.27(5)	57.1(1)
∡ D-B	66.95(8)	85.07(3)	75.5(1)

The molecular structure of trimer **4-14b** is shown in Figure 4-13, and selected bond distances and angles are listed in Table 4-14. The trimer **4-14b** crystallizes in the triclinic space group $P\bar{1}$.

For trimer **4-13b**, the bond distances in ring A range from 1.381(2) – 1.397(2) Å, for ring B from 1.391(2) – 1.414(2) Å, for ring C from 1.389(2) – 1.399(2) Å, for ring D from 1.381(2) – 1.397(2) Å and for ring E from 1.382(3) – 1.398(2) Å. The C1-C2, C8-C9 and C10-C11 bond lengths are 1.495(3), 1.493(3) and 1.490(3) Å, respectively. The bond lengths of C12-C13 and C13-C14 are 1.519(3) and 1.527(3) Å, respectively. The distance from the sulfur-substituents to the carbon atoms of the aryl moieties are in the range of 1.763(3) – 1.780(2) Å. The distance from the methyl groups to the sulfur atoms are in the 1.783(3) – 1.796(3) Å range. The rings A, C and D are rotated with respect to ring B by 62.3(1), 62.9(1) and 72.7(1)°, respectively.

The data for the other half of the molecule is not greatly different from the data already discussed. All obtained bond lengths are consistent with the literature[208] and are similar to those of **4-13a**.

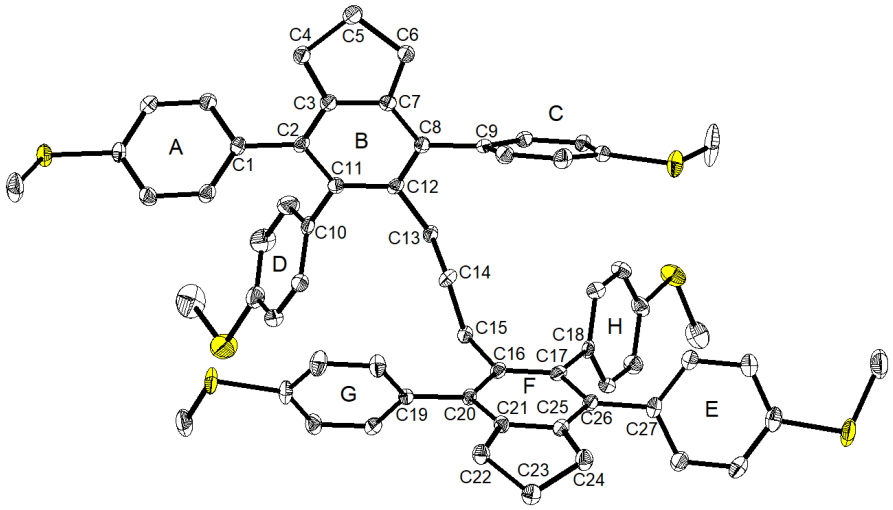

Figure 4-13: Molecular structure of trimer **4-13b** in the solid state at 100 K. Hydrogen atoms and minor disordered parts (SMe group for aryl moiety G) are omitted for clarity. Atomic displacement ellipsoids are drawn at the 50% probability level.

The rotation of rings A, C and D with respect to ring B are in the 62.3(1) – 72.7(1)° range, and for rings E, G and H with respect to ring F, in the 60.7(1) – 75.6(1)° range.

Table 4-10: Selected bond lengths [Å] and angles [°] of trimer **4-13b** determined by single-crystal X-ray diffraction at 100 K with esd's in parentheses.

	4-13b		**4-13b**
C1-C2	1.495(3)	C17-C18	1.493(3)
C2-C3	1.387(3)	C19-C20	1.497(3)
C2-C11	1.414(3)	C20-C21	1.390(3)
C3-C7	1.395(3)	C16-C20	1.409(3)
C7-C8	1.396(3)	C17-C26	1.414(3)
C8-C9	1.493(3)	C21-C25	1.394(3)
C8-C12	1.407(3)	C25-C26	1.392(3)
C11-C12	1.407(3)	C26-C27	1.495(3)
C10-C11	1.490(3)	∡ A-B	62.3(1)
C12-C13	1.519(3)	∡ C-B	62.9(1)
C13-C14	1.527(3)	∡ D-B	72.7(1)
C14-C15	1.534(3)	∡ E-F	60.7(1)
C15-C16	1.510(3)	∡ G-F	68.2(1)
C16-C17	1.407(3)	∡ H-F	75.6(1)

4.3.3 Reaction of $[Rh_2(ox)(P(p\text{-tolyl})_3)_4]$ with CO_2Me-substituted α,ω-tetrayne

As $[Rh_2(ox)(P(p\text{-tolyl})_3)_4]$ **4-5** has two rhodium(I) centers, reactions on both sides are expected. Therefore, compound **4-5** and the CO_2Me-substituted α,ω-tetrayne **1-47d** were reacted in a 1:2 ratio in THF (Scheme 4-9). Surprisingly, one equivalent of unbound α,ω-tetrayne remained unreacted in solution. After heating the reaction mixture to 60°C for 24 hours, additional signals were observed in the ^1H NMR spectrum, which correspond to cycloisomerization products of the α,ω-tetrayne. In the $^{31}P\{^1H\}$ NMR spectrum, there are two doublets at 54.1 ppm ($^1J_{Rh\text{-}P}$ = 201 Hz) and 26.2 ppm ($^1J_{Rh\text{-}P}$ = 115 Hz), the coupling constants indicating oxidation states of +1 and +3, respectively, for the two rhodium centers.

Rhodacycle **4-15** was synthesized in the reaction of $[Rh_2(ox)(P(p\text{-tolyl})_3)_4]$ **4-5** with CO_2Me-substituted α,ω-tetrayne **1-47d** in equimolar amounts at 60 °C for three days. Analytically pure **4-15** was obtained by recrystallization from **4-15** in toluene layered with *n*-hexane at -30 °C in a yield of 26%.

Inspection of the NMR spectroscopic data in C_6D_6 revealed the formation of complex **4-15**, which was characterized by elemental analysis, HRMS, multinuclear NMR spectroscopy, and by single-crystal X-ray diffraction analysis.

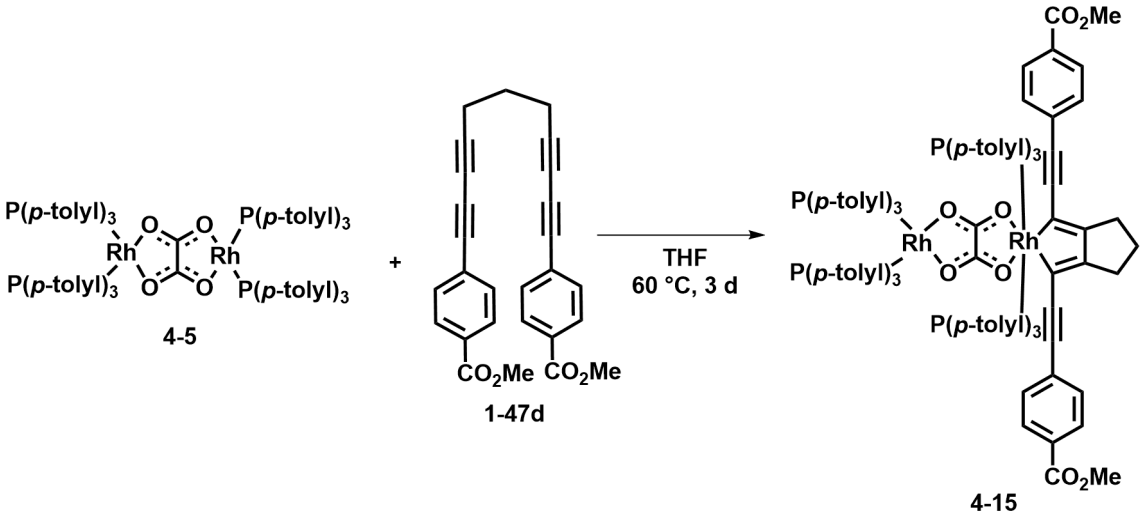

Scheme 4-9: Synthesis of rhodacycle **4-15** *via* reaction of $[Rh_2(ox)(P(p\text{-tolyl})_3)_4]$ **4-5** with CO_2Me-substituted α,ω-tetrayne **1-47d**.

The ^1H NMR spectra revealed for rhodacycle **4-15** to have C_{2v} symmetry, as indicated by a single resonance at 3.55 ppm that integrates to six for the CO_2Me groups. The methyl groups of the two chemically inequivalent sets of tri(*p*-tolyl)phosphine ligands give rise to two singlets at 2.12 and 1.95 ppm with an integral of 18. The signals for the backbone of the α,ω-tetrayne are displayed at 1.69 ppm ($^3J_{H\text{-}H}$ = 7.6 Hz) as a quintet with an integral of two and at 2.02 –

1.99 ppm as a multiplet with an integral of four. In the aromatic region, two multiplets at 8.23 – 8.21 and 7.77 – 7.75 ppm with an integral of four are *α,ω*-assigned to the CH groups of the tetrayne ligand. Four multiplets with an integral of twelve are displayed between 8.01 – 7.99, 7.54 – 7.51, 7.01 – 7.00 and 6.76 – 6.75 ppm, respectively, and are assigned to the aromatic CH groups of the tri(*p*-tolylphosphine) ligands.

HRMS and elemental analysis are consistent with the formulation of rhodacycle **4-15**.

Single-crystals suitable for X-ray diffraction analysis were obtained *via* diffusion of *n*-pentane into a solution of **4-15** in toluene. Complex **4-15** crystallizes in the triclinic space group $P\bar{1}$ and the molecular structure is shown in Figure 4-14. Due to poor crystal quality, the structure only serves as a proof of connectivity.

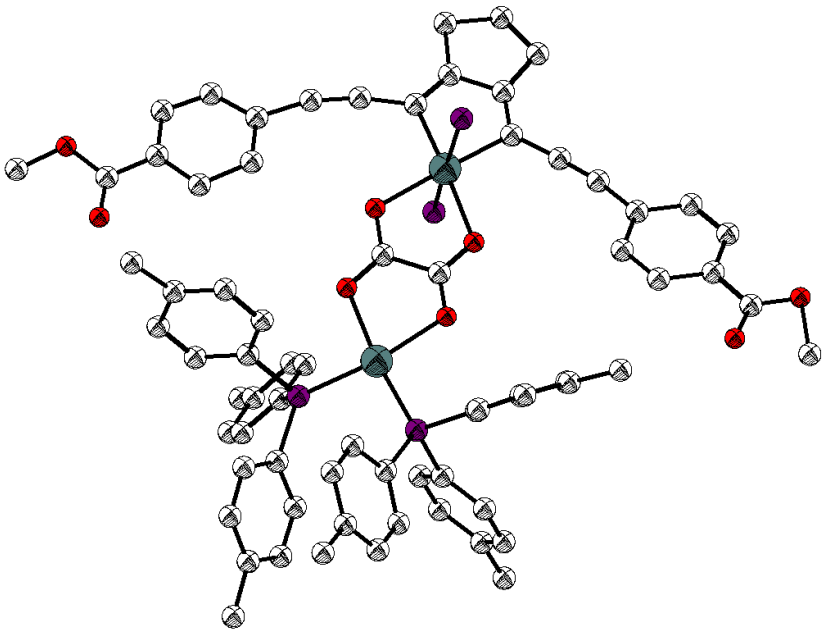

Figure 4-14: Molecular structure of complex **4-15** in the solid state at 100 K. Hydrogen atoms and the *p*-tolyl moieties of the rhodium(III) center are omitted for clarity. The structure is represented in the "ball-and-stick"-model. The representation only serves as a proof of connectivity.

Attempts to replace the tri(*p*-tolyl)phosphine ligands in **4-15** with PMe_3 at 60 °C were not successful and resulted, as indicated by NMR spectroscopy, in multiple species.

Attempted synthesis of a PMe_3 analogue of **4-5** by adding PMe_3 to $[Rh_2(ox)(COE)_4]$ **4-4** also resulted in multiple species according to $^{31}P\{^1H\}$ NMR spectroscopy. However, it was possible to isolate orange single-crystals of the salt $[Rh(PMe_3)_4][Rh(ox)(PMe_3)_2]$ **4-16** from a concentrated THF solution at -30 °C. Compound **4-16** crystallizes in the monoclinic space group $P2_1/c$, and its molecular structure is shown in Figure 4-15 with selected bond lengths and angles listed in Table 4-11.

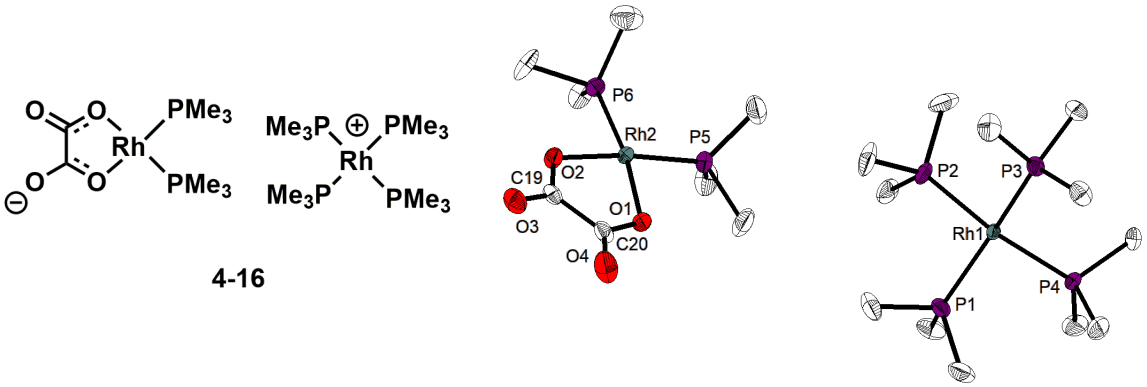

Figure 4-15: Schematic and molecular structure of salt $[Rh(PMe_3)_4][Rh(ox)(PMe_3)_2]$ **4-16** in the solid state at 100 K. Hydrogen atoms, THF solvent molecule and a second molecule in the unit cell are omitted for clarity. Atomic displacement ellipsoids drawn at the 50% probability level.

The salt **4-16** is composed of two square planar rhodium(I) moieties. The cationic rhodium(I) center is bound to four trimethylphosphine ligands and the anionic rhodium(I) species contains two trimethylphosphine and one oxalate ligand. The Rh-P bond distances in the cationic rhodium moiety are ca. 2.298 Å. The P2-Rh1-P4 and P1-Rh1-P3 angles are 157.90(4) and 158.31(4)°, respectively. The Rh-P distances are identical and the P-Rh-P angles are comparable with the values reported for $[Rh(PMe_3)_4]Cl$, which are 2.295 Å and 163.987(4)°, respectively.[317] The Rh-P and Rh-O distances in the anionic moiety are 2.178 and 2.105 Å, respectively. The P5-Rh2-P6 and O1-Rh2-O2 angles are 95.61(4) and 78.84(9)°, respectively. The Rh-P bond lengths are shorter and the Rh-O bond lengths are longer, than those in $[Rh(acac)(PMe_3)_2]$ **1-51**,[305] whereas the P5-Rh2-P6 angle of 94.716(15)° is comparable. The O1-Rh2-O2 angle of 78.84(19)° is comparable to the angles in $[Rh_2(ox)(COE)_4]$ **4-4** and $[Rh_2(ox)(P(p\text{-tolyl})_3)_4]$ **4-5** which are 79.20(17) and 77.84(8)°, respectively (see Table 4-2).

Table 4-11: Selected bond lengths [Å] and angles [°] of salt $[Rh(PMe_3)_4][Rh(ox)(PMe_3)_2]$ **4-16** determined by single-crystal X-ray diffraction at 100 K with esd's in parentheses.

	4-16		**4-16**
Rh1-P1	2.3005(11)	C20-O4	1.220(4)
Rh1-P2	2.2929(11)	C19-O3	1.229(4)
Rh1-P3	2.3005(11)	P1-Rh1-P3	158.31(4)
Rh1-P4	2.2965(11)	P2-Rh1-P4	157.90(4)
Rh2-P5	2.1785(10)	P1-Rh1-P4	92.21(4)
Rh2-P6	2.1784(10)	P2-Rh1-P3	92.46(4)
Rh2-O1	2.106(2)	O1-Rh1-O2	78.84(9)
Rh2-O2	2.103(2)	P5-Rh2-P6	95.61(4)
O1-C20	1.290(4)	O1-Rh2-P6	170.64(7)
O2-C19	1.279(4)	O2-Rh2-P5	172.28(6)
C18-C19	1.553(5)		

4.4 Photophysical studies of the luminescent products

Compound **4-11a** shows an intense absorption band with $\lambda_{abs,max}$ = 265 nm and a small shoulder at ca. 278 nm in THF with an extinction coefficient ε of 56000 M^{-1} cm^{-1}. An emission band is observed between 325 – 500 nm with $\lambda_{em,max}$ = 356 nm and the apparent Stokes shift is ca. 9645 cm^{-1} (Figure 4-16, left). Compound **4-11a** exhibits a low quantum yield Φ = 0.08 and very short emission lifetime τ_F = 1.14 ns at room temperature. The short lifetime strongly indicates fluorescence.[318]

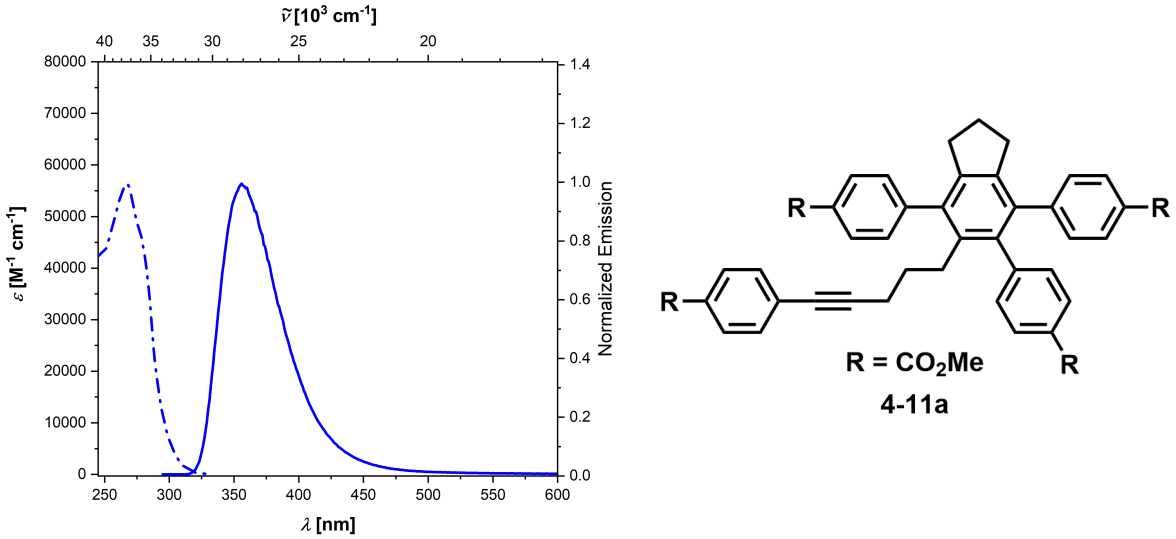

Figure 4-16: Absorption (dashed line) and emission spectra (solid line) of dimer **4-11a** in dry, degassed THF at room temperature (left). Chemical structure of dimer **4-11a** (right).

The absorption and emission spectra of compound **4-11a** in different solvents are displayed in Figure 4-17. Absorption maxima $\lambda_{abs,max}$ in *n*-hexane, dichloromethane (DCM), THF, and acetonitrile (ACN) are at 266, 268, 265 and 266 nm, respectively. The compound is emissive, with $\lambda_{em,max}$ in *n*-hexane at 351 nm, in DCM at 359 nm, in THF at 356 nm, and in ACN at 367 nm. The apparent Stokes shift is 9103 cm^{-1} in *n*-hexane, 9458 cm^{-1} in DCM, 9645 cm^{-1} in THF, and 10346 cm^{-1} in ACN. A small bathochromic solvatochromic shift of the emission is observed with increasing solvent polarity.

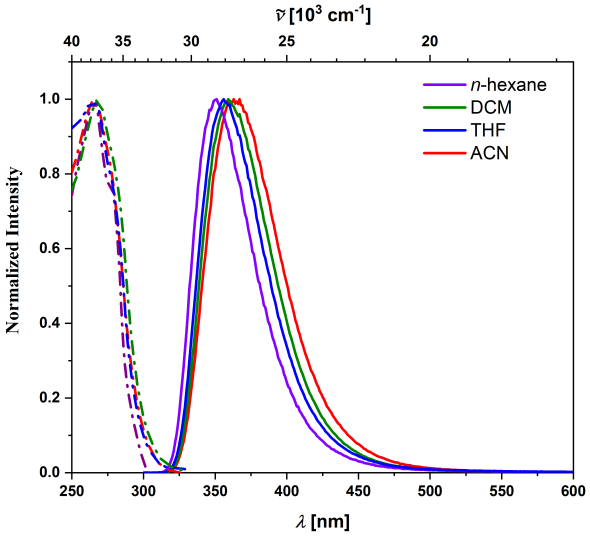

Figure 4-17: Absorption (dashed lines) and emission spectra (solid lines) of dimer **4-11a** in dry, degassed *n*-hexane (purple), DCM (green), THF (blue) and ACN (red) at room temperature.

Compound **4-11b** shows an intense absorption band with $\lambda_{abs,max}$ = 264 nm in THF with an extinction coefficient ε of 41000 M^{-1} cm^{-1}. An emission band is observed between 325 – 500 nm with $\lambda_{em,max}$ = 357 nm and the apparent Stokes shift is 9867 cm^{-1} (Figure 4-18, left). The quantum yield was determined to be Φ = 0.17 and a very short emission lifetime τ_F = 1.72 ns was determined at room temperature. The short lifetime strongly indicates fluorescence.[318]

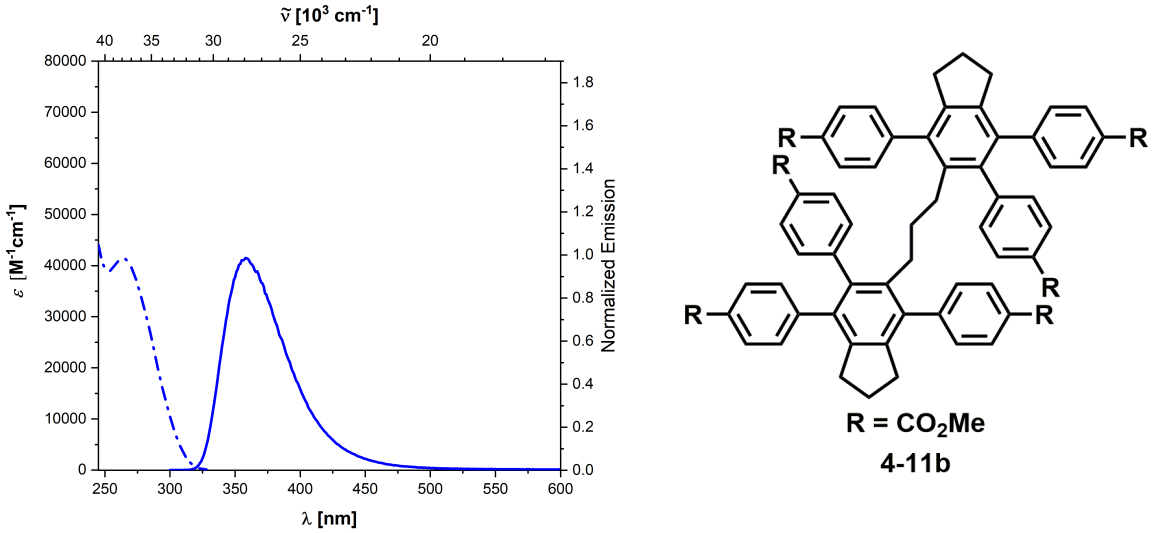

Figure 4-18: Absorption (dashed line) and emission spectra (solid line) of trimer **4-11b** in dry, degassed THF at room temperature (left). Chemical structure of trimer **4-11b** (right).

Absorption and emission spectra of **4-11b** in different solvents are displayed in Figure 4-19. The absorption maximum $\lambda_{abs,max}$ in DCM is at 265 nm, in THF at 264 nm, and in ACN at 266 nm. The emission maximum $\lambda_{em,max}$ in DCM is at 359 nm, in THF at 357 nm, and at 362 nm in ACN. The apparent Stokes shift is 9880 cm^{-1} in DCM, 9867 cm^{-1} in THF, and 9969 cm^{-1} in ACN. No solvatochromic effect is observed.

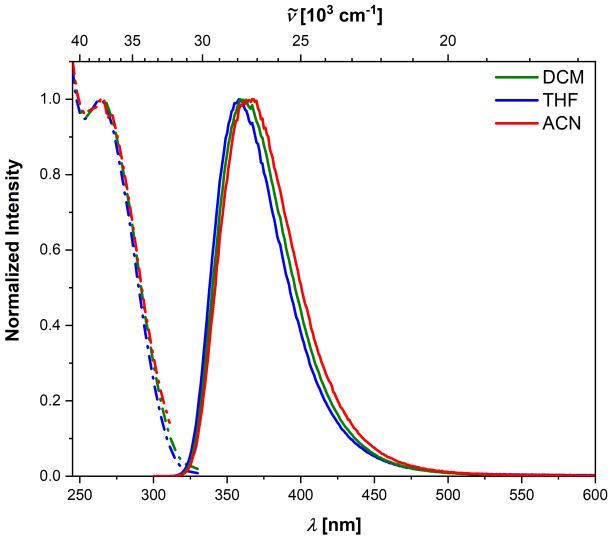

Figure 4-19: Absorption (dashed lines) and emission spectra (solid lines) of trimer **4-11b** in dry, degassed DCM (green), THF (blue) and ACN (red) at room temperature.

Compound **4-13a** shows an intense absorption band at $\lambda_{abs,max}$ = 273 nm in THF with an extinction coefficient ε of 60000 M^{-1} cm^{-1}. An emission band is observed between 325 – 500 nm with $\lambda_{em,max}$ = 359 nm and the apparent Stokes shift is 8774 cm^{-1} (Figure 4-20, left). Compound **4-13a** exhibits a quantum yield of Φ = 0.12 and very short emission lifetime of τ_F = 1.18 ns at room temperature. The short lifetime strongly indicates fluorescence.[318]

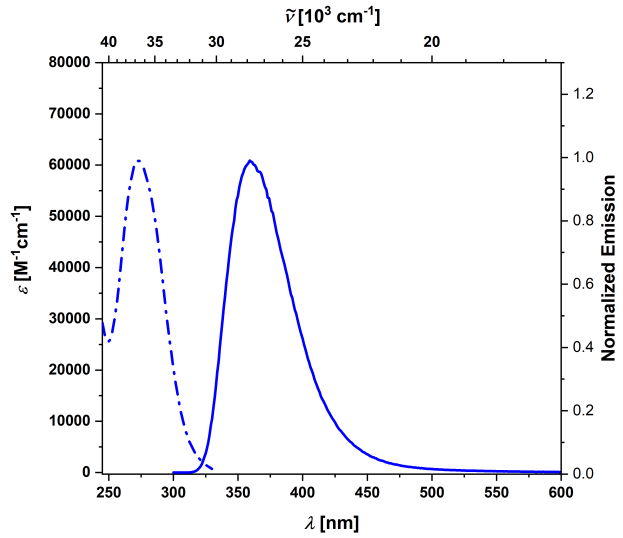

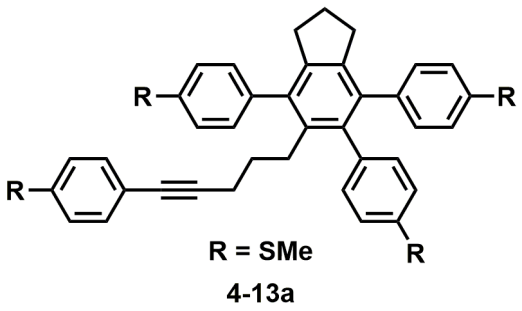

Figure 4-20: Absorption (dashed line) and emission spectra (solid line) of dimer **4-13a** in dry, degassed THF at room temperature (left). Chemical structure of dimer **4-13a** (right).

Compound **4-13b** shows an intense absorption band with $\lambda_{abs,max}$ = 266 nm in THF with an extinction coefficient ε of 75000 M^{-1} cm^{-1}. An emission band is observed between 325 – 500 nm with $\lambda_{em,max}$ = 360 nm and the apparent Stokes shift is 9816 cm^{-1} (Figure 4-21, left). The quantum yield was determined to be Φ = 0.16 and very short emission lifetime of τ_F < 1 ns was determined at room temperature. The short lifetime strongly indicates fluorescence.[318]

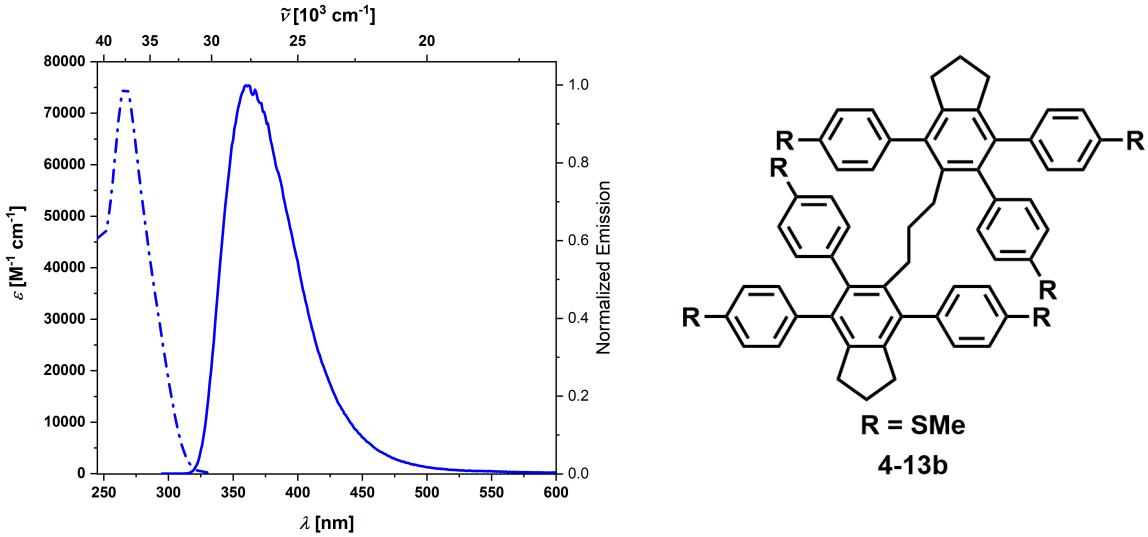

Figure 4-21: Absorption (dashed line) and emission spectra (solid line) (left) of trimer **4-13b** in dry, degassed THF at room temperature. Chemical structure of trimer **4-13b** (right).

The compound *para*-terphenyl shows an intense absorption band with $\lambda_{abs,max}$ = 281 nm in THF and an emission band between 300 – 425 nm with two local emission maxima at $\lambda_{em,max}$ = 325 and 339 nm, and two shoulders at ca. 355 and 375 nm. The apparent Stokes shift is 4817 cm^{-1} (Figure 4-22, left). *Para*-terphenyl exhibits a quantum yield of Φ = 0.82 and very short emission lifetime of τ_F = 1.03 ns at room temperature. The short lifetime and the small apparent Stokes shift strongly indicates fluorescence.[318]

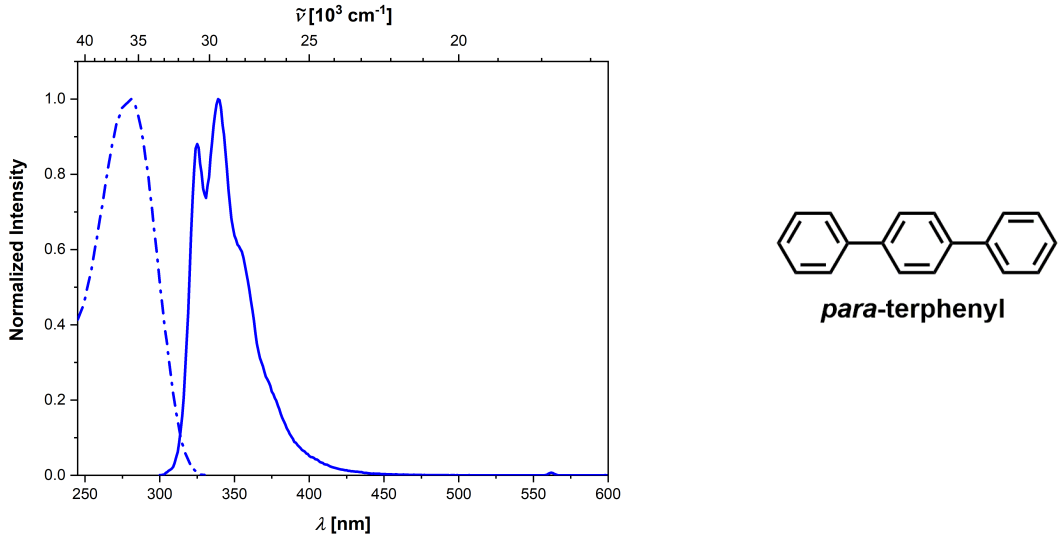

Figure 4-22: Absorption (dashed line) and emission spectra (solid line) of *para*-terphenyl in dry, degassed THF at room temperature (left). Chemical structure of *para*-terphenyl (right).

The compounds **4-11a**,**b** and **4-13a**,**b** display $\lambda_{abs,max}$ in the 264 – 273 nm range, $\lambda_{exc,max}$ in the 267 – 272 nm range and $\lambda_{em,max}$ in the 356 – 360 nm range (Table 4-12). The extinction coefficients for the CO_2Me-substituted compounds are smaller than for the SMe-substituted compounds and the apparent Stokes shifts are comparable. The quantum yields Φ are in the 0.08 – 0.17 range and the fluorescence lifetimes τ_F < 2 ns, indicative of fluorescence. The apparent Stokes shifts are in the range of 8774 – 9867 cm^{-1}.

The small apparent Stokes shift of *para*-terphenyl of 4817 cm^{-1} compared to **4-11a**,**b** and **4-13a**,**b** arises from a red-shift of $\lambda_{abs,max}$ of ca. 1600 cm^{-1} and a blue-shift of $\lambda_{em,max}$ of ca. 1600 cm^{-1}. The quantum yield is larger for *para*-terphenyl than for **4-11a**,**b** and **4-13a**,**b**, likely due to the smaller Stokes shift. However, the fluorescence lifetimes of all five compounds are τ_F < 2 ns. The lower quantum yield of the dimers and trimers may arise from the larger twist of the aryl rings attached to the central benzene moiety (see Table 4-9 and 4-10, also Figure 4-12 and 4-13).

Table 4-12: Photophysical data of compounds **4-11a**,**b**, **4-13a**,**b** and *para*-terphenyl in dry, degassed THF at room temperature.

Compound	$\lambda_{abs,max}$ [nm]	$\lambda_{exc,max}$ [nm]	$\lambda_{em,max}$ [nm]	ε [M^{-1} cm^{-1}]	Φ	τ_F [ns]	Stokes shift [cm^{-1}]
4-11a	265	267	356	56000 (265 nm)	0.08	1.14	9645
4-11b	264	267	357	41000 (264 nm)	0.17	1.72	9867
4-13a	273	272	359	60000 (273 nm)	0.12	1.18	8774
4-13b	266	268	360	75000 (266 nm)	0.16	< 1	9816
p-terphenyl	281	280	325	-	0.82	1.03	4817

Schwenk reported that the dimers of the α,ω-tetraynes absorb with $\lambda_{abs,max}$ in the 297 – 332 nm range in DCM with extinction coefficients ε of 55000 – 95000 M^{-1} cm^{-1}. Emission was observed with $\lambda_{em,max}$ in the 377 – 438 nm range, resulting in Stokes shifts of 3600 – 7900 cm^{-1}. The fluorescence quantum yields Φ were determined to be in the 0.09 – 0.78 range and the fluorescence lifetimes τ_F in the 0.83 – 2.36 ns range (Figure 4-23 and Table 4-13).[68]

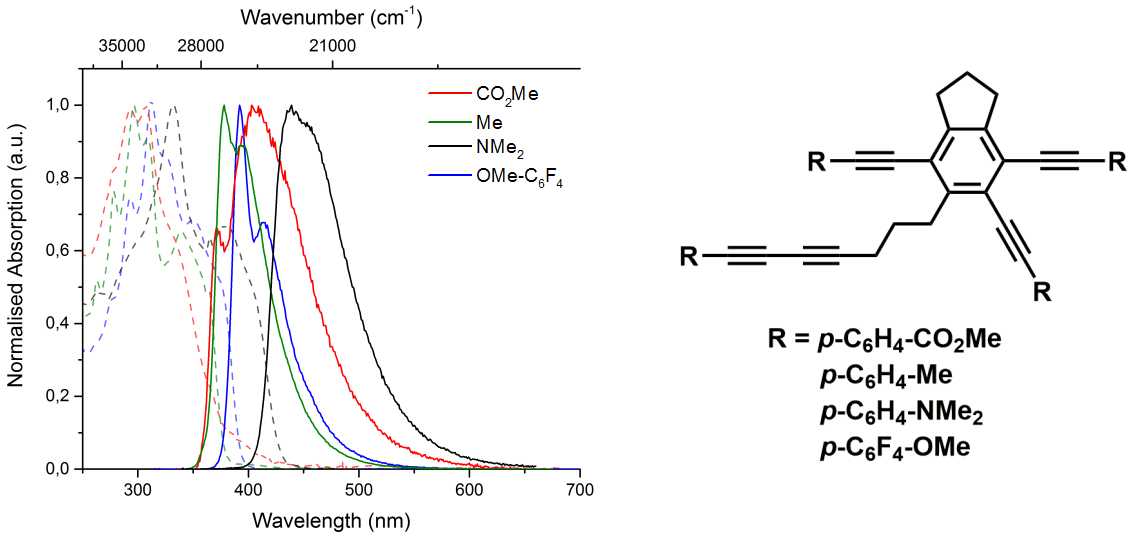

Figure 4-23: Absorption (dashed lines) and emission spectra (solid lines) of dimers of α,ω-tetraynes in DCM at room temperature previously reported by Schwenk (left).[68] Chemical structure of dimers of α,ω-tetraynes (right).

The trimers of the α,ω-tetraynes absorb with $\lambda_{abs,max}$ in the 305 – 325 nm range in DCM with extinction coefficients ε of 84000 – 131000 M^{-1} cm^{-1}. Emission was observed $\lambda_{em,max}$ in the 378 – 400 nm range, resulting in Stokes shifts of 5300 – 7800 cm^{-1}. The fluorescence quantum yields Φ were determined to be in the 0.12 – 0.72 range and the fluorescence lifetimes τ_F in the 1.57 – 2.60 ns range (Figure 4-24 and Table 4-13).[68]

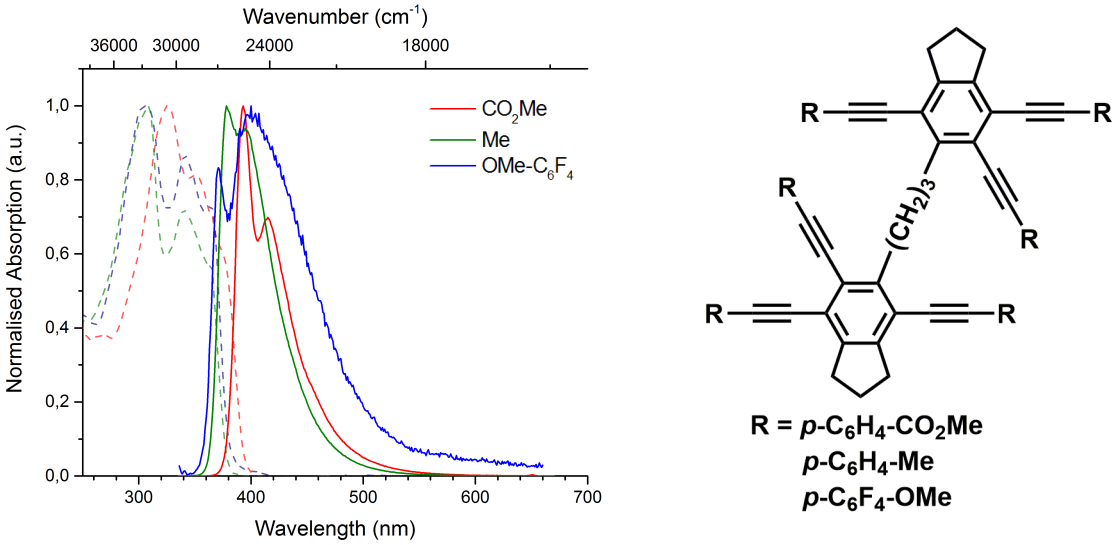

Figure 4-24: Absorption (dashed lines) and emission spectra (solid lines) of trimers of α,ω-tetraynes in DCM at room temperature previously reported by Schwenk (left).[68] Chemical structure of trimers of α,ω-tetraynes (right).

The photophysical data for the dimers and trimers investigated by Schwenk are summarized in Table 4-13.

As the dimer **4-11a** and the trimer **4-11b** exhibit only a small and almost no solvatochromic effect, respectively, it is possible to compare **4-11a** and **4-11b**, measured in THF, with CO_2Me-substituted dimer and trimer of the *α,ω*-tetraynes, measured in DCM. The absorption and emission of **4-11a**,**b** are hypsochromically shifted, the extinction coefficient *ε* and the fluorescence quantum yields are smaller, whereas the Stokes shift is larger, compared to the data obtained by Schwenk.

Table 4-13: Photophysical data of dimers and trimers of *α,ω*-tetraynes in dichloromethane at room temperature previously reported by Schwenk.[68]

R	$\lambda_{abs,max}$ [nm]	$\lambda_{em,max}$ [nm]	ε [M^{-1} cm^{-1}]	Φ	τ_F [ns]	Stokes shift [cm^{-1}]
			Dimer			
***p*-C_6H_4-CO_2Me**	307	406	77000	0.78	0.83	7900
***p*-C_6H_4-Me**	297	377	74000	0.66	2.36	7100
***p*-C_6H_4-NMe_2**	332	438	95000	0.27	1.22	3600
***p*-C_6F_4-OMe**	311	391	55000	0.09	1.61	6600
			Trimer			
***p*-C_6H_4-CO_2Me**	325	392	131000	0.72	1.57	5300
***p*-C_6H_4-Me**	310	378	115000	0.24	2.60	5800
***p*-C_6F_4-OMe**	305	400	84000	0.12	1.60	7800

Complex **4-15** shows a low-energy absorption band in the visible region of the electromagnetic spectrum with absorption maxima at $\lambda_{abs,max}$ = 517 and 555 nm in THF and extinction coefficients ε of 27000 M^{-1} cm^{-1} and 29000 M^{-1} cm^{-1}, respectively. A broad emission band is observed between 525 – 800 nm with two local emission maxima at $\lambda_{em,max}$ = 587 and 632 nm. The apparent Stokes shift is 982 cm^{-1} (Figure 4-25, left). Complex **4-15** exhibits a low quantum yield $\Phi < 0.01$ and very short emission lifetime of < 1 ns at room temperature. The short lifetime and the small apparent Stokes shift strongly indicate fluorescence.

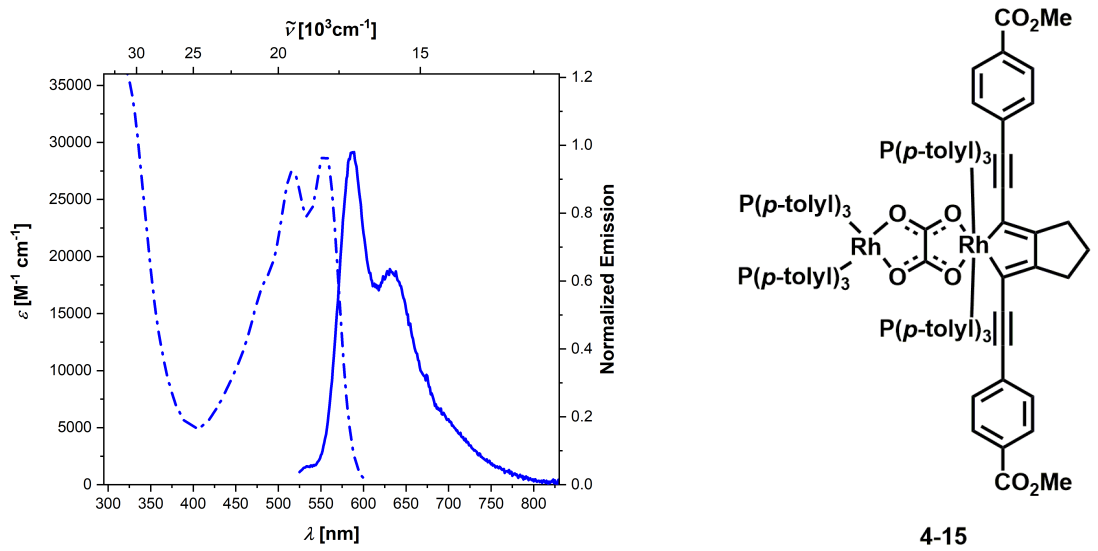

Figure 4-25: Absorption (dashed line) and emission spectra (solid line) (left) of complex **4-15** in dry, degassed THF at room temperature. Chemical structure of complex **4-15** (right).

The CO_2Me- and tri(*p*-tolyl)phosphine-substituted 2,5-bis(arylethynyl)rhodacyclopentadiene **1-57d** synthesized by Sieck displays an absorption band in toluene with $\lambda_{abs,max}$ = 563 nm, a broad emission band with $\lambda_{em,max}$ = 583 nm, an apparent Stokes shift of 609 cm^{-1}, a low quantum yield $\Phi < 0.01$ and very short emission lifetime of less than 1 ns at room temperature. The molar extinction coefficient ε is 32500 M^{-1} cm^{-1}.(Figure 4-26, left).[71-72]

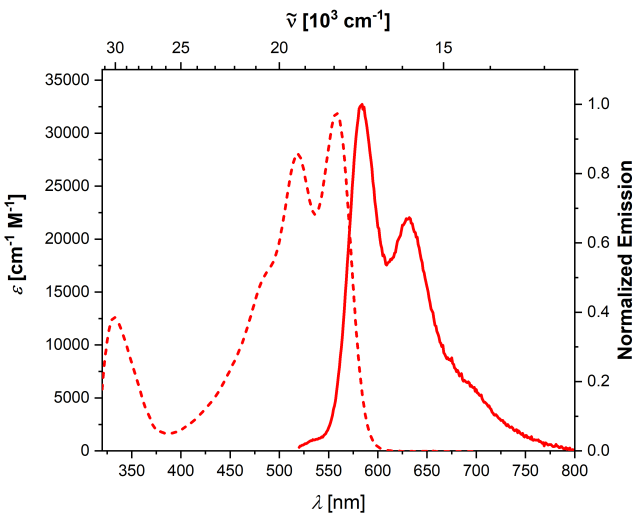

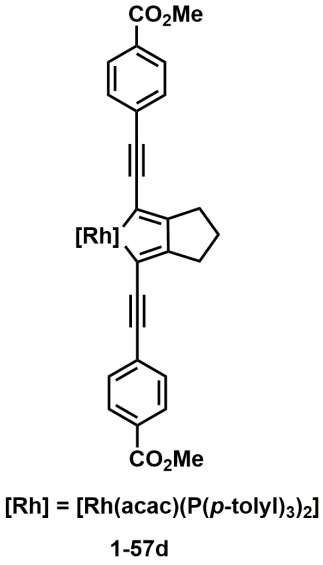

Figure 4-26: Absorption (dashed line) and emission spectra (solid line) of **1-57d** in degassed toluene at room temperature (left)[71-72] and chemical structure of rhodacycle **1-57d**.

Only negligible differences in $\lambda_{abs,max}$, $\lambda_{em,max}$, ε, the apparent Stokes shift, quantum yield and the emission lifetime are observed for **4-15** in comparison with **1-57d** (see Table 4-14). Hence, the additional rhodium(I) center in the complex has no influence on the photophysical properties of **4-15**.

Table 4-14: Photophysical data of complex **4-15** in dry, degassed THF and of complex **1-57d**[72], previously reported by Sieck, in dry, degassed toluene at room temperature.

Compound	$\lambda_{abs,max}$ [nm]	$\lambda_{em,max}$ [nm]	ε [M^{-1} cm^{-1}]	Φ	τ_F [ns]	Stokes shift [cm^{-1}]
4-15	517, 555	587, 632	29000	< 0.01	< 1	982
1-57d	519, 563	583, 632	32500	< 0.01	< 1	609

Chapter 5

5 Summary

5.1 Summary of Chapter 2

In the reaction of [Rh(acac)(PMe_3)$_2$] **1-51** with two equivalents of *para*-substituted 1,4-diphenylbuta-1,3-diynes **2-1a**,**b** at room temperature, the complexes **2-2a**,**b** and **2-3a**,**b** were formed. It was possible to separate the minor products **2-3a**,**b** from the major products **2-2a**,**b** (Scheme 5-1) *via* flash column chromatography, resulting in blue (**2-3a**) and blue/green (**2-3b**) complexes. Compounds **2-2a**,**b** contain a bidentate organic fulvene moiety, composed of two diynes, σ-bound to the rhodium center and were formed in a [3+2] cyclization. Whereas complexes **2-3a**,**b** contain an organic indene moiety, composed of three diynes, attached to the rhodium center in a bis-σ-manner and were formed in a [3+2+3] cyclization process.

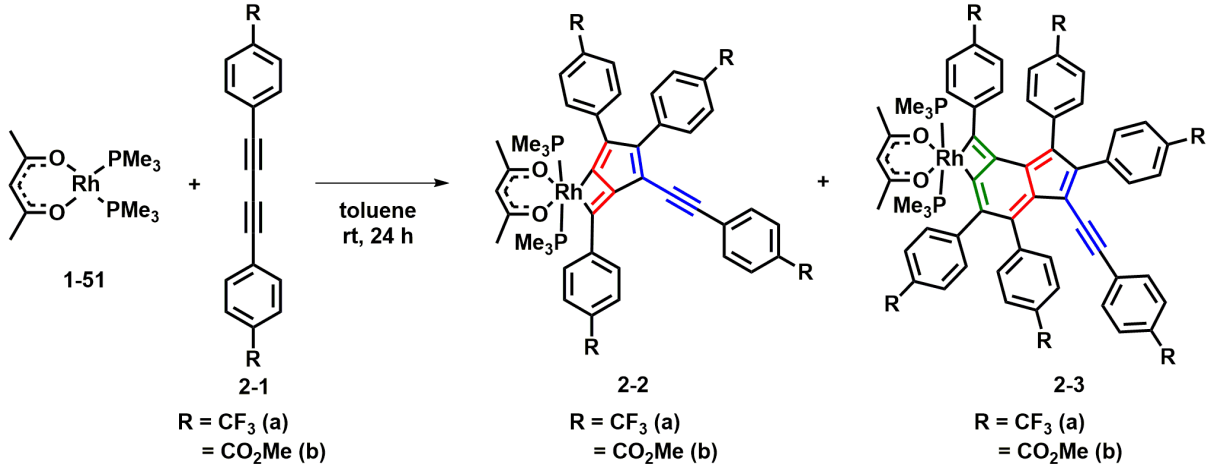

Scheme 5-1: Synthesis of the complexes **2-2a**,**b** and **2-3a**,**b** *via* reaction of [Rh(acac)(PMe_3)$_2$] **1-51** with *para*-substituted 1,4-diphenylbuta-1,3-diynes **2-1a**,**b**. The former 1,3-butadiyne units are highlighted in different colors.

For reactions at 100 °C, more than two equivalents of *para*-CF_3-substituted 1,4-diphenylbuta-1,3-diyne **2-1a** are necessary for a complete consumption of [Rh(acac)(PMe_3)$_2$] **1-51**, and that with three equivalents of **2-1a** present, more of complex **2-3a** was formed than with five equivalents of **2-1a**. Additional studies revealed the possibility of the formation of complex **2-3a** from the reaction of complex **2-2a** with **2-1a** at 100 °C. Furthermore, a 2,5-bis(arylethynyl)rhodacyclopentadiene **2-SYM^{CF3}** and a 2,4-bis(arylethynyl)rhodacyclopentadiene **2-UNSYM^{CF3}** were formed in the reactions of [Rh(acac)(PMe_3)$_2$] **1-51** with **2-1a** and complex **2-2a** with **2-1a**, respectively, at 100 °C.

A crossover experiment of complex **2-2a** with *para*-CO_2Me-substituted 1,4-diphenylbuta-1,3-diyne **2-1b** was conducted, resulting in complex **2-3c**, in addition to **2-SYM^{CO2Me}** and **2-UNSYM^{CO2Me}**. In compound **2-3c**, the third *para*-substituted 1,4-diphenylbuta-1,3-diyne

2-1b was incorporated between the rhodium center and the bis-*σ*-bound organic fulvene fragment of complex **2-2a** (Scheme 5-2).

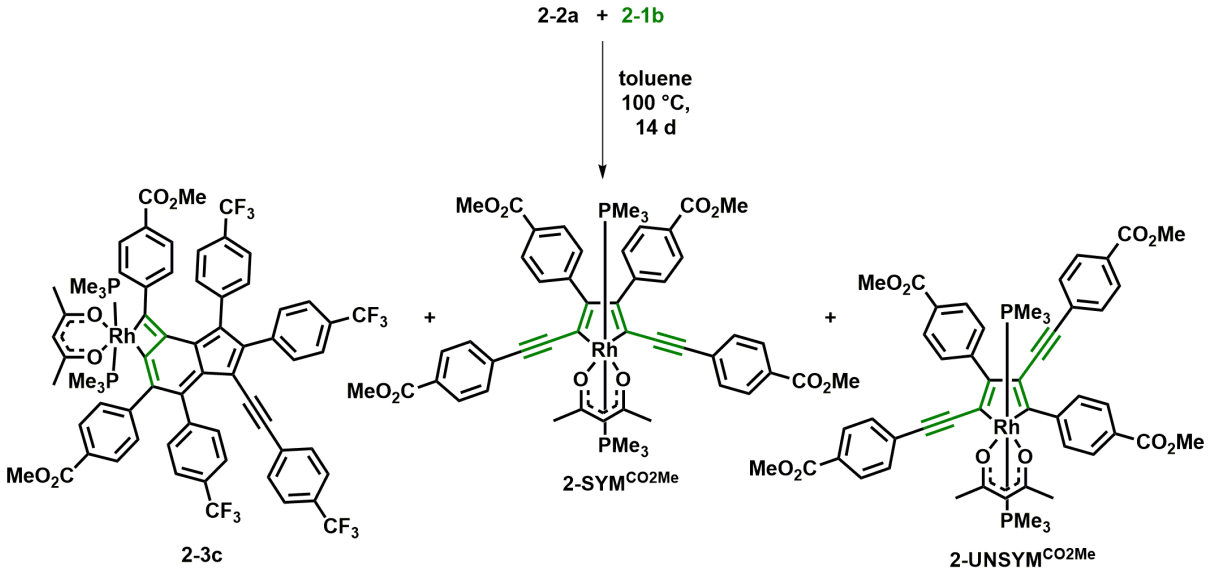

Scheme 5-2: Formation of complexes **2-3c**, **2-SYM**^{CO2Me} and **2-UNSYM**^{CO2Me} *via* reaction of complex **2-2a** with *para*-substituted 1,4-diphenylbuta-1,3-diyne **2-1b**. The former 1,3-butadiyne units of **2-1b** are highlighted in green.

This unique type of [3+2] cyclization can be used for the synthesis of highly conjugated organic molecules, which are hard to access or even inaccessible by conventional methods. At 80 °C, in the reaction of complex **2-2a** with *para*-tolyl isocyanate **2-4**, the formation of a purple pure organic compound **2-5**, comprising of the organic fulvene structure and one equivalent of *para*-tolyl isocyanate was formed. Orange-colored single-crystals, suitable for X-ray diffraction analysis, of **2-9**, a formal dimer of **2-5**, were also obtained (Scheme 5-3).

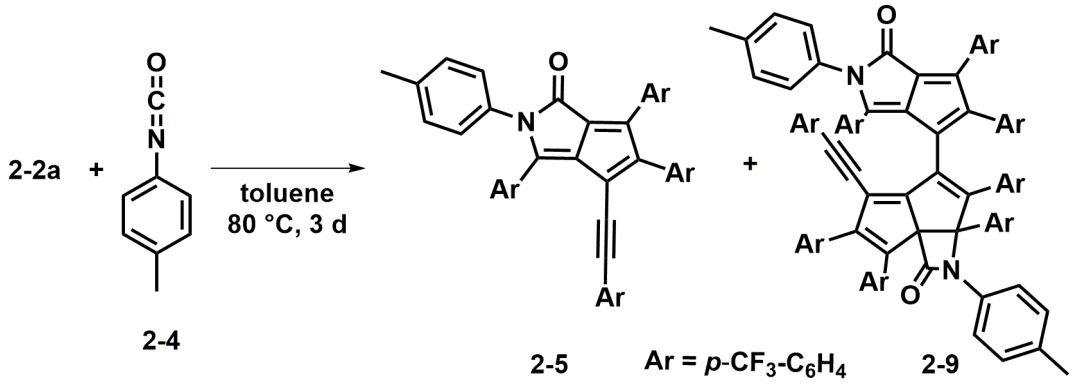

Scheme 5-3: Synthesis of **2-5** and **2-9** *via* reaction of complex **2-2a** with four equivalents of *para*-tolyl isocyanate **2-4**.

In addition to the products **2-5** and **2-9** in Scheme 5-3, 1,3,5-tris(*p*-tolyl)-1,3,5-triazine-2,4,6-trione **2-8**, a cyclotrimerization product of *para*-tolyl isocyanate **2-4**, was also isolated (Scheme 5-4). This finding led to the conclusion that some participant in the reaction of complex **2-2a** with *para*-tolyl isocyanate **2-4** catalyzes the isocyanate trimerization.

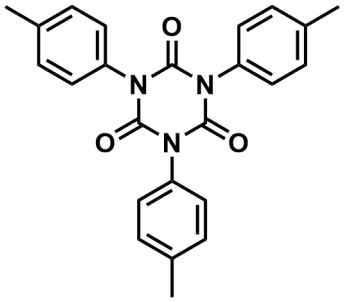

2-8

Scheme 5-4: Chemical structure of 1,3,5-tris(*p*-tolyl)-1,3,5-triazine-2,4,6-trione **2-8**.

As the starting material [Rh(acac)(PMe_3)$_2$] **1-51** is released after removing the organic fulvene part from the rhodium center, in the reaction of complex **2-2a** with *para*-tolyl isocyanate **2-4**, its catalytic activity for the trimerization of **2-4** was investigated. The reaction of [Rh(acac)(PMe_3)$_2$] **1-51** with four equivalents of **2-4** gave mainly *cis*-phosphine rhodium complexes, and small amounts of **2-8**. The predominant rhodium complex isolated being, according to single-crystal X-ray diffraction, *cis*-[Rh(acac)(PMe_3)$_2$(2-4)$_2$] **2-10a**, with an isocyanate dimer bound to the rhodium center by one carbon and one oxygen atom (Scheme 5-5).

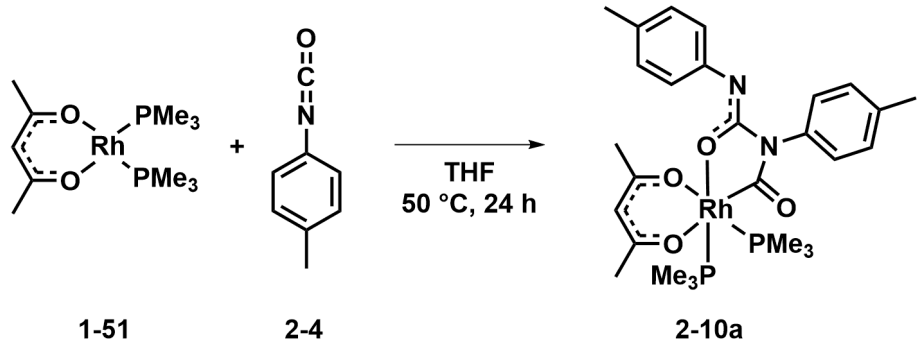

1-51 **2-4** **2-10a**

Scheme 5-5: Synthesis of complex **2-10a** *via* reaction of [Rh(acac)(PMe_3)$_2$] **1-51** with *para*-tolyl isocyanate **2-4**.

Formation of cyclotrimerization product **2-8** was observed in the reaction of complex **2-10a** with *para*-tolyl isocyanate **2-4** at elevated temperatures. However, the activity of [Rh(acac)(PMe_3)$_2$] **1-51** and complex **2-10a** in the catalytic trimerization of **2-4** remains unclear, as when trimethylphosphine was added to *para*-tolyl isocyanate **2-4** in C_6D_6, precipitation of the trimer **2-8** began at room temperature. Therefore, it is likely that liberated PMe_3 is the catalytic species in the reaction.

When the NHC-substituted rhodium(I) precursor [Rh(acac)(Me_2Im)$_2$] **2-21** was used instead of [Rh(acac)(PMe_3)$_2$] **1-51** in the reaction with *para*-substituted 1,4-diphenylbuta-1,3-diynes **2-1a**,**b**, the outcome was drastically altered (Scheme 5-6). The reaction pathway was proposed

on the basis of NMR spectroscopic studies in C_6D_6 and THF-d_8, and a single-crystal X-ray structure of complex **2-I$_{cis}$b**.

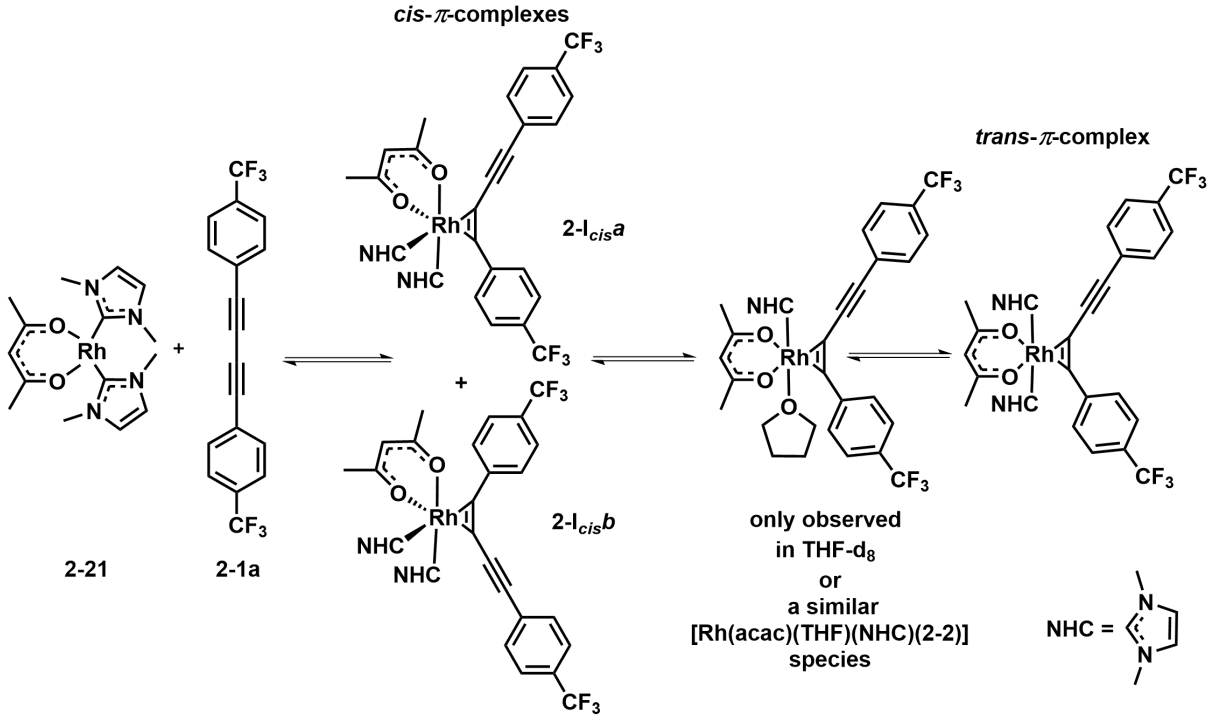

Scheme 5-6: Proposed reaction pathway for the formation of *trans*-[Rh(acac)(Me$_2$Im$_2$)$_2$(2-2a)].

While the formation of a *trans*-NHC complex proceeds at least *via* one *cis*-π-complex, similar to the reaction of [Rh(acac)(PMe$_3$)$_2$] **1-51** with the *para*-substituted 1,4-diphenylbuta-1,3-diynes **2-1a**,**b**, the formation of a complex similar to **2-2a**,**b** or **2-3(a-c)** could not unambiguously be assigned *via* NMR spectroscopy. An NHC-substituted analogue of **2-2a**,**b** was identified only by HRMS. Furthermore, an equilibrium between the different species was observed.

The photophysical properties of **2-2a**,**b**, **2-3(a-c)** and **2-5** are limited to absorption, as no emission was observed in THF at room temperature or in 2-Me-THF at room temperature or at 77 K in a glass matrix.

Complexes **2-2a**,**b** show broad absorptions with four local maxima in the 214 – 540 nm range with extinction coefficients ε of up to ca. 45000 M^{-1} cm^{-1} in THF. The absorption band of complex **2-2a** with the highest energy is hypsochromically shifted compared to that of complex **2-2b**, while the other absorption bands are all bathochromically shifted. The extinction coefficients ε are all in the same range, and both compounds display weak absorptions tailing to 700 nm with small extinction coefficients ε of up to ca. 2000 M^{-1} cm^{-1}.

Complexes **2-3(a-c)** show a broad high energy absorption with a maximum at ca. 350 nm with extinction coefficients ε of up to ca. 70000 M^{-1} cm^{-1} and a broad absorption from ca.

500 – 1000 nm with extinction coefficients ε of ca. 11000 M^{-1} cm^{-1} in THF. The high energy absorption band from the pure CF_3-substituted complex **2-3a** is hypsochromically shifted compared to the mixed CO_2Me-CF_3-substituted complex **2-3c**, and to the pure CO_2Me-substituted complex **2-3b**.
The UV-visible absorption spectrum of the pure organic compound **2-5** shows a broad absorption from 214 – 750 nm with extinction coefficients ε of up to 40500 M^{-1} cm^{-1} in THF.

TD-DFT studies show that the first three transitions are HOMO, HOMO-1 and HOMO-2 to LUMO transitions. These π-π* excitations exhibit moderate to weak charge-transfer character. The incorporation of the nitrogen donor and the carbonyl acceptor in conjunction with the large conjugated π-system results in the low energies of the transitions.

Cyclic voltammetry measurements on compound **2-2a** show that the first reduction at $E_{1/2}$ = -1.89 V and oxidation at $E_{1/2}$ = 0.29 V, relative to the Fc/Fc^+ couple, are reversible. Similarly, complex **2-3a** shows only one reversible reduction at $E_{1/2}$ = -1.42 V and one reversible oxidation at $E_{1/2}$ = 0.13 V, relative to the Fc/Fc^+ couple. Inspection of the pure organic compound **2-5** in THF reveals two fully reversible reductions at $E_{1/2}$ = -1.05 and -1.70 V, relative to the Fc/Fc^+ couple, respectively, and no oxidation.

5.2 Summary of Chapter 3

Various *α,ω*-diynes with different backbones were synthesized, with **3-1**, **3-2**, **3-3** and **3-5** having a fixed u-shape in contrast to the flexible w-shape of **3-4** and **3-8** (Scheme 5-7).

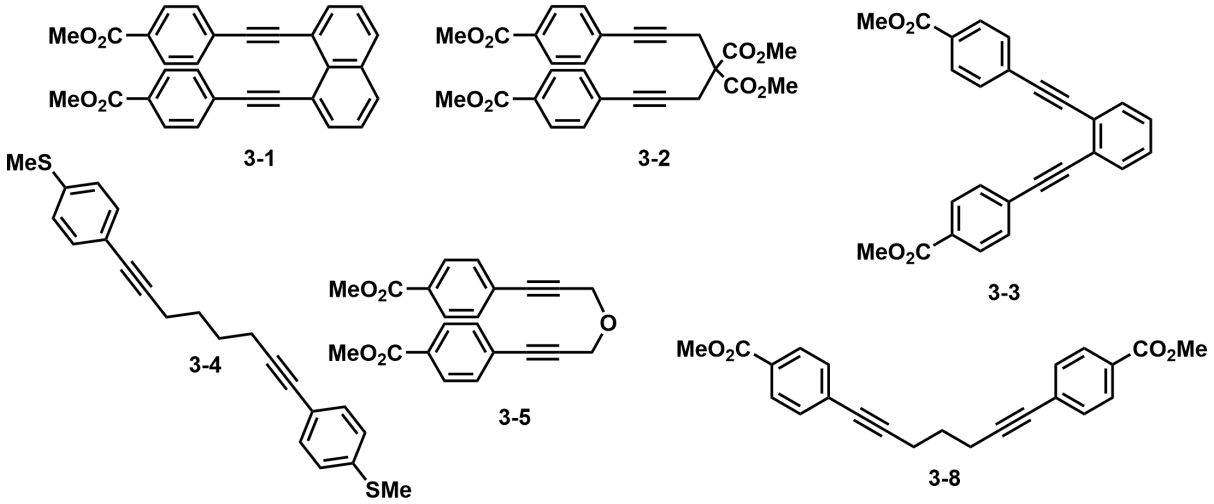

Scheme 5-7: Chemical structures of dimethyl 4,4'-(naphthalene-1,8-diylbis(ethyne-2,1-diyl))dibenzoate **3-1**, dimethyl 2,2-bis(3-(4-(methoxycarbonyl)phenyl)prop-2-yn-1-yl)malonate **3-2**, dimethyl 4,4'-(1,2-phenylenebis(ethyne-2,1-diyl))dibenzoate **3-3**, 1,8-bis(4-(methylthio)phenyl)octa-1,7-diyne **3-4**, dimethyl 4,4'-(oxybis(prop-1-yne-3,1-diyl))dibenzoate **3-5** and dimethyl 4,4'-(hepta-1,6-diyne-1,7-diyl)dibenzoate **3-8**.

The influence of the *α,ω*-diynes on the reaction with [Rh(acac)(PMe_3)$_2$] **1-51** and [Rh(acac)(P(*p*-tolyl)$_3$)$_2$] **1-56** in equimolar amounts leading to the formation of 2,5-bis(aryl)rhodacyclopentadienes in C_6D_6 was investigated.

In the reaction of [Rh(acac)(PMe_3)$_2$] **1-51** with *α,ω*-diynes **3-1**, **3-2** and **3-8** at room temperature, preorganization of the *α,ω*-diyne was able to enhance the rate of consumption of the rhodium(I) starting material. Additionally, at 60 °C, smooth conversion to the desired 2,5-bis(aryl)rhodacyclopentadienes was observed with *α,ω*-diynes **3-1** and **3-8**, while reaction with *α,ω*-diyne **3-2** also gave minor byproducts.

Only very slow conversion to the desired rhodacyclopentadiene was observed in the reaction of [Rh(acac)(PMe_3)$_2$] **1-51** with *α,ω*-diyne **3-5**, even at elevated temperatures, although the rhodium(I) starting material was completely consumed.

With *α,ω*-diynes **3-3** and **3-4**, only very slow consumption of [Rh(acac)(PMe_3)$_2$] **1-51** was observed, even at elevated temperatures. It remains unclear, if the desired rhodacyclopentadienes were formed.

However, in reactions of [Rh(acac)(PMe_3)$_2$] **1-51** with *α,ω*-diynes **3-1** and **3-2** the unknown 2,5-bis(aryl)rhodacyclopentadienes **3-6** and **3-7** were obtained (Scheme 5-8).

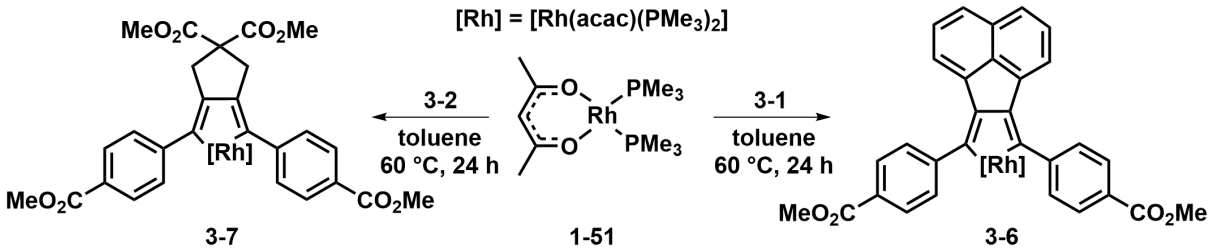

Scheme 5-8: Synthesis of 2,5-bis(aryl)rhodacyclopentadienes **3-6** and **3-7** *via* reaction of [Rh(acac)(PMe_3)$_2$)] **1-51** with *α,ω*-diynes **3-1** and **3-2**.

Reaction of [Rh(acac)(P(*p*-tolyl)$_3$)$_2$] **1-56** with *α,ω*-diynes **3-2**, **3-5** and **3-8** in equimolar amounts showed similar reaction behavior. According to $^{31}P\{^1H\}$ NMR spectroscopy at room temperature, in addition to [Rh(acac)(P(*p*-tolyl)$_3$)$_2$] **1-56**, the respective rhodacyclopentadienes, an additional rhodium(I)-phosphine complex at ca. 30 ppm with $^1J_{Rh\text{-}P}$ = 170 Hz, and a resonance for unbound tri(*p*-tolyl)phosphine were observed. After heating, resonances for the complexes at ca. 30 ppm and unbound tri(*p*-tolyl)phosphine were diminished. The amounts of remaining **1-56** were quite small for the reactions with *α,ω*-diynes **3-2** and **3-5**, while for *α,ω*-diyne **3-8**, larger amounts remained. Cycloisomerization products were observed in the ^1H NMR spectra for all three *α,ω*-diynes. Complex **1-56** is known to be a catalyst for the cycloisomerization of aryl-substituted *α,ω*-diynes and *α,ω*-tetraynes, and was used in the Marder group previously.

The reaction of [Rh(acac)(P(*p*-tolyl)$_3$)$_2$] **1-56** with *α,ω*-diyne **3-4** shows similar signals to those of *α,ω*-diynes **3-2**, **3-5** and **3-8**, in their $^{31}P\{^1H\}$ NMR spectra, whereas the resonances are downfield shifted, the coupling constants are larger and the quantities of the compounds formed smaller. After heating, only traces of cycloisomerization products and no rhodacyclopentadiene were observed.

Reaction of [Rh(acac)(P(*p*-tolyl)$_3$)$_2$] **1-56** with *α,ω*-diyne **3-1** at room temperature resulted in the observation of resonances for the starting material and the desired rhodacyclopentadiene complex, according to $^{31}P\{^1H\}$ NMR spectroscopy. After heating, the rhodacyclopentadiene **3-15** was obtained (Scheme 5-9).

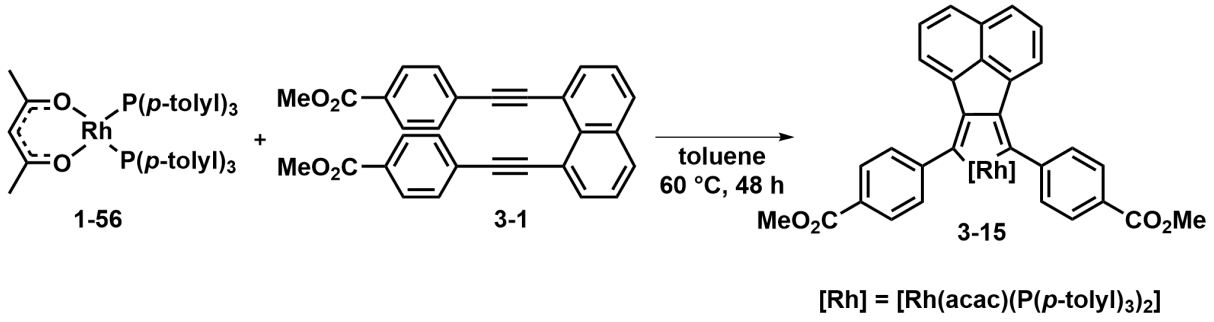

Scheme 5-9: Synthesis of 2,5-bis(aryl)rhodacyclopentadiene **3-15** *via* reaction of [Rh(acac)(P(*p*-tolyl$_3$)$_2$)] **1-56** with *α,ω*-diyne **3-1**.

Reaction of [Rh(acac)(Me_2Im)$_2$] **2-21** with α,ω-diyne **3-1**, resulted in the formation of *trans*- and *cis*-NHC-substituted 2,5-bis(aryl)rhodacyclopentadienes as observed by ^{1}H and ^{13}C{^{1}H} NMR spectroscopy (Scheme 5-10). At room temperature after 14 days, the rhodium(I) starting material was completely consumed, resulting in a ratio of *cis*:*trans* complexes of 1:0.83. Heating the reaction at 60 °C for six days resulted in a *cis*:*trans* ratio of 1:0.25. Further heating at 80 °C for 24 hours resulted in a *cis*:*trans* ratio of 1:0.10. Additional heating did not change the ratio but resulted in decomposition. While in the reaction of [Rh(acac)(Me_2Im)$_2$] **2-21** with *para*-substituted 1,4-diphenylbuta-1,3-diynes **2-1a**,**b** the *trans*-species was the thermodynamic favored species, in this reaction the *cis*-species was favored.

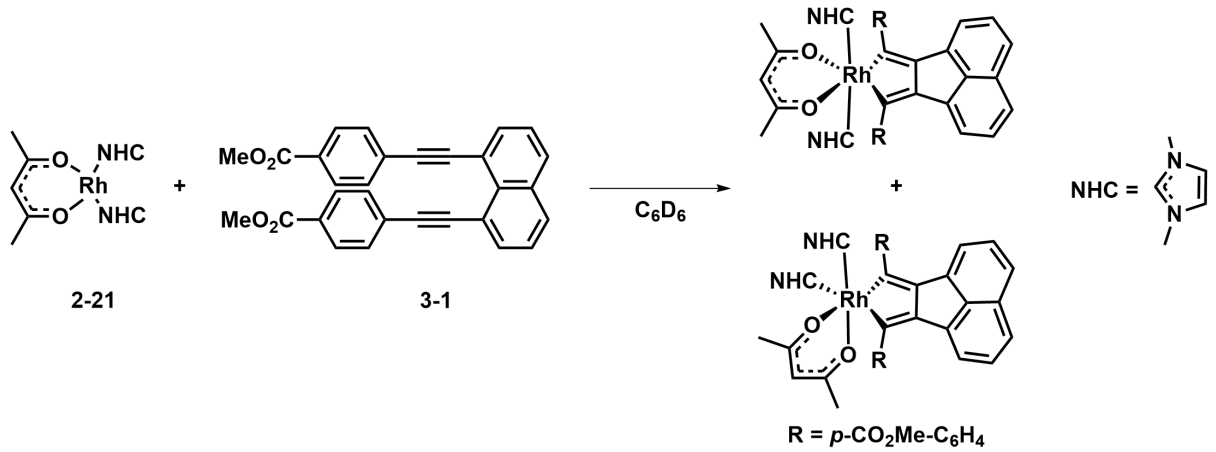

Scheme 5-10: Reaction of [Rh(acac)(Me_2Im)$_2$] **2-21** with α,ω-diyne **3-1** resulting in a *trans*- and *cis*-NHC-substituted 2,5-bis(aryl)rhodacyclopentadiene.

Rhodacyclopentadienes **3-6** and **3-7** exhibit small apparent Stokes shifts, low quantum yields Φ of < 0.01, and very short emission lifetimes τ_F of less than 1 ns at room temperature. Such short lifetimes and the small apparent Stokes shifts strongly indicate fluorescence. Compared to compound **3-7**, complex **3-6** displays a bathochromic shift in excitation, absorption and emission spectra.

Comparing complex **3-7**, with a similar 2,5-bis(aryl)rhodacyclopentadiene **3-10** synthesized in the group previously, shows that they have similar photophysical properties. Thus, replacing the CH_2 with a $C(CO_2Me)_2$ group in the rhodacyclopentadiene backbone does not significantly affect the photophysical properties of the compound.

Compound **3-15** shows a small apparent Stokes shift, a quantum yield of Φ = 0.02, and multiple emission lifetimes τ_F of 1.79 ns (32%), 5.81 ns (63%) and 13.12 ns (5%) in THF. Such short lifetimes and the small Stokes shift strongly indicate fluorescence. The excitation and the absorption spectra differ remarkably. It was not possible to detect any emission from compound **3-15** in toluene.

Compounds **3-6** and **3-15**, bearing different phosphine ligands, differ substantially in their photophysical properties. Additionally, the different absorption and excitation spectra lead to the conclusion that different species may be present. This finding has not been observed previously for any other rhodacycles. As the P(*p*-tolyl)$_3$ ligand is more labile than the trimethylphosphine ligand, and is therefore readily dissociable from rhodacycle **3-15**, it cannot be excluded that the recorded photophysical data for this compound result from a mixture of dissociation products.

5.3 Summary of Chapter 4

Various acac- and diethyldithiocarbamate-substituted rhodium(I) complexes bearing the phosphines dmpe, dcpe, dppe and P(*p*-tolyl)$_3$ were synthesized. Furthermore, it was found that by adding sodium diethyldithiocarbamate to the acac-substituted rhodium(I) compounds, the acac ligand is replaced by the diethyldithiocarbamate ligand at elevated temperatures (Scheme 5-11).

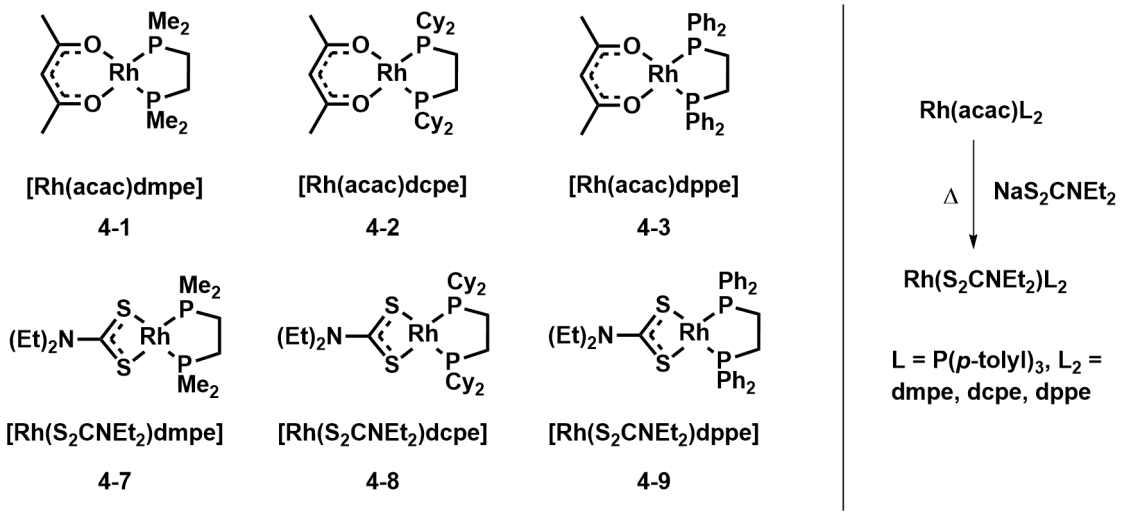

Scheme 5-11: Acac- and diethyldithiocarbamate-substituted rhodium(I) complexes bearing the chelating phosphines dmpe (**4-1** and **4-7**), dcpe (**4-2** and **4-8**) and dppe (**4-3** and **4-9**). Additionally, a convenient route to [Rh(S$_2$CNEt$_2$)L$_2$] *via* [Rh(acac)L$_2$] by an acac/diethyldithiocarbamate exchange.

Rhodium(I) complexes [Rh(acac)dmpe] **4-1**, [Rh(acac)dcpe] **4-2**, [Rh(acac)dppe] **4-3**, [Rh(acac)(P(*p*-tolyl)$_3$)$_2$] **1-56**, [Rh(S$_2$CNEt$_2$)dcpe] **4-8**, [Rh(S$_2$CNEt$_2$)dppe] **4-9** and [Rh(S$_2$CNEt$_2$)(P(*p*-tolyl)$_3$)$_2$] **4-10** were investigated as catalysts for the [2+2+2] cyclization of *α,ω*-diynes **4-11** and **4-13** resulting in dimers and trimers (Scheme 5-12). Different catalyst loadings (1 and 10 mol%) and temperatures (room temperature and 60 °C) in C$_6$D$_6$ were applied. A temperature of 60 °C and a catalyst loading of 10 mol% were found to be the best conditions for smooth conversion within 12 hours, using [Rh(acac)(P(*p*-tolyl)$_3$)$_2$] **1-56**. The dimers **4-11a** – **4-14a** and trimers **4-11b** – **4-14b** , which have a *para*-terphenyl core structure, were obtained.

Low catalytic activity was observed for the dcpe- and dppe-substituted rhodium(I) catalysts [Rh(acac)dcpe] **4-2**, [Rh(S$_2$CNEt$_2$)dcpe] **4-8**, [Rh(acac)dppe] **4-3** and [Rh(S$_2$CNEt$_2$)dppe] **4-9** with *α*,*ω*-diynes **4-11** and **4-13**, resulting only in trace amounts of dimer. However, the dmpe- and acac-substituted rhodium(I) complex [Rh(acac)dmpe] **4-1** was able to catalyze the cycloisomerization of *α*,*ω*-diyne **4-11** to dimer and trimer. The steric influence of the chelating phosphine seems to play an important role in the catalytic reaction with *α*,*ω*-diynes.

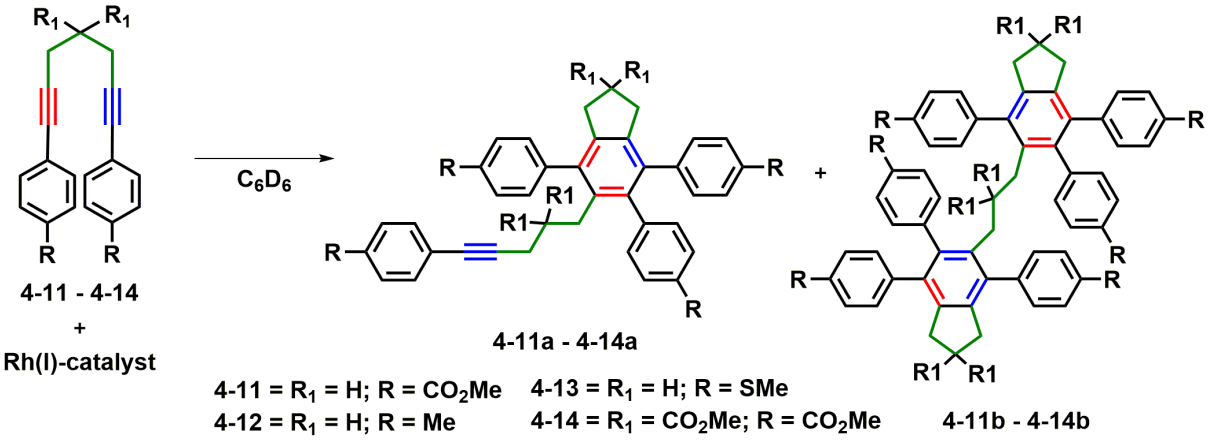

Scheme 5-12: Reaction of α,ω-diynes **4-11** – **4-14** with a rhodium(I)-catalyst forming dimers **4-11a** – **4-14a** and trimers **4-11b** – **4-14b**.

Reactions of [Rh(acac)dcpe] **4-2** and [Rh(S_2CNEt_2)dppe] **4-9** with an OMe-substituted α,ω-tetrayne resulted in complete conversion to dimer and trimer, indicating that the neighboring triple bond plays also an important role in the catalytic cycloisomerization.

Reaction of the phosphine-substituted bimetallic rhodium(I) complex **4-5** with α,ω-tetrayne **1-47d** gave rhodacycle **4-15**, in which the rhodium(III) center of the rhodacyclopentadiene is connected to an unreacted rhodium(I) center *via* an oxalate bridge. Additional diyne and heating did not result in a reaction with the α,ω-tetrayne at the remaining rhodium(I) center (Scheme 5-13).

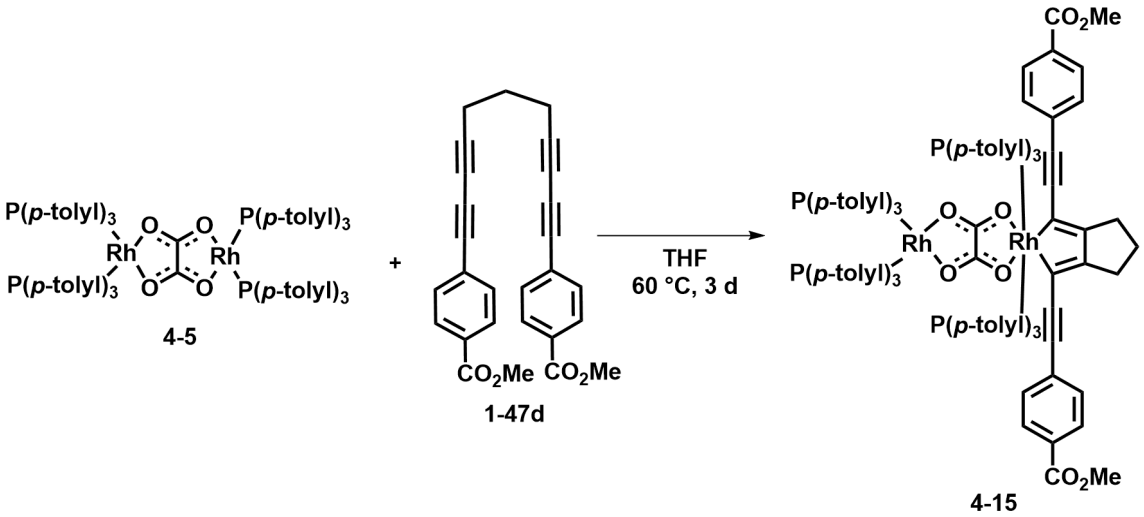

Scheme 5-13: Synthesis of the bimetallic complex **4-15** *via* reaction of [Rh_2(ox)(P(*p*-tolyl)$_3$)$_4$] **4-5** and CO_2Me-substituted α,ω-tetrayne **1-47d.**

Dimers **4-11a** and **4-13a** show small apparent Stokes shifts, low quantum yields of Φ = 0.08 and 0.12, respectively, and very short emission lifetimes τ_F of 1.14 and 1.18 ns at room temperature. A small bathochromic solvatochromic shift for **4-11a** was observed with increasing solvent polarity.

Trimers **4-11b** and **4-13b** also show small apparent Stokes shifts, low quantum yields of $\Phi = 0.17$ and 0.16, respectively, and very short emission lifetimes τ_F of 1.72 and less than 1 ns at room temperature. Increasing solvent polarity did not result in a solvatochromic shift for trimer **4-11b**. The short lifetimes and small apparent Stokes shifts of the dimers and trimers strongly indicate fluorescence. The extinction coefficients for the CO_2Me-substituted compounds are smaller than for the SMe-substituted compounds.

Complex **4-15** shows a small apparent Stokes shift, a low quantum yield of $\Phi < 0.01$, and short emission lifetime τ_F of less than 1 ns at room temperature. The short lifetime and the small apparent Stokes shift strongly indicate the expected fluorescence as observed for other rhodacyclopentadienes.

Only negligible differences in absorption, emission, extinction coefficient, in the apparent Stokes shift, lifetime and quantum yield are observed for complex **4-15** in comparison with rhodacyclopentadiene **1-57d**. Hence, the additional rhodium(I) center in the complex has no influence on the photophysical properties.

Chapter 6

6 Zusammenfassung

6.1 Zusammenfassung Kapitel 2

Durch die Umsetzung von [Rh(acac)(PMe_3)$_2$] **1-51** mit zwei Äquivalenten des *para*-substituierten 1,4-Diphenylbuta-1,3-diins **2-1a**,**b** bei Raumtemperatur, wurden die Komplexe **2-2a**,**b** und **2-3a**,**b** gebildet. Mittels Flash-Säulenchromatographie konnten diese separiert und als blauer (**2-3a**) bzw. blau/grüner (**2-3b**) Feststoff erhalten werden. Die Komplexe **2-2a**,**b** bilden sich in einer [3+2] Zyklisierung und zeigen eine Fulveneinheit, bestehend aus zwei Diinen, verbunden über zwei σ-Bindungen mit dem Rhodiumzentralatom. Die Komplexe **2-3a**,**b** hingegen bilden sich in einer [3+2+3] Zyklisierung und zeigen eine Indeneinheit, bestehend aus drei Diinen, welche durch zwei σ-Bindungen mit dem Rhodiumzentralatom verbunden ist (Schema 6-1).

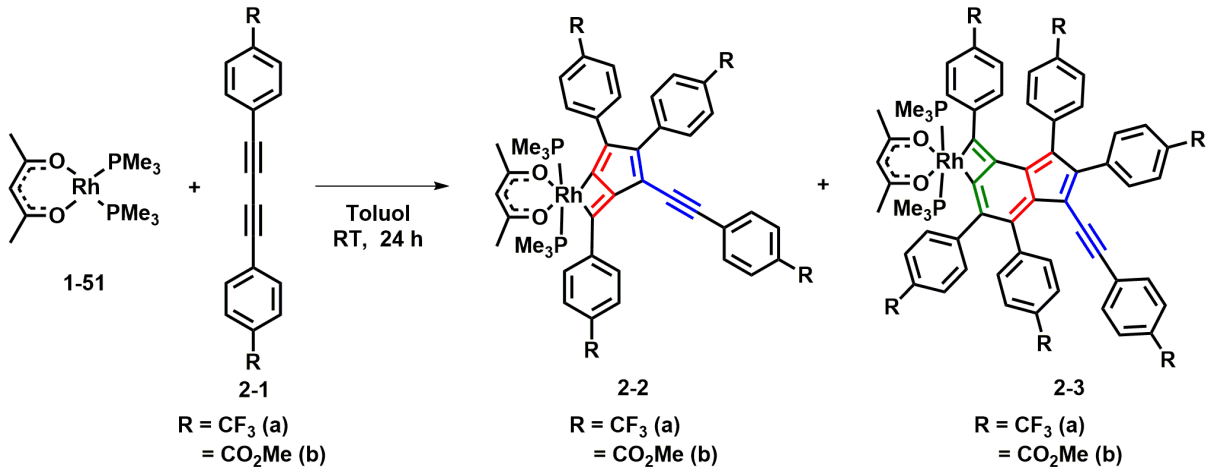

Schema 6-1: Darstellung der Komplexe **2-2a**,**b** und **2-3a**,**b** durch die Umsetzung von [Rh(acac)(PMe_3)$_2$] **1-51** mit *para*-substituierten 1,4-Diphenylbuta-1,3-diinen **2-1a**,**b**. Die ehemaligen 1,3-Butadiin-Einheiten sind farbig hervorgehoben.

Experimente bei 100 °C zeigen, dass für eine quantitative Umsetzung von [Rh(acac)(PMe_3)$_2$] **1-51** mehr als zwei Äquivalente des *para*-CF_3-substituierten 1,4-Diphenylbuta-1,3-diins **2-1a** benötigt werden, und dass in der Reaktion mit drei Äquivalenten von **2-1a** mehr Komplex **2-3a** gebildet wurde als mit fünf Äquivalenten von **2-1a**. Ebenso wurde gezeigt, dass sich Komplex **2-3a** auch durch die Reaktion von Komplex **2-2a** mit **2-1a** bei 100 °C darstellen lässt. Zusätzlich bilden sich in der Umsetzung von [Rh(acac)(PMe_3)$_2$] **1-51** bzw. Komplex **2-2a** mit *para*-substituierten 1,4-Diphenylbuta-1,3-diin **2-1a** bei 100 °C die Verbindungen 2,5-Bis(arylethinyl)rhodazyklopentadien **2-SYM^{CF3}** und 2,4-Bis(arylethinyl)rhodazyklopentadien **2-UNSYM^{CF3}**.

Bei einem Kreuzungsexperiment mit Komplex **2-2a** und **2-1b** wurden die Verbindung **2-3c**, neben **2-SYM**^{CO2Me} und **2-UNSYM**^{CO2Me} dargestellt. Es konnte gezeigt, dass sich das dritte *para*-substituierte 1,4-Diphenylbuta-1,3-diin **2-1b** zwischen dem Rhodiumzentralatom und der Fulveneinheit einlagert (Schema 6-2).

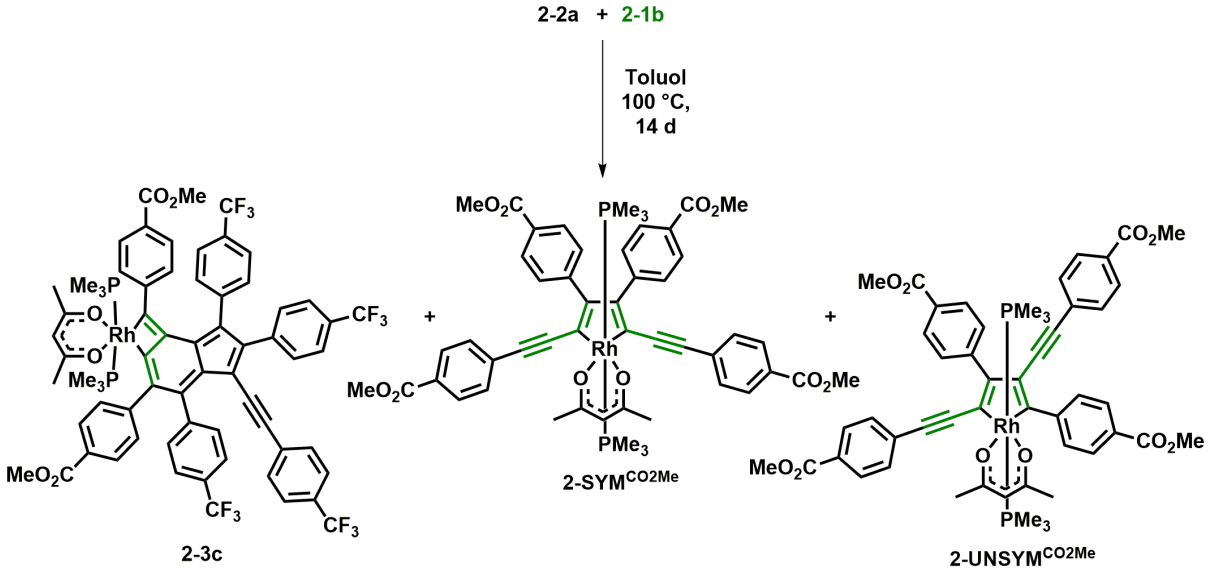

Schema 6-2: Darstellung der Komplexe **2-3c**, **2-SYM**^{CO2Me} und **2-UNSYM**^{CO2Me} durch die Umsetzung von Komplex **2-2a** mit *para*-substituierten 1,4-Diphenylbuta-1,3-diin **2-1b**. Die ehemaligen 1,3-Butadiin-Einheiten von **2-1b** sind in grün hervorgehoben.

Diese seltene [3+2] Zyklisierungsreaktion kann benutzt werden um konjugierte, organische Moleküle darzustellen, welche sonst nur schwer oder gar nicht mit bisher bekannten Synthesemethoden zugänglich sind. In der Umsetzung von Komplex **2-2a** mit *para*-Tolylisocyanat **2-4** bei 80 °C konnte ein violetter, rein organischer Feststoff **2-5** erhalten werden, bestehend aus der organischen Fulveneinheit von **2-2a** und einem Äquivalent des *para*-Tolylisocyanats. Zusätzlich wurden orangene Kristalle der Verbindung **2-9** erhalten. Mittels Röntgenstrukturanalyse konnte gezeigt werden, dass die Verbindung **2-9** ein Dimer von **2-5** darstellt (Schema 6-3).

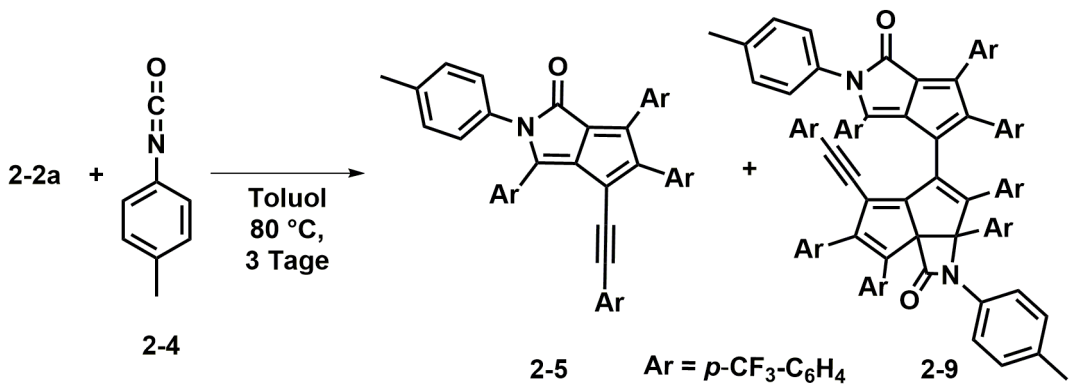

Schema 6-3: Darstellung der Verbindungen **2-5** und **2-9** in der Reaktion von Komplex **2-2a** mit *para*-Tolylisocyanat **2-4**.

Neben den beiden oben genannten Produkten **2-5** und **2-9**, wurde zusätzlich 1,3,5-Tris(*p*-tolyl)-1,3,5-triazin-2,4,6-trion **2-8** erhalten, welches ein Zyklotrimerisierungsprodukt des *para*-Tolylisocyanats **2-4** darstellt (Schema 6-4). Demnach katalysiert ein Reaktand, in der gezeigten Reaktion in Schema 6-3, die Trimerisierung des Isocyanats.

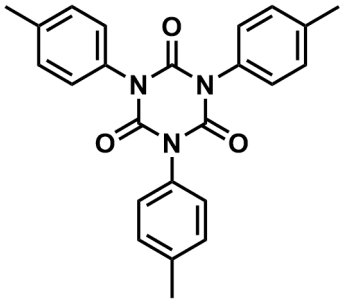

2-8

Schema 6-4: Struktur von 1,3,5-Tris(*p*-tolyl)1,3,5-triazin-2,4,6-trion **2-8**.

Da während der Reaktion von Komplex **2-2a** und *para*-Tolylisocyanat **2-4** das Startmaterial [Rh(acac)(PMe_3)$_2$] **1-51** freigesetzt wird, wurde dessen katalytische Aktivität gegenüber der Trimerisierung von **2-4** näher untersucht. Bei der Umsetzung von [Rh(acac)(PMe_3)$_2$] **1-51** mit vier Äquivalenten **2-4** wurden hauptsächlich Rhodiumkomplexe mit *cis*-ständigen Phosphanen erhalten, neben kleinen Mengen an Zyklotrimerisierungsprodukt **2-8**. Die vorherrschende *cis*-Spezies in Lösung konnte isoliert, und mittels Röntgenstrukturanalyse als *cis*-[Rh(acac)(PMe_3)$_2$(2-4)$_2$] **2-10a** identifiziert werden, bei dem ein *para*-Tolylisocyanat-Dimer über ein Kohlenstoff- und ein Sauerstoffatom an das Rhodiumzentralatom koordiniert (Schema 6-5).

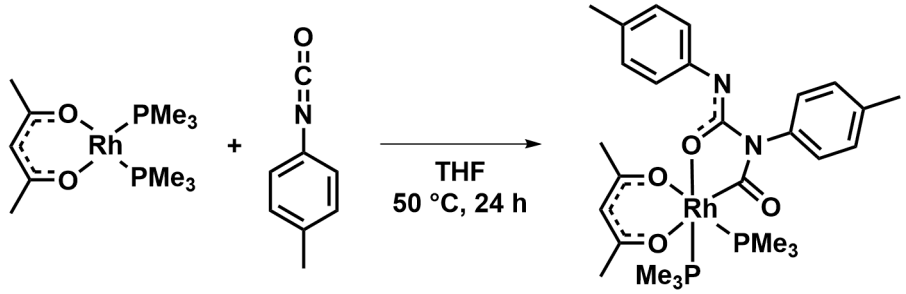

1-51 **2-4** **2-10a**

Schema 6-5: Darstellung des Komplexes **2-10a** durch die Umsetzung von [Rh(acac)(PMe_3)$_2$] **1-51** mit *para*-Tolylisocyanat **2-4**.

Bei höheren Temperaturen konnte eine Umsetzung von Komplex **2-10a** mit *para*-Tolylisocyanat **2-4** zum Zyklotrimerisierungsprodukt **2-8** beobachtet werden. Allerdings konnte [Rh(acac)(PMe_3)$_2$] **1-51** und Komplex **2-10a** keine eindeutige katalytische Wirkung zugeschrieben werden. In dieser Arbeit durchgeführte Experimente zeigen, dass die Zugabe

von Trimethylphosphan zu *para*-Tolylisocyanat **2-4** in C_6D_6 bei Raumtemperatur, zu einer Niederschlagsbildung führt, bei der das Trimer **2-8**, das Hauptprodukt darstellt. Demnach kann nicht ausgeschlossen werden, dass das bei höheren Temperaturen dissoziierende Phosphan die katalytisch aktive Spezies darstellt.

Wenn anstelle des Rhodium(I)-Komplexes [Rh(acac)(PMe_3)$_2$] **1-51**, ein NHC-substituierter Komplex [Rh(acac)(Me_2Im)$_2$] **2-21** mit den *para*-substituierten 1,4-Diphenylbuta-1,3-diinen **2-1a**,**b** umgesetzt wird, kann ein zu Schema 6-1 unterschiedlicher Reaktionsverlauf beobachtet werden. Der in Schema 6-6 postulierte Verlauf wurde durch NMR Spektroskopie in C_6D_6 und THF-d_8, sowie Röntgenstrukturanalyse der Verbindung **2-I$_{cis}$b** aufgestellt.

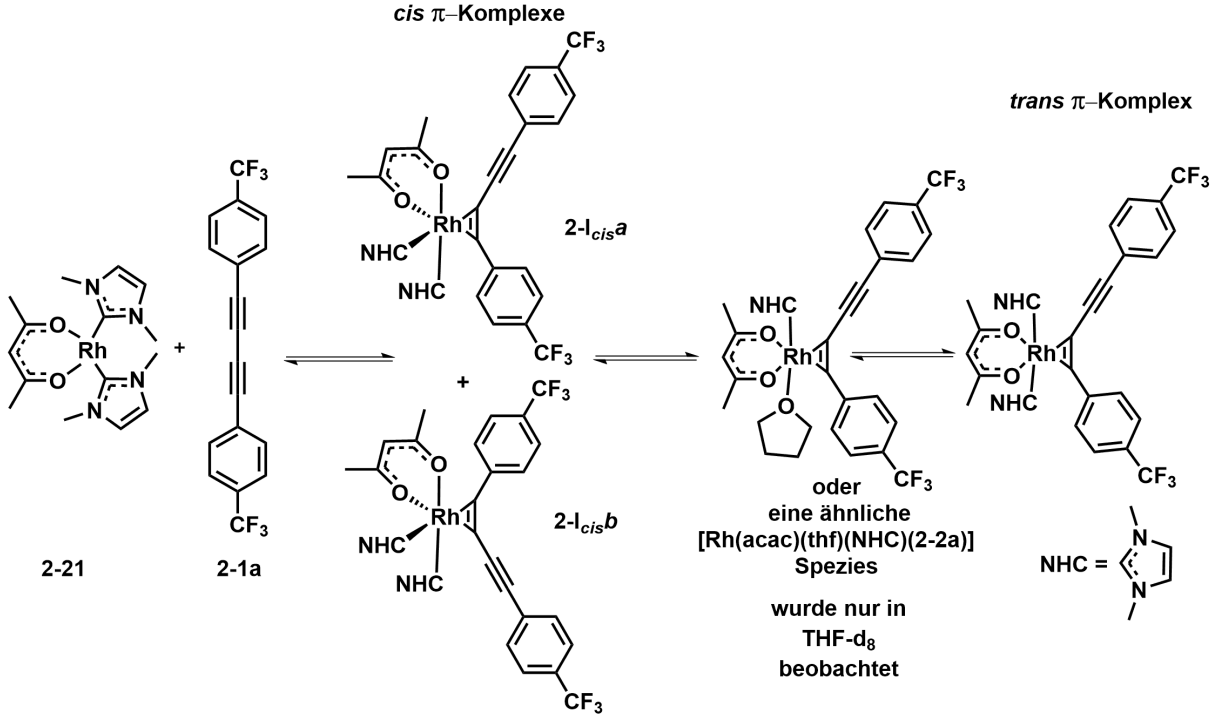

Schema 6-6: Möglicher Reaktionsverlauf für die Bildung von *trans*-[Rh(acac)(Me_2Im)$_2$(2-2)].

Während der Bildung des *trans*-NHC Komplexes, ähnlich der Reaktion von [Rh(acac)(PMe_3)$_2$] **1-51** mit den *para*-substituierten 1,4-Diphenylbuta-1,3-diinen **2-1a**,**b**, über mindestens einen *cis*-π-Komplex als Intermediat abläuft, konnte mittels NMR Spektroskopie die Bildung von Verbindungen ähnlich zu den Komplexen **2-2a**,**b** und **2-3(a-c)** nicht verifiziert werden. Eine zu den Komplexen **2-2a**,**b** analoge Spezies konnte nur durch hochaufgelöste Massenspektroskopie bestätigt werden. Zusätzlich konnte gezeigt werden, dass es sich um eine Gleichgewichtsreaktion handelt.

Für die Verbindungen **2-2a**,**b**, **2-3(a-c)** und **2-5** können nur die Absorptionsspektren diskutiert werden, da keine Emission in THF bei Raumtemperatur oder in 2-Me-THF bei Raumtemperatur oder bei 77 K in einer Glas-Matrix beobachtet werden konnte.

Die Komplexe **2-2a**,**b** zeigen eine breite Absorption mit vier lokalen Maxima zwischen 214 – 500 nm mit Extinktionskoeffizienten ε von bis zu 45000 $M^{-1}\,cm^{-1}$ in THF. Die höchstenergetische Absorptionsbande von Komplex **2-2a** ist hypsochrom verschoben, verglichen mit der von **2-2b**, wohingegen die anderen Banden bathochrom verschoben sind. Die Extinktionskoeffizienten ε sind alle in der gleichen Größenordnung. Zusätzlich zeigen beide Komplexe eine schwache Absorption von 540 – 700 nm mit Extinktionskoeffizienten ε von bis zu 2000 $M^{-1}\,cm^{-1}$.
Die Komplexe **2-3(a-c)** zeigen eine breite, hochenergetische Absorption mit einem Maximum bei ca. 350 nm und Extinktionskoeffizienten ε von ca. 70000 $M^{-1}\,cm^{-1}$, sowie eine breite Absorption im Bereich von 500 – 1000 nm und Extinktionskoeffizienten ε von ca. 11000 $M^{-1}\,cm^{-1}$ in THF. Das Absorptionsmaximum des CF_3-substitutierten Komplexes **2-3a** ist hypsochrom verschoben im Vergleich zum gemischt CO_2Me-CF_3-substituierten Komplex **2-3c**, sowie zum reinen CO_2Me-substituierten Komplex **2-3b**.
Die rein organische Verbindung **2-5** zeigt eine breite Absorption von 214 – 750 nm mit Extinktionskoeffizienten ε von bis zu 40500 $M^{-1}\,cm^{-1}$ in THF.

Mittels TD-DFT Studien konnte gezeigt werden, dass die ersten drei Übergänge alle HOMO, HOMO-1 und HOMO-2 zu LUMO Übergänge sind. Diese π-π* Übergänge haben einen moderaten Ladungstransfercharakter. Die Übergänge bei niedrigen Energien resultieren aus der Einbindung der Stickstoff-Donor- und der Carbonyl-Akzeptor-Einheit in Verbindung mit dem ausgedehnten π-System.

Cyclovoltammetriemessungen an Komplex **2-2a** zeigen, dass die erste Reduktion bei $E_{1/2}$ = -1.89 V und Oxidation bei $E_{1/2}$ = 0.29 V, bezogen auf das Fc/Fc^+ Redoxpaar, reversibel sind. Komplex **2-3a** zeigt eine reversible Reduktion bei $E_{1/2}$ = -1.42 V, sowie eine Oxidation bei $E_{1/2}$ = 0.13 V, bezogen auf das Fc/Fc^+ Redoxpaar. Die rein organische Verbindung **2-5** zeigt zwei reversible Reduktionen bei $E_{1/2}$ = -1.05 und -1.70 V, bezogen auf das Fc/Fc^+ Redoxpaar, jedoch keine Oxidation.

6.2 Zusammenfassung Kapitel 3

Mehrere *α,ω*-Diine mit unterschiedlichem Rückgrat wurden synthetisiert, wobei die Verbindungen **3-1**, **3-2**, **3-3** und **3-5** eine starre U-Form, und die Verbindungen **3-4** und **3-5** eine flexible W-Form aufweisen (Schema 6-7).

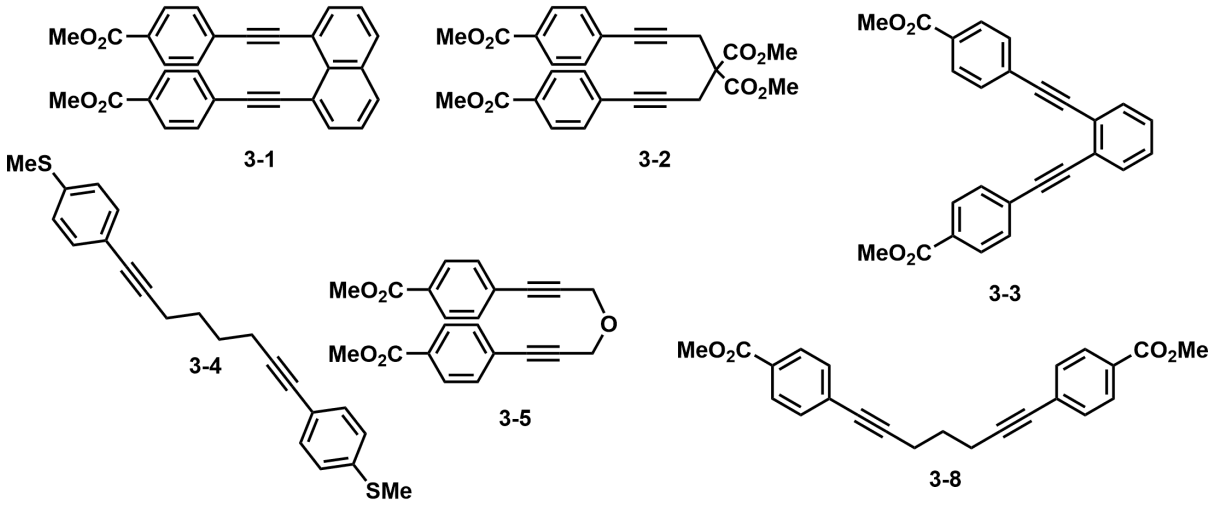

Schema 6-7: Strukturen von: Dimethyl 4,4'-(naphthalen-1,8-diylbis(ethin-2,1-diyl))dibenzoat **3-1**, Dimethyl 2,2-bis(3-(4-(methoxycarbonyl)phenyl)prop-2-in-1-yl)malonat **3-2**, Dimethyl 4,4'-(1,2-phenylenebis(ethin-2,1-diyl))dibenzoat **3-3**, 1,8-Bis(4-(methylthio)phenyl)octa-1,7-diin **3-4**, Dimethyl 4,4'-(oxybis(prop-1-in-3,1-diyl))dibenzoat **3-5** and Dimethyl 4,4'-(hepta-1,6-diin-1,7-diyl)dibenzoat **3-8**.

Der Einfluss der *α,ω*-Diine auf die Reaktion mit [Rh(acac)(PMe_3)$_2$] **1-51** und [Rh(acac)(P(*p*-tolyl)$_3$)$_2$] **1-56** in äquimolaren Mengen auf die Bildung von 2,5-Bis(aryl)rhodazyklopentadiene in C_6D_6 wurde untersucht.

In der Umsetzung von [Rh(acac)(PMe_3)$_2$] **1-51** mit den *α,ω*-Diinen **3-1**, **3-2** und **3-8** bei Raumtemperatur konnte gezeigt werden, dass durch die starre U-Form des *α,ω*-Diins die Rhodium(I)-Verbindung schneller aufgebraucht wurde als bei den *α,ω*-Diinen mit einer flexiblen W-Form. Bei 60 °C erfolgt selektiv die Bildung des entsprechenden 2,5-Bis(aryl)rhodazyklopentadiens für die *α,ω*-Diine **3-1** und **3-8**. Für das *α,ω*-Diin **3-2** wurden zusätzlich noch kleine Mengen an nichtidentifizierbaren Nebenprodukten erhalten.

In der Reaktion von [Rh(acac)(PMe_3)$_2$] **1-51** mit dem *α,ω*-Diin **3-5** zeigt sich ein sehr langsame Umsetzung zu dem gewünschten Rhodazyklopentadien bei erhöhten Temperaturen, obwohl das Rhodium(I)-Startmaterial bereits aufgebraucht wurde.

In der Umsetzung von [Rh(acac)(PMe_3)$_2$] **1-51** mit den *α,ω*-Diinen **3-3** und **3-4** konnte ein langsamer Reaktionsfortschritt, sogar bei erhöhten Temperaturen, beobachtet werden. Die Bildung der gewünschten Rhodazyklopentadiene konnte nicht zweifelsfrei bestätigt werden.

Die bisher unbekannten Rhodazyklopentadiene **3-6** und **3-7** konnten in die Umsetzung von [Rh(acac)(PMe$_3$)$_2$] **1-51** mit den *α,ω*-Diinen **3-1** bzw. **3-2** isoliert werden (Schema 6-8).

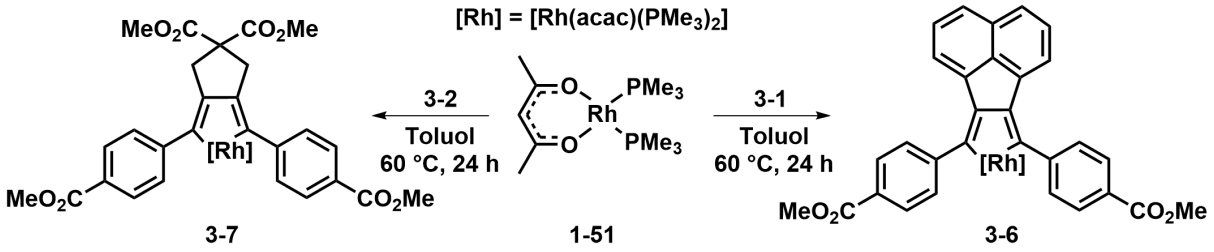

Schema 6-8: Darstellung der 2,5-Bis(aryl)rhodazyklopentadiene **3-6** und **3-7** durch die Umsetzung von [Rh(acac)(PMe$_3$)$_2$] **1-51** mit den *α,ω*-Diinen **3-1** und **3-2**.

Die Umsetzungen von [Rh(acac)(P(*p*-tolyl)$_3$)$_2$] **1-56** mit den *α,ω*-Diinen **3-2**, **3-5** und **3-8** in äquimolaren Mengen zeigten ein ähnliches Reaktionsverhalten. Mittels ^{31}P{^{1}H} NMR Spektroskopie konnte gezeigt werden, dass neben [Rh(acac)(P(*p*-tolyl)$_3$)$_2$] **1-56**, dem entsprechendem Rhodazyklopentadien und ungebundenem Tri(*p*-tolyl)phosphan sich auch eine Rhodium(I)-spezies bei ca. 30 ppm mit $^1J_{\text{Rh-P}}$ = 170 Hz bildet. Nach Erwärmen der Reaktionslösung konnten die Signale für die Spezies bei ca. 30 ppm und das ungebundene Tri(*p*-tolyl)phosphan nicht mehr detektiert werden. Die Intensität des Signals für [Rh(acac)(P(*p*-tolyl)$_3$)$_2$] **1-56** war für die Reaktion mit den *α,ω*-Diinen **3-2** und **3-5** wenig intensiv, wohingegen bei der Reaktion mit dem *α,ω*-Diin **3-8** eine deutlich größere Intensität beobachtet wurde. Mittels ^{1}H NMR Spektroskopie konnten für alle drei Reaktionen Zykloisomerisierungsprodukte nachgewiesen werden. Die Verbindung **1-56** ist bekannt dafür, als Katalysator für die Zykloisomerisierung von *α,ω*-Diinen und *α,ω*-Tetrainen zu dienen, und wurde dafür im Arbeitskreis Marder bereits eingesetzt.

Die Reaktion zwischen [Rh(acac)(P(*p*-tolyl)$_3$)$_2$] **1-56** und dem *α,ω*-Diin **3-4**, zeigt ähnliche Signale im ^{31}P{^{1}H} NMR Spektrum wie sie in der Reaktion zwischen **1-56** mit *α,ω*-Diinen **3-2**, **3-5** und **3-8** gefunden wurden, allerdings zeigen die Resonanzen eine Verschiebung zu Tieffeld, die Kopplungskonstanten sind größer und die Intensität der gebildeten Signale ist deutlich geringer. Nach Erwärmen der Reaktionslösung konnten Signale für die Startmaterialien und geringe Mengen an Zykloisomerisierungsprodukt identifiziert werden, jedoch kein Rhodazyklopentadien.

Bei der Umsetzung von [Rh(acac)(P(*p*-tolyl)$_3$)$_2$] **1-56** mit dem *α,ω*-Diin **3-1** bei Raumtemperatur konnten im ^{31}P{^{1}H} NMR Spektrum nur Signale von **1-56** und dem gewünschten Rhodazyklopentadien detektiert werden. Nach Erwärmen der Reaktionslösung wurde der Rhodazyklopentadien **3-15** erhalten (Schema 6-9).

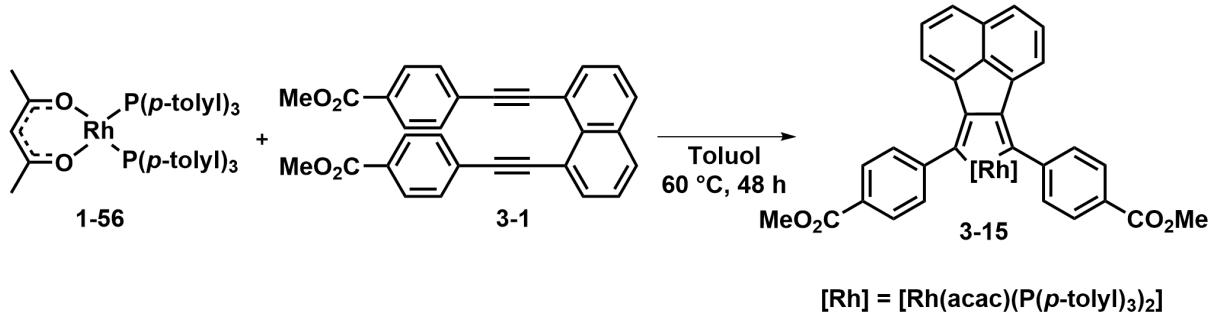

Schema 6-9: Darstellung des 2,5-Bis(aryl)rhodazyklopentadiens **3-15** in der Umsetzung von [Rh(acac)(P(*p*-tolyl)$_3$)$_2$] **1-56** mit dem *α,ω*-Diin **3-1**.

Die Reaktion von [Rh(acac)(Me$_2$Im)$_2$] **2-21** mit dem *α,ω*-Diin **3-1** (Schema 6-10) resultiert, gemäß ^{1}H und ^{13}C{^{1}H} NMR Spektroskopie, in der Bildung von *trans*- und *cis*-NHC-substituierten 2-5-Bis(aryl)rhodazyklopentadienen. Nach 14 Tagen bei Raumtemperatur ist das Startmaterial [Rh(acac)(Me$_2$Im)$_2$] **2-21** aufgebraucht und es stellt sich ein Verhältnis von *cis*:*trans* Komplex von 1:0.83 ein. Ein Erwärmen der Reaktionslösung für sechs Tage bei 60 °C resultiert in ein *cis*:*trans* Verhältnis von 1:0.25 und für 24 h bei 80 °C in ein *cis*:*trans* Verhältnis von 1:0.10. Weiteres Erwärmen führt zu Zersetzung. Während in der Reaktion von [Rh(acac)(Me$_2$Im)$_2$] **2-21** und den *para*-substituierten 1,4-Diphenylbuta-1,3-diinen **2-1a**,**b** der *trans*-Komplex die thermodynamisch begünstigte Verbindung ist, ist es bei dieser Reaktion der *cis*-Komplex.

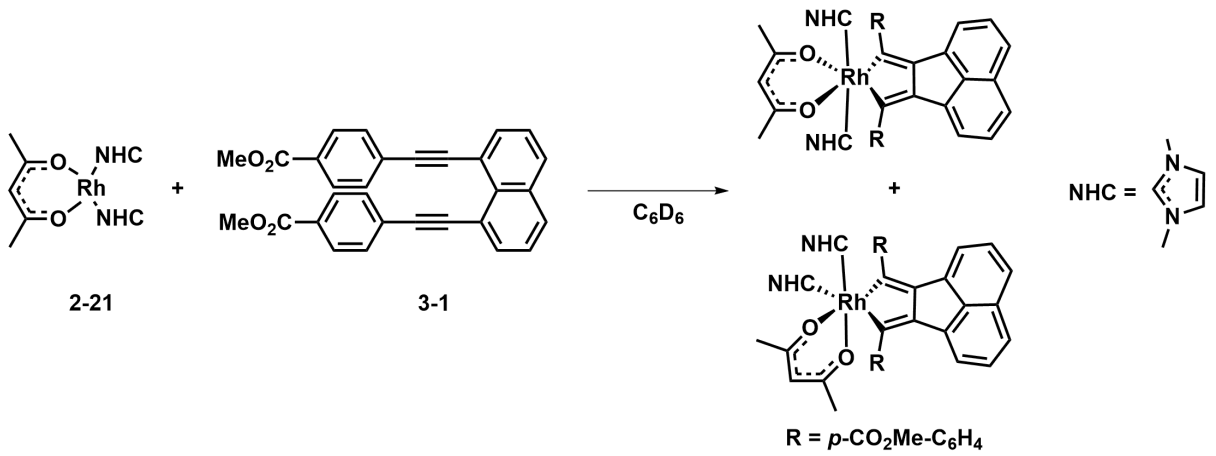

Schema 6-10: Reaktion zwischen [Rh(acac)(Me$_2$Im)$_2$] **2-21** und dem *α,ω*-Diin **3-1** resultierend in *trans*- und *cis*-NHC-substituierten 2-5-Bis(aryl)rhodazyklopentadienen.

Die Rhodazyklopentadiene **3-6** und **3-7** zeigen eine kleine Stokes-Verschiebung, geringe Quantenausbeuten von $\Phi < 0.01$, sowie sehr kurze Lebenszeiten τ_F von weniger als 1 ns bei Raumtemperatur. Die kurzen Lebenszeiten, wie auch die kleine Stokes-Verschiebung weisen auf Fluoreszenz hin. Komplex **3-6**, zeigt, verglichen zu Komplex **3-7**, eine bathochrome Verschiebung des Anregungs-, Absorptions- und Emissionsspektrums.

Der Vergleich mit den bereits zuvor im Arbeitskreis Marder dargestellten Rhodazyklopentadien **3-10** zeigt, dass die Substitution im Rückgrat von CH_2 mit $C(CO_2Me)_2$ keinen Einfluss auf die photophysikalischen Eigenschaften des Rhodazyklopentadiens hat.

Der Rhodazyklopentadien **3-15** zeigt eine kleine Stokes-Verschiebung, geringe Quantenausbeute von $\Phi = 0.02$, sowie mehrere, sehr kurze Lebenszeiten τ_F von 1.79 ns (32%), 5.81 ns (63%) und 13.12 ns (5%) bei Raumtemperatur in THF. Unterschiedliche Anregungs- und Absorptionsspektren sind eindeutig zu erkennen. Die kurzen Lebenszeiten weisen auf Fluoreszenz hin. Die Verbindung zeigte keine Emission in Toluol.

Die beiden Rhodazyklopentadiene **3-6** und **3-15**, welche verschiedene Phosphanliganden tragen, unterscheiden sich grundlegend in ihren photophysikalischen Eigenschaften. Die unterschiedlichen Anregungs- und Absorptionsspektren deuten zusätzlich auf verschiedene Spezies hin. Dieses Phänomen wurde zuvor noch nicht für andere Rhodazyklopentadiene beschrieben. Da der P(*p*-tolyl)$_3$-ligand weniger stark als der PMe_3-ligand an das Rhodiumzentralatom gebunden ist und daher leichter dissoziieren kann, kann nicht ausgeschlossen werden, dass die erhaltenen photophysikalischen Daten eine Mischung aus mehreren Dissoziationsprodukten darstellen.

6.3 Zusammenfassung Kapitel 4

In Kapitel 4 wurde die Synthese mehrerer acac- und diethyldithiocarbamat-substituierter Rhodium(I)-Komplexe mit den Phosphanen dmpe, dcpe, dppe und P(*p*-tolyl)$_3$ beschrieben. Des Weiteren wurde gezeigt, dass es möglich ist durch Zugabe von Natriumdiethyldithiocarbamat zu einer acac-substituierten Rhodium(I)-Verbindung, den acac Liganden durch den diethyldithiocarbamat Liganden bei erhöhten Temperaturen auszutauschen (Schema 6-11).

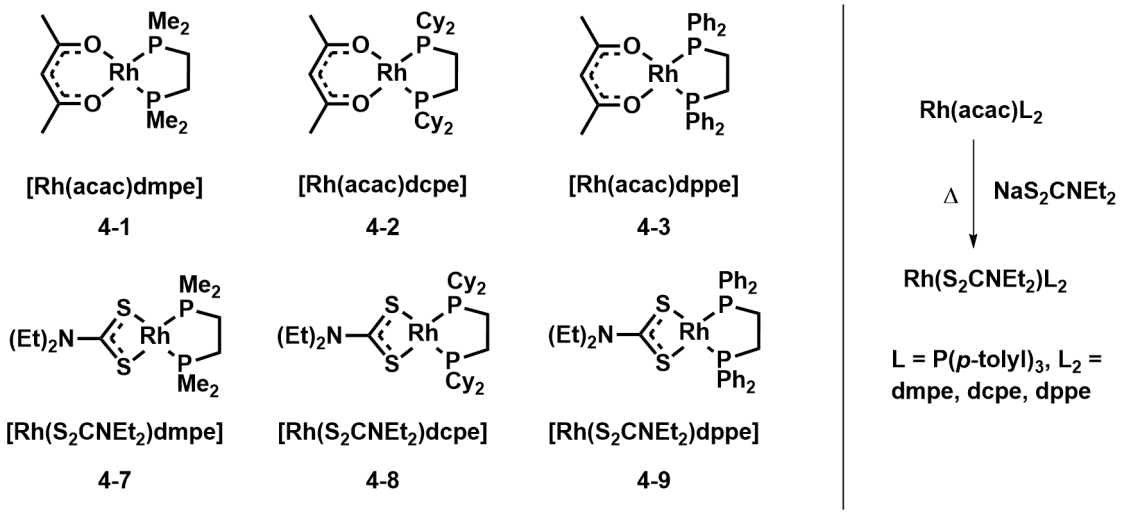

Schema 6-11: Acac- und diethyldithiocarbamat-substituierte Rhodium(I)-Komplexe mit den chelatisierenden Phosphanen dmpe (**4-1** und **4-7**), dcpe (**4-2** und **4-8**) und dppe (**4-3** und **4-9**). Zusätzliche eine komfortable Syntheseroute um [Rh(S$_2$CNEt$_2$)L$_2$] aus [Rh(acac)L$_2$]-Komplexen durch einen acac/diethyldithiocarbamat Austausch zu erhalten.

Die Rhodium(I)-Komplexe [Rh(acac)dmpe] **4-1**, [Rh(acac)dcpe] **4-2**, [Rh(acac)dppe] **4-3**, [Rh(acac)(P(*p*-tolyl)$_3$)$_2$] **1-56**, [Rh(S$_2$CNEt$_2$)dcpe] **4-8**, [Rh(S$_2$CNEt$_2$)dppe] **4-9** und [Rh(S$_2$CNEt$_2$)(P(*p*-tolyl)$_3$)$_2$] **4-10** wurden auf katalytische Aktivität in der [2+2+2] Zyklisierung der *α,ω*-Diine **4-11** und **4-13** zu Dimer und Trimer untersucht (Schema 6-12). Dabei wurden verschiedene Katalysatormengen (1 und 10 mol%) und Temperaturen (Raumtemperatur und 60 °C) in C$_6$D$_6$ getestet. Bei 60 °C mit 10 mol% des Katalysators [Rh(acac)(P(*p*-tolyl)$_3$)$_2$] **1-56** zeigte sich eine quantitative Umsetzung der beiden *α,ω*-Diine **4-11** und **4-13** innerhalb von 12 Stunden.

Die erhaltenen Dimere **4-11a** – **4-14a** und Trimere **4-11b** – **4-14b** weisen einen *para*-Terphenyl Grundkörper auf. Eine geringe katalytische Aktivität wurden für die Rhodium(I)-Komplexe mit den chelatisierenden dcpe und dppe Phosphanen [Rh(acac)dcpe] **4-2**, [Rh(S$_2$CNEt$_2$)dcpe] **4-8**, [Rh(acac)dppe] **4-3** und [Rh(S$_2$CNEt$_2$)dppe] **4-9** in der Umsetzung mit den *α,ω*-Diinen **4-11** und **4-13** festgestellt. Bei den Reaktionen konnten nur Spuren des Dimers nachgewiesen werden.

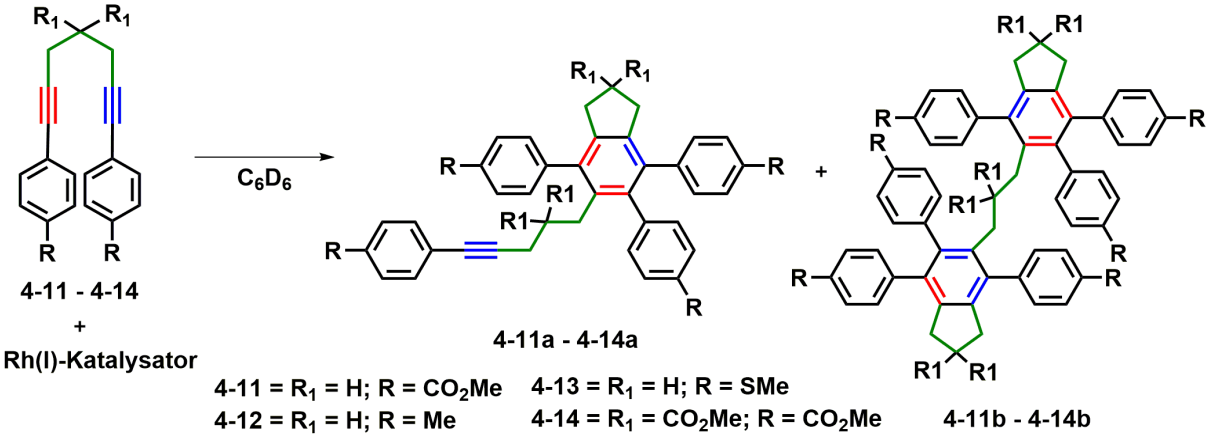

Schema 6-12: Umsetzung der *α,ω*-Diine **4-11** – **4-14** mit einem Rhodium(I)-Katalysator zu den Dimeren **4-11a** – **4-14a** und zu den Trimeren **4-11b** – **4-14b**.

Der dmpe- und acac-substituierte Rhodium(I)-Komplex [Rh(acac)dmpe] **4-1** hingegen, zeigt eine vollständige Zykloisomerisierung von *α,ω*-Diin **4-11** zu Dimer und Trimer. Der sterische Anspruch der chelatisierenden Phosphanliganden scheint einen großen Einfluss auf die katalytische Aktivität in der Zykloisomerisierung der *α,ω*-Diine zu haben.

Die Rhodium(I)-Komplexe [Rh(acac)dcpe] **4-2** und [Rh(S_2CNEt_2)dppe] **4-9** zeigen mit einem OMe-substituierten *α,ω*-Tetrain die gewünschte Umsetzung zu Dimer und Trimer. Folglich spielt bei der Katalyse durch die Rhodium(I)-Komplexe mit chelatisierenden Phosphanen die zusätzliche Dreifachbindung in dem *α,ω*-Tetrain eine tragende Rolle.

In der Umsetzung des Tri(*p*-tolyl)posphan-substituierten bimetallischen Rhodium(I)-Komplexes **4-5** mit dem *α,ω*-Tetrain **1-47d** konnte der Rhodazyklus **4-15** dargestellt werden. Bei dieser Verbindung ist das Rhodium(III)-Zentralatom über eine Oxalatbrücke mit einem Rhodium(I)-Zentralatom verbunden. Weitere Zugabe von Tetrain bei erhöhten Temperaturen führt zu keiner Reaktion mit dem Rhodium(I)-Zentrum (Schema 6-13).

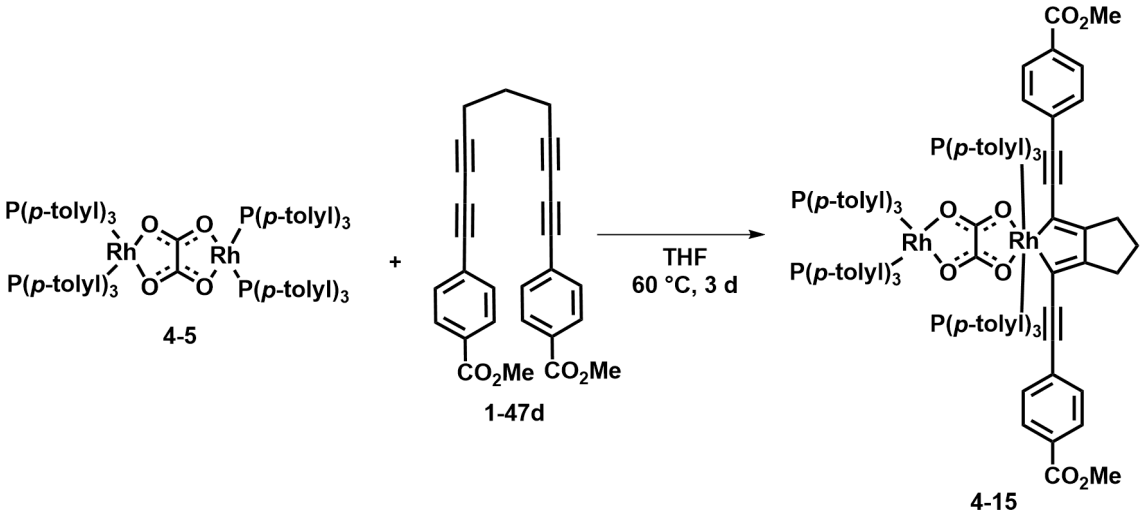

Schema 6-13: Umsetzung von [Rh_2(ox)(P(*p*-tolyl)$_3$)$_4$] **4-5** mit dem CO_2Me-substituierten *α,ω*-Tetrain **1-47d** zu dem bimetallischen Rhodiumkomplex **4-15**.

Die Dimere **4-11a** und **4-13a** zeigen eine kleine Stokes-Verschiebung, geringe Quantenausbeuten von $\Phi = 0.08$ und 0.12, sowie sehr kurze Fluoreszenzlebenszeiten τ_F von 1.14 und 1.18 ns bei Raumtemperatur. Eine kleine bathochrome-Verschiebung mit steigender Lösemittelpolarität wurde für **4-11a** beobachtet.

Die Trimere **4-11b** und **4-13b** zeigen eine kleine Stokes-Verschiebung, geringe Quantenausbeuten von $\Phi = 0.17$ and 0.16, sowie sehr kurze Lebenszeiten τ_F von 1.72 weniger als 1 ns bei Raumtemperatur. Ein solvatochromer Effekt mit steigender Lösemittelpolarität wurde für **4-11b** nicht beobachtet. Die kurzen Lebenszeiten, wie auch die kleine Stokes-Verschiebung der Dimere und Trimere weisen auf Fluoreszenz hin. Die Extinktionskoeffizienten der CO_2Me-substituierten Verbindungen sind kleiner als die der SMe-substituierten Verbindungen.

Komplex **4-15** zeigt eine kleine Stokes-Verschiebung, geringe Quantenausbeute von $\Phi < 0.01$, sowie sehr kurze Lebenszeiten τ_F von weniger als 1 ns bei Raumtemperatur. Die kurze Lebenszeit, als auch die kleine Stokes-Verschiebung weisen auf Fluoreszenz, wie in anderen Rhodazyklopentadienen, hin. Der Komplex **4-15** zeigt nur geringe Unterschiede in seinen photophysikalischen Eigenschaften, verglichen mit dem CO_2Me- und tri(*p*-tolyl)phoshan-substituiertem Rhodazyklopentadien **1-57d**. Demnach führt die zusätzliche Rhodium(I)-Einheit zu keiner Veränderung in den photophysikalischen Eigenschaften.

Chapter 7

7 Experimental section

7.1 General considerations

The compounds $[RhCl(COE)_2]_2$,[319] $[Pd(PPh_3)_2Cl_2]$,[320] PMe_3[321], 3-(prop-2-yn-1-yloxy)prop-1-yne[287], 1,8-diiodonapthalene[285] and sodium diethyldithiocarbamate[322] were prepared according to the literature. Me_2Im was kindly provided by Michael Dömling and synthesized according to the literature.[323] All other starting materials were purchased from commercial sources and used without further purification.

All solvents for synthetic reactions were HPLC grade, further treated to remove traces of water using an Innovative Technology Inc. Pure Solvent Purification System and deoxygenated by bubbling with argon. C_6D_6, THF-d_8 and toluene-d_8 were dried according to standard procedures and deoxygenated using the freeze-pump-thaw method, and vacuum transferred into sealed vessels. Unless otherwise stated, all reactions and subsequent manipulations were performed under an atmosphere of dry argon in an Innovative Technology Inc. glovebox or using standard Schlenk techniques. Only oven-dried and flame-dried glassware were used.
Reaction progress was monitored using thin layer chromatography (TLC) plates precoated with a layer of silica (Polygram® Sil G/UV254) with fluorescent indicator UV254 purchased from Marchery-Nagel or by GC/MS analyses using an Agilent 7890A gas chromatograph (column: HP-5MS 5% phenyl methyl siloxane, 10 m, 0.25 mm, film 0.25 μm; injector: 250 °C; oven: 40 °C; 40 °C – 180 °C (20 °C/min), 180 °C – 280 °C (50 °C/min); carrier gas: He (1.2 mL/min) equipped with an Agilent 5975C inert MSD detector operating in EI mode and an Agilent 7693A series liquid handling system functioning as an auto sampler.
Automated flash column chromatography was performed using a Biotage® Isolera Four system with silica gel (Biotage SNAP cartridge KP-Sil 10 g, KP-Sil 25 g or KP-Sil 50 g obtained from Biotage) as the stationary phase and the solvent system indicated. Solvents were generally removed *in vacuo* using a rotary evaporator at a maximum temperature of 50 °C.
^1H, ^{13}C, ^{19}F and $^{31}P\{^1H\}$ NMR spectroscopic data were obtained at 298.15 K (25 °C), unless otherwise indicated, *vide infra*, using a Bruker Avance I 200 NMR spectrometer (operating at 200 MHz for ^1H and 188 MHz for ^{19}F), a Bruker DRX-300 (operating at 300 MHz for ^1H, 75 MHz for $^{13}C\{^1H\}$ and 121 MHz for $^{31}P\{^1H\}$), a Bruker Avance Neo 400 NMR spectrometer (operating at 400 MHz for ^1H, 100 MHz for $^{13}C\{^1H\}$, 377 MHz for ^{19}F and 162 MHz for $^{31}P\{^1H\}$) or a Bruker Avance 500 NMR spectrometer (operating at 500 MHz for ^1H, 125 MHz for $^{13}C\{^1H\}$, 470 MHz for ^{19}F and 202 MHz for $^{31}P\{^1H\}$).^{13}C and ^{31}P NMR spectra were broad-

band proton-decoupled ($^{13}C\{^1H\}$ and $^{31}P\{^1H\}$). Chemical shifts are listed in parts per million (ppm) and were referenced to external trimethylsilane (^1H and ^{13}C), Cl_3CF (^{19}F) and 85% H_3PO_4 (^{31}P). ^1H NMR spectra were internally referenced *via* residual proton resonance of $CDCl_3$ (^1H, 7.26 ppm), toluene-d_8 (^1H, 7.09, 7.01, 6.97 and 2.08 ppm), C_6D_6 (^1H, 7.16 ppm) and THF-d_8 (^1H, 1.72 and 3.58 ppm). $^{13}C\{^1H\}$ spectra were internally referenced using the signals from $CDCl_3$ (^{13}C, 77.16 ppm), C_6D_6 (^{13}C, 128.06 ppm) and THF-d_8 (^{13}C, 67.21 and 25.31 ppm). Coupling constants (*J*) are quoted in Hertz (Hz). Assignment of the ^1H and ^{13}C NMR resonances was supported by two-dimensional methods where necessary. $^{13}C\{^1H\}$ resonances are singlets, if not otherwise indicated. $^{13}C\{^1H\}$ signals that are not singlets are expanded as insets or as separate figures. Coupling constants are ^1H-^1H coupling constants if not otherwise indicated. NMR signals are given as s: singlet, d: doublet, dd: doublet of doublets, dt: doublet of triplets, t: triplet, q: quartet, qui: quintet, vt: virtual triplet, vdt: virtual doublet of triplets and m: multiplet. For the higher order spin systems of the PMe_3 groups, *N* (with $N = |^1J_{P\text{-}C} + {}^3J_{P\text{-}C}|$) is given instead of *J*.[324-325]

VT-NMR spectroscopic data were obtained at various temperatures using a Bruker Avance III HD 300 NMR spectrometer (operating at 300 MHz for ^1H and 121 MHz for $^{31}P\{^1H\}$). The temperature was calibrated using a sample of 4% MeOH in CD_3OD for temperatures below 298 K or a sample of 80% 1,2-ethanediol in d_6-DMSO for temperatures above 298 K.[326]

Elemental analyses were performed by the microanalytical laboratory of the Institute of Inorganic Chemistry of the University of Würzburg with an Elementar vario micro cube.

High-resolution mass spectrometry (HRMS) was performed with a Thermo Fisher Scientific Exactive Plus Orbitrap MS System with either an atmospheric-pressure chemical ionization (APCI) or liquid injection field desorption ionization (LIFDI).

Cyclic voltammetry was performed in 0.1 M tetrabutylammonium hexafluorophosphate THF solutions using a Gamry Reference 600 Potentiostat and a three electrode cell setup. A 3 mm Pt working electrode and a Pt wire counter electrode was used. The Ag pseudo reference electrode was immersed in electrolyte solution and separated from the cell using a vycore tip. All potentials are referenced against the ferrocene/ferrocenium redox couple using ferrocene or decamethyl ferrocene as an internal standard.[327-328]

Single-crystals suitable for X-ray diffraction were selected, coated in perfluoropolyether oil, and mounted on MiTeGen sample holders. Diffraction data of **2-5**, **2-3a**, **2-3c**, **3-7**, **4-1**, **4-4**, **4-9**, **4-13a**, **4-14a** were collected on a Bruker X8-APEX II diffractometer with a CCD area detector and multi-layer mirror monochromated Mo-K_α radiation. Diffraction data of **2-10a**, **2-SYM^{CO2Me}**, **2-21**, **3-1**, **3-6**, **3-15**, **4-2**, **4-7**, **4-5**, **4-10**, **4-12a**, **4-16** were collected on a Bruker

X8-APEX II diffractometer with a CCD area detector and graphite monochromated Mo-K_α radiation. The crystals were cooled using Oxford Cryostream open-flow N_2 gas cryostats. The images were processed and corrected for Lorentz-polarization effects and absorption as implemented in the Bruker software packages. Diffraction data of **2-9**, **2-I$_{cis}$b** and **4-3** were collected on a Rigaku Oxford Diffraction XtaLAB Synergy diffractometer with a semiconductor HPA-detector (HyPix-6000) and multi-layer mirror monochromated Cu-K_α radiation. The crystals were cooled using an Oxford Cryostream 800 low-temperature device. The images were processed and corrected for Lorentz-polarization effects and absorption as implemented in the CrysAlis^{Pro} software.

The structure was solved using intrinsic phasing method (ShelXT),[329] and Fourier expansion technique. All non-hydrogen atoms were refined in anisotropic approximation, with hydrogen atoms 'riding' on idealized positions by full-matrix least squares against F^2 of all data, using SHELXL[330] software and the SHELXLE graphical user interface.[331] The program DIAMOND was used for graphical representation.[332]

General color code: carbon (white), sulfur (yellow), oxygen (red), phosphorus (purple), rhodium (dark green), nitrogen (blue).

All photophysical measurements were performed in standard quartz cuvettes (1 cm x 1 cm cross-section) under an argon atmosphere unless otherwise stated.

UV-visible absorption spectra were recorded using an Agilent 8453 diode array UV-visible spectrophotometer. The molar extinction coefficients were calculated from three independently prepared samples in dry, degassed THF solutions.

The Stokes shift is defined as the energy difference between the 0-0 transitions of the absorption and the emission. However, as the first transition is broad, the band maxima of the absorption and emission have been used to determine the Stokes shift throughout the paper. Consequently, the term "apparent Stokes shift" is used.

The emission spectra were recorded using an Edinburgh Instruments FLSP920 spectrometer equipped with a 450 W Xenon arc lamp, with a double monochromator for both excitation and emission, operating in right-angle geometry mode and a red-sensitive R928-P or Hamamatsu R13456-P photomultiplier tube (PMT) as the detector. All spectra were fully corrected for the spectral response of the instrument. All solutions used in photophysical measurements had an optical density lower than 0.15 to minimize inner filter effects during fluorescence measurements.

The fluorescence quantum yields were measured using a calibrated integrating sphere (inner diameter: 150 mm) from Edinburgh Instruments combined with the FLSP920 spectrometer

described above. For solution-state measurements, the longest-wavelength absorption maximum of the compound in the respective solvent was chosen as the excitation wavelength, unless stated otherwise.

Fluorescence lifetimes were recorded using the time-correlated single-photon counting (TCSPC) method using an Edinburgh Instruments FLSP920 spectrometer equipped with a picosecond pulsed laser diode (λ_{ex} = 505 nm, 472 nm and 273 nm). The emission was collected at right angles to the excitation source with the emission wavelength selected using a double grated monochromator and detected by a R928-P or Hamamatsu R13456-P PMT. Data were collected to 10000 counts in the peak channel and were fitted over >1000 channels. The instrument response function (IRF) was measured using a scattering sample (LUDOX) and setting the emission monochromator at the wavelength of the excitation beam. The resulting intensity decay is a convolution of the luminescence decay with the IRF, and iterative reconvolution of the IRF with one or two decay function(s) and non-linear least squares analysis was used to analyze the convoluted data. A bi-exponential decay fit was chosen only when the fit was significantly better than that obtained with a single function. The quality of all decay fits was judged to be satisfactory, based on the calculated values of the reduce χ^2 and Durbin-Watson parameters and visual inspection of the weighted residuals.

Low temperature measurements were performed in an Oxford Instruments Optistat DN N_2 cryostat controlled by an Oxford Instruments Mercury iTC temperature controller. Samples were allowed to equilibrate at 77 K before measurements were conducted. 2-Me-THF solutions were observed to form clear glasses below T_g.

All calculations (DFT and TD-DFT) were carried out with the Gaussian 09 (9.E.01)[333] program package and were performed on a parallel cluster system. GaussView (6.0.16) and multiwfn[334] were used to visualize the results, to measure calculated structural parameters, and to plot orbital surfaces (isovalue: ± 0.030 [e a_0^{-3}]$^{1/2}$). The ground-state geometries were optimized using the B3LYP functional[335] in combination with the 6-31+G(d) basis set.[336-337] The ultrafine integration grid and symmetry constraints were used for all molecules. Frequency calculations were performed on the optimized structures to confirm them to be local minima showing no negative (imaginary) frequencies. Based on these optimized structures, the lowest-energy vertical transitions (gas-phase and solvent correction using the polarizable continuum model) were calculated (singlets, 25 states) by TD-DFT, using the B3LYP in combination with the 6-31G+(d) basis set.

7.2 Synthetic routes

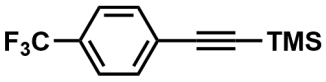

Trimethyl((4-(trifluoromethyl)phenyl)ethynyl)silane. A bright yellow suspension of $[Pd(PPh_3)_2Cl_2]$ (1.09 g, 1.55 mmol) and CuI (592 mg, 3.11 mmol) in dry, degassed triethylamine (350 mL) was treated with degassed ethynyltrimethylsilane (11.7 g, 119 mmol) and degassed 4-bromobenzotrifluoride (23.3 g, 104 mmol). The suspension turned gradually dark grey and was stirred at room temperature for 18 h. All volatiles were removed *in vacuo*, the grey residue was then suspended in *n*-hexane (500 mL) and filtered through a pad of silica (10 cm). Removing the solvent under reduced pressure resulted in a yellowish liquid (24.9 g, 103 mmol, 99%).

^{1}H NMR (300 MHz, $CDCl_3$): δ = 7.56 (s, 4H) and 0.27 (s, 9H) ppm.

^{13}C{^{1}H} NMR (75 MHz, $CDCl_3$): δ = 132.3, 130.3 (q, $^2J_{C\text{-}F}$ = 33 Hz), 127.1 (q, $^5J_{C\text{-}F}$ = 1 Hz, 125.3 (q, $^3J_{C\text{-}F}$ = 4 Hz), 124.1 (q, $^1J_{C\text{-}F}$ = 272 Hz), 103.6 (m), 97.3 and -0.1 ppm.

^{19}F NMR (188 MHz, $CDCl_3$): δ = -62.9 ppm.

The data are consistent with those in the literature.[284]

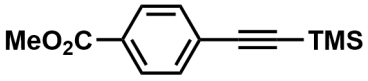

Methyl 4-((trimethylsilyl)ethynyl)benzoate. A bright yellow suspension of $[Pd(PPh_3)_2Cl_2]$ (1.00 g, 1.43 mmol) and CuI ((545 mg, 2.86 mmol) in dry, degassed triethylamine (400 mL) was treated with degassed ethynyltrimethylsilane (9.84 g, 100 mmol) and methyl-4-iodobenzoate (25.0 g, 95.4 mmol). The suspension turned gradually dark grey and was stirred at room temperature for 18 h. All volatiles were removed *in vacuo*, the grey residue was then suspended in *n*-hexane (900 mL) and filtered through a pad of silica (8 cm). Removing the solvent under reduced pressure resulted in an off-white solid (21.1 g, 90.8 mmol, 95%).

^{1}H NMR (300 MHz, $CDCl_3$): δ = 7.98-7.94 (m, 2H), 7.53-7.49 (m, 2H), 3.91 (s, 3H) and 0.26 (s, 9H) ppm.

^{13}C{^{1}H} NMR (75 MHz, $CDCl_3$): δ = 166.6, 132.0, 129.8, 129.5, 127.9, 104.2, 97.8, 52.4 and 0.0 ppm.

The data are consistent with those in the literature.[284]

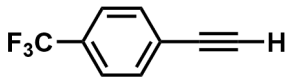

1-Ethynyl-4-(trifluoromethyl)benzene. Trimethyl((4-(trifluoromethyl)phenyl)ethynyl-silane (7.00 g, 28.9 mmol) in MeOH (50 mL) was treated with finely powdered KOH (2.43 g, 43.3 mmol), and stirred at room temperature for 1 hour. The reaction was quenched by adding Et_2O (100 mL) and dest. water (100 mL) to the mixture. Then, the crude product was extracted with Et_2O (60 mL x 5). The combined organic phases were dried over Na_2SO_4, filtered and the solvent removed *in vacuo* to give a light orange liquid (3.30 g, 19.4 mmol, 67%).

^{1}H NMR (500 MHz, $CDCl_3$): δ = 7.59 (s, 4H) and 3.20 (s, 1H) ppm.
^{13}C{^{1}H} NMR (125 MHz, $CDCl_3$): δ = 132.6, 130.8 (q, $^2J_{C\text{-}F}$ = 33 Hz), 126.1 (q, $^5J_{C\text{-}F}$ = 1 Hz), 125.4 (q, $^3J_{C\text{-}F}$ = 4 Hz), 124.0 (q, $^1J_{C\text{-}F}$ = 272 Hz), 82.3 (m) and 79.7 ppm.
^{19}F NMR (470 MHz, $CDCl_3$): δ = -63.0 ppm.
The data are consistent with those in the literature.[284]

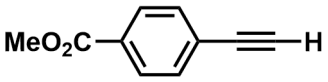

Methyl 4-ethynylbenzoate. Methyl 4-((trimethylsilyl)ethynyl)benzoate (21.10 g, 90.8 mmol) in MeOH (250 mL) was treated with finely powdered KOH (7.64 g, 136 mmol) and stirred at room temperature for 1 hour. The reaction was quenched by adding CH_2Cl_2 (150 mL) and dest. water (150 mL) to the mixture. Then, the crude product was extracted with CH_2Cl_2 (150 mL x 3). The combined organic phases were dried over Na_2SO_4, filtered and the solvent removed *in vacuo* to give an off-white solid (7.05 g, 44.0 mmol, 48%).

^{1}H NMR (300 MHz, $CDCl_3$): δ = 8.00-7.96 (m, 2H), 7.56-7.52 (m, 2H), 3.91 (s, 3H) and 3.23 (s, 1H) ppm.
^{13}C{^{1}H} NMR (75 MHz, $CDCl_3$): δ = 166.5, 132.2, 130.2, 129.6, 126.9, 82.9, 80.2 and 52.4 ppm.
The data are consistent with those in the literature.[284]

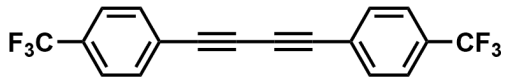

1,4-Bis(4-(trifluoromethyl)phenyl)buta-1,3-diyne 2-1a. 1-Ethynyl-4-(trifluoromethyl)-benzene (5.03 g, 29.6 mmol) in MeOH (50 mL) and pyridine (100 mL) was treated with $Cu(OAc)_2$ monohydrate (8.85 g, 44.4 mmol), and the blue suspension was vigorously stirred for 24 h. All volatiles were removed *in vacuo* and the residue was suspended in *n*-hexane (1.50 L) and filtered through a pad of silica (5 cm). Removing the solvent *in vacuo*, washing the residue with cold *n*-hexane (-30 °C; 15 mL x 4) and recrystallization from *n*-hexane (-30 °C) resulted in a colorless solid (4.30 g, 12.7 mmol, 86%).

^{1}H NMR (300 MHz, $CDCl_3$): δ = 7.66-7.59 (m, 8H) ppm.

^{13}C{^{1}H} NMR (75 MHz, $CDCl_3$): δ = 133.0, 131.3 (q, $^2J_{C\text{-}F}$ = 33 Hz), 125.6 (q, $^3J_{C\text{-}F}$ = 4 Hz), 125.4 (q, $^5J_{C\text{-}F}$ = 1 Hz), 123.8 (q, $^1J_{C\text{-}F}$ = 272 Hz), 81.1 and 75.8 ppm.

^{19}F NMR (377 MHz, $CDCl_3$): δ = -63.0 ppm.

The data are consistent with those in the literature.[284]

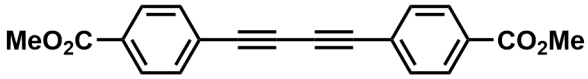

Dimethyl 4,4'-(buta-1,3-diyne-1,4-diyl)dibenzoate 2-1b. Methyl 4-ethynylbenzoate (7.05 g, 44.0 mmol) in MeOH (70 mL) and pyridine (70 mL) was treated with $Cu(OAc)_2$ monohydrate (13.2 g, 66 mmol), and the blue suspension was vigorously stirred for 48 h. The suspension was filtered, and the residue was washed with MeOH, which resulted in a colorless solid (6.49 g, 20.4 mmol, 93%).

^{1}H NMR (300 MHz, CD_2Cl_2): δ = 8.03-7.99 (m, 4H), 7.63-7.59 (m, 4H) and 3.90 (s, 6H) ppm.

^{13}C{^{1}H} NMR (75 MHz, CD_2Cl_2): δ = 166.4, 132.9, 131.2, 129.9, 126.3, 82.1, 76.3 and 52.6 ppm.

The data are consistent with those in the literature.[284]

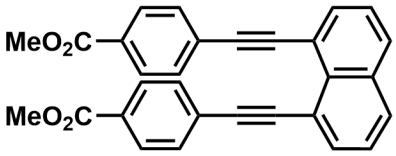

Dimethyl 4,4'-(naphthalene-1,8-diylbis(ethyne-2,1-diyl))dibenzoate 3-1. A bright yellow suspension of $[Pd(PPh_3)_2Cl_2]$ (67.7 mg, 96.5 µmol) and CuI (36.8 mg, 193 µmol) in dry, degassed triethylamine (250 mL) was treated with 1,8-diiodonaphthalene (1.83 g, 4.82 mmol) and stirred for 5 min before methyl 4-ethynylbenzoate (1.70 g, 10.6 mmol) was added. The suspension turned gradually dark grey and was stirred at room temperature for 24 h. All volatiles were removed *in vacuo*, and the crude product was then suspended in toluene and filtered through a pad of silica (10 cm). The filtrate was evaporated and purified by flash column chromatography using a gradient of CH_2Cl_2 in *n*-hexane (0 – 80% CH_2Cl_2) as the eluent. Removing the solvent *in vacuo* resulted in a colorless solid (2.10 g, 4.72 mmol, 98%).

^{1}H NMR (300 MHz, $CDCl_3$): δ = 7.89-7.88 (m, 2H), 7.87-7.86 (m, 2H), 7.77-7.75 (m, 4H), 7.51-7.46 (m, 2H), 7.39-7.36 (m, 4H) and 3.90 (s, 6H) ppm.

^{13}C{^{1}H} NMR (75 MHz, $CDCl_3$): δ = 166.6, 135.2, 134.2, 131.5, 131.4, 130.3, 129.27, 129.25, 128.4, 125.8, 120.3, 95.9, 92.8 and 52.3 ppm.

Elem. Anal. Calc. (%) for $C_{30}H_{20}O_4$: C, 81.07; H, 4.54; found: C, 81.07; H, 4.61.

HRMS (APCI$^+$): *m/z* calc. for $[C_{30}H_{21}O_4]^+$ 445.1434; found: 445.1427 $[M+H]^+$.

The data are consistent with those in the literature.[338]

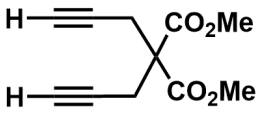

Dimethyl 2,2-di(prop-2-yn-1-yl)malonate. A suspension of sodiumhydride (60% in mineral oil, 8.01 g, 200 mmol) in THF (250 mL) was treated dropwise with dimetyl malonate (12.0 g, 91.0 mmol) at 0 °C and stirred for 30 min, before allowed to warm to room temperature. The suspension was again cooled to 0 °C and propargyl bromide (80 wt% in toluene, 29.8 g, 200 mmol) was added dropwise under vigorously stirring for 2 h. The color of the suspension turned from colorless to yellow. The reaction mixture was allowed to warm to room temperature and stirred for additional 15 h over night. The mixture was quenched with dest. water (150 mL) and the product extracted with ethyl acetate (50 mL x 3). The combined organic layers were dried over $MgSO_4$, filtered and concentrated *in vacuo*. The remaining yellow liquid was placed in a freezer (-30 °C) over night, during which a precipitate formed, which was filtered, washed with *n*-pentane (20 mL x 3) and recrystallized from *n*-hexane (-30 °C), resulting in a colorless solid (4.00 g, 19.2 mmol, 21%).

^{1}H NMR (300 MHz, $CDCl_3$): δ = 3.76 (s, 6H), 3.00-2.99 (m, 4H) and 2.04-2.02 (m, 2H) ppm.
^{13}C{^{1}H} NMR (75 MHz, $CDCl_3$): δ = 169.2, 78.4, 71.9, 56.6, 53.3 and 22.8 ppm.
The data are consistent with those in the literature.[339]

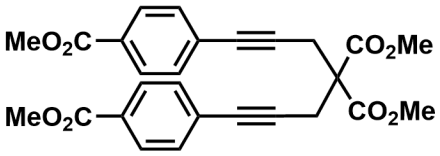

Dimethyl-2,2-bis(3-(4-(methoxycarbonyl)phenyl)prop-2-yn-1-yl)malonate 3-2/4-14. A bright yellow suspension of $[Pd(PPh_3)_2Cl_2]$ (142 mg, 202 μmol) and CuI (76.9 mg, 404 μmol) in dry, degassed triethylamine (50 mL) was treated with methyl-4-idodobenzoate (5.29 g, 20.2 mmol) and stirred for 5 min before dimethyl-2,2-di(prop-2-yn-1-yl)malonate (2.06 g, 9.89 mmol) was added. The suspension turned gradually dark grey and was stirred at room temperature for 24 h. All volatiles were removed *in vacuo*, the crude product suspended in toluene and filtered through a pad of silica (10 cm). The filtrate was evaporated and purified by flash column chromatography using a gradient of THF in *n*-hexane (0 – 30% THF) as the eluent. Removing the solvent *in vacuo* and recrystallization from THF/*n*-hexane at room temperature resulted in a colorless solid (3.13 g, 6.57 mmol, 66%).

^{1}H NMR (300 MHz, $CDCl_3$): δ = 7.96-7.93 (m, 4H), 7.44-7.41 (m, 4H), 3.90 (s, 6H), 3.81 (s, 6H) and 3.28 (s, 4H) ppm.

^{13}C{^{1}H} NMR (75 MHz, $CDCl_3$): δ = 169.3, 166.6, 131.8, 129.6, 129.5, 127.8, 87.1, 83.5, 57.1, 53.4, 52.3 and 24.1 ppm.

Elem. Anal. Calc. (%) for $C_{27}H_{24}O_8$: C, 68.06; H, 5.08; found: C, 68.02; H, 5.22.

HRMS ($APCI^+$): *m/z* calc. for $[C_{27}H_{25}O_8]^+$ 477.1544; found: 477.1536 $[M+H]^+$.

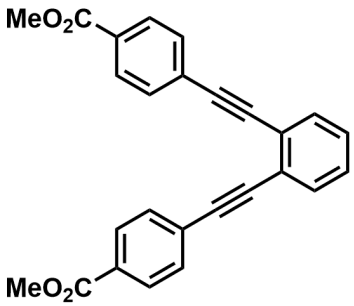

Dimethyl 4,4'-(1,2-phenylenebis(ethyne-2,1-diyl))dibenzoate 3-3. A bright yellow suspension of $[Pd(PPh_3)_2Cl_2]$ (88.9 mg, 127 µmol) and CuI (48.3 mg, 253 µmol) in dry, degassed triethylamine (150 mL) was treated with 1,2-diiodobenzene (2.09 g, 6.34 mmol) and stirred for 5 min before methyl 4-ethynylbenzoate (2.13 g, 13.3 mmol) was added. The suspension turned gradually dark grey and was stirred at room temperature for 24 h. All volatiles were removed *in vacuo*, the crude product suspended in a mixture of CH_2Cl_2/*n*-hexane and filtered through a pad of silica (10 cm). The filtrate was evaporated and purified by flash column chromatography using a gradient of THF in *n*-hexane (0 – 80% THF) as the eluent. Removing the solvent *in vacuo* and washing the residue with MeOH resulted in a colorless solid (2.33 g, 5.91 mmol, 93%).

^{1}H NMR (300 MHz, $CDCl_3$): δ = 8.04-8.00 (m, 4H), 7.63-7.55 (m, 6H), 7.38-7.32 (m, 2H) and 3.93 (s, 6H) ppm.

^{13}C{^{1}H} NMR (75 MHz, $CDCl_3$): δ = 166.6, 132.1, 131.6, 129.9, 129.7, 128.7, 127.9, 125.6, 93.1, 91.1 and 52.4 ppm.

Elem. Anal. Calc. (%) for $C_{26}H_{18}O_4$: C, 79.17; H, 4.60; found: C, 78.80; H, 4.68.

HRMS (APCI$^-$): *m/z* calc. for $[C_{26}H_{18}O_4]^-$ 394.1211; found: 394.1199 $[M]^-$.

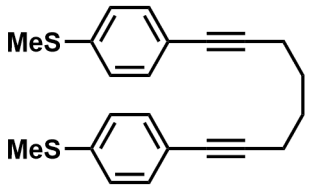

1,8-Bis(4-(methylthio)phenyl)octa-1,7-diyne 3-4. A bright yellow suspension of $[Pd(PPh_3)_2Cl_2]$ (70.2 mg, 100 µmol) and CuI (38.1 mg, 200 µmol) in dry, degassed triethylamine (250 mL) was treated with 4-iodothioanisole (3.00 g, 12.0 mmol) and stirred for 5 min before degassed 1,7-octadiyne (0.76 mL, 5.76 mmol) was added by syringe. The suspension turned gradually dark grey and was stirred at room temperature for 24 h. All volatiles were removed *in vacuo*, the crude product was then suspended in a mixture of *n*-hexane and CH_2Cl_2 (3:1) and filtered through pad of silica (4 cm). Removing the solvent *in vacuo* and washing the residue with *n*-hexane resulted in a colorless solid (1.23 g, 3.51 mmol, 61%).

^{1}H NMR (300 MHz, C_6D_6) δ = 7.36-7.32 (m, 4H), 6.93-6.89 (m, 4H), 2.25-2.21 (m, 4H), 1.87 (s, 6H) and 1.62-1.57 (m, 4H) ppm.

^{13}C{^{1}H} NMR (75 MHz, C_6D_6) δ = 139.1, 132.3, 126.3, 121.0, 90.2, 81.5, 28.3, 19.4 and 15.0 ppm.

Elem. Anal. Calc. (%) for $C_{22}H_{22}S_2$: C, 75.38; H, 6.33; S, 18.29; found: C, 75.76; H, 6.29; S, 18.58.

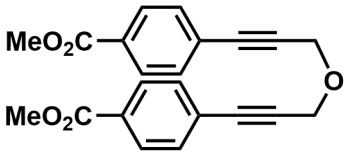

Dimethyl 4,4'-(oxybis(prop-1-yne-3,1-diyl))dibenzoate 3-5. A bright yellow suspension of $[Pd(PPh_3)_2Cl_2]$ (1.55 g, 2.21 mmol) and CuI (843 mg, 4.43 mmol) in dry, degassed triethylamine (300 mL) was treated with methyl-4-iodobenzoate (14.5 g, 55.3 mmol) and stirred for 5 min before degassed 3-(prop-2-yn-1-yloxy)prop-1-yne (2.60 g, 27.7 mmol) was added by syringe. The suspension turned gradually dark grey and was stirred at room temperature for 48 h. All volatiles were removed *in vacuo*, the crude product was suspended in a mixture of *n*-hexane and E_2O (1:1, 500 mL) and filtered through a pad of silica (10 cm). The filtrate was evaporated and purified by flash column chromatography using a gradient of THF in *n*-hexane (0 – 10% THF) as eluent. Removing the solvent *in vacuo* and recrystallization from THF (-30 °C) resulted in a colorless solid (280 mg, 0.77 mmol, 3%).

^{1}H NMR (300 MHz, $CDCl_3$) δ = 7.99-7.96 (m, 4H), 7.52-7.49 (m, 4H), 4.56 (s, 4H) and 3.90 (s, 6H) ppm.

^{13}C{^{1}H} NMR (75 MHz, $CDCl_3$) δ = 166.5, 131.8, 130.0, 129.6, 127.2, 87.4, 86.3, 57.6 and 52.4 ppm.

Elem. Anal. Calc. (%) for $C_{22}H_{18}O_5$: C, 72.92; H, 5.01; found: C, 73.14; H, 5.15.

The data are consistent with those in the literature.[340]

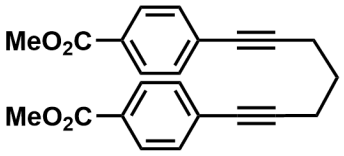

Dimethyl-4,4'-(hepta-1,6-diyne-1,7-diyl)dibenzoate 3-8/4-11. A bright yellow suspension of $[Pd(PPh_3)_2Cl_2]$ (804 mg, 1.14 mmol) and CuI (363 mg, 1.91 mmol) in dry, degassed triethylamine (300 mL) was treated with methyl-4-iodobenzoate (10.0 g, 38.2 mmol) and stirred for 5 min before degassed 1,6-heptadiyne (2.11 mL, 18.7 mmol) was added. The suspension turned gradually dark grey and was stirred at room temperature for 24 h. All volatiles were removed *in vacuo*, the crude product was then suspended in a mixture of *n*-hexane and Et_2O (2:1) and filtered through pad of silica (10 cm). The filtrate was evaporated and purified by flash column chromatography using a gradient of CH_2Cl_2 in *n*-hexane (0 – 66% CH_2Cl_2) as the eluent. Removing the solvent *in vacuo* resulted in a colorless solid (5.29 g, 14.7 mmol, 79%).

^{1}H NMR (300 MHz, $CDCl_3$) δ = 7.97-7.93 (m, 4H), 7.46-7.43 (m, 4H), 3.91 (s, 6H), 2.62 (t, ^3J = 7.0 Hz, 4H) and 1.93 (qui, ^3J = 7.0 Hz, 2H) ppm.

^{13}C{^{1}H} NMR (75 MHz, $CDCl_3$) δ = 166.7, 131.6, 129.6, 129.2, 128.7, 92.6, 81.0, 52.3, 27.7 and 18.9 ppm.

Elem. Anal. Calc. (%) for $C_{23}H_{20}O_4$: C, 76.65; H, 5.59; found: C, 76.42; H, 5.64.

The data are consistent with those in the literature.[341]

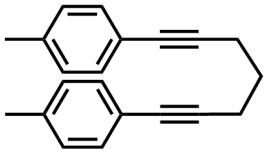

1,7-Di-*p*-tolylhepta-1,6-diyne 3-9/4-12. A bright yellow suspension of [$Pd(PPh_3)_2Cl_2$] (217 mg, 309 µmol,) and CuI (39.3 mg, 206 µmol) in dry, degassed triethylamine (300 mL) was treated with 4-iodotoluene (9.00 g, 41.3 mmol) and stirred for 5 min before degassed 1,6-heptadiyne (2.30 mL, 20.4 mmol) was added. The suspension turned gradually dark grey and was stirred at room temperature for 24 h. All volatiles were removed *in vacuo*, the residue was suspended in *n*-hexane (200 mL) and then filtered through a pad of silica (10 cm). The yellow filtrate was evaporated and purified by flash column chromatography using a gradient of CH_2Cl_2 in *n*-hexane (0 – 30% DCM) as the eluent. Removing the solvent *in vacuo* resulted in a colorless solid (4.09 g, 15.0 mmol, 73%).

^{1}H NMR (300 MHz, C_6D_6)**:** δ = 7.43-7.39 (m, 4H), 6.85-6.81 (m, 4H), 2.41 (t, ^3J = 7.0 Hz, 4H), 2.00 (s, 6H) and 1.70 (qui, ^3J = 7.0 Hz, 2H) ppm.

^{13}C{^{1}H} NMR (75 MHz, C_6D_6): δ = 137.6, 132.0, 129.3, 121.7, 88.9, 82.1, 28.5, 21.3 and 19.0 ppm.

Elem. Anal. Calc. (%) for $C_{21}H_{20}$: C, 92.60; H, 7.40; found: C, 92.68; H, 7.51.

The data are consistent with those in the literature.[342]

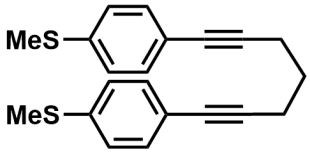

1,7-Bis(methylthio)phenylhepta-1,6-diyne 4-13. A bright yellow suspension of $[Pd(PPh_3)_2Cl_2]$ (269 mg, 384 µmol,) and CuI (146 mg, 768 µmol) in dry and degassed triethylamine (300 mL) was treated with 4-iodothioanisole (4.80 g, 19.2 mmol) and stirred for 5 min before degassed 1,6-heptadiyne (1.06 mL, 9.40 mmol) was added. The suspension turned gradually dark grey and was stirred at room temperature for 24 h. All volatiles were removed *in vacuo*, the residue suspended in *n*-hexane (120 mL) and filtered through a pad of silica (5 cm). The yellow filtrate was evaporated and recrystallized from *n*-hexane/MeOH (-30 °C), which resulted in a colorless solid (2.34 g, 6.95 mmol, 74%).

^{1}H NMR (300 MHz, C_6D_6) δ = 7.34-7.30 (m, 4H), 6.93-6.89 (m, 4H), 2.40 (t, ^3J = 7.0 Hz, 4H), 1.88 (s, 6H) and 1.69 (qui, ^3J = 7.0 Hz, 2H) ppm.
^{13}C{^{1}H} NMR (75 MHz, C_6D_6) δ = 139.2, 132.3, 126.3, 120.8, 89.6, 81.8, 28.4, 19.0 and 15.0 ppm.
Elem. Anal. Calc. (%) for $C_{21}H_{20}S_2$: C, 74.95; H, 5.99; S, 19.05; found: C, 75.29; H, 5.83; S, 18.97.

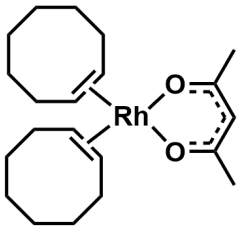

Acetylacetonatobis(cyclooctene)rhodium(I) [Rh(acac)(COE)$_2$]. A suspension of degassed acetylacetone (614 mg, 6.13 mmol) and KOH (344 mg, 6.13 mmol) in THF (60 mL) was stirred 5 min at room temperature before solid [Rh(μ-Cl)(COE)$_2$]$_2$ (2.00 g, 2.79 mmol) was added and the yellow suspension was stirred at room temperature for 3 h. Then, all volatiles were removed *in vacuo* and the product was extracted into *n*-hexane (150 mL) and filtered *via* filter cannulation, which gave the product as a yellow solid (2.04 g, 4.83 mmol, 87%).

^{1}H NMR (500 MHz, C_6D_6): δ = 5.04 (s, 1H), 2.52-2.43 (m, 11H) and 1.69-1.41 (m, 23H) ppm.
^{13}C{^{1}H} NMR (125 MHz, C_6D_6): δ = 185.4, 99.1 (m), 78.3 (d, $^1J_{Rh\text{-}C}$ = 13 Hz), 30.6, 28.3, 27.3 and 27.1 ppm.
The data are consistent with those in the literature.[304]

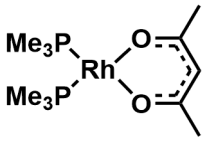

Acetylacetonatobis(trimethylphosphine)rhodium(I) 1-51. Acetylacetonatobis-(cyclooctene)rhodium(I) (4.00 g, 9.47 mmol) in *n*-hexane (200 mL) was treated with PMe_3 (1.51 g, 19.9 mmol) and the resulting yellow solution was stirred for 45 min at 40 °C. Removing all volatiles *in vacuo* resulted in a yellow solid (3.30 g, 9.32 mmol, 98%).

^{1}H NMR (300 MHz, C_6D_6): δ = 5.41 (s, 1H), 1.88 (s, 6H) and 1.21-1.17 (m, 18H) ppm.
^{13}C{^{1}H} NMR (75 MHz, C_6D_6): δ = 184.4 (m), 100.0 (m), 27.9 (m) and 18.7 (m) ppm.
^{31}P{^{1}H} NMR (121 MHz, C_6D_6): δ = 7.4 (d, $^1J_{Rh\text{-}P}$ = 186 Hz) ppm.
The data are consistent with those in the literature.[305]

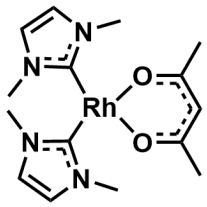

Acetylacetonatobis(1,3-dimethylimidazol-2-ylidene)rhodium(I) 2-21. Acetylacetonatobis-(cyclooctene)rhodium(I) (331 mg, 784 µmol) in THF (5 mL) was treated dropwise with bis(1,3-dimethyl-imidazol-2-ylidene) (151 mg, 1.57 mmol) in THF (4 mL) and stirred at room temperature for 16 h. Removing all volatiles *in vacuo*, washing the residue with *n*-hexane (2 mL x 3) and recrystallization from THF/*n*-hexane resulted in an orange solid (297 mg, 753 µmol, 96%).

^{1}H NMR (300 MHz, C_6D_6): δ = 6.09 (m, 4H), 5.54 (s, 1H), 3.52 (s, 12H) and 1.91 (s, 6H) ppm.
^{13}C{^{1}H} NMR (75 MHz, C_6D_6) δ = 192.3 (d, J_{Rh-C} = 66 Hz), 182.8 (m), 119.4 (m), 99.7 (m), 37.0 (m) and 28.2 (m) ppm.
Elem. Anal. Calc. (%) for $C_{15}H_{23}O_2N_4Rh$: C, 45.69; H, 5.88; N, 14.21; found: C, 45.68; H, 5.83; N 14.21.
HRMS(LIFDI): *m/z* calc. for $[C_{15}H_{23}O_2N_4Rh]^+$ 394.0871; found: 394.0869 $[M]^+$.

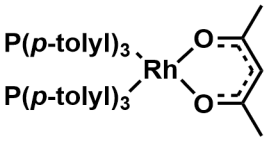

Acetylacetonatobis(tri(*p*-tolyl)phosphine)rhodium(I) 1-56. Acetylacetonatobis(cyclo-octene)rhodium(I) (1.00 g, 2.37 mmol) in THF (50 mL) was treated with tri(*p*-tolyl)phosphine (1.44 g, 4.73 mmol) and the resulting yellow solution stirred at room temperature for 18 h. Removing all volatiles *in vacuo* and recrystallization from THF/EtOH (-35 °C) resulted a yellow solid (1.80 g, 2.22 mmol, 94%).

^{1}H NMR (300 MHz, C_6D_6): δ = 7.89-7.83 (m, 12H), 6.82-6.80 (m, 12H), 5.39 (s, 1H), 2.00 (s, 18H) and 1.58 (s, 6H) ppm.
^{13}C{^{1}H} NMR (75 MHz, C_6D_6) δ = 184.3, 138.3 (m), 135.5 (m), 134.1 (m), 128.0 (m), 99.8 (m), 27.2 (m) and 21.2 ppm.
^{31}P{^{1}H} NMR (121 MHz, C_6D_6) δ = 54.8 (d, $^{1}J_{Rh-P}$ = 195 Hz) ppm.
HRMS (LIFDI): *m/z* calc. for $[C_{47}H_{49}O_2P_2Rh]^+$ 810.2257; found: 810.2239 $[M]^+$.
The data are consistent with those in the literature.[71]

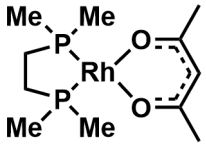

Acetylacetonato(1,2-ethanediylbis(dimethylphosphine)rhodium(I) 4-1. Acetylacetonatobis(cyclooctene)rhodium(I) (250 mg, 592 µmol) in THF (15 mL) was treated dropwise with 1,2-bis(dimethylphosphino)ethane (88.9 mg, 592 µmol) in THF (5 mL) and stirred at room temperature for 24 h. Removing all volatiles *in vacuo*, washing the residue with *n*-hexane (2 mL x 3) and recrystallization from THF/*n*-hexane resulted in a yellow solid (183 mg, 520 µmol, 88%).

^{1}H NMR (300 MHz, C_6D_6): δ = 5.41 (s, 1H), 1.96 (s, 6H), 1.31-1.27 (m, 12H) and 1.01-0.95 (m, 4H) ppm.

^{13}C{^{1}H} NMR (75 MHz, C_6D_6) δ = 184.7 (m), 99.9 (m), 29.7 (m), 28.4 (m) and 16.5 (m) ppm.

^{31}P{^{1}H} NMR (121 MHz, C_6D_6) δ = 51.5 (d, $^{1}J_{Rh\text{-}P}$ = 190 Hz) ppm.

Elem. Anal. Calc. (%) for $C_{11}H_{23}O_2P_2Rh$: C, 37.52; H, 6.58; found: C, 37.47; H, 6.68.

HRMS (LIFDI): *m/z* calc. for $[C_{11}H_{23}O_2P_2Rh]^+$ 352.0223; found: 352.0211 $[M]^+$.

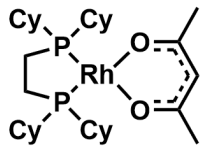

Acetylacetonato(1,2-ethanediylbis(dicyclohexylphosphine)rhodium(I) 4-2. Acetylacetonatobis(cyclooctene)rhodium(I) (250 mg, 592 µmol) in THF (10 mL) was treated dropwise with 1,2-bis(dicyclohexylphosphino)ethane (250 mg, 592 µmol) in THF (10 mL) and stirred at room temperature for 24 h. Removing all volatiles *in vacuo* and washing the residue with EtOH (2 mL x 3) resulted in a yellow solid (300 mg, 480 µmol, 81%).

^{1}H NMR (400 MHz, C_6D_6): δ = 5.38 (s, 1H), 2.50-2.47 (m, 4H), 1.94 (s, 6H), 1.90-1.58 (m, 28H) and 1.33-1.16 (m, 16H) ppm.

^{13}C{^{1}H} NMR (100 MHz, C_6D_6) δ = 184.0, 99.5 (m), 36.1 (m), 29.8 (s, br), 29.4, 28.1 (m), 27.9 (m), 27.7 (m), 26.9 and 22.7 (m) ppm.

^{31}P{^{1}H} NMR (162 MHz, C_6D_6) δ = 91.7 (d, $^{1}J_{RhP}$ = 194 Hz) ppm.

Elem. Anal. Calc. (%) for $C_{31}H_{55}O_2P_2Rh$: C, 59.61; H, 8.88; found: C, 59.82; H, 8.97.

HRMS (LIFDI): *m/z* calc. for $[C_{31}H_{55}O_2P_2Rh]^+$ 624.2727; found: 624.2710 $[M]^+$.

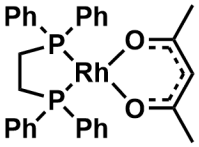

Acetylacetonato(1,2-ethanediylbis(diphenylphosphine)rhodium(I) 4-3. Acetylacetonato-bis(cyclooctene)rhodium(I) (500 mg, 1.18 mmol) in THF (5 mL) was treated dropwise with 1,2-bis(diphenylphosphino)ethane (472 mg, 1.18 mmol) in THF (5 mL) and stirred at room temperature for 48 h. Removing all volatiles *in vacuo*, washing with *n*-hexane (2 mL x 3) and recrystallization from THF/*n*-hexane resulted in a yellow solid (680 mg, 1.13 mmol, 96%).

^{1}H NMR (300 MHz, C_6D_6): δ = 8.07-8.01 (m, 8H), 7.12-7.01 (m, 12H), 5.41 (s, 1H) and 1.86-1.80 (m, 10H) ppm.

^{13}C{^{1}H} NMR (75 MHz, C_6D_6) δ = 185.0 (m), 137.5 (m), 133.4 (m), 129.4 (m), 128.2 (m), 99.8 (m), 28.1 (m) and 27.8 (m) ppm.

^{31}P{^{1}H} NMR (121 MHz, C_6D_6) δ = 70.2 (d, $^{1}J_{Rh\text{-}P}$ = 193 Hz) ppm.

HRMS (LIFDI): *m/z* calc. for $[C_{31}H_{31}O_2P_2Rh]^+$ 600.0849; found: 600.0832 $[M]^+$.

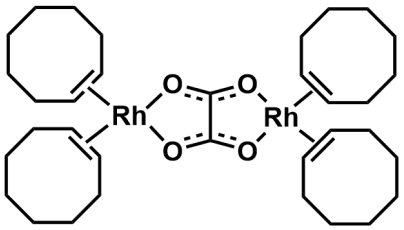

Oxalatobis(cyclooctene)rhodium(I) dimer 4-4. Acetylacetonatobis(cyclooctene)-rhodium(I) (968 mg, 2.29 mmol) in THF (20 mL) was treated with oxalic acid dihydrate (138 mg, 1.09 mmol) and stirred at room temperature for 24 h. Removing all volatiles *in vacuo* and washing the residue with *n*-hexane (10 mL x 3) resulted in a yellow solid (744 mg, 1.01 mmol, 93%).

^{1}H NMR (400 MHz, THF-d_8): δ = 2.51 (s(br), 8H), 2.10-2.06 (m, 8H), 1.92-1.87 (m, 8H), 1.65-1.60 (m, 8H) and 1.50-1.29 (m, 24H) ppm.

^{13}C{^{1}H} NMR (100 MHz, THF-d_8) δ = 174.5, 77.1 (m), 30.3, 27.7 and 27.1 ppm.

Elem. Anal. Calc. (%) for $C_{34}H_{56}O_4Rh_2$: C, 55.59; H, 7.68; found: C, 55.48; H, 7.83.

HRMS(LIFDI): *m/z* calc. for $[M\text{-}COE+THF]^+$ 696.1763; found: 696.1754 $[C_{30}H_{50}O_5Rh_2]^+$.

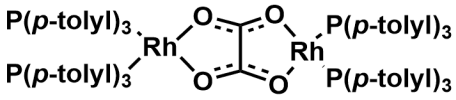

Oxalatotetra(tris(*p*-tolylphoshpine))bisrhodium(I) 4-5. Oxalatobis(cyclooctene)rhodium(I) dimer **4-4** (250 mg, 340 µmol) in THF (15 mL) was treated with tri(*p*-tolyl)phosphine (456 mg, 1.50 mmol) and stirred at 60 °C for 12 h. Removing all volatiles *in vacuo*, washing the residue with *n*-hexane (5 mL x 3), and recrystallization from THF/*n*-hexane resulted in an orange solid (460 mg, 304 µmol, 89%).

^{1}H NMR (300 MHz, THF-d_8): δ = 7.37-7.31 (m, 24H), 6.83-6.81 (m, 24H) and 2.25 (s, 36H) ppm.

^{13}C{^{1}H} NMR (75 MHz, THF-d_8) δ = 173.1, 138.8, 135.2 (m), 133.4 (m), 128.2 (m) and 21.2 ppm.

^{31}P{^{1}H} NMR (121 MHz, THF-d_8) δ = 53.7 (d, $^{1}J_{Rh\text{-}P}$ = 201 Hz) ppm.

Elem. Anal. Calc. (%) for $C_{86}H_{84}O_4P_4Rh_2$: C, 68.35; H, 5.60; found: C, 68.13; H, 5.83.

HRMS(LIFDI): *m/z* calc. for $[C_{86}H_{84}O_4P_4Rh_2]^+$ 1510.3425; found: 1510.3411 $[M]^+$.

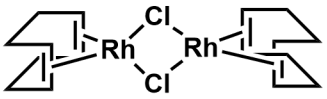

Bis(1,5-cyclooctadiene)dirhodium(I)-dichloride [RhCl(COD)]$_2$. Chlorobis(cyclooctene)-rhodium(I) dimer (250 mg, 348 µmol) in THF (8 mL) was treated with cyclooctadiene (77.3 mg, 714 µmol) and stirred at room temperature for 12 h. Removing all volatiles *in vacuo* resulted in a yellow solid (170 mg, 345 µmol, 99%).

^{1}H NMR (500 MHz, C_6D_6): δ = 4.31 (s, 8H), 2.09-2.06 (m, 8H) and 1.32-1.30 (m, 8H) ppm.

^{13}C{^{1}H} NMR (125 MHz, C_6D_6) δ = 78.5 (d, $J_{Rh\text{-}C}$ = 14 Hz) and 30.9 ppm.

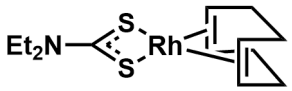

Diethyldithiocarbamato(1,5-cyclooctadiene)rhodium(I) [Rh(S$_2$CNEt$_2$)(COD)]. A suspension of bis(1,5-cyclooctadiene)dirhodium(I) dichloride (300 mg, 609 µmol) in THF (10 mL) was treated with sodium diethyldithiocarbamate (219 mg, 1.28 mmol) and stirred at room temperature for 48 h. Removing all volatiles *in vacuo* and washing the residue with ethanol (3 mL x 3) resulted in a yellow solid (210 mg, 584 µmol, 96%).

^{1}H NMR (500 MHz, C_6D_6): δ = 4.58 (s, 4H), 3.21 (q, ^3J = 7.1 Hz, 4H), 2.28-2.25 (m, 4H), 1.69-1.64 (m, 4H) and 0.75 (t, ^3J = 7.1 Hz, 6H) ppm.

^{13}C{^{1}H} NMR (125 MHz, C_6D_6) δ = 209.8 (d, J = 6 Hz), 80.9 (d, $J_{Rh\text{-}C}$ = 12 Hz), 44.0, 31.8 and 12.4 ppm.

Only limited spectroscopic data was reported previously.[309]

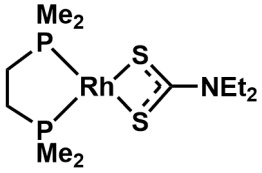

Diethyldithiocarbamato(1,2-ethanediylbis(dimethylphosphine)rhodium(I) 4-7. Diethyldithiocarbamate(cyclooctadiene)rhodium(I) (151 mg, 420 µmol) in THF (10 mL) was treated dropwise with 1,2-bis(dimethylphosphino)ethane (63 mg, 420 µmol) in THF (5 mL) and stirred at room temperature for 24 h. Removing all volatiles *in vacuo* and washing the residue with ethanol (2 mL x 1) resulted in a yellow solid (135 mg, 336 µmol, 80%).

^{1}H NMR (300 MHz, C_6D_6): δ = 3.50 (q, ^3J = 7.1 Hz, 4H), 1.29-1.25 (m, 12H), 1.04-0.98 (m, 4H) and 0.92 (t, ^3J = 7.1 Hz, 6H) ppm.

^{13}C{^{1}H} NMR (75 MHz, C_6D_6) δ = 216.2 (d, J = 5 Hz), 43.8, 30.4 (m), 17.9 (m) and 12.7 ppm.

^{31}P{^{1}H} NMR (121 MHz, C_6D_6) δ = 45.1 (d, $^1J_{Rh\text{-}P}$ = 174 Hz) ppm.

HRMS (LIFDI): *m/z* calc. for $[C_{11}H_{26}NS_2P_2Rh]^+$ 401.0031; found: 401.0023 $[M]^+$.

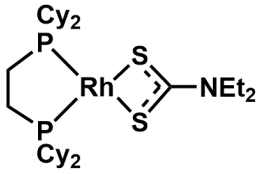

Diethyldithiocarbamato(1,2-ethanediylbis(dicyclohexylphosphine)rhodium(I) 4-8. Diethyldithiocarbamate(cyclooctadiene)rhodium(I) (213 mg, 592 µmol) in THF (10 mL) was treated dropwise with 1,2-bis(dicyclohexylphosphino)ethane (250 mg, 592 µmol) in THF (10 mL) and stirred at room temperature for 24 h. Removing all volatiles *in vacuo* and washing with ethanol (2 mL x 3) resulted a yellow solid (355 mg, 527 µmol, 89%).

^{1}H NMR (500 MHz, C_6D_6): δ = 3.47 (q, ^{3}J = 7.1 Hz, 4H), 2.49-2.46 (m, 4H), 1.86-1.61 (m, 28H), 1.30-1.18 (m, 16H) and 0.87 (t, ^{3}J = 7.1 Hz, 6H) ppm.

^{13}C{^{1}H} NMR (125 MHz, C_6D_6) δ = 216.3 (d, J = 5 Hz), 43.2, 37.4 (m), 30.2 (m), 29.6, 27.8 (m), 27.7 (m), 26.9, 23.4 (m) and 12.7 ppm.

^{31}P{^{1}H} NMR (202 MHz, C_6D_6) δ = 91.1 (d, $^{1}J_{Rh\text{-}P}$ = 181 Hz) ppm.

Elem. Anal. Calc. (%) for $C_{31}H_{58}NS_2P_2Rh$: C, 55.26; H, 8.68; N, 2.08; S, 9.52; found: C, 55.58; H, 8.50; N, 2.37; S, 9.33.

HRMS (LIFDI): *m/z* calc. for $[C_{31}H_{58}NS_2P_2Rh]^+$ 673.2535; found: 673.2524 $[M]^+$.

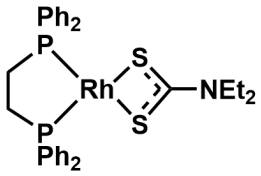

Diethyldithiocarbamato-(1,2-ethanediylbis(diphenylphosphine)rhodium(I) 4-9. Diethyldithiocarbamate(cyclooctadiene)rhodium(I) (100 mg, 278 µmol) in THF (5 mL) was treated dropwise with 1,2-bis(diphenylphosphino)ethane (111 mg, 278 µmol) in THF (5 mL) and stirred at room temperature for 24 h. Removing all volatiles *in vacuo* and washing the residue with ethanol (2 mL x 3) resulted in a yellow solid (161 mg, 248 µmol, 89%).

^{1}H NMR (400 MHz, THF-d_8): δ = 7.84-7.79 (m, 8H), 7.28-7.27 (m, 12H), 3.78 (q, ^{3}J = 7.1 Hz, 4H), 2.14-2.09 (4H, m) and 1.21 (t, ^{3}J = 7.1 Hz, 6H) ppm.

^{1}H NMR (300 MHz, C_6D_6): δ = 8.00-7.94 (m, 8H), 7.09-6.98 (m, 12H), 3.38 (q, ^{3}J = 7.1 Hz, 4H), 1.96-1.89 (4H, m) and 0.81 (t, ^{3}J = 7.1 Hz, 6H) ppm.

^{13}C{^{1}H} NMR (100 MHz, THF-d_8) δ = 215.5 (d, J = 5 Hz), 138.6 (m), 133.6 (m), 129.7 (m), 128.6 (m), 43.9, 29.2 (m) and 12.9 ppm.

^{13}C{^{1}H} NMR (75 MHz, C_6D_6) δ = 215.1 (d, J = 5 Hz), 138.1 (m), 133.3 (m), 129.3 (m), 128.3 (m), 43.4, 28.7 (m) and 12.6 ppm.

^{31}P{^{1}H} NMR (162 MHz, THF-d_8) δ = 69.9 (d, $^{1}J_{Rh\text{-}P}$ = 178 Hz) ppm.

^{31}P{^{1}H} NMR (121 MHz, C_6D_6) δ = 70.2 (d, $^{1}J_{Rh\text{-}P}$ = 178 Hz) ppm.

Elem. Anal. Calc. (%) for $C_{31}H_{34}NS_2P_2Rh$: C, 57.32; H, 5.28; N, 2.16; S, 9.87; found: C, 57.47; H, 5.31; N, 2.22; S, 9.79.

HRMS (LIFDI): *m/z* calc. for $[C_{31}H_{34}NS_2P_2Rh]^+$ 649.0657; found: 649.0644 $[M]^+$.

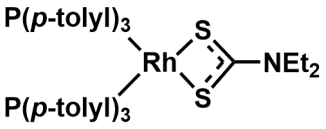

Diethyldithiocarbamatobis(tri(*p*-tolyl)phosphine)rhodium(I) 4-10. Acetylacetonato-bis(tri(*p*-tolyl)phosphine)rhodium(I) **1-56** (300 mg, 370 µmol) in THF (7 mL) was treated with sodium diethyldithiocarbamate (95 mg, 555 µmol) and stirred at 60 °C for 24 h. The solvent was removed *in vacuo* and the product was then extracted into toluene and filtered over a thin pad of Celite (2 cm). Removing the solvent *in vacuo* and washing the residue with ethanol (2 mL x 3) resulted in a yellow solid (280 mg, 326 µmol, 88%).

^{1}H NMR (300 MHz, THF-d_8): δ = 7.42-7.36 (m, 12H), 6.85-6.82 (m, 12H), 3.60 (q, J = 7.1 Hz, 4H), 2.23 (s, 18H) and 1.08 (t, J = 7.1 Hz, 6H) ppm.

^{1}H NMR (300 MHz, C_6D_6): δ = 7.93-7.87 (m, 12H), 6.85-6.82 (m, 12H), 3.22 (q, J = 7.1 Hz, 4H), 1.98 (s, 18H) and 0.68 (t, J = 7.1 Hz, 6H) ppm.

^{13}C{^{1}H} NMR (75 MHz, THF-d_8) δ = 213.3 (d, J = 5 Hz), 138.4 (m), 135.2 (m), 135.0 (m), 128.1 (m), 42.8, 21.1 and 12.6 ppm.

^{13}C{^{1}H} NMR (75 MHz, C_6D_6) δ = 213.1 (d, J = 5 Hz), 138.2 (m), 135.2 (m), 135.0 (m), 128.3 (m), 42.4, 21.2 and 12.6 ppm.

^{31}P{^{1}H} NMR (121 MHz, THF-d_8) δ = 46.9 (d, $^{1}J_{Rh\text{-}P}$ = 179 Hz) ppm.

^{31}P{^{1}H} NMR (121 MHz, C_6D_6) δ = 47.5 (d, $^{1}J_{Rh\text{-}P}$ = 178 Hz) ppm.

Elem. Anal. Calc. (%) for $C_{47}H_{52}NS_2P_2Rh$: C, 65.65; H, 6.10; N, 1.63; S, 7.46; found: C, 65.54; H, 6.12; N, 1.72; S, 7.47.

HRMS (LIFDI): *m/z* calc. for $[C_{47}H_{52}NS_2P_2Rh]^+$ 859.2066; found: 859.2044 $[M]^+$.

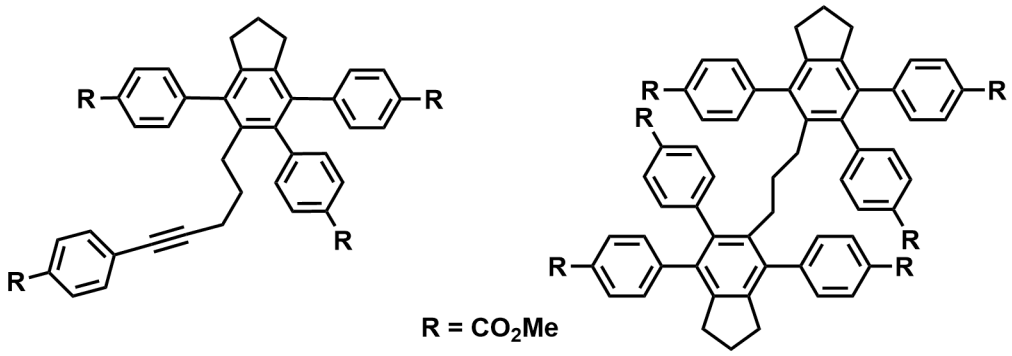

Dimer 4-11a and Trimer 4-11b. Dimethyl-4,4'-(hepta-1,6-diyne-1,7-diyl)dibenzoate **4-11** (1.00 g, 2.77 mmol) in toluene (100 mL) was treated with acetylacetonato-bis(tri(*p*-tolyl)phosphine)rhodium(I) **1-56** (225 mg, 277 µmol) and stirred at 60 °C for 72 h. The solvent was removed *in vacuo* and the residue was separated by flash column chromatography using a gradient of CH_2Cl_2 in *n*-hexane (0 – 90% CH_2Cl_2) as the eluent. All volatiles were removed *in vacuo*. The dimer was further purified by recrystallization from acetone/*n*-pentane (-30 °C) and the trimer from CH_2Cl_2/MeOH (-30 °C) resulting in dimer and trimer as colorless solids (dimer: 404 mg, 560 µmol, 40%; trimer: 294 mg, 272 µmol, 30%).

Dimer 4-11a:

^{1}H NMR (500 MHz, C_6D_6) δ = 8.19-8.18 (m, 2H), 8.01-8.00 (m, 2H), 7.97-7.94 (m, 4H), 7.24-7.22 (m, 2H), 7.19-7.17 (m, 2H), 7.12-7.10 (m, 2H), 6.97-6.95 (m, 2H), 3.59 (s, 3H), 3.45 (s, 3H), 3.39 (s, 3H), 3.37 (s, 3H), 2.65-2.62 (m, 2H), 2.59 (t, 2H, ^3J = 7.4 Hz), 2.52 (t, 2H, ^3J = 7.4 Hz), 1.79 (t, 2H, ^3J = 6.5 Hz), 1.73 (qui, 2H, ^3J = 7.4 Hz) and 1.47-1.42 (m, 2H) ppm.

^{13}C{^{1}H} NMR (125 MHz, C_6D_6) δ = 166.5, 166.31, 166.28, 166.2, 145.8, 145.51, 145.46, 143.0, 140.8, 139.0, 138.1, 137.3, 135.8, 131.8, 131.2, 130.3, 130.1, 129.8, 129.7, 129.6, 129.5, 129.4, 129.2, 129.0, 128.9, 92.6, 81.2, 51.8, 51.6, 51.51, 51.47, 33.5, 33.4, 30.6, 30.0, 25.2 and 19.8 ppm.

Elem. Anal. Calc. (%) for $C_{46}H_{40}O_8$: C, 76.65; H, 5.59; found: C, 76.94; H, 5.64.

HRMS (APCI$^+$): *m/z* calc. for $[C_{46}H_{41}O_8]^+$ 721.2796; found: 721.2774 $[M+H]^+$.

Trimer 4-11b:

^{1}H NMR (500 MHz, C_6D_6) δ = 8.21-8.19 (m, 4H), 7.96-7.92 (m, 8H), 7.04-7.02 (m, 4H), 6.92-6.88 (m, 8H), 3.68 (s, 6H), 3.50 (s, 6H), 3.36 (s, 6H), 2.50 (t, 4H, ^{3}J = 7.4 Hz), 2.42 (t, 4H, ^{3}J = 7.4 Hz), 2.08-2.04 (m, 4H), 1.64 (qui, 4H, ^{3}J = 7.4 Hz), 1.23-1.18 (m, 2H, overlapping with *n*-hexane CH_2 groups) ppm.

^{13}C{^{1}H} NMR (125 MHz, C_6D_6) δ = 166.7, 166.4, 166.3, 146.0, 145.7, 145.5, 142.9, 140.7, 138.5, 137.6, 137.1, 136.0, 131.2, 130.1, 130.0, 129.6, 129.5, 129.4, 129.3, 129.0, 128.9, 51.9, 51.6, 51.4, 33.5, 33.3, 32.4, 30.9 and 25.1 ppm.

Elem. Anal. Calc. (%) for $C_{69}H_{60}O_{12}$: C, 76.65; H, 5.54; found: C, 76.60; H, 5.78.

HRMS (APCI^{+}): *m/z* calc. for $[C_{69}H_{61}O_{12}]^{+}$ 1081.4158; found: 1081.4123 $[M+H]^{+}$.

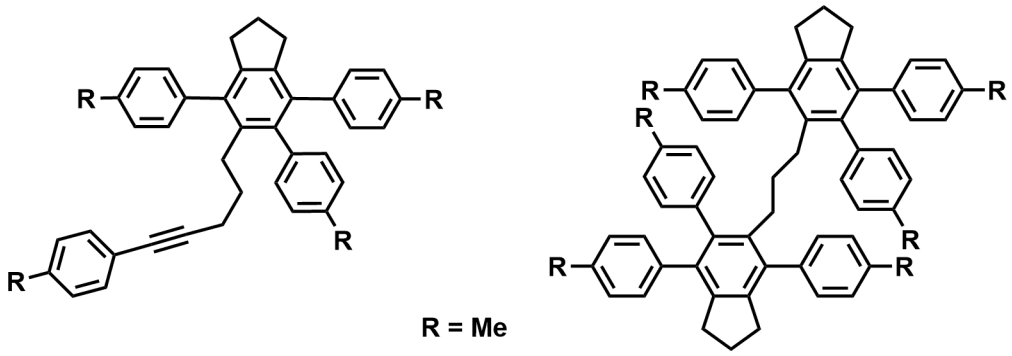

Dimer 4-12a and Trimer 4-12b.1,7-Di-*p*-tolylhepta-1,6-diyne **4-12** (1.27 g, 4.66 mmol) in toluene (15 mL) was treated with acetylacetonatobis(tri(*p*-tolyl)phosphine)rhodium(I) **1-56** (182 mg, 0.33 mmol) and stirred at 60 °C for 72 h. The solvent was removed *in vacuo* and the residue recrystallized from THF/*n*-hexane (-30 °C), whereas most of the dimer was in solution and most of the trimer precipitated. The dimer was further purified by flash column chromatography using *n*-hexane as the eluent, which gave the dimer as a colorless solid. The trimer was further purified by washing with acetone, which resulted in a colorless solid (dimer: 375 mg, 677 µmol, 30%; trimer: 478 mg, 585 µmol, 38%).

Dimer 4-12a:

^{1}H NMR (500 MHz, C_6D_6) δ = 7.29-7.25 (m, 4H), 7.21-7.19 (m, 2H), 7.09-7.07 (m, 4H), 6.88-6.86 (m, 4H), 6.83-6.81 (m, 2H), 2.88-2.85 (m, 2H), 2.83 (t, ^{3}J = 7.4 Hz, 2H), 2.76 (t, ^{3}J = 7.4 Hz, 2H), 2.15 (s, 3H), 2.00 (s, 3H), 1.95 (t, ^{3}J = 7.4 Hz, 2H and s, 3H), 1.92 (s, 3H), 1.81 (qui, 2H, ^{3}J = 7.4 Hz) and 1.77-1.71 (m, 2H) ppm.

^{13}C{^{1}H} NMR (125 MHz, C_6D_6) δ = 142.7, 140.8, 140.2, 138.84, 138.83, 138.7, 138.4, 138.2, 137.1, 137.0, 136.3, 135.6, 135.4, 131.9, 131.2, 130.1, 129.53, 129.45, 129.1, 2 x 128.68, 122.1, 89.4, 81.4, 34.0, 33.9, 31.1, 30.8, 25.4, 21.25, 21.23, 21.10, 21.07 and 20.0 ppm.

Elem. Anal. Calc. (%) for $C_{42}H_{40}$: C, 92.60; H, 7.40; found: C, 92.26; H, 7.61.

HRMS (APCI^{+}): *m/z* calc. for $[C_{42}H_{41}]^{+}$ 545.3203; found: 545.3192 $[M+H]^{+}$.

Trimer 4-12b:

^{1}H NMR (500 MHz, C_6D_6) δ = 7.07 (s, 8H), 7.01-6.99 (m, 4H), 6.97-6.95 (m, 4H), 6.85-6.82 (m, 8H), 2.72 (t, ^{3}J = 7.4 Hz, 4H), 2.67 (t, ^{3}J = 7.4 Hz, 4H), 2.31-2.27 (m, 10H, overlapping CH_3 and CH_2 group), 2.06 (s, 6H), 1.93 (s, 6H), 1.72 (qui, ^{3}J = 7.4 Hz, 4H) and 1.67-1.61 (m, 2H) ppm.

^{13}C{^{1}H} NMR (125 MHz, C_6D_6) δ = 142.4, 140.3, 139.8, 139.2, 139.0, 138.9, 138.0, 137.9, 137.8, 135.8, 135.2, 135.1, 131.2, 130.1, 129.5, 129.3, 128.6, 128.5, 33.84, 33.76, 31.6, 25.3, 21.4, 21.3 and 21.1 ppm.

Elem. Anal. Calc. (%) for $C_{63}H_{60}$: C, 92.60; H, 7.40; found: C, 92.36; H, 7.50.

HRMS (APCI^{+}): *m/z* calc. for $[C_{63}H_{61}]^{+}$ 817.4768; found: 817.4719 $[M+H]^{+}$.

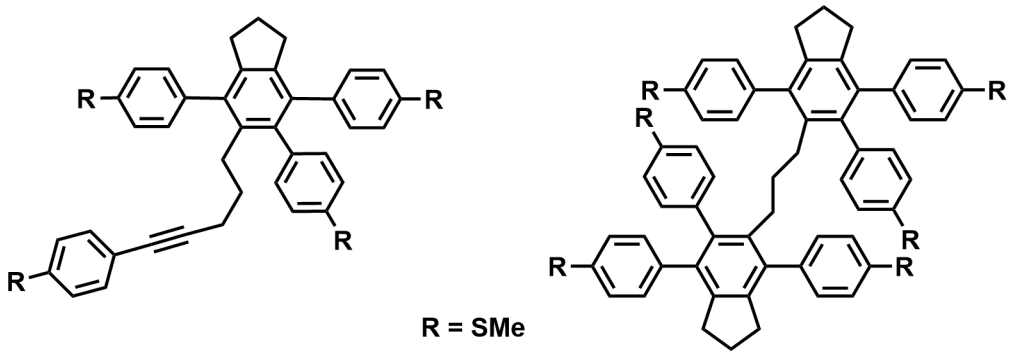

Dimer 4-13a and Trimer 4-13b. 1,7-Bis(methylthio)phenylhepta-1,6-diyne **4-13** (1.10 g, 3.30 mmol) in toluene (15 mL) was treated with acetylacetonato-bis(tri(*p*-tolyl)phosphine)rhodium(I) **1-56** (267 mg, 0.33 mmol) and stirred at 60 °C for 72 h. The solvent was removed *in vacuo* and the residue was separated by flash column chromatography using a gradient of CH_2Cl_2 in *n*-hexane (0 – 20% CH_2Cl_2) as eluent. All volatiles were removed *in vacuo.* The dimer and trimer were further purified by recrystallization from THF/MeOH resulting in colorless solids (dimer: 490 mg, 728 µmol, 44%; trimer: 440 mg, 436 µmol, 40%).

Dimer 4-13a:

^{1}H NMR (500 MHz, C_6D_6) δ = 7.25-7.20 (m, 4H), 7.17-7.15 (m, 2H, overlapping with solvent signal), 7.12-7.09 (m, 2H), 7.02-7.00 (m, 2H), 6.98-6.94 (m, 6H), 2.85-2.82 (m, 2H), 2.77 (t, 2H, ^3J = 7.4 Hz), 2.69 (t, 2H, ^3J = 7.4 Hz), 2.00 (s, 3H), 1.93 (t, ^3J = 7.0 Hz, 2H), 1.91 (s, 3H), 1.84 (s, 3H), 1.81 (s, 3H), 1.80 (qui, ^3J = 7.4 Hz, 2H) and 1.68-1.62 (m, 2H) ppm.

^{13}C{^{1}H} NMR (125 MHz, C_6D_6) δ = 143.1, 141.0, 139.6, 138.7, 138.1, 138.0, 137.9, 137.79, 137.76, 137.7, 137.2, 137.0, 136.9, 132.3, 131.7, 130.6, 130.0, 126.7, 126.4, 126.0, 125.8, 121.1, 90.0, 81.3, 33.9, 33.8, 31.0, 30.5, 25.4, 20.0, 15.2, 15.1, 15.0 and 14.9 ppm.

Elem. Anal. Calc. (%) for $C_{42}H_{40}S_4$: C, 74.95; H, 5.99; S, 19.05; found: C, 75.02; H, 6.10; S, 18.67.

HRMS (APCI$^+$): *m/z* calc. for $[C_{42}H_{41}S_4]^+$ 673.2086; found: 673.2078 $[M+H]^+$.

Trimer 4-13b:

^{1}H NMR (500 MHz, C_6D_6) δ = 7.27-7.25 (m, 4H), 7.02-7.00 (m, 8H), 6.92-6.89 (m, 12H), 2.65 (t, 4H, ^{3}J = 7.4 Hz), 2.60 (t, 4H, ^{3}J = 7.4 Hz), 2.24-2.20 (m, 4H), 2.20 (s, 6H), 1.98 (s, 6H), 1.81 (s, 6H), 1.74-1.68 (qui, 4H, ^{3}J = 7.4 Hz) and 1.58-1.51 (m, 2H) ppm.

^{13}C{^{1}H} NMR (125 MHz, C_6D_6) δ = 142.9, 140.6, 139.1, 138.3, 138.1, 138.0, 137.5, 137.4, 136.79, 136.78, 131.6, 130.6, 130.0, 126.7, 125.9, 125.8, 125.8, 125.7, 33.79, 33.77, 33.6, 31.7, 25.3, 15,4, 15.1 and 15.0 ppm.

Elem. Anal. Calc. (%) for $C_{63}H_{60}S_6$: C, 74.95; H, 5.99; S, 19.05; found: C, 74.65; H, 6.35; S, 17.97.

HRMS (APCI^{+}): *m/z* calc. for $[C_{63}H_{59}S_6]^{+}$ 1007.2936; found: 1007.2930 $[M-H]^{+}$.

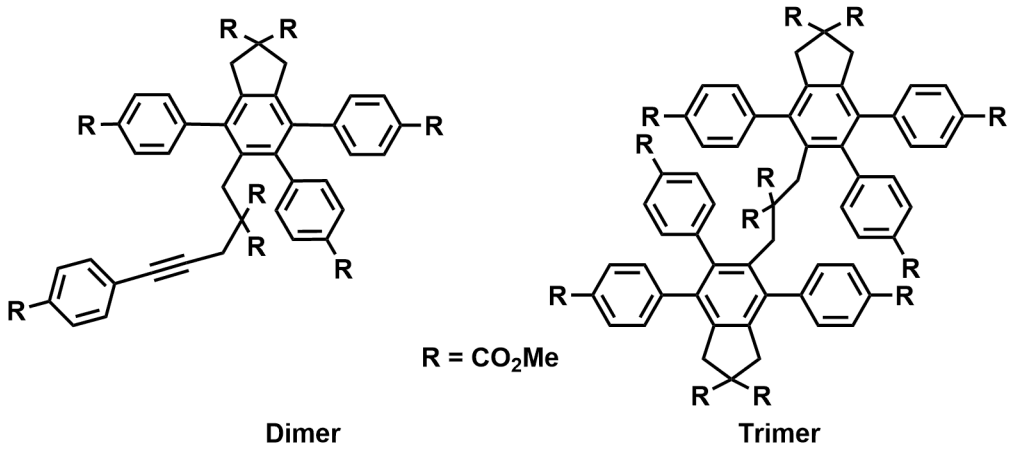

Dimer 4-14a and Trimer 4-14b. Dimethyl 2,2-bis(3-(4-(methoxycarbonyl)phenyl)prop-2-yn-1-yl)malonate **4-14** (1.00 g, 2.10 mmol) in toluene (50 mL) was treated with acetylacetonatobis(tri(*p*-tolyl)phosphine)rhodium(I) **1-56** (170 mg, 210 µmol) and stirred at 60 °C for 14 h. All volatiles were removed *in vacuo* and the residue was further purified by flash column chromatography using a gradient of THF in *n*-hexane (0 – 50% THF) as the eluent. The dimer was further purified by recrystallization from MeOH (-35 °C) resulting in a colorless solid (550 mg, 577 µmol, 55%) and the trimer was further purified by recrystallization from MeOH (-35 °C) and THF/MeOH (-35 °C) resulting in a colorless solid (300 mg, 210 µmol, 30%).

Dimer 4-14a:

^{1}H NMR (500 MHz, THF-d_8): δ = 8.14-8.12 (m, 2H), 7.89-7.86 (m, 2H), 7.81-7.79 (m, 4H), 7.51-7.49 (m, 2H), 7.24-7.05(m, 6H), 3.88 (s, 3H), 3.84 (s, 3H), 3.80 (s, 3H), 3.77 (s, 3H), 3.71 (s, 2H), 3.59 (s, 6H), 3.32-3.29 (m, 10H, overlapping CH_3 with CH_2 groups) and 2.28 (s, 2H) ppm.

^{13}C{^{1}H} NMR (125 MHz, THF-d_8): δ = 171.8, 170.0, 166.7, 166.52, 166.48, 166.3, 145.3, 145.13, 145.08, 141.9, 140.2, 139.7, 138.9, 137.8, 133.2, 132.8 (br), 132.1, 131.2 (br), 130.34, 130.29, 130.14, 130.12, 129.8, 129.6, 129.34, 129.33, 129.32, 128.7, 88.9, 82.6, 60.1, 59.2, 52.7, 52.4, 52.0, 51.9, 51.80, 51.77, 41.5, 41.3, 32.7 and 27.6 ppm.

Elem. Anal. Cal. (%) for $C_{54}H_{48}O_{16}$: C, 68.06; H, 5.08; found: C, 68.27; H, 5.56.

HRMS (APCI$^+$): *m/z* calc. for $[C_{54}H_{49}O_{16}]^+$ 953.3015; found: 953.3003 $[M+H]^+$.

Trimer 4-14b:

^{1}H NMR (500 MHz, THF-d_8): δ = 8.11-8.10 (m, 4H), 7.79-7.73 (m, 8H), 7.12-7.10 (m, 4H), 6.94 (s(br), 4H), 6.83-6.81 (m, 4H), 3.95 (s, 6H), 3.85 (s, 6H), 3.77 (s, 6H), 3.54 (s, 12H), 3.16-3.14 (m, 8H), 2.87 (s, 6H), 2.48 (s, 4H) ppm.

^{13}C{^{1}H} NMR (125 MHz, THF-d_8): δ = 171.7, 170.0, 166.8, 166.7, 166.4, 145.10, 145.08, 141.4, 139.8, 139.0, 138.0, 137.1, 134.5, 132.6, 131.0, 130.2, 130.0, 129.9, 129.5, 129.2, 129.1, 61.4, 60.1, 52.7, 52.0, 51.84, 51.77, 51.6, 41.1, 41.0 and 38.9 ppm.

Elem. Anal. Calc. (%) for $C_{81}H_{72}O_{24}$: C, 68.06; H, 5.08; found: C, 67.74; H, 5.14.

HRMS (APCI$^+$): *m/z* calc. for $[C_{81}H_{73}O_{24}]^+$ 1429.4497; found: 1429.4475 $[M+H]^+$.

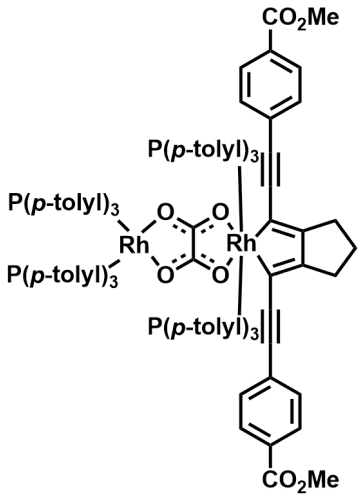

Rhodacycle 4-15. Oxalatotetra(tris(*p*-tolylphoshpine))bisrhodium(I**)** (240 mg, 159 µmol) in THF (10 mL) was treated with dimethyl 4,4'-(undeca-1,3,8,10-tetrayne-1,11-diyl)dibenzoate **1-47d** (64.9 mg, 159 µmol) and stirred at 60 °C for 3 d. The solvent was removed *in vacuo*, the product was extracted into toluene and then recrystallized from toluene/*n*-hexane (-30 °C) resulting in a dark red solid (80.0 mg, 41.7 µmol, 26%).

^{1}H NMR (500 MHz, C_6D_6): δ= 7.37-7.31 (m, 24H), 6.83-6.81 (m, 24H) and 2.25 (s, 36H) ppm.
^{31}P{^{1}H} NMR (202 MHz, C_6D_6) δ= 54.1 (d, $^{1}J_{Rh\text{-}P}$ = 201 Hz) and 26.2 (d, $^{1}J_{Rh\text{-}P}$ = 115 Hz) ppm.
Elem. Anal. Calc. (%) for $C_{113}H_{104}O_8P_4Rh_2$: C, 70.70; H, 5.46; Found: C, 70.60; H, 5.54.
HRMS(LIFDI): *m/z* calc. for $[C_{113}H_{104}O_8P_4Rh_2]^+$ 1919.4793, found: 1919.4820 $[M]^+$.

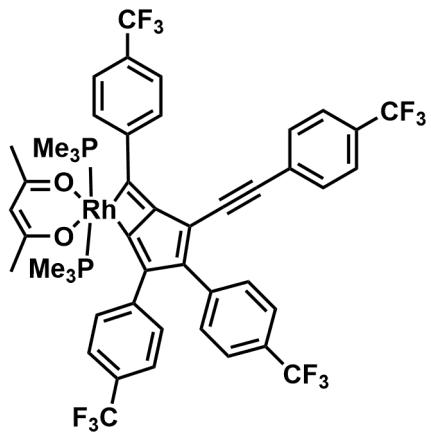

2-2a

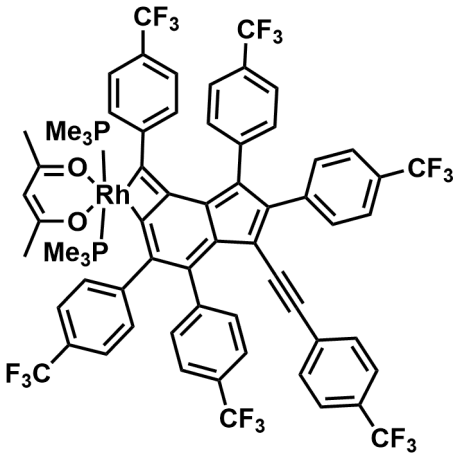

2-3a

Rhodacycles 2-2a and 2-3a. Acetylacetonatobis(trimethylphosphine)rhodium(I) **1-51** (335 mg, 956 µmol) in toluene (3 mL) was treated dropwise with 1,4-bis(4-(trifluoromethyl)phenyl)buta-1,3-diyne **2-1a** (640 mg, 1.89 mmol) in toluene (20 ml) and stirred at room temperature for 24 h. The solvent was removed *in vacuo* and the crude product was separated *via* flash column chromatography using a gradient of THF in *n*-hexane (0 – 30% THF). This led to a dark yellow solid **2-2a** (718 mg, 696 µmol, 74%) and 74 mg of a blue solid **2-3a**. The isolated complex **2-3a** was further purified by washing with *n*-hexane (3 x 2 mL) and recrystallization from THF/*n*-hexane (-30 °C). The solid obtained was dissolved in *n*-hexane and filtered through a thin pad of Celite (2 cm). The solvent was removed *in vacuo* and **2-3a** was obtained as an analytically pure, blue solid (50 mg, 36.5 µmol, 4%).

Rhodacycle 2-2a:

^{1}H NMR (500 MHz, THF-d_8): δ = 8.81-8.79 (m, 2H), 7.72-7.70 (m, 4H), 7.66-7.63 (m, 6H), 7.45-7.43 (m, 2H), 7.39-7.37 (m, 2H), 5.33 (s, 1H), 2 x 2.01 (2 x s, 6H) and 1.16 (vt, 18H, N = 6.8 Hz) ppm.

^{13}C{^{1}H} NMR (125 MHz, THF-d_8): δ = 189.0, 188.4, 161.5 (dt, $^{1}J_{Rh-C}$ = 25 Hz, $^{2}J_{P-C}$ = 10 Hz), 158.9 (m), 158.3 (td, $^{3}J_{P-C}$ = 6 Hz, $^{2}J_{Rh-C}$ = 4 Hz), 145.2 (m), 142.1 (m), 141.7 (m) 136.5, 131.7, 131.4, 130.4 (q, $^{2}J_{F-C}$ = 32 Hz), 130.3, 129.6 (q, $^{5}J_{F-C}$ = 1 Hz), 129.4 (q, $^{2}J_{F-C}$ = 32 Hz), 128.9 (q, $^{2}J_{F-C}$ = 32 Hz), 128.3, 128.0 (dt, $^{1}J_{Rh-C}$ = 27 Hz, $^{2}J_{P-C}$ = 10 Hz), 126.3 (q, $^{2}J_{F-C}$ = 32 Hz), 126.1 (q, $^{3}J_{F-C}$ = 4 Hz), 125.8 (q, $^{1}J_{F-C}$ = 271 Hz), 125.4 (2 x q, $^{1}J_{F-C}$ = 271 Hz), 125.4 (q, $^{1}J_{F-C}$ = 271 Hz), 125.4 and 125.1 (2 x q, $^{3}J_{F-C}$ = 4 Hz), 125.1 (q, $^{1}J_{F-C}$ = 271 Hz), 124.8 (q, $^{3}J_{F-C}$ = 4 Hz), 111.1 (m), 98.9, 93.9 (m), 93.0, 28.3, 28.2 and 12.4 (vtd, N = 29 Hz) ppm.

^{19}F NMR (470 MHz, THF-d_8): δ = -62.7, -62.9, -63.3 and -63.4 ppm.

^{31}P{^{1}H} NMR (202 MHz, THF-d_8): δ = 1.1 (d, $^{1}J_{Rh-P}$ = 109 Hz) ppm.

HRMS (LIFDI): *m*/*z* calc. for $[C_{47}H_{41}F_{12}O_2P_2Rh]^+$ 1030.1440; found: 1030.1418 $[M]^+$.

Rhodacycle 2-3a:

^{1}H NMR (500 MHz, THF-d_8): δ = 7.56-7.53 (m, 4H), 7.49-7.48 (m, 2H), 7.40-7.34 (m, 8H), 7.20-7.10 (m, 2H), 7.09-7.07 (m, 2H), 7.03-7.01 (m, 2H), 6.92-6.91 (m, 2H), 6.71-6.69 (m, 2H), 5.09 (s, 1H), 1.88 (s, 3H), 1.51 (s, 3H) and 1.15 (vt, 18H, N = 6.8 Hz) ppm.

^{13}C{^{1}H} NMR (125 MHz, THF-d_8): δ = 189.3, 188.2, 177.2 (dt, $^1J_{Rh\text{-}C}$ = 23 Hz, $^2J_{P\text{-}C}$ = 11 Hz), 152.3 (m), 149.9 (dt, $^1J_{Rh\text{-}C}$ = 24 Hz, $^2J_{P\text{-}C}$ = 9 Hz) 147.3 (m), 146.9 (m), 146.7, 145.9 (m), 143.6 (m), 143.8 (m), 141.9 (q, $^5J_{F\text{-}C}$ = 1 Hz), 134.12, 134.07, 132.7, 131.9, 131.8, 131.1, 130.1 (q, $^2J_{F\text{-}C}$ = 32 Hz), 129.8 (q, $^2J_{F\text{-}C}$ = 32 Hz), 129.6, 129.4 (q, $^5J_{F\text{-}C}$ = 1 Hz), 129.1, 128.7 (q, $^2J_{F\text{-}C}$ = 32 Hz), 128.3 (q, $^2J_{F\text{-}C}$ = 32 Hz), 128.1 (q, $^2J_{F\text{-}C}$ = 32 Hz), 128.0 (q, $^2J_{F\text{-}C}$ = 32 Hz), 126.3, 125.5 (q, $^1J_{F\text{-}C}$ = 271 Hz), 125.4 (q, $^1J_{F\text{-}C}$ = 271 Hz), 125.2 (q, $^1J_{F\text{-}C}$ = 271 Hz), 125.1 (q, $^1J_{F\text{-}C}$ = 271 Hz), 125.0 (q, $^1J_{F\text{-}C}$ = 271 Hz), 124.9 (q, $^1J_{F\text{-}C}$ = 271 Hz), 125.3 (q, $^3J_{F\text{-}C}$ = 4 Hz), 125.0 (q, $^3J_{F\text{-}C}$ = 4 Hz), 124.8 (q, 2C, $^3J_{F\text{-}C}$ = 4 Hz), 124.3 (q, $^3J_{F\text{-}C}$ = 4Hz), 123.9 (q, $^3J_{F\text{-}C}$ = 4 Hz), 108.2, 98.8, 94.8, 93.4, 28.1, 27.4 and 12.4 (vtd, N = 29 Hz) ppm.

^{19}F NMR (470 MHz, THF-d_8): δ = -62.9 (q, $^{ts}J_{F\text{-}F}$ = 3.7 Hz), -62.9, -63.0, -63.1, -63.4 (q, $^{ts}J_{F\text{-}F}$ = 3.7 Hz) and -63.5 ppm. ts = through space.

^{31}P{^{1}H} NMR (202 MHz, THF-d_8): δ = 0.50 (d, $^1J_{Rh\text{-}P}$ = 111 Hz) ppm.

Elem. Anal. Calc. (%) for $C_{65}H_{49}F_{18}O_2P_2Rh$: C, 57.03; H, 3.61; found: C, 56.78; H, 3.26.

HRMS (LIFDI): *m*/*z* calc. for $[C_{65}H_{49}F_{18}O_2P_2Rh]^+$ 1368.1970; found: 1368.1952 $[M]^+$.

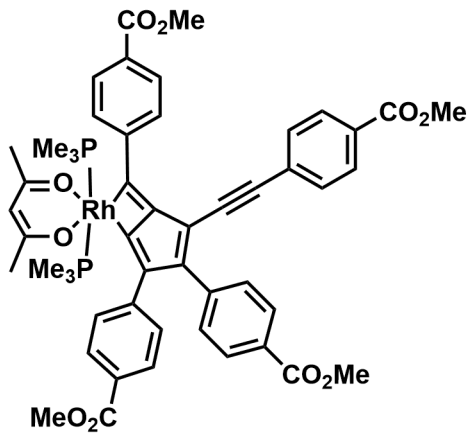

2-2b

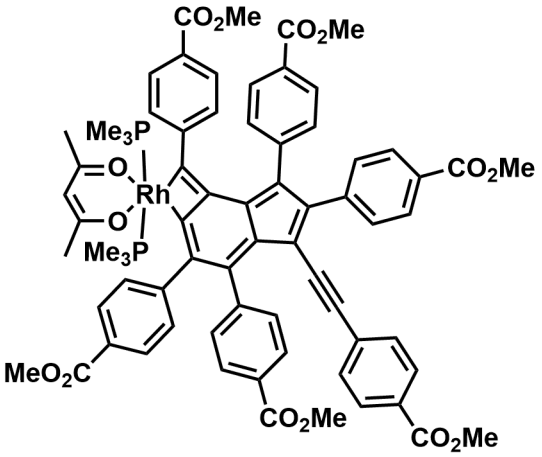

2-3b

Rhodacycles 2-2b and 2-3b. Acetylacetonatobis(trimethylphosphine)rhodium(I) **1-51** (300 mg, 847 µmol) in toluene (6 mL) was dropwise treated with dimethyl 4,4'-(buta-1,3-diyne-1,4-diyl)dibenzoate **2-1b** (566 mg, 1.78 mmol) in toluene (30 ml) and stirred at room temperature for 24 h. The solvent was removed *in vacuo* and the crude product was separated *via* flash column chromatography using a gradient of THF in *n*-hexane (0 – 50% THF) resulting in **2-2b** as a dark yellow solid (421 mg, 425 µmol, 51%) and **2-3b** as a blue/green solid (90 mg, 69 µmol, 8%).

Rhodacycles 2-2b:

^{1}H NMR (300 MHz, THF-d_8): δ = 8.74-8.70 (m, 2H), 8.05-8.01 (m, 4H), 7.98-7.94 (m, 2H), 7.74-7.70 (m, 2H), 7.56-7.51 (m, 4H), 7.39-7-35 (m, 2H), 5.30 (s, 1H), 3.89 (s, 3H), 3.88 (s, 3H), 3.85 (s, 3H), 3.78 (s, 3H), 2 x 2.00 (s, 3H) and 1.14 (vt, 18H, N = 6.8 Hz) ppm.

^{13}C{^{1}H} NMR (75 MHz, THF-d_8): δ= 188.9, 188.3, 167.0, 166.8, 166.7, 166.4, 161.8 (dt, $^{1}J_{Rh-C}$ = 26 Hz, $^{2}J_{P-C}$ = 11 Hz), 159.0 (m), 158.6 (m), 145.9 (m), 143.1, 142.5 (m), 142.1, 137.3, 131.3, 130.6, 130.4, 130.1, 129.9, 129.6, 129.5, 129.3, 129.2, 129.0, 128.4 (m), 128.0, 126.5, 111.1 (m), 98.8, 94.7, 94.0, 52.0, 51.9, 51.8, 51.4, 28.3, 28.2 and 12.5 (vtd, N_{P-C} = 29 Hz) ppm.

^{31}P{^{1}H} NMR (121 MHz, THF-d_8): δ= 1.09 (d, $^{1}J_{Rh-P}$ = 109 Hz) ppm.

Elem. Anal. Calc. (%) for $C_{51}H_{53}O_{10}P_2Rh$: C, 61.82; H, 5.39; found: C, 61.81; H, 5.71.

HRMS (LIFDI): *m/z* calc. for $[C_{51}H_{53}O_{10}P_2Rh]^+$ 990.2164; found: 990.2156 $[M]^+$.

Rhodacycle 2-3b:

^{1}H NMR (500 MHz, THF-d_8): δ = 7.85-7.83 (m, 4H), 7.74-7.72 (m, 2H), 7.65-7.63 (m, 2H), 7.41-7.39 (m, 2H), 7.34-7.32 (m, 2H), 7.30-7.28 (m, 2H), 7.20-7.17 (m, 4H), 7.05-7.03 (m, 2H), 6.67-6.62 (m, 4H), 5.07 (s, 1H), 3.81 (s, 6H), 3.80 (s, 3H), 3.79 (s, 3H), 3.77 (s, 3H), 3.74 (s, 3H), 1.85 (s, 3H), 1.51 (s, 3H) and 1.14 (vt, 18H, N = 6.7 Hz) ppm.

^{13}C{^{1}H} NMR (125 MHz, THF-d_8): δ = 188.4, 187.3, 176.9 (m), 166.1, 166.0, 165.9, 165.73, 165.71, 165.6, 151.6 (m), 148.8 (m), 147.5 (m), 146.90, 146,88, 146.1, 146.0 (m), 144.0, 143.7, 142.0, 133.6, 133.5, 131.5, 130.7, 130.5, 130.1, 129.6, 129.4, 128.6, 128.5, 128.3, 128.2, 128.12, 128.07, 127.9, 127.8, 127.4, 127.2, 127.1, 127.0, 126.6, 126.2 (m), 125.1 (m), 107.5, 97.8, 94.6, 93.6, 51.02, 50.96, 50.94, 50.86, 50.8, 50.7, 27.3, 26.7 and 11.6 (vtd, $N_{P\text{-}C}$ = 28 Hz) ppm.

^{31}P{^{1}H} NMR (202 MHz, THF-d_8): δ = 0.55 (d, $^{1}J_{Rh\text{-}P}$ = 112 Hz) ppm.

Elem. Anal. Calc. (%) for $C_{71}H_{67}O_{14}P_2Rh$: C, 65.14; H, 5.16; found: C, 64.81; H, 5.18.

HRMS (LIFDI): m/z calc. for $[C_{71}H_{67}O_{14}P_2Rh]^+$ 1308.3056; found: 1308.3064 $[M]^+$.

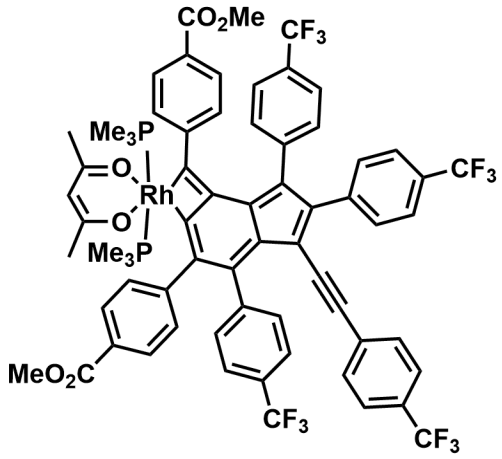

Rhodacycle 2-3c. Complex **2-2a** (580 mg, 563 µmol) and dimethyl 4,4'-(buta-1,3-diyne-1,4-diyl)dibenzoate **2-1b** (896 mg, 2.81 mmol) in toluene (30 mL) were stirred at 100 °C for 14 d. The solvent was removed *in vacuo* and the crude product separated *via* flash column chromatography using a gradient of THF in *n*-hexane (0 – 15% THF) resulted in **2-3c** as a green solid (105 mg, 76.4 µmol, 14%) and a mixture of **2-SYM^{CO2Me}** and **2-UNSYM^{CO2Me}** as an orange solid (17 mg).

^{1}H NMR (500 MHz, THF-d$_8$): δ = 7.75-7.74 (m, 2H), 7.56-7.49 (m, 6H), 7.41-7.39 (m, 4H), 7.35-7.33 (m, 2H), 7.19-7.17 (m, 2H), 7.13-7.12 (m, 2H), 6.94-6.93(m, 2H), 6.83-6.81 (m, 2H), 6.72-6.70 (m, 2H), 5.07 (s, 1H), 3.80 (s, 3H), 3.78 (s, 3H), 1.86 (s, 3H), 1.50 (s, 3H) and 1.14 (vt, 18H, N = 7 Hz) ppm.

^{13}C{^{1}H} NMR (125 MHz, THF-d$_8$): δ = 189.3, 188.1, 176.3 (dt, $^{1}J_{Rh-C}$ = 23 Hz, $^{2}J_{P-C}$ = 10 Hz), 166.9, 166.3, 152.5 (m), 150.0 (dt, $^{1}J_{Rh-C}$ = 25 Hz, $^{2}J_{P-C}$ = 10 Hz), 147.9 (m), 147.2 (m), 146.7, 146.5, 144.1 (m), 143.6, 142.1 (m), 134.6, 134.1, 132.3, 132.0, 131.9, 131.1, 129.9, 129.7 (q, $^{2}J_{F-C}$ = 32 Hz), 129.5, 128.7, 128.6 (q, $^{2}J_{F-C}$ = 32 Hz), 128.4, 128.2 (m), 128.1, 128.0, 127.8 (q, $^{2}J_{F-C}$ = 32Hz), 126.0 (m), 125.9 (m), 125.5 (q, $^{1}J_{F-C}$ = 271 Hz), 125.29 (q, $^{1}J_{F-C}$ = 271 Hz), 125.26 (q, $^{3}J_{F-C}$ = 4 Hz), 125.2 (q, $^{1}J_{F-C}$ = 271 Hz), 125.1 (q, $^{1}J_{F-C}$ = 271 Hz), 124.78 (q, $^{3}J_{F-C}$ = 4 Hz), 124.75 (q, $^{3}J_{F-C}$ = 4 Hz), 107.8, 98.7, 94.7, 93.6, 51.7, 51.6, 28.0, 27.4 and 12.3 (vtd, N_{P-C} = 28 Hz) ppm.

^{19}F NMR (470 MHz, THF-d$_8$): δ = -62.7, -62.9, -62.9, -63.5 ppm.

^{31}P{^{1}H} NMR (202 MHz, THF-d$_8$): δ = 0.55 (d, $^{1}J_{Rh-P}$ = 112 Hz) ppm.

Elem. Anal. Calc. (%) for $C_{67}H_{55}F_{12}O_6P_2Rh$: C, 59.65; H, 4.11; found: C, 60.39; H, 4.32.

HRMS (LIFDI): *m*/*z* calc. for $[C_{67}H_{55}F_{12}O_6P_2Rh]^+$ 1348.2332; found: 1348.2322 $[M]^+$.

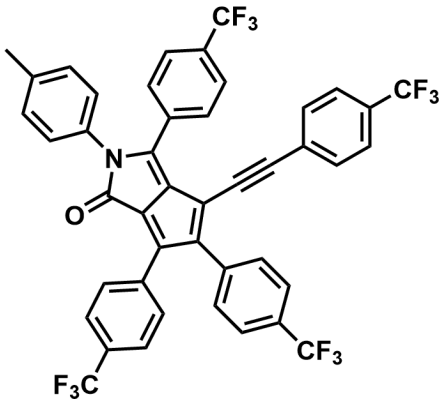

2-(*p*-Tolyl)-3,5,6-tris(4-(trifluoromethyl)phenyl)-4-((4-(trifluoromethyl)phenyl)ethynyl)-cyclopenta[c]pyrrol-1(2H)-one 2-5. Complex **2-2a** (350 mg, 339 µmol) in toluene (20 mL) was treated with degassed *para*-tolyl isocyanate **2-4** (181 mg, 1.36 mmol) and stirred at 80 °C for 3 d. After cooling to room temperature, all volatiles were removed *in vacuo*, and the crude product was separated *via* flash column chromatography using a gradient of CH_2Cl_2 in *n*-hexane (0 – 20% CH_2Cl_2). Removing the solvent *in vacuo*, washing with *n*-hexane (3 x 2 mL) and recrystallization from THF/*n*-hexane (-30 °C) resulted in a purple solid (35 mg, 43 µmol, 13%).

^{1}H NMR (500 MHz, C_6D_6): δ= 7.69-7.67 (m, 2H), 7.42-7.34 (m, 6H), 7.27-7.25 (m, 2H), 7.19-7.17 (m, 2H, overlapping with C_6D_6), 7.10-7.08 (m, 2H), 6.89-6.88 (m, 2H), 6.82-6.80 (m, 2H), 6.77-6.75 (m, 2H) and 1.95 (s, 3H) ppm.

^{13}C{^{1}H} NMR (125 MHz, C_6D_6): δ= 163.1, 156.1, 146.7, 145.2, 138.9 (q, $^5J_{F\text{-}C}$ = 1 Hz), 138.3, 136.1 (q, $^5J_{F\text{-}C}$ = 1 Hz), 133.2 (q, $^2J_{F\text{-}C}$ = 32 Hz), 131.9, 131.6, 131.3 (q, $^2J_{F\text{-}C}$ = 32 Hz), 131.20 (m), 131.16, 130.7 (q, $^2J_{F\text{-}C}$ = 32 Hz), 130.5, 130.1 (q, $^2J_{F\text{-}C}$ = 32 Hz), 130.0, 127.6, 126.5 (q, $^5J_{F\text{-}C}$ = 1 Hz), 125.7 (q, $^3J_{F\text{-}C}$ = 4 Hz), 125.5 (m), 125.3 (q, $^3J_{F\text{-}C}$ = 4 Hz), 124.9 (q, $^1J_{F\text{-}C}$ = 272 Hz), 124.6 (q, $^1J_{F\text{-}C}$ = 272 Hz), 124.4 (q, $^1J_{F\text{-}C}$ = 272 Hz), 124.0 (q, $^1J_{F\text{-}C}$ = 272 Hz), 122.3, 116.9, 96.4, 88.4 and 20.9 ppm.

^{19}F NMR (470 MHz, C_6D_6): δ= -62.1, -62.5, -62.7 and -63.1 ppm.

Elem. Anal. Calc. (%) for $C_{44}H_{23}F_{12}NO$: C, 65.27; H, 2.86; N, 1.73; found: C, 65.47; H, 2.95; N, 1.72.

HRMS (LIFDI): *m*/*z* calc. for $[C_{44}H_{23}F_{12}NO]^+$ 809.1583; found: 809.1572 $[M]^+$.

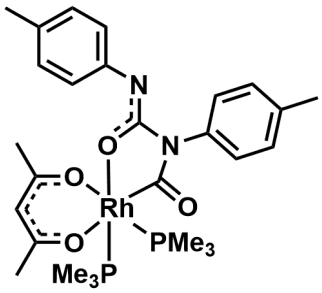

Rhodacycle 2-10a. Acetylacetonatobis(trimethylphosphine)rhodium(I) **1-51** (400 mg, 1.13 mmol) in THF (20 mL) was treated with degassed *para*-tolyl isocyanate **2-4** (301 mg, 2.26 mmol) and stirred at 50 °C for 24 h. The color of the mixture changed from yellow to pale yellow during the reaction. Removing all volatiles *in vacuo*, recrystallization from THF/*n*-hexane (-30 °C) and washing with cold mixtures of THF/*n*-hexane 1:3 (1 mL x 9) and toluene/*n*-hexane 1:2 (1 mL x 7) resulted in a colorless solid (250 mg, 403 µmol, 36%).

^{1}H NMR (300 MHz, C_6D_6): δ = 7.78-7.75 (m, 2H), 7.54-7.51 (m, 2H), 7.09-7.08 (m, 4H), 5.20 (s, 1H), 2.17 (s, 3H), 2.11 (s, 3H), 1.87 (s, 3H), 1.79 (s, 3H), 1.03 (m, 9H) and 0.93 (m, 9H) ppm.

^{13}C{^{1}H} NMR (75 MHz, C_6D_6): δ = 188.4, 187.2 (m), 160.91, 160.86, 149.4, 139.2, 135.6, 130.0, 129.0, 128.8, 128.7, 125.1, 98.9 (m), 28.6, 28.5 (m), 21.2, 21.1, 13.7 (m) and 13.4 (m) ppm.

^{31}P{^{1}H} NMR (121 MHz, C_6D_6): δ = 15.8 (dd, $^{1}J_{Rh\text{-}P}$ = 136 Hz, $^{2}J_{P\text{-}P}$ = 40 Hz), 12.3 (dd, $^{1}J_{Rh\text{-}P}$ = 143 Hz, $^{2}J_{P\text{-}P}$ = 40 Hz) ppm.

Elem. Anal. Calc. (%) for $C_{27}H_{39}N_2O_4P_2Rh$ x THF: C, 53.76; H, 6.84; N, 4.04; found: C, 53.26; H, 6.80; N, 3.99.

HRMS (LIFDI): *m/z* calc. for $[C_{27}H_{39}N_2O_4P_2Rh]^+$ 620.1435; found: 620.1426 $[M]^+$.

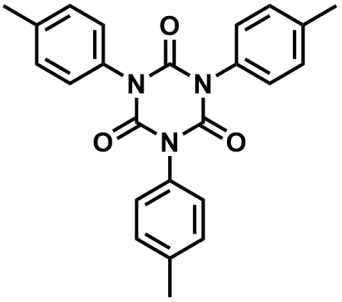

1,3,5-Tris(*p*-tolyl)-1,3,5-triazine-2,4,6-trione 2-8. *para*-Tolylisocyanate **2-4** (100 mg, 751 µmol) in C_6D_6 (0.7 mL) in a J. Young's tap NMR tube was treated with PMe_3 (2.86 mg, 37.6 µmol) and allowed to rest at room temperature for 24 h. During this time, the product precipitated. The suspension was filtered, and the residue was washed with *n*-pentane (3 mL x 3) and recrystallized from THF/*n*-pentane, which resulted in a colorless solid (45 mg, 113 µmol, 45%).

^{1}H NMR (300MHz, $CDCl_3$): δ = 7.27-7.26 (m, 12H) and 2.39 (s, 9H) ppm.

^{1}H NMR (200MHz, C_6D_6): δ = 7.20-6.92 (m, 12H) and 2.00 (s, 9H) ppm.

^{13}C{^{1}H} NMR (75 MHz, $CDCl_3$): δ = 149.0, 139.4, 131.2, 130.1, 128.2 and 21.4 ppm.

HRMS (LIFDI): *m/z* calc. for $[C_{24}H_{21}N_3O_3]^+$ 399.1577; found: 399.1574 $[M]^+$.

The data are consistent with those in the literature.[343]

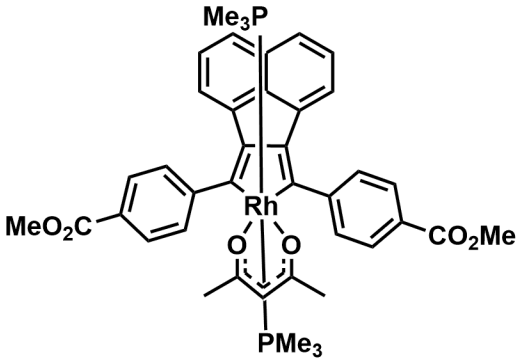

Rhodacycle 3-6. Dimethyl 4,4'-(naphthalene-1,8-diylbis(ethyne-2,1-diyl))dibenzoate **3-1** (197 mg, 443 µmol) and acetylacetonatobis(trimethylphosphine)rhodium(I) **1-51** (160 mg, 452 µmol) were dissolved in toluene (20 mL) and stirred at 60 °C for 24 h. Removing the solvent *in vacuo*, washing the orange residue with *n*-hexane (4 mL x 3) and recrystallization from THF/*n*-hexane (-35 °C) resulted in an orange solid (166 mg, 208 µmol, 47%).

^{1}H NMR (500 MHz, THF-d_8): δ = 7.98-7.96 (m, 4H), 7.75-7.72 (m, 4H), 7.36-7.35 (m, 2H), 7.19-7.18 (m, 2H), 7.10-7.07 (m, 2H), 5.18 (s, 1H), 3.87 (s, 6H), 1.77 (m, 6H; overlapping with THF-d_8 signal) and 1.09 (vt, 18H, N = 7 Hz) ppm.

^{1}H NMR (500 MHz, C_6D_6): δ = 8.37-8.33 (m, 4H), 7.86-7.82 (m, 4H), 7.68-7.65 (m, 2H), 7.47-7.44 (m, 2H), 7.24-7.19 (m, 2H), 4.89 (s, 1H), 3.60 (s, 6H), 1.55 (s, 6H) and 0.75 (vt, 18H, N = 7 Hz) ppm.

^{13}C{^{1}H} NMR (125 MHz, THF-d_8) δ = 187.7, 167.2, 162.1 (dt, $^{1}J_{Rh-C}$ = 32 Hz, $^{2}J_{P-C}$ = 11 Hz), 154.7 (m), 152.0 (m), 143.0 (m), 136.5 (m), 133.8, 129.6, 129.1, 127.7, 127.5, 122.6, 115.7, 99.1, 51.6, 28.1 and 12.4 (vtd, N = 29 Hz) ppm.

^{31}P{^{1}H} NMR (202 MHz, THF-d_8) δ = -2.6 (d, $^{1}J_{Rh-P}$ = 113 Hz) ppm.

^{31}P{^{1}H} NMR (202 MHz, C_6D_6) δ = -3.4 (d, $^{1}J_{Rh-P}$ = 113 Hz) ppm.

Elem. Anal. Calc. (%) for $C_{41}H_{45}O_6P_2Rh$ x 2 THF: C, 62.42; H, 6.52; found: C, 62.74; H, 6.40.

HRMS (LIFDI): *m/z* calc. for $[C_{41}H_{45}O_6P_2Rh]^+$ 798.1741; found: 798.1731 $[M]^+$.

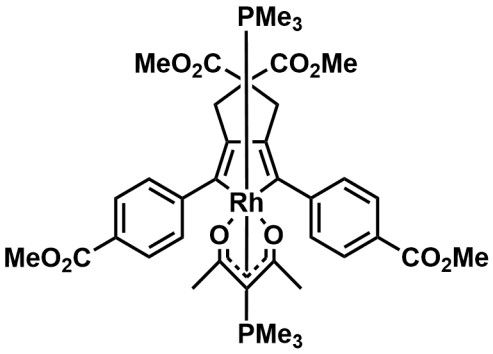

Rhodacycle 3-7. Dimethyl-2,2-bis(3-(4-(methoxycarbonyl)phenyl)prop-2-yn-1-yl)malonate **3-2** (197 mg, 414 µmol) and acetylacetonatobis(trimethylphosphine)rhodium(I) **1-51** (152 mg, 429 µmol) in toluene (10 mL) were stirred at 60 °C for 24 h. Removing the solvent *in vacuo*, washing the orange residue washed with *n*-hexane (1 mL x 3), recrystallization from THF/*n*-hexane (-35 °C) and washing with a mixture of THF/*n*-hexane (3:7) resulted in an orange solid (240 mg, 289 µmol, 70%).

^{1}H NMR (300 MHz, C_6D_6): δ = 8.27-8.25 (m, 4H), 7.63-7.60 (m, 4H), 4.95 (s, 1H), 3.56 (s, 6H), 3.54-3.52 (m, 4H), 3.33 (s, 6H), 1.60 (s, 6H) and 0.80 (vt, 18H, N = 7 Hz) ppm.

^{13}C{^{1}H} NMR (75 MHz, C_6D_6) δ = 186.8, 172.6, 167.3, 153.7 (m), 151.9 ($^{1}J_{Rh\text{-}C}$ = 33 Hz, $^{2}J_{P\text{-}C}$ = 11 Hz), 151.8 (m), 129.2, 129.0, 126.5, 98.6, 64.0, 52.2, 51.4, 37.6, 28.2 and 12.3 (vtd, N = 29 Hz) ppm.

^{31}P{^{1}H} NMR (121 MHz, C_6D_6) δ = -2.9 (d, $^{1}J_{Rh\text{-}P}$ = 113 Hz) ppm.

Elem. Anal. Calc. (%) for $C_{38}H_{49}O_{10}P_2Rh$: C, 54.95; H, 5.95; found: C, 55.30; H, 6.01.

HRMS (LIFDI): *m/z* calc. for $[C_{38}H_{49}O_{10}P_2Rh]^+$ 830.1851; found: 830.1844 $[M]^+$.

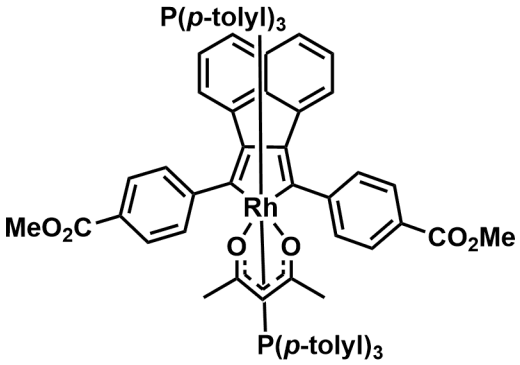

Rhodacycle 3-15. Dimethyl 4,4'-(naphthalene-1,8-diylbis(ethyne-2,1-diyl))dibenzoate **3-1** (124 mg, 278 µmol) and acetylacetonatobis(tri(*p*-tolyl)phosphine)rhodium(I) **1-56** (230 mg, 284 µmol) were dissolved in toluene (15 mL) and stirred for 2 d at 60 °C. Removing the solvent *in vacuo*, washing the residue with *n*-hexane (4 mL x 3) and recrystallization from THF/*n*-hexane (-35 °C) resulted in an orange-red solid (267 mg, 213 µmol, 77%).

^{1}H NMR (300 MHz, THF-d_8): δ = 7.58-7.56 (m, 4H), 7.29-7.23 (m, 2H), 7.08-6.99 (m, 20H), 6.67-6.64 (m, 12H), 5.07 (s, 1H), 3.88 (s, 6H), 2.05 (s, 18H) and 1.51 (s, 6H) ppm.

^{1}H NMR (300 MHz, C_6D_6): δ = 8.19-8.16 (m, 4H), 7.54-7.51 (m, 4H), 7.46-7.31 (m, 16H), 7.08-7.03 (m, 2H), 6.65-6.62 (m, 12H), 5.15 (s, 1H), 3.61 (s, 6H), 1.79 (s, 18H) and 1.64 (s, 6H) ppm.

^{13}C{^{1}H} NMR (75 MHz, THF-d_8) δ = 187.7, 167.4, 161.0 (dt, $^{1}J_{Rh\text{-}C}$ = 29 Hz, $^{2}J_{P\text{-}C}$ = 10 Hz), 157.6 (m), 152.2, 142.7, 140.0, 136.6 (m), 135.6 (m), 133.2, 130.5, 128.5, 128.2 (m), 128.1 (m), 127.3, 126.8, 122.2, 115.4, 101.0, 51.5, 29.0 and 20.9 ppm.

^{13}C{^{1}H} NMR (75 MHz, C_6D_6) δ = 187.4, 167.5, 160.6 (dt, $^{1}J_{Rh\text{-}C}$ = 29 Hz, $^{2}J_{P\text{-}C}$ = 11 Hz), 157.7 (m), 152.3, 142.6, 139.9, 136.4 (m), 135.5 (m), 132.9, 130.7, 128.7, 128.2 (m), 128.1 (m), 127.5, 127.1, 122.3, 115.4, 101.1, 51.4, 29.2 and 20.9 ppm.

^{31}P{^{1}H} NMR (121 MHz, C_6D_6) δ = 19.8 (d, $^{1}J_{Rh\text{-}P}$ = 117 Hz) ppm.

Elem. Anal. Calc. (%) for $C_{77}H_{69}O_6P_2Rh$: C, 73.68; H, 5.54; found: C, 73.95; H, 5.79.

HRMS (LIFDI): *m/z* calc. for $[C_{77}H_{69}O_6P_2Rh]^+$ 1254.3619; found: 1254.3616 $[M]^+$.

8 References

[1] V. Prautzsch, S. Ibach, *J. Incl. Phenom. Macrocycl. Chem.* **1999**, *33*, 427-458.
[2] IUPAC, *IUPAC - Compendium of Chemical Terminology*, Blackwell Scientific Publications, Oxford, **1997**.
[3] I. Halduc, *J. Struct. Chem.* **1961**, *2*, 350-358.
[4] U. Rosenthal, V. V. Burlakov, M. A. Bach, T. Beweries, *Chem. Soc. Rev.* **2007**, *36*, 719-728.
[5] B. J. Frogley, L. J. Wright, *Chem. Eur. J.* **2018**, *24*, 2025-2038.
[6] Y. Chauvin, *Angew. Chem. Int. Ed.* **2006**, *45*, 3740-3747.
[7] G. Zi, *Chem. Commun.* **2018**, *54*, 7412-7430.
[8] W. Ma, C. Yu, T. Chen, L. Xu, W.-X. Zhang, Z. Xi, *Chem. Soc. Rev.* **2017**, *46*, 1160-1192.
[9] J. P. Collman, J. W. Kang, *J. Am. Chem. Soc.* **1967**, *89*, 844-851.
[10] E. O. Greaves, C. J. L. Lock, P. M. Maitlis, *Can. J. Chem.* **1968**, *46*, 3879-3891.
[11] P. J. Low, M. I. Bruce, in *Advances in Organometallic Chemistry, Vol. 48* (Eds.: R. West, A. F. Hill), Academic Press, **2001**, p. 71-288.
[12] U. Rosenthal, V. V. Burlakov, P. Arndt, W. Baumann, A. Spannenberg, *Organometallics* **2003**, *22*, 884-900.
[13] U. Rosenthal, V. V. Burlakov, P. Arndt, W. Baumann, A. Spannenberg, *Organometallics* **2005**, *24*, 456-471.
[14] C. P. Casey, J. T. Brady, T. M. Boller, F. Weinhold, R. K. Hayashi, *J. Am. Chem. Soc.* **1998**, *120*, 12500-12511.
[15] J. Wolf, H. Werner, *Organometallics* **1987**, *6*, 1164-1169.
[16] T. Rappert, O. Nuernberg, H. Werner, *Organometallics* **1993**, *12*, 1359-1364.
[17] H. Werner, O. Gevert, P. Steinert, J. Wolf, *Organometallics* **1995**, *14*, 1786-1791.
[18] H. Werner, M. Schäfer, J. Wolf, K. Peters, H. G. von Schnering, *Angew. Chem. Int. Ed.* **1995**, *34*, 191-194.
[19] H. Werner, O. Gevert, P. Haquette, *Organometallics* **1997**, *16*, 803-806.
[20] H. Werner, R. W. Lass, O. Gevert, J. Wolf, *Organometallics* **1997**, *16*, 4077-4088.
[21] R. M. Ward, A. S. Batsanov, J. A. K. Howard, T. B. Marder, *Inorg. Chim. Acta* **2006**, *359*, 3671-3676.
[22] G. M. Lee, A. S. C. Leung, D. J. Harrison, I. Korobkov, R. P. Hughes, R. T. Baker, *Organometallics* **2017**, *36*, 2853-2860.
[23] F. N. Tebbe, R. L. Harlow, *J. Am. Chem. Soc.* **1980**, *102*, 6149-6151.
[24] R. J. McKinney, T. H. Tulip, D. L. Thorn, T. S. Coolbaugh, F. N. Tebbe, *J. Am. Chem. Soc.* **1981**, *103*, 5584-5586.
[25] Y.-C. Cheng, Y.-K. Chen, T.-M. Huang, C.-I. Yu, G.-H. Lee, Y. Wang, J.-T. Chen, *Organometallics* **1998**, *17*, 2953-2957.
[26] R. C. Hemond, R. P. Hughes, D. J. Robinson, A. L. Rheingold, *Organometallics* **1988**, *7*, 2239-2241.
[27] R. P. Hughes, M. E. King, D. J. Robinson, J. M. Spotts, *J. Am. Chem. Soc.* **1989**, *111*, 8919-8920.
[28] C. P. Casey, C. S. Yi, *J. Am. Chem. Soc.* **1992**, *114*, 6597-6598.
[29] C. P. Casey, J. R. Nash, C. S. Yi, A. D. Selmeczy, S. Chung, D. R. Powell, R. K. Hayashi, *J. Am. Chem. Soc.* **1998**, *120*, 722-733.
[30] J. M. O'Connor, H. L. Ji, A. L. Rheingold, *J. Am. Chem. Soc.* **1993**, *115*, 9846-9847.
[31] E. J. Derrah, R. McDonald, L. Rosenberg, *Chem. Commun.* **2010**, *46*, 4592-4594.
[32] C. Bianchini, C. Mealli, A. Meli, M. Sabat, *Organometallics* **1985**, *4*, 421-422.
[33] E. T. Knight, L. K. Myers, M. E. Thompson, *Organometallics* **1992**, *11*, 3691-3696.

[34] M. Westerhausen, M. H. Digeser, C. Gückel, H. Nöth, J. Knizek, W. Ponikwar, *Organometallics* **1999**, *18*, 2491-2496.
[35] D. J. Sikora, M. D. Rausch, R. D. Rogers, J. L. Atwood, *J. Am. Chem. Soc.* **1979**, *101*, 5079-5081.
[36] H. tom Dieck, C. Munz, C. Müller, *J. Organomet. Chem.* **1990**, *384*, 243-255.
[37] H. Suzuki, K. Itoh, Y. Ishii, K. Simon, J. A. Ibers, *J. Am. Chem. Soc.* **1976**, *98*, 8494-8500.
[38] J. P. Collman, J. W. Kang, W. F. Little, M. F. Sullivan, *Inorg. Chem.* **1968**, *7*, 1298-1303.
[39] C. S. Yi, J. R. Torres-Lubian, N. Liu, A. L. Rheingold, I. A. Guzei, *Organometallics* **1998**, *17*, 1257-1259.
[40] L. J. Canoira, J. L. Davidson, G. Douglas, K. W. Muir, *J. Organomet. Chem.* **1989**, *362*, 135-146.
[41] T. V. Harris, J. W. Rathke, E. L. Muetterties, *J. Am. Chem. Soc.* **1978**, *100*, 6966-6977.
[42] R. Usón, J. Vicente, M. T. Chicote, P. G. Jones, G. M. Sheldrick, *J. Chem. Soc., Dalton Trans.* **1983**, 1131-1136.
[43] C. Bianchini, A. Meli, M. Peruzzini, A. Vacca, F. Vizza, *Organometallics* **1991**, *10*, 645-651.
[44] Y. Wakatsuki, T. Kuramitsu, H. Yamazaki, *Tetrahedron Lett.* **1974**, *15*, 4549-4552.
[45] T.-i. Shimura, A. Ohkubo, K. Aramaki, H. Uekusa, T. Fujita, S. Ohba, H. Nishihara, *Inorg. Chim. Acta* **1995**, *230*, 215-218.
[46] Y. Wakatsuki, O. Nomura, K. Kitaura, K. Morokuma, H. Yamazaki, *J. Am. Chem. Soc.* **1983**, *105*, 1907-1912.
[47] M. Horáček, I. Císařová, J. Kubišta, A. Spannenberg, K. Dallmann, U. Rosenthal, K. Mach, *J. Organomet. Chem.* **2004**, *689*, 4592-4600.
[48] V. V. Burlakov, A. Ohff, C. Lefeber, A. Tillack, W. Baumann, R. Kempe, U. Rosenthal, *Chem. Ber.* **1995**, *128*, 967-971.
[49] M. I. Bruce, N. N. Zaitseva, B. W. Skelton, A. H. White, *Inorg. Chim. Acta* **1996**, *250*, 129-138.
[50] A. F. Hill, A. D. Rae, M. Schultz, A. C. Willis, *Organometallics* **2007**, *26*, 1325-1338.
[51] A. Steffen, R. M. Ward, W. D. Jones, T. B. Marder, *Coord. Chem. Rev.* **2010**, *254*, 1950-1976.
[52] H. Braunschweig, C. W. Chiu, K. Radacki, P. Brenner, *Chem. Commun.* **2010**, *46*, 916-918.
[53] A. J. Boydston, Y. Yin, B. L. Pagenkopf, *J. Am. Chem. Soc.* **2004**, *126*, 3724-3725.
[54] Y. Matano, H. Imahori, *Org. Biomol. Chem.* **2009**, *7*, 1258-1271.
[55] S. H. Eichhorn, A. J. Paraskos, K. Kishikawa, T. M. Swager, *J. Am. Chem. Soc.* **2002**, *124*, 12742-12751.
[56] A. Steffen, R. M. Ward, M. G. Tay, R. M. Edkins, F. Seeler, M. van Leeuwen, L. O. Pålsson, A. Beeby, A. S. Batsanov, J. A. Howard, T. B. Marder, *Chem. Eur. J.* **2014**, *20*, 3652-3666.
[57] J. P. Rourke, A. S. Batsanov, J. A. K. Howard, T. B. Marder, *Chem. Commun.* **2001**, 2626-2627.
[58] A. Steffen, M. G. Tay, A. S. Batsanov, J. A. K. Howard, A. Beeby, K. Q. Vuong, X.-Z. Sun, M. W. George, T. B. Marder, *Angew. Chem. Int. Ed.* **2010**, *49*, 2349-2353.
[59] C. Sieck, M. G. Tay, M. H. Thibault, R. M. Edkins, K. Costuas, J. F. Halet, A. S. Batsanov, M. Haehnel, K. Edkins, A. Lorbach, A. Steffen, T. B. Marder, *Chem. Eur. J.* **2016**, *22*, 10523-10532.
[60] I. Ojima, M. Tzamarioudaki, Z. Li, R. J. Donovan, *Chem. Rev.* **1996**, *96*, 635-662.
[61] M. Lautens, W. Klute, W. Tam, *Chem. Rev.* **1996**, *96*, 49-92.
[62] H. Bönnemann, *Angew. Chem. Int. Ed.* **1985**, *24*, 248-262.

[63] B. Heller, M. Hapke, *Chem. Soc. Rev.* **2007**, *36*, 1085-1094.
[64] J. K. Vandavasi, W.-P. Hu, C.-T. Hsiao, G. C. Senadi, J.-J. Wang, *RSC Adv.* **2014**, *4*, 57547-57552.
[65] K.-P. Wang, S. Y. Yun, P. Mamidipalli, D. Lee, *Chem. Sci.* **2013**, *4*, 3205-3211.
[66] N. K. Lee, S. Y. Yun, P. Mamidipalli, R. M. Salzman, D. Lee, T. Zhou, Y. Xia, *J. Am. Chem. Soc.* **2014**, *136*, 4363-4368.
[67] S. Y. Yun, K. P. Wang, N. K. Lee, P. Mamidipalli, D. Lee, *J. Am. Chem. Soc.* **2013**, *135*, 4668-4671.
[68] N. Schwenk, Ph.D. Thesis, Julius-Maximilians-Universität Würzburg **2017**.
[69] S. McKnight, M.Sc. Thesis, Heriot-Watt University Edinburgh **2015**.
[70] F. Kerner, M.Sc. Thesis, Julius-Maximilians-Universität Würzburg **2016**.
[71] C. Sieck, D. Sieh, M. Sapotta, M. Haehnel, K. Edkins, A. Lorbach, A. Steffen, T. B. Marder, *J. Organomet. Chem.* **2017**, *847*, 184-192.
[72] C. Sieck, Ph.D. Thesis, Julius-Maximilians-Universität Würzburg **2017**.
[73] M. Berthelot, *C. R. Hebd. Seances Acad. Sci.* **1866**, *62*, 905.
[74] W. Reppe, S. W. J., *Liebigs Ann. Chem.* **1948**, *560*, 104.
[75] R. B. Woodward, R. Hoffmann, *Angew. Chem. Int. Ed.* **1969**, *8*, 781-853.
[76] K. N. Houk, R. W. Gandour, R. W. Strozier, N. G. Rondan, L. A. Paquette, *J. Am. Chem. Soc.* **1979**, *101*, 6797-6802.
[77] R. D. Bach, G. J. Wolber, H. B. Schlegel, *J. Am. Chem. Soc.* **1985**, *107*, 2837-2841.
[78] S. Kotha, E. Brahmachary, K. Lahiri, *Eur. J. Org. Chem.* **2005**, *2005*, 4741-4767.
[79] S. Saito, Y. Yamamoto, *Chem. Rev.* **2000**, *100*, 2901-2916.
[80] V. Gandon, C. Aubert, M. Malacria, *Chem. Commun.* **2006**, 2209-2217.
[81] P. R. Chopade, J. Louie, *Adv. Synth. Catal.* **2006**, *348*, 2307-2327.
[82] Y. Shibata, K. Tanaka, in *Rhodium Catalysis in Organic Synthesis* (Ed.: K. Tanaka), Wiley-VCH, Weinheim, **2019**, p. 183-228.
[83] G. N. Schrauzer, P. Glockner, S. Eichler, *Angew. Chem. Int. Ed.* **1964**, *3*, 185-191.
[84] L. S. Meriwether, M. F. Leto, E. C. Colthup, G. W. Kennerly, *J. Org. Chem.* **1962**, *27*, 3930-3941.
[85] R. Diercks, B. E. Eaton, S. Gürtzgen, S. Jalisatgi, A. J. Matzger, R. H. Radde, K. P. C. Vollhardt, *J. Am. Chem. Soc.* **1998**, *120*, 8247-8248.
[86] J. A. Varela, C. Saá, *J. Organomet. Chem.* **2009**, *694*, 143-149.
[87] S. H. Lecker, N. H. Nguyen, K. P. C. Vollhardt, *J. Am. Chem. Soc.* **1986**, *108*, 856-858.
[88] B. C. Berris, G. H. Hovakeemian, Y. H. Lai, H. Mestdagh, K. P. C. Vollhardt, *J. Am. Chem. Soc.* **1985**, *107*, 5670-5687.
[89] K. P. C. Vollhardt, *Angew. Chem. Int. Ed.* **1984**, *23*, 539-556.
[90] R. L. Funk, K. P. C. Vollhardt, *J. Am. Chem. Soc.* **1980**, *102*, 5253-5261.
[91] H. Yamazaki, Y. Wakatsuki, *J. Organomet. Chem.* **1977**, *139*, 157-167.
[92] R. L. Hillard, K. P. C. Vollhardt, *J. Am. Chem. Soc.* **1977**, *99*, 4058-4069.
[93] R. L. Funk, K. P. Vollhardt, *J. Am. Chem. Soc.* **1977**, *99*, 5483-5484.
[94] K. P. C. Vollhardt, *Acc. Chem. Res.* **1977**, *10*, 1-8.
[95] L. P. McDonnell Bushnell, E. R. Evitt, R. G. Bergman, *J. Organomet. Chem.* **1978**, *157*, 445-456.
[96] K. Jonas, E. Deffense, D. Habermann, *Angew. Chem. Int. Ed.* **1983**, *22*, 716-717.
[97] U. Kölle, B. Fuss, *Chem. Ber.* **1986**, *119*, 116-128.
[98] D. R. McAlister, J. E. Bercaw, R. G. Bergman, *J. Am. Chem. Soc.* **1977**, *99*, 1666-1668.
[99] J. H. Hardesty, J. B. Koerner, T. A. Albright, G.-Y. Lee, *J. Am. Chem. Soc.* **1999**, *121*, 6055-6067.
[100] N. Agenet, V. Gandon, K. P. Vollhardt, M. Malacria, C. Aubert, *J. Am. Chem. Soc.* **2007**, *129*, 8860-8871.
[101] R. Xu, P. Winget, T. Clark, *Eur. J. Inorg. Chem.* **2008**, *2008*, 2874-2883.

[102] K. Kirchner, M. J. Calhorda, R. Schmid, L. F. Veiros, *J. Am. Chem. Soc.* **2003**, *125*, 11721-11729.
[103] Y. Yamamoto, T. Arakawa, R. Ogawa, K. Itoh, *J. Am. Chem. Soc.* **2003**, *125*, 12143-12160.
[104] M. O. Albers, D. J. A. De Waal, D. C. Liles, D. J. Robinson, E. Singleton, M. B. Wiege, *J. Chem. Soc., Chem. Commun.* **1986**, 1680-1682.
[105] M. Paneque, M. L. Poveda, N. Rendón, K. Mereiter, *J. Am. Chem. Soc.* **2004**, *126*, 1610-1611.
[106] E. Álvarez, M. Gómez, M. Paneque, C. M. Posadas, M. L. Poveda, N. Rendón, L. L. Santos, S. Rojas-Lima, V. Salazar, K. Mereiter, C. Ruiz, *J. Am. Chem. Soc.* **2003**, *125*, 1478-1479.
[107] M. Ping, L. Xiubin, W. Yuankai, *J. Chem. Educ.* **1990**, *67*.
[108] V. N. Sapunov, R. Schmid, K. Kirchner, H. Nagashima, *Coord. Chem. Rev.* **2003**, *238-239*, 363-382.
[109] P. Cioni, P. Diversi, G. Ingrosso, A. Lucherini, P. Ronca, *J. Mol. Catal. B. Enzym.* **1987**, *40*, 337-357.
[110] P. Diversi, L. Ermini, G. Ingrosso, A. Lucherini, *J. Organomet. Chem.* **1993**, *447*, 291-298.
[111] L. Orian, J. N. P. van Stralen, F. M. Bickelhaupt, *Organometallics* **2007**, *26*, 3816-3830.
[112] L. F. Veiros, G. Dazinger, K. Kirchner, M. J. Calhorda, R. Schmid, *Chem. Eur. J.* **2004**, *10*, 5860-5870.
[113] N. E. Schore, *Chem. Rev.* **1988**, *88*, 1081-1119.
[114] K. Abdulla, B. L. Booth, C. Stacey, *J. Organomet. Chem.* **1985**, *293*, 103-114.
[115] W. J. Bowyer, J. W. Merkert, W. E. Geiger, A. L. Rheingold, *Organometallics* **1989**, *8*, 191-198.
[116] S. T. Belt, M. Helliwell, W. D. Jones, M. G. Partridge, R. N. Perutz, *J. Am. Chem. Soc.* **1993**, *115*, 1429-1440.
[117] A. R. Katritzky, *Chem. Rev.* **2004**, *104*, 2125-2126.
[118] A. V. Gulevich, A. S. Dudnik, N. Chernyak, V. Gevorgyan, *Chem. Rev.* **2013**, *113*, 3084-3213.
[119] K. Tanaka, *Transition-Metal-Mediated Aromatic Ring Construction*, John Wiley & Sons, Inc., **2013**.
[120] E. Müller, R. Thomas, M. Sauerbier, E. Langer, D. Streichfuß, *Tetrahedron Lett.* **1971**, *12*, 521-524.
[121] E. Müller, *Synthesis* **1974**, *1974*, 761-774.
[122] R. Grigg, R. Scott, P. Stevenson, *Tetrahedron Lett.* **1982**, *23*, 2691-2692.
[123] K. Tanaka, K. Toyoda, A. Wada, K. Shirasaka, M. Hirano, *Chem. Eur. J.* **2005**, *11*, 1145-1156.
[124] S. Nishigaki, Y. Shibata, K. Tanaka, *J. Org. Chem.* **2017**, *82*, 11117-11125.
[125] Y. Wakatsuki, H. Yamazaki, *J. Chem. Soc., Chem. Commun.* **1973**, 280a-280a.
[126] J. A. Varela, C. Saá, *Chem. Rev.* **2003**, *103*, 3787-3802.
[127] G. Dominguez, J. Perez-Castells, *Chem. Soc. Rev.* **2011**, *40*, 3430-3444.
[128] P. Diversi, G. Ingrosso, A. Lucherini, A. Minutillo, *J. Mol. Catal. B. Enzym.* **1987**, *40*, 359-377.
[129] K. Tanaka, N. Suzuki, G. Nishida, *Eur. J. Org. Chem.* **2006**, *2006*, 3917-3922.
[130] A. Wada, K. Noguchi, M. Hirano, K. Tanaka, *Org. Lett.* **2007**, *9*, 1295-1298.
[131] K. Tanaka, H. Hara, G. Nishida, M. Hirano, *Org. Lett.* **2007**, *9*, 1907-1910.
[132] Y. Komine, K. Tanaka, *Org. Lett.* **2010**, *12*, 1312-1315.
[133] M. Ishii, F. Mori, K. Tanaka, *Chem. Eur. J.* **2014**, *20*, 2169-2174.
[134] P. Braunstein, D. Nobel, *Chem. Rev.* **1989**, *89*, 1927-1945.
[135] Y. Yamamoto, H. Takagishi, K. Itoh, *Org. Lett.* **2001**, *3*, 2117-2119.

[136] H. A. Duong, M. J. Cross, J. Louie, *J. Am. Chem. Soc.* **2004**, *126*, 11438-11439.
[137] P. Hong, H. Yamazaki, *Tetrahedron Lett.* **1977**, *18*, 1333-1336.
[138] H. Hoberg, B. W. Oster, *Synthesis* **1982**, *1982*, 324-325.
[139] H. A. Duong, J. Louie, *J. Organomet. Chem.* **2005**, *690*, 5098-5104.
[140] Y. Yamamoto, K. Kinpara, T. Saigoku, H. Takagishi, S. Okuda, H. Nishiyama, K. Itoh, *J. Am. Chem. Soc.* **2005**, *127*, 605-613.
[141] T. Kondo, M. Nomura, Y. Ura, K. Wada, T.-a. Mitsudo, *Tetrahedron Lett.* **2006**, *47*, 7107-7111.
[142] K. M. Oberg, E. E. Lee, T. Rovis, *Tetrahedron* **2009**, *65*, 5056-5061.
[143] T. Takahashi, F.-Y. Tsai, Y. Li, K. Nakajima, M. Kotora, *J. Am. Chem. Soc.* **1999**, *121*, 11093-11100.
[144] D. Suzuki, H. Urabe, F. Sato, *J. Am. Chem. Soc.* **2001**, *123*, 7925-7926.
[145] R. Tanaka, Y. Nakano, D. Suzuki, H. Urabe, F. Sato, *J. Am. Chem. Soc.* **2002**, *124*, 9682-9683.
[146] V. Gevorgyan, U. Radhakrishnan, A. Takeda, M. Rubina, M. Rubin, Y. Yamamoto, *J. Org. Chem.* **2001**, *66*, 2835-2841.
[147] H. Ryuichiro, G. Qiaoxia, T. Tamotsu, *Chem. Lett.* **2000**, *29*, 140-141.
[148] D. M. Duckworth, S. Lee-Wong, A. M. Z. Slawin, E. H. Smith, D. J. Williams, *J. Chem. Soc., Perkin Trans. 1* **1996**.
[149] P. Bhatarah, E. H. Smith, *J. Chem. Soc., Perkin Trans. 1* **1992**.
[150] P. Bhatarah, E. H. Smith, *J. Chem. Soc., Chem. Commun.* **1991**.
[151] K. P. C. Vollhardt, R. G. Bergman, *J. Am. Chem. Soc.* **1974**, *96*, 4996-4998.
[152] R. Grigg, R. Scott, P. Stevenson, *J. Chem. Soc., Perkin Trans. 1* **1988**, 1357-1364.
[153] H. Nishiyama, E. Niwa, T. Inoue, Y. Ishima, K. Aoki, *Organometallics* **2002**, *21*, 2572-2574.
[154] Y. Yamamoto, A. Nagata, Y. Arikawa, K. Tatsumi, K. Itoh, *Organometallics* **2000**, *19*, 2403-2405.
[155] B. Witulski, C. Alayrac, *Angew. Chem. Int. Ed.* **2002**, *41*, 3281-3284.
[156] Y. Komine, A. Kamisawa, K. Tanaka, *Org. Lett.* **2009**, *11*, 2361-2364.
[157] T. Shibata, Y.-k. Tahara, R. Matsubara, *Heterocycles* **2015**, *90*.
[158] K. Tanaka, A. Wada, K. Noguchi, *Org. Lett.* **2005**, *7*, 4737-4739.
[159] G. Nishida, S. Ogaki, Y. Yusa, T. Yokozawa, K. Noguchi, K. Tanaka, *Org. Lett.* **2008**, *10*, 2849-2852.
[160] A. C. Marco Montalti, Luca Prodi, M. Teresa Gandolfi, *Handbook of Photochemistry*, 3rd ed., CRC Press, **2006**.
[161] V. Balzani, A. Credi, M. Venturi, *Coord. Chem. Rev.* **1998**, *171*, 3-16.
[162] P. G. Bomben, K. C. D. Robson, B. D. Koivisto, C. P. Berlinguette, *Coord. Chem. Rev.* **2012**, *256*, 1438-1450.
[163] A. S. Polo, M. K. Itokazu, N. Y. Murakami Iha, *Coord. Chem. Rev.* **2004**, *248*, 1343-1361.
[164] A. Hagfeldt, G. Boschloo, L. Sun, L. Kloo, H. Pettersson, *Chem. Rev.* **2010**, *110*, 6595-6663.
[165] M. Grätzel, *J. Photochem. Photobiol. C* **2003**, *4*, 145-153.
[166] M. Grätzel, *Acc. Chem. Res.* **2009**, *42*, 1788-1798.
[167] W.-Y. Wong, C.-L. Ho, *Acc. Chem. Res.* **2010**, *43*, 1246-1256.
[168] H. Yersin, A. F. Rausch, R. Czerwieniec, T. Hofbeck, T. Fischer, *Coord. Chem. Rev.* **2011**, *255*, 2622-2652.
[169] S. Sato, T. Morikawa, T. Kajino, O. Ishitani, *Angew. Chem. Int. Ed.* **2013**, *52*, 988-992.
[170] Y.-J. Yuan, J.-Y. Zhang, Z.-T. Yu, J.-Y. Feng, W.-J. Luo, J.-H. Ye, Z.-G. Zou, *Inorg. Chem.* **2012**, *51*, 4123-4133.
[171] W. C. H. Choy, W. K. Chan, Y. Yuan, *Adv. Mater.* **2014**, *26*, 5368-5399.

[172] C. A. Bignozzi, R. Argazzi, R. Boaretto, E. Busatto, S. Carli, F. Ronconi, S. Caramori, *Coord. Chem. Rev.* **2013**, *257*, 1472-1492.
[173] N. A. Smith, P. J. Sadler, *Philos. Trans. A. Math. Phys. Eng. Sci.* **2013**, *371*, 20120519.
[174] M. R. Gill, J. A. Thomas, *Chem. Soc. Rev.* **2012**, *41*, 3179-3192.
[175] U. Schatzschneider, *Inorg. Chim. Acta* **2011**, *374*, 19-23.
[176] W. Huber, R. Linder, J. Niesel, U. Schatzschneider, B. Spingler, P. C. Kunz, *Eur. J. Inorg. Chem.* **2012**, *2012*, 3140-3146.
[177] P. C. Ford, *Acc. Chem. Res.* **2008**, *41*, 190-200.
[178] F. Marquele-Oliveira, D. C. Santana, S. F. Taveira, D. M. Vermeulen, A. R. de Oliveira, R. S. da Silva, R. F. Lopez, *J. Pharm. Biomed. Anal.* **2010**, *53*, 843-851.
[179] J. R. Lakowicz, *Principles of Fluorescence Spectroscopy*, 3 ed., Springer, **2006**.
[180] V. Balzani, S. Campagna, *Photochemistry and Photophysics of Coordination Compounds I*, **2007**.
[181] H. Saigusa, T. Azumi, M. Sumitani, K. Yoshihara, *J. Chem. Phys.* **1980**, *72*, 1713-1715.
[182] A. Steffen, K. Costuas, A. Boucekkine, M.-H. Thibault, A. Beeby, A. S. Batsanov, A. Charaf-Eddin, D. Jacquemin, J.-F. Halet, T. B. Marder, *Inorg. Chem.* **2014**, *53*, 7055-7069.
[183] J. Huheey, E. Keiter, R. Keiter, *Anorganische Chemie*, 5 ed., De Gruyter, **2014**.
[184] M. T. Indelli, C. Chiorboli, F. Scandola, in *Photochemistry and Photophysics of Coordination Compounds I* (Eds.: V. Balzani, S. Campagna), Springer **2007**, p. 215-255.
[185] A. Damas, B. Ventura, J. Moussa, A. D. Esposti, L.-M. Chamoreau, A. Barbieri, H. Amouri, *Inorg. Chem.* **2012**, *51*, 1739-1750.
[186] W. L. Su, Y. Cheng Yu, M. Ching Tseng, S. P. Wang, W. L. Huang, *Dalton Trans.* **2007**, 3440-3449.
[187] K. K.-W. Lo, C.-K. Li, K.-W. Lau, N. Zhu, *Dalton Trans.* **2003**, 4682-4689.
[188] L. Ghizdavu, O. Lentzen, S. Schumm, A. Brodkorb, C. Moucheron, A. Kirsch-De Mesmaeker, *Inorg. Chem.* **2003**, *42*, 1935-1944.
[189] D. H. W. Carstens, G. A. Crosby, *J. Mol. Spectrosc.* **1970**, *34*, 113-135.
[190] J. S. Siddle, R. M. Ward, J. C. Collings, S. R. Rutter, L. Porrès, L. Applegarth, A. Beeby, A. S. Batsanov, A. L. Thompson, J. A. K. Howard, A. Boucekkine, K. Costuas, J.-F. Halet, T. B. Marder, *New J. Chem.* **2007**, *31*, 841-851.
[191] D. Ashen-Garry, M. Selke, *Photochemistry and Photobiology* **2014**, *90*, 257-274.
[192] S. W. Buckner, M. J. Fischer, P. A. Jelliss, R. Luo, S. D. Minteer, N. P. Rath, A. Siemiarczuk, *Inorg. Chem.* **2006**, *45*, 7339-7347.
[193] C.-C. Hsu, C.-C. Lin, P.-T. Chou, C.-H. Lai, C.-W. Hsu, C.-H. Lin, Y. Chi, *J. Am. Chem. Soc.* **2012**, *134*, 7715-7724.
[194] Y.-M. Cheng, Y.-S. Yeh, M.-L. Ho, P.-T. Chou, P.-S. Chen, Y. Chi, *Inorg. Chem.* **2005**, *44*, 4594-4603.
[195] G. Volpi, C. Garino, L. Salassa, J. Fiedler, K. I. Hardcastle, R. Gobetto, C. Nervi, *Chem. Eur. J.* **2009**, *15*, 6415-6427.
[196] D. Tapu, C. Owens, D. VanDerveer, K. Gwaltney, *Organometallics* **2009**, *28*, 270-276.
[197] P. Datta, D. Sardar, P. Mitra, C. Sinha, *Polyhedron* **2011**, *30*, 1516-1523.
[198] F. Cicogna, M. Colonna, J. L. Houben, G. Ingrosso, F. Marchetti, *J. Organomet. Chem.* **2000**, *593-594*, 251-266.
[199] G.-J. Zhao, F. Yu, M.-X. Zhang, B. H. Northrop, H. Yang, K.-L. Han, P. J. Stang, *J. Phys. Chem. A* **2011**, *115*, 6390-6393.
[200] J. J. Wilson, S. J. Lippard, *Inorg. Chim. Acta* **2012**, *389*, 77-84.
[201] M.-H. Nguyen, J. H. K. Yip, *Organometallics* **2011**, *30*, 6383-6392.
[202] K. Horst, P. Valeri, V. Arnd, *Z. Naturforsch. B* **2008**, *63*, 963-967.
[203] P. Valeri, K. Horst, V. Arnd, *Z. Naturforsch. B* **2005**, *60*, 359-362.

[204] K. Horst, V. Arnd, *Z. Naturforsch. B* **2011**, *66*, 828-832.
[205] C. Cardozo, A. Mendoza, G. Farías, A. L. B. Formiga, D. Peña, F. Fuentes, A. Arce, Y. Otero, *J. Organomet. Chem.* **2019**, *881*, 34-44.
[206] D. Sieh, F. Kerner, K. Murata, M.-H. Thibault, N. Schwenk, M.-L. Lechner, S. McKnight, J. Weinmann, A. Okorn, A. S. Batsanov, K. Fucke, M. Hähnel, R. Bertermann, A. Eichhorn, Z. Yu, Z. Lin, A. Steffen, T. B. Marder, *unpublished work*, **2020**.
[207] A. Okorn, M.Sc. Thesis, Julius-Maximilians-Universität Würzburg **2017**.
[208] F. H. Allen, O. Kennard, D. G. Watson, L. Brammer, A. G. Orpen, R. Taylor, *J. Chem. Soc., Perkin Trans. 2* **1987**, S1 - S19.
[209] C. Hartmann, M.Sc. Thesis, Julius-Maximilians-Universität Würzburg **2018**.
[210] K. Murata, T. B. Marder, *unpublished results*, Julius-Maximilians-Universität Würzburg, **2014**.
[211] R. A. Earl, K. P. C. Vollhardt, *J. Am. Chem. Soc.* **1983**, *105*, 6991-6993.
[212] Y. Yamamoto, H. Kitahara, R. Ogawa, H. Kawaguchi, K. Tatsumi, K. Itoh, *J. Am. Chem. Soc.* **2000**, *122*, 4310-4319.
[213] K. Ziegler, B. Schnell, *Liebigs Ann. Chem.* **1925**, *445*, 266-282.
[214] D. G. Farnum, G. Mehta, G. G. I. Moore, F. P. Siegal, *Tetrahedron Lett.* **1974**, *15*, 2549-2552.
[215] T. Yamagata, J. Kuwabara, T. Kanbara, *Tetrahedron* **2014**, *70*, 1451-1457.
[216] S. Frebort, Z. Elias, A. Lycka, S. Lunak, J. Vynuchal, L. Kubac, R. Hrdina, L. Burgert, *Tetrahedron Lett.* **2011**, *52*, 5769-5773.
[217] S. Griesbeck, E. Michail, C. Wang, H. Ogasawara, S. Lorenzen, L. Gerstner, T. Zang, J. Nitsch, Y. Sato, R. Bertermann, M. Taki, C. Lambert, S. Yamaguchi, T. B. Marder, *Chem. Sci.* **2019**, *10*, 5405-5422.
[218] R. L. Riggs, C. J. H. Morton, A. M. Z. Slawin, D. M. Smith, N. J. Westwood, W. S. D. Austen, K. E. Stuart, *Tetrahedron* **2005**, *61*, 11230-11243.
[219] E. D. Głowacki, H. Coskun, M. A. Blood-Forsythe, U. Monkowius, L. Leonat, M. Grzybowski, D. Gryko, M. S. White, A. Aspuru-Guzik, N. S. Sariciftci, *Org. Electron.* **2014**, *15*, 3521-3528.
[220] J. Mizuguchi, A. Grubenmann, G. Rihs, *Acta Crystallogr. B* **1993**, *49*, 1056-1060.
[221] A. Iqbal, M. Jost, R. Kirchmayr, J. Pfenninger, A. Rochat, O. Wallquist, *Bull. Soc. Chim. Belg.* **1988**, *97*, 615-644.
[222] J. Mizuguchi, *Acta Crystallogr. C* **1998**, *54*, 1482-1484.
[223] J. Goodman, V. V. Grushin, R. B. Larichev, S. A. Macgregor, W. J. Marshall, D. C. Roe, *J. Am. Chem. Soc.* **2010**, *132*, 12013-12026.
[224] J. M. Kenny, L. Torre, L. M. Chiacchiarelli, *J. Appl. Polym. Sci.* **2015**, *132*.
[225] G. Wegener, M. Brandt, L. Duda, J. Hofmann, B. Klesczewski, D. Koch, R.-J. Kumpf, H. Orzesek, H.-G. Pirkl, C. Six, C. Steinlein, M. Weisbeck, *Appl. Catal. A,* **2001**, *221*, 303-335.
[226] P. Gibbons, D. Love, T. Craig, C. Budke, *Vet. Parasitol.* **2016**, *218*, 1-4.
[227] A. Bosco, L. Rinaldi, G. Cappelli, A. Saratsis, L. Nisoli, G. Cringoli, *Vet. Parasitol.* **2015**, *212*, 408-410.
[228] A. P. Murray, M. J. Miller, *J. Org. Chem.* **2003**, *68*, 191-194.
[229] M. Ghosh, M. J. Miller, *J. Org. Chem.* **1994**, *59*, 1020-1026.
[230] E. Preis, N. Schindler, S. Adrian, U. Scherf, *ACS Macro Lett.* **2015**, *4*, 1268-1272.
[231] Y. Zhang, S. N. Riduan, J. Y. Ying, *Chem. Eur. J.* **2009**, *15*, 1077-1081.
[232] A. Zhou, L. Cao, H. Li, Z. Liu, H. Cho, W. P. Henry, J. C. U. Pittman, *Tetrahedron* **2006**, *62*, 4188-4200.
[233] T. H. Brown, P. J. Green, *J. Am. Chem. Soc.* **1970**, *92*, 2359-2362.

[234] A. L. Spek, M. A. Siegler, J. Meeuwissen, R. N. H. Reek, *Experimental Crystal Structure Determination* **2015**, *CCDC 1058712*.
[235] S. Hasegawa, K. Itoh, Y. Ishii, *Inorg. Chem.* **2002**, *13*, 2675-2679.
[236] H. Werner, J. Wolf, U. Schubert, *Chem. Ber.* **1983**, *116*, 2848-2854.
[237] A. Hernán-Gómez, T. D. Bradley, A. R. Kennedy, Z. Livingstone, S. D. Robertson, E. Hevia, *Chem. Commun.* **2013**, *49*, 8659-8661.
[238] Q. Liu, Z. Guo, H. Han, H. Tong, X. Wei, *Polyhedron* **2015**, *85*, 15-19.
[239] Z. Guo, S. Wang, H. Tong, J. Chao, X. Wei, *Inorg. Chem. Commun.* **2013**, *33*, 68-72.
[240] B. Srinivas, C.-C. Chang, C.-H. Chen, M. Y. Chiang, I. T. Chen, Y. Wang, G.-H. Lee, *J. Chem. Soc., Dalton Trans.* **1997**, 957-964.
[241] Y. Wu, S. Wang, X. Zhu, G. Yang, Y. Wei, L. Zhang, H.-b. Song, *Inorg. Chem.* **2008**, *47*, 5503-5511.
[242] Y. Sun, Z. Zhang, X. Wang, X. Li, L. Weng, X. Zhou, *Organometallics* **2009**, *28*, 6320-6330.
[243] X. Zhu, J. Fan, Y. Wu, S. Wang, L. Zhang, G. Yang, Y. Wei, C. Yin, H. Zhu, S. Wu, H. Zhang, *Organometallics* **2009**, *28*, 3882-3888.
[244] W. Yi, J. Zhang, L. Hong, Z. Chen, X. Zhou, *Organometallics* **2011**, *30*, 5809-5814.
[245] H.-M. Wang, H.-X. Li, X.-Y. Yu, Z.-G. Ren, J.-P. Lang, *Tetrahedron* **2011**, *67*, 1530-1535.
[246] O. Blacque, H. Brunner, M. M. Kubicki, J.-C. Leblanc, W. Meier, C. Moise, Y. Mugnier, A. Sadorge, J. Wachter, M. Zabel, *J. Organomet. Chem.* **2001**, *634*, 47-54.
[247] Y. Li, H. Matsumura, M. Yamanaka, T. Takahashi, *Tetrahedron* **2004**, *60*, 1393-1400.
[248] S. R. Foley, G. P. A. Yap, D. S. Richeson, *Organometallics* **1999**, *18*, 4700-4705.
[249] S. R. Foley, Y. Zhou, G. P. A. Yap, D. S. Richeson, *Inorg. Chem.* **2000**, *39*, 924-929.
[250] H. Wang, H.-S. Chan, J. Okuda, Z. Xie, *Organometallics* **2005**, *24*, 3118-3124.
[251] H. R. Sharpe, A. M. Geer, H. E. Williams, T. J. Blundell, W. Lewis, A. J. Blake, D. L. Kays, *Chem. Commun.* **2017**, *53*, 937-940.
[252] W. Beck, W. Rieber, S. Cenini, F. Porta, G. La Monica, *J. Chem. Soc., Dalton Trans.* **1974**, 298-304.
[253] A. G. Giuglio-Tonolo, C. Spitz, T. Terme, P. Vanelle, *Tetrahedron Lett.* **2014**, *55*, 2700-2702.
[254] J. Tang, T. Mohan, J. G. Verkade, *J. Org. Chem.* **1994**, *59*, 4931-4938.
[255] T. Yoichi, S. Isao, Y. Masahiko, T. Tohru, Y. Katsumi, *Bull. Chem. Soc. Jpn.* **1990**, *63*, 3486-3489.
[256] Y. Nambu, T. Endo, *J. Org. Chem.* **1993**, *58*, 1932-1934.
[257] H. A. Duong, M. J. Cross, J. Louie, *Org. Lett.* **2004**, *6*, 4679-4681.
[258] H. Hoberg, B. W. Oster, C. Krüger, Y. H. Tsay, *J. Organomet. Chem.* **1983**, *252*, 365-373.
[259] H. Hoberg, K. Radine, A. Milchereit, *J. Organomet. Chem.* **1985**, *280*, c60-c62.
[260] H. Hoberg, J. Korff, *J. Organomet. Chem.* **1978**, *150*, C20-C22.
[261] H. Hoberg, K. Sümmermann, A. Milchereit, *J. Organomet. Chem.* **1985**, *288*, 237-248.
[262] H. Hoberg, K. Sümmermann, A. Milchereit, *Angew. Chem. Int. Ed.* **1985**, *24*, 325-326.
[263] H. Hoberg, E. Hernandez, *J. Chem. Soc., Chem. Commun.* **1986**, 544-545.
[264] H. Hoberg, E. Hernandez, *J. Organomet. Chem.* **1986**, *311*, 307-312.
[265] E. Hernandez, H. Hoberg, *J. Organomet. Chem.* **1987**, *328*, 403-412.
[266] H. Hoberg, *J. Organomet. Chem.* **1988**, *358*, 507-517.
[267] H. Hoberg, D. Guhl, *J. Organomet. Chem.* **1990**, *384*, C43-C46.
[268] S. G. Lee, K. Y. Choi, Y. J. Kim, S. Park, S. W. Lee, *Dalton Trans.* **2015**, *44*, 6537-6545.
[269] F. Paul, S. Moulin, O. Piechaczyk, P. Le Floch, J. A. Osborn, *J. Am. Chem. Soc.* **2007**, *129*, 7294-7304.

[270] A. W. Hofmann, *Ber. d. Dt. Chem. Ges.* **1885**, *18*, 764-766.
[271] A. W. Hofmann, *Ber. d. Dt. Chem. Ges.* **1871**, *4*, 246-251.
[272] A. W. Hofmann, O. Olshausen, *Ber. d. Dt. Chem. Ges.* **1870**, *3*, 269-276.
[273] L. C. Raiford, H. B. Freyermuth, *J. Org. Chem.* **1943**, *08*, 230-238.
[274] G. A. Grasa, Z. Moore, K. L. Martin, E. D. Stevens, S. P. Nolan, V. Paquet, H. Lebel, *J. Organomet. Chem.* **2002**, *658*, 126-131.
[275] D. M. Khramov, V. M. Lynch, C. W. Bielawski, *Organometallics* **2007**, *26*, 6042-6049.
[276] H. V. Huynh, *Chem. Rev.* **2018**, *118*, 9457-9492.
[277] U. Radius, J. Nitsch, M. J. Krahfuß, F. M. Bickelhaupt, T. B. Marder, *Chem. Eur. J.* **2020**.
[278] Y. Matsusaka, S. Shitaya, K. Nomura, A. Inagaki, *Inorg. Chem.* **2017**.
[279] S. Chen, K. Li, F. Zhao, L. Zhang, M. Pan, Y.-Z. Fan, J. Guo, J. Shi, C.-Y. Su, *Nat. Commun.* **2016**, *7*, 13169.
[280] M. Grzybowski, D. T. Gryko, *Adv. Optical Mater.* **2015**, *3*, 280-320.
[281] J. Dhar, N. Venkatramaiah, A. A, S. Patil, *J. Mater. Chem. C* **2014**, *2*, 3457-3466.
[282] M. Grzybowski, E. Glodkowska-Mrowka, T. Stoklosa, D. T. Gryko, *Org. Lett.* **2012**, *14*, 2670-2673.
[283] E. Müller, E. Langer, H. Jäkle, H. Muhm, W. Hoppe, R. Graziani, A. Gieren, F. Brandl, *Z. Naturforsch. B* **1971**, *26*, 305-307.
[284] R. M. Ward, Ph.D. Thesis, University of Durham **2007**.
[285] X. Liu, Q. Yi, Y. Han, Z. Liang, C. Shen, Z. Zhou, J.-l. Sun, Y. Li, W. Du, R. Cao, *Angew. Chem. Int. Ed.* **2015**, *54*, 1846-1850.
[286] Y. Yoshida, S. Takizawa, H. Sasai, *Tetrahedron Lett.* **2011**, *52*, 6877-6879.
[287] A.-F. Tran-Van, E. Huxol, J. M. Basler, M. Neuburger, J.-J. Adjizian, C. P. Ewels, H. A. Wegner, *Org. Lett.* **2014**, *16*, 1594-1597.
[288] P. J. Garratt, K. P. C. Vollhardt, *J. Am. Chem. Soc.* **1972**, *94*, 7087-7092.
[289] V. Engelhardt, J. Garcia, A. Hubaud, K. Lyssenko, S. Spyroudis, T. Timofeeva, P. Tongwa, K. Vollhardt, *Synlett* **2010**, *2011*, 280-284.
[290] W. C. Lothrop, *J. Am. Chem. Soc.* **1941**, *63*, 1187-1191.
[291] B. C. Berris, Y.-H. Lai, K. P. C. Vollhardt, *J. Chem. Soc., Chem. Commun.* **1982**, 953-954.
[292] C. D. Campbell, C. W. Rees, *J. Chem. Soc. C* **1969**, 742-747.
[293] S. M. Humayun Kabir, M. Hasegawa, Y. Kuwatani, M. Yoshida, H. Matsuyama, M. Iyoda, *J. Chem. Soc., Perkin Trans. 1* **2001**, 159-165.
[294] S.-L. Wang, M.-L. Pan, W.-S. Su, Y.-T. Wu, *Angew. Chem. Int. Ed.* **2017**, *56*, 14694-14697.
[295] R. Boese, D. Blaser, R. Latz, *Acta Crystallogr. C* **1999**, *55*.
[296] S. Hashimoto, K. Tahara, *J. Org. Chem.* **2019**, *84*, 9850-9858.
[297] A. Kondoh, H. Yorimitsu, K. Oshima, *J. Am. Chem. Soc.* **2007**, *129*, 6996-6997.
[298] H. Y. Jang, M. J. Krische, *J. Am. Chem. Soc.* **2004**, *126*, 7875-7880.
[299] K. Tanaka, K. Takeishi, K. Noguchi, *J. Am. Chem. Soc.* **2006**, *128*, 4586-4587.
[300] Y. Badrieh, J. Blum, I. Amer, K. Peter, C. Vollhardt, *J. Mol. Catal. B. Enzym.* **1991**, *66*, 295-312.
[301] P. J. Fennis, P. H. M. Budzelaar, J. H. G. Frijns, A. G. Orpen, *J. Organomet. Chem.* **1990**, *393*, 287-298.
[302] A. V. D. Ent, A. L. Onderdelinden, R. A. Schunn, in *Inorganic Syntheses, Vol. 28*, John Wiley & Sons, Inc., **1990**, p. 90-92.
[303] T. G. Schenck, J. M. Downes, C. R. C. Milne, P. B. Mackenzie, T. G. Boucher, J. Whelan, B. Bosnich, *Inorg. Chem.* **1985**, *24*, 2334-2337.
[304] M. A. Esteruelas, F. J. Lahoz, E. Oñate, L. A. Oro, L. Rodríguez, P. Steinert, H. Werner, *Organometallics* **1996**, *15*, 3436-3444.

[305] M.-H. Thibault, M. G. Tay, A. S. Batsanov, J. A. K. Howard, T. B. Marder, *J. Organomet. Chem.* **2013**, *730*, 104-107.
[306] Z. Duan, M. J. Hampden-Smith, E. N. Duesler, A. L. Rheingold, *Polyhedron* **1994**, *13*, 609-623.
[307] J. G. Leipoldt, G. J. Lamprecht, G. J. Van Zyl, *Inorg. Chim. Acta* **1985**, *96*, L31-L34.
[308] G. J. Van Zyl, G. J. Lamprecht, J. G. Leipoldt, *Inorg. Chim. Acta* **1985**, *102*, L1-L4.
[309] M. H. J. M. de Croon, H. L. M. van Gaal, A. van der Ent, *Inorg. Nucl. Chem. Lett.* **1974**, *10*, 1081-1086.
[310] A. D. Hunter, T. R. Williams, B. M. Zarzyczny, H. W. Bottesch, S. A. Dolan, K. A. McDowell, D. N. Thomas, C. H. Mahler, *Organometallics* **2016**, *35*, 2701-2706.
[311] R. Joe Gerald Jesu, *Rev. Inorg. Chem.* **2015**, *35*, 25-56.
[312] P. E. Garrou, *Chem. Rev.* **1981**, *81*, 229-266.
[313] M. J. Bennett, P. B. Donaldson, *Inorg. Chem.* **1977**, *16*, 655-660.
[314] J. A. Codelli, J. M. Baskin, N. J. Agard, C. R. Bertozzi, *J. Am. Chem. Soc.* **2008**, *130*, 11486-11493.
[315] J. M. Baskin, J. A. Prescher, S. T. Laughlin, N. J. Agard, P. V. Chang, I. A. Miller, A. Lo, J. A. Codelli, C. R. Bertozzi, *Proc. Natl. Acad. Sci.* **2007**, *104*, 16793-16797.
[316] J. L. Baudour, H. Cailleau, W. B. Yelon, *Acta Crystallogr. B* **1977**, *33*, 1773-1780.
[317] K. Osakada, T.-a. Koizumi, S. Sarai, T. Yamamoto, *Organometallics* **1998**, *17*, 1868-1872.
[318] M. Zhu, C. Yang, *Chem. Soc. Rev.* **2013**, *42*, 4963-4976.
[319] A. v. d. Ent, A. L. Onderdelinden, R. A. Schunn, in *Inorganic Syntheses, Vol. 14* (Eds.: A. Wold, J. K. Ruff), McGraw-Hill, Inc., **1973**, p. 92-95.
[320] N. Miyaura, A. Suzuki, *Org. Synth.* **1990**, *68*, 130.
[321] W. Wolfsberger, H. Schmidbaur, *Synth. React. Inorg. M.* **2007**, *4*, 149-156.
[322] R. M. Golding, P. C. Healy, P. W. G. Newman, E. Sinn, A. H. White, *Inorg. Chem.* **1972**, *11*, 2435-2440.
[323] A. J. Arduengo, H. V. R. Dias, R. L. Harlow, M. Kline, *J. Am. Chem. Soc.* **1992**, *114*, 5530-5534.
[324] P. S. Pregosin, *NMR in Organometallic Chemistry*, Wiley-VCH, Weinheim, **2012**.
[325] U. Weber, H. Thiele, *NMR Spectroscopy: Modern Spectral Analysis*, Wiley-VCH, Weinheim, **1998**.
[326] S. Berger, S. Braun, *200 and More NMR Experiments: A Practical Course, Vol. 1*, Wiley-VCH, Weinheim, **2004**.
[327] I. Noviandri, K. N. Brown, D. S. Fleming, P. T. Gulyas, P. A. Lay, A. F. Masters, L. Phillips, *J. Phys. Chem. B* **1999**, *103*, 6713-6722.
[328] N. G. Connelly, W. E. Geiger, *Chem. Rev.* **1996**, *96*, 877-910.
[329] G. Sheldrick, *Acta Crystallogr. C* **2015**, *71*, 3-8.
[330] G. Sheldrick, *Acta Crystallogr. A* **2008**, *64*, 112-122.
[331] C. B. Hubschle, G. M. Sheldrick, B. Dittrich, *J. Appl. Crystallogr.* **2011**, *44*, 1281-1284.
[332] *Diamond - Crystal and Molecular Structure Visualization*, 4.6.0 ed., Crystal Impact - Dr. H. Putz & Dr. K. Brandenburg GbR, Bonn, **2020**.
[333] G. W. T. M. J. Frisch, H. B. Schlegel, G. E. Scuseria, M. A. Robb, J. R. Cheeseman, G. Scalmani, V. Barone, G. A. Petersson, H. Nakatsuji, X. Li, M. Caricato, A. Marenich, J. Bloino, B. G. Janesko, R. Gomperts, B. Mennucci, H. P. Hratchian, J. V. Ortiz, A. F. Izmaylov, J. L. Sonnenberg, D. Williams-Young, F. Ding, F. Lipparini, F. Egidi, J. Goings, B. Peng, A. Petrone, T. Henderson, D. Ranasinghe, V. G. Zakrzewski, J. Gao, N. Rega, G. Zheng, W. Liang, M. Hada, M. Ehara, K. Toyota, R. Fukuda, J. Hasegawa, M. Ishida, T. Nakajima, Y. Honda, O. Kitao, H. Nakai, T. Vreven, K. Throssell, J. A. Montgomery, Jr., J. E. Peralta, F. Ogliaro, M. Bearpark, J. J. Heyd, E. Brothers, K. N. Kudin, V. N. Staroverov, T. Keith, R. Kobayashi, J. Normand, K. Raghavachari, A.

Rendell, J. C. Burant, S. S. Iyengar, J. Tomasi, M. Cossi, J. M. Millam, M. Klene, C. Adamo, R. Cammi, J. W. Ochterski, R. L. Martin, K. Morokuma, O. Farkas, J. B. Foresman, and D. J. Fox, *Gaussian 09, Revision E.01*, Gaussian, Inc., Wallingford CT, **2016**.

[334] T. Lu, F. Chen, *J. Comput. Chem.* **2012**, *33*, 580-592.

[335] C. Lee, W. Yang, R. G. Parr, *Phys. Rev. B: Condens. Matter Mater. Phys.* **1988**, *37*, 785-789.

[336] G. A. Petersson, M. A. Al-Laham, *J. Chem. Phys.* **1991**, *94*, 6081-6090.

[337] G. A. Petersson, A. Bennett, T. G. Tensfeldt, M. A. Al-Laham, W. A. Shirley, J. Mantzaris, *J. Chem. Phys.* **1988**, *89*, 2193-2218.

[338] Y. T. Wu, T. Hayama, K. K. Baldridge, A. Linden, J. S. Siegel, *J. Am. Chem. Soc.* **2006**, *128*, 6870-6884.

[339] L. Severa, J. Vávra, A. Kohoutová, M. Čížková, T. Šálová, J. Hývl, D. Šaman, R. Pohl, L. Adriaenssens, F. Teplý, *Tetrahedron Lett.* **2009**, *50*, 4526-4528.

[340] P. A. Wender, J. P. Christy, A. B. Lesser, M. T. Gieseler, *Angew. Chem. Int. Ed.* **2009**, *48*, 7687-7690.

[341] C.-C. Cheng, C.-S. Chang, Y.-L. Hsu, T.-Y. Lee, L.-C. Chang, S.-H. Liu, Y.-T. Wu, *Eur. J. Org. Chem.* **2010**, *2010*, 672-679.

[342] G. Wang, C. Chen, J. Peng, *Chem. Commun.* **2016**, *52*, 10277-10280.

[343] J. Shi, Z. Guo, X. Wei, D. Liu, M. F. Lappert, *Synlett* **2011**, *2011*, 1937-1939.

9 Appendix

9.1 Determination of the yield in section 2.3.1.2

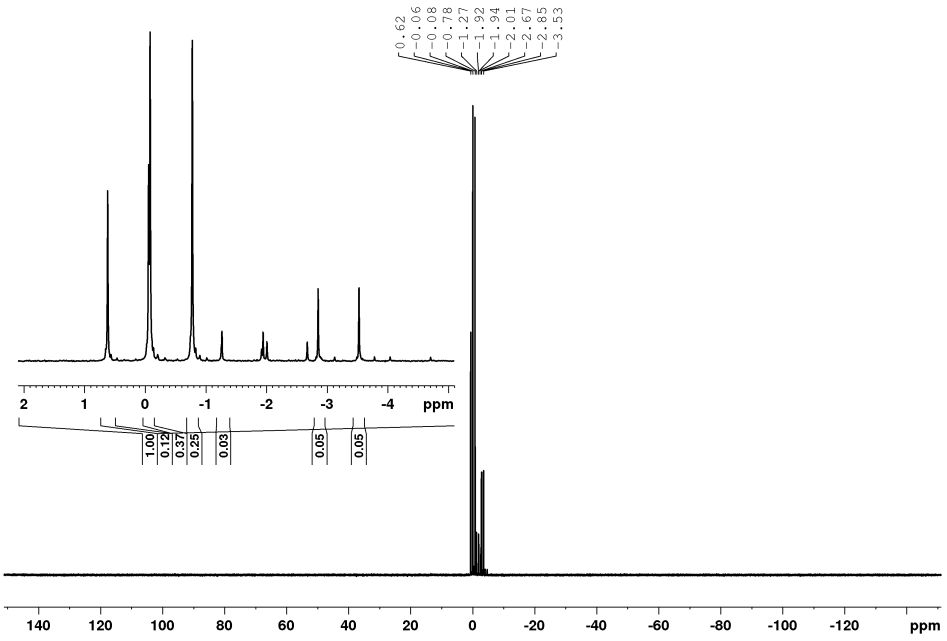

Figure A1: $^{31}P\{^{1}H\}$ NMR spectrum (120 MHz, toluene-d_8) of the reaction of **1-51** with **2-1a** in a 1:3 ratio at 100 °C after 24 h.

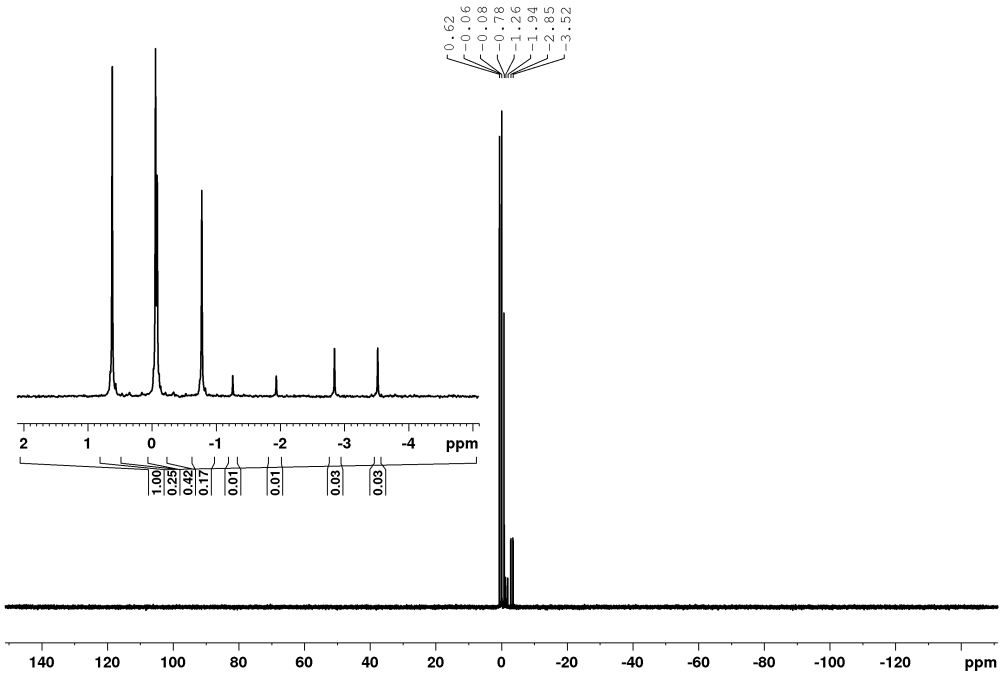

Figure A2: $^{31}P\{^{1}H\}$ NMR spectrum (120 MHz, toluene-d_8) of the reaction of **2-2a** with **2-1a** in a 1:3 ratio at 100 °C after 24 h.

9.2 List of compounds

9.2.1 Compounds of Chapter 1

Important chemical structures of Chapter 1:

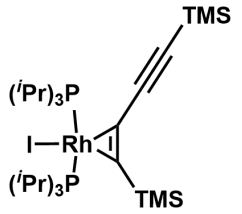

1-4

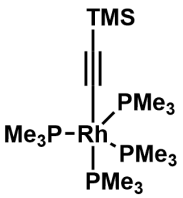

1-28a

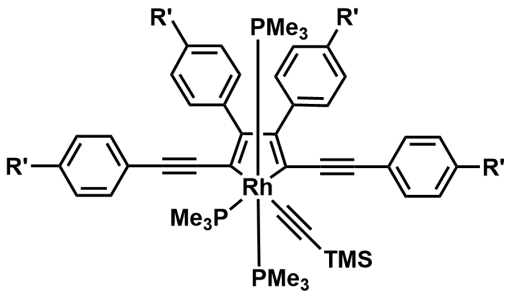

1-29a - 1-37a

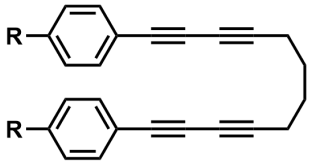

a: R = H
b: R = SMe
c: R = $BMes_2$
d: R = CO_2Me

1-43(a-d)

1-29: R' = H 1-32: R' = SMe 1-35: R' = CO_2Me
1-30: R' = Me 1-33: R' = NMe_2 1-36: R' = CN
1-31: R' = OMe 1-34: R' = CF_3 1-37: R' = NO_2

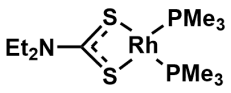

1-44

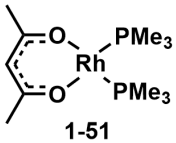

1-51

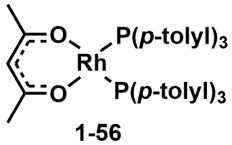

1-56

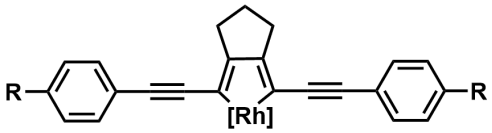

[Rh] = [Rh(S_2CNEt_2)(PMe_3)$_2$]

1-48(a-e)

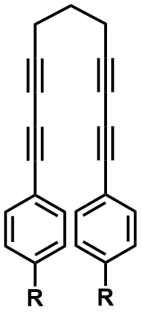

1-47(a-e)

a: R = Me
b: R = SMe
c: R = NMe_2
d: R = CO_2Me
e: R = NO_2

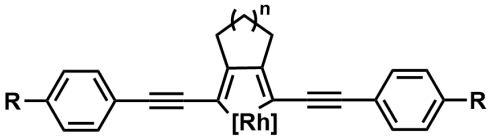

[Rh] = [Rh(acac)(PMe_3)$_2$]

n = 1 (1-52b,d)
n = 2 (1-53b,d)

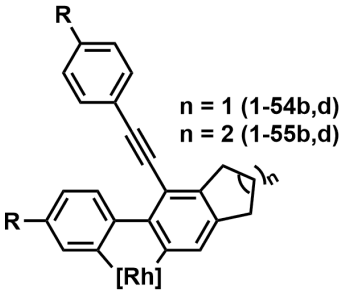

[Rh] = [Rh(acac)(PMe_3)$_2$]

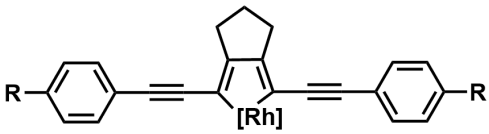

[Rh] = [Rh(acac)(P(*p*-tolyl$_3$)$_2$]

1-57b,d

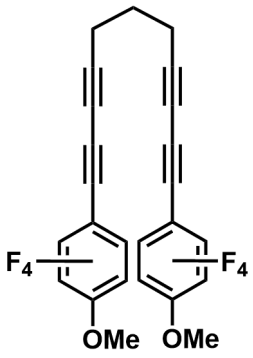

1-47f

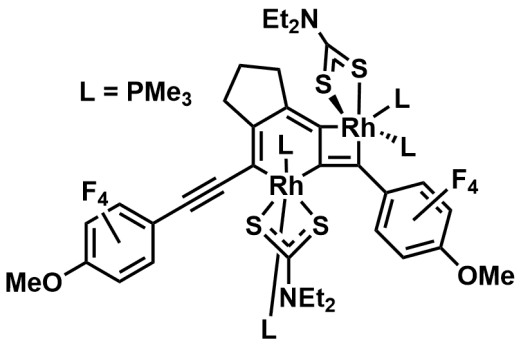

1-50

9.2.2 Compounds of Chapter 2

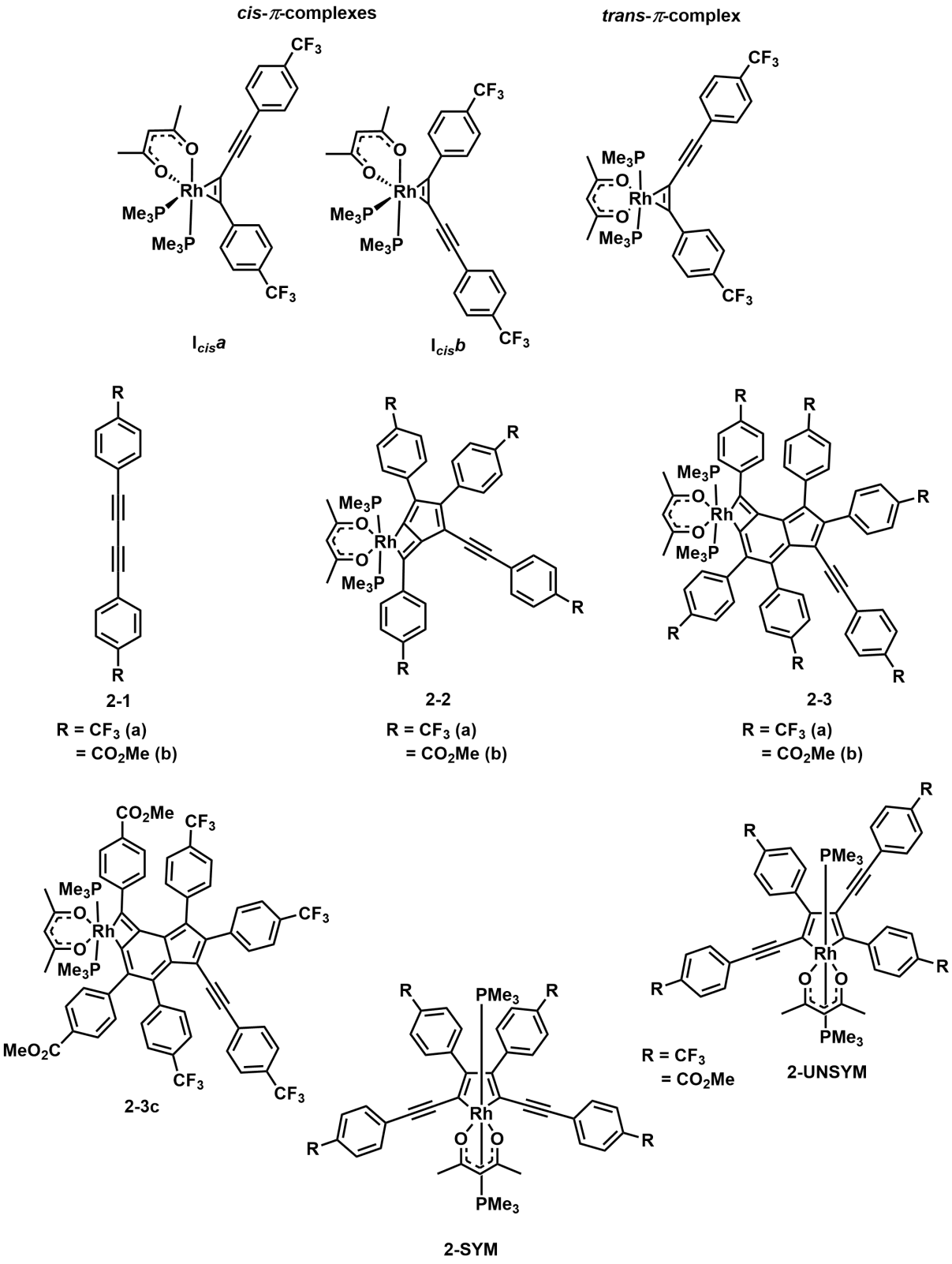

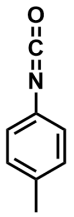

2-4

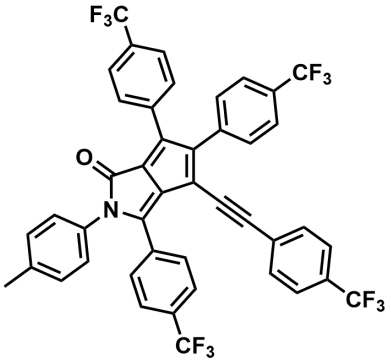

2-5

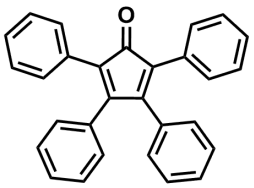

2-6

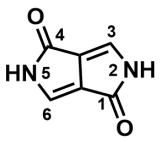

2-7

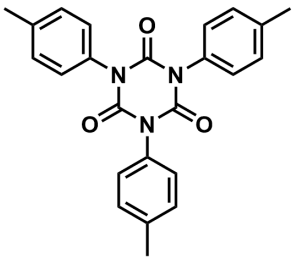

2-8

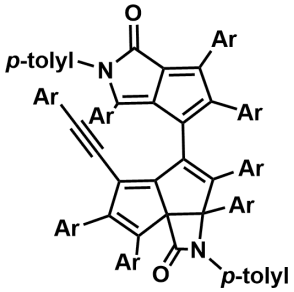

Ar = *p*-CF_3-C_6H_4

2-9

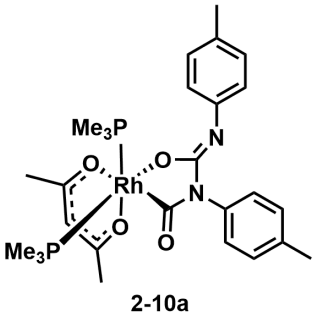

2-10a

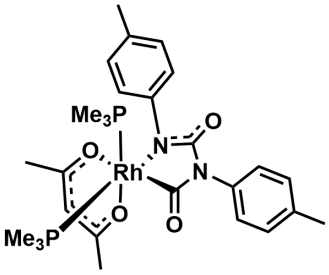

2-10b

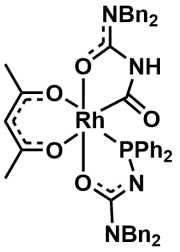

2-11

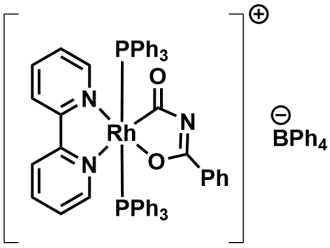

2-12

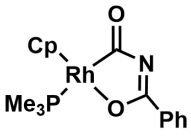

2-13

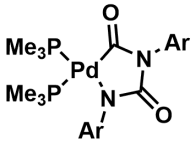

Ar = C_6H_5, *p*-Me-C_6H_4, *p*-Cl-C_6H_4 2-14 2-15

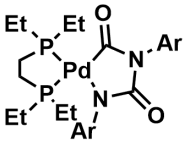

Ar = *p*-Cl-C_6H_4 2-16

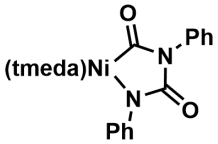

2-17

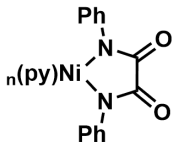

2-18

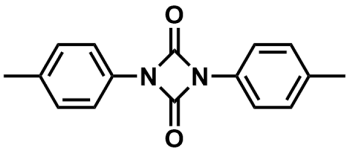

2-19

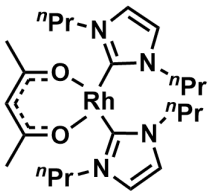

2-20

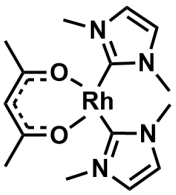

2-21

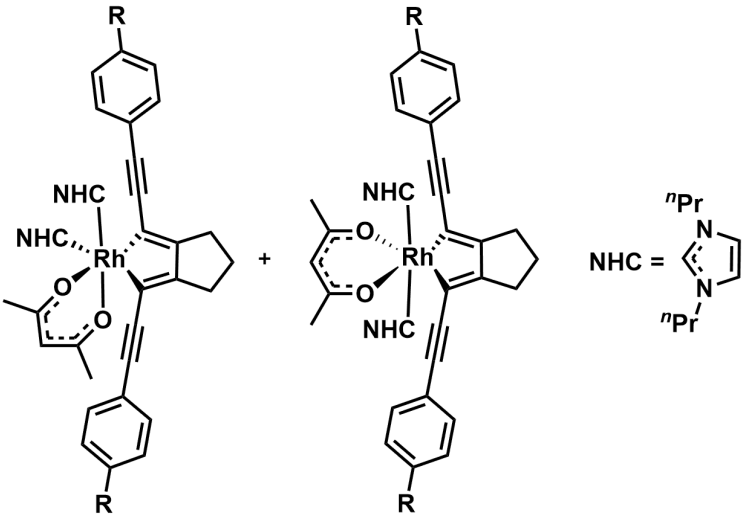

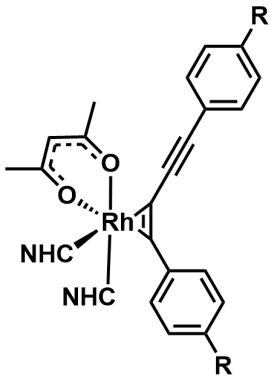

2-I$_{cis}$*a*

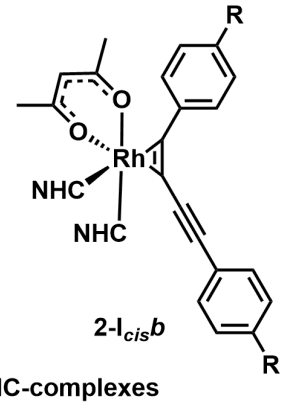

2-I$_{cis}$*b*

cis-NHC-complexes

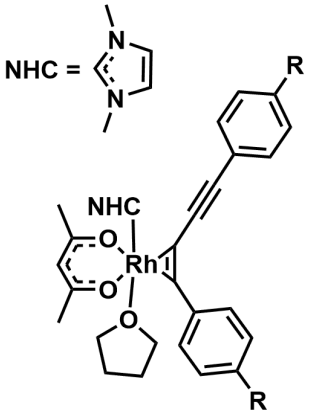

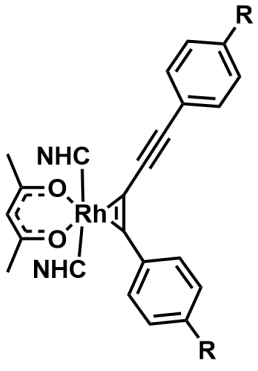

trans-NHC-complex

9.2.3 Compounds of Chapter 3

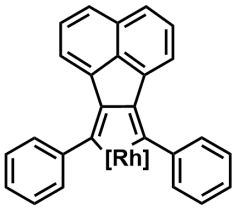

3-I

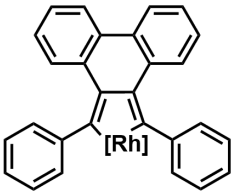

3-II

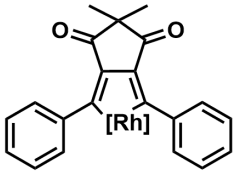

3-III

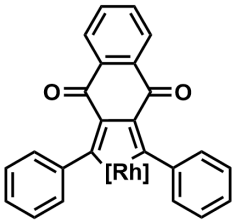

3-IV

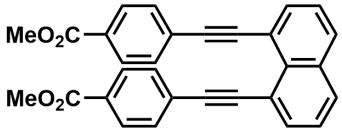

3-1

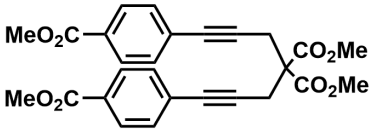

3-2

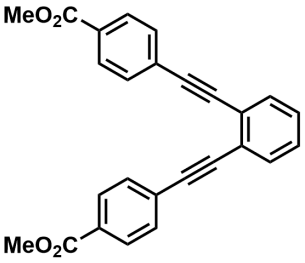

3-3

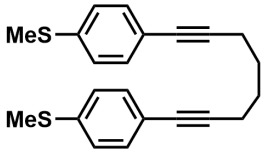

3-4

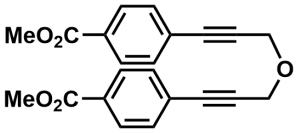

3-5

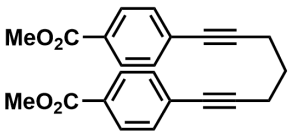

3-8

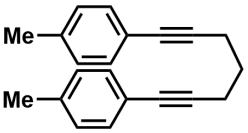

3-9

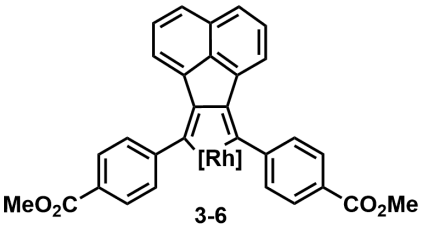

3-6

[Rh] = [Rh(acac)(PMe$_3$)$_2$]

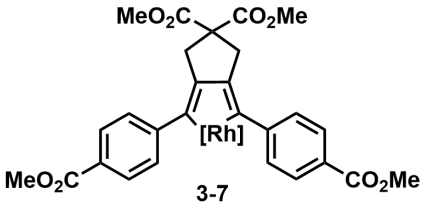

3-7

[Rh] = [Rh(acac)(PMe$_3$)$_2$]

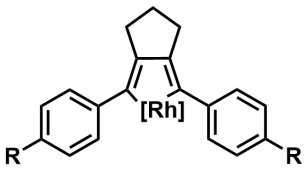

[Rh] = [Rh(acac)(PMe$_3$)$_2$]

R = CO_2Me 3-10
Me 3-11

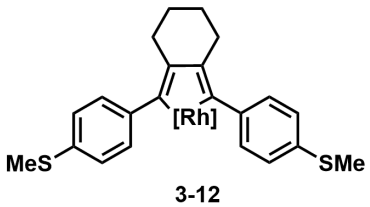

3-12

[Rh] = [Rh(acac)(PMe$_3$)$_2$]

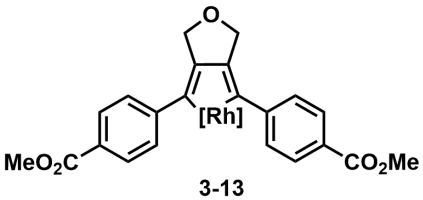

3-13

[Rh] = [Rh(acac)(PMe$_3$)$_2$]

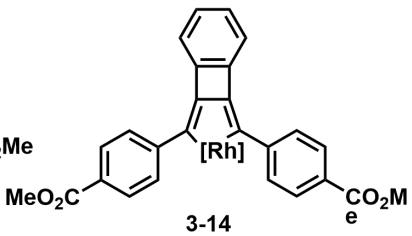

3-14

[Rh] = [Rh(acac)(PMe$_3$)$_2$]

"outside"

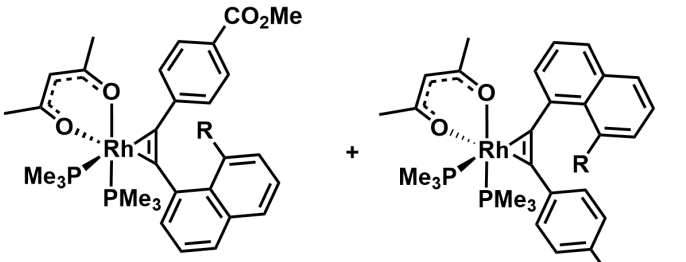

3-I$_{cis}$a + 3-I$_{cis}$b

"inside"

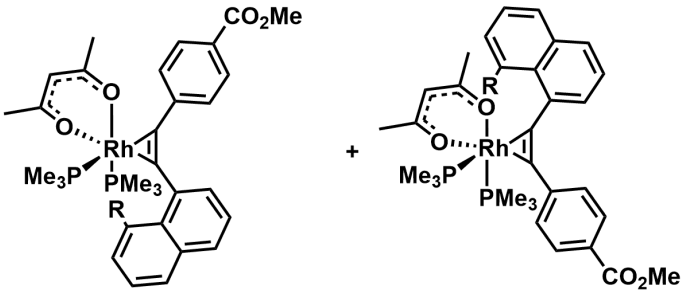

3-I$_{cis}$a + 3-I$_{cis}$b

R = *p*-CO$_2$Me-C$_6$H$_4$-CC-

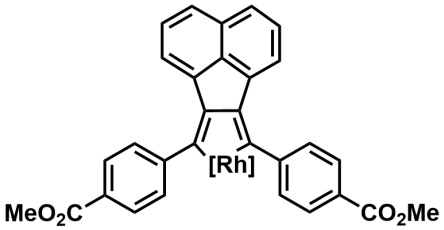

3-15

[Rh] = [Rh(acac)(P(*p*-tolyl)$_3$)$_2$]

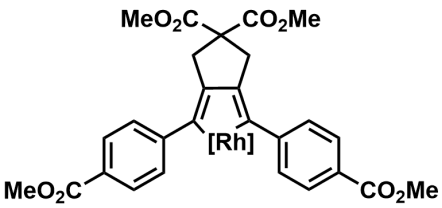

3-16

[Rh] = [Rh(acac)(P(*p*-tolyl)$_3$)$_2$]

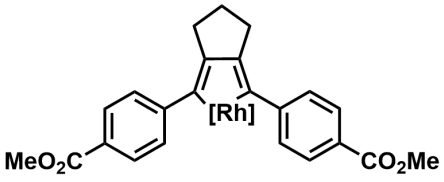

3-17

[Rh] = [Rh(acac)(P(*p*-tolyl)$_3$)$_2$]

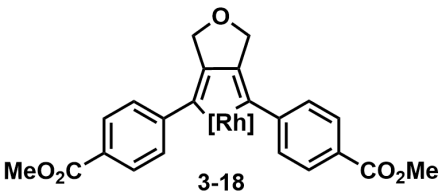

3-18

[Rh] = [Rh(acac)(P(*p*-tolyl)$_3$)$_2$]

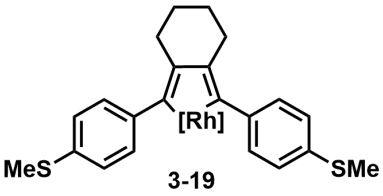

3-19

[Rh] = [Rh(acac)(P(*p*-tolyl)$_3$)$_2$]

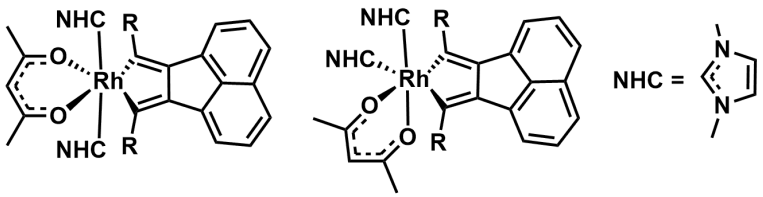

R = *p*-CO$_2$Me-C$_6$H$_4$

9.2.4 Compounds of Chapter 4

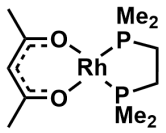

4-1

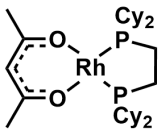

4-2

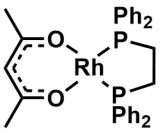

4-3

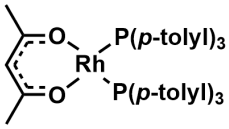

1-56

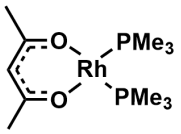

1-51

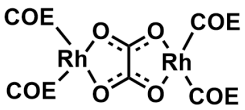

4-4

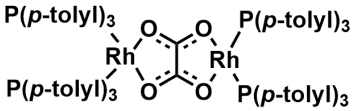

4-5

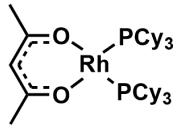

4-6

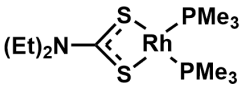

1-44

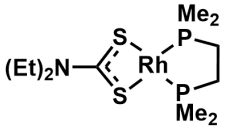

4-7

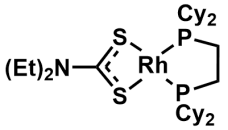

4-8

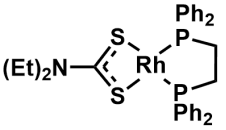

4-9

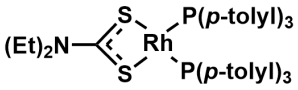

4-10

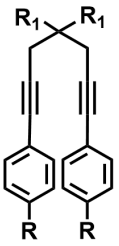

4-11 - 4-14

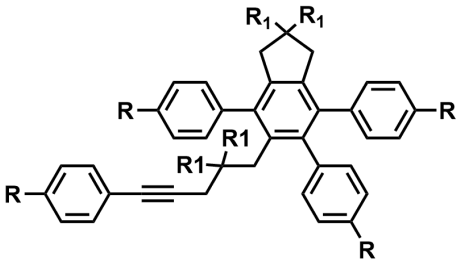

4-11a - 4-14a

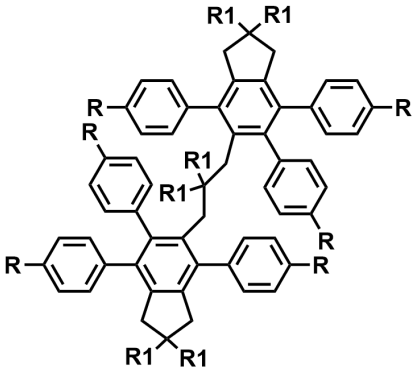

4-11b - 4-14b

4-11 (3-8) = R_1 = H; R = CO_2Me
4-12 = R_1 = H; R = Me
4-13 = R_1 = H; R = SMe
4-14 (3-2) = R_1 = CO_2Me; R = CO_2Me

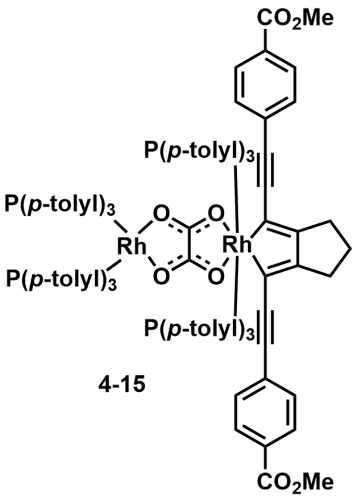

4-15

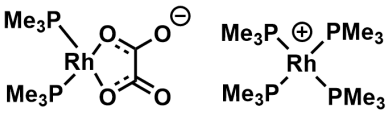

4-16

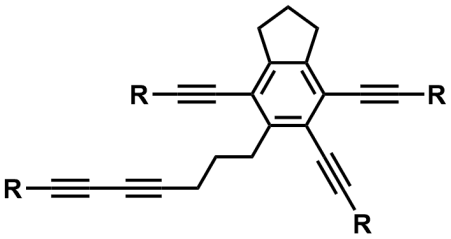

R = *p*-C_6H_4-CO_2Me
p-C_6H_4-Me
p-C_6H_4-NMe_2
p-C_6F_4-OMe

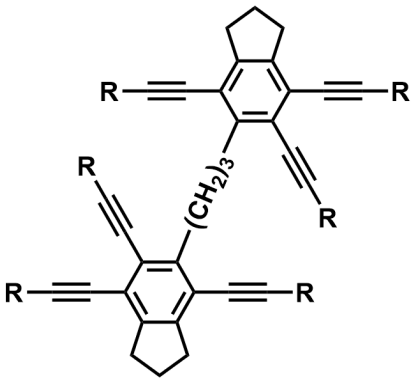

R = *p*-C_6H_4-CO_2Me
p-C_6H_4-Me
p-C_6F_4-OMe

9.3 NMR spectra

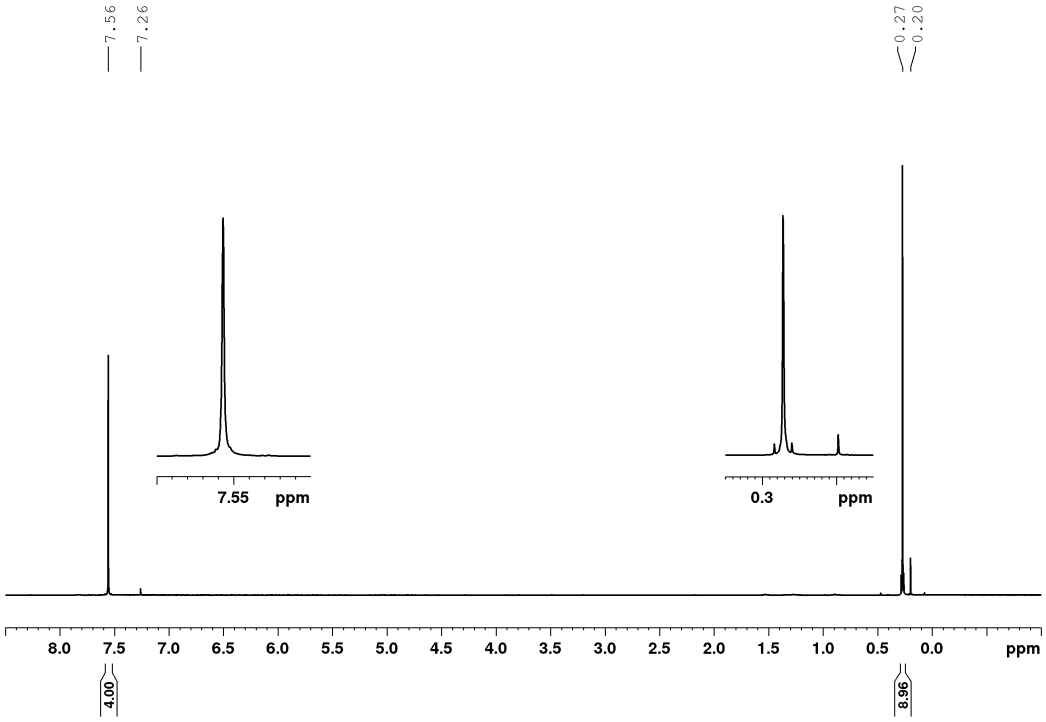

Figure A3: ^{1}H NMR spectrum of **trimethyl((4-(trifluoromethyl)phenyl)ethynyl)silane** in $CDCl_3$ at 300 MHz. Additionally, residual amounts of homocoupled TMSA at 0.20 ppm.

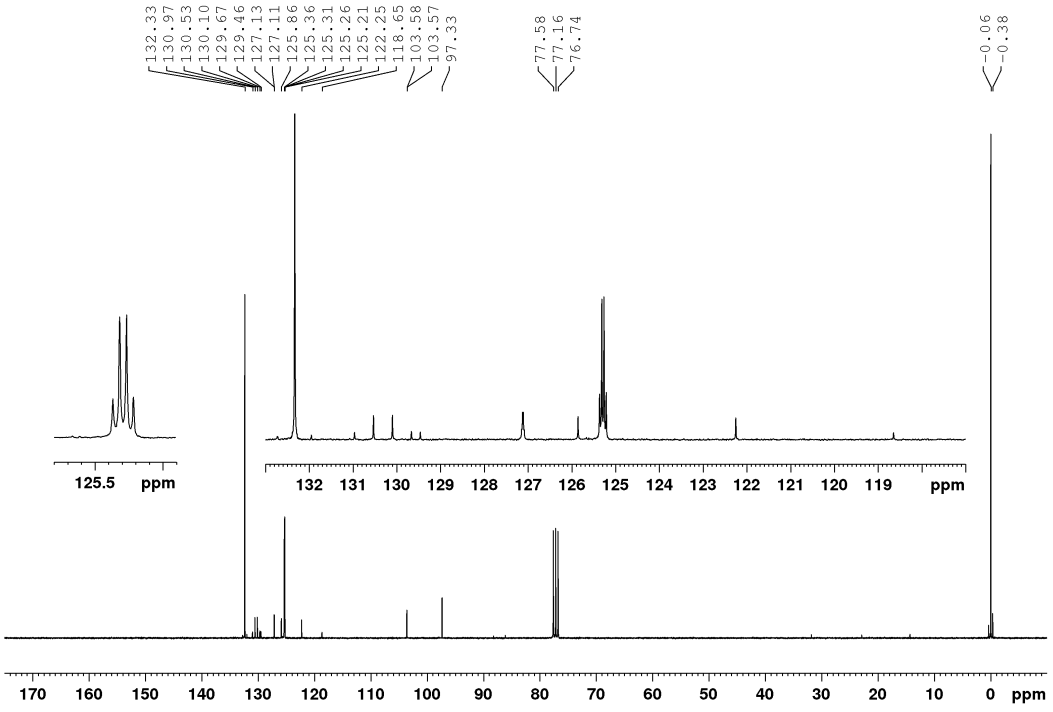

Figure A4: ^{13}C{^{1}H} NMR spectrum of **trimethyl((4-(trifluoromethyl)phenyl)ethynyl)silane** in $CDCl_3$ at 75 MHz.

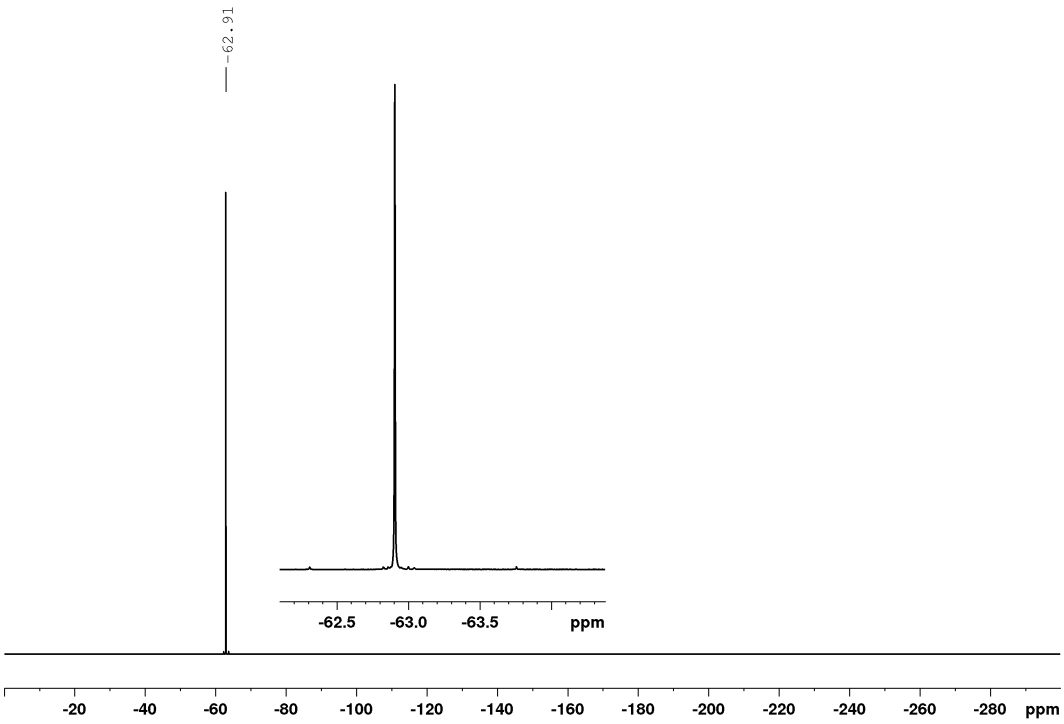

Figure A5: ^{19}F NMR spectrum of **trimethyl((4-(trifluoromethyl)phenyl)ethynyl)silane** in $CDCl_3$ at 188 MHz.

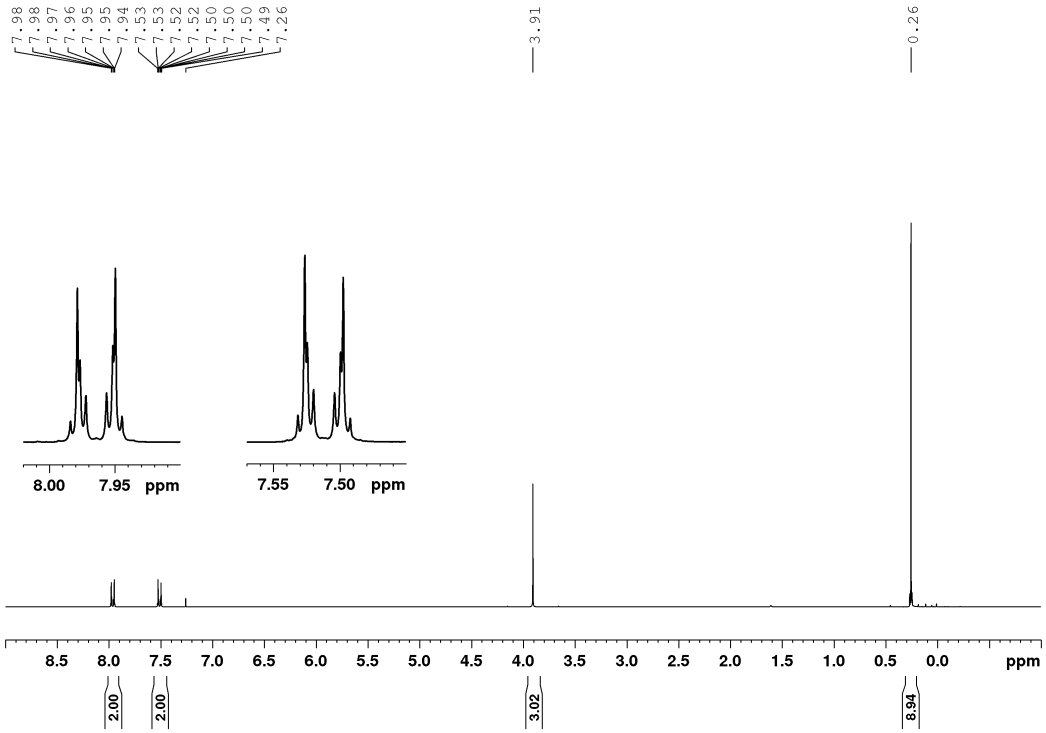

Figure A6: ^{1}H NMR spectrum of **methyl 4-((trimethylsilyl)ethynyl)benzoate** in $CDCl_3$ at 300 MHz.

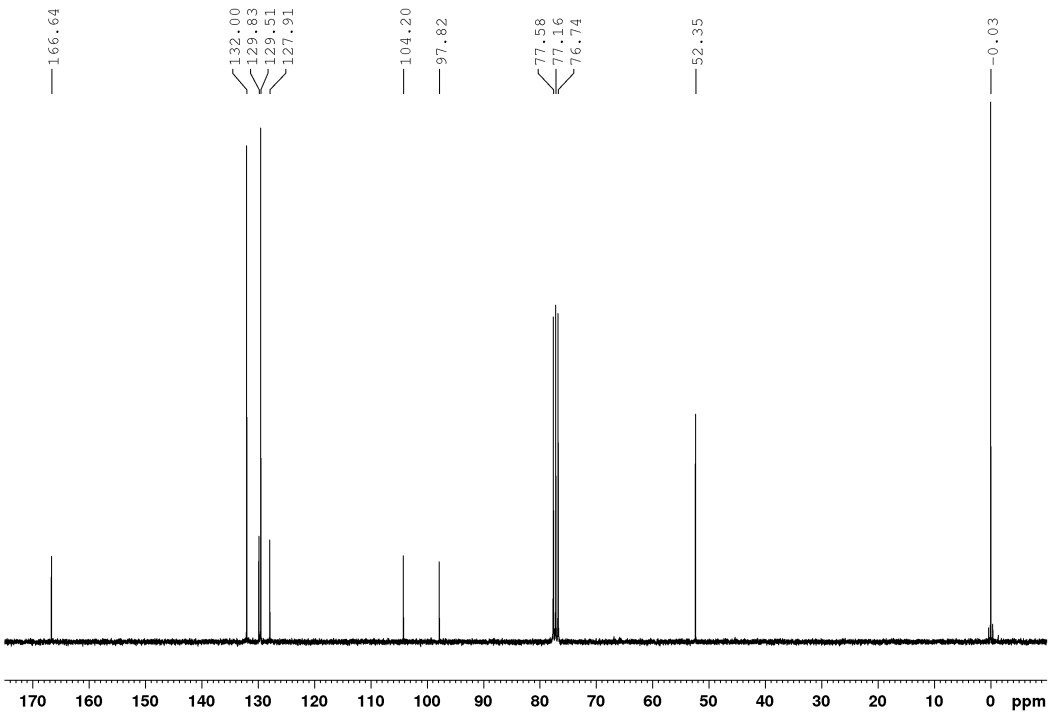

Figure A 7: $^{13}C\{^{1}H\}$ NMR spectrum of **methyl 4-((trimethylsilyl)ethynyl)benzoate** in $CDCl_3$ at 75 MHz.

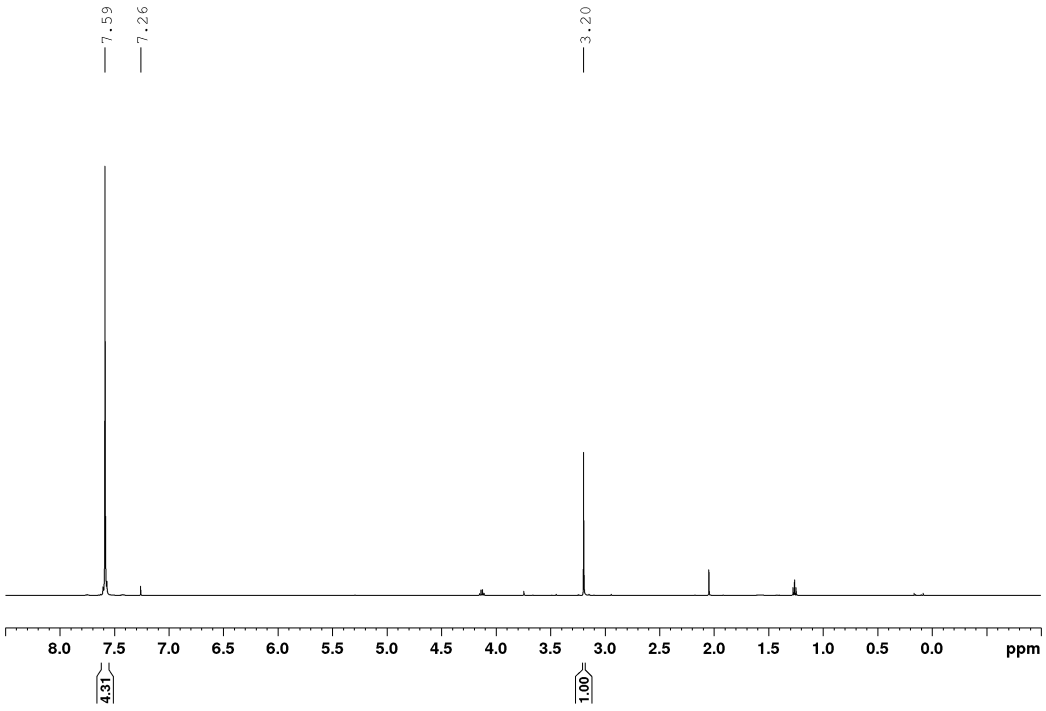

Figure A8: ^{1}H NMR spectrum of **1-ethynyl-4-(trifluoromethyl)benzene** in $CDCl_3$ at 500 MHz. Additionally, residual amounts of ethyl acetate (1.26, 2.05 and 4.12 ppm).

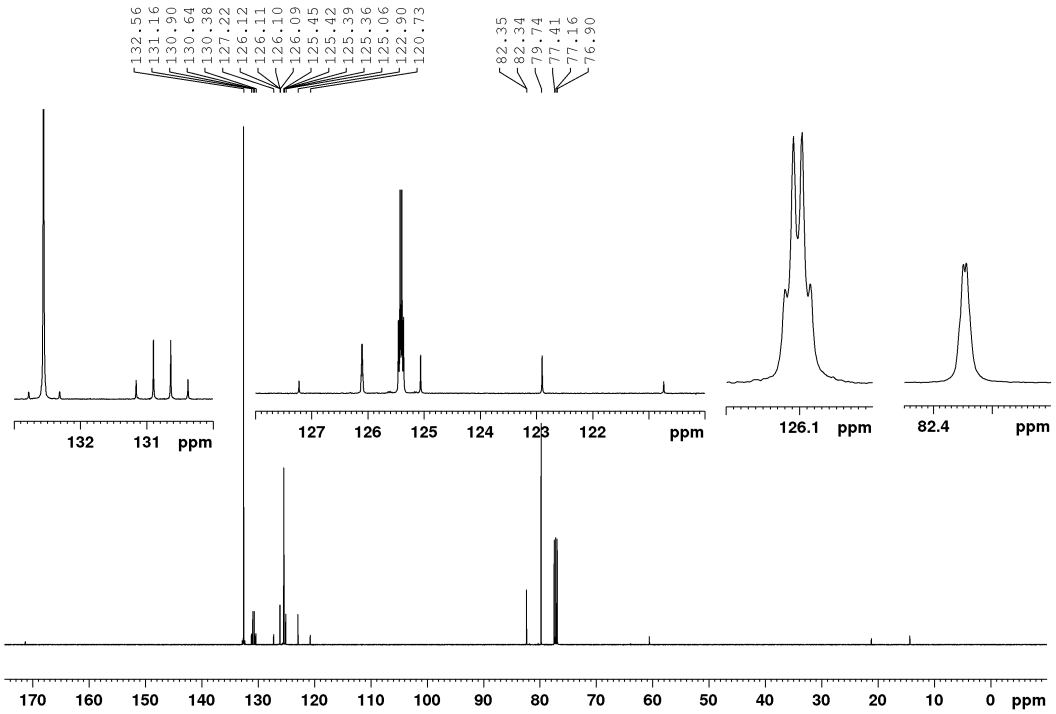

Figure A9: $^{13}C\{^{1}H\}$ NMR spectrum of **1-ethynyl-4-(trifluoromethyl)**benzene in $CDCl_3$ at 125 MHz. Additionally, residual amounts of ethyl acetate (14.2, 21.0, 60.5 and 171.4 ppm).

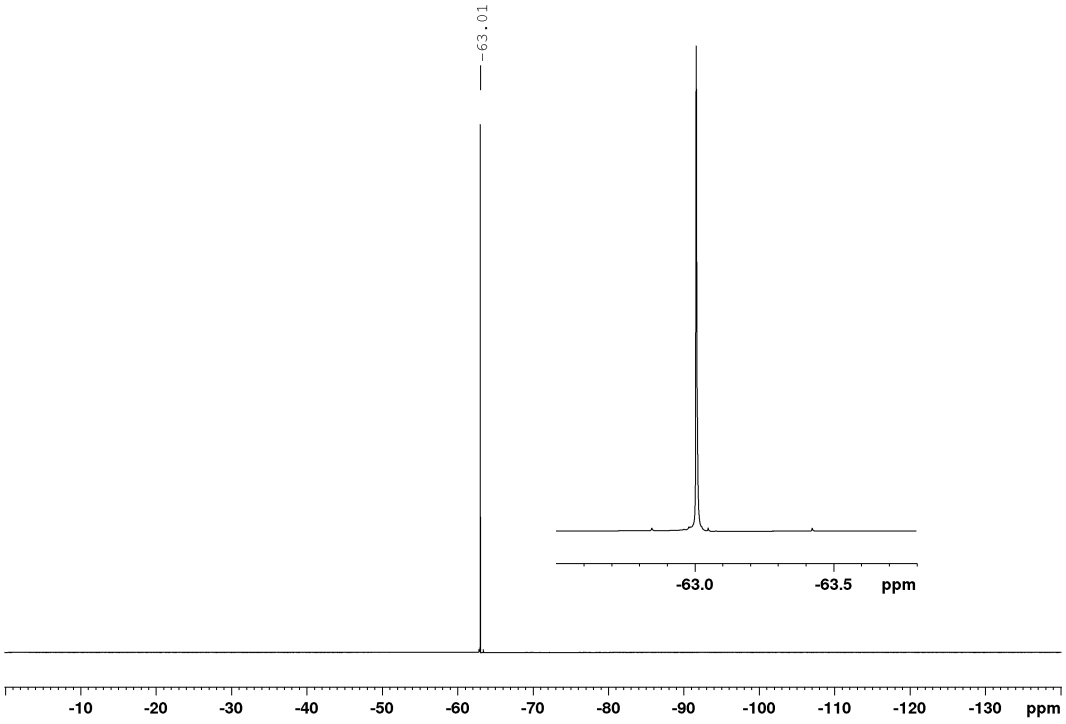

Figure A10: ^{19}F NMR spectrum of **1-ethynyl-4-(trifluoromethyl)benzene** in $CDCl_3$ at 470 MHz.

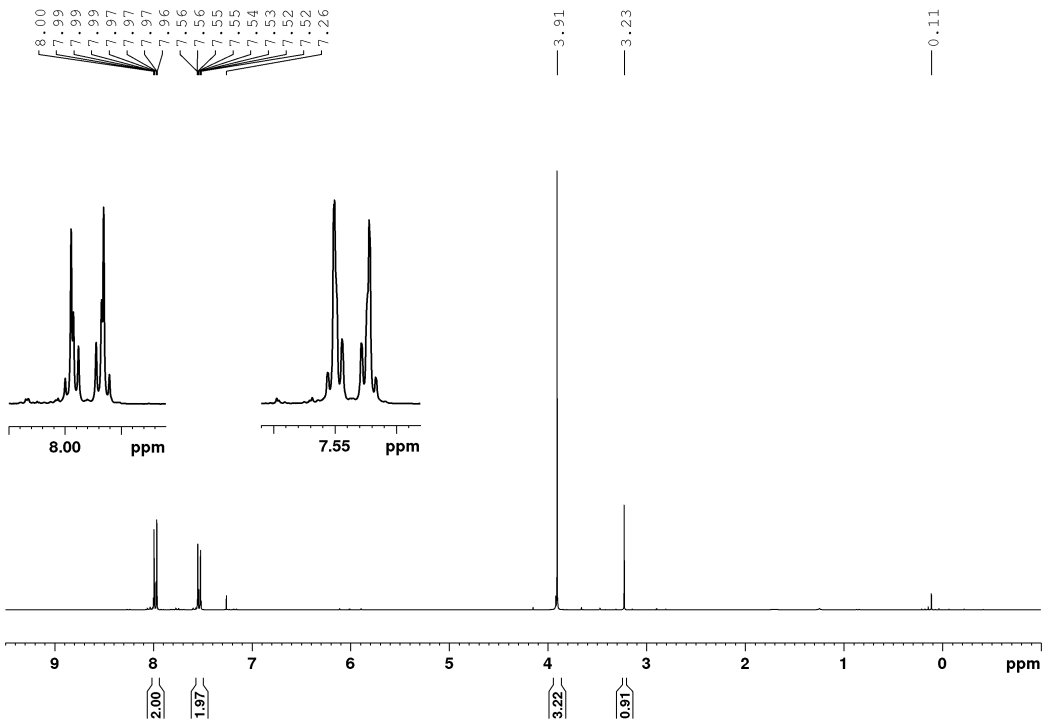

Figure A11: ^{1}H NMR spectrum of **methyl 4-ethynylbenzoate** in $CDCl_3$ at 300 MHz.

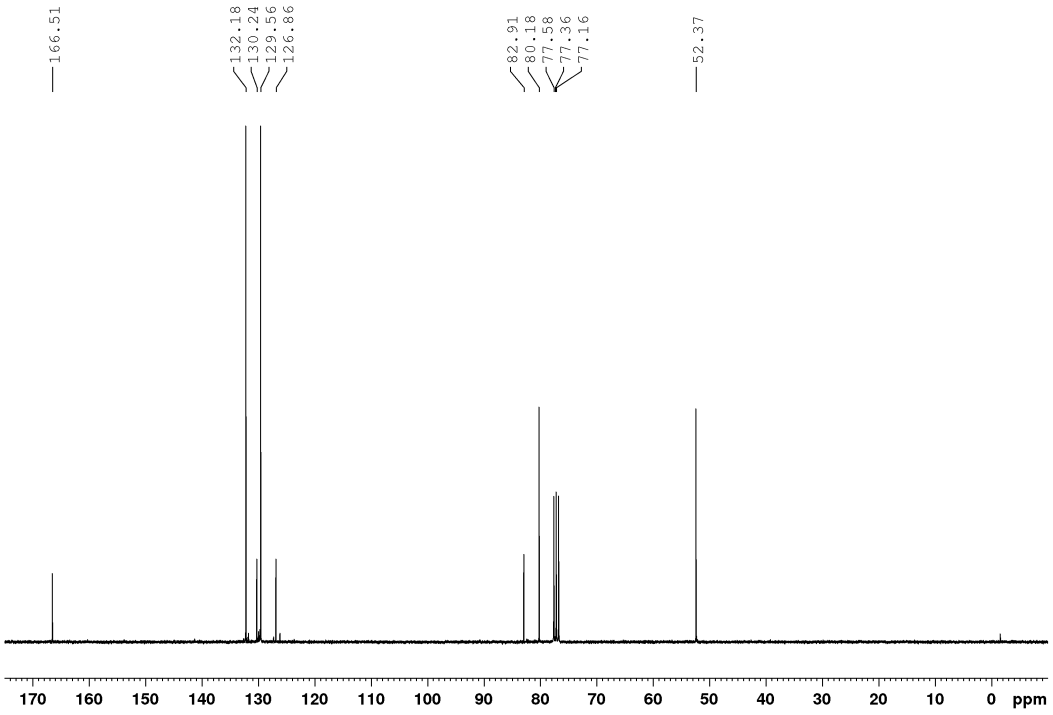

Figure A12: $^{13}C\{^{1}H\}$ NMR spectrum of **methyl 4-ethynylbenzoate** in $CDCl_3$ at 75 MHz.

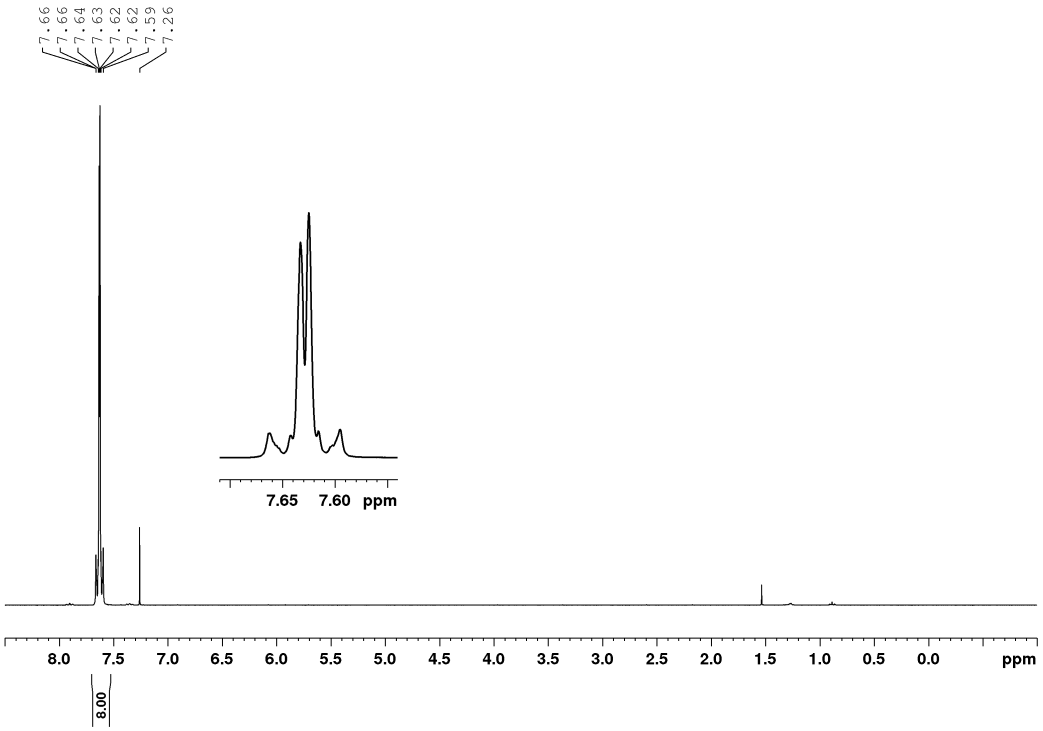

Figure A13: ^{1}H NMR spectrum of **2-1a** in $CDCl_3$ at 300 MHz. Additionally, residual amounts for water (1.56 ppm).

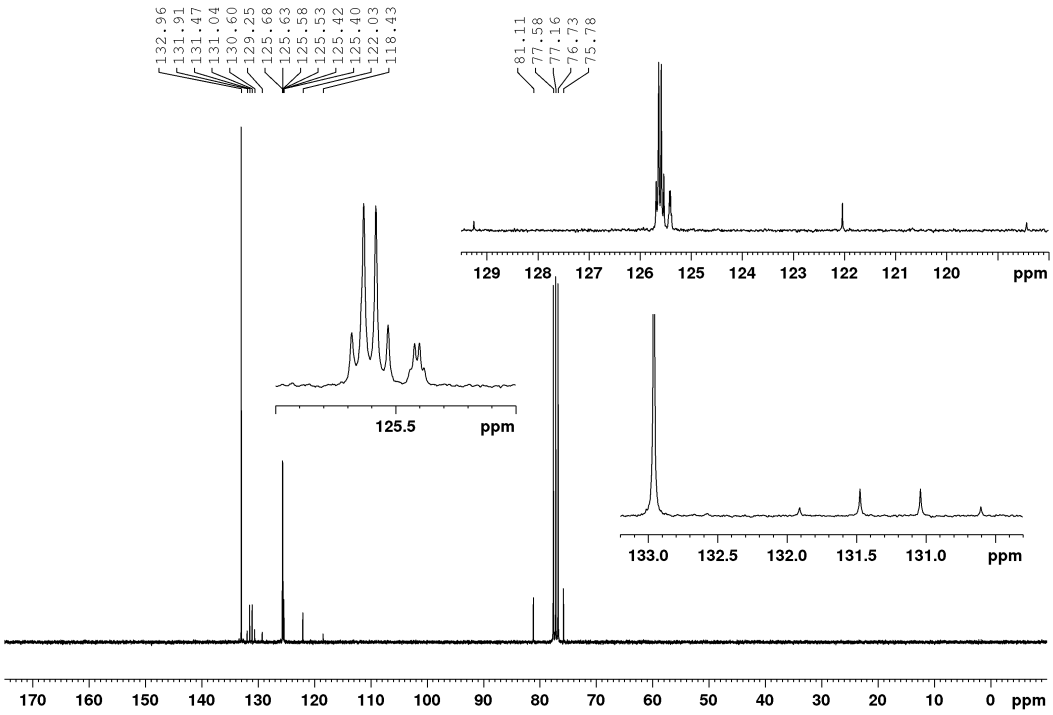

Figure A14: $^{13}C\{^{1}H\}$ NMR spectrum of **2-1a** in $CDCl_3$ at 75 MHz.

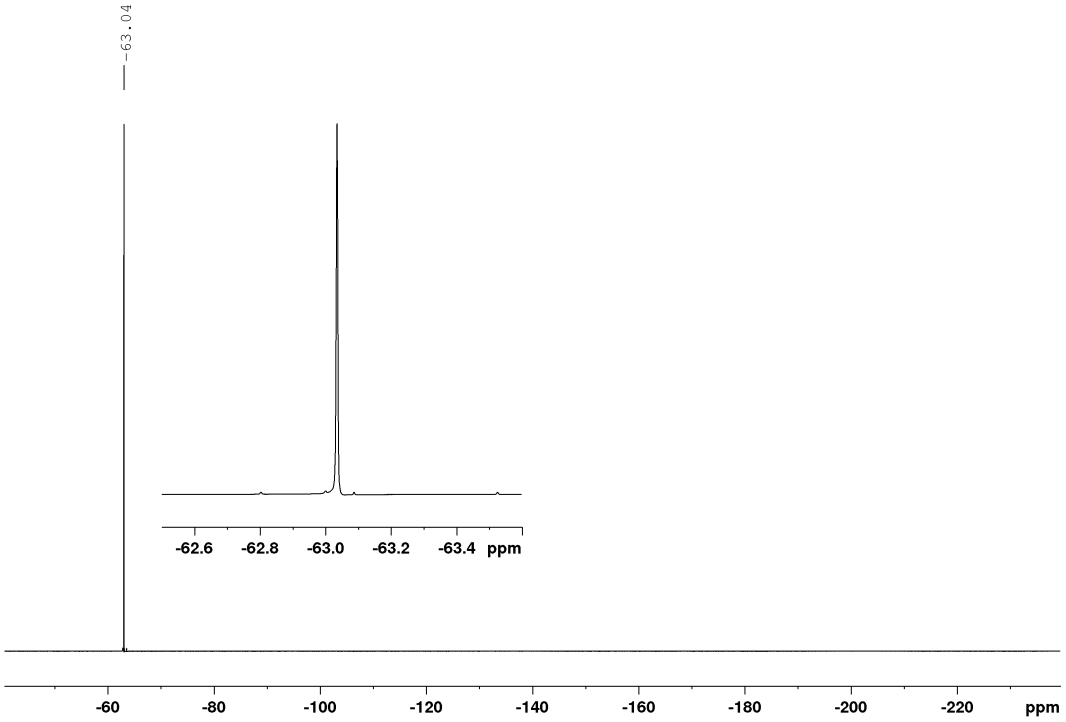

Figure A15: ^{19}F NMR spectrum of **2-1a** in $CDCl_3$ at 377 MHz.

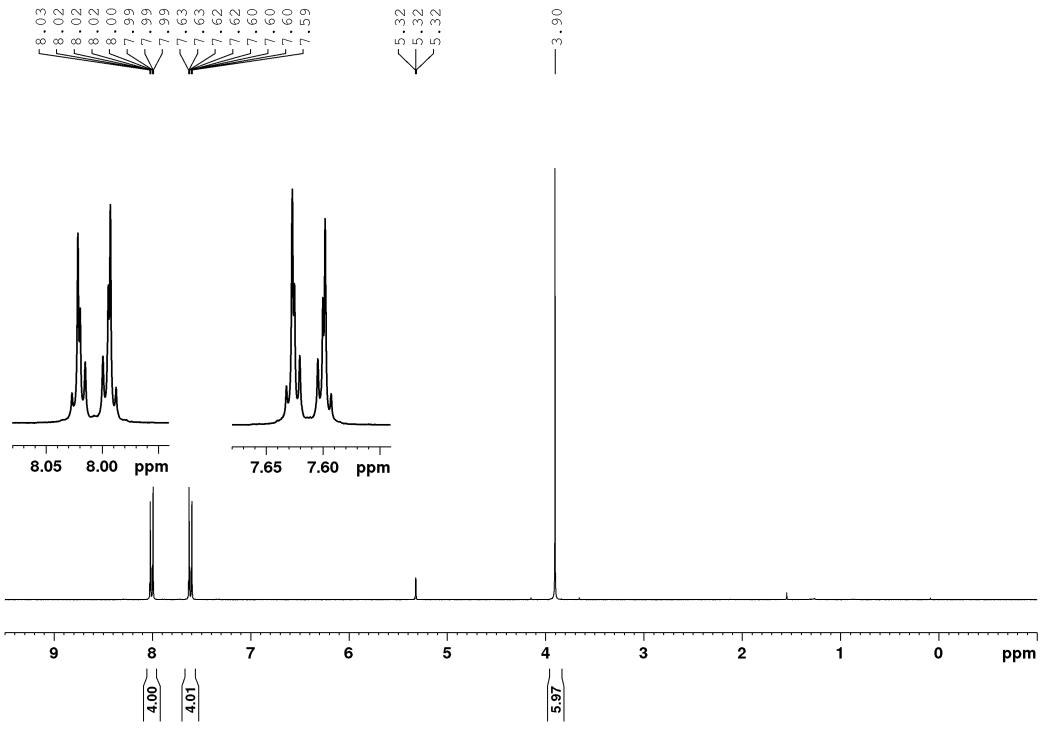

Figure A16: ^{1}H NMR spectrum of **2-1b** in CD_2Cl_2 at 300 MHz. Additionally, residual amounts of water (1.52 ppm).

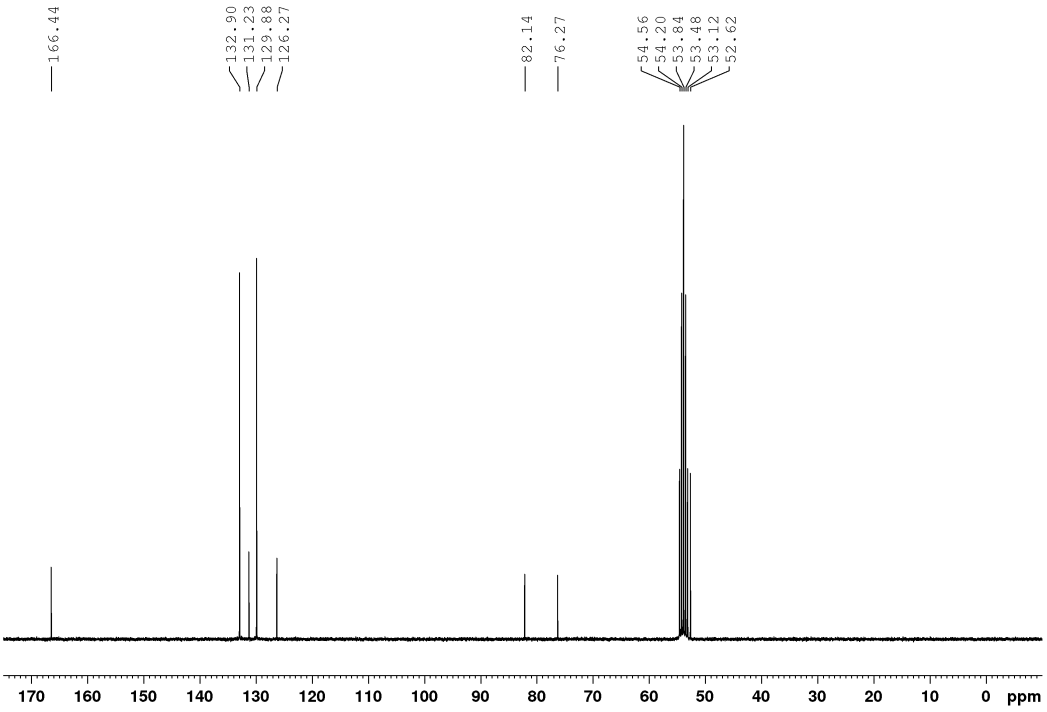

Figure A17: $^{13}C\{^{1}H\}$ NMR spectrum of **2-1b** in CD_2Cl_2 at 75 MHz.

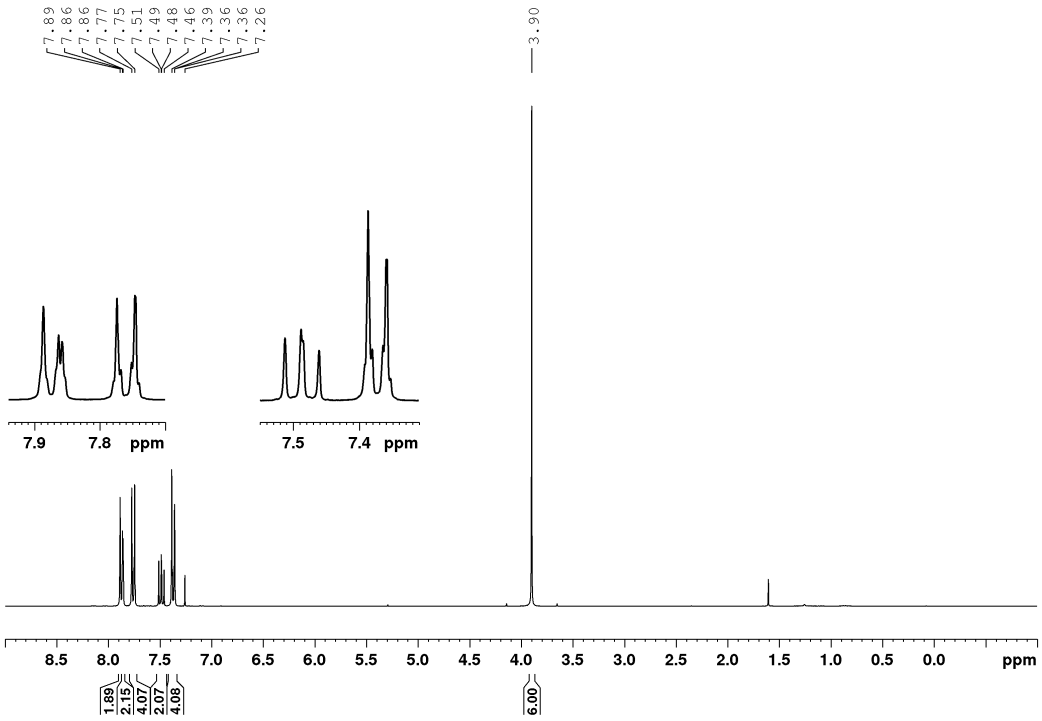

Figure A18: ^{1}H NMR spectrum of **3-1** in $CDCl_3$ at 300 MHz. Additionally, residual amounts of water (1.56 ppm).

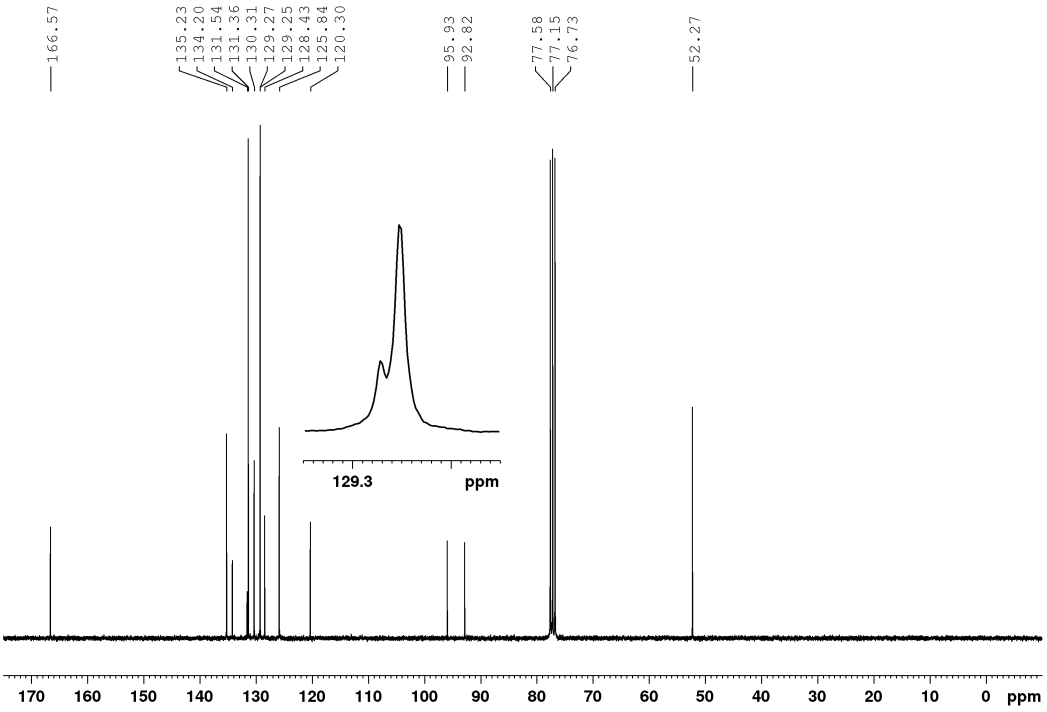

Figure A19: $^{13}C\{^{1}H\}$ NMR spectrum of **3-1** in $CDCl_3$ at 75 MHz.

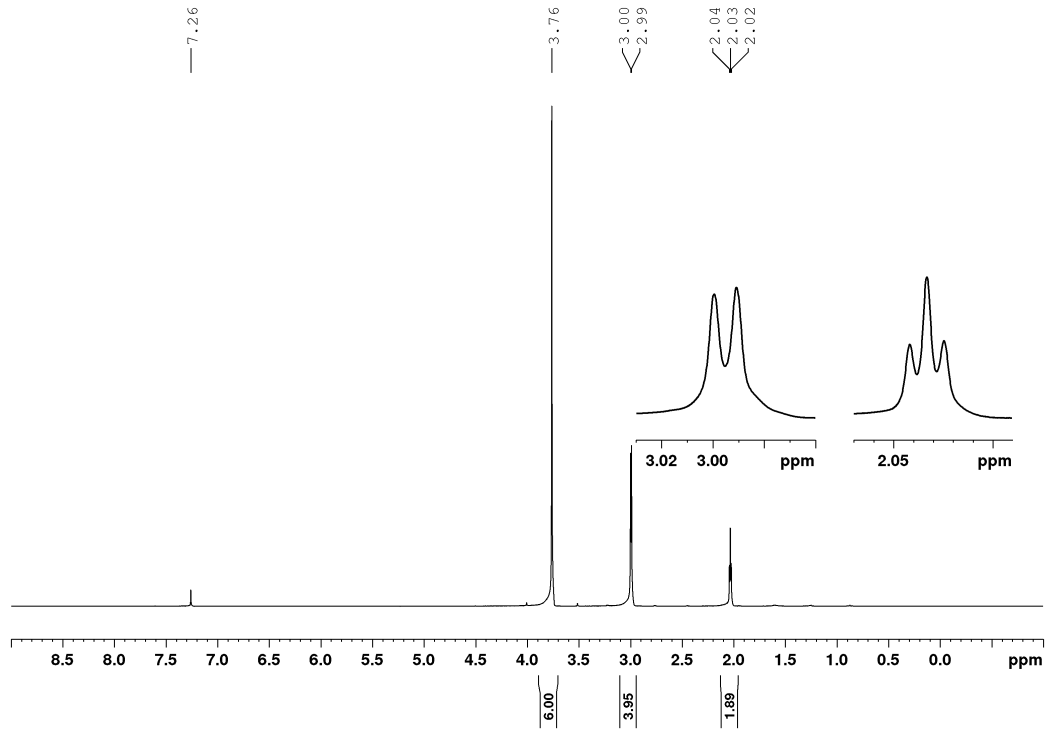

Figure A20: ^{1}H NMR spectrum of **dimethyl 2,2-di(prop-2-yn-1-yl)malonate** in $CDCl_3$ at 300 MHz.

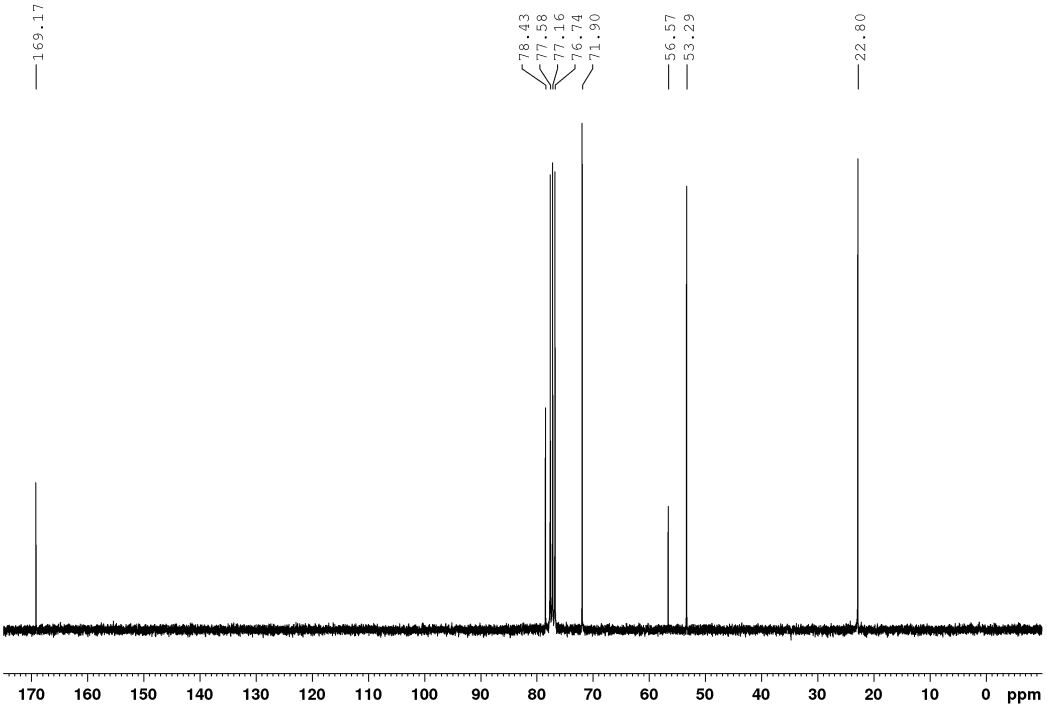

Figure A21: $^{13}C\{^{1}H\}$ NMR spectrum of **dimethyl 2,2-di(prop-2-yn-1-yl)malonate** in $CDCl_3$ at 75 MHz.

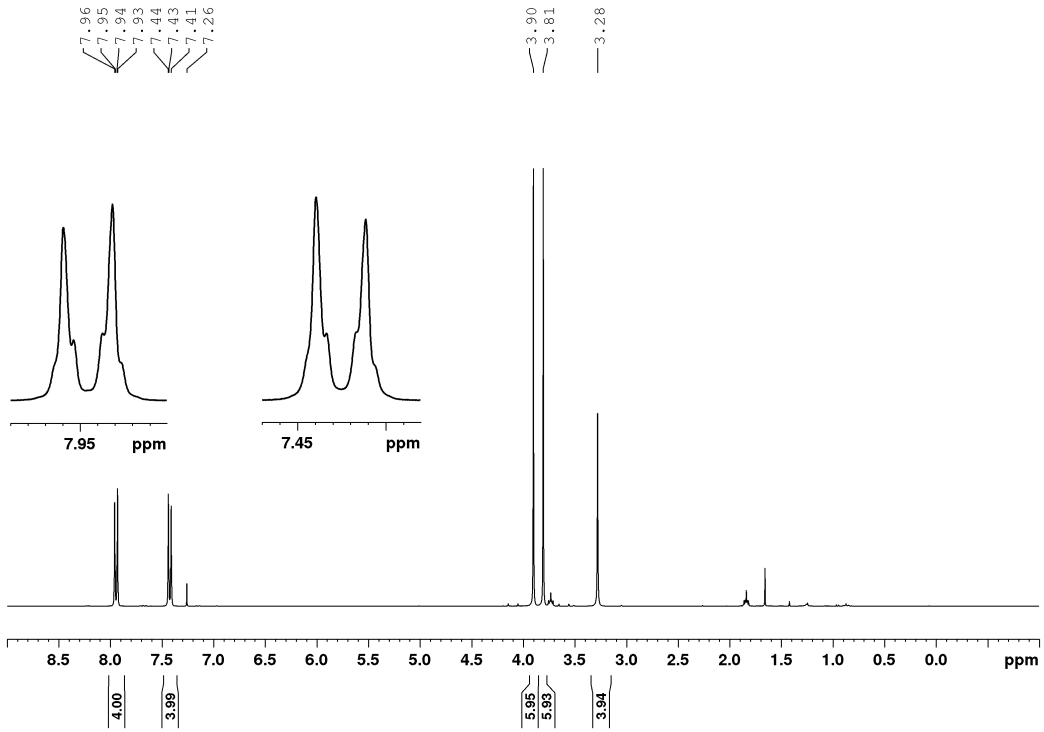

Figure A22: ^{1}H NMR spectrum of **3-2/4-14** in $CDCl_3$ at 300 MHz. Additionally, residual amounts of THF (3.76 and 1.85 ppm), *n*-hexane (0.88 and 1.26 ppm) and water (1.56 ppm).

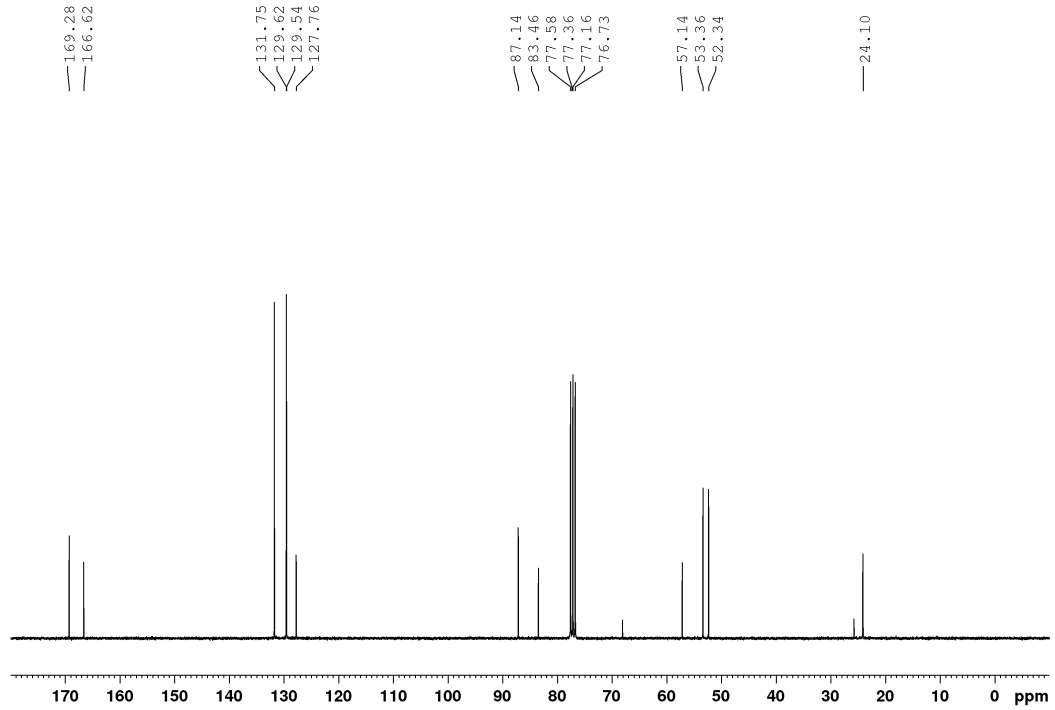

Figure A23: $^{13}C\{^{1}H\}$ NMR spectrum of **3-2/4-14** in $CDCl_3$ at 75 MHz. Additionally, residual amounts of THF (25.6 and 68.0 ppm).

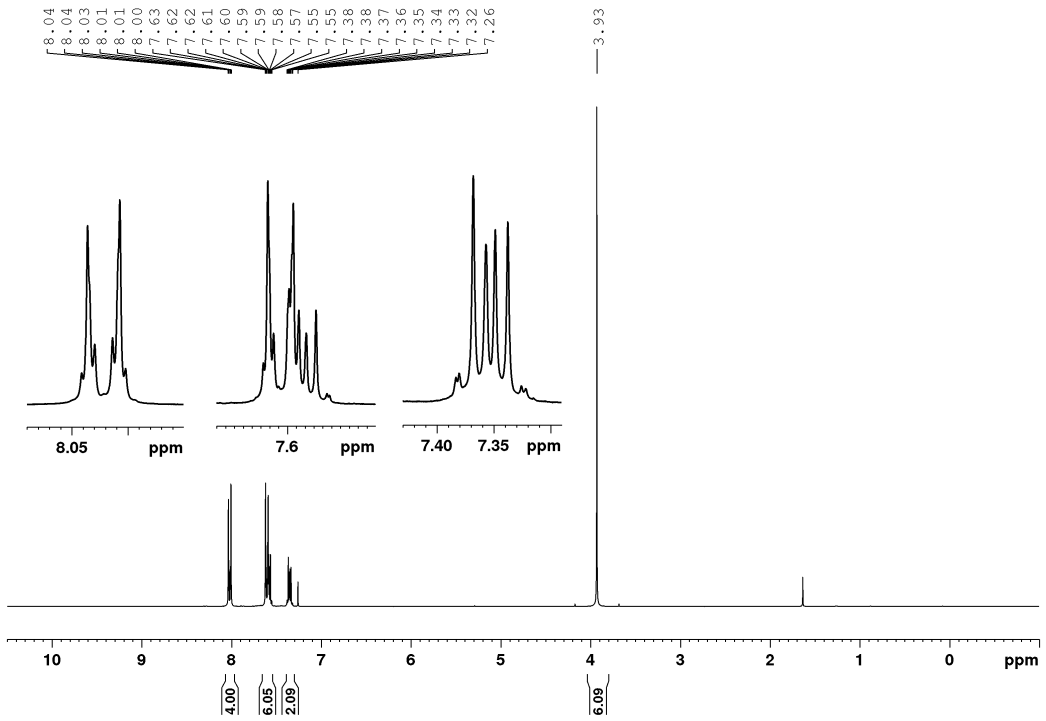

Figure A24: ^{1}H NMR spectrum of **3-3** in $CDCl_3$ at 300 MHz. Additionally, residual amounts of water (1.56 ppm).

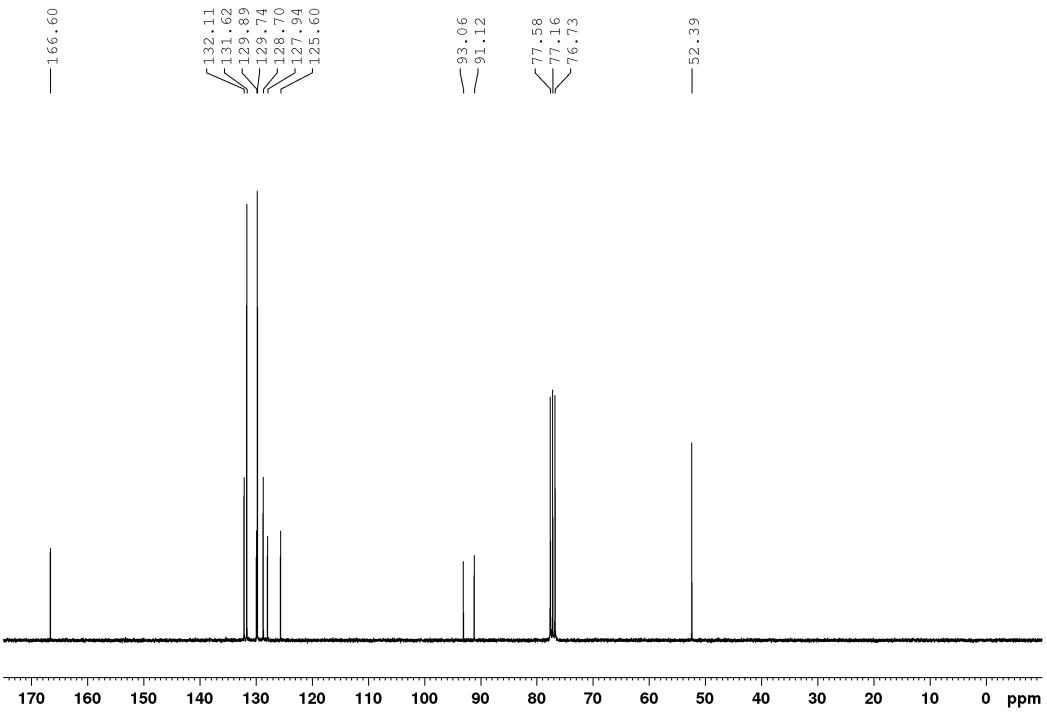

Figure A25: $^{13}C\{^{1}H\}$ NMR spectrum of **3-3** in $CDCl_3$ at 75 MHz.

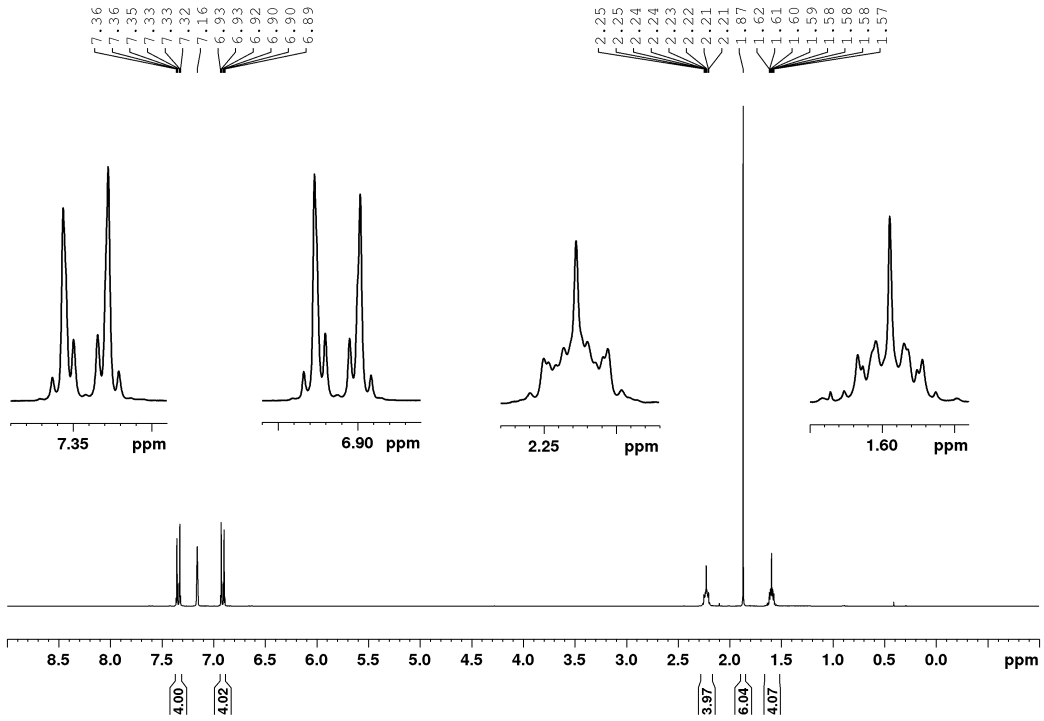

Figure A26: ^{1}H NMR spectrum of **3-4** in C_6D_6 at 300 MHz.

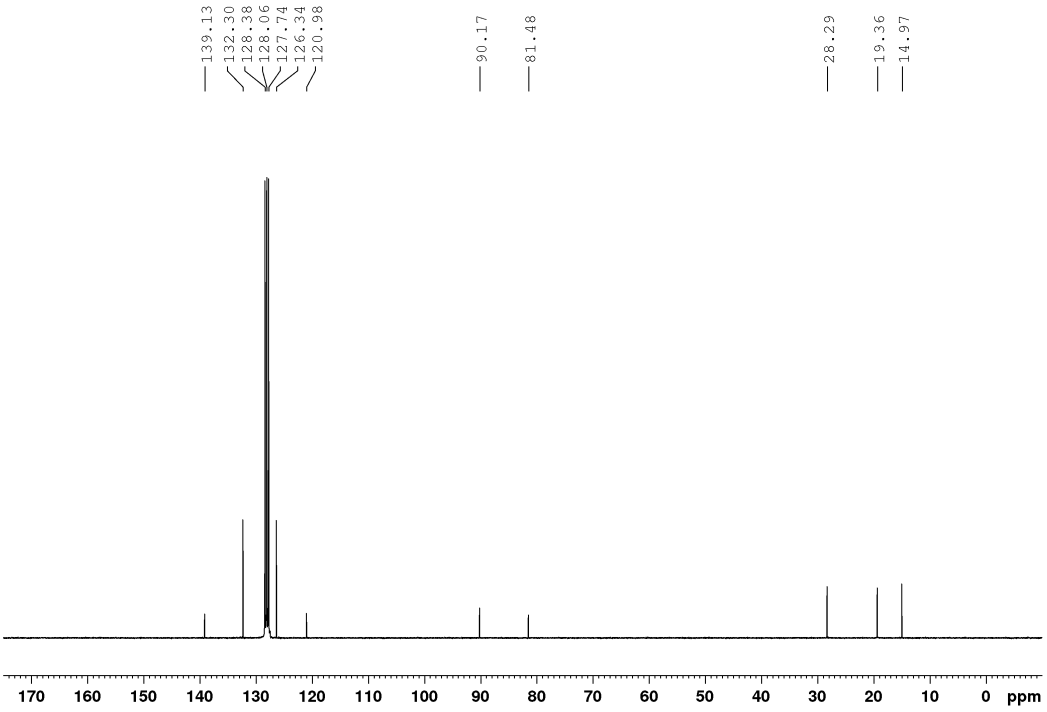

Figure A27: $^{13}C\{^{1}H\}$ NMR spectrum of **3-4** in C_6D_6 at 75 MHz.

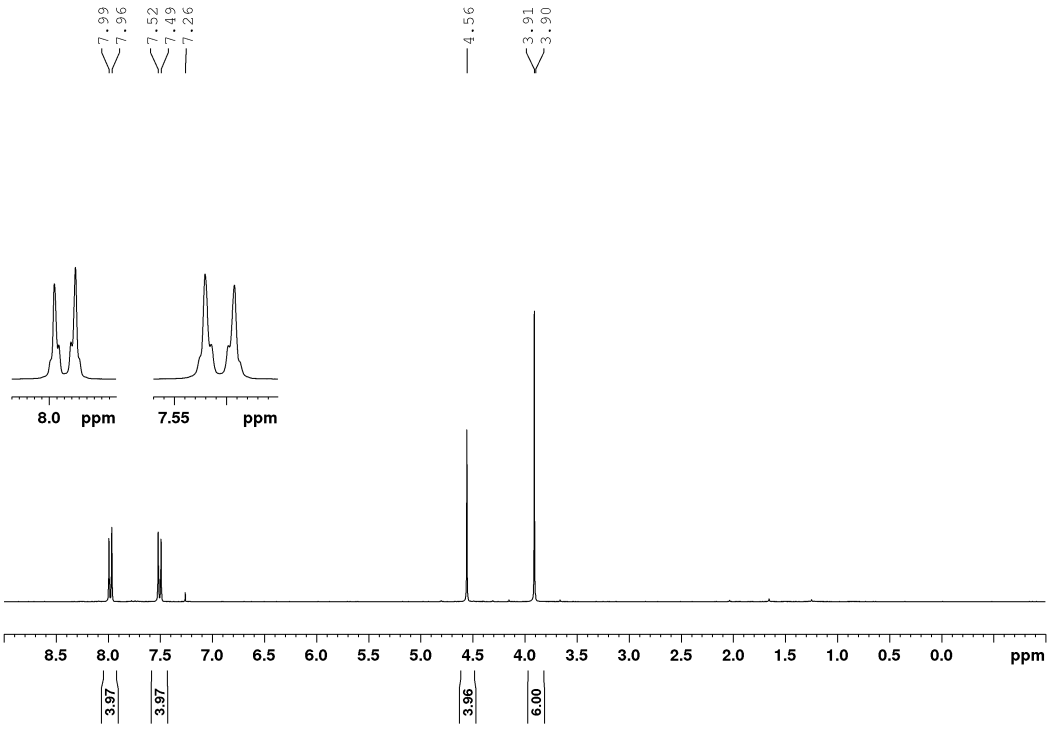

Figure A28: ^{1}H NMR spectrum of **3-5** in $CDCl_3$ at 300 MHz.

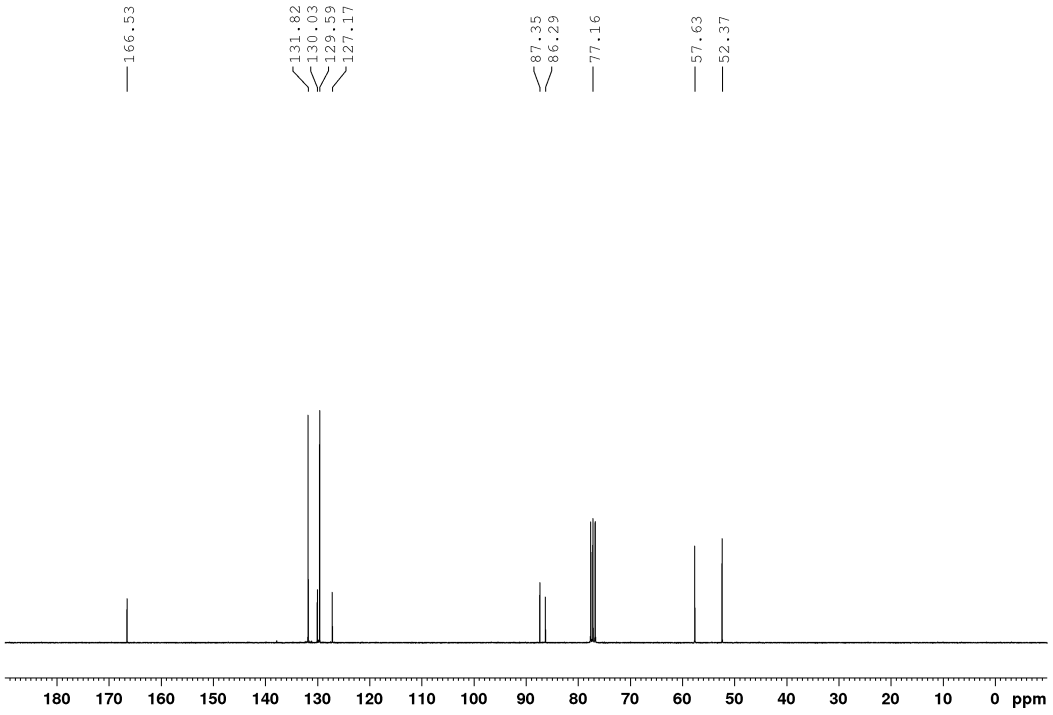

Figure A29: $^{13}C\{^{1}H\}$ NMR spectrum of **3-5** in $CDCl_3$ at 75 MHz.

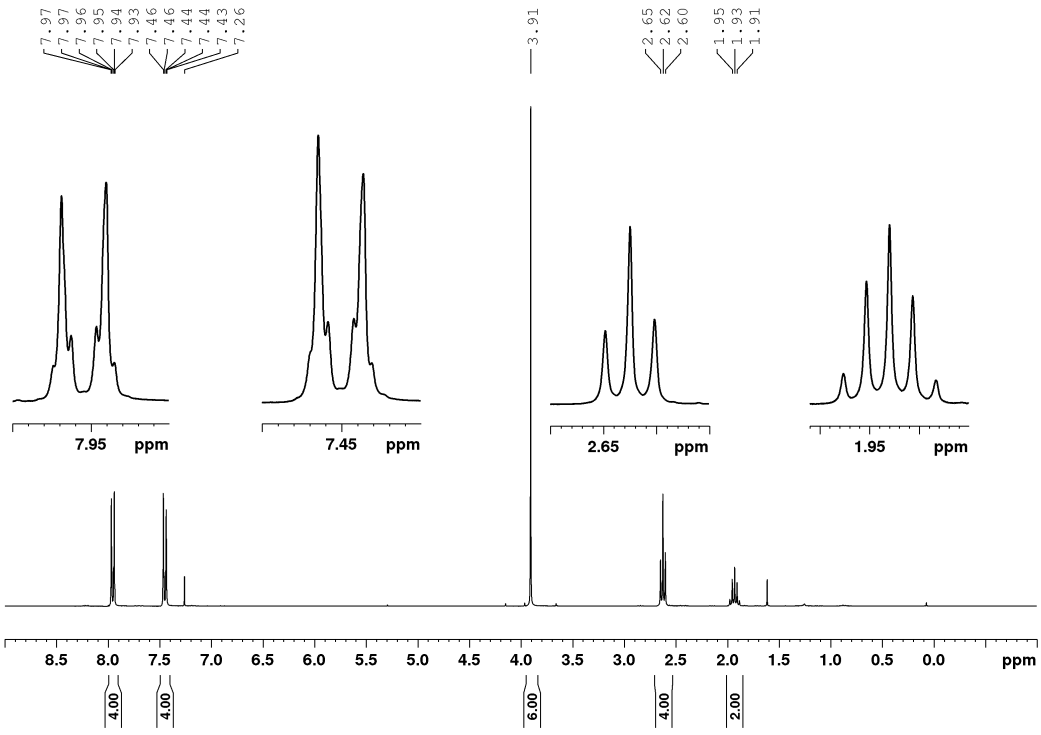

Figure A30: ^{1}H NMR spectrum of **3-8/4-11** in $CDCl_3$ at 300 MHz. Additionally, residual amounts of water (1.56 ppm).

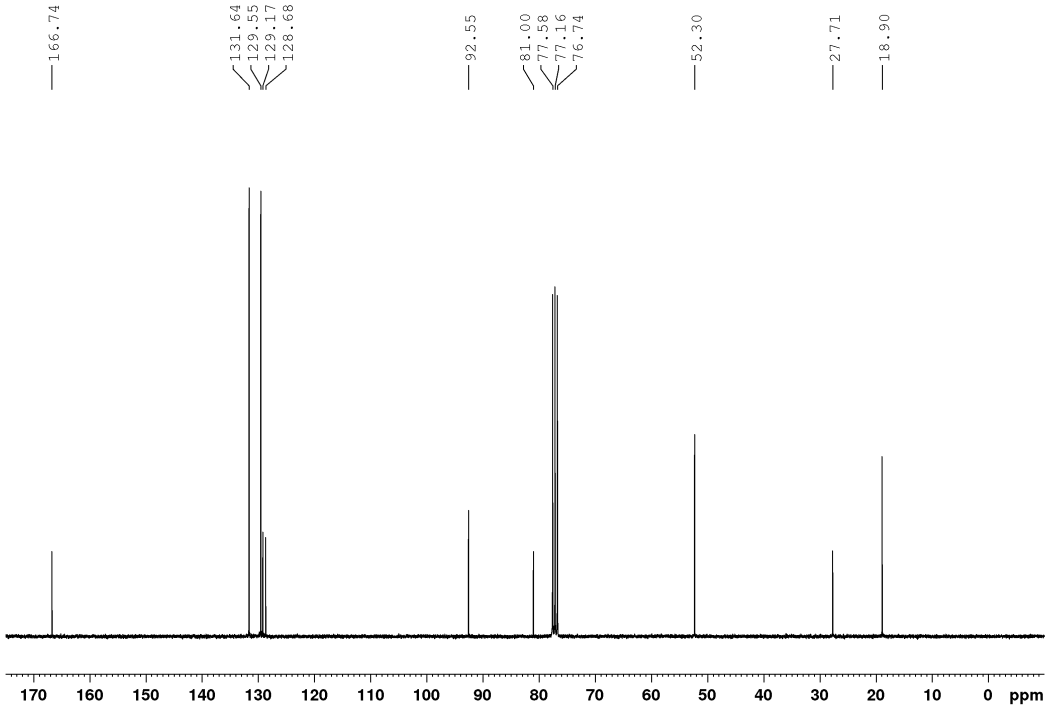

Figure A31: $^{13}C\{^{1}H\}$ NMR spectrum of **3-8/4-11** in $CDCl_3$ at 75 MHz.

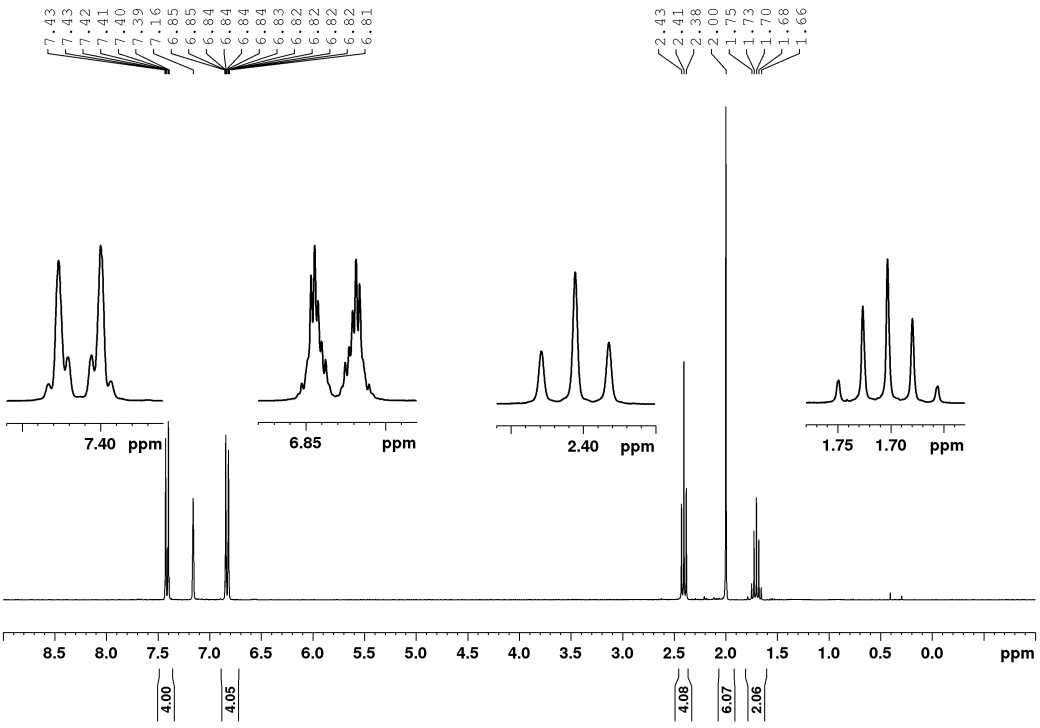

Figure A32: ^{1}H NMR spectrum of **3-9/4-12** in C_6D_6 at 300 MHz. Additionally, residual amounts of water (0.40 ppm).

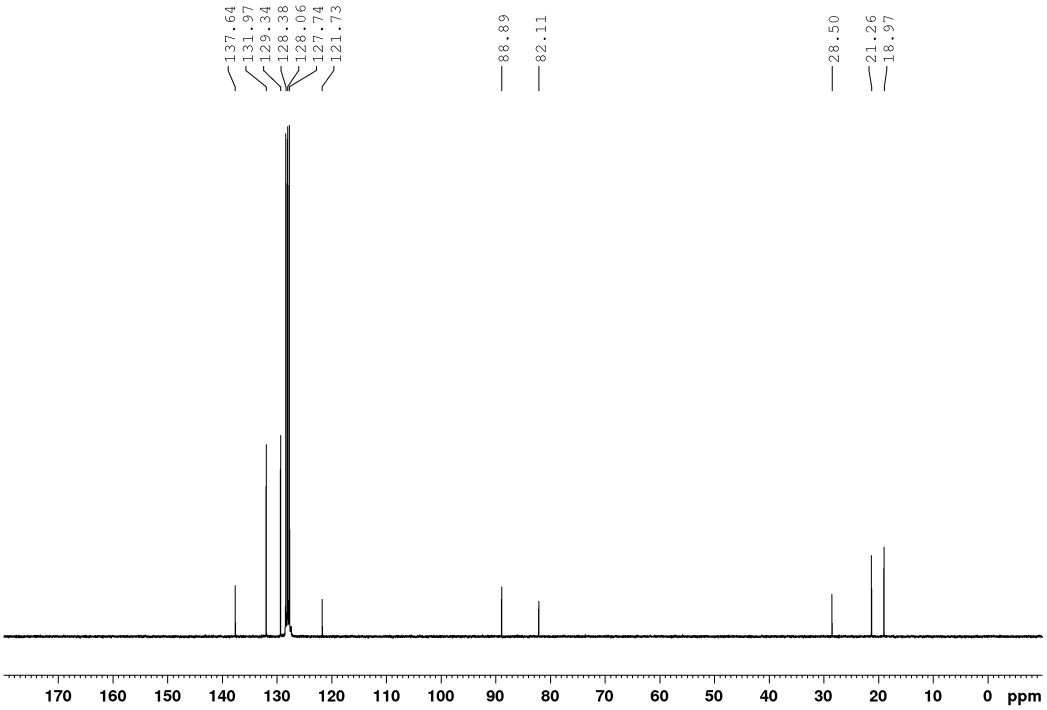

Figure A33: $^{13}C\{^{1}H\}$ NMR spectrum of **3-9/4-12** in C_6D_6 at 75 MHz.

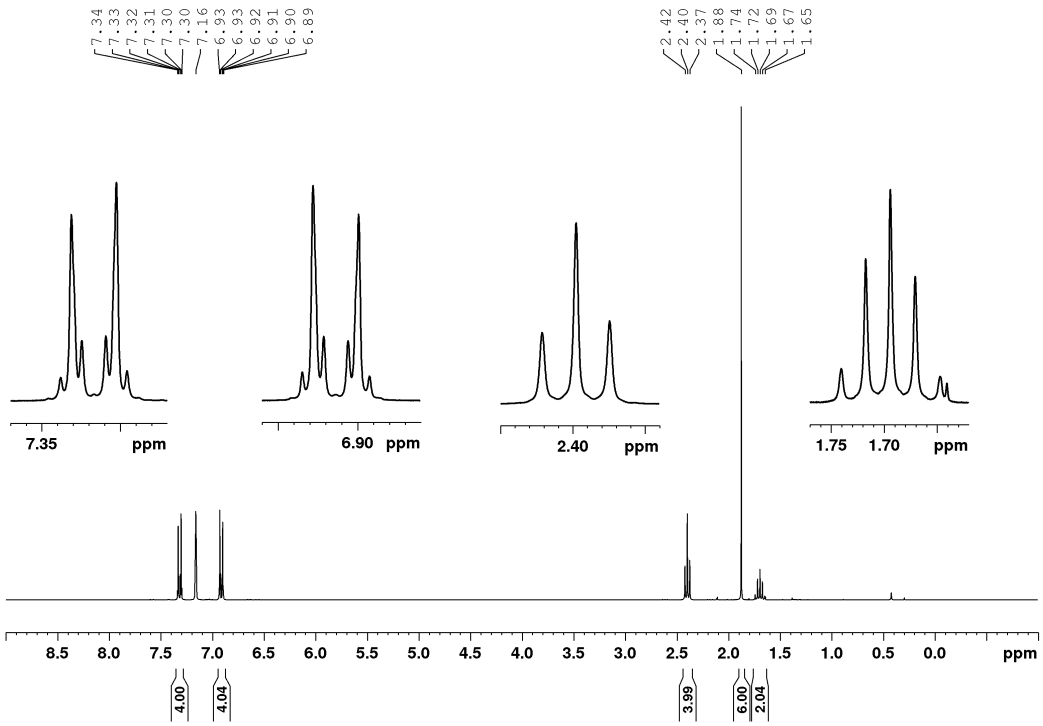

Figure A34: ^{1}H NMR spectrum of **4-13** in C_6D_6 at 300 MHz. Additionally, residual amounts of water (0.40 ppm).

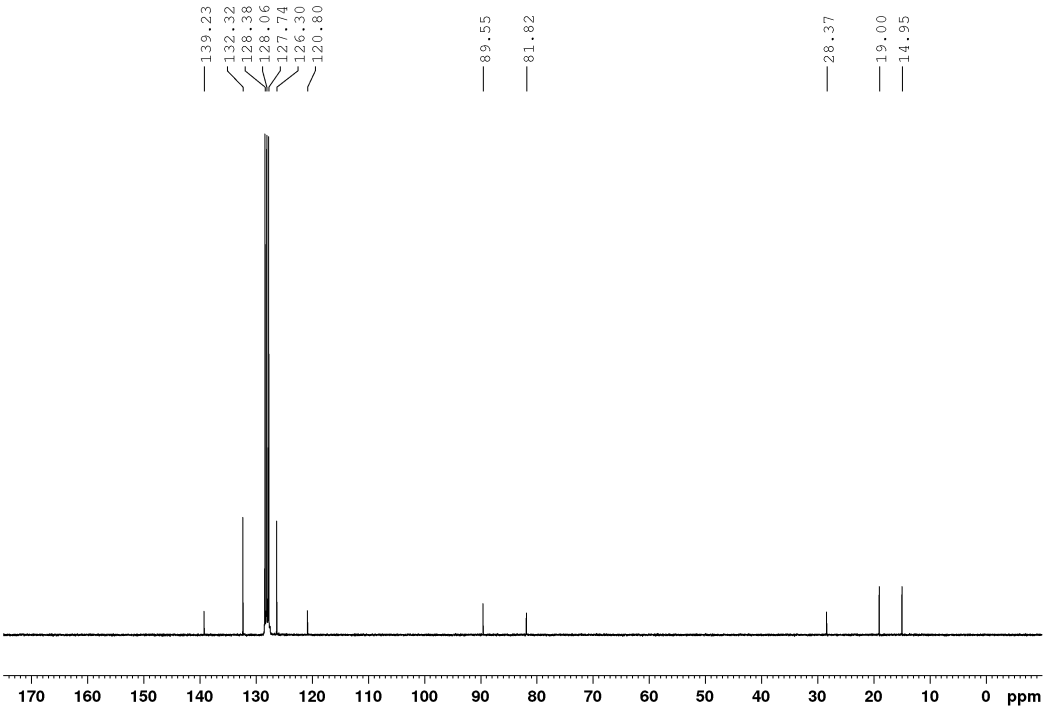

Figure A35: $^{13}C\{^{1}H\}$ NMR spectrum of **4-13** in C_6D_6 at 75 MHz.

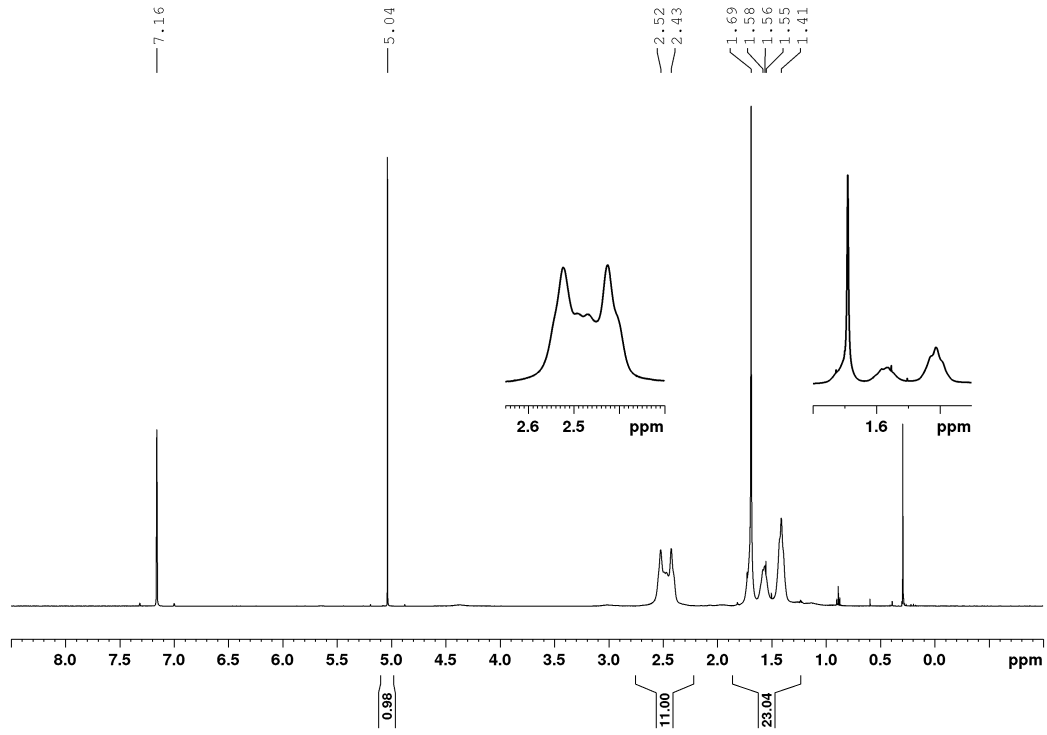

Figure A36: ^{1}H NMR spectrum of **[Rh(acac)(COE)$_2$]** in C_6D_6 at 500 MHz. Additionally, residual amounts of silicon grease (0.29 ppm) and *n*-hexane (0.89 and 1.24 ppm).

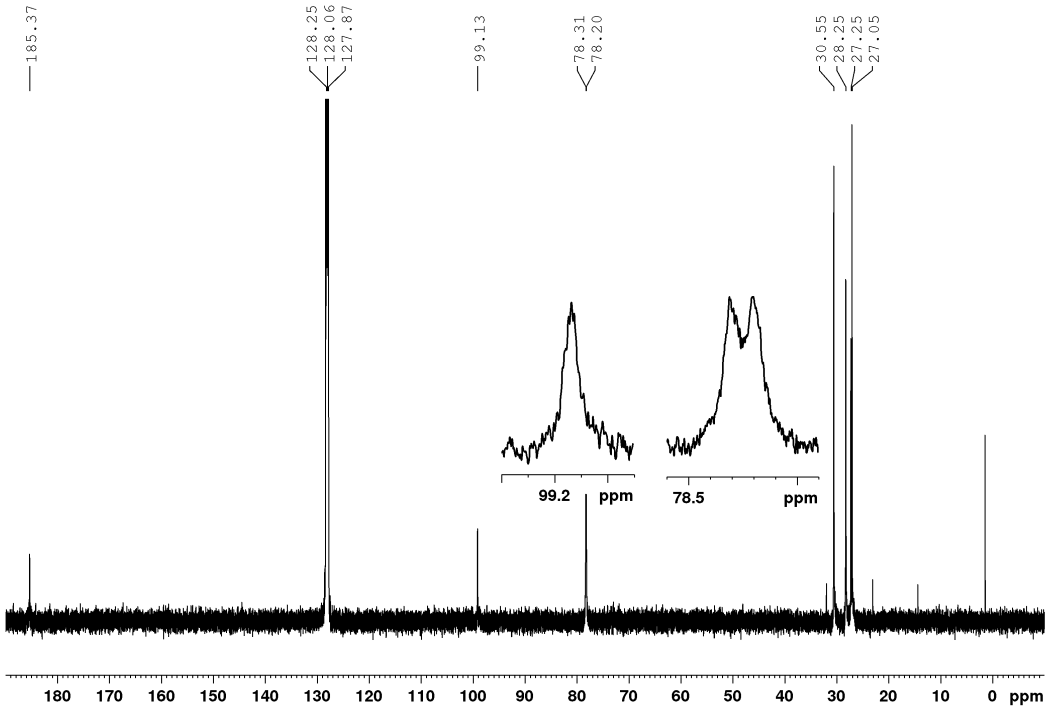

Figure A37: $^{13}C\{^{1}H\}$ NMR spectrum of **[Rh(acac)(COE)$_2$]** in C_6D_6 at 125 MHz. Additionally, residual amounts of silicon grease (1.38 ppm) and *n*-hexane (14.3, 23.0 and 32.0 ppm).

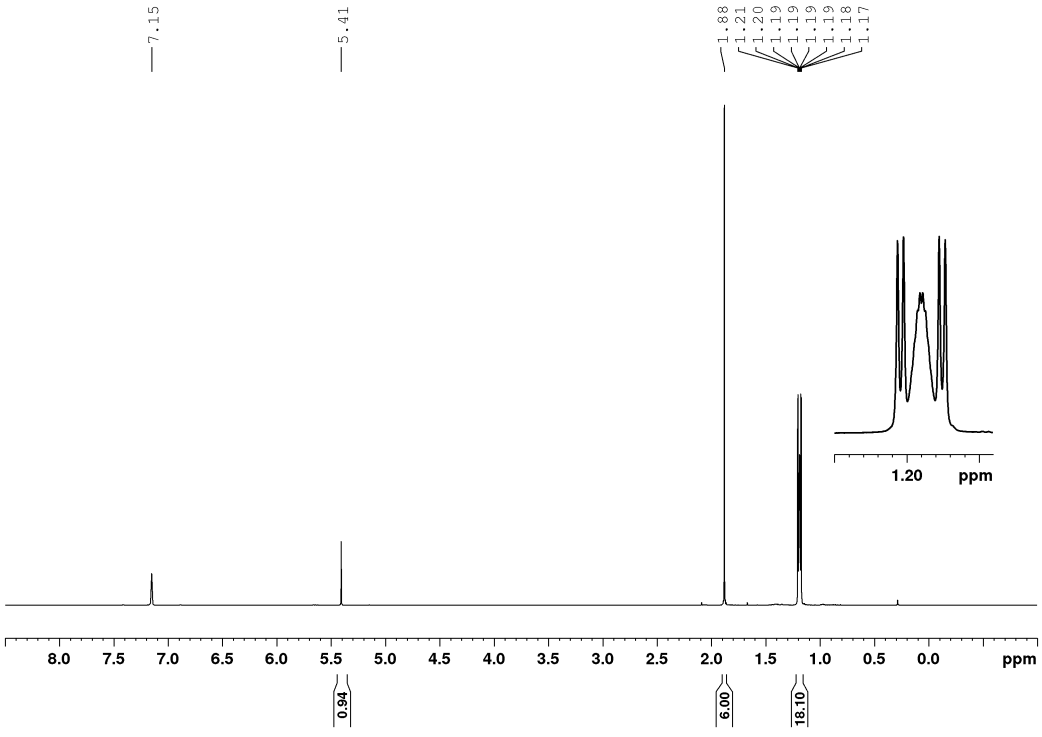

Figure A38: ^{1}H NMR spectrum of **1-51** in C_6D_6 at 300 MHz.

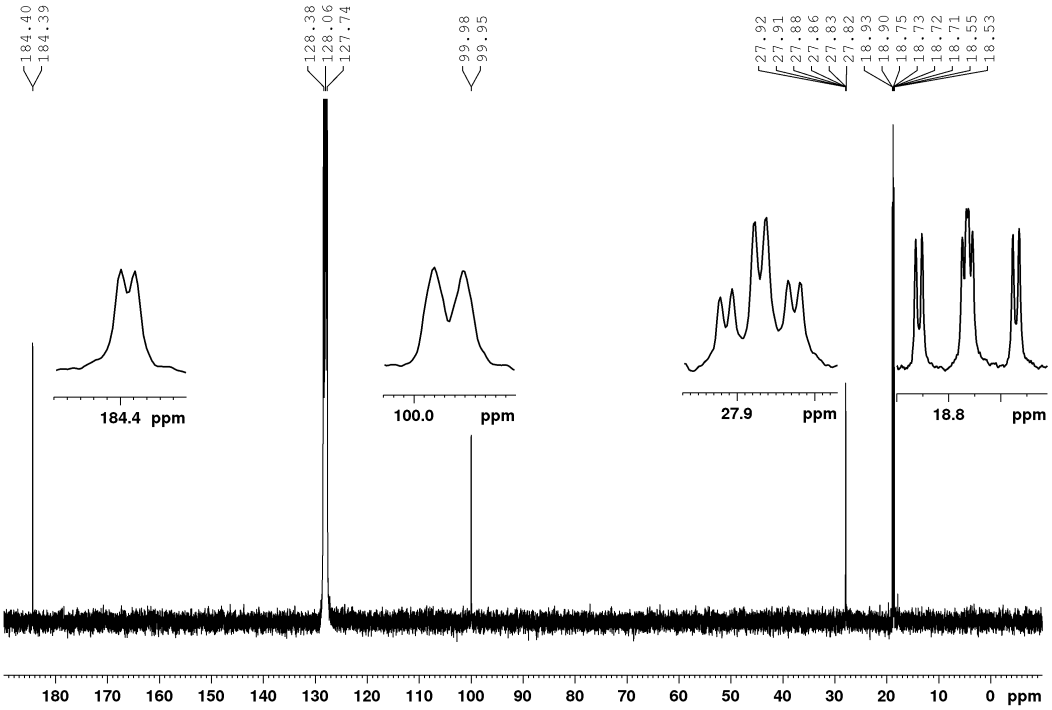

Figure A39: $^{13}C\{^{1}H\}$ NMR spectrum of **1-51** in C_6D_6 at 75 MHz.

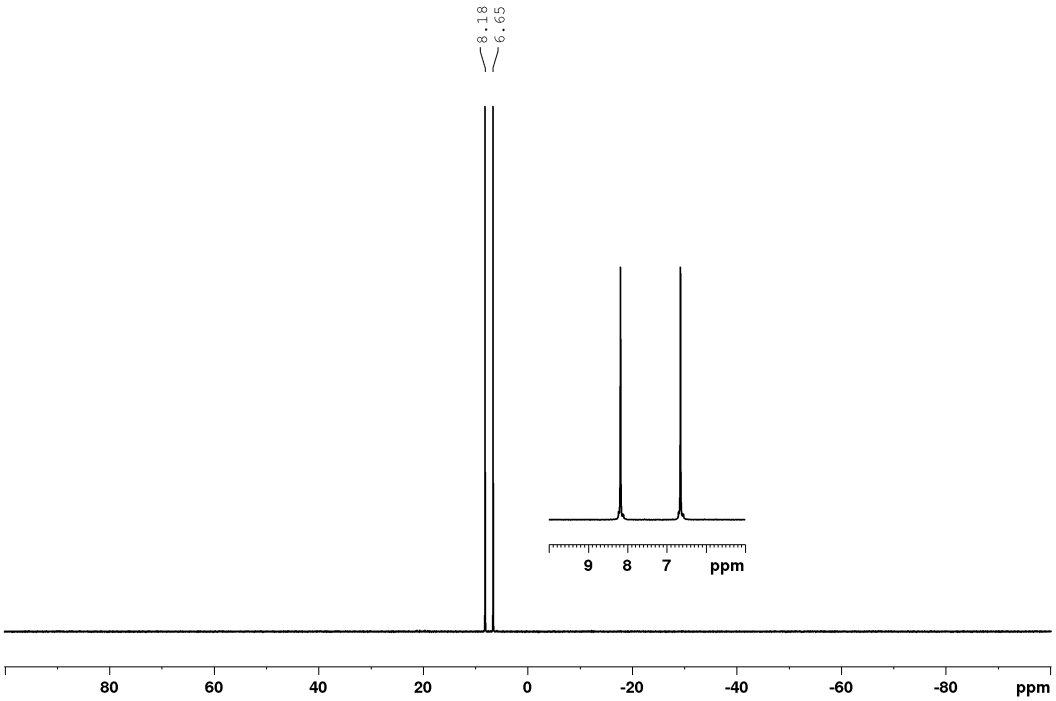

Figure A40: $^{31}P\{^{1}H\}$ NMR spectrum of **1-51** in C_6D_6 at 121 MHz.

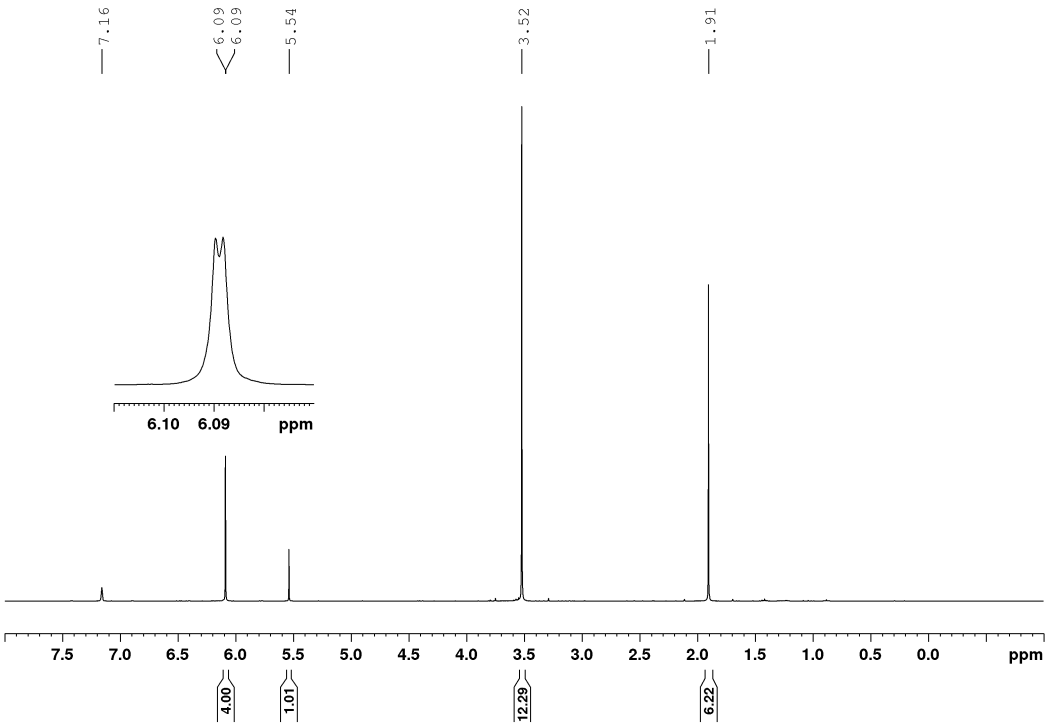

Figure A41: ^{1}H NMR spectrum of **2-21** in C_6D_6 at 300 MHz.

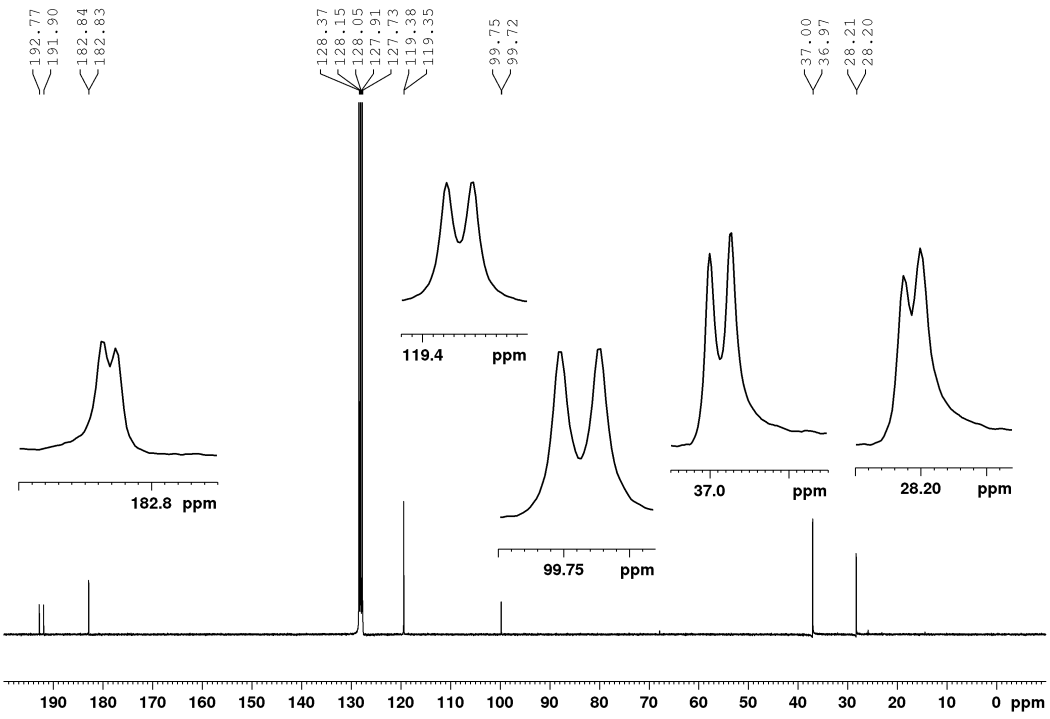

Figure A42: $^{13}C\{^{1}H\}$ NMR spectrum of **2-21** in C_6D_6 at 75 MHz.

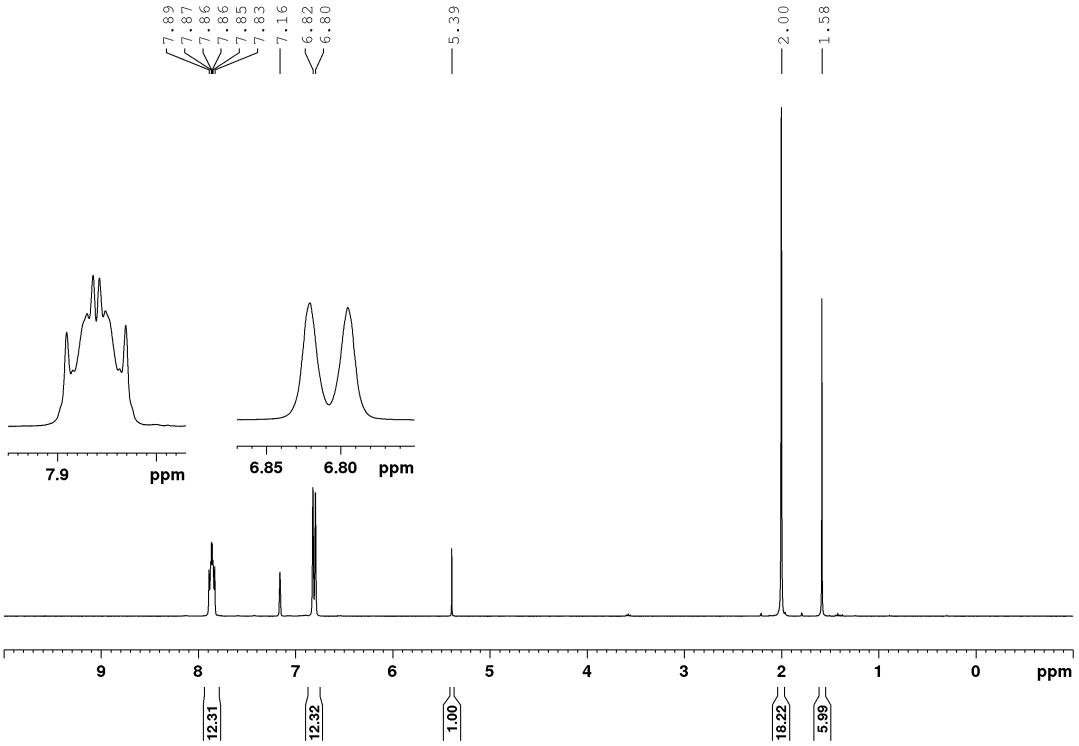

Figure A43: ^{1}H NMR spectrum of **1-56** in C_6D_6 at 300 MHz.

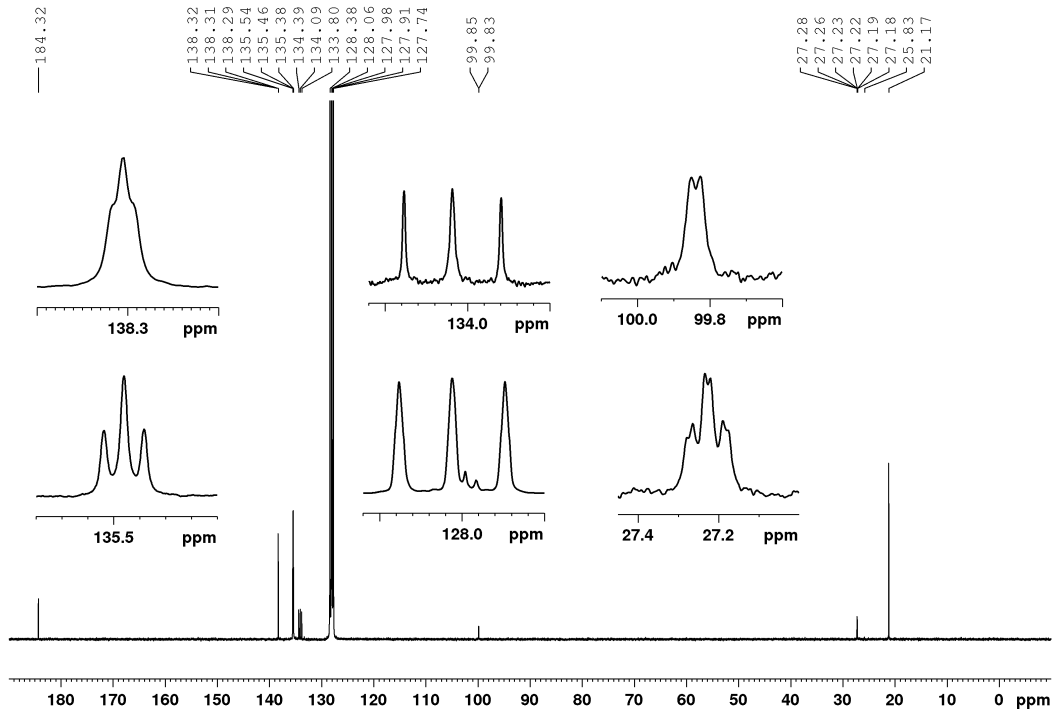

Figure A44: $^{13}C\{^{1}H\}$ NMR spectrum of **1-56** in C_6D_6 at 75 MHz.

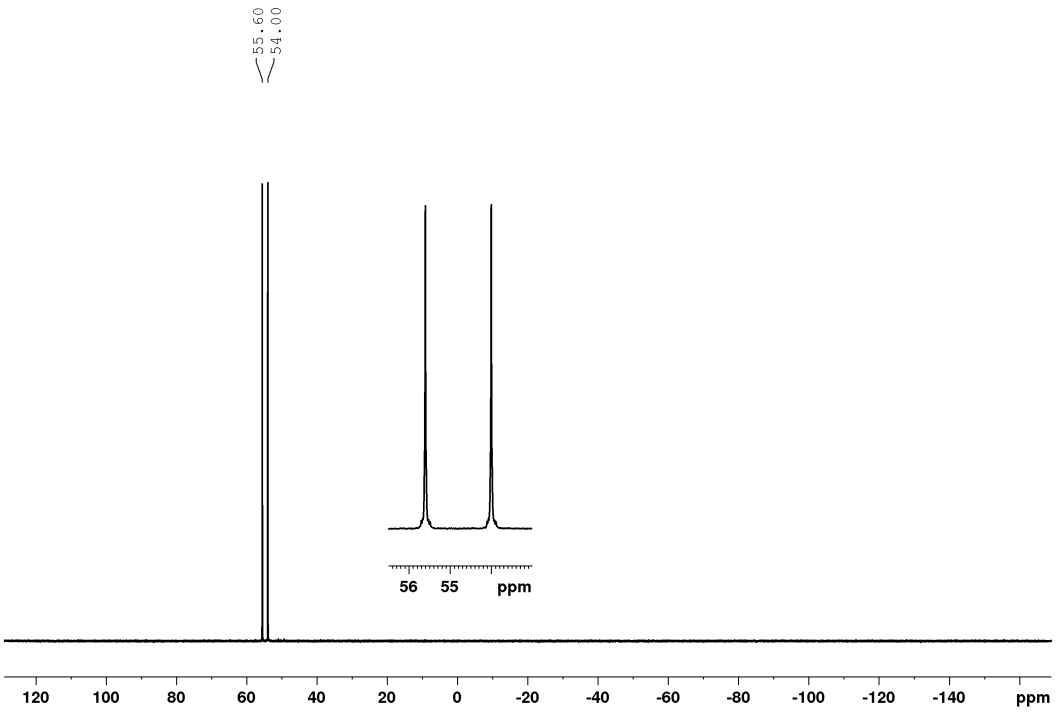

Figure A45: $^{31}P\{^{1}H\}$ NMR spectrum of **1-56** in C_6D_6 at 121 MHz.

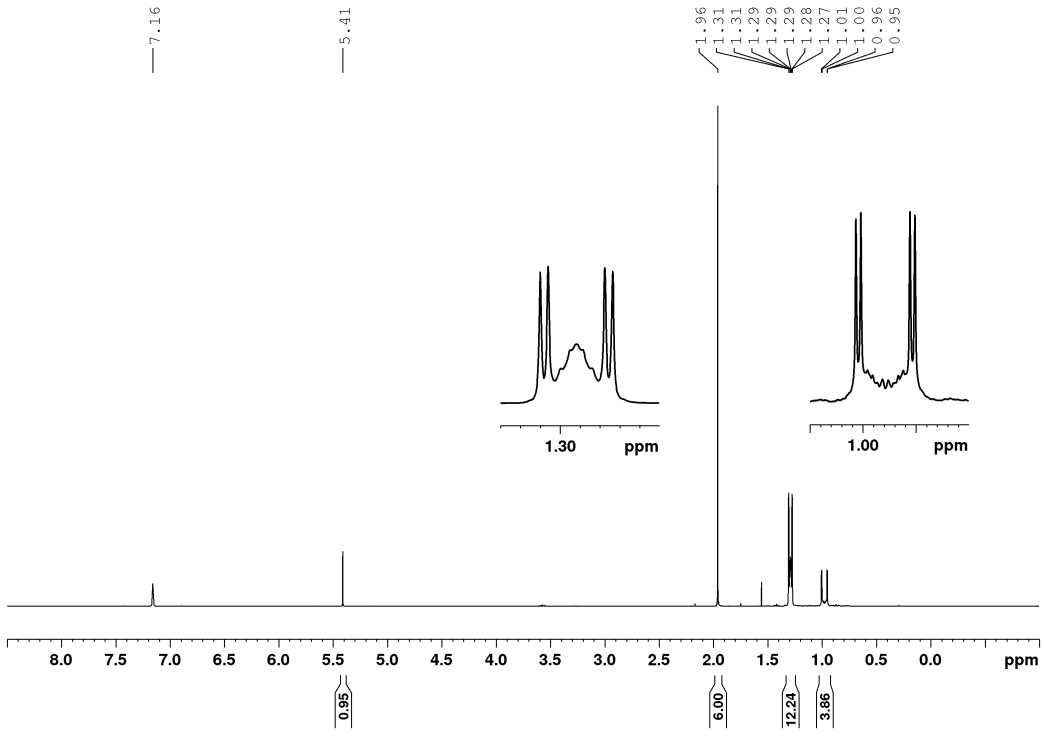

Figure A46: ^{1}H NMR spectrum of **4-1** in C_6D_6 at 300 MHz. Additionally, residual amounts of acetone (1.55 ppm).

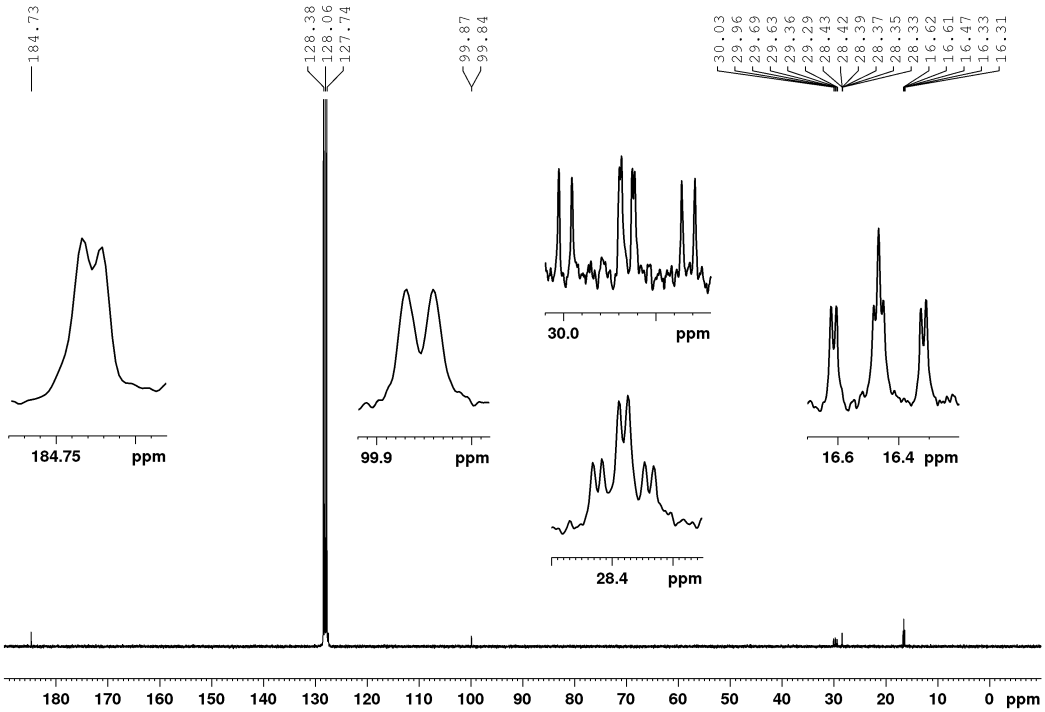

Figure A47: $^{13}C\{^{1}H\}$ NMR spectrum of **4-1** in C_6D_6 at 75 MHz.

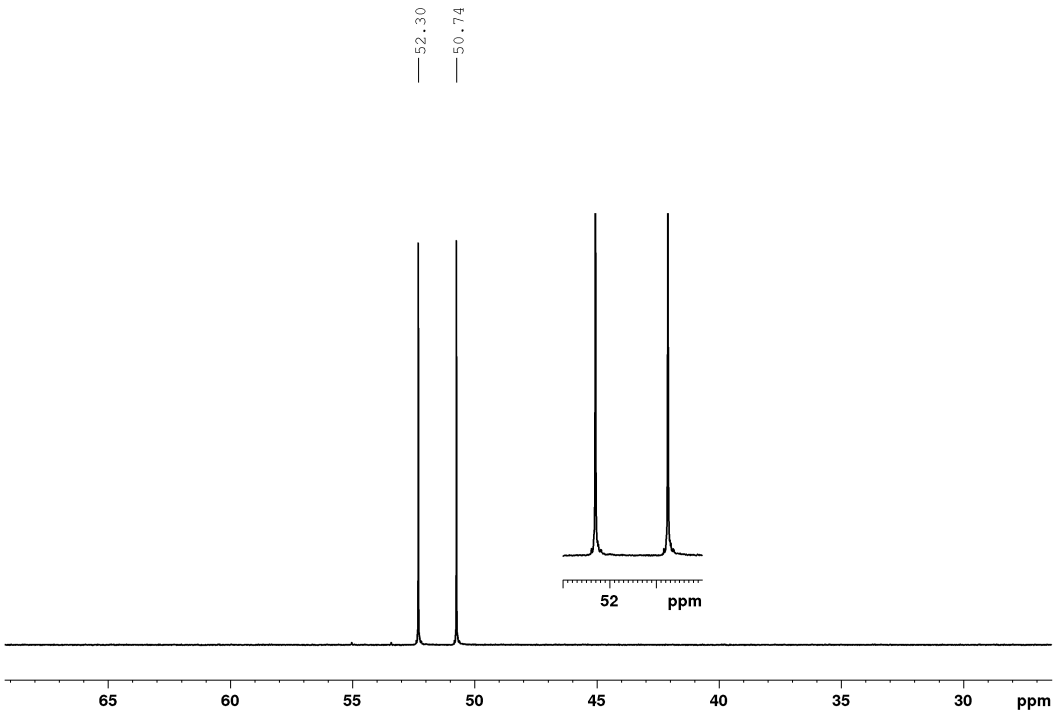

Figure A48: $^{31}P\{^{1}H\}$ NMR spectrum of **4-1** in C_6D_6 at 121 MHz.

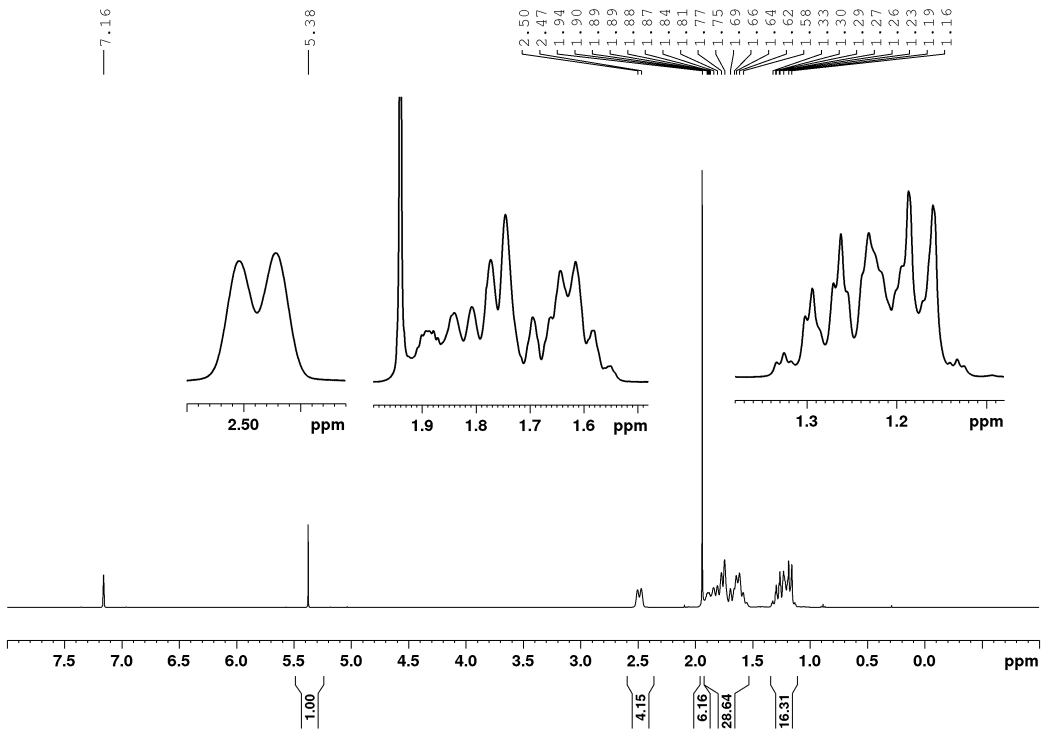

Figure A49: ^{1}H NMR spectrum of **4-2** in C_6D_6 at 400 MHz.

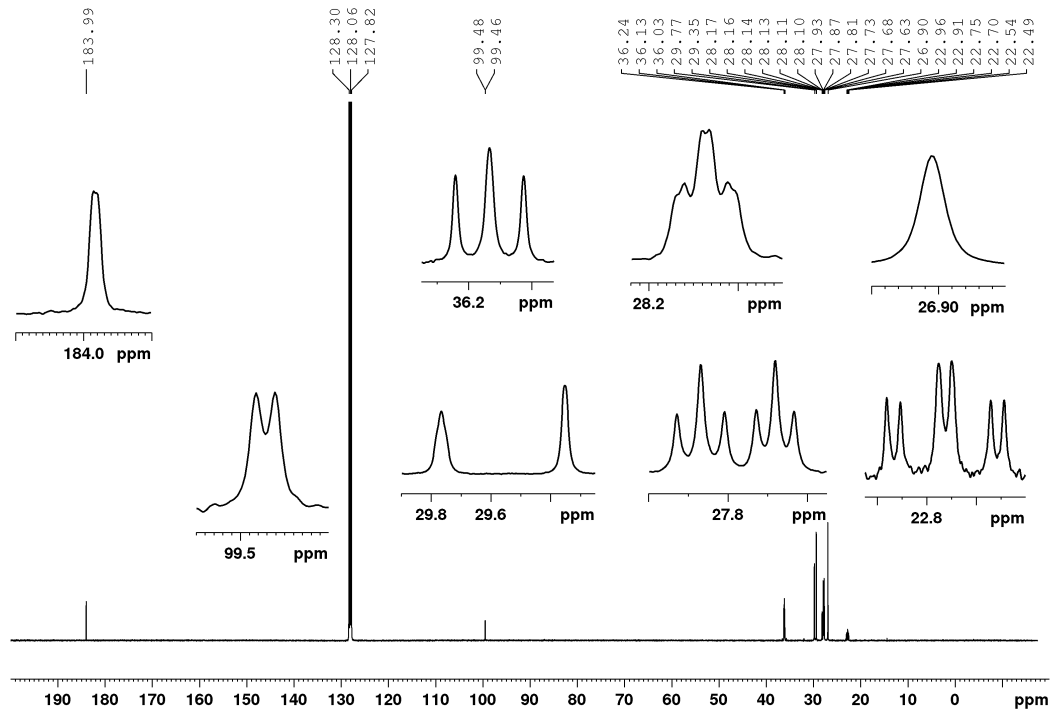

Figure A50: $^{13}C\{^{1}H\}$ NMR spectrum of **4-2** in C_6D_6 at 100 MHz.

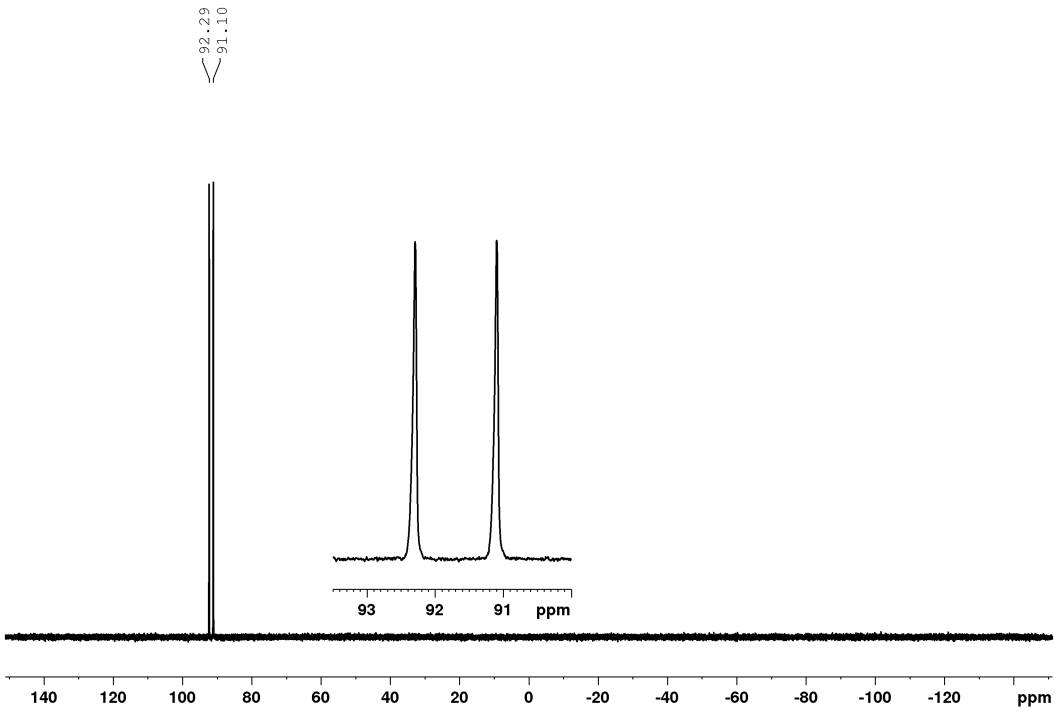

Figure A51: $^{31}P\{^{1}H\}$ NMR spectrum of **4-2** in C_6D_6 at 162 MHz.

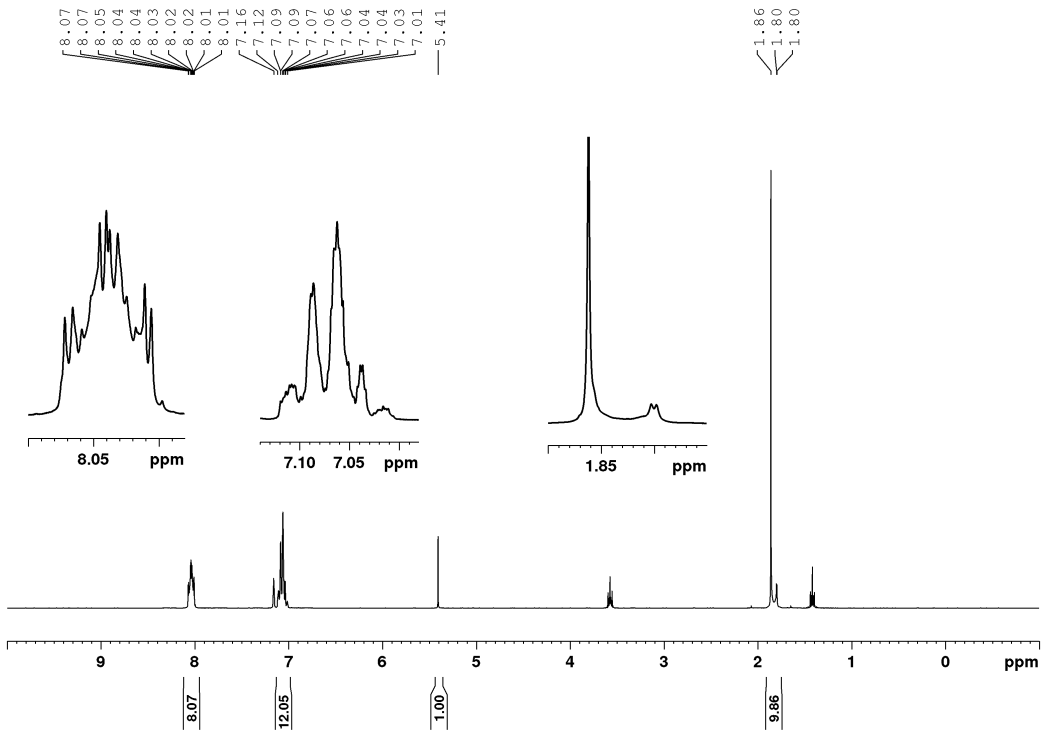

Figure A52: ^{1}H NMR spectrum of **4-3** in C_6D_6 at 300 MHz. Additionally, residual amounts of THF (3.57 and 1.40 ppm).

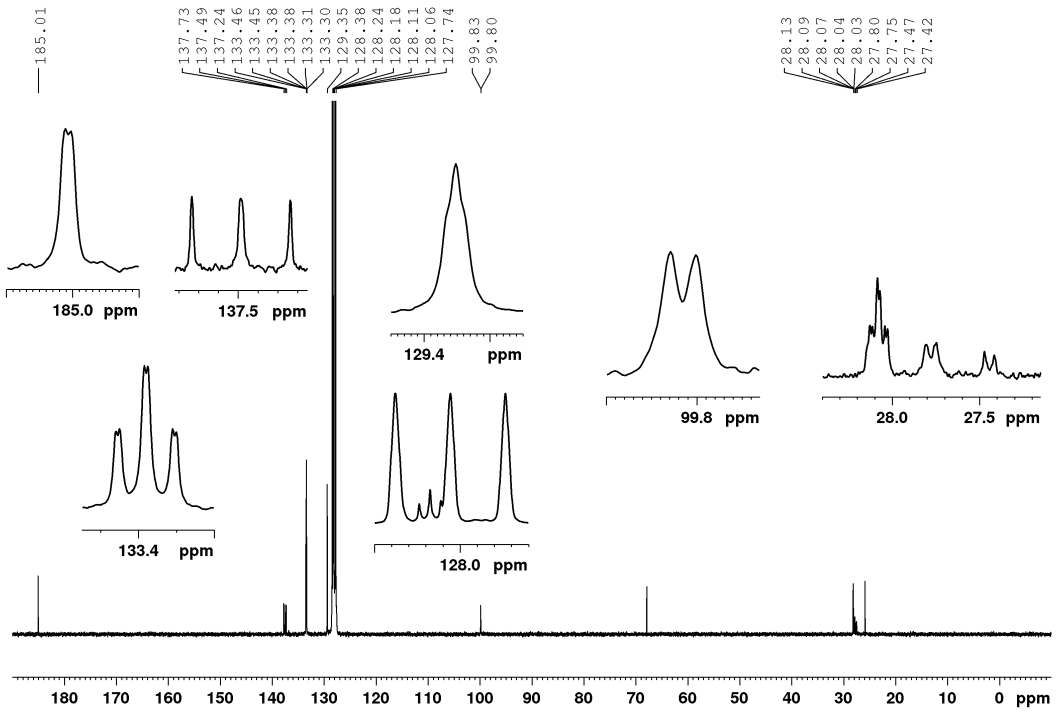

Figure A53: $^{13}C\{^{1}H\}$ NMR spectrum of **4-3** in C_6D_6 at 75 MHz. Additionally, residual amounts of THF (67.8 and 25.7 ppm).

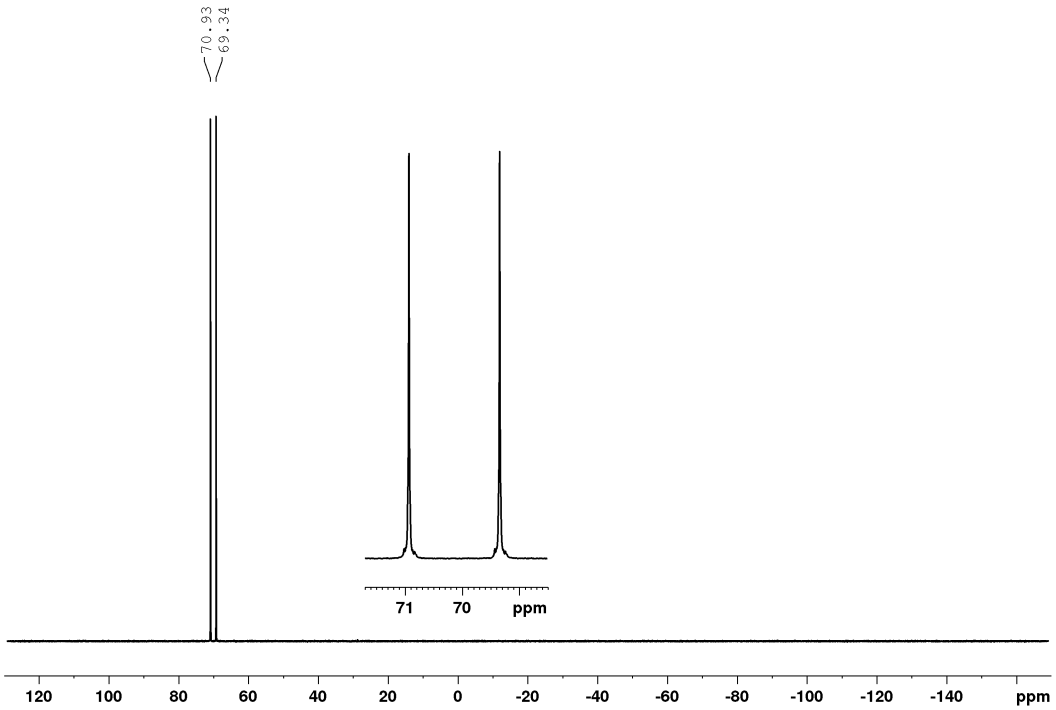

Figure A54: $^{31}P\{^{1}H\}$ NMR spectrum of **4-3** in C_6D_6 at 121 MHz.

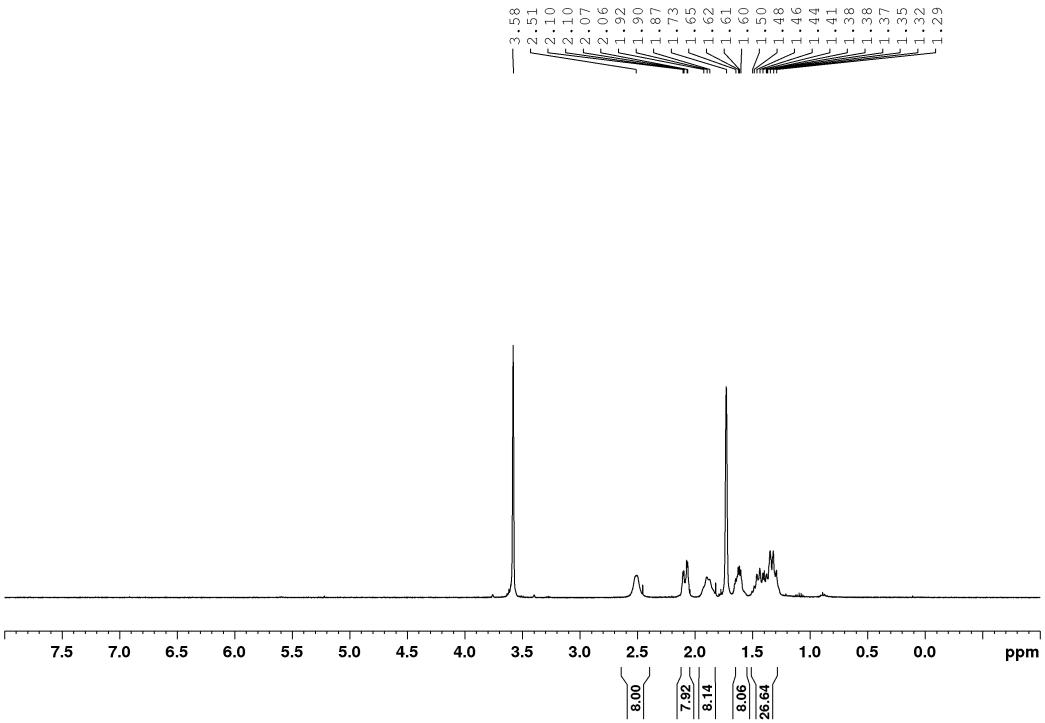

Figure A55: ^{1}H NMR spectrum of **4-4** in THF-d_8 at 400 MHz. Additionally, residual amounts of water (2.46 ppm) and *n*-hexane (0.89 and 1.29 ppm).

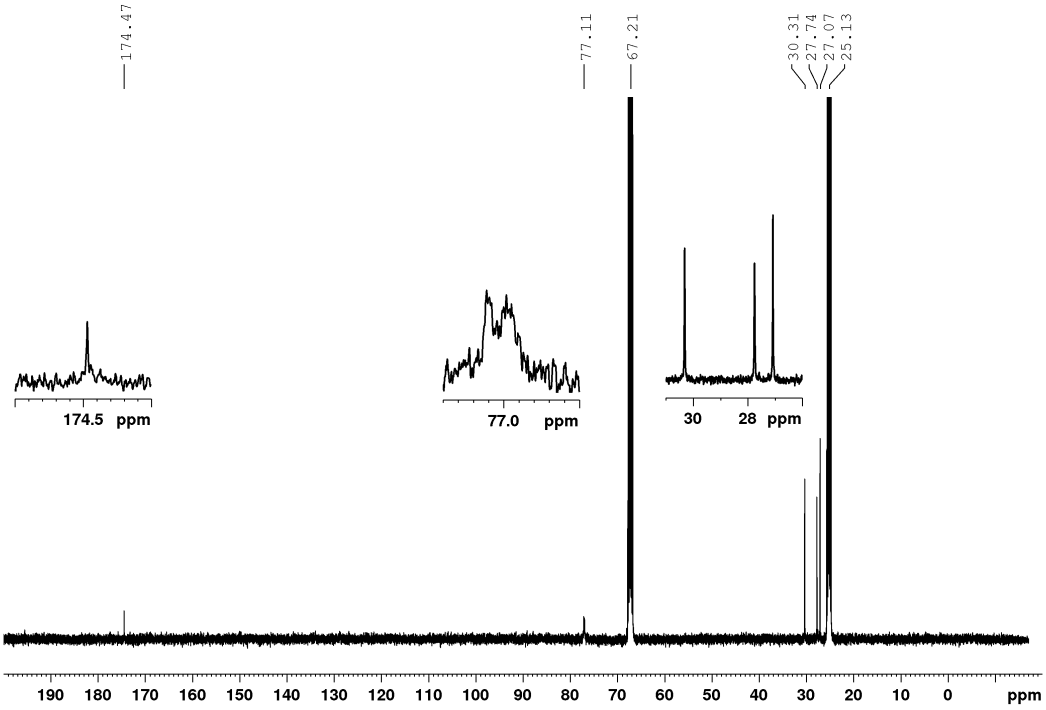

Figure A56: ^{13}C{^{1}H} NMR spectrum of **4-4** in THF-d_8 at 100 MHz.

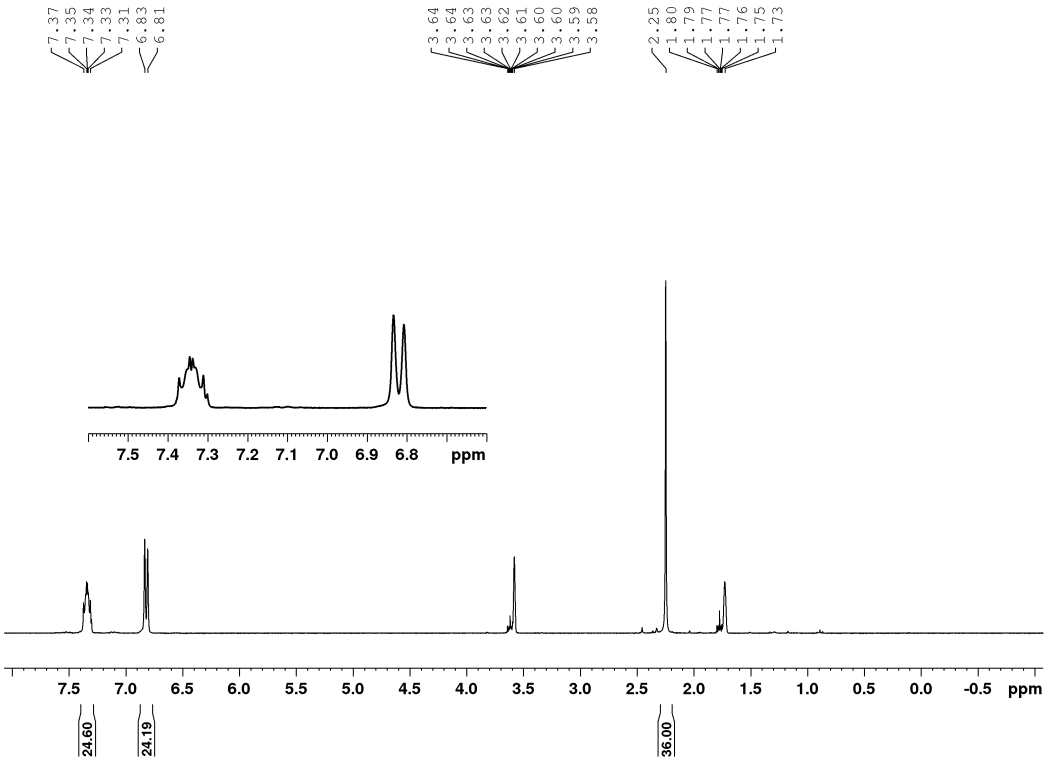

Figure A57: ^{1}H NMR spectrum of **4-5** in THF-d_8 at 300 MHz.

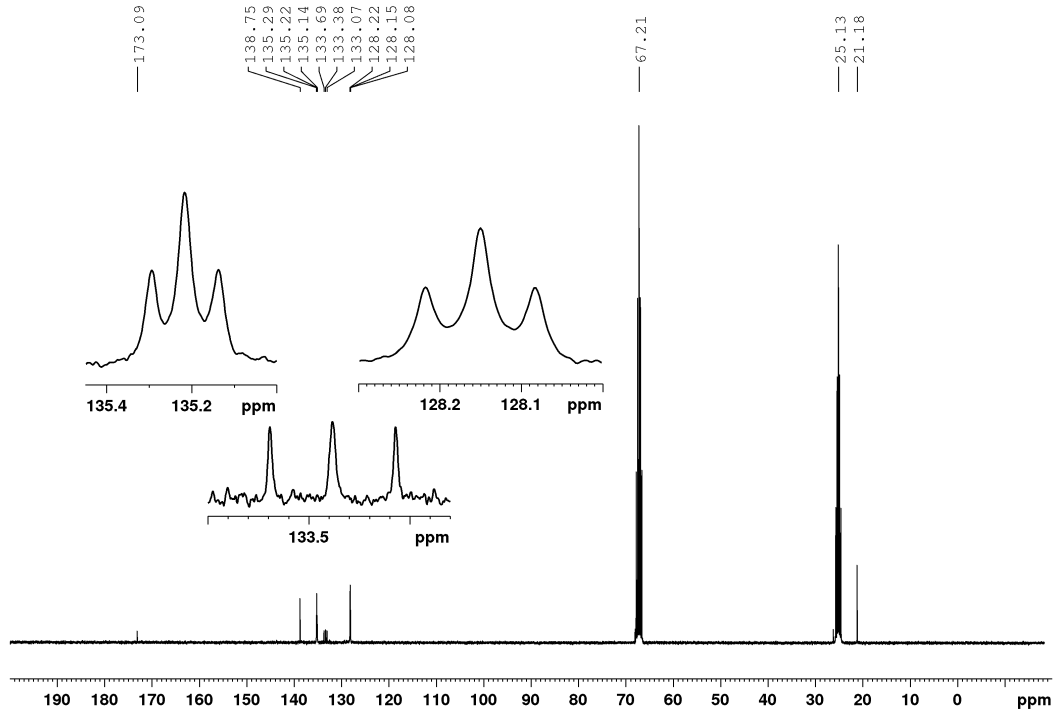

Figure A58: $^{13}C\{^{1}H\}$ NMR spectrum of **4-5** in THF-d_8 at 75 MHz.

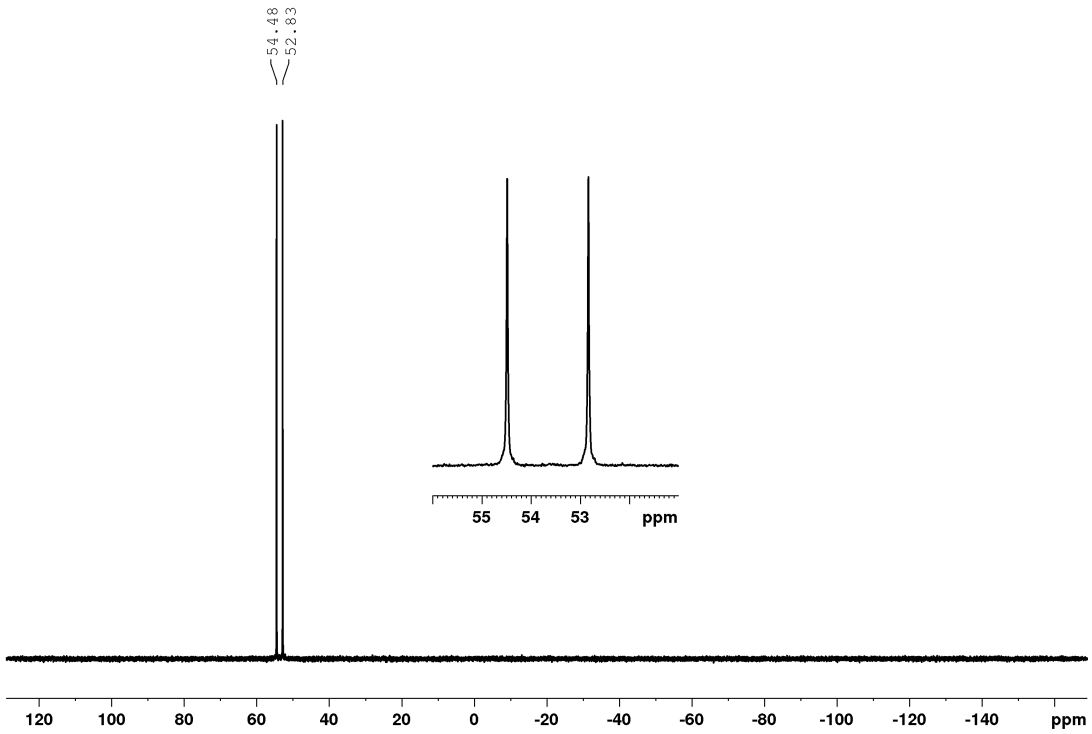

Figure A59: $^{31}P\{^{1}H\}$ NMR spectrum of **4-5** in THF-d_8 at 121 MHz.

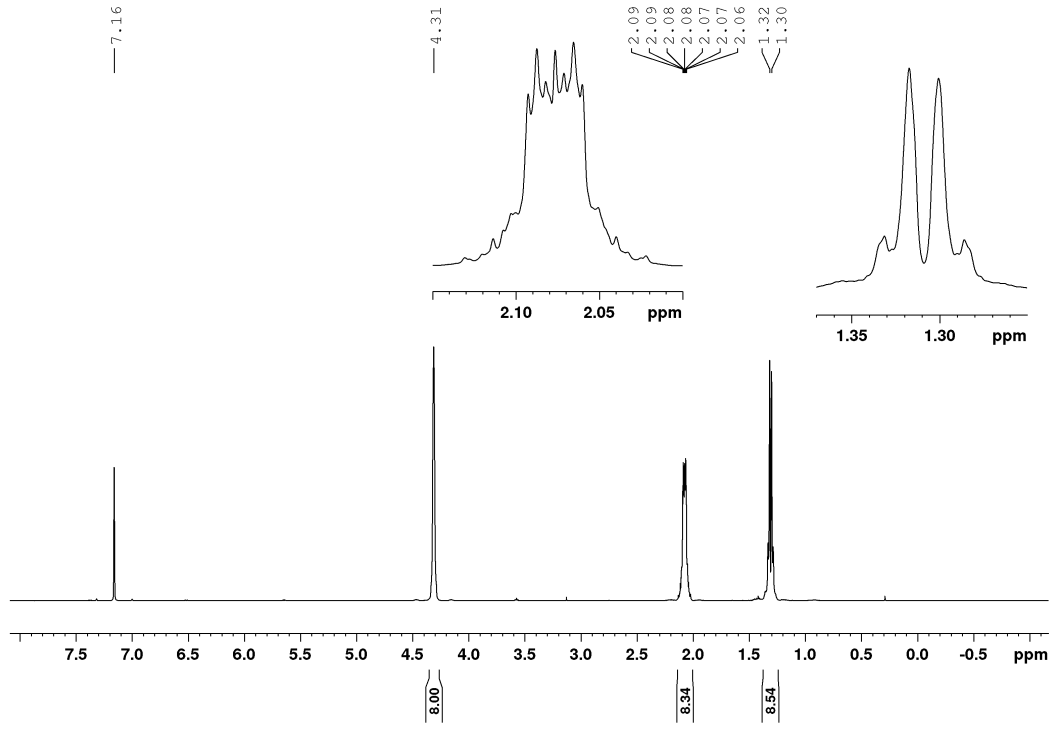

Figure A60: ^{1}H NMR spectrum of **[RhClCOD]$_2$** in C_6D_6 at 500 MHz.

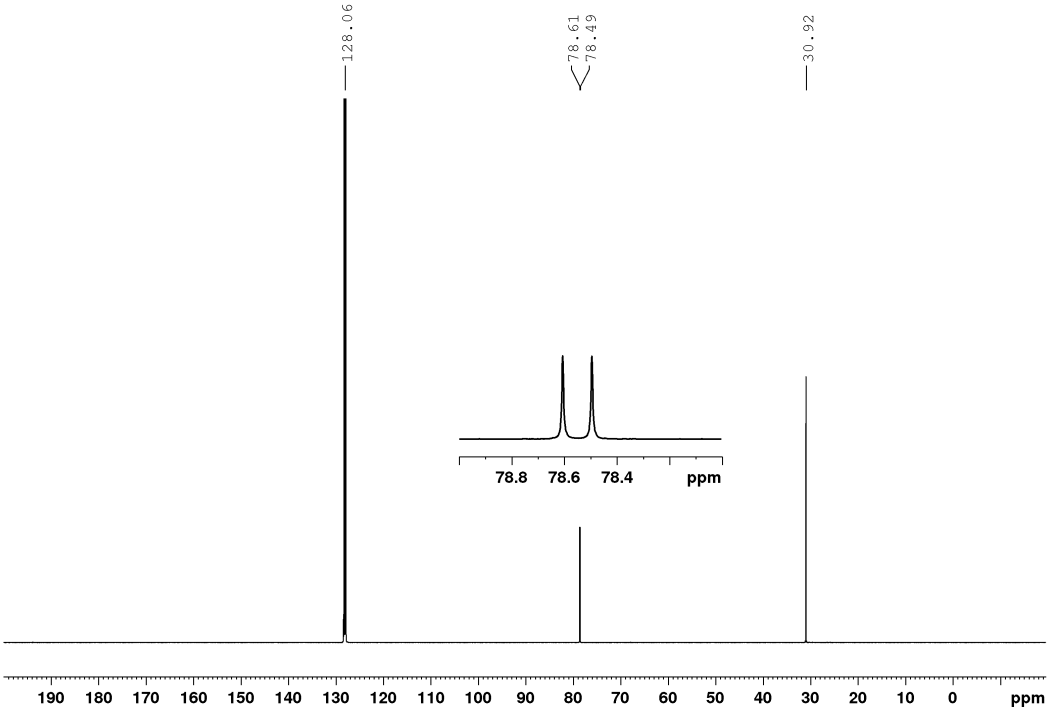

Figure A61: $^{13}C\{^{1}H\}$ NMR spectrum of **[RhClCOD]$_2$** in C_6D_6 at 125 MHz.

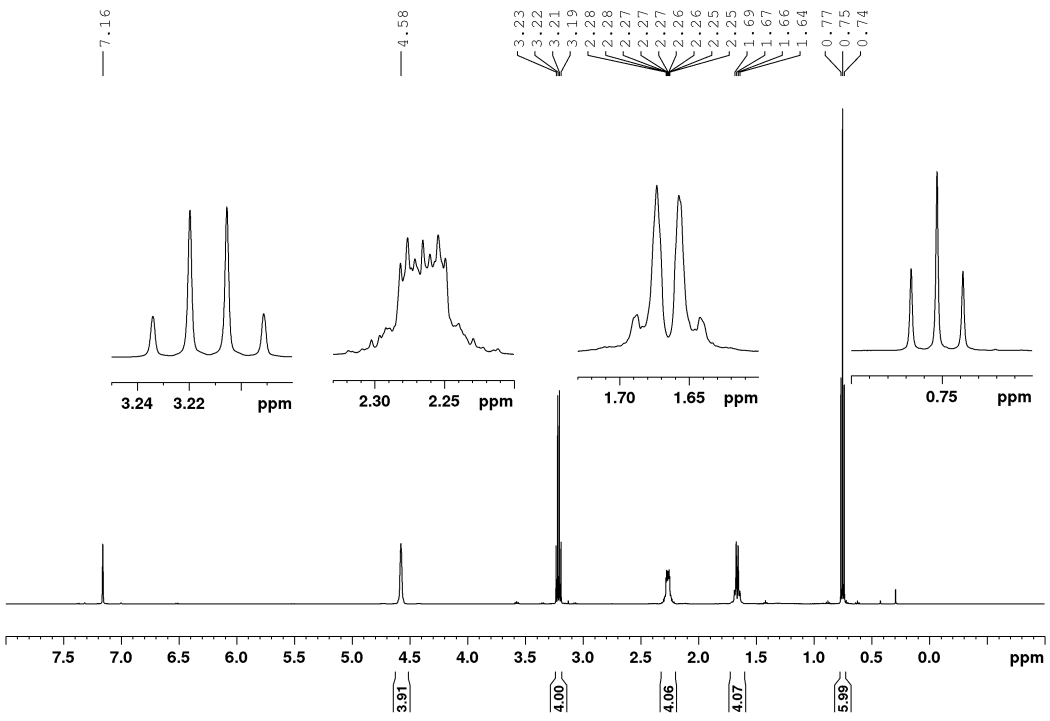

Figure A62: ^{1}H NMR spectrum of **[Rh(S$_2$CNEt$_2$)COD]** in C_6D_6 at 500 MHz.

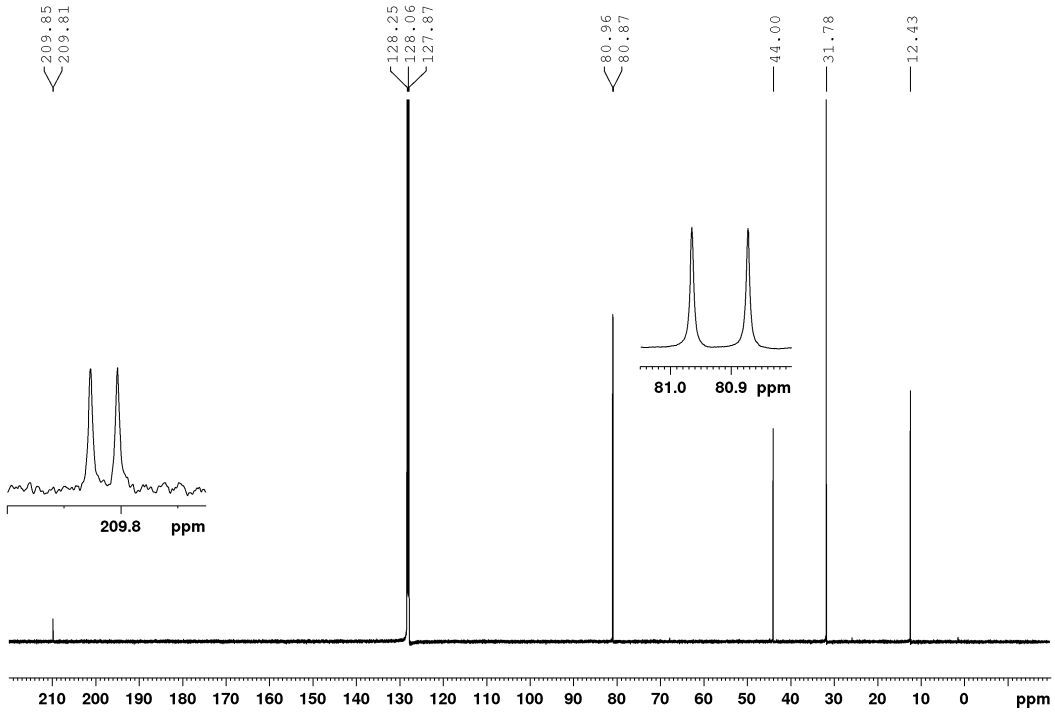

Figure A63: $^{13}C\{^{1}H\}$ NMR spectrum of **[Rh(S$_2$CNEt$_2$)COD]** in C_6D_6 at 125 MHz.

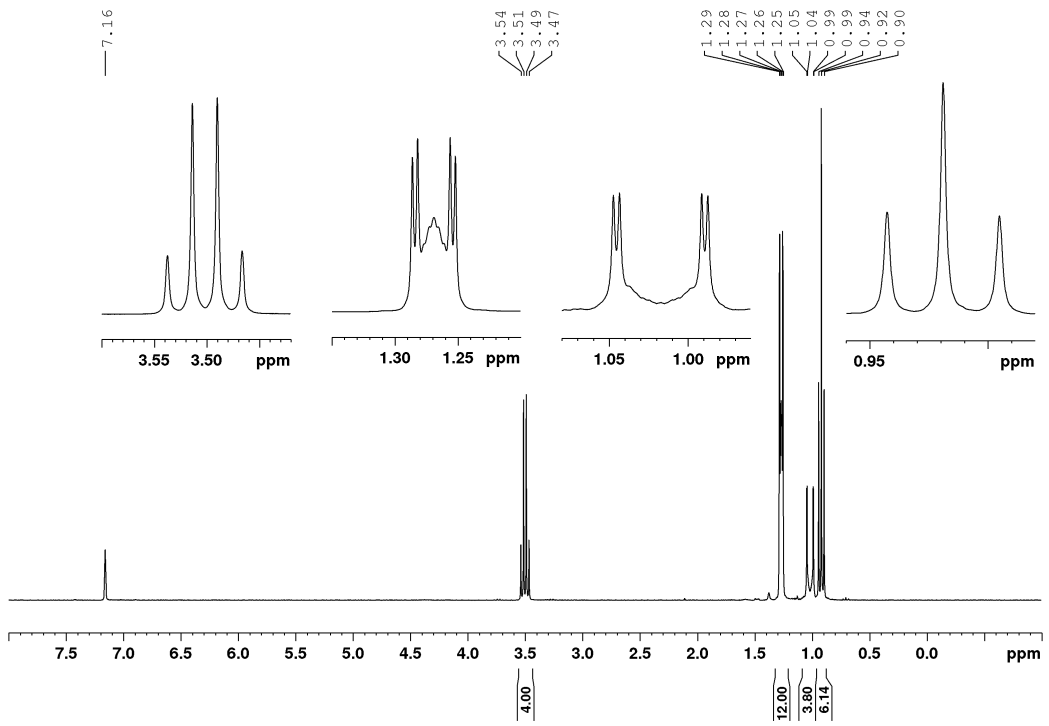

Figure A64: ^{1}H NMR spectrum of **4-7** in C_6D_6 at 300 MHz.

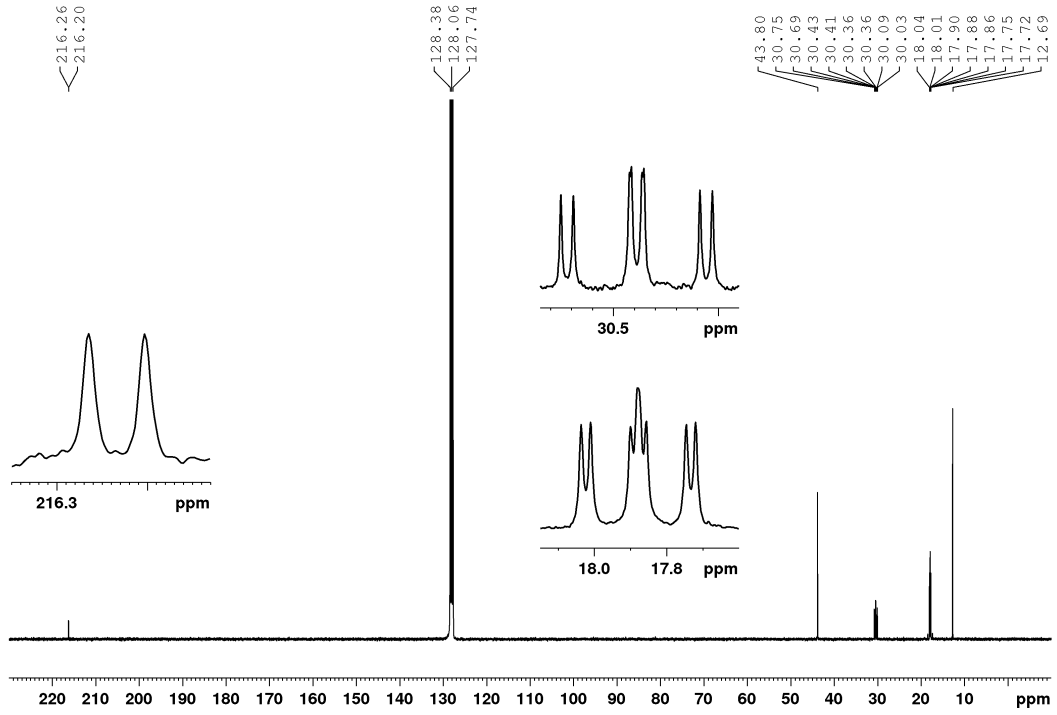

Figure A65: $^{13}C\{^{1}H\}$ NMR spectrum of **4-7** in C_6D_6 at 75 MHz.

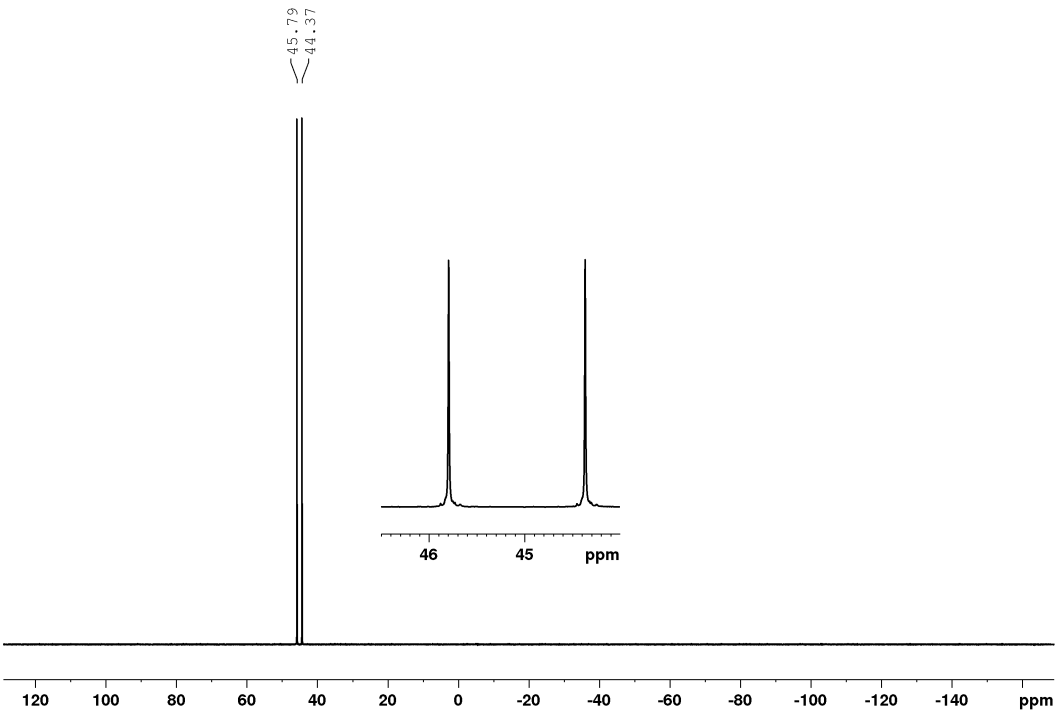

Figure A66: $^{31}P\{^{1}H\}$ NMR spectrum of **4-7** in C_6D_6 at 121 MHz.

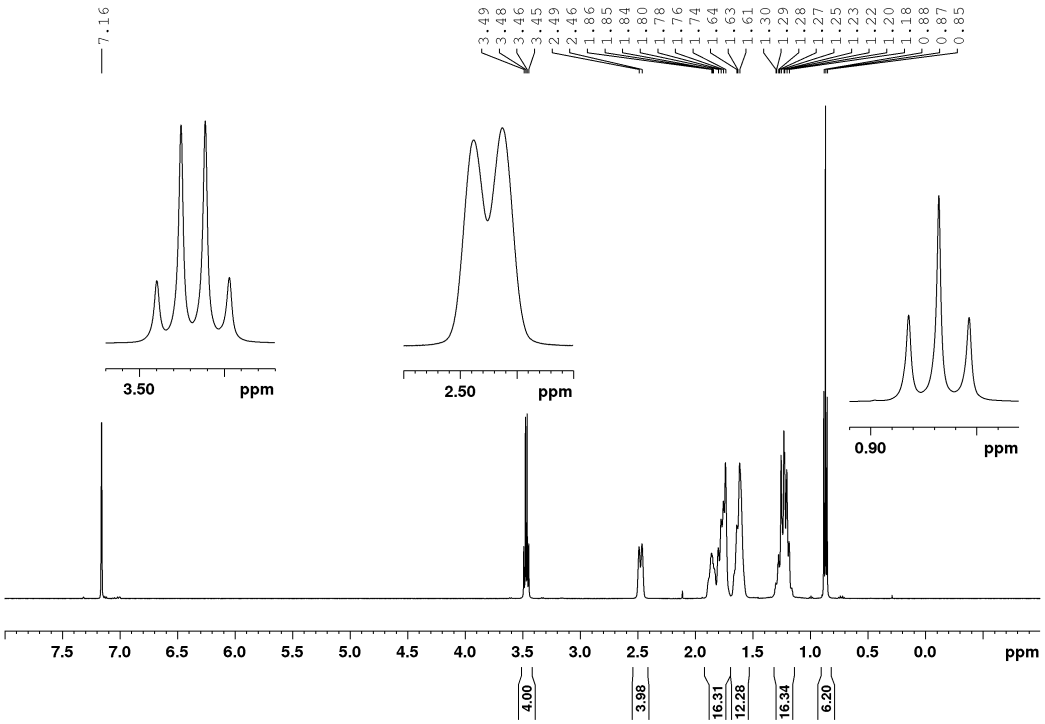

Figure A67: ^{1}H NMR spectrum of **4-8** in C_6D_6 at 500 MHz. Additionally, residual amounts of toluene (2.11, 7.02 and 7.13 ppm).

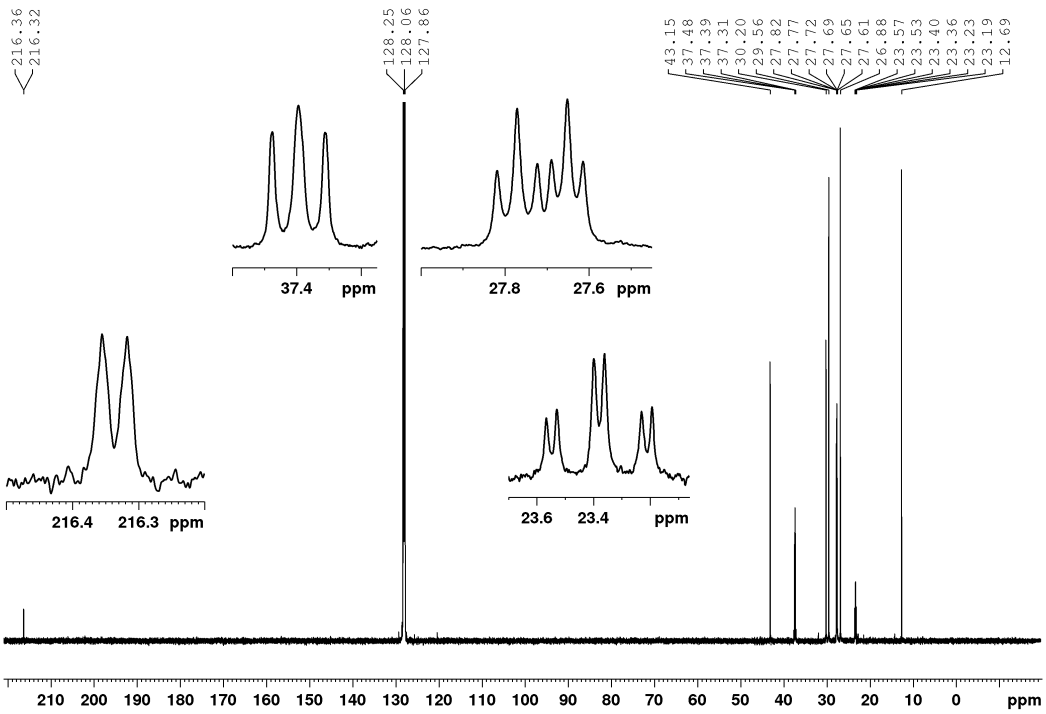

Figure A68:^{13}C{^{1}H} NMR spectrum of **4-8** in C_6D_6 at 125 MHz.

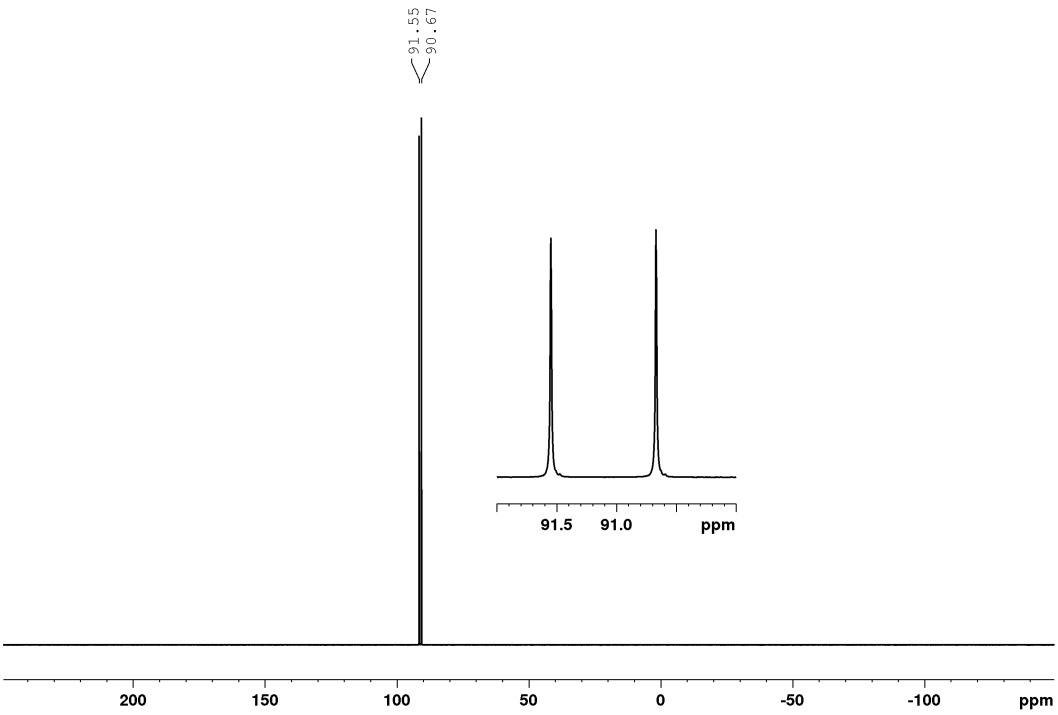

Figure A69: $^{31}P\{^{1}H\}$ NMR spectrum of **4-8** in C_6D_6 at 202 MHz.

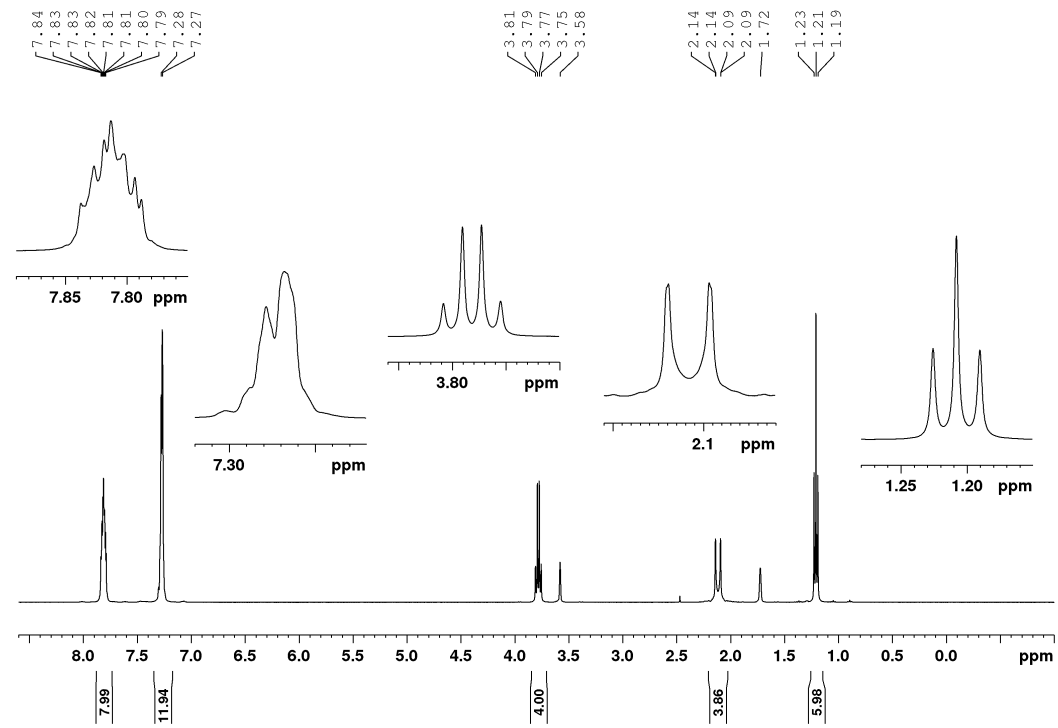

Figure A70: ^{1}H NMR spectrum of **4-9** in THF-d_8 at 400 MHz. Additionally, residual amounts of water (2.46 ppm).

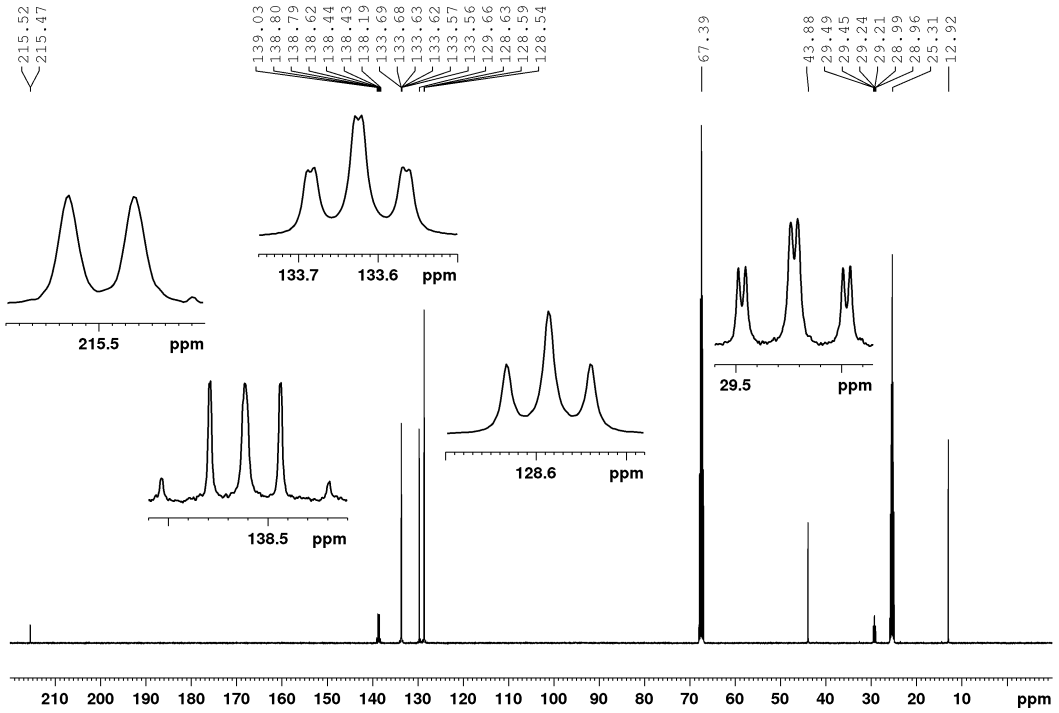

Figure A71: $^{13}C\{^{1}H\}$ NMR spectrum of **4-9** in THF-d_8 at 100 MHz.

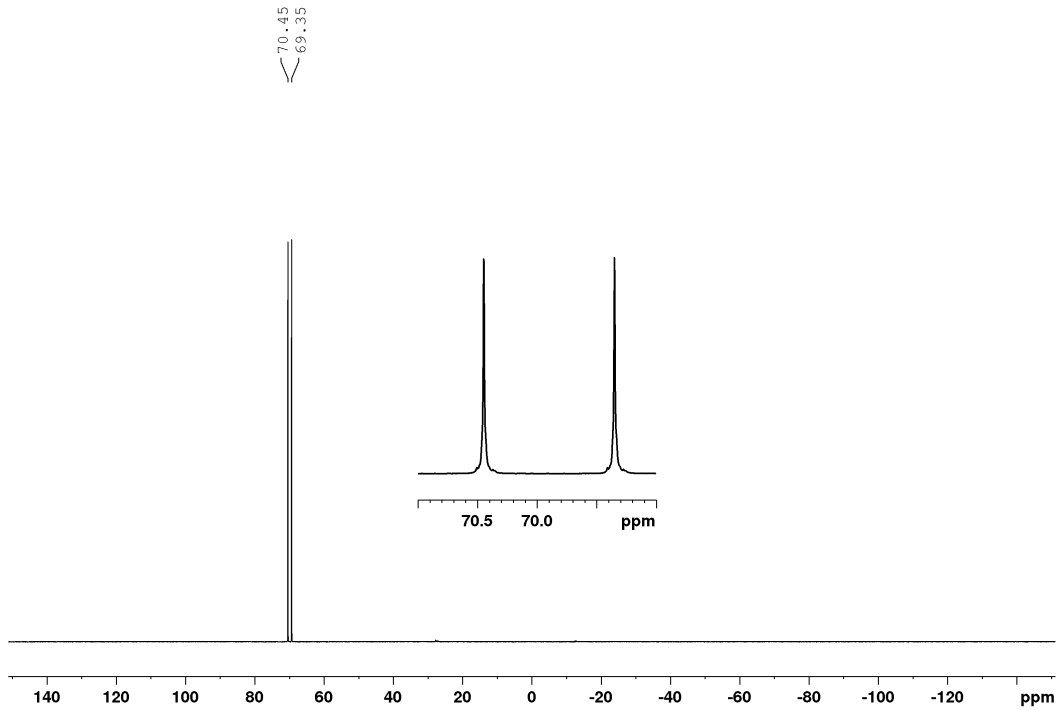

Figure A72: $^{31}P\{^{1}H\}$ NMR spectrum of **4-9** in THF-d_8 at 162 MHz.

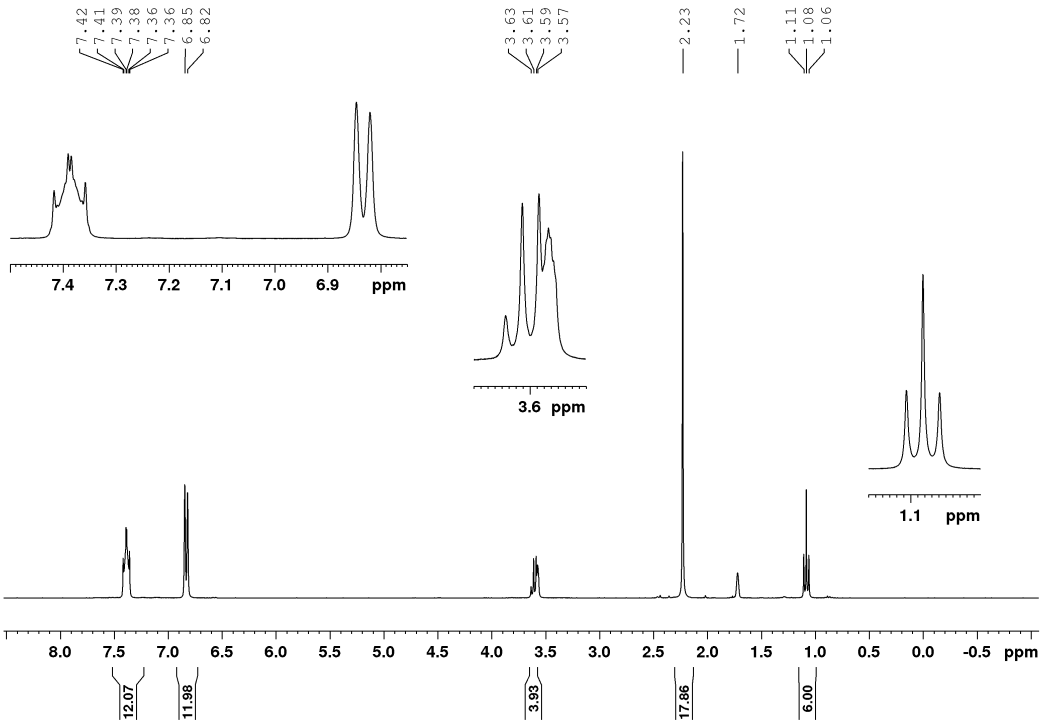

Figure A73: ^{1}H NMR spectrum of **4-10** in THF-d$_8$ at 300 MHz.

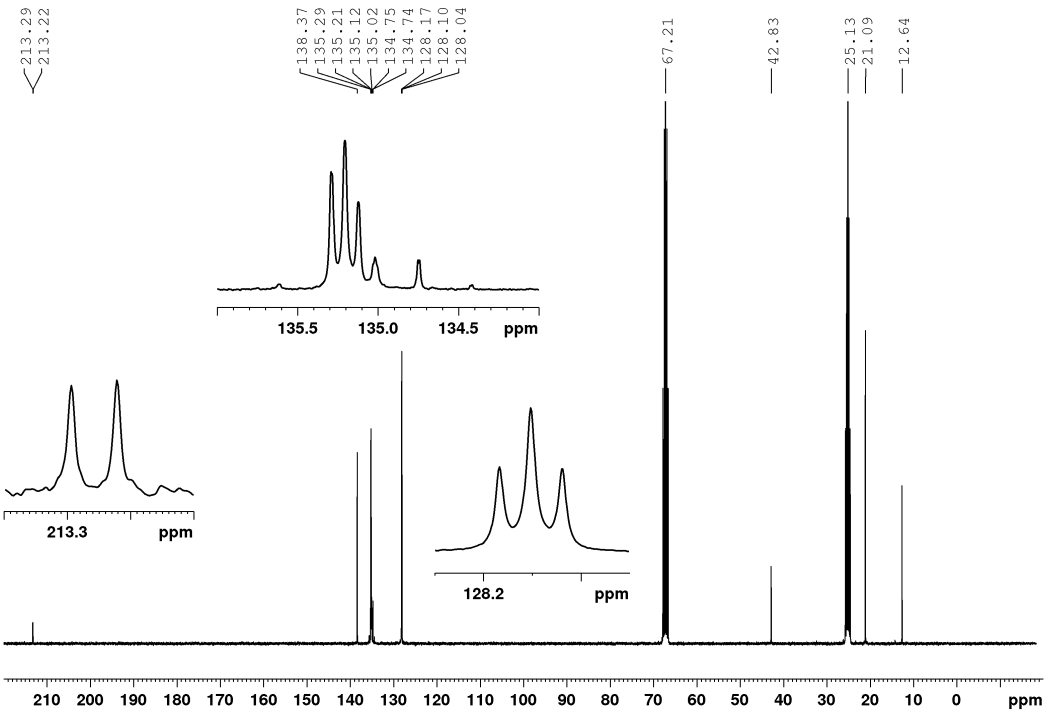

Figure A74: ^{13}C{^{1}H} NMR spectrum of **4-10** in THF-d$_8$ at 75 MHz.

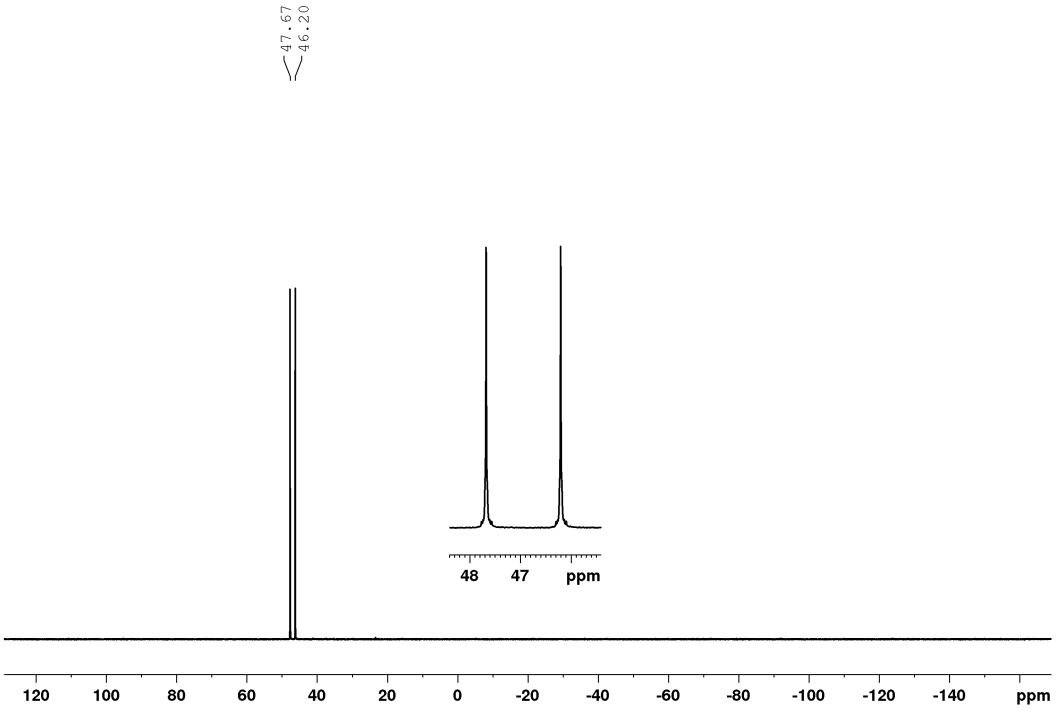

Figure A75: $^{31}P\{^{1}H\}$ NMR spectrum of **4-10** in THF-d_8 at 121 MHz.

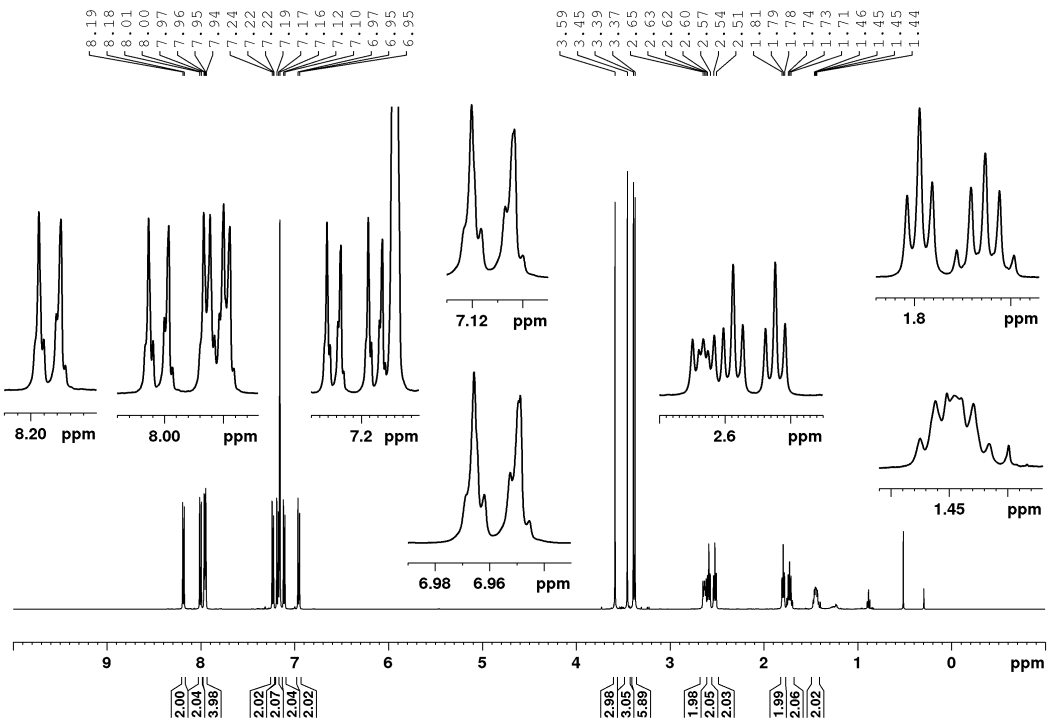

Figure A76: ^{1}H NMR spectrum of **4-11a** in C_6D_6 at 500 MHz. Additionally, residual amounts of silicon grease (0.29 ppm), water (0.40 ppm) and *n*-hexane (0.89 and 1.24 ppm).

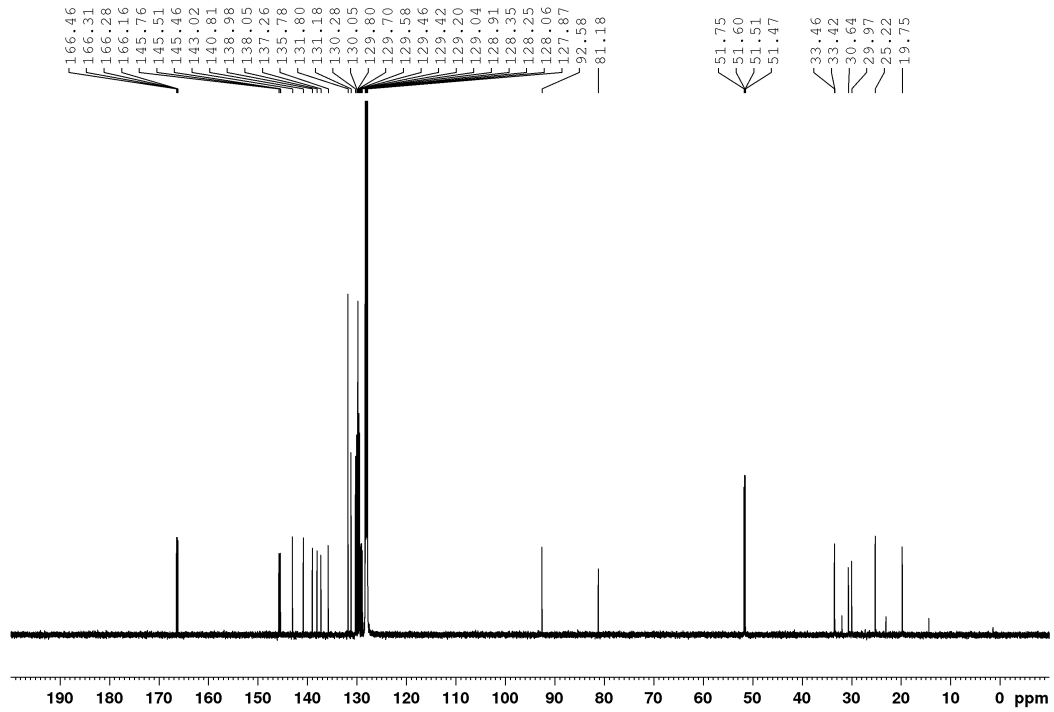

Figure A77: $^{13}C\{^{1}H\}$ NMR spectrum of **4-11a** in C_6D_6 at 125 MHz. Additionally, residual amounts of silicon grease (1.38 ppm) and *n*-hexane (14.3, 23.0 and 32.0 ppm).

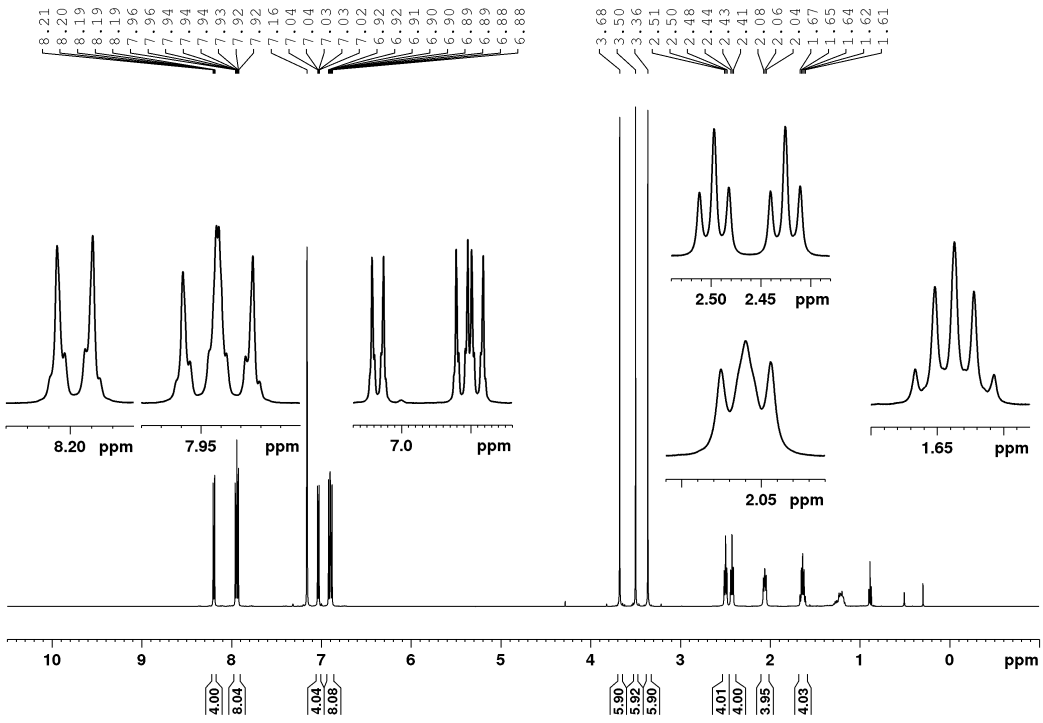

Figure A78: ^{1}H NMR spectrum of **4-11b** in C_6D_6 at 500 MHz. Additionally, residual amounts of silicon grease (0.29 ppm), water (0.40 ppm) and *n*-hexane (0.89 and 1.24 ppm).

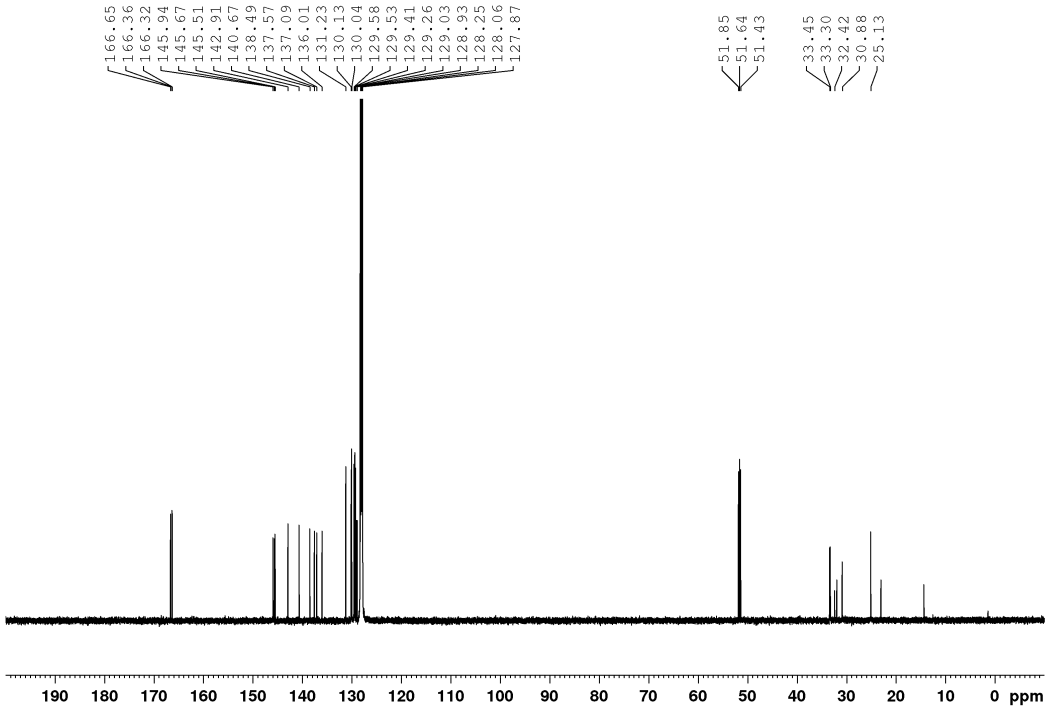

Figure A79: $^{13}C\{^{1}H\}$ NMR spectrum of **4-11b** in C_6D_6 at 125 MHz. Additionally, residual amounts of silicon grease (1.38 ppm) and *n*-hexane (14.3, 23.0 and 32.0 ppm).

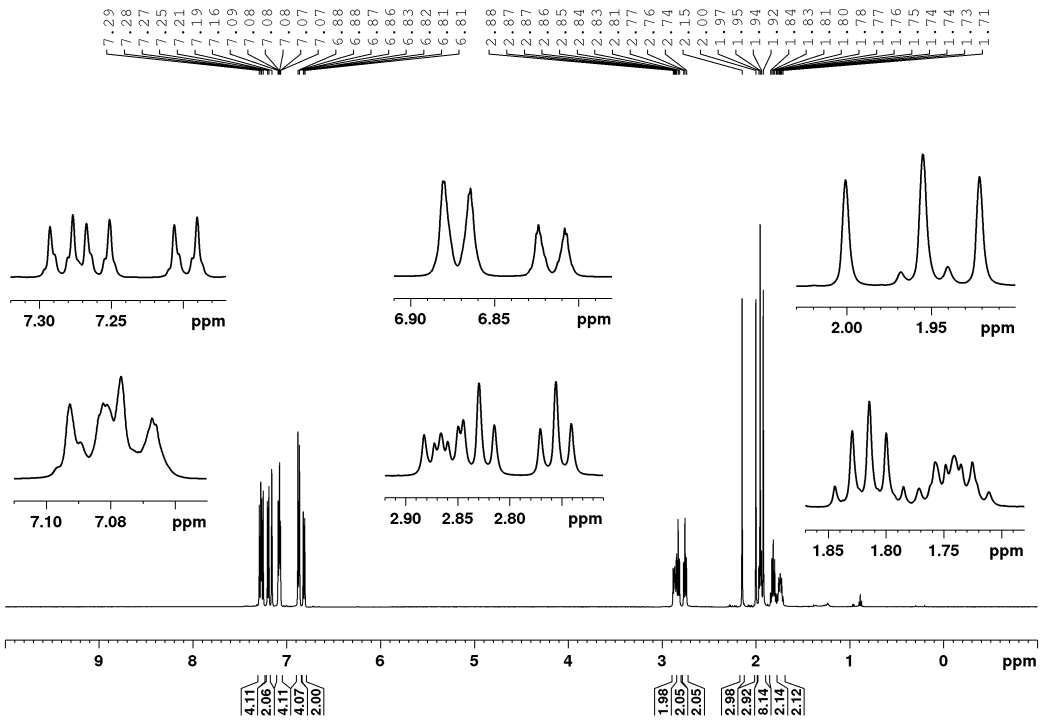

Figure A80: ^{1}H NMR spectrum of **4-12a** in C_6D_6 at 500 MHz. Additionally, residual amounts of *n*-hexane (0.89 and 1.24 ppm).

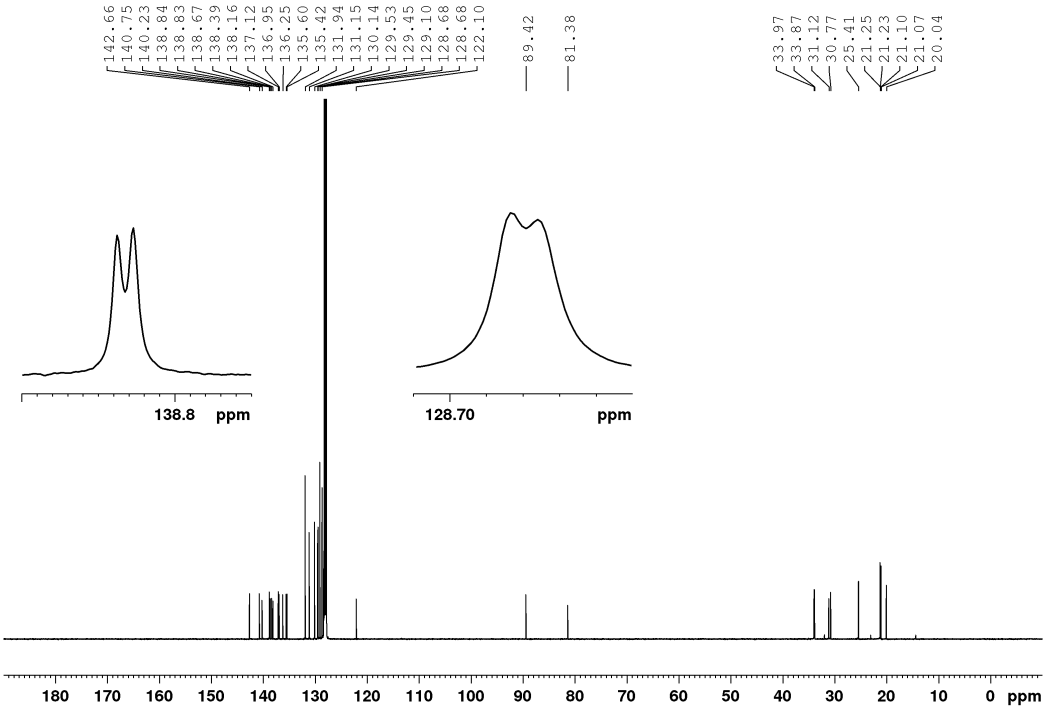

Figure A81: $^{13}C\{^{1}H\}$ NMR spectrum of **4-12a** in C_6D_6 at 125 MHz. Additionally, residual amounts of *n*-hexane (14.3, 23.0 and 32.0 ppm).

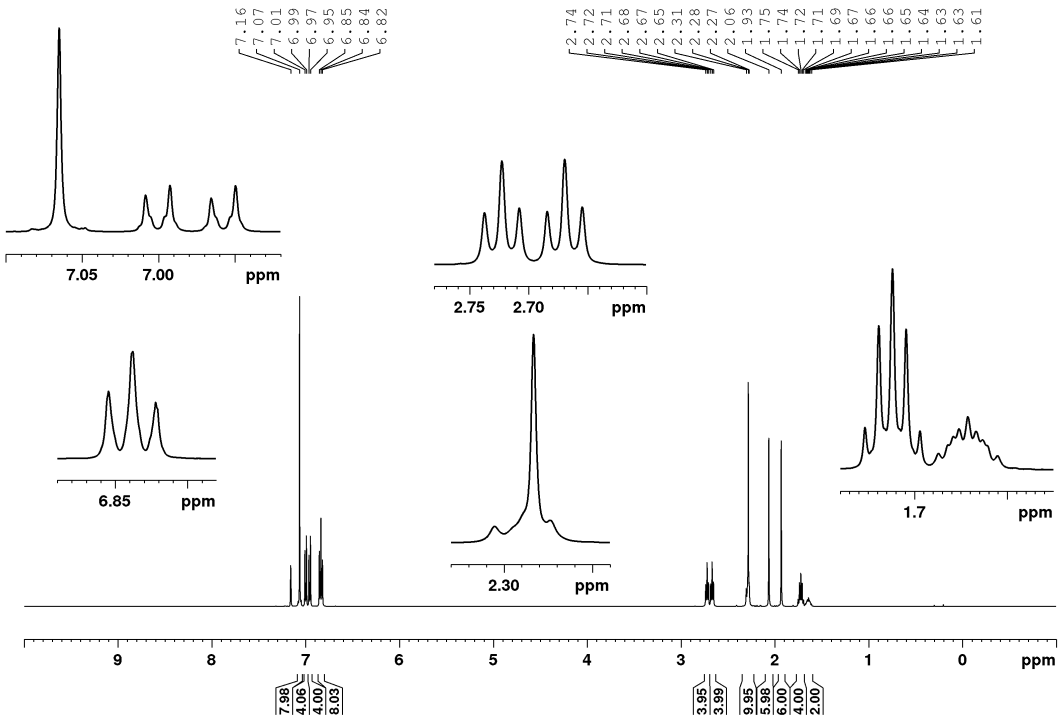

Figure A82: ^{1}H NMR spectrum of **4-12b** in C_6D_6 at 500 MHz.

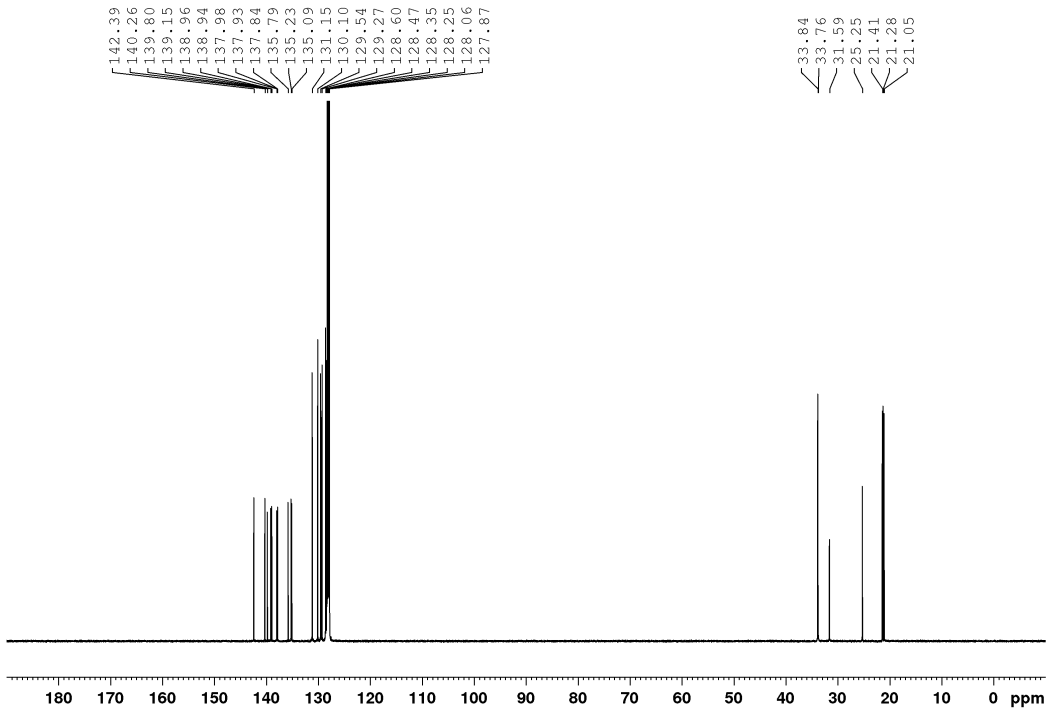

Figure A83: $^{13}C\{^{1}H\}$ NMR spectrum of **4-12b** in C_6D_6 at 125 MHz.

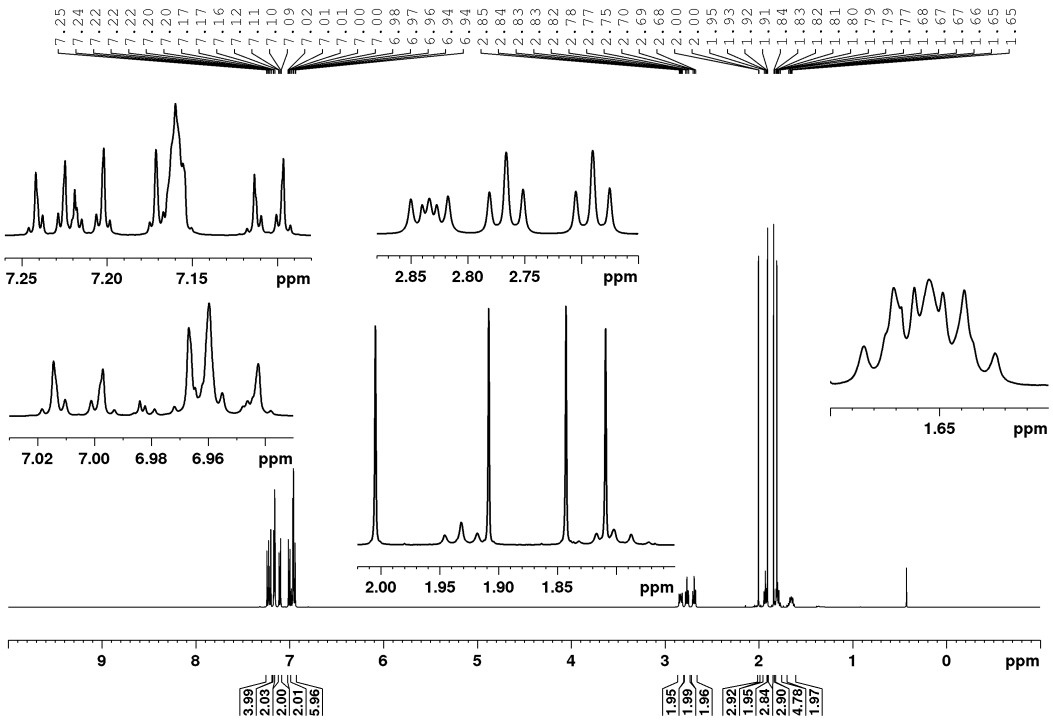

Figure A84: ^{1}H NMR spectrum of **4-13a** in C_6D_6 at 500 MHz. Additionally, residual amounts of water (0.40 ppm).

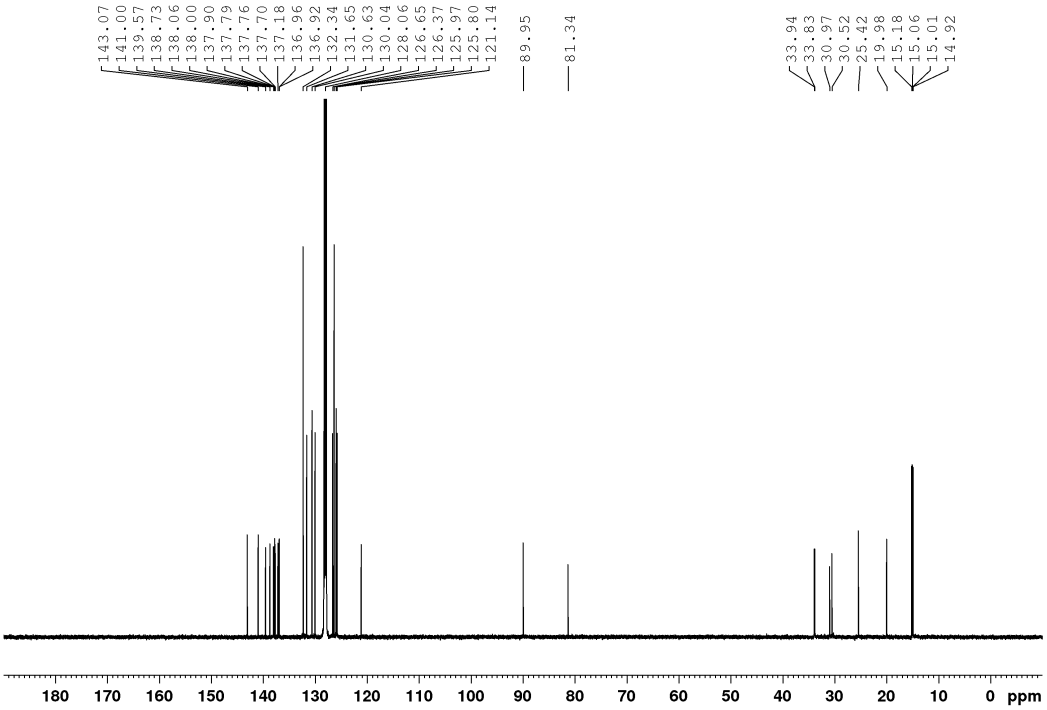

Figure A85: $^{13}C\{^{1}H\}$ NMR spectrum of **4-13a** in C_6D_6 at 125 MHz.

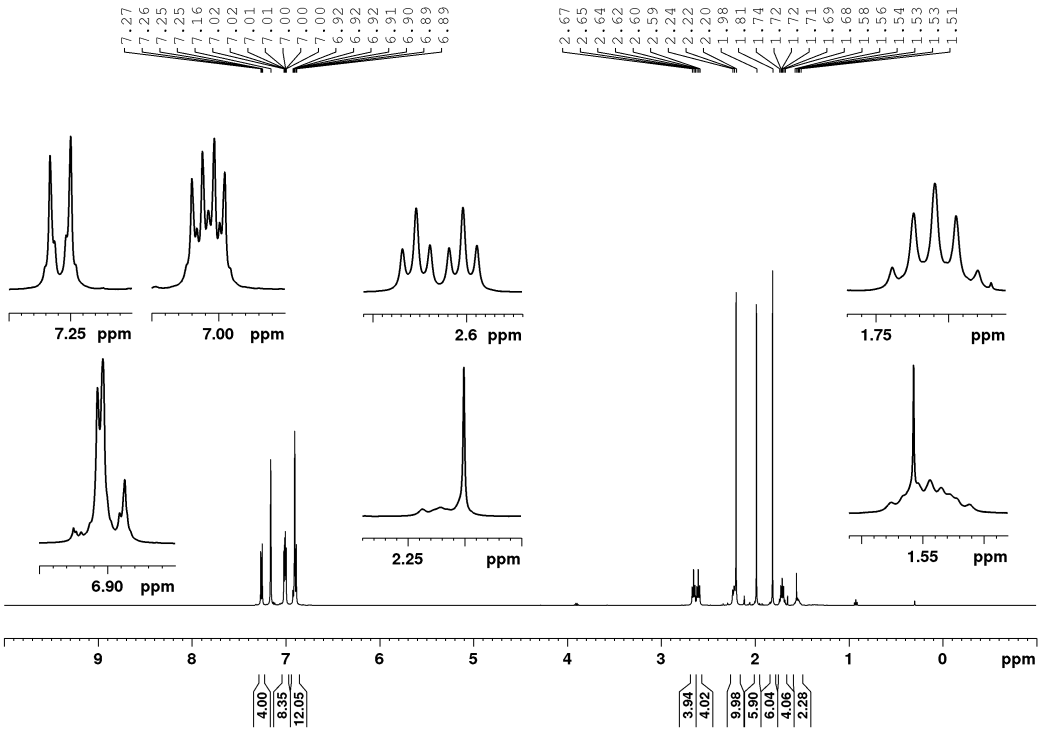

Figure A86: ^{1}H NMR spectrum of **4-13b** in C_6D_6 at 500 MHz. Additionally, residual amounts of acetone (1.55 ppm), toluene (2.11, 7.02 and 7.13 ppm) and ethylacetate (1.65, 3.89 and 0.92 ppm).

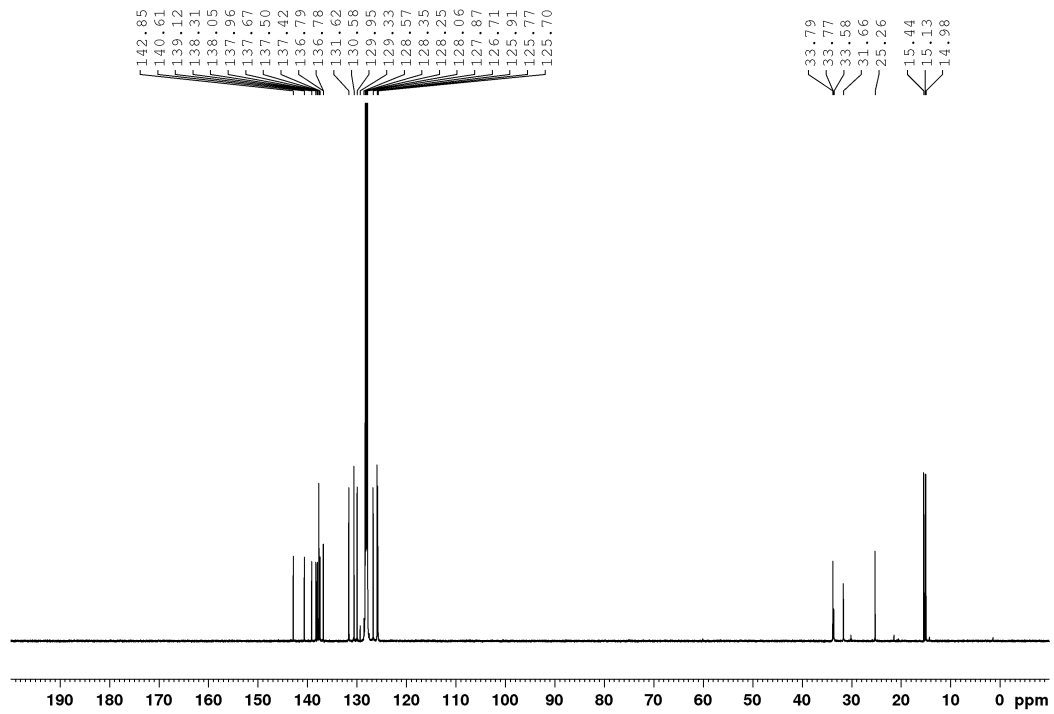

Figure A87: $^{13}C\{^{1}H\}$ NMR spectrum of **4-13b** in C_6D_6 at 125 MHz. Additionally, resonances for acetone (30.1 ppm), toluene (21.1, 137.9, 129.3, 128.6 and 125.7 ppm) and ethylacetate (20.6, 170.4, 60.2 and 14.9 ppm).

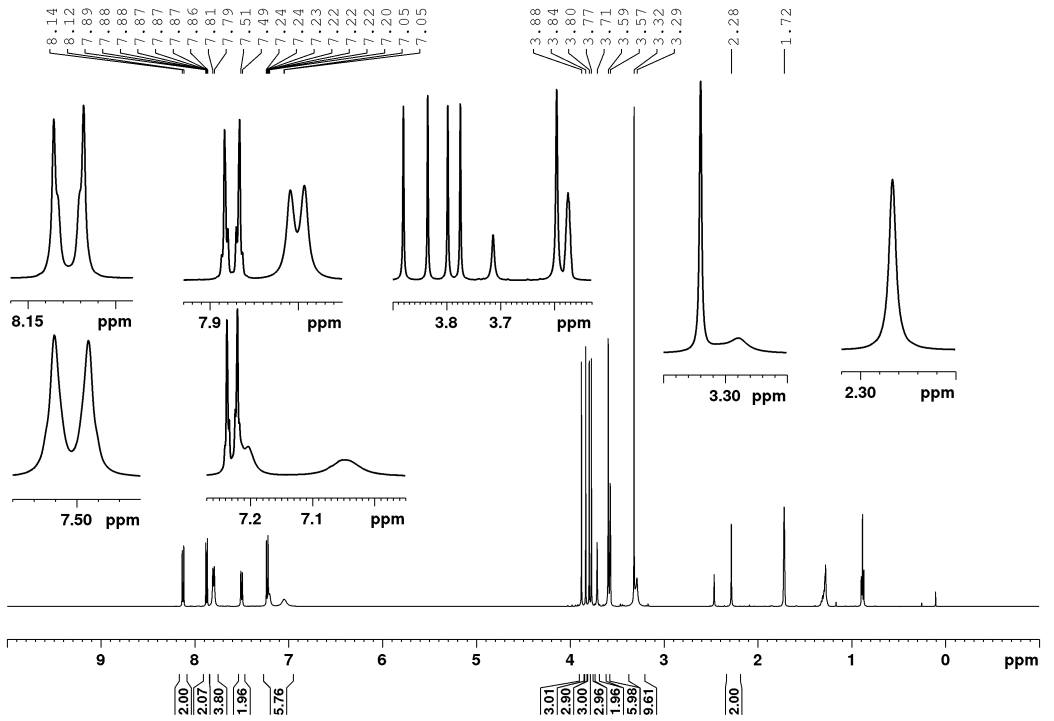

Figure A88: ^{1}H NMR spectrum of **4-14a** in THF-d_8 at 500 MHz. Additionally, residual amounts of silicon grease (0.11 ppm), water (2.46 ppm) and *n*-hexane (0.89 and 1.29 ppm).

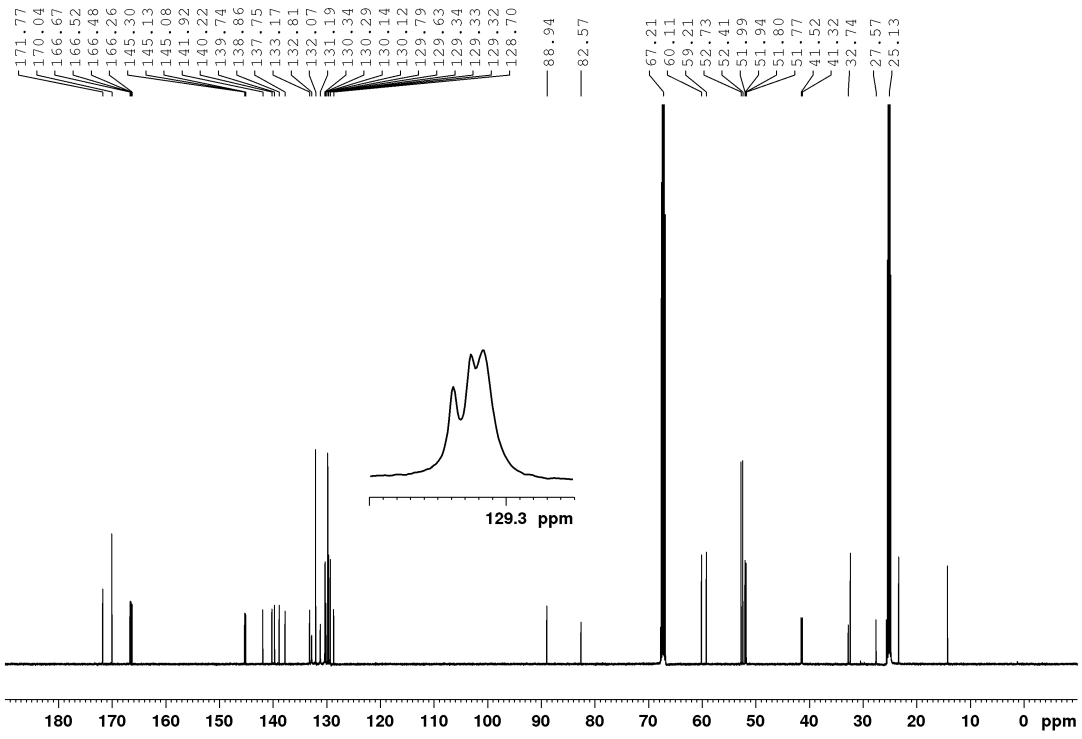

Figure A89: $^{13}C\{^{1}H\}$ NMR spectrum of **4-14a** in THF-d_8 at 125 MHz. Additionally, residual amounts of *n*-hexane (14.2, 23.3 and 32.3 ppm).

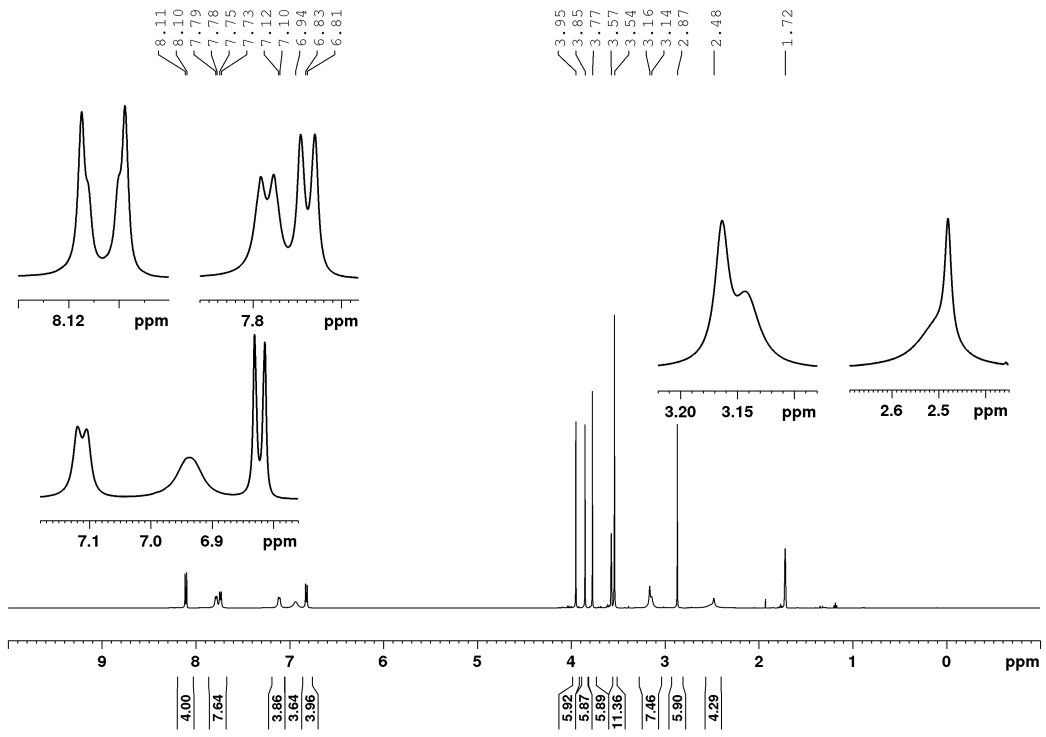

Figure A90: ^{1}H NMR spectrum of **4-14b** in THF-d_8 at 500 MHz. Additionally, residual amounts of ethylacetate (1.94, 4.04 and 1.19 ppm).

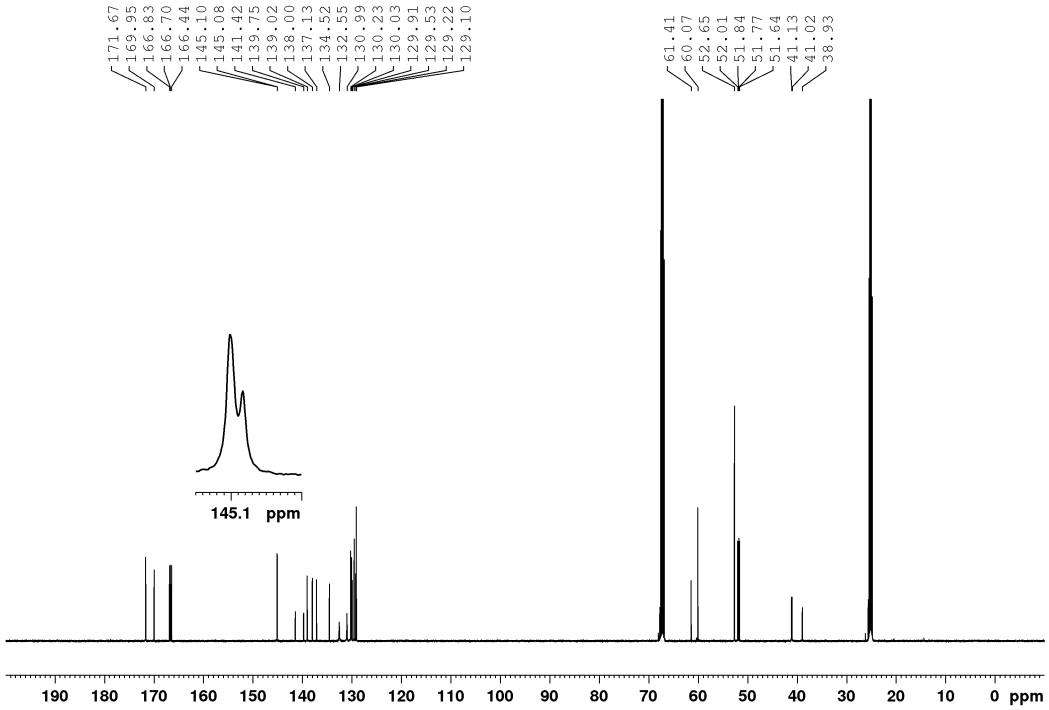

Figure A91: $^{13}C\{^{1}H\}$ NMR spectrum of **4-14b** in THF-d_8 at 125 MHz.

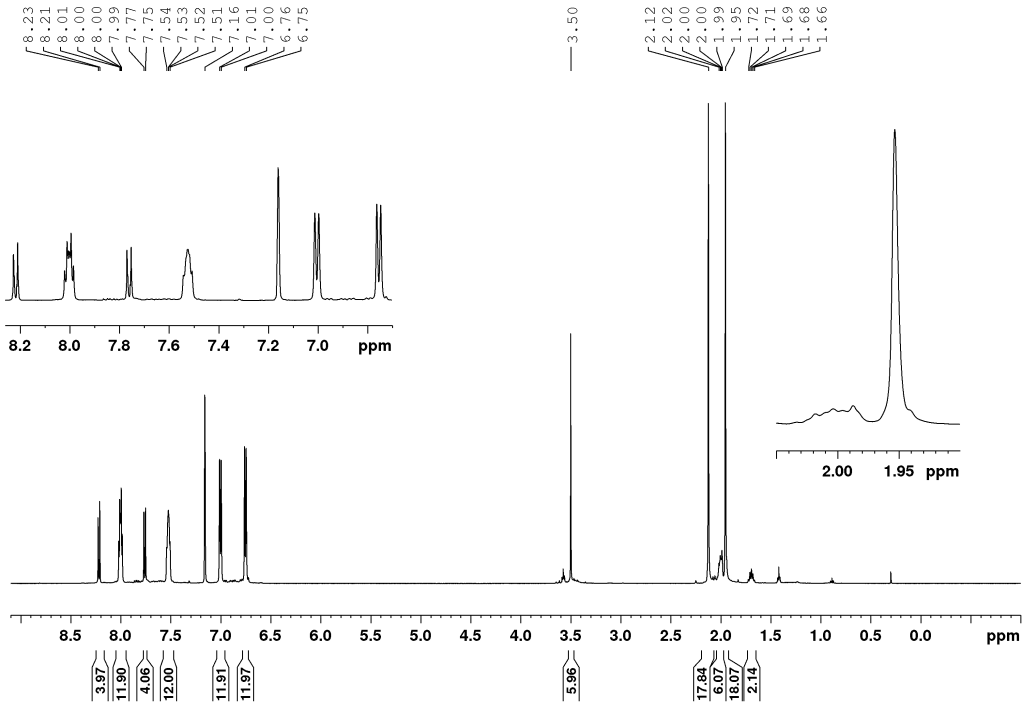

Figure A92: ^{1}H NMR spectrum of **4-15** in C_6D_6 at 500 MHz. Additionally, residual amounts of water (0.40 ppm), *n*-hexane (0.89 and 1.24 ppm) and THF (1.40 and 3.57 ppm).

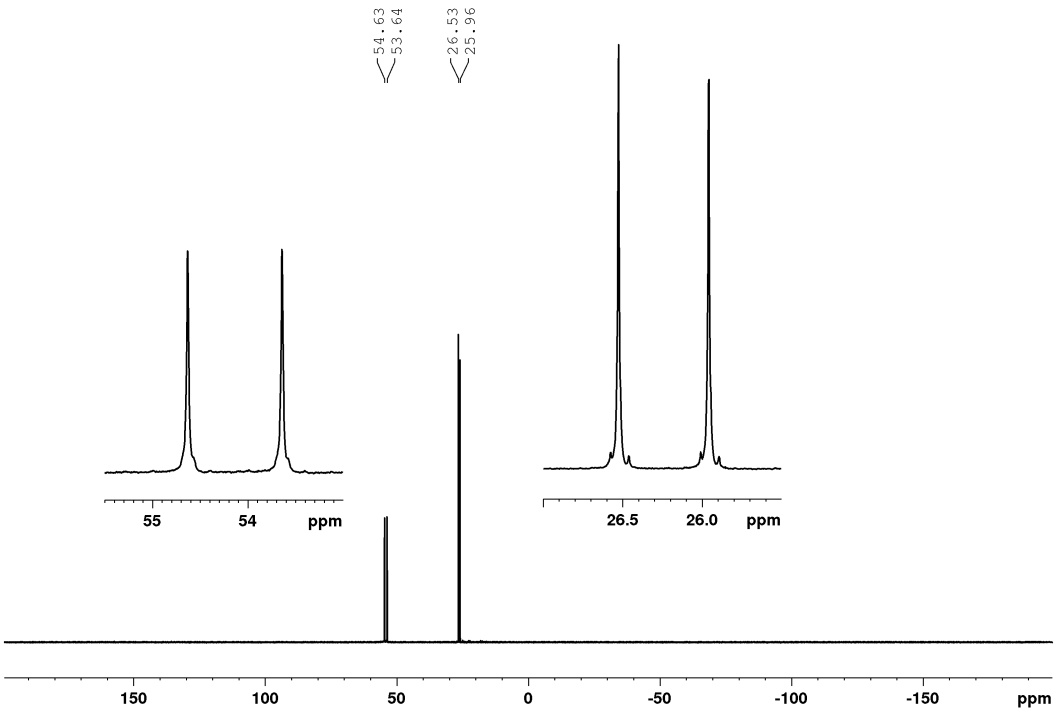

Figure A93: $^{31}P\{^{1}H\}$ NMR spectrum of **4-15** in C_6D_6 at 202 MHz.

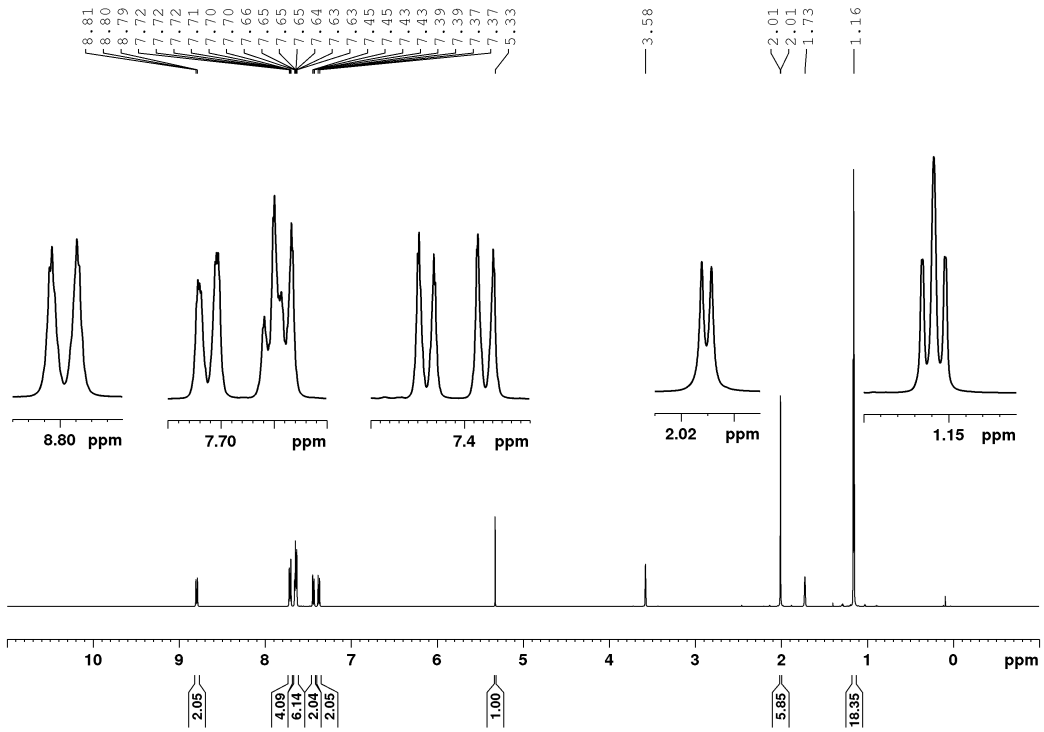

Figure A94: ^{1}H NMR spectrum of **2-2a** in THF-d_8 at 500 MHz.

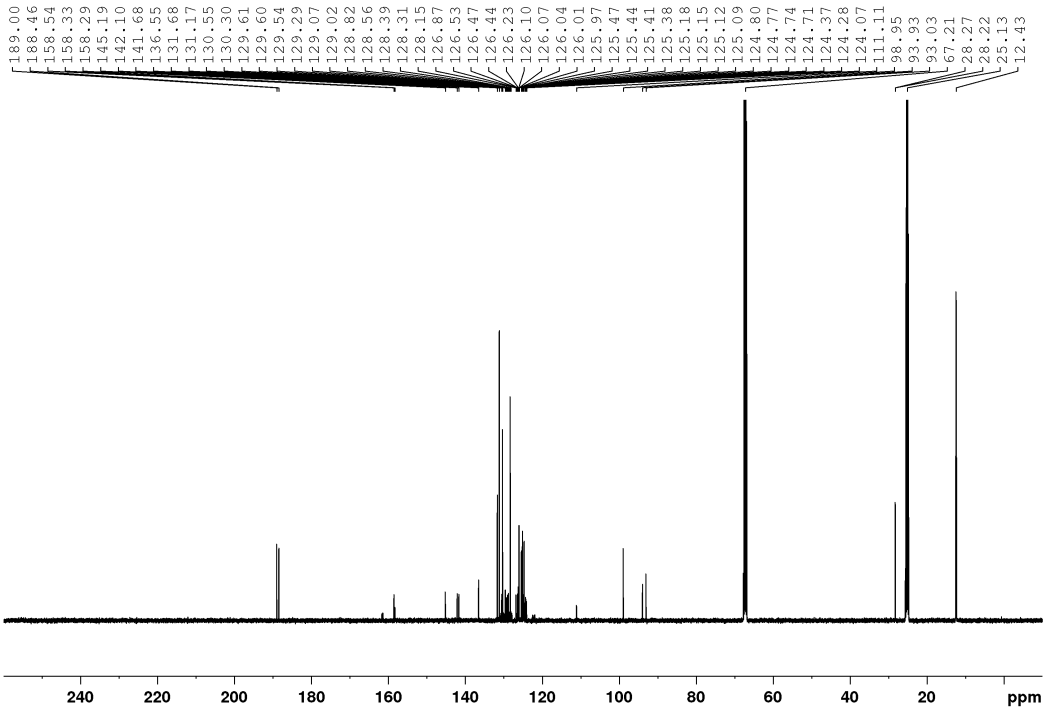

Figure A95: $^{13}C\{^{1}H\}$ NMR spectrum of **2-2a** in THF-d_8 at 125 MHz.

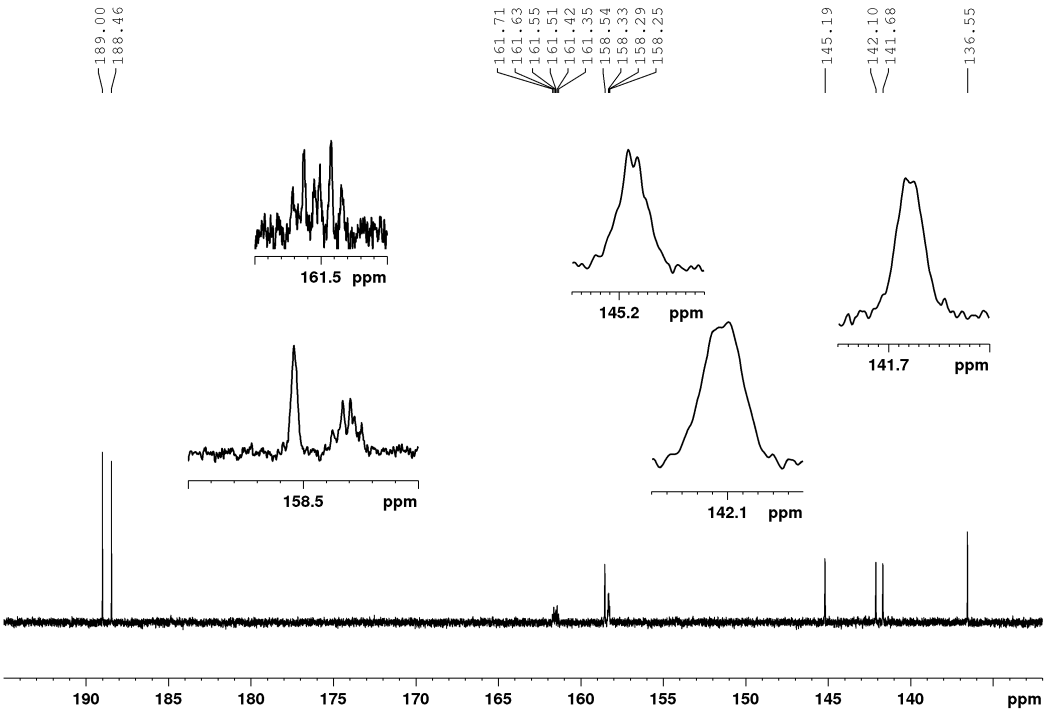

Figure A96: Portion of the $^{13}C\{^{1}H\}$ NMR spectrum (195 – 132 ppm) of **2-2a** in THF-d_8 at 125 MHz.

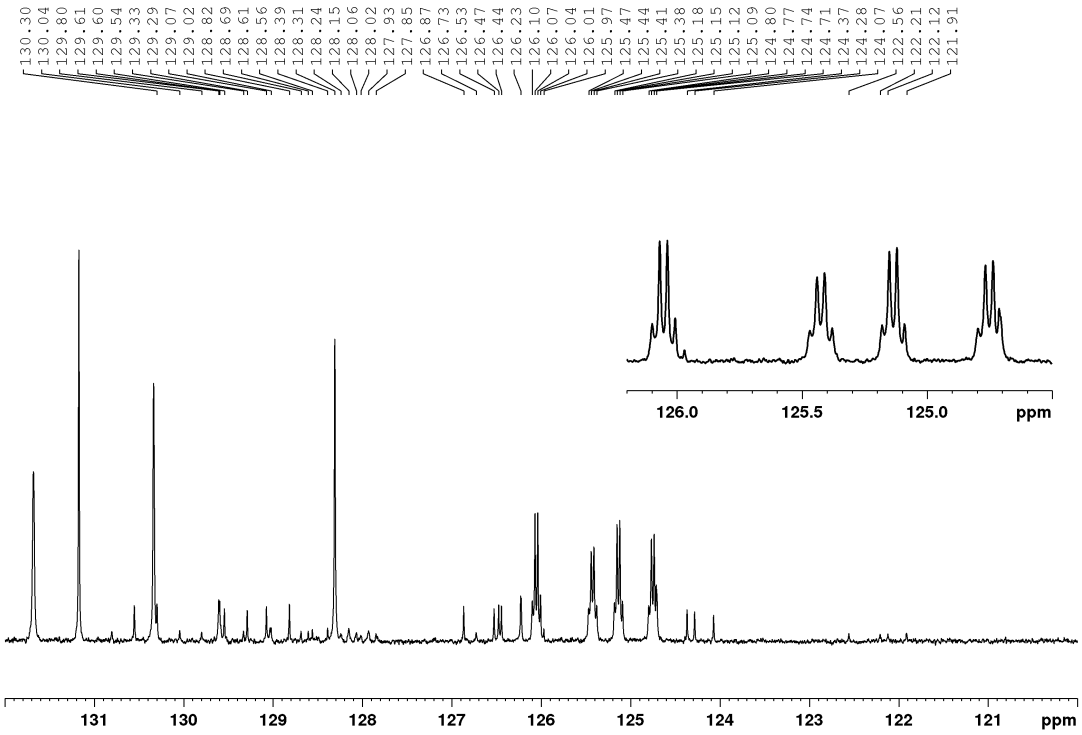

Figure A97: Portion of the $^{13}C\{^{1}H\}$ NMR spectrum (132 – 120 ppm) of **2-2a** in THF-d_8 at 125 MHz.

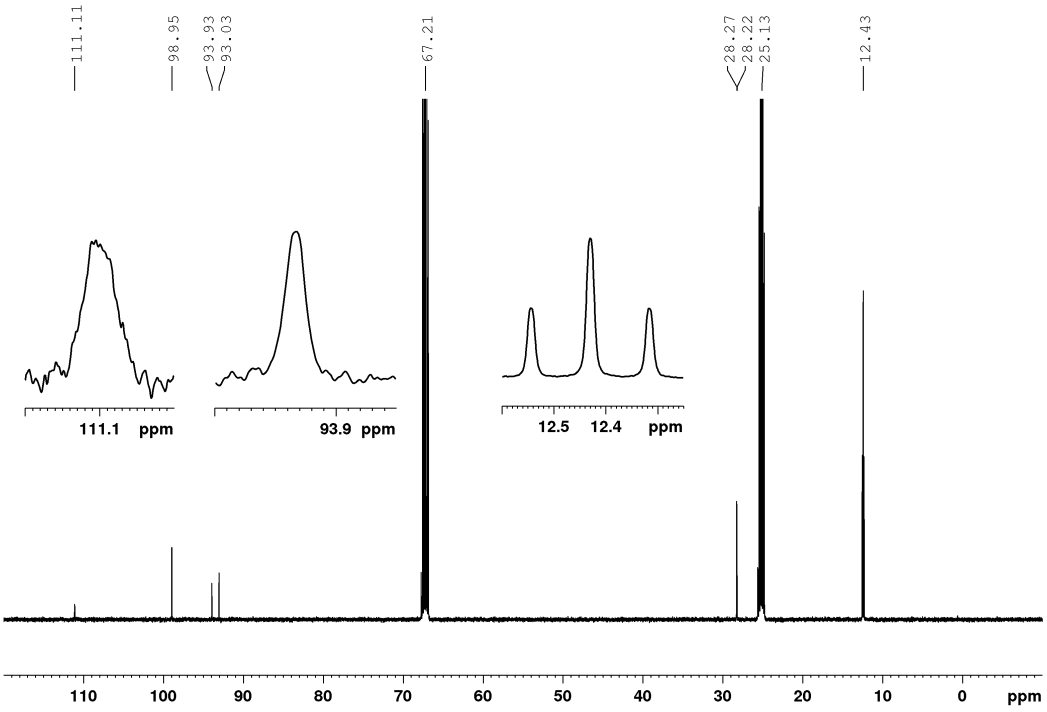

Figure A98: Portion of the $^{13}C\{^{1}H\}$ NMR spectrum (120 – -10 ppm) of **2-2a** in THF-d_8 at 125 MHz.

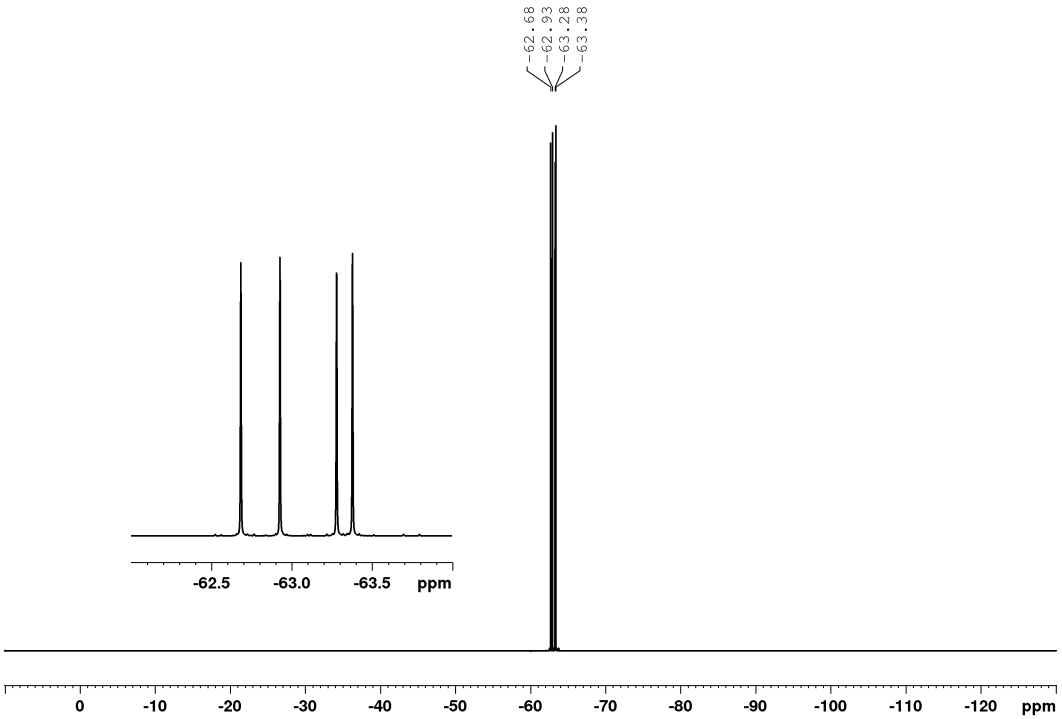

Figure A99: ^{19}F NMR spectrum of **2-2a** in THF-d_8 at 470 MHz.

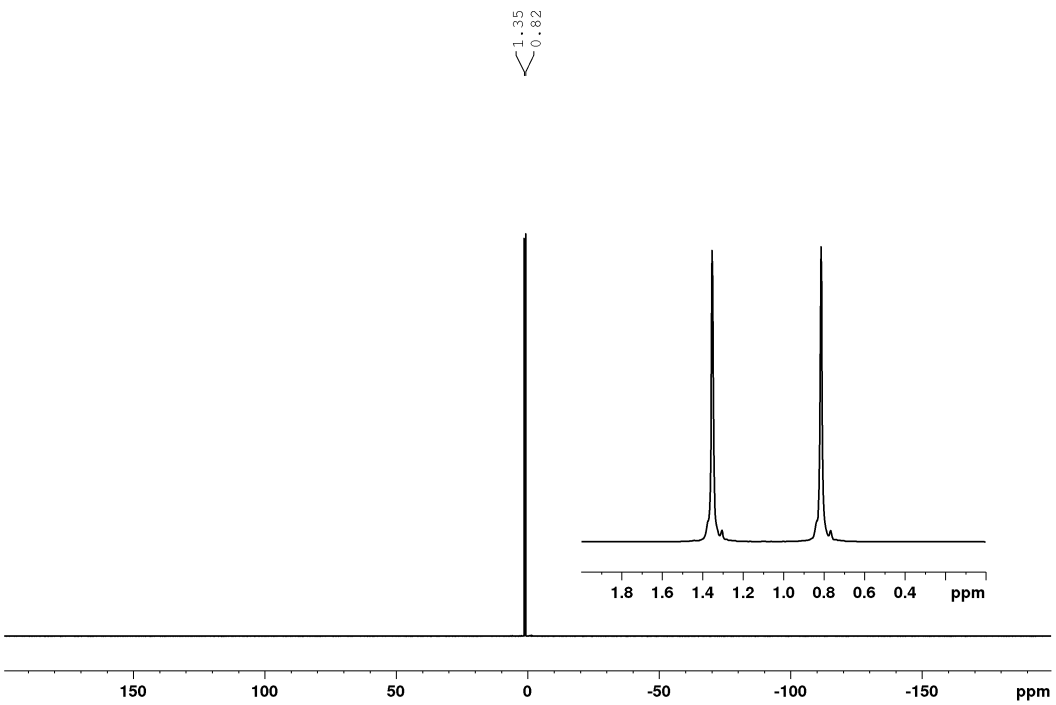

Figure A100: $^{31}P\{^1H\}$ NMR spectrum of **2-2a** in THF-d_8 at 202 MHz.

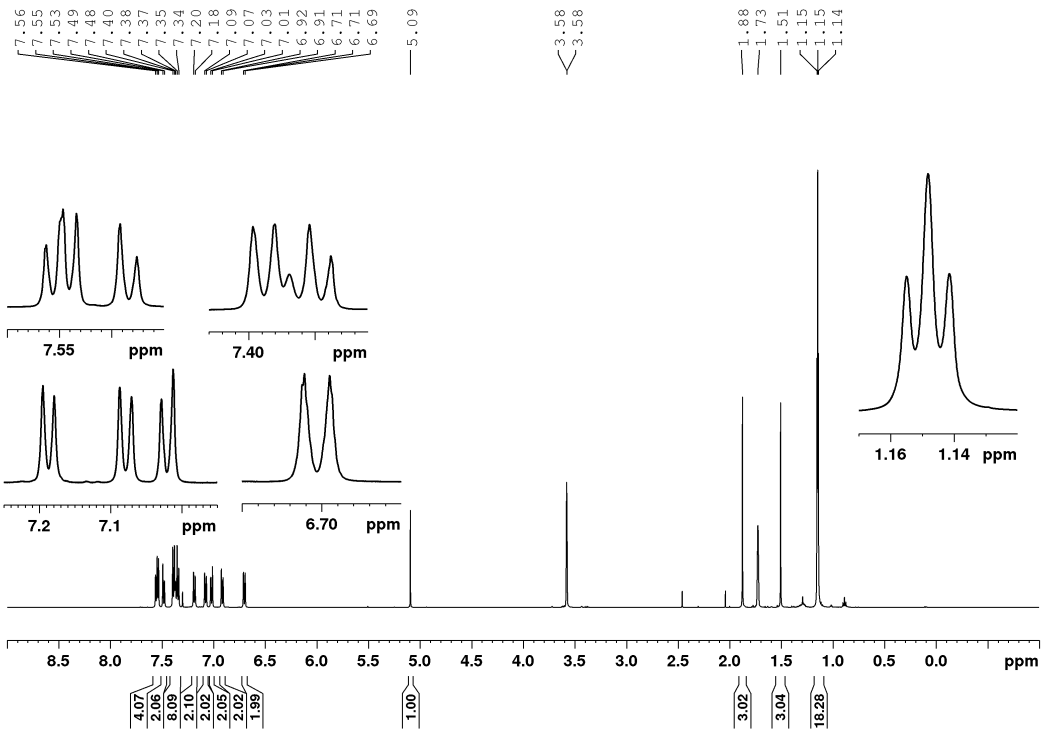

Figure A101: ^{1}H NMR spectrum of **2-3a** in THF-d_8 at 500 MHz. Additionally, residual amounts of water (2.46 ppm), acetone (2.05 ppm) and *n*-hexane (0.89 and 1.29 ppm).

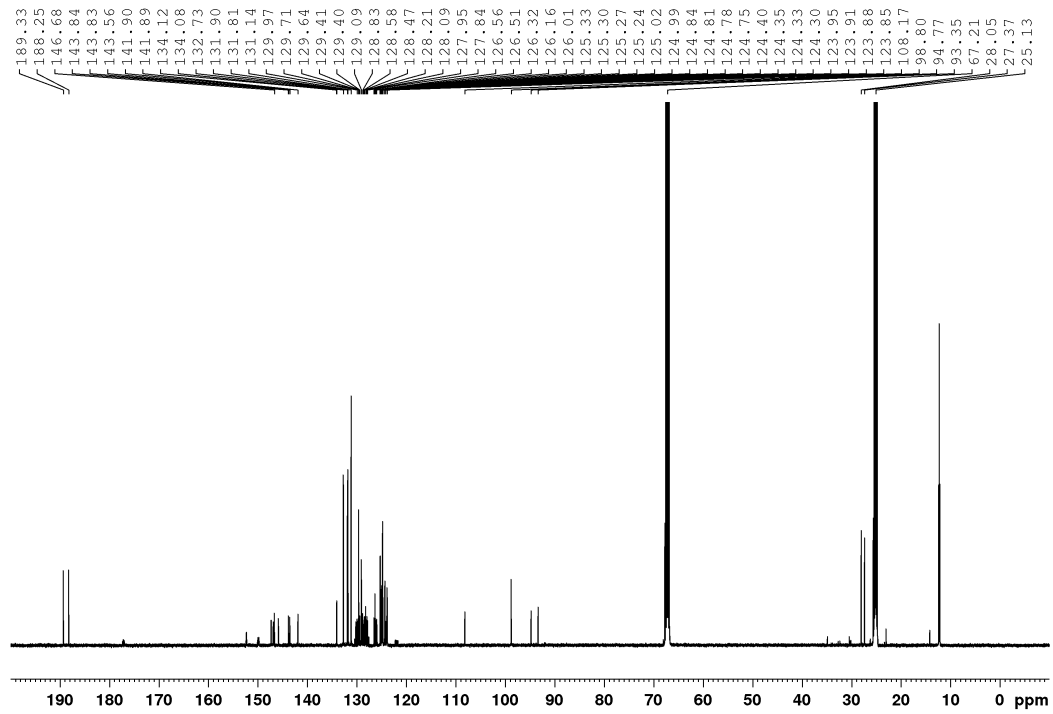

Figure A102: ^{13}C{^{1}H} NMR spectrum of **2-3a** in THF-d_8 at 125 MHz. Additionally, residual amounts of acetone (30.2 ppm) and *n*-hexane (14.2, 23.3 and 32.4 ppm).

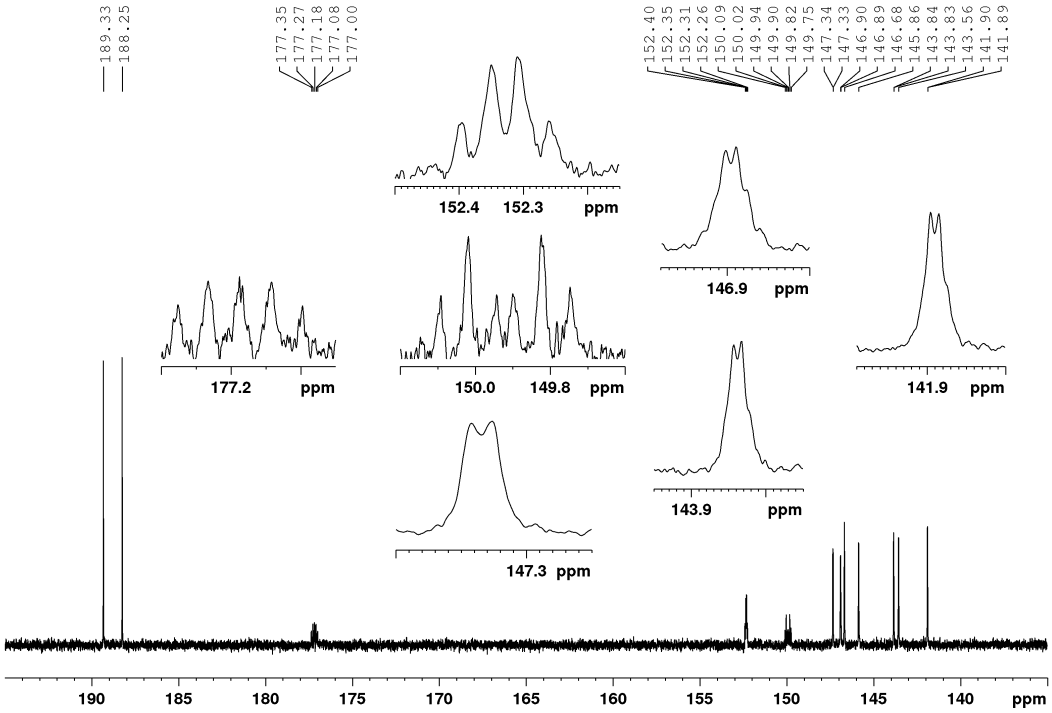

Figure A103: Portion of the $^{13}C\{^{1}H\}$ NMR spectrum (195 – 135 ppm) of **2-3a** in THF-d_8 at 125 MHz.

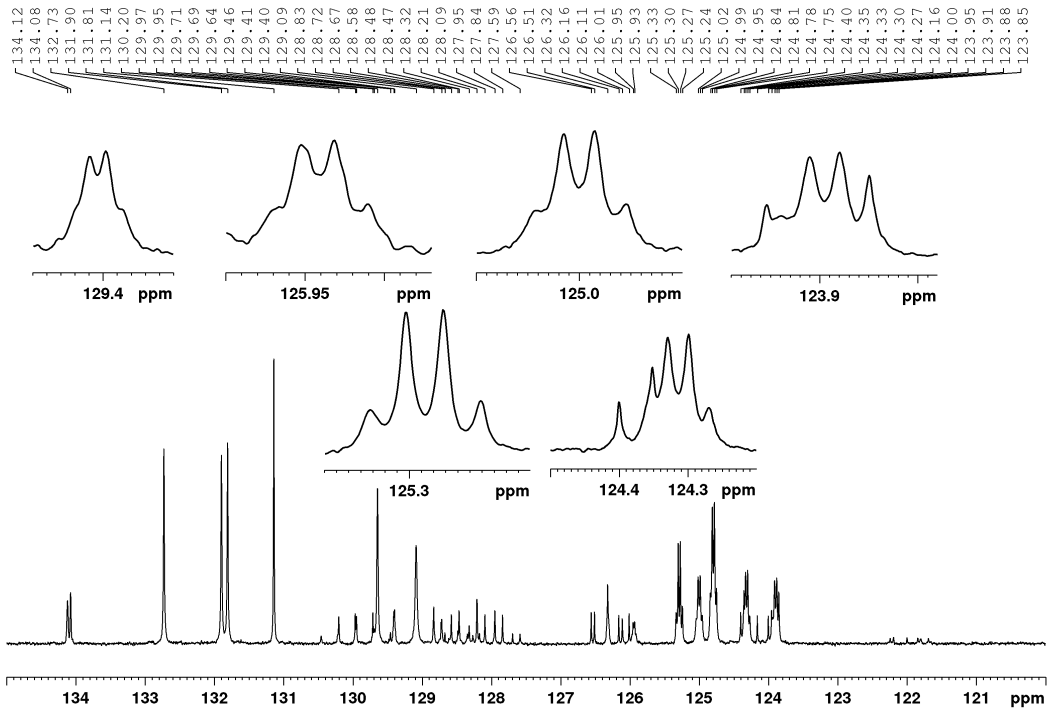

Figure A104: Portion of the $^{13}C\{^{1}H\}$ NMR spectrum (135 – 120 ppm) of **2-3a** in THF-d_8 at 125 MHz.

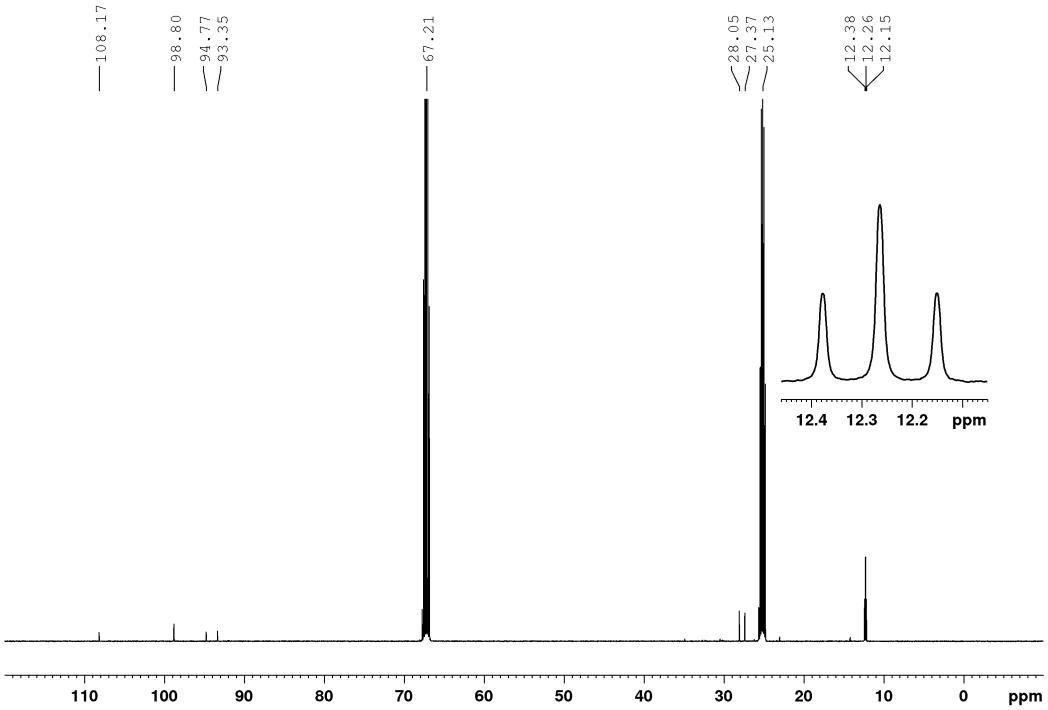

Figure A105: Portion of the $^{13}C\{^{1}H\}$ NMR spectrum (120 – -10 ppm) of **2-3a** in THF-d_8 at 125 MHz. Additionally, residual amounts of acetone (30.2 ppm) and *n*-hexane (14.2, 23.3 and 32.4 ppm).

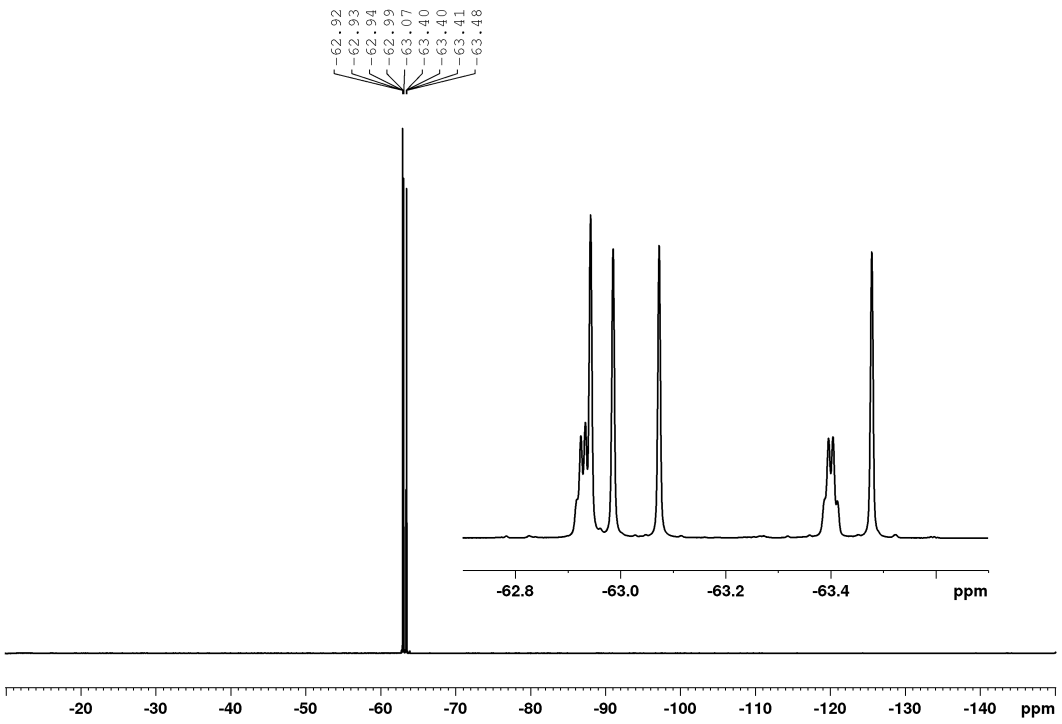

Figure A106: ^{19}F NMR spectrum of **2-3a** in THF-d_8 at 470 MHz.

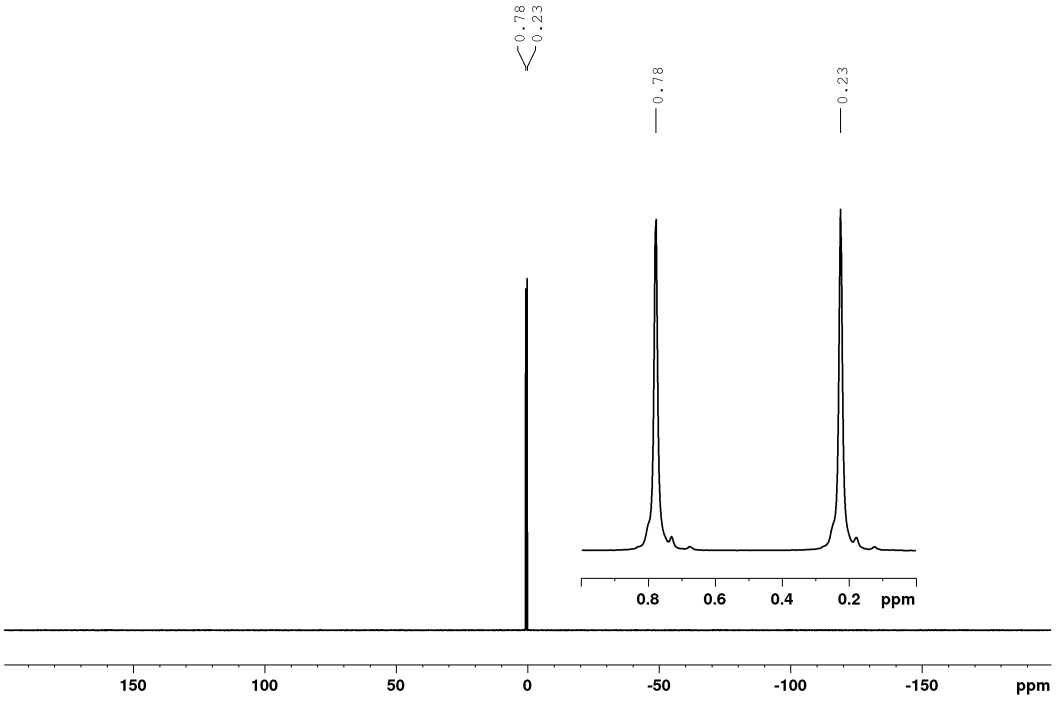

Figure A107: $^{31}P\{^{1}H\}$ NMR spectrum of **2-3a** in THF-d_8 at 202 MHz.

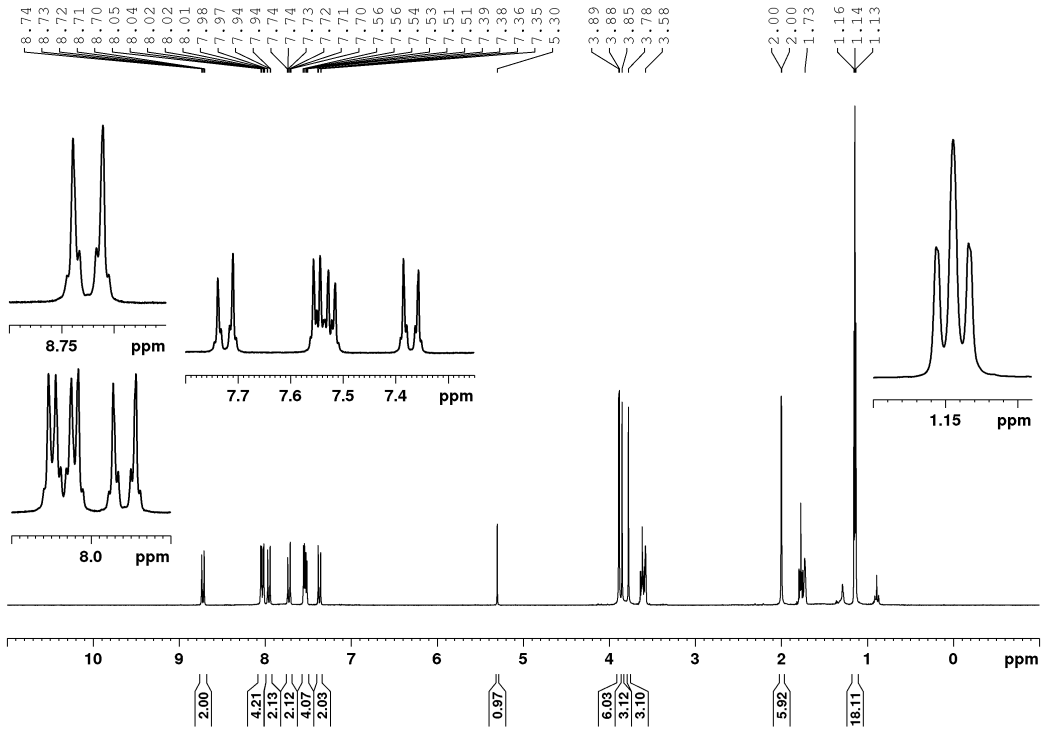

Figure A108: ^{1}H NMR spectrum of **2-2b** in THF-d_8 at 300 MHz. Additionally, residual amounts of n-hexane (0.89 and 1.29 ppm).

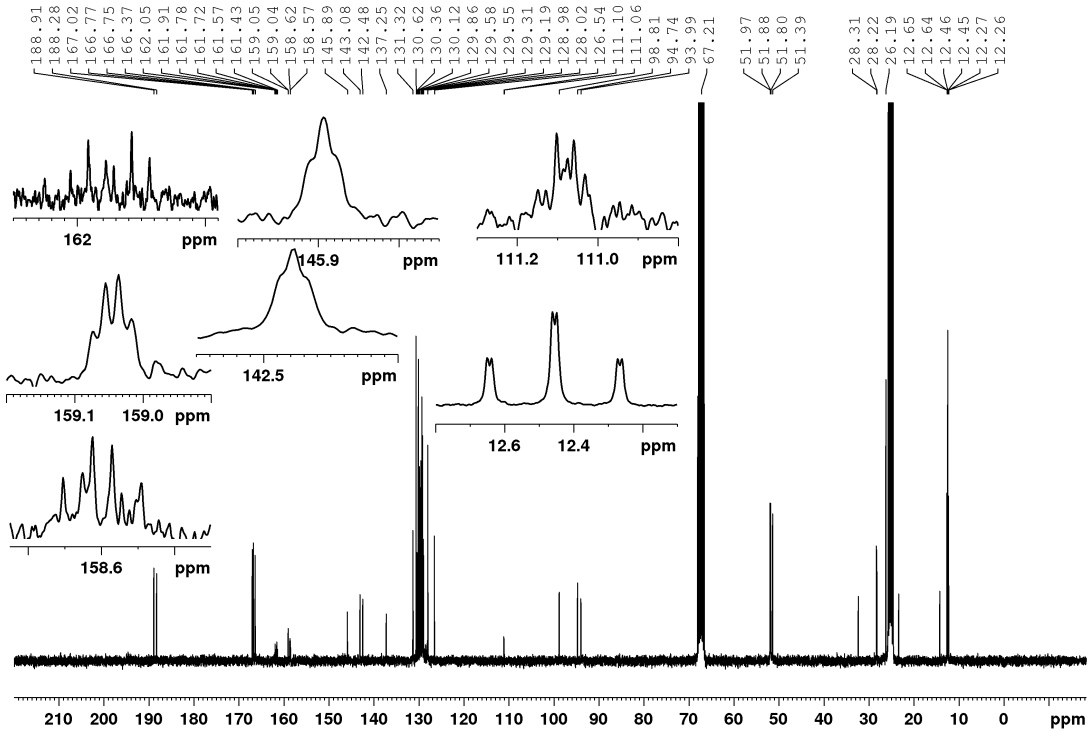

Figure A109: $^{13}C\{^{1}H\}$ NMR spectrum of **2-2b** in THF-d_8 at 75 MHz. Additionally, residual amounts of *n*-hexane (14.2, 23.3 and 32.3 ppm).

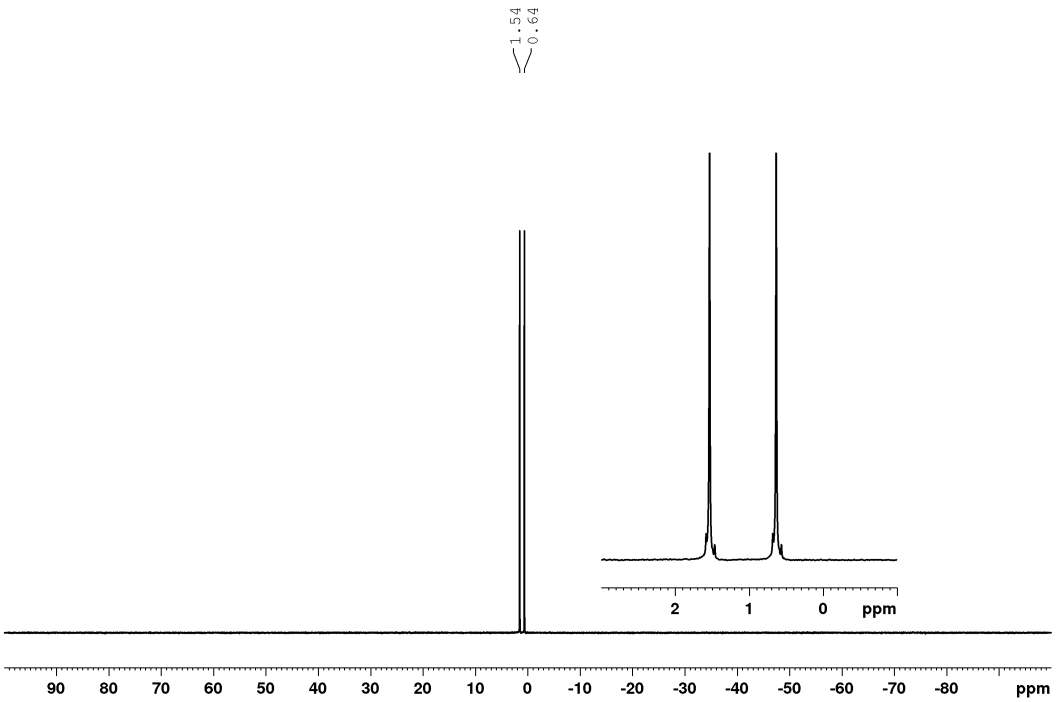

Figure A110: $^{31}P\{^{1}H\}$ NMR spectrum of **2-2b** in THF-d_8 at 121 MHz.

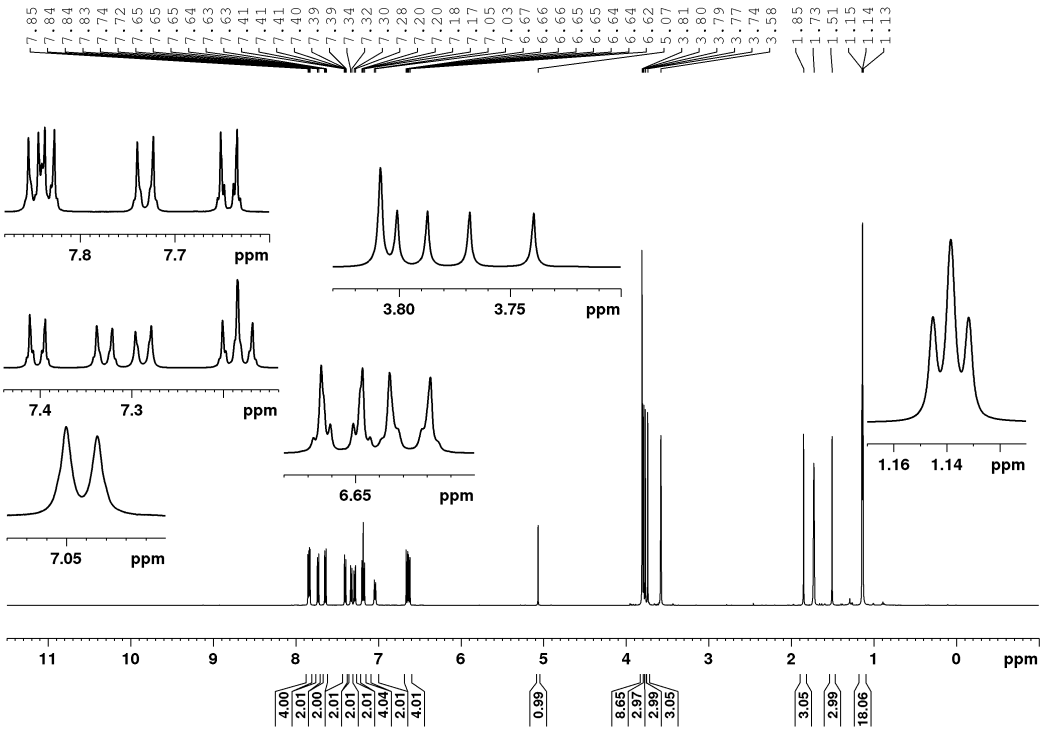

Figure A111: ^{1}H NMR spectrum of **2-3b** in THF-d_8 at 500 MHz.

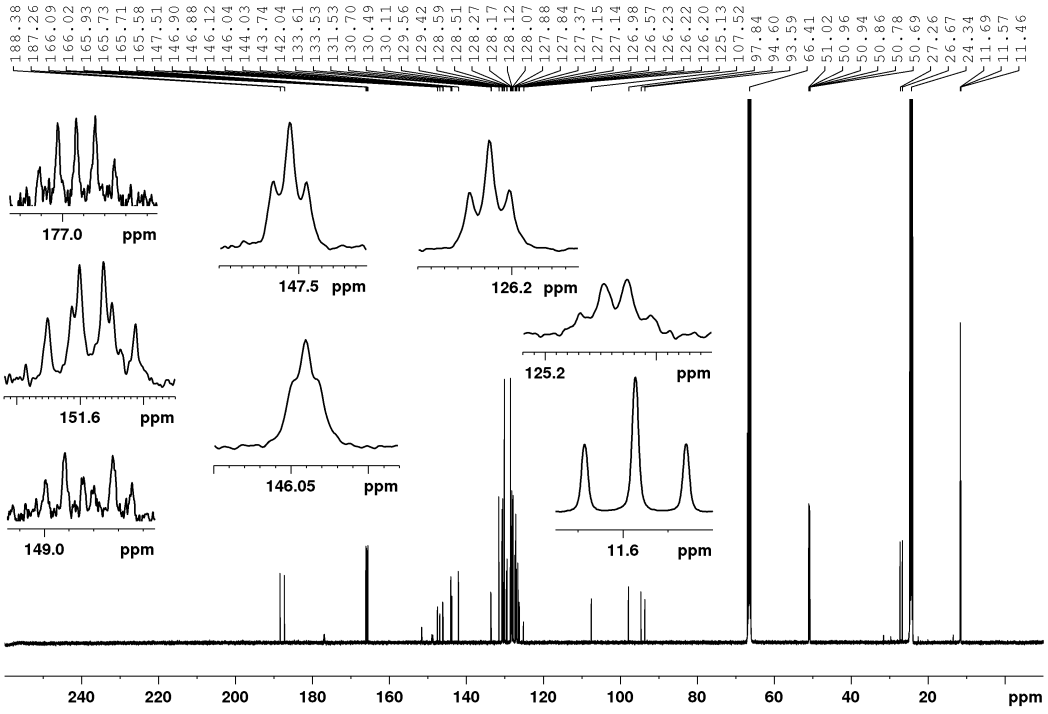

Figure A112: $^{13}C\{^{1}H\}$ NMR spectrum of **2-3b** in THF-d_8 at 125 MHz.

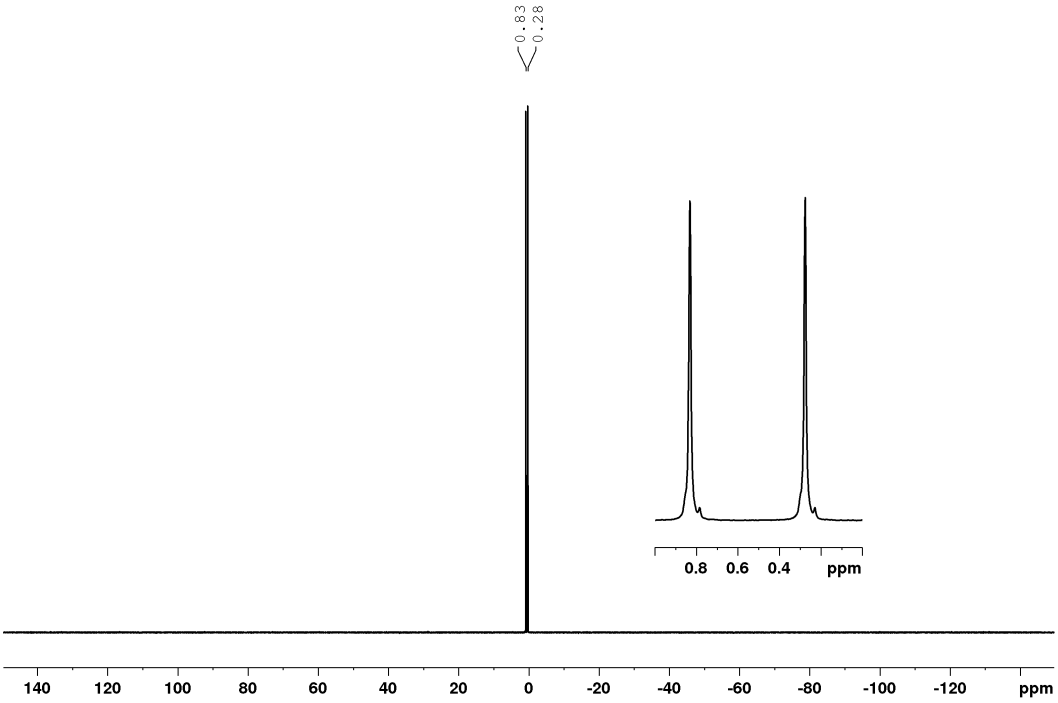

Figure A113: $^{31}P\{^{1}H\}$ NMR spectrum of **2-3b** in THF-d_8 at 202 MHz.

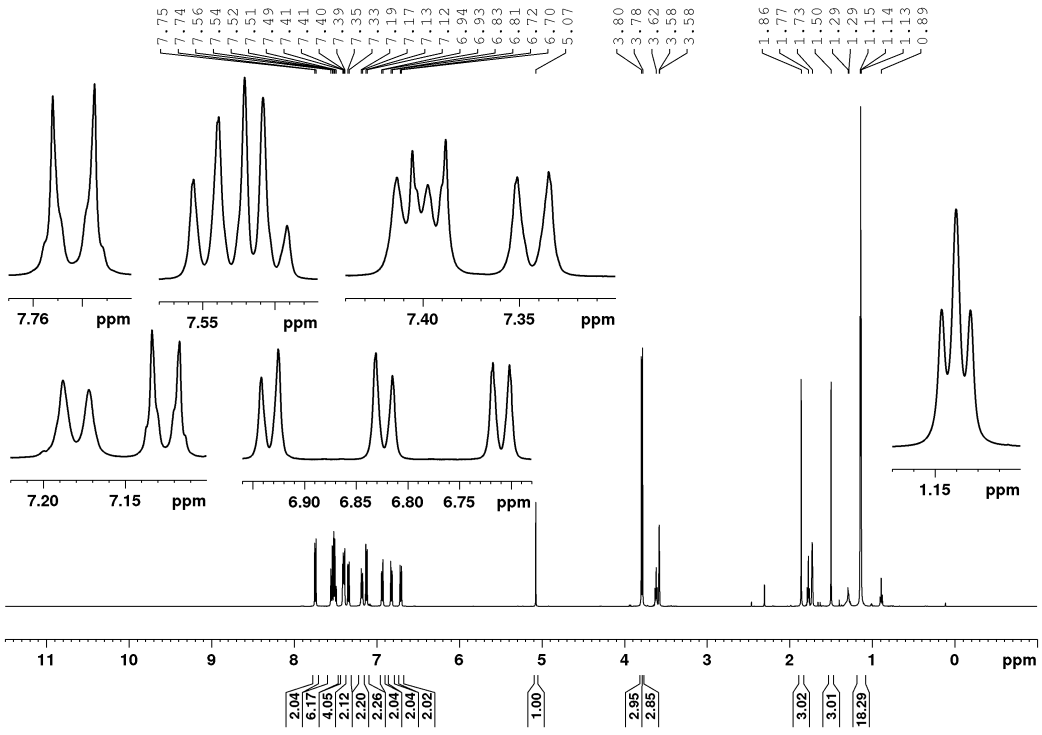

Figure A114: ^{1}H NMR spectrum of **2-3c** in THF-d_8 at 500 MHz. Additionally, residual amounts of water (2.46 ppm) and *n*-hexane (0.89 and 1.29 ppm).

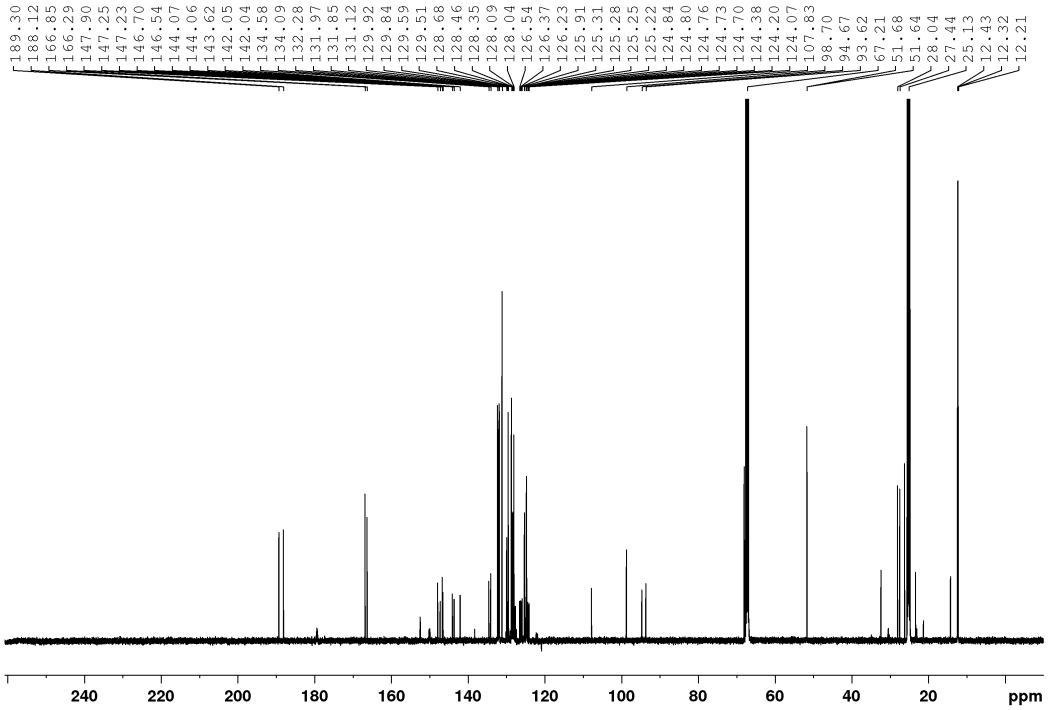

Figure A115: $^{13}C\{^{1}H\}$ NMR spectrum of **2-3c** in THF-d_8 at 125 MHz. Additionally, residual amounts of *n*-hexane (14.2, 23.3 and 32.3 ppm).

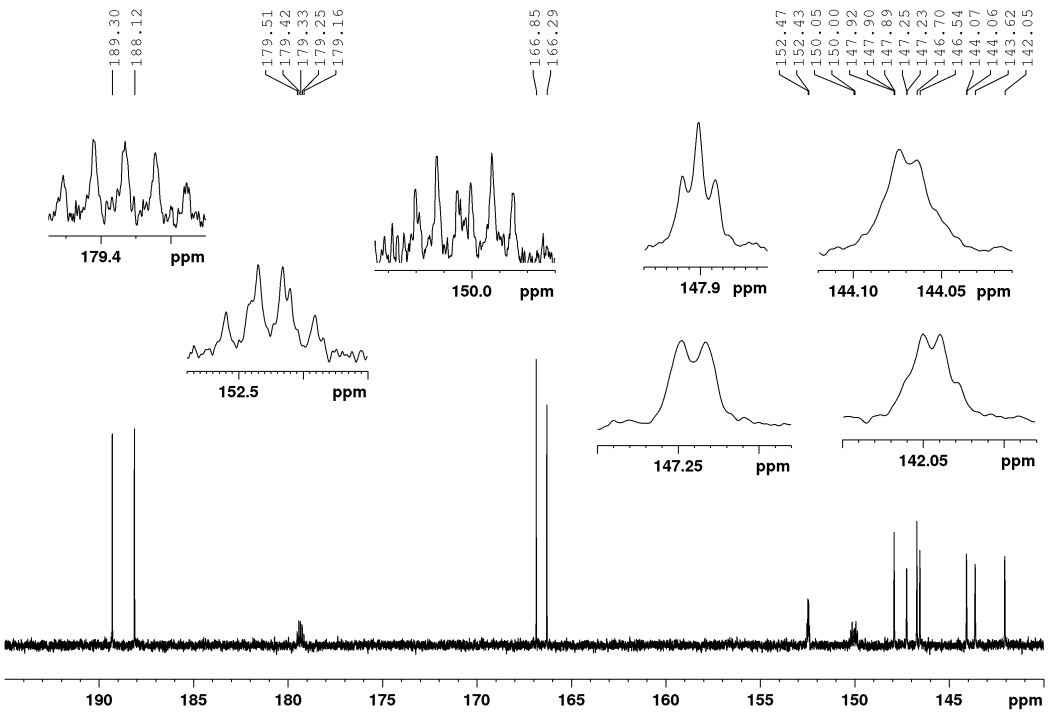

Figure A116: Portion of the $^{13}C\{^{1}H\}$ NMR spectrum (195 – 140 ppm) of **2-3c** in THF-d_8 at 125 MHz.

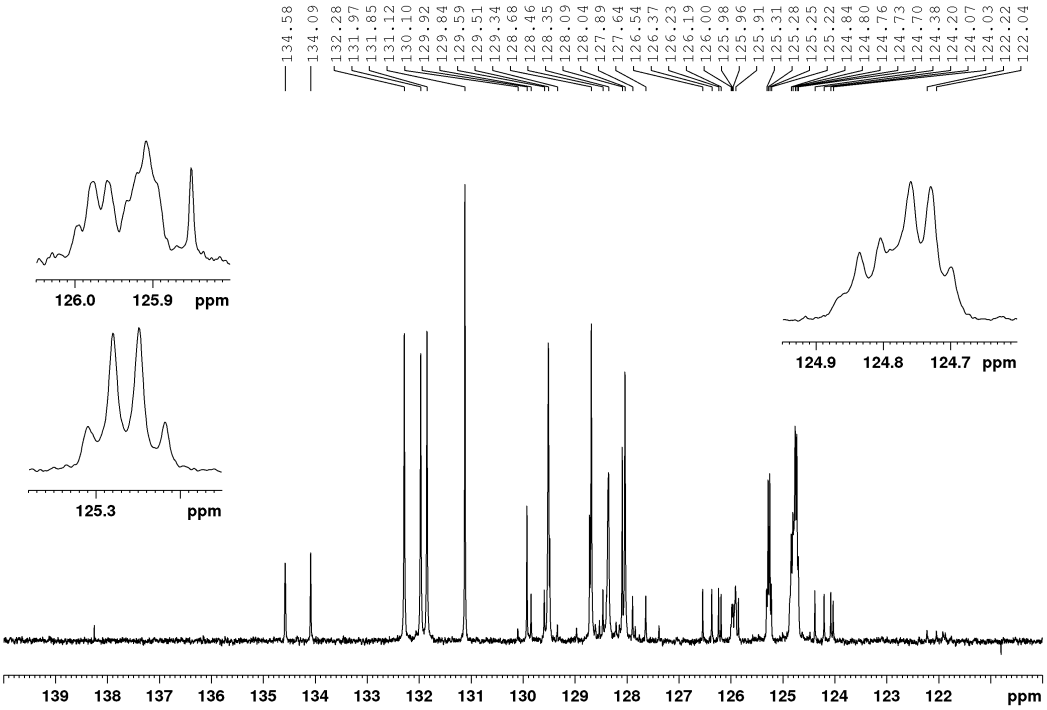

Figure A117: Portion of the $^{13}C\{^{1}H\}$ NMR spectrum (140 – 120 ppm) of **2-3c** in THF-d_8 at 125 MHz.

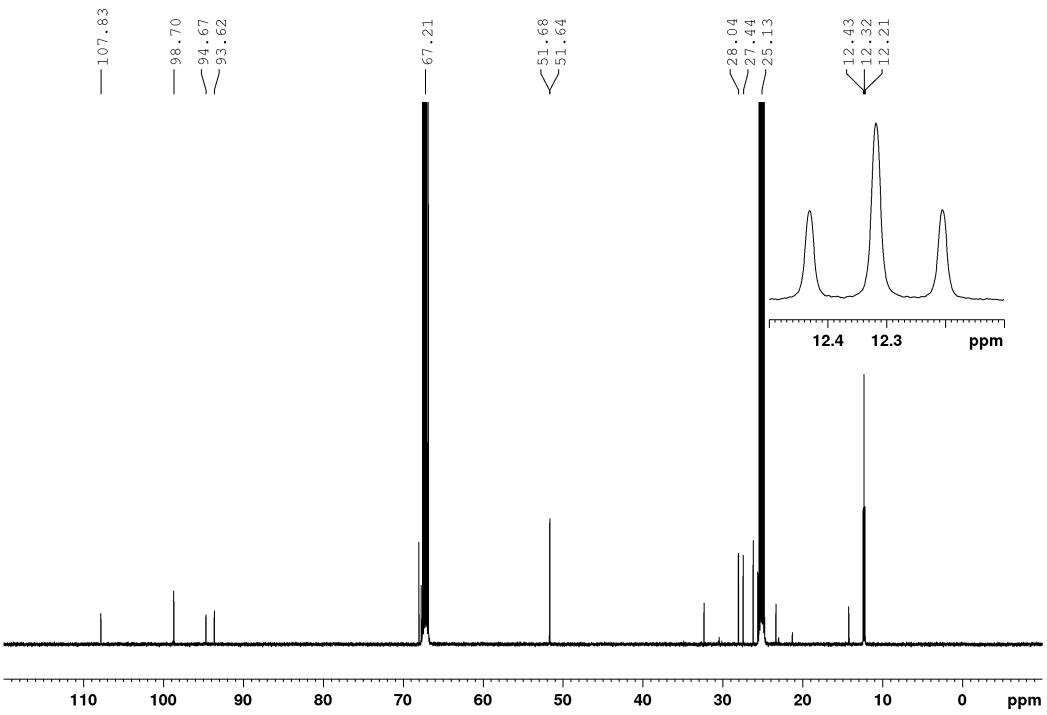

Figure A118: Portion of the $^{13}C\{^{1}H\}$ NMR spectrum (120 – -10 ppm) of **2-3c** in THF-d_8 at 125 MHz. Additionally, residual amounts of *n*-hexane (14.2, 23.3 and 32.3 ppm).

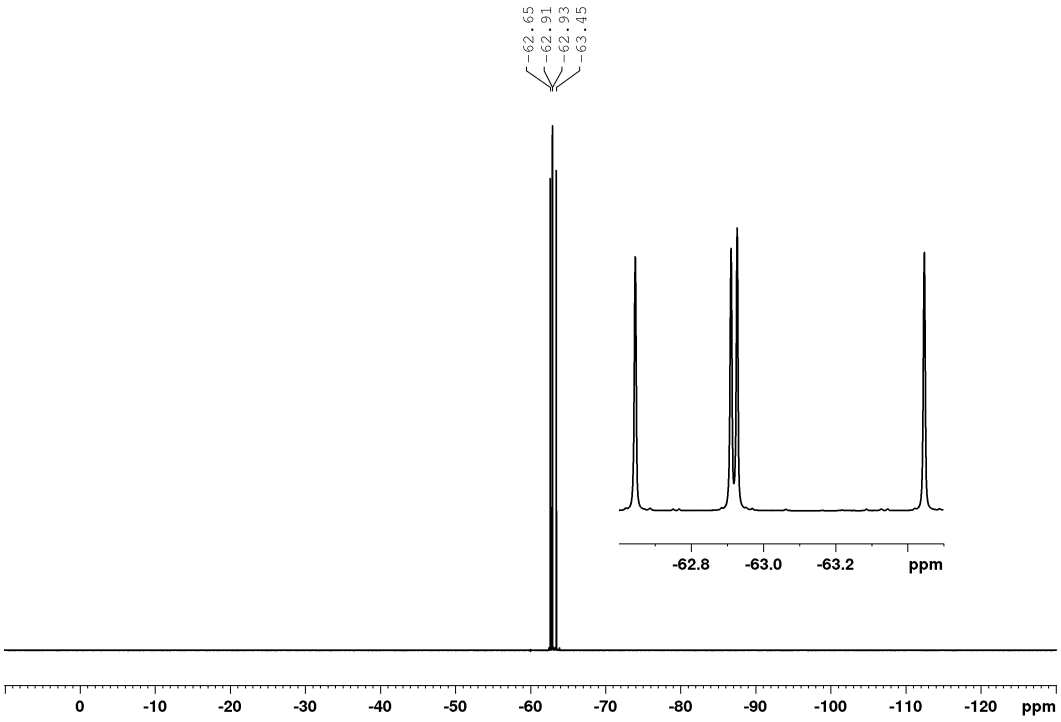

Figure A119: ^{19}F NMR spectrum of **2-3c** in THF-d_8 at 470 MHz.

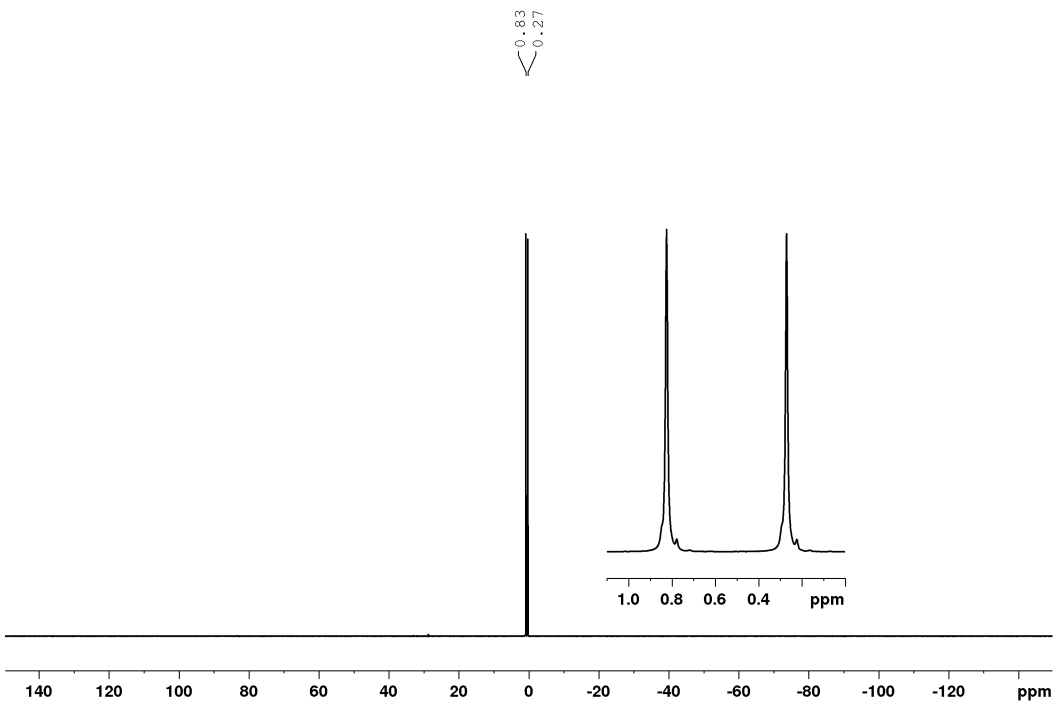

Figure A120: $^{31}P\{^1H\}$ NMR spectrum of **2-3c** in THF-d_8 at 202 MHz.

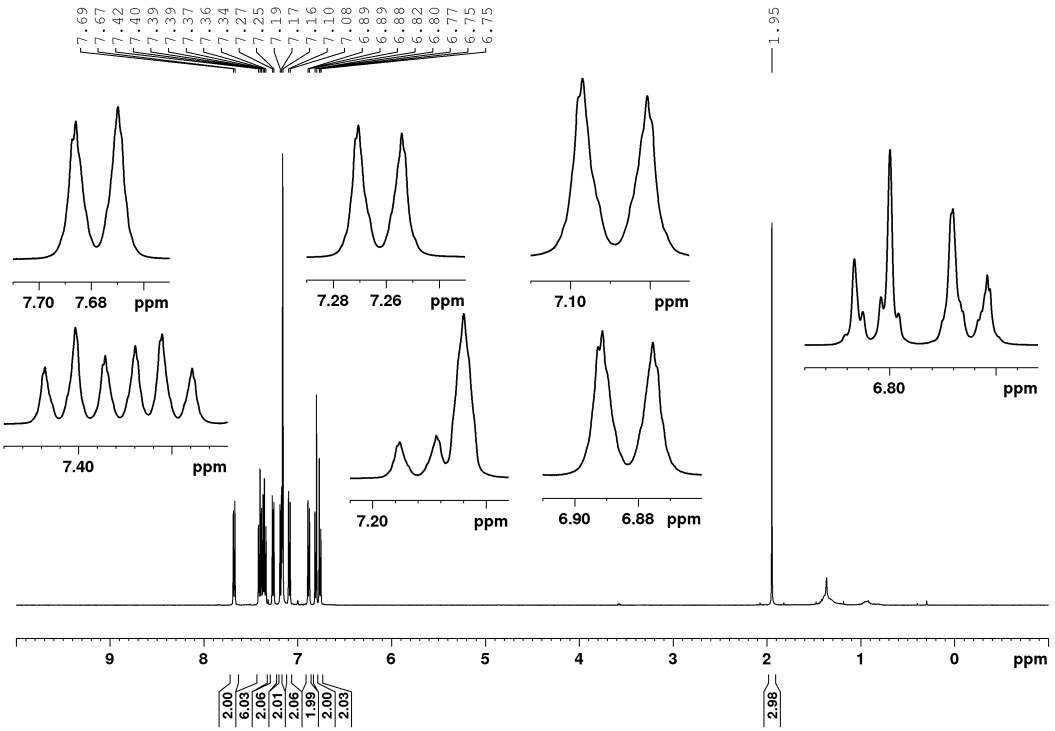

Figure A121: ^{1}H NMR spectrum of **2-5** in C_6D_6 at 500 MHz. Additionally, residual amounts of *n*-hexane (0.89 and 1.24 ppm) and acetone (1.55 ppm).

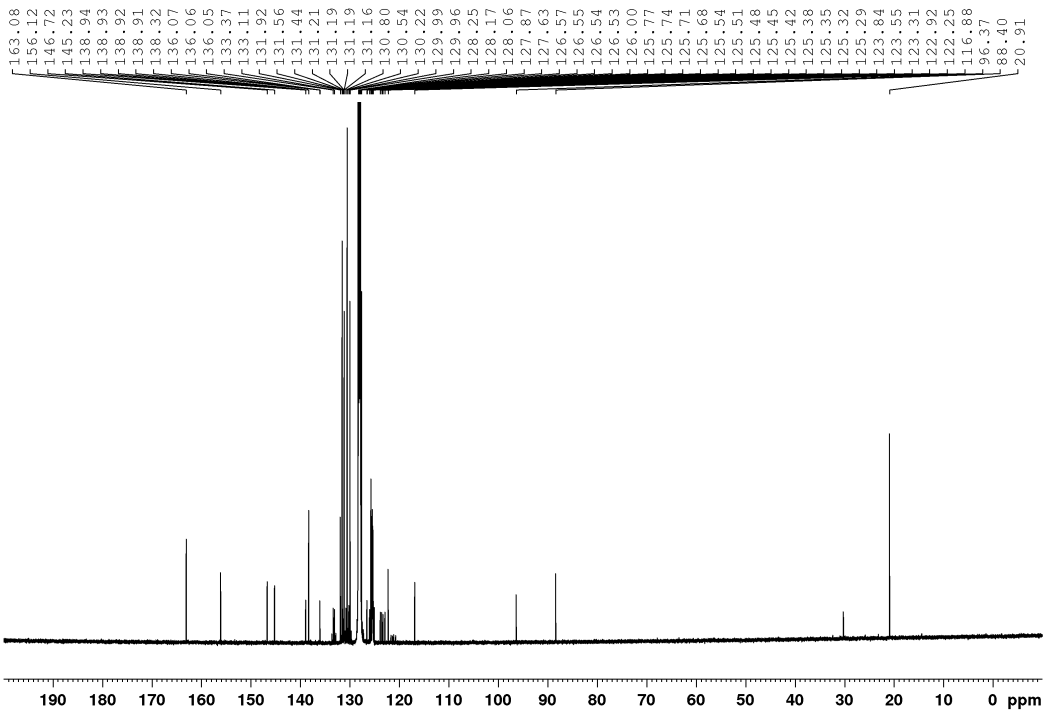

Figure A122: ^{13}C{^{1}H} NMR spectrum of **2-5** in C_6D_6 at 125 MHz. Additionally, residual amounts of acetone (30.1 ppm).

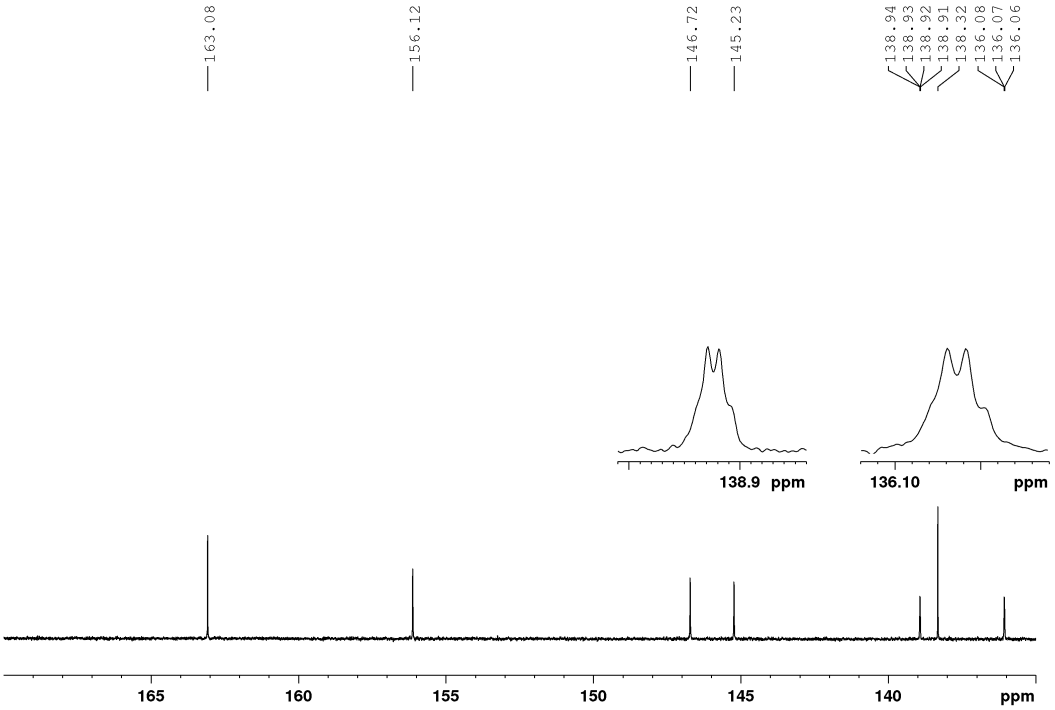

Figure A123: Portion of the $^{13}C\{^{1}H\}$ NMR spectrum (170 – 135 ppm) of **2-5** in C_6D_6 at 125 MHz.

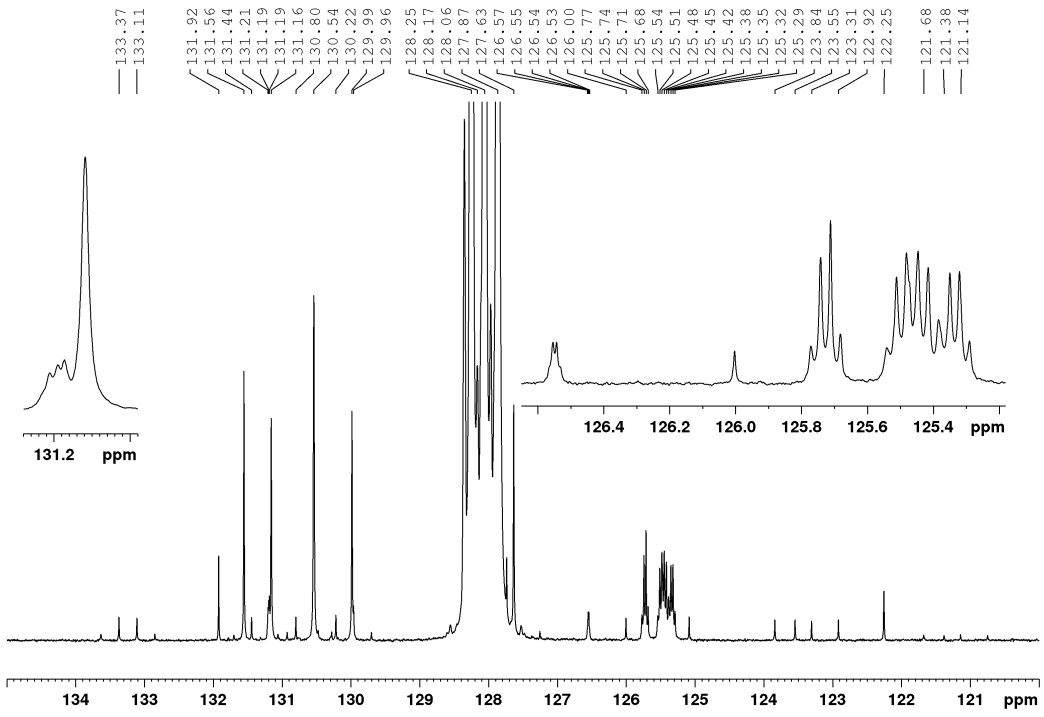

Figure A124: Portion of the $^{13}C\{^{1}H\}$ NMR spectrum (135 – 120 ppm) of **2-5** in C_6D_6 at 125 MHz.

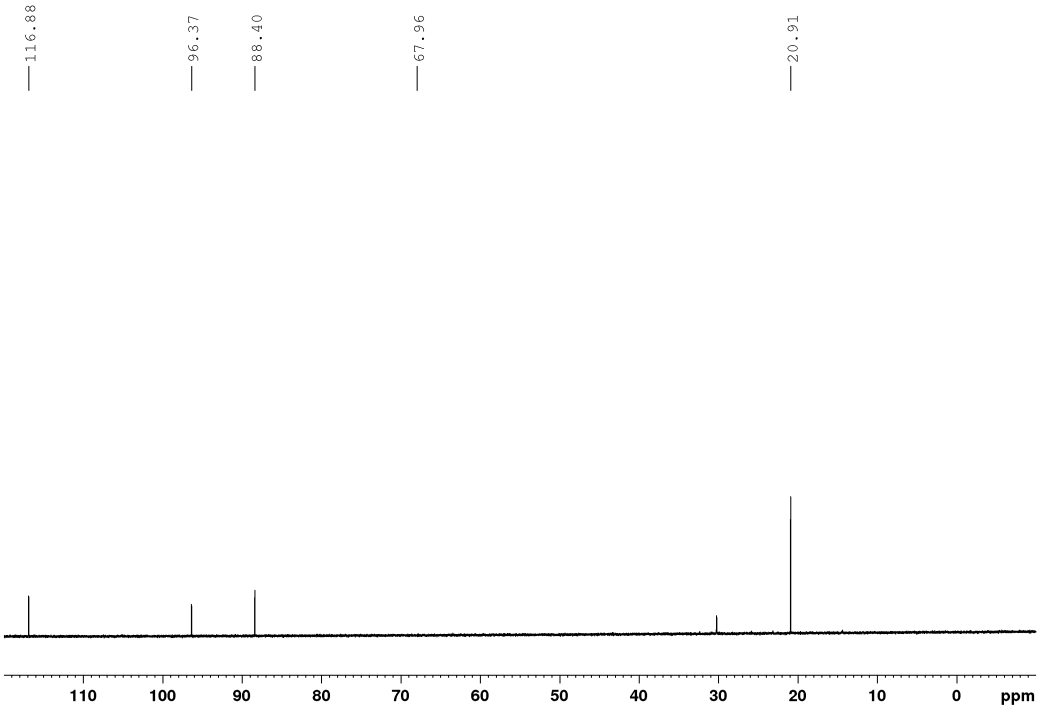

Figure A125: Portion of the $^{13}C\{^{1}H\}$ NMR spectrum (120 – -10 ppm) of **2-5** in C_6D_6 at 125 MHz. Additionally, residual amounts of acetone (30.1 ppm).

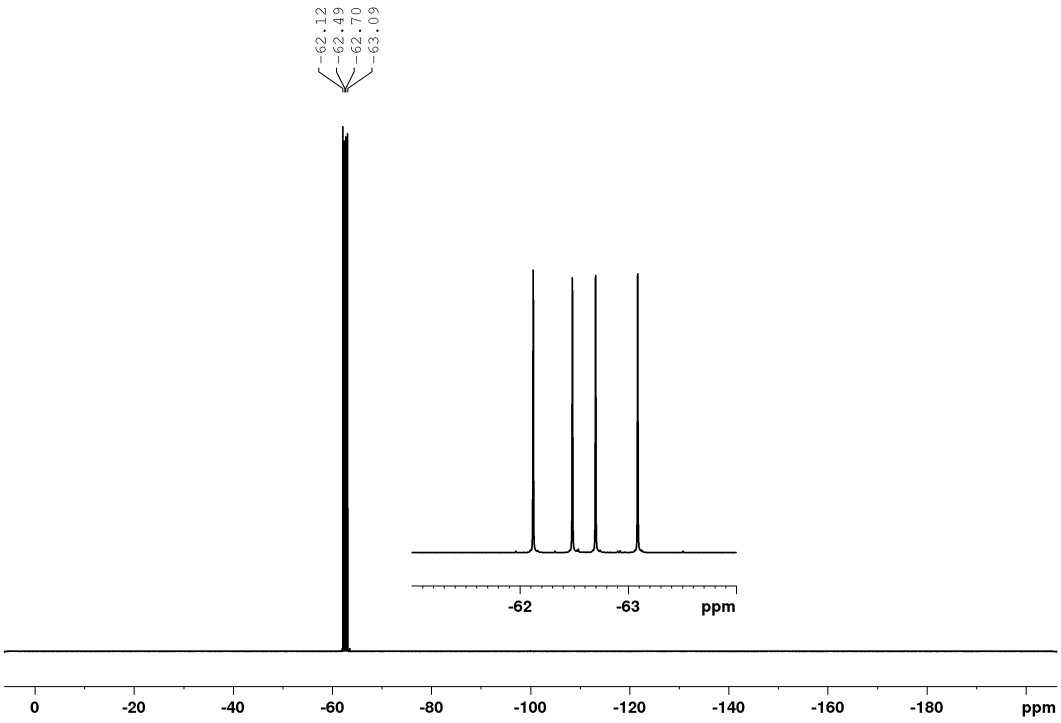

Figure A126: ^{19}F NMR spectrum of **2-5** in C_6D_6 at 470 MHz.

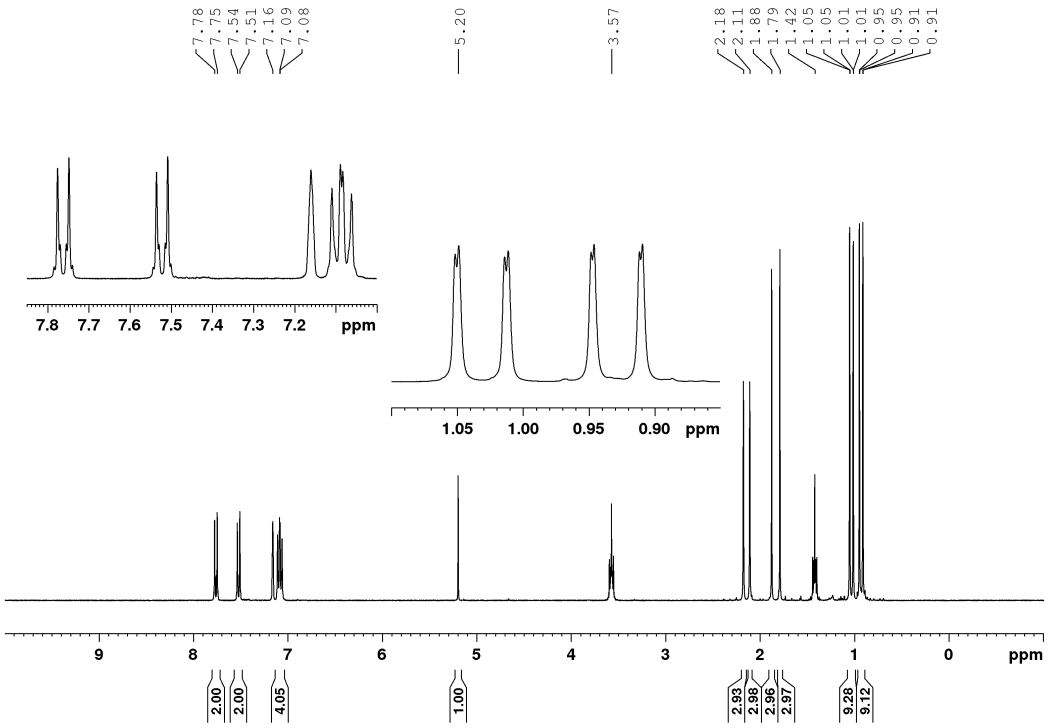

Figure A127: ^{1}H NMR spectrum of **2-10a** in C_6D_6 at 300 MHz. Additionally, residual amounts of THF (1.40 and 3.57 ppm).

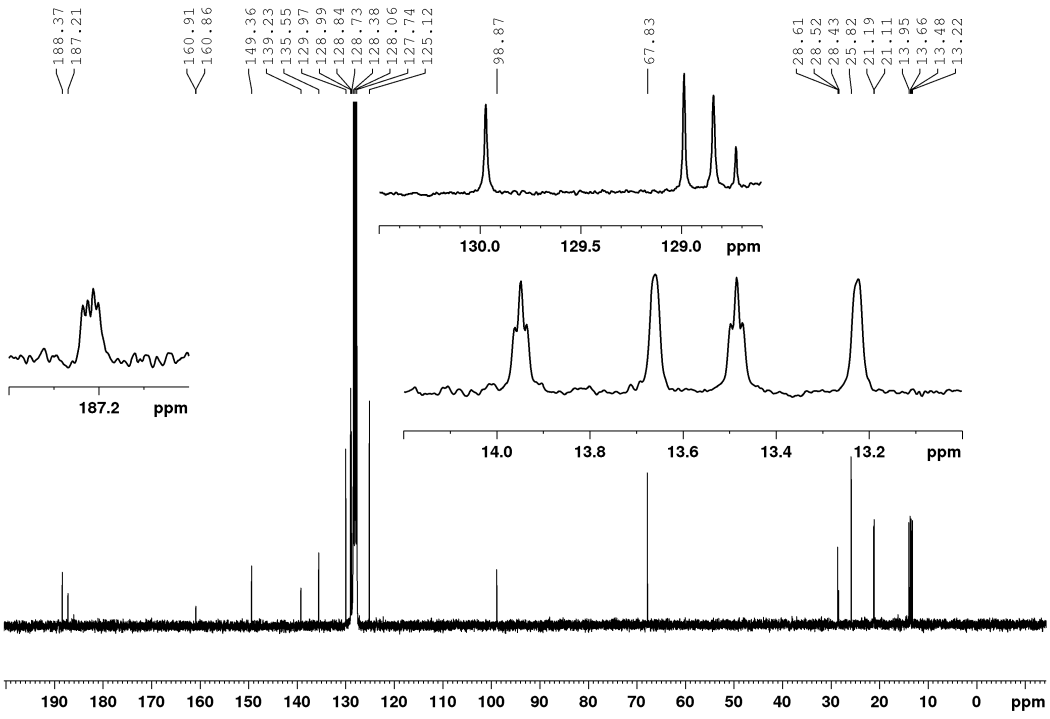

Figure A128: $^{13}C\{^{1}H\}$ NMR spectrum of **2-10a** in C_6D_6 at 75 MHz. Additionally, residual amounts of THF (26.2 and 68.0 ppm).

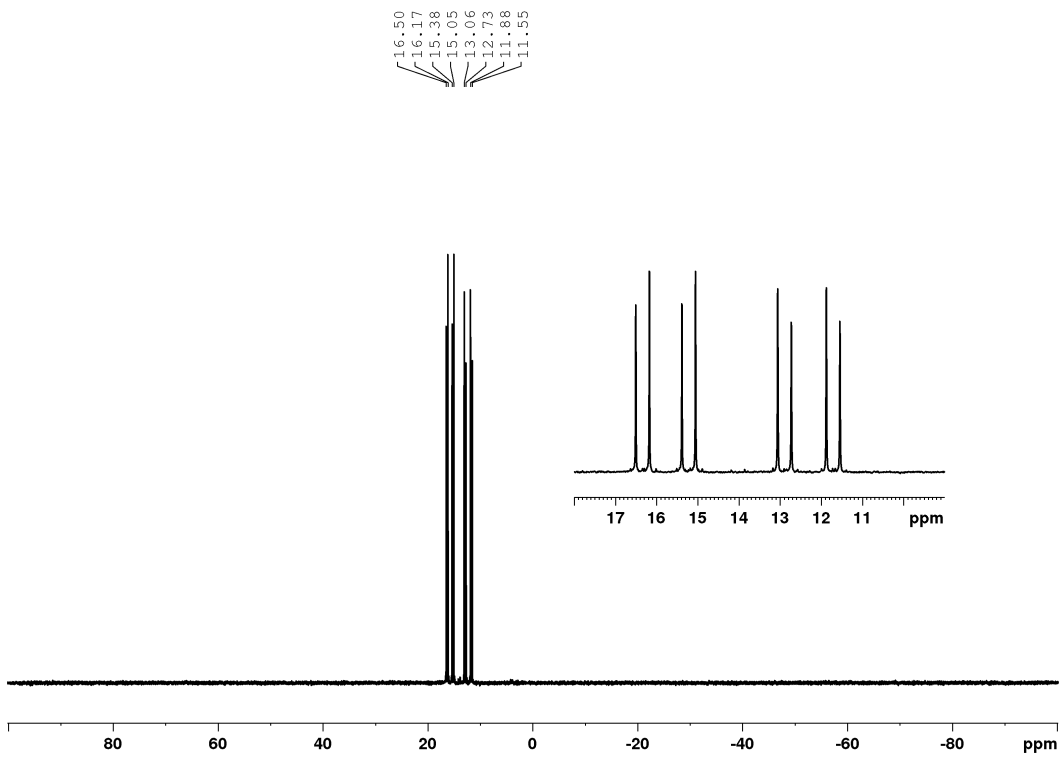

Figure A129: $^{31}P\{^{1}H\}$ NMR spectrum of **2-10a** in C_6D_6 at 121 MHz.

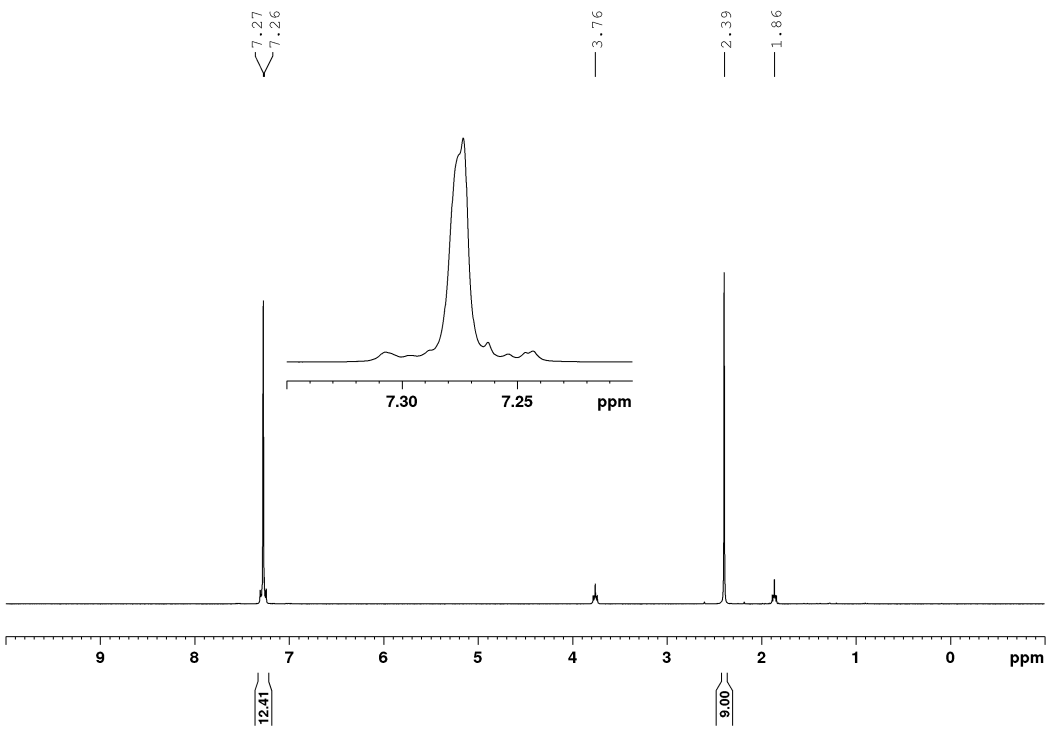

Figure A130: ^{1}H NMR spectrum of **2-8** in $CDCl_3$ at 300 MHz. Additionally, residual amounts of THF (3.76 and 1.85 ppm).

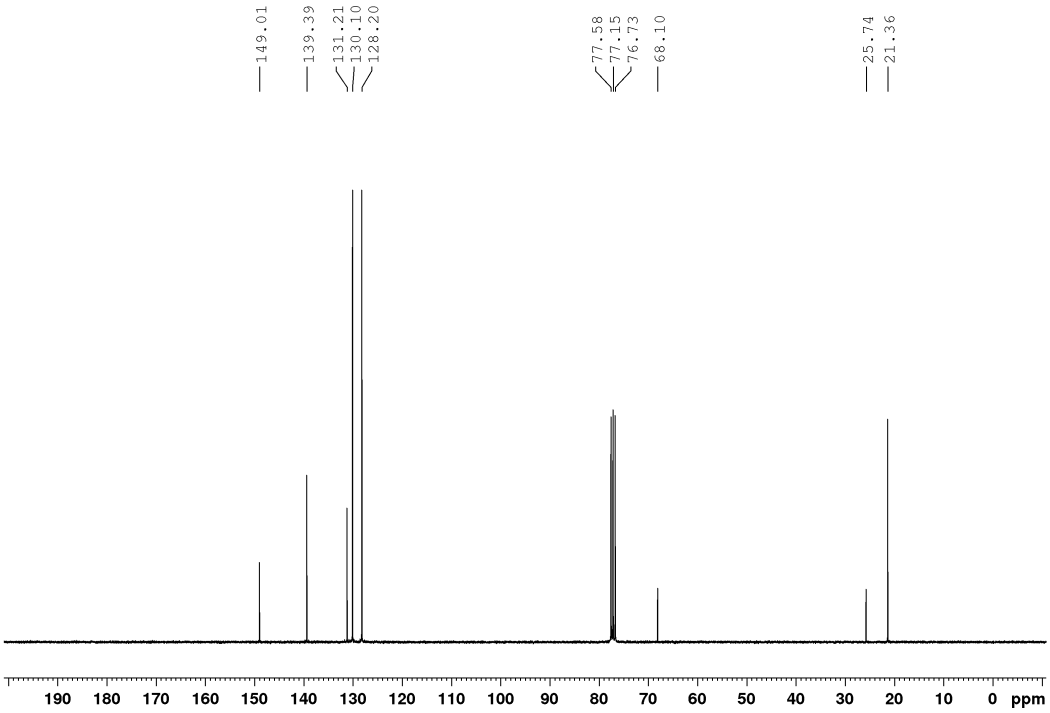

Figure A131: $^{13}C\{^{1}H\}$ NMR spectrum of **2-8** in $CDCl_3$ at 75 MHz. Additionally, residual amounts of THF (68.0 and 25.6 ppm).

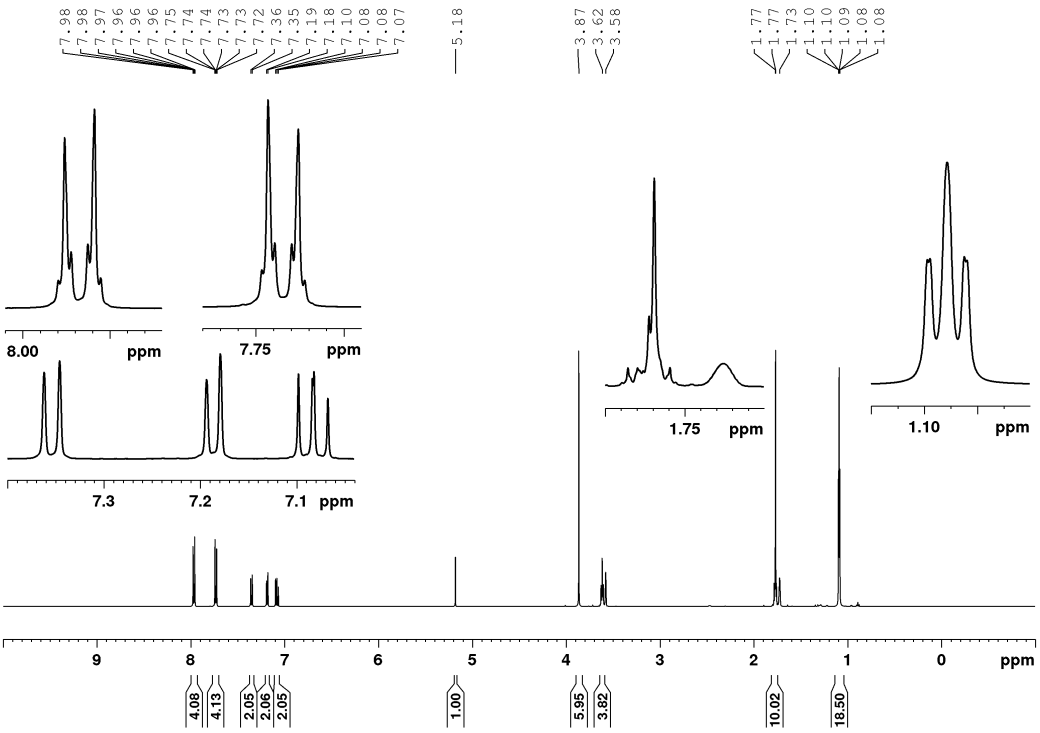

Figure A132: ^{1}H NMR spectrum of **3-6** in THF-d_8 at 500 MHz.

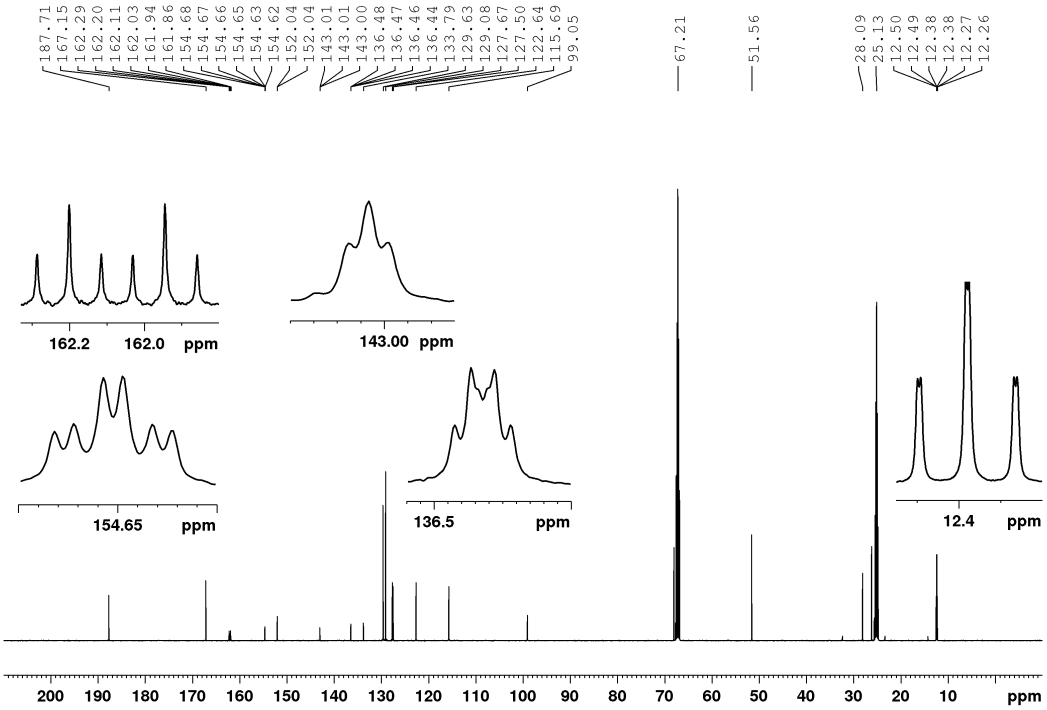

Figure A133: $^{13}C\{^{1}H\}$ NMR spectrum of **3-6** in THF-d_8 at 125 MHz.

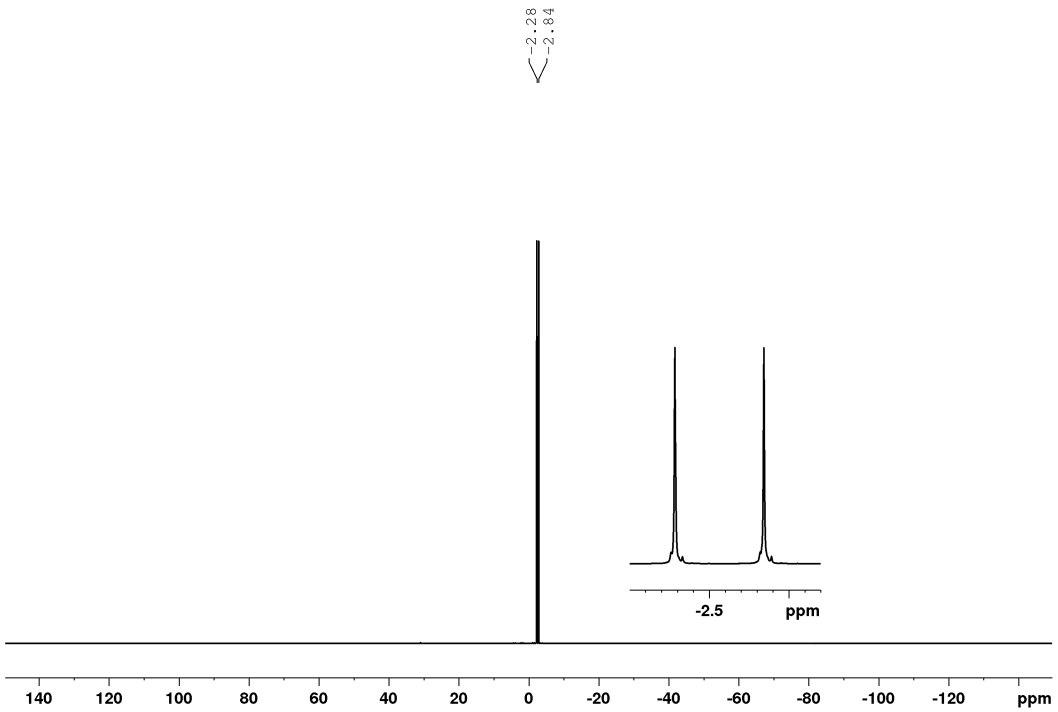

Figure A134: $^{31}P\{^{1}H\}$ NMR spectrum of **3-6** in THF-d_8 at 202 MHz.

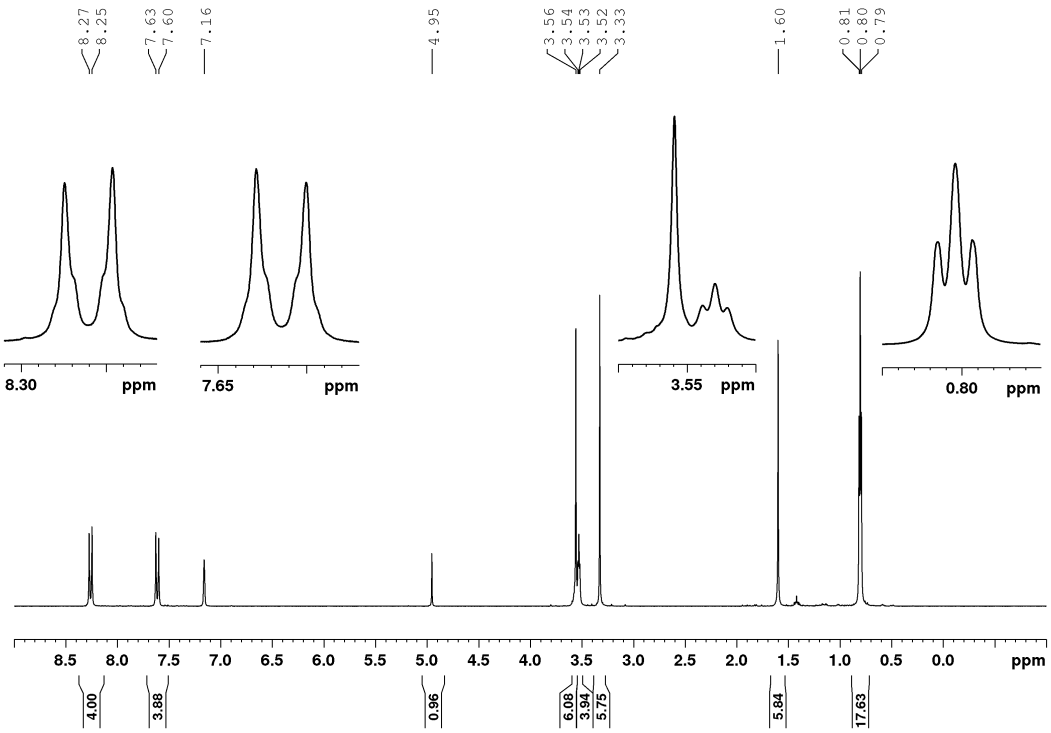

Figure A135: ^{1}H NMR spectrum of **3-7** in C_6D_6 at 300 MHz. Additionally, residual amounts of THF (3.57 and 1.40 ppm).

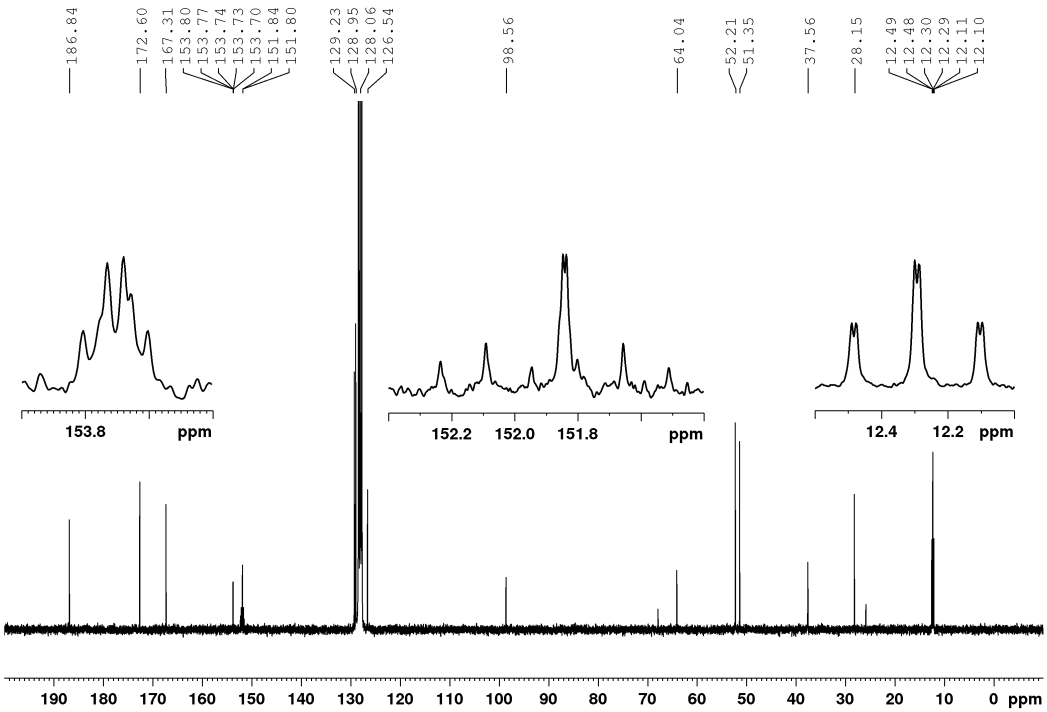

Figure A136: $^{13}C\{^{1}H\}$ NMR spectrum of **3-7** in C_6D_6 at 75 MHz. Additionally, residual amounts of THF (67.8 and 25.7 ppm).

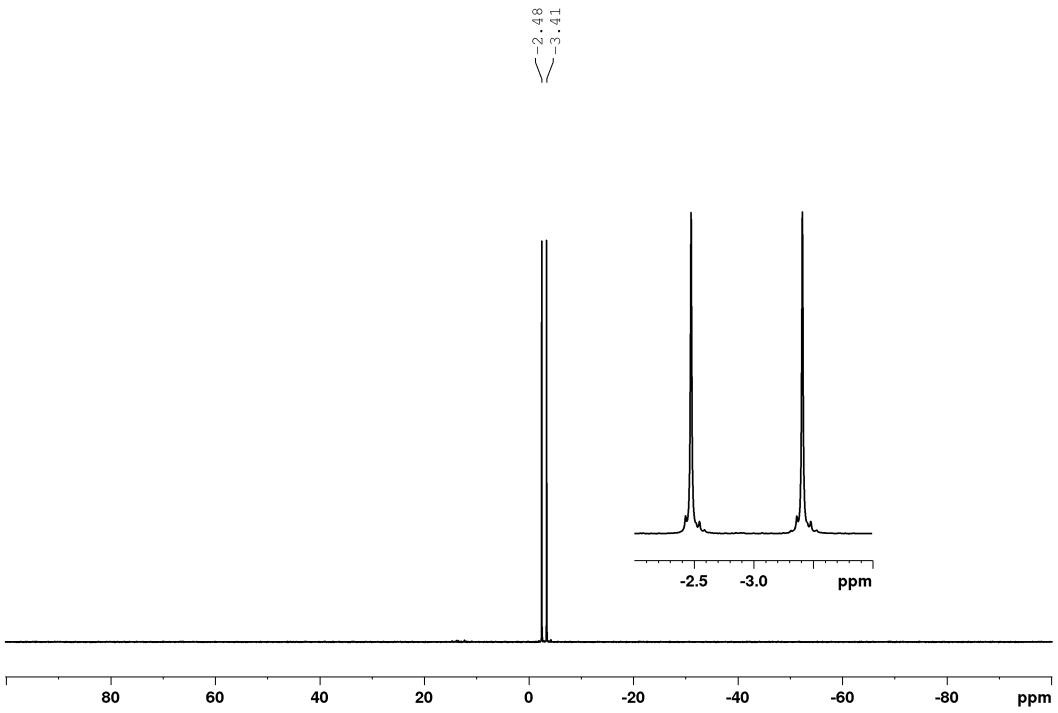

Figure A137: $^{31}P\{^{1}H\}$ NMR spectrum of **3-7** in C_6D_6 at 121 MHz.

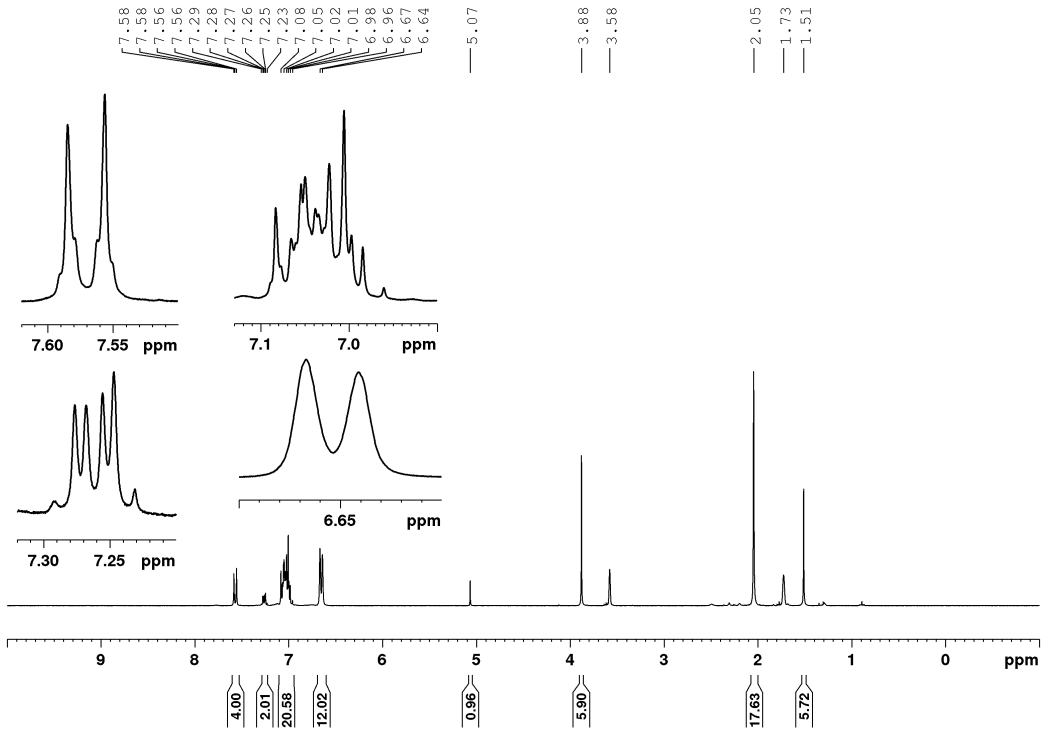

Figure A138: ^{1}H NMR spectrum of **3-15** in THF-d_8 at 300 MHz.

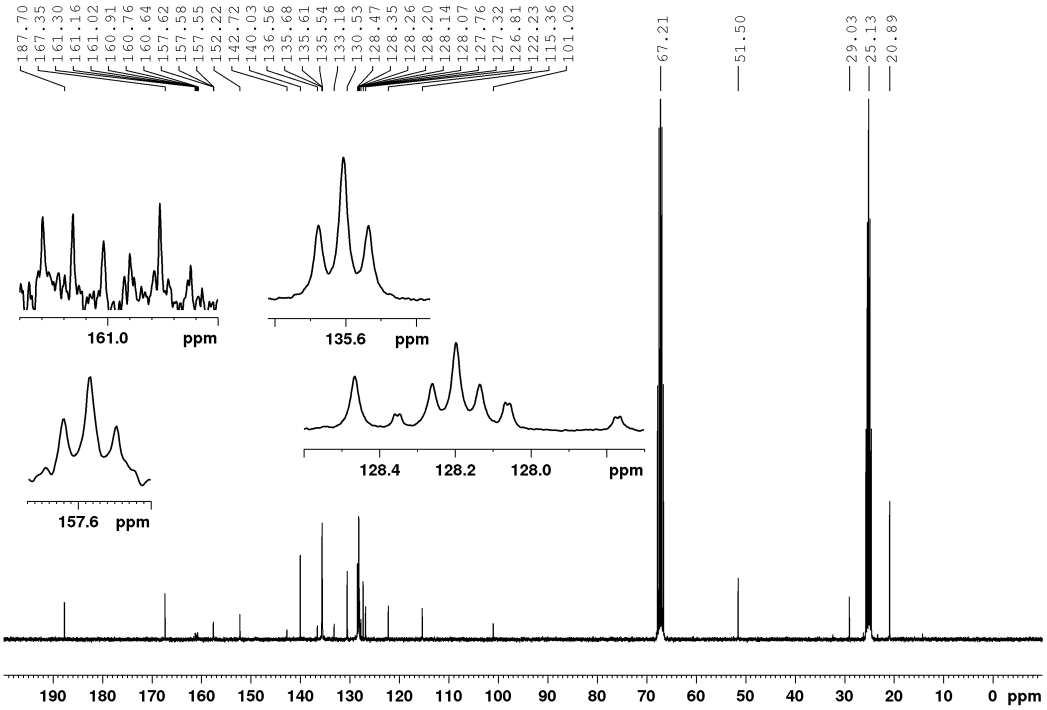

Figure A139: $^{13}C\{^{1}H\}$ NMR spectrum of **3-15** in THF-d_8 at 75 MHz.

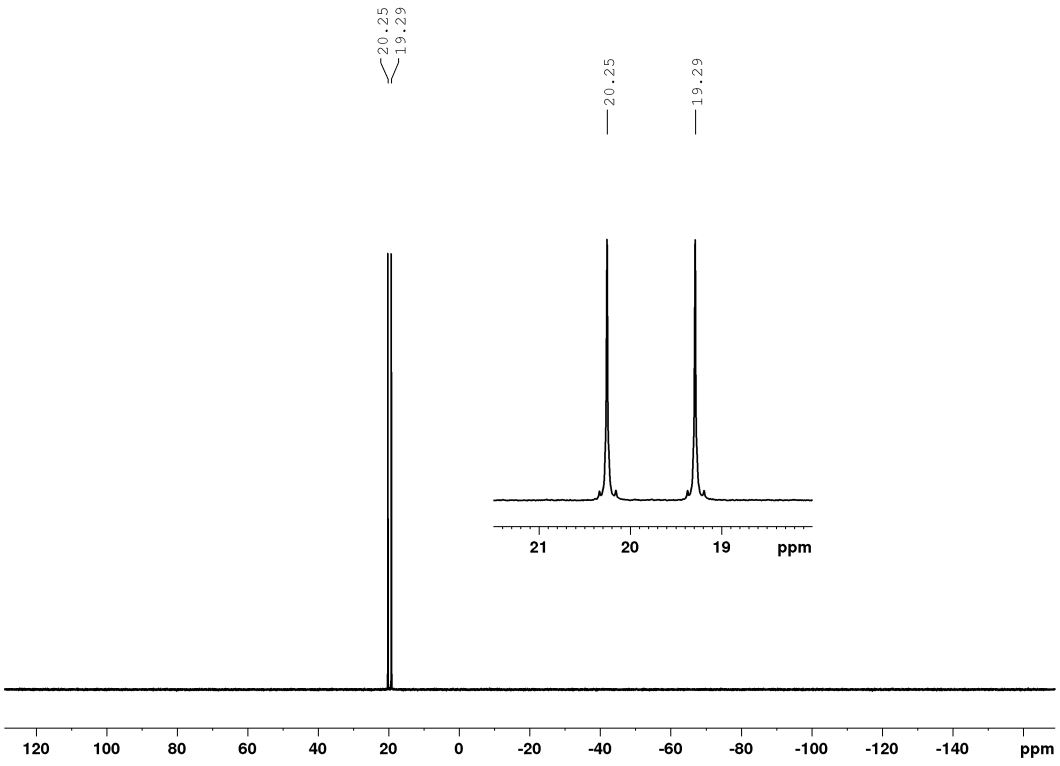

Figure A140: $^{31}P\{^{1}H\}$ NMR spectrum of **3-15** in C_6D_6 at 121 MHz.

9.4 Crystallographic data

Table A1: Single-crystal X-ray data of Chapter 2.

Compound	**2-3a**	**SYM^{CO2Me}**	**2-3c**
Empirical formula	$C_{81}H_{81}F_{18}O_6P_2Rh$	$C_{51}H_{53}O_{10}P_2Rh$	$C_{77}H_{75}F_{12}O_{8.50}P_2Rh$
Color and shape	green needle	orange block	green plate
Formula weight ($g \cdot mol^{-1}$)	1657.30	990.78	1529.22
Temperature (K)	100(2)	100(2)	100(2)
Radiation, λ (Å)	Mo-K$_\alpha$, 0.71073	Mo-K$_\alpha$, 0.71073	Mo-K$_\alpha$, 0.71073
Crystal system	monoclinic	triclinic	monoclinic
Space group	$P2_1/n$	$P\bar{1}$	$C2/c$
a (Å)	15.239(10)	13.132(4)	33.973(13)
b (Å)	9.682(7)	13.189(3)	17.794(7)
c (Å)	51.66(3)	16.564(4)	24.462(12)
α (°)	90	81.974(16)	90
β (°)	95.77(2)	73.51(3)	100.171(8)
γ (°)	90	60.307(14)	90
Volume (Å^3)	7584(8)	2389.7(11)	14555(11)
Z	4	2	8
Calculated density ($Mg \cdot m^{-3}$)	1.451	1.377	1.396
Absorption coefficient (mm^{-1})	0.365	0.482	0.365
F(000)	3408	1028	6304
Theta range for collection	2.140 to 26.354°	1.777 to 27.875°	1.218 to 25.195°
Reflections collected	65796	41342	118293
Independent reflections	15430	11400	13020
Minimum/maximum transmission	0.6819/0.7454	0.6707/0.7457	0.6677/0.7452
Data/parameters/restrains	15430/1020/407	11400/804/360	13020/1096/389
Goodness-of-fit on F^2	1.113	1.040	1.064
Final R indices [I>2σ(I)]	R_1 = 0.0721, wR_2 = 0.1343	R_1 = 0.0510, wR_2 = 0.1089	R_1 = 0.0616, wR_2 = 0.1498
R indices (all data)	R_1 = 0.1086, wR_2 = 0.1484	R_1 = 0.0983, wR_2 = 0.1290	R_1 = 0.0902, wR_2 = 0.1674
Maximum/minimum residual electron density ($e \cdot Å^{-3}$)	1.040 / –1.838	0.541 / –0.858	1.363 / –0.754

Table A2: Single-crystal X-ray data of Chapter 2.

Data	**2-5**	**2-9**	**2-10a**
Empirical formula	$C_{58}H_{39}F_{12}NO$	$C_{88}H_{46}N_2O_2F_{24}$	$C_{15.50}H_{23.50}NO_{2.50}PRh_{0.50}$
Color and shape	purple needle	orange plate	colorless block
Formula weight ($g \cdot mol^{-1}$)	993.90	1619.27	346.28
Temperature (K)	100(2)	100(2)	100(2)
Radiation, λ (Å)	Mo-Kα, 0.71073	Cu-Kα, 1.54184	Mo-Kα, 0.71073
Crystal system	triclinic	monoclinic	triclinic
Space group	$P\ \bar{1}$	$P2_1/n$	$P\ \bar{1}$
a (Å)	9.175(8)	13.14431(13)	10.670(4)
b (Å)	15.920(13)	35.4427(3)	11.530(5)
c (Å)	16.570(13)	17.79556(18)	14.237(5)
α (°)	82.57(3)	90	93.379(17)
β (°)	87.25(4)	107.0145(11)	97.60(3)
γ (°)	78.23(2)	90	104.876(17)
Volume ($Å^3$)	2349(3)	7927.54(14)	1670.2(11)
Z	2	4	4
Calculated density ($Mg \cdot m^{-3}$)	1.405	1.357	1.377
Absorption coefficient (mm^{-1})	0.116	1.052	0.646
F(000)	1020	3280.0	724
Theta range for collection	1.316 to 25.237°	2.493 to 74.503	1.836 to 33.180°
Reflections collected	46407	84557	61035
Independent reflections	8373	16144	12732
Minimum/maximum transmission	0.5906/0.7452	0.746/1.000	0.7140/0.7465
Data/parameters/restrains	8373/679/42	16144/1193/399	12732/399/95
Goodness-of-fit on F^2	1.020	1.052	1.023
Final R indices [I>2σ(I)]	R_1 = 0.0707, wR_2 = 0.1331	R_1 = 0.0662 wR_2 =0.1820	R_1 = 0.0349, wR_2 = 0.0829
R indices (all data)	R_1 = 0.1721, wR_2 = 0.1623	R_1 = 0.0714 wR_2 = 0.1865	R_1 = 0.0504, wR_2 = 0.0906
Maximum/minimum residual electron density ($e \cdot Å^{-3}$)	0.275 / –0.330	0.52/-0.47	0.903 / –0.967

Table A3: Single-crystal X-ray data of Chapter 2.

Compound	**2-21**	**2-I_{cis}b**	
Empirical formula	$C_{15}H_{23}N_4O_2Rh$	$C_{80}H_{78}N_8O_4F_{12}Rh_2$	
Color and shape	red block	orange block	
Formula weight ($g \cdot mol^{-1}$)	394.28	1649.32	
Temperature (K)	100(2)	104(6)	
Radiation, λ (Å)	Mo-K_α, 0.71073	Cu-K_α, 1.54184	
Crystal system	triclinic	monoclinic	
Space group	$P\ \bar{1}$	$P2_1/n$	
a (Å)	13.933(3)	20.19606(19)	
b (Å)	14.656(6)	15.70507(10)	
c (Å)	17.026(9)	25.3727(2	
α (°)	75.66(3)	90	
β (°)	88.54(2)	103.0994(9)	
γ (°)	88.329(18)	90	
Volume ($Å^3$)	3366(2)	7838.32(11)	
Z	8	4	
Calculated density ($Mg \cdot m^{-3}$)	1.556	1.398	
Absorption coefficient (mm^{-1})	1.027	4.067	
F(000)	1616	3376	
Theta range for collection	1.462 to 30.032°	2.534 to 76.969	
Reflections collected	44407	84342	
Independent reflections	19662	16305	
Minimum/maximum transmission	0.6750/0.7461	0.393/1.000	
Data/parameters/restrains	19662/883/100	16305/985/342	
Goodness-of-fit on F^2	1.027	1.051	
Final R indices [I>2σ(I)]	R_1 = 0.0274, wR_2 = 0.0605	R_1 = 0.0486, wR_2 =0.1345	
R indices (all data)	R_1 = 0.0360, wR_2 = 0.0642	R1 = 0.0559, wR_2 = 0.1396	
Maximum/minimum residual electron density ($e \cdot Å^{-3}$)	0.601 / –0.645	1.96/-0.98	

2-I_{cis}b: Despite exhaustive attempts to model a toluene disorder, no acceptable (chemically reasonable) structure could be obtained, therefore the program “squeeze” was used.

Table A4: Single-crystal X-ray data of Chapter 3.

Compound	**3-1**	**3-6**	**3-7**
Empirical formula	$C_{30}H_{20}O_4$	$C_{48}H_{53}O_6P_2Rh$	$C_{38}H_{49}O_{10}P_2Rh$
Color and shape	colorless block	orange block	orange block
Formula weight ($g \cdot mol^{-1}$)	444.46	890.75	830.62
Temperature (K)	100(2)	100(2)	100(2)
Radiation, λ (Å)	Mo-Kα, 0.71073	Mo-Kα, 0.71073	Mo-Kα, 0.71073
Crystal system	monoclinic	triclinic	monoclinic
Space group	*C*2/*c*	$P\ \bar{1}$	$P2_1/c$
a (Å)	16.357(6)	9.2094(16)	19.356(7)
b (Å)	15.519(7)	12.694(5)	11.745(3)
c (Å)	10.019(4)	20.053(3)	18.360(6)
α (°)	90	76.635(17)	90
β (°)	121.143(8)	77.943(10)	110.649(19)
γ (°)	90	75.33(2)	90
Volume ($Å^3$)	2176.7(15)	2178.0(10)	3906(2)
Z	4	2	4
Calculated density ($Mg \cdot m^{-3}$)	1.356	1.358	1.413
Absorbtion coefficient (mm^{-1})	0.090	0.513	0.574
F(000)	928	928	1728
Theta range for collection	1.959 to 27.481°	1.816 to 27.875°	1.124 to 28.700°
Reflections collected	19736	45628	51817
Independent reflections	2503	10371	10091
Minimum/maximum transmission	0.7198/0.7461	0.6948/0.7461	0.6626/0.7460
Data/parameters/restrains	2503/156/0	10371/525/0	10091 / 492 / 27
Goodness-of-fit on F^2	1.045	1.020	1.036
Final R indices [I>2σ(I)]	R_1 = 0.0365, wR_2 = 0.0892	R_1 = 0.0331, wR_2 = 0.0739	R_1 = 0.0343, wR_2 = 0.0880
R indices (all data)	R_1 = 0.0499, wR_2 = 0.0965	R_1 = 0.0491, wR_2 = 0.0800	R_1 = 0.0437, wR_2 = 0.0936
Maximum/minimum residual electron density ($e \cdot Å^{-3}$)	0.299 / –0.233	0.474 / –0.568	1.007 / –0.589

Table A5: Single-crystal X-ray data of Chapter 3.

Compound	**3-15**
Empirical formula	$C_{92.50}H_{101}O_6P_2Rh$
Color and shape	orange plate
Formula weight ($g \cdot mol^{-1}$)	1473.58
Temperature (K)	100(2)
Radiation, λ (Å)	Mo-Kα, 0.71073
Crystal system	monoclinic
Space group	$P2_1/c$
a (Å)	15.015(9)
b (Å)	23.803(14)
c (Å)	21.968(13)
α (°)	90
β (°)	98.655(17)
γ (°)	90
Volume ($Å^3$)	7762(8)
Z	4
Calculated density ($Mg \cdot m^{-3}$)	1.261
Absorbtion coefficient (mm^{-1})	0.316
F(000)	3116
Theta range for collection	1.372 to 26.371°
Reflections collected	95209
Independent reflections	15866
Minimum/maximum transmission	0.6844/0.7455
Data/parameters/restrains	15866/1009/309
Goodness-of-fit on F^2	1.056
Final R indices [I>2σ(I)]	R_1 = 0.0564, wR_2 = 0.1307
R indices (all data)	R_1 = 0.1031, wR_2 = 0.1533
Maximum/minimum residual electron density ($e \cdot Å^{-3}$)	0.799 / –0.869

Table A6: Single-crystal X-ray data of Chapter 4.

Compound	**4-1**	**4-2**	**4-3**
Empirical formula	$C_{11}H_{23}O_2P_2Rh$	$C_{31}H_{55}O_2P_2Rh$	$C_{528}H_{560}O_{40}P_{32}Rh_{16}$
Color and shape	yellow, block	yellow, block	yellow, block
Formula weight ($g \cdot mol^{-1}$)	352.15	624.60	1272.92
Temperature (K)	100(2)	100(2)	100(2)
Radiation, λ (Å)	Mo-Kα, 0.71073	Mo-Kα, 0.71073	Cu-Kα, 1.54184
Crystal system	orthorhombic	monoclinic	tetragonal
Space group	$P2_12_12_1$	$P2_1/n$	$I4_1/a$
a (Å)	9.7783(3)	11.573(7)	26.56669(11)
b (Å)	10.3626(3)	17.291(3)	26.56669(11)
c (Å)	15.2869(5) Å	16.292(5)	16.35191(11)
α (°)	90	90	90
β (°)	90	101.747(10)	90
γ (°)	90	90	90
Volume ($Å^3$)	1549.00(8)	3192(2)	11541.00(10)
Z	4	4	8
Calculated density ($Mg \cdot m^{-3}$)	1.5099	1.300	1.465
Absorbtion coefficient (mm^{-1})	1.295	0.660	2.998
F(000)	720	1328	5248
Theta range for collection	2.374 to 38.999	1.981 to 31.505°	3.197 to 76.391
Reflections collected	26905	56890	24819
Independent reflections	8627	10612	5960
Minimum/maximum transmission	0.6691/0.7481	0.6646/0.7465	0.609/1.000
Data/parameters/restrains	8627/151/0	10612/382/337	5960/350/0
Goodness-of-fit on F^2	1.003	1.026	1.061
Final R indices [I>2σ(I)]	R_1 = 0.0305, wR_2 = 0.0514	R_1 = 0.0291, wR_2 = 0.0654	R_1 = 0.0292, wR_2 = 0.0792
R indices (all data)	R_1 = 0.0414, wR_2 = 0.0547	R_1 = 0.0389, wR_2 = 0.0701	R_1 = 0.0305, wR_2 = 0.0801
Maximum/minimum residual electron density ($e \cdot Å^{-3}$)	0.978/-0.567	0.571 / –0.829	0.91/-0.89

Table A7: Single-crystal X-ray data of Chapter 4.

Compound	**4-4**	**4-5**	**4-7**
Empirical formula	$C_{44}H_{76}O_{6.50}Rh_2$	$C_{102}H_{116}O_8P_4Rh_2$	$C_{11}H_{26}NP_2RhS_2$
Color and shape	yellow, block	orange, needle	yellow, block
Formula weight ($g \cdot mol^{-1}$)	914.86	1799.64	401.30
Temperature (K)	100(2)	100(2)	100(2)
Radiation, λ (Å)	Mo-Kα, 0.71073	Mo-Kα, 0.71073	Mo-Kα, 0.71073
Crystal system	triclinic	triclinic	orthorhombic
Space group	$P\ \bar{1}$	$P\ \bar{1}$	*Pbca*
a (Å)	11.843(4)	11.647(7)	11.052(3)
b (Å)	13.491(5)	13.859(6)	10.556(3)
c (Å)	15.253(6)	15.751(9)	29.657(10)
α (°)	113.484(19)	89.67(2)	90
β (°)	94.73(2)	68.75(3)	90
γ (°)	103.66(2)	71.561(8)	90
Volume ($Å^3$)	2128.9(15)	2231(2)	3459.9(18)
Z	2	1	8
Calculated density ($Mg \cdot m^{-3}$)	1.427	1.340	1.541
Absorbtion coefficient (mm^{-1})	0.822	0.499	1.396
F(000)	964	942	1648
Theta range for collection	1.485 to 26.022°	1.951 to 26.022°	2.298 to 30.508°
Reflections collected	12436	49436	65890
Independent reflections	12436	8790	5265
Minimum/maximum transmission	0.598602/0.745431	0.6657/0.7454	0.5276/0.6774
Data/parameters/restrains	12436/616/481	8790/673/560	5265/160/0
Goodness-of-fit on F^2	1.083	1.063	1.219
Final R indices [I>2σ(I)]	R_1 = 0.0572, wR_2 = 0.1288	R_1 = 0.0370, wR_2 = 0.0919	R_1 = 0.0233, wR_2 = 0.0453
R indices (all data)	R_1 = 0.0777, wR_2 = 0.1473	R_1 = 0.0456, wR_2 = 0.0963	R_1 = 0.0257, wR_2 = 0.0461
Maximum/minimum residual electron density ($e \cdot Å^{-3}$)	2.213 / –1.059	0.875 / –0.612	0.541 / –0.987

4-4: The crystal was a non-merohedral twin with domains rotated by 179.9 ° around real axis [1.000 0.532 0.722]. The BASF parameter was refined to 25%.The structure was refined using TWIN keyword.

Table A8: Single-crystal X-ray data of Chapter 4.

Compound	**4-9**	**4-10**	**4-16**
Empirical formula	$C_{31}H_{34}NP_2RhS_2$	$C_{47}H_{52}NS_2P_2Rh$	$C_{22}H_{58}O_{4.50}P_6Rh_2$
Color and shape	yellow, block	yellow, plate	orange, block
Formula weight ($g \cdot mol^{-1}$)	649.56	859.91	786.32
Temperature (K)	100(2)	100(2)	100(2)
Radiation, λ (Å)	Mo-Kα, 0.71073	Mo-Kα, 0.71073	Mo-Kα, 0.71073
Crystal system	monoclinic	monoclinic	monoclinic
Space group	$P2_1/c$	$C2/c$	$P2_1/c$
a (Å)	11.645(7)	35.822(9)	18.940(5)
b (Å)	14.808(15)	11.966(3)	20.425(10)
c (Å)	17.624(13)	25.109(7)	19.255(9)
α (°)	90	90	90
β (°)	103.72(3)	122.058(13)	108.425(11)
γ (°)	90	90	90
Volume ($Å^3$)	2952(4)	9122(4)	7067(5)
Z	4	8	8
Calculated density ($Mg \cdot m^{-3}$)	1.461	1.305	1.478
Absorbtion coefficient (mm^{-1})	0.850	0.570	1.231
F(000)	1336	3752	3248
Theta range for collection	1.800 to 36.359°	1.829 to 28.282°	1.496 to 27.877°
Reflections collected	59242	119490	78387
Independent reflections	14354	11316	16855
Minimum/maximum transmission	0.6681/0.7471	0.6295/0.7460	0.6648/0.7457
Data/parameters/restrains	14354/336/0	11316/553/78	16855/833/410
Goodness-of-fit on F^2	1.025	1.031	1.044
Final R indices [I>2σ(I)]	R_1 = 0.0288, wR_2 = 0.0669	R_1 = 0.0406, wR_2 = 0.0868	R_1 = 0.0326, wR_2 = 0.0714
R indices (all data)	R_1 = 0.0393, wR_2 = 0.0719	R_1 = 0.0750, wR_2 = 0.1017	R_1 = 0.0518, wR_2 = 0.0803
Maximum/minimum residual electron density ($e \cdot Å^{-3}$)	1.002 / –0.380	0.705 / –0.608	0.998 / –0.843

Table A9: Single-crystal X-ray data of Chapter 4.

Compound	**4-12a**	**4-13a**	**4-13b**
Empirical formula	$C_{42}H_{40}$	$C_{42}H_{40}S_4$	$C_{63}H_{60}S_6$
Color and shape	colorless block	colorless block	colorless block
Formula weight ($g \cdot mol^{-1}$)	544.74	672.98	1009.47
Temperature (K)	100(2)	100(2)	100(2)
Radiation, λ (Å)	Mo-Kα, 0.71073	Mo-Kα, 0.71073	Mo-Kα, 0.71073
Crystal system	triclinic	triclinic	triclinic
Space group	$P\ \bar{1}$	$P\ \bar{1}$	$P\ \bar{1}$
a (Å)	9.9755(13)	10.052(3)	12.541(3)
b (Å)	10.5241(15)	10.853(4)	14.182(3)
c (Å)	15.978(2)	17.462(5)	15.096(4)
α (°)	91.459(20)	75.888(16)	87.231(11)
β (°)	102.941(14)	87.380(14)	84.187(17)
γ (°)	96.54(2)	70.131(8)	76.208(11)
Volume ($Å^3$)	1621.9(4)	1736.1(9)	2593.5(11)
Z	2	2	2
Calculated density ($Mg \cdot m^{-3}$)	1.115	1.287	1.293
Absorbtion coefficient (mm^{-1})	0.063	0.304	0.305
F(000)	584	712	1068
Theta range for collection	1.309 to 29.574°	1.203 to 30.508°	1.679 to 26.879°
Reflections collected	44115	129627	56700
Independent reflections	9105	10610	11076
Minimum/maximum transmission	0.7142/0.7462	0.6807/0.7461	0.7041/0.7454
Data/parameters/restrains	9105 / 476 / 500	10610/419/0	11076 / 648 / 72
Goodness-of-fit on F^2	1.050	1.037	1.015
Final R indices [I>2σ(I)]	R_1 = 0.0802, wR_2 = 0.2359	R_1 = 0.0411, wR_2 = 0.1067	R_1 = 0.0507, wR_2 = 0.1091
R indices (all data)	R_1 = 0.1075, wR_2 = 0.2640	R_1 = 0.0489, wR_2 = 0.1124	R_1 = 0.0879, wR_2 = 0.1245
Maximum/minimum residual electron density ($e \cdot Å^{-3}$)	1.986 / –0.477	0.638 / –0.293	0.616 / –0.466

The structure of **4-12a** contained a large residual electron density of 1.986 $e \cdot Å^{-3}$, presumably a solvent molecule. Despite exhaustive attempts to model this disorder, no acceptable (chemically reasonable) structure could be obtained.

Table A10: Single-crystal X-ray data of Chapter 4.

Compound	**4-14a**
Empirical formula	$C_{56.50}H_{54}O_{16}$
Color and shape	colorless block
Formula weight ($g \cdot mol^{-1}$)	988.99
Temperature (K)	100(2)
Radiation, λ (Å)	Mo-K_α, 0.71073
Crystal system	Monoclinic
Space group	*C*2/*c*
a (Å)	25.422(18)
b (Å)	15.654(13)
c (Å)	28.559(19)
α (°)	90
β (°)	113.99(3)
γ (°)	90
Volume ($Å^3$)	10384(14)
Z	8
Calculated density ($Mg \cdot m^{-3}$)	1.265
Absorbtion coefficient (mm^{-1})	0.093
F(000)	4168
Theta range for collection	1.946 to 27.877°
Reflections collected	53007
Independent reflections	12367
Minimum/maximum transmission	0.6617/0.7457
Data/parameters/restrains	12367 / 686 / 84
Goodness-of-fit on F^2	1.057
Final R indices [I>2σ(I)]	R_1 = 0.0475, wR^2 = 0.1281
R indices (all data)	R_1 = 0.0739, wR_2 = 0.1432
Maximum/minimum residual electron density ($e \cdot Å^{-3}$)	0.708 / –0.282

9.5 Theoretical calculations: Cartesian coordinates

2-5

DFT B3LYP/6-31G+(d), gas phase, S_0

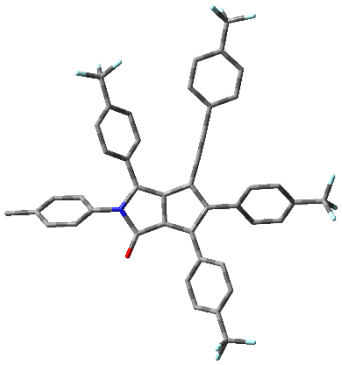

Point group: C_1

Total energy: –1,894,418.90 kcal mol^{-1}

Dipole moment: 7.02 D

Imaginary frequencies: 0

C	1.77776900	1.67512300	0.23164600
C	2.59821000	0.54710900	0.13670800
C	1.71543600	-0.61583700	0.12688200
C	0.37553100	-0.17668700	0.15409600
C	0.41236800	1.26532100	0.23662000
C	-0.40033100	2.38417300	0.11113400
N	0.39852800	3.51083100	0.01378500
C	1.81625900	3.12593500	0.10685300
O	2.71385000	3.94411500	0.09517400
C	4.05524300	0.54550600	-0.01292200
C	2.12460000	-2.02780300	0.17528900
C	-0.77898000	-0.97650200	0.11960900
C	-1.86094400	2.42318900	0.02121700
C	-2.61831700	1.59791900	0.86897900
C	-4.00553200	1.58181300	0.77849000
C	-4.64748900	2.37819900	-0.17528000
C	-3.90459100	3.20744500	-1.02109500
C	-2.51724800	3.24115500	-0.91293500
C	1.53000800	-2.98087600	-0.66915500
C	1.89955000	-4.32228900	-0.60453600
C	2.87123900	-4.73391600	0.31185400
C	3.47428500	-3.79828600	1.15929900
C	3.10161400	-2.45982300	1.09044700
C	4.82558900	1.55934600	0.58520300
C	6.21014300	1.58192700	0.44142100
C	6.84773300	0.59362700	-0.31247500
C	6.09499200	-0.40987700	-0.93324900
C	4.71382000	-0.43426000	-0.78256800
C	8.33697400	0.62633200	-0.51480800
C	3.30990900	-6.17036000	0.34608800
C	-6.14285400	2.28108400	-0.31140300
F	-6.50488400	1.12048300	-0.93075200
F	-6.76428200	2.28108300	0.89288800
F	-6.66847300	3.29233800	-1.03779800
F	2.31617700	-7.02095300	-0.01501200
F	4.34573300	-6.40454700	-0.50762000
F	3.73356900	-6.55092600	1.57686400
F	8.97211000	1.37477600	0.41859400
F	8.88393700	-0.61577800	-0.47133200
F	8.67008400	1.14859100	-1.72746900
C	-1.80392900	-1.63329400	0.06277100
C	-3.01581500	-2.36952700	-0.00765000
C	-4.19466300	-1.75047100	-0.47407900
C	-5.38702900	-2.46202600	-0.53479400
C	-5.41934800	-3.80387900	-0.13878400
C	-4.25618400	-4.43214500	0.31974800
C	-3.06163300	-3.72288700	0.38466000
C	-6.72182600	-4.55496200	-0.15512900
F	-7.54218300	-4.13761100	-1.15026300
F	-6.54453700	-5.88936300	-0.31405600
F	-7.41104000	-4.39146600	1.00829500
H	-2.11601400	0.97858700	1.60283500
H	-4.58584600	0.94774700	1.44065800
H	-4.40710500	3.82575000	-1.75647400
H	-1.94075800	3.88995600	-1.56311300
H	0.78230500	-2.66453600	-1.38843400
H	1.43417700	-5.04578300	-1.26597700
H	4.22433000	-4.11706100	1.87556900
H	3.56452500	-1.73925600	1.75689700
H	4.33479500	2.33574500	1.16026400

H	6.79056500	2.36585800	0.91536200
H	6.58857900	-1.16972600	-1.53064400
H	4.13998700	-1.20949400	-1.27618700
H	-4.16275200	-0.71453300	-0.79156600
H	-6.28768100	-1.97618000	-0.89532300
H	-4.28463900	-5.47379300	0.62134200
H	-2.15646600	-4.20444300	0.74026400
C	-0.02863900	4.85987100	0.17551200
C	-0.87095800	5.21871800	1.23184900
C	-1.29757100	6.53924100	1.35880700
C	-0.87508200	7.52843300	0.45949700
C	-0.01467400	7.15061400	-0.58101900
C	0.40526000	5.82973300	-0.73092100
H	-1.19565000	4.46696100	1.94463700
H	-1.96190500	6.80662100	2.17691700
H	0.32888700	7.89989000	-1.28996500
H	1.06806300	5.54731400	-1.54160900
C	-1.30540900	8.96520400	0.62783000
H	-2.28809100	9.03578000	1.10591500
H	-0.59355300	9.51550100	1.25734500
H	-1.35706000	9.48283800	-0.33587700

9.6 Theoretical calculations: Lowest energy singlet electronic transitions

Table A11: Lowest energy singlet electronic transitions of **2-5** (TD-DFT B3LYP/6-31+G(d), gas phase)

State	E [eV]	λ [nm]	*f*	Symmetry	Major contributions	Λ
1	1.88	658.02	0.0703	A	H-1->LUMO (14%), HOMO->LUMO (84%)	0.65
2	2.30	538.36	0.2782	A	H-1->LUMO (81%), HOMO->LUMO (15%)	0.72
3	2.90	427.90	0.1528	A	H-2->LUMO (91%)	0.52
4	3.12	396.83	0.001	A	H-3->LUMO (78%)	0.46
5	3.24	382.83	0.0167	A	H-4->LUMO (91%)	0.35
6	3.32	373.06	0.0019	A	H-5->LUMO (88%)	0.48
7	3.41	363.17	0.0077	A	H-10->LUMO (17%), H-6->LUMO (68%)	0.40
8	3.47	357.74	0.0032	A	H-10->LUMO (21%), H-9->LUMO (19%), H-8->LUMO (17%), H-6->LUMO (19%)	0.50
9	3.55	348.83	0.3855	A	H-8->LUMO (17%), HOMO->L+1 (75%)	0.61
10	3.64	340.24	0.0093	A	H-10->LUMO (24%), H-8->LUMO (34%), H-7->LUMO (19%)	0.48
11	3.67	337.72	0.0857	A	H-1->L+1 (73%)	0.53
12	3.72	333.30	0.2016	A	H-9->LUMO (10%), H-8->LUMO (17%), H-7->LUMO (49%), H-1->L+1 (11%)	0.39
13	3.75	330.71	0.1207	A	H-9->LUMO (34%), H-7->LUMO (21%), HOMO->L+2 (27%)	0.46
14	3.77	328.59	0.2528	A	H-9->LUMO (18%), H-1->L+1 (10%), HOMO->L+2 (49%)	0.50
15	3.87	320.74	0.0193	A	H-1->L+2 (78%)	0.60
16	3.97	311.93	0.0179	A	H-11->LUMO (74%)	0.55
17	4.06	305.26	0.0491	A	HOMO->L+3 (88%)	0.33
18	4.11	301.69	0.0876	A	H-12->LUMO (28%), HOMO->L+4 (44%)	0.51
19	4.17	297.52	0.0009	A	H-1->L+3 (77%)	0.38
20	4.18	296.49	0.1996	A	H-12->LUMO (33%), HOMO->L+4 (36%)	0.53
21	4.24	292.17	0.0451	A	H-13->LUMO (60%), H-1->L+4 (20%)	0.55
22	4.30	288.40	0.0799	A	H-13->LUMO (14%), H-1->L+4 (69%)	0.48
23	4.38	283.24	0.0277	A	HOMO->L+5 (85%)	0.37
24	4.47	277.21	0.0011	A	HOMO->L+6 (84%)	0.37
25	4.52	274.10	0.017	A	H-1->L+5 (12%), HOMO->L+7 (79%)	0.47

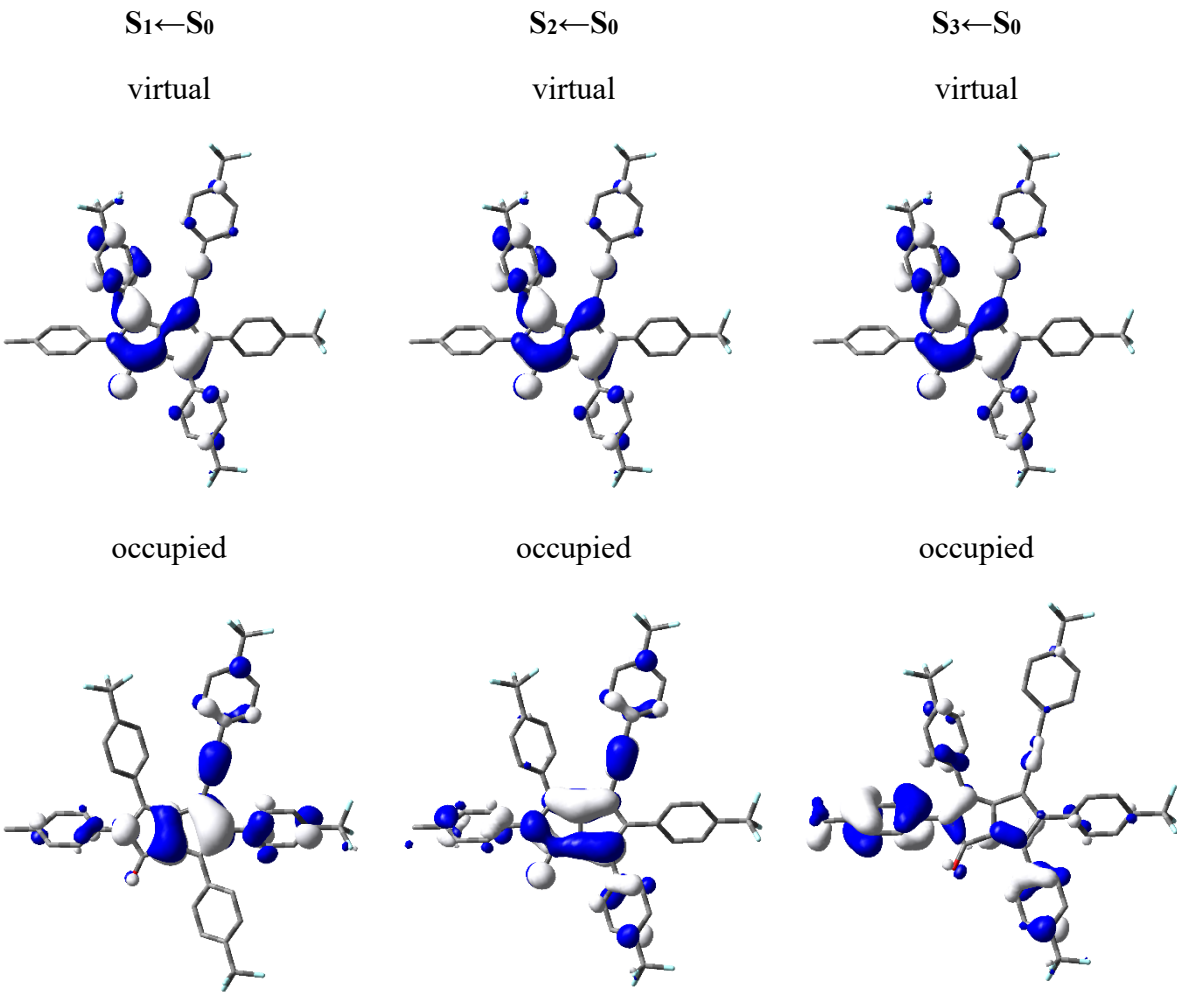

Figure A141: Frontier orbital contour plots of $S_1 \leftarrow S_o$, $S_2 \leftarrow S_o$ and $S_3 \leftarrow S_0$.

Orbitals relevant to the $S_1 \leftarrow S_0$, $S_2 \leftarrow S_0$, $S_3 \leftarrow S_0$ transitions

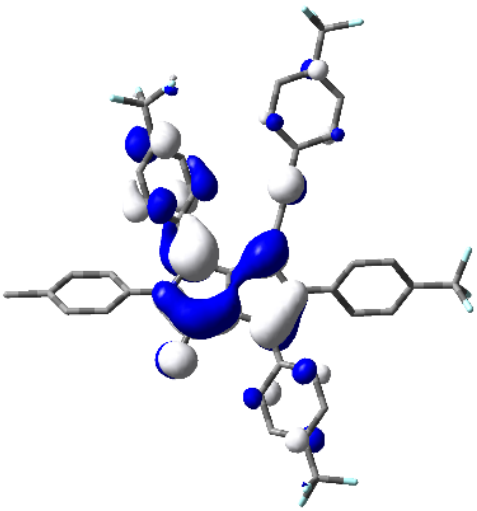

LUMO: -3.754 eV

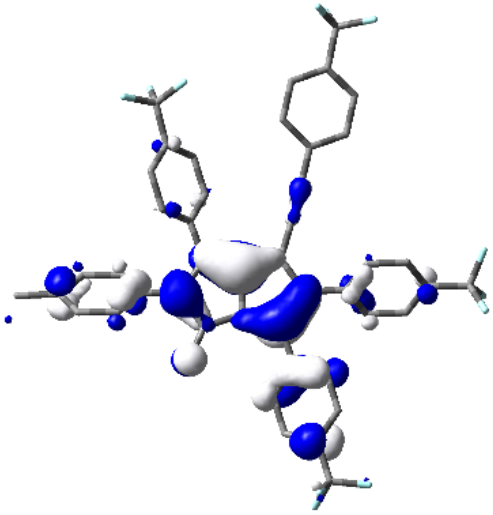

HOMO–1: –6.364 eV

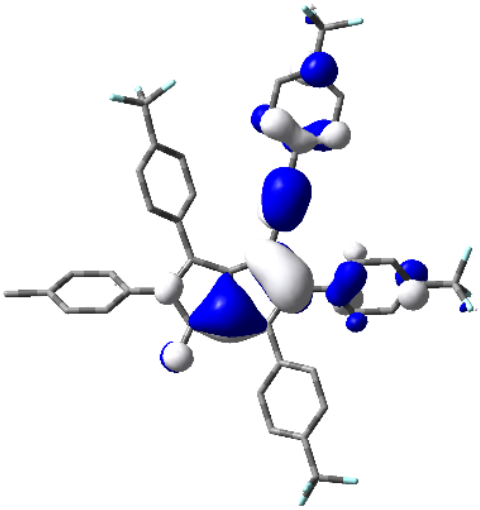

HOMO: –6.229 eV

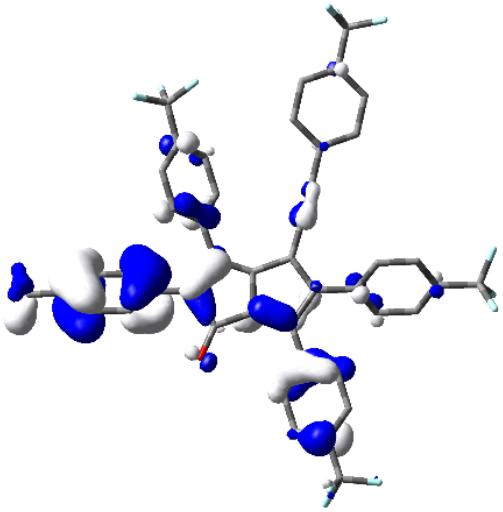

HOMO–2: –7.183 eV

Figure A142: Relevant orbitals to the $S_1 \leftarrow S_0$, $S_2 \leftarrow S_0$, $S_3 \leftarrow S_0$ transitions.

10 Acknowledgement

First of all, thank you Prof. Dr. Dr. h. c. Todd B. Marder for the chance to undertake my PhD in your group and under your supervision, for the scientific freedom that I had over the last couple of years, for your patience, endless support and time your offered to me. I am delighted to have had such an interesting topic to work on. I enjoyed learning new things and how to get a vision from all points of views on a special issue. Your passion for chemistry was always motivating. Thank you, for being an awesome teacher, mentor and boss.

Thanks to the people from the Rhodacycle/Metallacycle Group: Dr. Nicola Schwenk, Dr. Carolin Sieck, Dr. Hashem Amini, Dr. Daniel Sieh, Dr. Shishir Ghosh, Jan Maier, Robert Ricker and Charlotte Hartmann; it was a great time!

I would also like to acknowledge Dr. Alexandra Friedrich, Dr. Daniel Sieh and Johannes Krebs for the X-ray measurements.

Dr. Stefan Wagner and Christoph Mahler for measuring high-resolution mass spectra. Many thanks to the NMR-service, Dr. Rüdiger Bertermann, Marie-Luise Schäfer and Laura Wolz for numerous measurements. Thank you Rüdiger, for answering all my questions about NMR.
Thanks to Liselotte Michels and Sabine Timmroth, the elemental analysis service.
And also many thanks to Sabine Lorenzen, Christoph Mahler, Hildegard Holzinger, Yannik Reuß and Charlotte Scheufler for help, endless starting materials and keeping the group running.

I would like thank AK Steffen, especially, Prof. Dr. Andreas Steffen, Dr. Benjamin Hupp and Markus Gernert for taking care of the fluorescence spectrometer in the old building and for the introduction to the beautiful world of photophysics.

Thanks to all my internship students, bachelor and master students: Sebastian Vettermann, Tim Görlich, Daniel Gillung, Meltem Yildirim and Max Passargus.

Thanks to our secretaries Bianca Putz, Stefanie Ziegler, Maria Eckhardt and Conny Walter for all the administrative tasks and help!

I also want to thank Gertrud Wunderling for keeping our community room/kitchen representable. Thanks to Alfred Schertzer and the technical service for solving all technical problems, any time. Thanks to our glassblowers Berthold Fertig and Bernhard Werner, the

workshop crew Alois Ruf, Wolfgang Obert, Manfred Reinhardt, Michael Ramold, for the technical service and maintenance.

Furthermore, I would like to thank Dr. Stefanie Griesbeck, Dr. Julia Merz, Dr. Jörn Nitsch, Florian Rauch, Matthias Ferger and Sarina Berger for always giving me a valuable second opinion on any photophysical problem that I had.

Thank you to everybody who proof-read my thesis and for all the valuable feedback.

I also want to thank the whole Marder group for the good time, support, help and funny working days.

A big thank you to each one of my friends, who I either met at the university or have known since forever. Thank you, Michael Dömling, Markus Gernert and Andreas Hock for the great time during my chemistry studies in Würzburg. Without you, it would have been not the same. Thank you for all the beers, barbecues, advice, chats, gym sessions, weddings and for all the other things we experienced together.

Last but certainly not least, I would like to thank my family and Lina who have been such great help and support. Thank you, for all of your love, encouragement and patience. I could not have done it without you. Thank you so much!

11 Affidavit

I hereby confirm that my thesis entitled "*Reactions of rhodium(I) with diynes and studies of the photophysical behavior of the luminescent products*" is the result of my own work. I did not receive any help or support from commercial consultants. All sources and/or materials applied are listed and specified in the thesis.

Furthermore, I confirm that this thesis has not yet been submitted as part of another examination process neither in identical nor similar form.

Würzburg, .06.2020	
Place, Date	Signature

12 Eidesstattliche Erklärung

Hiermit erkläre ich an Eides statt, die Dissertation "*Reactions of rhodium(I) with diynes and studies of the photophysical behavior of the luminescent products*" eigenständig, *d.h.* insbesondere selbstständig und ohne Hilfe eines kommerziellen Promotionsberaters angefertigt und keine anderen als die von mir angegebenen Quellen und Hilfsmittel verwendet zu haben.

Ich erkläre außerdem, dass die Dissertation weder in gleicher noch in ähnlicher Form bereits in einem anderen Prüfungsverfahren vorgelegen hat.

Würzburg, .06.2020	
Ort, Datum	Unterschrift

13 Publications

The thesis listed below is partly reproduced in this dissertation (under the supervision of Florian Kerner):

Reactions of Rh(I) complexes with α,ω-diynes and studies of the luminescent properties of the products, M. B. Passargus, Bachelor's Thesis, Julius-Maximilians-Universität Würzburg, **2019**.

Further publications:

X. Jia, J. Nitsch, L. Ji, Z. Wu, A. Friedrich, F. Kerner, M. Moos, C. Lambert, T. B. Marder, *Chem. Eur. J.* **2019**, *25*, 10845 – 10857.

X. Liu, W. Ming, A. Friedrich, F. Kerner, T. B. Marder, *Angew. Chem. Int. Ed.* **2020**, *59*, 304 – 309.

Y. P. Budiman, A. Jayaraman, A. Friedrich, F. Kerner, U. Radius, T. B. Marder, *J. Am. Chem. Soc.* **2020**, *142*, 6036 – 6050.

M. Gernert, L. Balles-Wolf, F. Kerner, U. Müller, A. Schmiedel, M. Holzapfel, C. M. Marian, J. Pflaum, C. Lambert, A. Steffen, *J. Am. Chem. Soc.* **2020**, *142*, 8897 – 8909.